ROOTS – THE HIDDEN PROVIDER

EDITED BY: Janin Riedelsberger and Michael R. Blatt
PUBLISHED IN: Frontiers in Plant Science

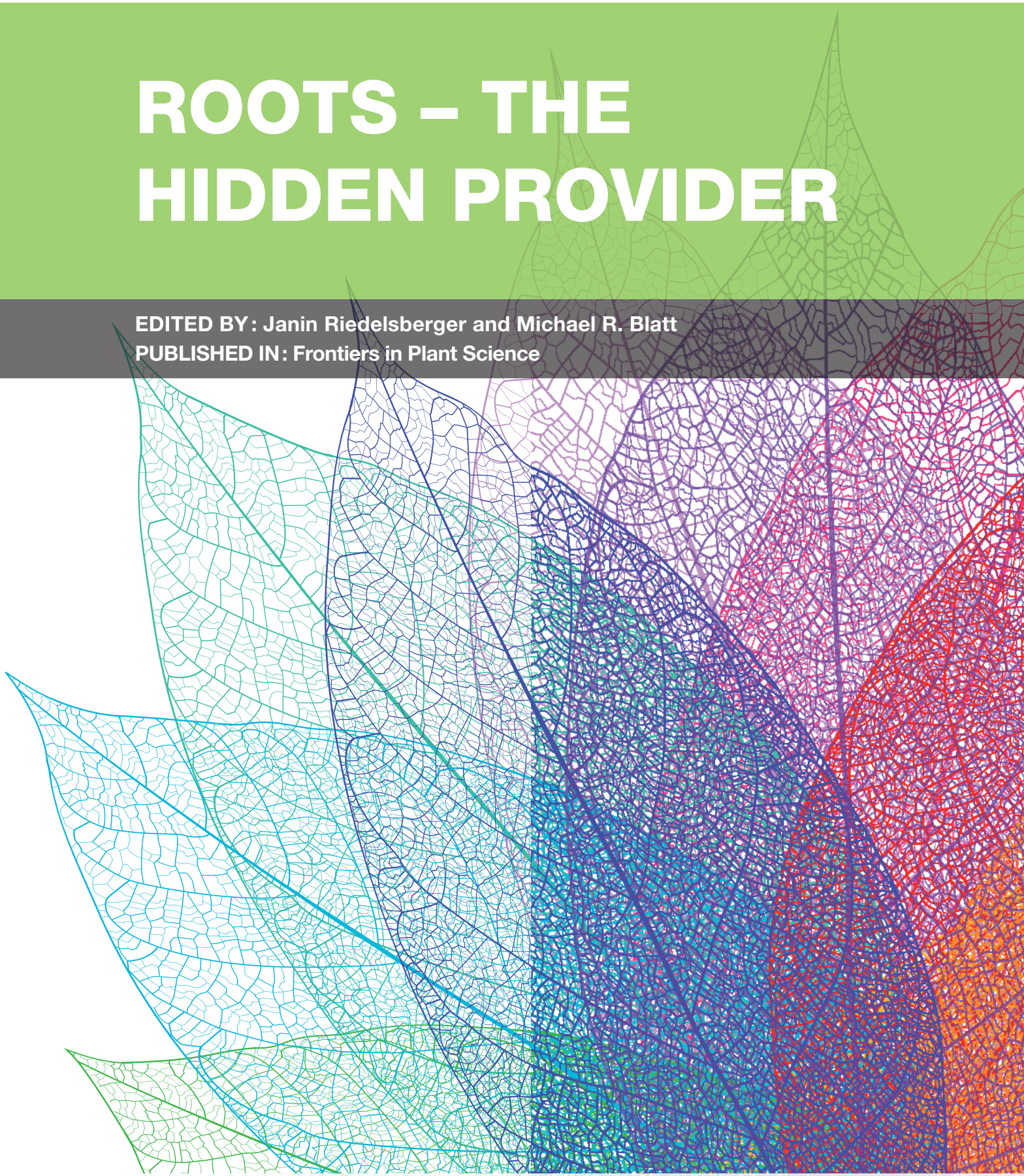

frontiers Research Topics

frontiers

ISSN 1664-8714
ISBN 978-2-88945-244-6
DOI 10.3389/978-2-88945-244-6

About Frontiers

Frontiers is more than just an open-access publisher of scholarly articles: it is a pioneering approach to the world of academia, radically improving the way scholarly research is managed. The grand vision of Frontiers is a world where all people have an equal opportunity to seek, share and generate knowledge. Frontiers provides immediate and permanent online open access to all its publications, but this alone is not enough to realize our grand goals.

Frontiers Journal Series

The Frontiers Journal Series is a multi-tier and interdisciplinary set of open-access, online journals, promising a paradigm shift from the current review, selection and dissemination processes in academic publishing. All Frontiers journals are driven by researchers for researchers; therefore, they constitute a service to the scholarly community. At the same time, the Frontiers Journal Series operates on a revolutionary invention, the tiered publishing system, initially addressing specific communities of scholars, and gradually climbing up to broader public understanding, thus serving the interests of the lay society, too.

Dedication to Quality

Each Frontiers article is a landmark of the highest quality, thanks to genuinely collaborative interactions between authors and review editors, who include some of the world's best academicians. Research must be certified by peers before entering a stream of knowledge that may eventually reach the public - and shape society; therefore, Frontiers only applies the most rigorous and unbiased reviews.
Frontiers revolutionizes research publishing by freely delivering the most outstanding research, evaluated with no bias from both the academic and social point of view.
By applying the most advanced information technologies, Frontiers is catapulting scholarly publishing into a new generation.

What are Frontiers Research Topics?

Frontiers Research Topics are very popular trademarks of the Frontiers Journals Series: they are collections of at least ten articles, all centered on a particular subject. With their unique mix of varied contributions from Original Research to Review Articles, Frontiers Research Topics unify the most influential researchers, the latest key findings and historical advances in a hot research area! Find out more on how to host your own Frontiers Research Topic or contribute to one as an author by contacting the Frontiers Editorial Office: **researchtopics@frontiersin.org**

ROOTS – THE HIDDEN PROVIDER

Topic Editors:
Janin Riedelsberger, Universidad de Talca, Chile
Michael R. Blatt, University of Glasgow, United Kingdom

Citation: Riedelsberger, J., Blatt, M. R., eds. (2017). Roots – The Hidden Provider. Lausanne: Frontiers Media. doi: 10.3389/978-2-88945-244-6

Table of Contents

Root-shoot communication

Modelling of nutrient transport

frontiers in Plant Science

EDITORIAL
published: 13 June 2017
doi: 10.3389/fpls.2017.01021

Editorial: Roots—The Hidden Provider

Janin Riedelsberger[1]* *and Michael R. Blatt*[2]*

[1] Centro de Bioinformática y Simulación Molecular, Universidad de Talca, Talca, Chile, [2] Laboratory of Plant Physiology and Biophysics, University of Glasgow, Glasgow, United Kingdom

Keywords: roots, ion transport, root system architecture (RSA), modeling biological systems

Editorial on the Research Topic

Roots—The Hidden Provider

Most plant roots are found hidden underground. They can form immense root systems with lengths of several kilometers featuring an architecture with up to millions of branch roots. Their versatile functions range from anchoring plants in soil via storing photosynthetic products to the vital uptake of water and nutrients. Plants build the basis of a food chain that ends with more than seven billion people who have to be fed every day. Therefore, it is vital to secure and enhance crop production, especially in terms of prevailing agricultural threats and climate change. The challenge must be to optimize plant's nutrient acquisition and stress tolerance. Understanding plant nutrition, homeostasis, and stress responses is a first step to directed and efficient manipulations and adjustments to counterbalance stress and deficiency symptoms. This knowledge must be used to optimize the use of fertilizer and water to achieve well-balanced nutrition acquisition as well as the use of pesticides to treat biotic stress. Such optimization is desirable as the constant use of fertilizer, irrigation, and pesticides is associated with negative long-term effects. Knowledge about nutrient uptake and signaling as well as behavior in stress situations will be valuable if we are to design adequate treatments to prepare plants for environmental challenges.

NUTRIENT UPTAKE AND SIGNALING

Nutrient uptake is the first step in the production of plant mass. It starts in the roots, which represent the main entrance for macro- and micronutrients that are crucial for elementary cell processes. Deficiency or excess nutrient uptake can result in severe damage to the point of yield loss or even plant death. Therefore, a balanced nutrient supply and its uptake are essential for optimal plant growth and crop production. Nutrient distribution in the soil is heterogeneous in space and time and affected by many factors, including binding and sequestration, groundwater level, pH, and salinity.

The three primary plant macronutrients are potassium, nitrate, and phosphorus. Over the course of evolution, transport systems with differing affinities for nutrients evolved to cope with variations in nutrient availability. Nieves-Cordones et al. and Noguero and Lacombe review high- and low-affinity uptake systems for potassium and nitrate, respectively. The uptake of phosphorus, which serves as well as nitrogen as constituent of macromolecules is reviewed by Gu et al. (2016).

Nitrate also acts as signaling molecule influencing lateral root primordia and root branching (Noguero and Lacombe). A more extensive signaling system is built upon calcium. The specificity of calcium signaling is determined by patterns of cytosolic calcium concentrations taking into account at least the amplitude and duration of calcium increases. Cytosolic free calcium concentration acts as a secondary messenger in the signaling of abiotic stress including nutrient deficiency. The

OPEN ACCESS

Edited by:
Hans-Henning Kunz, Washington State University, United States

Reviewed by:
Hans-Henning Kunz, Washington State University, United States
Karen A. Sanguinet, Washington State University, United States

***Correspondence:**
Janin Riedelsberger
jriedelsberger@utalca.cl
Michael R. Blatt
michael.blatt@glasgow.ac.uk

Specialty section:
This article was submitted to Plant Physiology, a section of the journal Frontiers in Plant Science

Received: *24 March 2017*
Accepted: *29 May 2017*
Published: *13 June 2017*

Citation:
Riedelsberger J and Blatt MR (2017) Editorial: Roots—The Hidden Provider. Front. Plant Sci. 8:1021. doi: 10.3389/fpls.2017.01021

comprehensive review of Wilkins and colleagues summarizes the state of the art of calcium's broad modes of operation. Besides, calcium transport systems, that are still an active field of investigation, are reviewed (Wilkins et al.).

Micronutrients often occur abundantly in solid earth but mainly in an insoluble form that is not suitable for uptake, meaning that plants may suffer nutrient deficiency despite their presence in the soil. One example is iron. Plants exhibit a number of special uptake strategies for iron. Poaceae use a chelation strategy to uptake iron by secreting phytosiderophores or precursors of phytosiderophores into the rhizosphere. Then, the chelated iron(III)-phytosiderophore complex is taken up into the plant by special transport systems. Non-Poaceae use an acidification-reduction strategy, which acidifies the rhizosphere to reduce iron(III) to iron(II), which can be taken up by plant roots. Phenolic compounds like coumarins, especially catechol coumarins, have been reported to play a role in iron recruitment showing iron(III) reducing and iron(II) chelating activity (Sisó-Terraza et al.).

Generally, acidic soils stimulate the uptake of micronutrients like iron. However, low pH also increases the solubility of toxic metals like aluminum, which directly affects the root system architecture (Rao et al., 2016). To control toxic metals plants developed quite sophisticated defense mechanisms. For example, plants chelate toxic aluminum ions with malate and export the aluminum-malate complex (Sharma et al.). ALMT channels have been identified to transport these malate-aluminum complexes. Latest research showed that the ALMT anion channel family has a far more versatile functional spectrum than initially thought. Sharma and colleagues give an extensive overview on ALMT's variable physiological and structural aspects including their input in mineral nutrition, ion homeostasis, and guard cell function among others.

PLANT ROOT—MICROBE INTERACTIONS

The most important plant-microbe interaction is the mycorrhizal symbiosis between plants and fungi. Plants benefit from enhanced nutrient uptake and stress resistance, while the fungi are provided with photosynthetical products. Schott and colleagues described a minimal network of transporters that is sufficient to describe realistically the bidirectional nutrient trade system (Schott et al.).

Another important plant symbiotic relationship is that between legumes and rhizobia, a type of nitrogen-fixing bacteria. Here, the plant benefits from the biological nitrogen fixation that is carried out by the rhizobial symbiont, while bacteria receive photosynthetically fixed carbon. Establishing such interactions between plant root hairs and microorganisms is initiated by chemical communication. Bacterial symbionts respond to plant signaling compounds with nod factor secretion that induces broad changes in the plant root transport machinery (Damiani et al.). Using high throughput RNA sequencing Damiani and colleagues identified a set of transport systems that are likely to be involved in early nodulation (Nod) factor signaling suggesting substantial rearrangements in the nutrient transport machinery after Nod factor perception.

Root exudates may also contain substances that function as allelochemicals for plant's defense. Infestation with pathogenic microorganisms can lead to substantial yield losses. It is thus essential to understand how plants are able to resist pathogen invasion if we are to enhance these defense mechanisms. A common signal on the part of bacteria is the bacterial protein flagellin flg22 that is recognized by the plant receptor kinase FLS2 and also induces ALMT transporter expression (Chen et al.; Sharma et al.).

ROOT SYSTEM ARCHITECTURE RESPONSES TO STRESS

Generally, plants are exposed to several stresses simultaneously. Although much attention is drawn to the characteristics of the shoot, effects on roots are often ignored. Though, root plasticity is highly flexible and its development is guided by environmental conditions like nutrient availability. Koevoets et al. address this gap in focus and summarize comprehensively the effects of nutrient deficiencies and other abiotic stresses on the root system architecture plasticity. In addition, the authors discuss challenges that have to be resolved to implement root system architecture evaluation in crop selection.

One of the major agricultural challenges is the increasing salinization of agricultural land. The majority of crop plants are salt-sensitive, which is why articles of this research topic concentrate on glycophytes. Nieves-Cordones and colleagues reviewed present knowledge on sodium uptake systems in plant roots and their regulations (Nieves-Cordones et al.). Sodium may be beneficial for plants, especially under potassium shortage, but it is not an essential nutrient. At high concentrations it causes stress that has far-reaching impact. Annunziata et al. and Jiang et al. present examples on how salt stress affects cytosolic metabolites and root growth.

ROOT-SHOOT COMMUNICATION

For centuries the increase in crop yield raise and quality has been achieved by transferring the scion of one plant to the rootstock of another plant. This process, known as grafting, may lead to increased nutrient uptake and stress tolerance among other benefits. Despite long and still actively utilized practice of grafting, physiological, and molecular bases are not fully understood yet. Nawaz et al. summarizes grating effects on ion uptake and accumulation. The authors discuss the enhanced expression of transport-related genes and changes in hormonal levels that influence the architecture of root systems.

The root structure not only responds to external stimuli, but also to partitioning patterns of photoassimilates in roots. Mudgil et al. discuss a possible signaling mechanism of photosynthetically fixed sugars that affect root system architecture. It is vital to understand root-shoot communication since seed production, the origin of the coming generation, depends on optimal grain filling that in part is achieved by

root carbon sources especially under dry conditions (Zhang et al.).

MODELING OF NUTRIENT TRANSPORT

Uptake and transport pathways of nutrients are well-organized for every mineral. These pathways intersect and result in complex networks that can be challenging to access experimentally. Modeling of transport processes, nutrient exchange and uptake processes have been subject to long-term investigations, which aim to predict and describe experimental data. Le Deunff and colleagues describe the advantage of the flow-force modeling approach over the enzyme-substrate approach by reviewing developments and advances carried out on modeling of nutrient uptake (Le Deunff et al.). Water and nutrient uptake into roots is non-uniform in space. Foster and Miklavcic illustrate root zone effects on passive water and nutrient uptake. Modeling approaches are advancing and more and more capable of reflecting biological realities. Schott and colleagues successfully reconstructed nutrient exchange processes between mycorrhizal symbionts and plant root cells. Their model furthermore permitted them to hypothesize about the potential mechanism behind symbiont-plant interactions (Schott et al.).

Modeling approaches go beyond the description of nutrient uptake and transport. Efforts have been made to simulate effects on whole root system architectures in response to nutrient availability (Postma et al., 2014a,b).

OUTLOOK

For future investigations it is crucial to combine studies of entire root systems and plants with modeling approaches. This ensures the assessment of systemic effects that result from changes in single traits. Advances in this field should be integrated into current experimental pipelines to refine and accelerate research. Further advances in the understanding of nutrient homeostasis are needed to enhance nutrient use efficiency and optimize the use of fertilizer as well as to improve and maintain soil quality and protect the environment from inefficient water and fertilizer use.

AUTHOR CONTRIBUTIONS

JR wrote the first draft of the manuscript. JR and MB revised and improved the manuscript.

FUNDING

This work was supported by grants from the Chilean Fondo Nacional de Desarrollo Científico y Tecnológico (http://www.conicyt.cl/fondecyt) to JR (No. 3150173).

REFERENCES

Gu, M., Chen, A., Sun, S., and Xu, G. (2016). Complex regulation of plant phosphate transporters and the gap between molecular mechanisms and practical application: what is missing? *Mol. Plant* 9, 396–416. doi: 10.1016/j.molp.2015.12.012

Postma, J. A., Dathe, A., and Lynch, J. P. (2014a). The optimal lateral root branching density for maize depends on nitrogen and phosphorus availability. *Plant Physiol.* 166, 590–602. doi: 10.1104/pp.113.233916

Postma, J. A., Schurr, U., and Fiorani, F. (2014b). Dynamic root growth and architecture responses to limiting nutrient availability: linking physiological models and experimentation. *Biotechnol. Adv.* 32, 53–65. doi: 10.1016/j.biotechadv.2013.08.019

Rao, I. M., Miles, J. W., Beebe, S. E., and Horst, W. J. (2016). Root adaptations to soils with low fertility and aluminium toxicity. *Ann. Bot.* 118, 593–605. doi: 10.1093/aob/mcw073

Conflict of Interest Statement: The authors declare that the research was conducted in the absence of any commercial or financial relationships that could be construed as a potential conflict of interest.

The reviewer KS and handling Editor declared their shared affiliation, and the handling Editor states that the process nevertheless met the standards of a fair and objective review.

frontiers in Plant Science

REVIEW
published: 05 July 2016
doi: 10.3389/fpls.2016.00992

Comparison between *Arabidopsis* and Rice for Main Pathways of K^+ and Na^+ Uptake by Roots

*Manuel Nieves-Cordones[1], Vicente Martínez[2], Begoña Benito[3] and Francisco Rubio[2]**

[1] *Biochimie et Physiologie Moléculaire des Plantes, Institut de Biologie Intégrative des Plantes, UMR 5004 CNRS/UMR 0386 INRA/Montpellier SupAgro/Université Montpellier 2, Montpellier, France,* [2] *Departamento de Nutrición Vegetal, Centro de Edafología y Biología Aplicada del Segura – Consejo Superior de Investigaciones Científicas, Murcia, Spain,* [3] *Centro de Biotecnología y Genómica de Plantas, Universidad Politécnica de Madrid, Madrid, Spain*

K^+ is an essential macronutrient for plants. It is acquired by specific uptake systems located in roots. Although the concentrations of K^+ in the soil solution are widely variable, K^+ nutrition is secured by uptake systems that exhibit different affinities for K^+. Two main systems have been described for root K^+ uptake in several species: the high-affinity HAK5-like transporter and the inward-rectifier AKT1-like channel. Other unidentified systems may be also involved in root K^+ uptake, although they only seem to operate when K^+ is not limiting. The use of knock-out lines has allowed demonstrating their role in root K^+ uptake in *Arabidopsis* and rice. Plant adaptation to the different K^+ supplies relies on the finely tuned regulation of these systems. Low K^+-induced transcriptional up-regulation of the genes encoding HAK5-like transporters occurs through a signal cascade that includes changes in the membrane potential of root cells and increases in ethylene and reactive oxygen species concentrations. Activation of AKT1 channels occurs through phosphorylation by the CIPK23/CBL1 complex. Recently, activation of the *Arabidopsis* HAK5 by the same complex has been reported, pointing to CIPK23/CBL as a central regulator of the plant's adaptation to low K^+. Na^+ is not an essential plant nutrient but it may be beneficial for some plants. At low concentrations, Na^+ improves growth, especially under K^+ deficiency. Thus, high-affinity Na^+ uptake systems have been described that belong to the HKT and HAK families of transporters. At high concentrations, typical of saline environments, Na^+ accumulates in plant tissues at high concentrations, producing alterations that include toxicity, water deficit and K^+ deficiency. Data concerning pathways for Na^+ uptake into roots under saline conditions are still scarce, although several possibilities have been proposed. The apoplast is a significant pathway for Na^+ uptake in rice grown under salinity conditions, but in other plant species different mechanisms involving non-selective cation channels or transporters are under discussion.

Keywords: potassium, sodium, uptake, roots, *Arabidopsis*, rice

OPEN ACCESS

Edited by:
Janin Riedelsberger, University of Talca, Chile

Reviewed by:
Vadim Volkov, London Metropolitan University, UK
Vicenta Salvador-Recatala, Ronin Institute, USA
Abdul Wakeel, University of Agriculture Faisalabad, Pakistan
Jose M. Pardo, Instituto de Bioquímica Vegetal y Fotosíntesis – Consejo Superior de Investigaciones Científicas, Spain

****Correspondence:***
Francisco Rubio
frubio@cebas.csic.es

Specialty section:
This article was submitted to Plant Physiology, a section of the journal Frontiers in Plant Science

Received: *31 March 2016*
Accepted: *22 June 2016*
Published: *05 July 2016*

Citation:
Nieves-Cordones M, Martínez V, Benito B and Rubio F (2016) Comparison between Arabidopsis and Rice for Main Pathways of K^+ and Na^+ Uptake by Roots. Front. Plant Sci. 7:992. doi: 10.3389/fpls.2016.00992

INTRODUCTION

Given the constant increase in world population, high-yield crop production has become a necessity for agriculture. As that the nutrient sources of the land are limited, the input of nutrients by the addition of fertilizers ensures a continuous supply for plants, circumventing reductions in plant yield. The use of fertilizers has raised crop yield considerably, for example, from 50 to 80%

of wheat and corn grain yield is attributable to nutrient fertilization (Stewart et al., 2005). However, this practice comes with high economic and environmental costs.

Potassium (K^+) is an essential macronutrient that is required by plants to complete their life cycle (Taiz and Zeiger, 1991). K^+ can make up to 10% of the total plant dry weight (Leigh and Wyn Jones, 1984) and fulfills important functions for metabolism, growth, and stress adaptation. Specifically, it acts as an enzyme activator, protein synthesis stabilizer, neutralization of protein negative charges, and it participates in cytoplasmic pH homeostasis as well (Marschner, 2012). An optimal K^+ concentration in the cytosol of around 100 mM is required for the performing of the functions mentioned above (Wyn Jones and Pollard, 1983), and plant cells maintain the cytosolic K^+ concentration around this value (Walker et al., 1996).

K^+ constitutes about 2.9% of the earth's crust but the concentration of K^+ in the soil solution is highly variable, in the 10^{-5} to 10^{-3} M range (Barraclough, 1989; Marschner, 2012). Since roots are able to take up K^+ at a higher rate than this cation can diffuse from the bulk soil solution, a K^+ depletion zone near the root surface can be formed with K^+ concentrations of just a few micromolar (Baldwin et al., 1973; Claassen and Jungk, 1982). More importantly, increasing areas of the world are currently described as being K^+ deficient for agricultural practices (Mengel et al., 2001; Moody and Bell, 2006; Römheld and Kirkby, 2010; Kirkby and Schubert, 2013).

K^+ deficiency has a negative impact on plant growth since cellular expansion and photosynthesis are severely affected under these conditions (Bednarz and Oosterhuis, 1999; Hafsi et al., 2014). This deficiency also correlates with a decrease in protein synthesis and subsequent decline in growth (Walker et al., 1996, 1998). K^+ deficiency has been shown to inhibit lateral root development in *Arabidopsis* (Armengaud et al., 2004; Shin and Schachtman, 2004; Kellermeier et al., 2014) and in barley (Drew, 1975) and in the up-regulation of genes involved in K^+ uptake (Ashley et al., 2006; Nieves-Cordones et al., 2014). In addition, K^+-deficient plants are more sensitive to abiotic and biotic stresses such as drought, cold, salinity, or fungal attacks (Marschner, 2012; Zörb et al., 2014).

Sodium (Na^+) is not an essential element for plants but, for some species it can be a beneficial element that stimulates growth (Wakeel et al., 2010, 2011; Kronzucker et al., 2013). In these cases, Na^+ can be regarded as a functional nutrient (Subbarao et al., 2003), that can partly replace K^+ in some functions such as osmotic adjustment of the large central vacuole, cell turgor regulation leading to cell enlargement, or long-distance transport of anions (Subbarao et al., 2003; Horie et al., 2007; Gattward et al., 2012; Battie-Laclau et al., 2013).

On the other hand, Na^+ has been extensively associated to its negative impact on crop yield. Excess of Na^+ salts in the soil results in both reduced soil water availability (due to the decrease in water potential) and ionic toxicity. When accumulated at high concentrations in the cytoplasm, Na^+ results in deleterious effects on cell biology, e.g., on photosynthetic activity or on membrane integrity (due to displacement of membrane-bound Ca^{2+} ions) (Cramer et al., 1985). Thus, Na^+ is usually compartmentalized outside the cytoplasm (Morgan et al., 2014), in vesicles such as the vacuole, where it is used as an osmoticum. Estimates of the area of salt-affected soils vary widely, ranging from 6 to 10% of the earth's land area (Eynard et al., 2005; Munns and Tester, 2008). Importantly, 20% of irrigated lands are affected by secondary salinization, limiting agriculture worldwide.

In the present review, we summarize recent advances in the field of K^+ and Na^+ uptake in the plant root, with special attention to the transport systems and their regulation mechanisms. We believe that the studies performed on the model plant *Arabidopsis* and the results of recent research in crops such as rice suggest that the results obtained with model species cannot be fully extended to other plant species.

K^+ AND Na^+ UPTAKE BY ROOTS: KINETIC FEATURES AND SENSITIVITY TO OTHER CATIONS

K^+ and Na^+ can enter the root apoplast and diffuse toward inner cell layers (Sattelmacher et al., 1998). However, this pathway is interrupted by the endodermis, where the Casparian strip, which is impermeable to water and ions, is located (Schreiber et al., 1999; Tester and Leigh, 2001; Marschner, 2012; Geldner, 2013; Barberon and Geldner, 2014). To cross this impermeable barrier, nutrient ions enter the cytosol of a root peripheral cell either from the epidermis, cortex or endodermis and move from cell to cell (symplastic pathway) through plasmodesmata (Burch-Smith and Zambryski, 2012). Diffusion within the symplasm beyond the endodermic barrier allows nutrient ions to reach the stele, where they will initiate their travel toward the aerial parts within the xylem vessels (Lauchli, 1972).

It is worth noting that the Casparian strip may be absent in some places (Maathuis, 2014) allowing ions to reach the root stele and xylem vessels through the apoplastic pathway via bypass flow (Kronzucker and Britto, 2011). Since this flow is relatively low, most of the ions that reach the root xylem vessels are probably taken up across the plasma membrane of a root peripheral cell (Tester and Leigh, 2001). Thus, their entry into the root symplasm would have been mediated by membrane transport systems, channels, transporters or cotransporters. It should be noted that the bypass flow was observed in rice at Na^+ external concentrations as low as 25 mM (Yeo et al., 1987) and it may contribute to salt stressing effects under high salinity by having an effect in shoot Na^+ content (Yeo et al., 1987; Faiyue et al., 2012; Maathuis, 2014). Na^+ bypass flow has been described in other species, besides rice, such as mangroves (Krishnamurthy et al., 2014), maize, and broad bean (Peterson et al., 1981), but not in *Arabidopsis* (Essah et al., 2003).

More than 60 years ago, through the application of the concept of enzyme kinetics for the study of root K^+ absorption (Epstein and Hagen, 1952), Epstein et al. (1963) suggested that at least two transport systems were involved in root K^+ uptake: a high-affinity system that operates at low external concentrations and a low-affinity system at higher concentrations. A similar scheme was also described for Na^+ uptake (Rains and Epstein, 1967a). This biphasic behavior has since been observed in many plant species, with some exceptions. Maize, for example, shows

a linear, non-saturating response to K^+ in the low-affinity range (Kochian and Lucas, 1982). More recently, it has been shown that this linear response is dominated by the apoplastic movement of K^+, and the "true" transmembrane flux saturates at modest rates (Coskun et al., 2016). In the high-affinity range of concentrations, K^+ uptake is an active process that takes place against the K^+ electrochemical potential, most likely by a K^+/H^+ symport, whilst the low-affinity uptake can take place by passive transport through inwardly rectifying K^+ channels (Maathuis and Sanders, 1996a; Maathuis et al., 1997; Rodríguez-Navarro, 2000). It should also be noted that the limits in K^+ concentrations for the operation of a symporter or a channel depend on the plasma membrane potential and the cytoplasmic pH and K^+ concentrations. Thus, assuming, for example, that a cytoplasmic K^+ concentration of 100 mM and a membrane potential of −240 mV exists, K^+ uptake could take place through a channel from an external K^+ concentration as low as 10 μM, which falls within the high-affinity system described by Epstein et al. (1963), Hirsch et al. (1998) and Spalding et al. (1999). High-affinity K^+ uptake becomes apparent when K^+ tissue concentrations decrease due to K^+ starvation (Glass, 1976; Kochian and Lucas, 1982; Siddiqi and Glass, 1986; Martínez-Cordero et al., 2005). Providing NH_4^+ to the nutrient solution used to grow the plants, has a large influence on the NH_4^+ sensitivity of high-affinity K^+ uptake. In some species such as barley (Santa-María et al., 2000), pepper (Martínez-Cordero et al., 2005), or *Arabidopsis* (Rubio et al., 2008), the presence of NH_4^+ in the growth solution induced an NH_4^+-insensitive high-affinity K^+ uptake component. In others, such as tomato (Nieves-Cordones et al., 2007), high-affinity K^+ uptake was dominated by an NH_4^+-sensitive component, irrespectively of the presence or the absence of NH_4^+ in the growth solution. By contrast, both Na^+ (Martínez-Cordero et al., 2005; Kronzucker et al., 2006, 2008; Nieves-Cordones et al., 2007, 2010; Alemán et al., 2009; Cheng et al., 2015) and Cs^+ (Rubio et al., 2000; White and Broadley, 2000; Qi et al., 2008) usually inhibit high-affinity K^+ uptake.

Regarding low-affinity K^+ transport, the role of TEA^+, Cs^+, and Ba^{2+}, in blocking animal and plant K^+ channels is well known, as these inhibit low-affinity K^+ uptake, supporting the idea of the channel-mediated nature of this transport (Ketchum and Poole, 1991; Blatt, 1992; Hille, 1992; Very and Sentenac, 2002; Hoopen et al., 2010; Coskun et al., 2013). Unlike high-affinity K^+ uptake, low-affinity K^+ uptake is not down-regulated at high external K^+ (Maathuis and Sanders, 1996b; Szczerba et al., 2006) and it is NH_4^+-insensitive (Spalding et al., 1999; Santa-María et al., 2000; Kronzucker et al., 2003; Szczerba et al., 2006). Na^+ suppresses K^+ uptake both in the low- and the high-affinity ranges, with low-affinity K^+ uptake being more sensitive to this inhibition (Epstein et al., 1963; Rains and Epstein, 1967a; Kronzucker et al., 2006, 2008). It is worth noting that K^+ uptake seems to be insensitive to Ca^{2+} in barley and *Arabidopsis* (Cramer et al., 1989; Caballero et al., 2012; Coskun et al., 2013).

As for Na^+ uptake, it has been shown that root high-affinity Na^+ uptake is significant when plants are starved of K^+ (Garciadeblas et al., 2003; Haro et al., 2010). Under these conditions, Na^+ is able to partially replace K^+ and support plant growth (Maathuis and Sanders, 1993; Garciadeblas et al., 2003; Horie et al., 2007; Wakeel et al., 2011; Wakeel, 2013). High-affinity Na^+ uptake has been shown to be sensitive to K^+ and Ca^{2+} in barley (Rains and Epstein, 1967b) and to K^+ and Ba^{2+} in rice (Garciadeblas et al., 2003). By contrast, low-affinity Na^+ uptake seems to be insensitive to Ca^{2+} and K^+ in rice (Malagoli et al., 2008) while it is sensitive to Ca^{2+} in *Arabidopsis*, barley, and wheat (Cramer et al., 1987, 1989; Essah et al., 2003; D'Onofrio et al., 2005). Na^+ uptake can be reduced by the application of K^+, and such reduction can alleviate salt stress effects to some extent (Wakeel, 2013). For example, a reduction in tissue Na^+ content due to increased K^+ application was observed in strawberry or in *Jatropha curcas* (Khayyat et al., 2009; Rodrigues et al., 2012).

IDENTIFICATION OF K^+ TRANSPORT SYSTEMS IN PLANTS

The molecular approaches developed in the last 25 years have led to the characterization of many K^+ and Na^+ transport systems in plants. The first K^+ uptake system identified in plants, AKT1, was isolated by complementing a K^+-uptake deficient yeast strain with an *Arabidopsis* cDNA library (Sentenac et al., 1992). Sequence analysis and heterologous expression in Sf9-insect cells showed that the AKT1 cDNA encoded an inward-rectifier K^+ channel belonging to the Shaker family (Gaymard et al., 1996). The gene encoding this channel showed specific constitutive expression in epidermal root cells (Lagarde et al., 1996) and AKT1 was proposed as the system mediating low-affinity K^+ uptake in the roots.

Later, a PCR-based approach led to the identification of a cDNA from barley, HvHAK1, that mediated high-affinity K^+ uptake in yeast (Santa-María et al., 1997). Specific expression of its mRNA in K^+-starved roots and its kinetic properties in yeast prompted researchers to propose it as the system mediating the high-affinity K^+ uptake observed in barley roots (Epstein et al., 1963). Subsequent studies led to the identification of an *Arabidopsis* homolog of HvHAK1, that was named AtHAK5 (Rubio et al., 2000).

In addition to AKT1 and AtHAK5-like transporters, other K^+ uptake systems could be involved in root K^+ uptake and in transmembrane K^+ movements in other plant organs. Moreover, the sequence of whole genomes of plants evidenced the existence of large gene families encoding putative K^+ transport systems (Grabov, 2007; Véry et al., 2014; Nieves-Cordones et al., 2016).

Initial Characterizations in *Arabidopsis*

The studies on heterologous systems and on gene expression patterns for AKT1 and AtHAK5 produced data suggesting that these two systems played important roles in K^+ acquisition by the root. However, a demonstration for the proposed roles was only possible when *Arabidopsis* knock-out mutants for these two genes became available (Spalding et al., 1999; Gierth et al., 2005; Rubio et al., 2008, 2010; Pyo et al., 2010). The studies showed that while *Arabidopsis* wild-type (WT) and *akt1* plants could deplete external K^+ (Rb^+) to values around 1 μM, the

athak5 plants did not diminish its concentration below 30 μM. In agreement with this, reduced growth was observed in *athak5* plants grown in the presence of 1 μM K^+ (Qi et al., 2008) or 10 μM K^+ (Pyo et al., 2010; Ragel et al., 2015). Moreover, K^+ (Rb^+) uptake in *athak5* plants was completely inhibited by the presence of Ba^{2+} in the external solution. By contrast, a complete inhibition of K^+ (Rb^+) depletion was observed in the presence of NH_4^+ in the *akt1* line. An *athak5 akt1* double mutant did not show K^+ (Rb^+) uptake at external concentrations below 50 μM, and it could only promote K^+ (Rb^+) uptake at concentrations higher than 100 μM. All these results demonstrated that in *Arabidopsis* plants, AtHAK5 was the only system mediating K^+ uptake at concentrations below 10 μM and that this system was inhibited by NH_4^+. At concentrations between 10 and 200 μM, both AtHAK5 and AKT1 contributed to K^+ uptake, defining AKT1 as a Ba^{2+}-sensitive component of K^+ uptake. Above 500 μM AtHAK5 contribution was negligible as the *AtHAK5* gene was repressed at this external K^+ concentration, and AKT1 role became more relevant. Unidentified systems could compensate for the lack of AKT1 since the *akt1* and the *athak5 akt1* lines grew at similar rates than the WT line when the external K^+ concentration was sufficiently high (∼10 mM).

The studies described for *Arabidopsis* allowed for depicting a model for the contribution of AtHAK5 and AKT1 to root K^+ uptake (Alemán et al., 2011). They also allowed for extending the studies to species where knock-out mutants were not available, through the use of NH_4^+ and Ba^{2+} as specific inhibitors of HAK5 and AKT1, respectively. Thus, it was shown that in tomato and pepper plants grown in the absence of NH_4^+, an NH_4^+-sensitive component, probably mediated by SlHAK5 (formerly LeHAK5) and CaHAK1, respectively, dominated K^+ uptake from concentrations corresponding to the high-affinity component (inhibition of K^+ uptake by NH_4^+ was close to 80% in tomato, for example; Martínez-Cordero et al., 2005; Nieves-Cordones et al., 2007). These results contrast with those obtained for *Arabidopsis*, where both AtHAK5 and AKT1 contribute to K^+ uptake within the range of the K^+ concentration assigned to the high-affinity component, as demonstrated by the use of single (Rubio et al., 2008), and double KO mutants (Rubio et al., 2010) in AtHAK5 and AKT1. Therefore, it can be concluded that the *Arabidopsis* model cannot be completely extended to other plant species, crops included, and highlights the need for the characterization of knock-out lines in each particular species to address the relevance of the different K^+ transport systems. In addition, the availability of whole genomes for many plant species revealed some differences with respect to *Arabidopsis*. In *Arabidopsis*, AtHAK5 is the only member that belongs to the cluster Ia of HAK transporters, which are involved in high-affinity K^+ uptake in roots (Nieves-Cordones et al., 2016). In tomato, a highly homologous gene to *SlHAK5* is located just 2580 bp downstream from it in the tomato genome (Fernandez-Pozo et al., 2015). In rice, the *OsHAK21* gene, also belonging to cluster Ia is induced by salinity, something that has not been described in other species for members of this cluster. This transporter has been linked to rice tolerance to salinity through the maintenance of Na^+/K^+ homeostasis, although the physiological mechanism remains unclear (Shen et al., 2015).

Rice Transport Systems Contributing to Root K^+ Uptake

The recent characterization of T-DNA insertion rice lines knocked-out for K^+ uptake systems such as OsHAK1, OsHAK5, and OsAKT1, has importantly contributed to increase our understanding of the relative contribution of such systems to K^+ uptake in a species different from *Arabidopsis*, which is of great importance in agriculture.

A T-DNA insertion mutant with OsAKT1 knocked-out (Golldack et al., 2003) showed reduced growth and decreased root and shoot K^+ concentrations when grown in the presence of 1 and 0.1 mM K^+ (Li et al., 2014). K^+ flux experiments and electrophysiological approaches showed an impairment of K^+ uptake in the *osakt1* line. Strong expression of *OsAKT1* was detected in epidermal root cells, but it was also found in cortex, endodermis, and vascular bundles, suggesting a direct or indirect role in K^+ translocation. In addition, slight expression was detected in shoots.

Knock-out mutants of the gene encoding the high-affinity K^+ transporter OsHAK1 (Bañuelos et al., 2002) were also characterized. The studies with *oshak1* lines showed that OsHAK1 contributed about 50–55% of high-affinity K^+ uptake in the range of 0.05–0.1 mM external K^+ and about 30% of K^+ uptake at 1 mM external K^+ (Chen et al., 2015). Root and shoot growth, cell size and internal K^+ concentrations were reduced in the *oshak1* mutant at both 0.1 and 1 mM K^+ and this deficient phenotype could not be rescued at high external K^+ (5 mM K^+). Transcripts of *OsHAK1* are preferentially accumulated in roots of K^+-starved plants, as it is observed with *AtHAK5* in *Arabidopsis*. In addition, *OsHAK1* is strongly expressed at the xylem parenchyma and phloem of root vascular tissues, shoot meristems and vascular bundles of leaf sheaths. Moreover, *oshak1* plants show reduced K^+ translocation from root to shoot. In addition, the *osakt1* and *oshak1* lines were inhibited throughout development, showing delayed grain filling and reduced grain yield, suggesting that they may play an important role in rice productivity.

OsHAK5 was isolated and characterized as a high-affinity transport system in heterologous systems (Horie et al., 2011). Expression studies showed that OsHAK5 localized to the plasma membrane and that under normal K^+ supply its transcripts were detected in root, root–shoot junction and leaf sheath. K^+ starvation enhanced its expression in root epidermis, parenchyma of stele tissue, primordials of lateral roots, mesophyll, and parenchyma cells of the vascular bundle. The expression pattern of *OsHAK5* supported its role in K^+ uptake, but also in K^+ distribution between roots and shoots, especially at low external K^+. The lower accumulation of K^+ in roots of overexpressing lines and the higher K^+ accumulation in the knock-out lines, grown in low K^+, supported this idea (Yang et al., 2014). These authors suggested that OsHAK5 may mediate K^+ accumulation in xylem parenchyma cells to enable K^+ channels to release K^+ efficiently into the xylem

sap. A role for OsHAK5 in K^+ signaling is also proposed, as K^+ in the phloem may act as a signal to convey the shoot demand of K^+ and K^+ xylem loading (Engels and Marschner, 1992), and *OsHAK5* is abundantly expressed in phloem tissue. A role for the AKT2 channel in K^+ signaling by modulating K^+ in the phloem has been also proposed (Deeken et al., 2002) and AKT2 has been recently suggested as a pathway for Na^+ entry into the roots (Salvador-Recatala, 2016). Since AKT2-mediated K^+ transport is Ca^{2+}-sensitive (Latz et al., 2007), interesting interactions between salt stress, Ca^{2+}, and AKT2 may emerge.

The differential abundance of *OsHAK1*, *OsHAK5*, and *OsAKT1* transcripts suggests that they play non-redundant functions. *OsHAK1* and *OsAKT1* are highly expressed in all cell types of roots and at low levels in shoots. However, while the *OsHAK1* gene was induced 8- to 12-fold by K^+ starvation (Chen et al., 2015), *OsAKT1* expression was not affected by the external K^+ concentrations (Li et al., 2014). By contrast, *OsHAK5* was less expressed in roots and strongly in shoots (Yang et al., 2014). It has been proposed that both OsHAK1 and OsAKT1 contribute to K^+ acquisition at low and high external concentrations. At low K^+, OsHAK1 dominates high-affinity K^+ uptake over OsAKT1 and OsHAK5. By contrast, OsHAK5 dominates K^+ transport from root to shoots (Yang et al., 2014).

The studies described above suggest that OsHAK1, OsHAK5, and OsAKT1 are involved in K^+ uptake at low and high concentrations as well as in K^+ translocation from root to shoot. Contribution to K^+ uptake over a wide range of K^+ concentrations by a unique system has been demonstrated for the *Arabidopsis* AKT1 (Alemán et al., 2011). For transporters of the HAK family, the overexpression of AtKUP1 in *Arabidopsis* suspension cells produced enhanced K^+ uptake at micromolar and millimolar K^+ concentrations (Kim et al., 1998). The rice studies reviewed here suggest that OsHAK1 and OsHAK5 may contribute to K^+ uptake at both low and high concentrations, which would explain why the growth of *oshak1* and *oshak5* lines is not rescued at high external K^+. However, the idea of dual affinity for HAK transporters should be taken with caution. It is possible that, in addition to K^+ uptake, the knock-out lines are affected in other processes. In fact, Yang et al. (2014) highlight the role of some HAK/KUP/KT transporters in auxin distribution, irrespective of K^+ supply. At this stage, it cannot be ruled out that OsHAK1 and OsHAK5 play a part in this process.

Role of HAK Transporters in K^+/Na^+ Homeostasis under NaCl Stress

K^+/Na^+ homeostasis has been shown to be crucial for tolerance of plants to salinity (Maathuis and Amtmann, 1999). Maintaining K^+ uptake rates at high external Na^+ is crucial for K^+/Na^+ homeostasis and salt tolerance (Munns and Tester, 2008; Cuin et al., 2012; Cheng et al., 2015). However, in the presence of high Na^+ concentrations, the low-K^+ induction of genes encoding high-affinity K^+ transporters is not observed (Nieves-Cordones et al., 2008, 2010). In addition, under salinity, K^+ transport through high-affinity HAK transporters is competitively inhibited (Santa-María et al., 1997; Rubio et al., 2000). In fact, OsHAK1 has been defined as the Na^+-sensitive high-affinity K^+ pathway in rice (Chen et al., 2015). Nonetheless, studies in low-K^+-grown *Arabidopsis* and rice plants showed that AtHAK5 and OsHAK1 function was still pivotal in maintaining K^+ uptake and plant growth in the presence of high Na^+ (Nieves-Cordones et al., 2010; Chen et al., 2015). In addition to OsHAK1, OsHAK5 may also play a role in salt tolerance, as high salt transiently enhances *OsHAK5* expression (Yang et al., 2014) and the transporter mediates Na^+-insensitive K^+ uptake (Horie et al., 2011). In the presence of salinity, OsHAK5-overexpressing lines accumulated more K^+ in shoots and showed enhanced growth as compared to WT. In contrast, *oshak5* lines accumulated more Na^+ in shoots and grew less than WT plants (Yang et al., 2014). The authors propose that the higher accumulation of Na^+ in shoots in *oshak5* may be due to a hyperpolarized membrane potential of mesophyll cells in knock-out mutants that would favor Na^+ accumulation in shoots. Therefore, the K^+ transport systems that contribute to maintaining a depolarized membrane potential of mesophyll cells to evade excessive Na^+ accumulation under salinity may play a role in salt tolerance. The function of another rice HAK transporter, OsHAK21, seems to be important for salt tolerance (Shen et al., 2015). The gene encoding this transporter is enhanced by salinity and the protein is localized to the plasma membrane of xylem parenchyma and endodermal cells (putative passage cells). It has been shown that the knock-out *oshak21* line is more salt sensitive because of a higher and a lower accumulation of Na^+ and K^+ respectively, which points to OsHAK21 as a key transporter needed for the maintenance of Na^+/K^+ homeostasis in rice under salt stress.

Other Systems That May Be Involved in Root K^+ Uptake

Recently, a T-DNA insertion mutant in the *Arabidopsis* KUP7, which belongs to cluster V of the HAK family (Nieves-Cordones et al., 2016) has been characterized (Han et al., 2016). The results showed that the *kup7* line was sensitive to low K^+ (<100 μM), showing lower internal K^+ concentrations. It could be rescued by higher K^+ concentrations or by complementing the mutant with the WT gene. The *KUP7* gene was ubiquitously expressed in many organs and the KUP7 protein was localized to the plasma membrane. KUP7 could complement a yeast strain deficient in K^+ uptake. K^+ transport studies showed that KUP7 was involved in root K^+ uptake and K^+ translocation to the shoot. It seemed to operate at higher concentrations than AtHAK5, and may be an alternative system involved in K^+ uptake in the *athak5 akt1 Arabidopsis* line (Caballero et al., 2012). The observed effect on K^+ translocation may be an indirect effect of a reduced uptake. However, Han et al. (2016) speculated that KUP7 may mediate K^+ release into the xylem sap. It should be noted that besides K^+ uptake, some HAK transporters have been shown to mediate K^+ efflux (Bañuelos et al., 2002; Garciadeblas et al., 2002; Osakabe et al., 2013). Thus, K^+ release into the xylem sap could take place through this type of transporters, if the electrochemical potential for K^+ allows for this movement. It is well known that K^+ loading of the xylem is mainly mediated by SKOR channels

and the possible specific contribution of HAK transporters to K^+ loading is yet to be determined.

All of the above described results can be summarized into two different models for the K^+ uptake systems in *Arabidopsis* and rice roots, shown in **Figure 1** and **Table 1**.

REGULATION OF K^+ UPTAKE

In general terms, the genes encoding HAK transporters that mediate high-affinity K^+ uptake in roots are strongly induced by K^+ deprivation, whereas the genes encoding AKT1 channels are not. Several elements in the signal transduction cascade that results in the activation of HAK transcription have been identified. One of the first events when a root faces K^+ deprivation is the hyperpolarization of the cell's plasma membrane (Amtmann and Blatt, 2009). A positive correlation has been found between the membrane potential and the expression levels of *SlHAK5* and *AtHAK5*, independent of the root's K^+ concentration (Nieves-Cordones et al., 2008; Rubio et al., 2014). Thus, it has been proposed that the hyperpolarization of the membrane potential may be the first element in the low-K^+ signal cascade. The mechanisms linking membrane potential and gene expression are unknown but, changes in cytoplasmic Ca^{2+} derived from the activity of hyperpolarization-activated Ca^{2+} channels, could provide a connecting mechanism (Véry and Davies, 2000). Increases in ethylene (Jung et al., 2009) and reactive oxygen species (ROS; Shin and Schachtman, 2004; Hernandez et al., 2012) are also involved, probably acting following the hyperpolarization of the membrane potential. Other hormones such as jasmonic acid (Armengaud et al., 2004, 2010; Takehisa et al., 2013; Schachtman, 2015) and cytokinins (Nam et al., 2012) may also play a role in K^+ signaling. At the end of the cascade, transcription factors such as DDF2, JLO, bHLH121, TFII_A for *Arabidopsis AtHAK5* (Kim et al., 2012; Hong et al., 2013), bind the gene's promoter to activate its expression.

Interestingly, some environmental conditions such as the lack of N, P, or S, that hyperpolarize root cell membrane potential (Rubio et al., 2014) and elevate ROS levels (Shin et al., 2005), also activate the transcription of *AtHAK5*-type genes. However, under such conditions, no HAK-mediated uptake is observed, suggesting a post-transcriptional regulation for these HAK transporters that is elicited specifically by K^+ starvation (Rubio

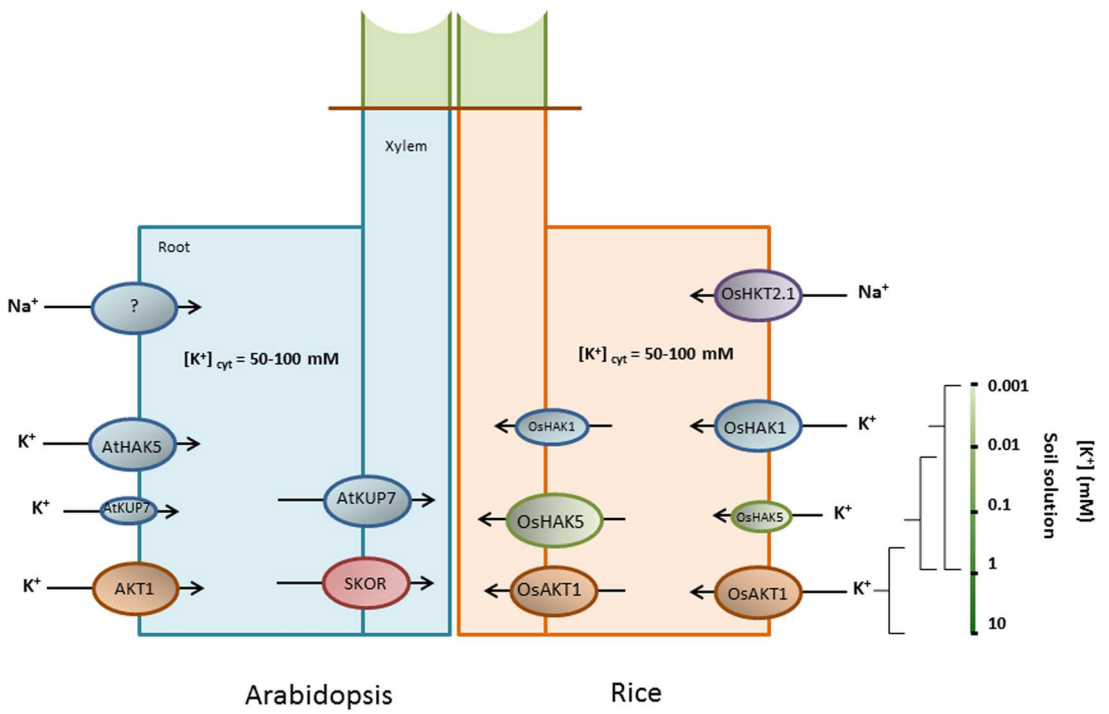

FIGURE 1 | Schematic comparison of the systems involved in K^+ and Na^+ movements in *Arabidopsis* and rice roots. The availability of knock-out mutants in *Arabidopsis* and rice plants for specific transport systems has allowed for elucidating their roles in K^+ transport. The figure shows the predicted function of each system for which knock-out mutants have been studied. AtHAK5 and AKT1 are the main systems for K^+ uptake in *Arabidopsis* plants. In addition, a member of the KT/HAK/KUP family, AtKUP7, seems to also be involved in K^+ uptake. K^+ release into the xylem is mainly mediated by SKOR and also partially by AtKUP7. In rice, AtHAK5 and AKT1 functions are fulfilled by the rice homologs OsHAK1 and OsAKT1. An additional system, OsHAK5, partially contributes to high-affinity K^+ uptake, but at higher concentrations than OsHAK1. These three rice systems may directly or indirectly facilitate K^+ release into the xylem, with the contribution by OsHAK5 to K^+ release into the xylem being more relevant. It is not clear if such contribution is a direct (by mediating K^+ efflux into xylem vessels) or indirect (by favoring K^+ accumulation in endodermal cells) outcome of the aforementioned transporters. Regarding Na^+ uptake, the genetic identity of Na^+ uptake systems in *Arabidopsis* remains to be elucidated. GLRs, CNGCs or other non-selective cation channels could be involved. In rice, OsHKT2;1 has been shown to mediate Na^+ uptake during K^+ deficiency. In the presence of K^+ or high external Na^+ concentrations other unknown systems should take part in Na^+ uptake.

TABLE 1 | Summary for K^+ and Na^+ uptake features observed in *Arabidopsis* and rice roots.

Species	Cation	Type of uptake†	K_m (μM)	Sensitivity	Transport systems involved	Reference
Arabidopsis	K^+	High-affinity	24*	(–) NH_4^+, Ba^{+2}, Cs^+ (=) Ca^{+2}	AtHAK5, AKT1	Spalding et al., 1999; Gierth et al., 2005; Rubio et al., 2008; Coskun et al., 2013
		Low-affinity	3,991*	(–) Ba^{+2}, Cs^+, TEA, La^{+3}, Na^+ (=) NH_4^+, Ca^{+2}	AKT1	Spalding et al., 1999; Gierth et al., 2005; Caballero et al., 2012
	Na^+	High-affinity	n.d.	n.d.	–	–
		Low-affinity	Linear response	(–) Ca^{+2}, Ba^{+2}, cyclic-nucleotides (+) La^{+3}, GABA (=) TEA, Cs^+	–	Maathuis and Sanders, 2001; Essah et al., 2003
Rice	K^+	High-affinity	11–18	(–) NH_4^+	OsHAK1, OsHAK5, OsAKT1	Bañuelos et al., 2002; Li et al., 2014; Yang et al., 2014; Chen et al., 2015
		Low-affinity	n.d.	n.d.	OsHAK1, OsAKT1	Li et al., 2014; Chen et al., 2015
	Na^+	High-affinity	60 or 477–655¶	(–) K^+, Ba^{+2}	OsHKT2;1	Garciadeblas et al., 2003; Horie et al., 2007; Haro et al., 2010
		Low-affinity	n.d.	(=) K^+, Ca^{2+}	OsHKT2;1	Horie et al., 2007; Malagoli et al., 2008

†*High-affinity uptake takes into account cation uptake observed at external concentrations <0.5 mM while the low-affinity one does so at >0.5 mM. *Obtained with Rb^+ as an analog for K^+. (+), (–), and (=) stand for activation, inhibition, or no effect on cation uptake, respectively. n.d., not determined. ¶ Only one component was identified in Horie et al. (2007) for external Na^+ concentrations up to 5 mM.*

et al., 2014). Recently, it has been shown that the *Arabidopsis* AtHAK5 transporter is activated by complexes that contain the CIPK23 kinase and CBL1, CBL8, CBL9, or CBL10 Ca^{2+} sensors. AtHAK5 phosphorylation by CIPK23 leads to increases in the maximal rate of transport (V_{max}) and the affinity for K^+ transport (Ragel et al., 2015). It can be assumed that a specific low-K^+-induced Ca^{2+} signal is registered by the CBL Ca^{2+} sensor, that in turn promotes phosphorylation of the transporter by CIPK23.

As a voltage-dependent inward-rectifier K^+ channel, AKT1 activity is regulated by the membrane potential (Gaymard et al., 1996; Xu et al., 2006). In addition, its activity is modulated by interaction with other proteins. AKT1 forms tetrameric channels by interacting with the AtKC1 subunit (Daram et al., 1997; Pilot et al., 2003; Duby et al., 2008; Geiger et al., 2009). Upon interaction with AtKC1 in root cells, the activation potential for AKT1-containing channels becomes more negative, in comparison with AKT1 homotetramers (Reintanz et al., 2002; Wang et al., 2010). Moreover, AtKC1 interacts, in turn, with the SNARE proteins SYP121 (Honsbein et al., 2009) and VAMP721 (Zhang et al., 2015). SYP121 was shown to activate K^+ uptake through AKT1/AtKC1 channels while VAMP721 negatively regulated this process. Phosphorylation also plays a role in AKT1 regulation. AKT1 activity is enhanced at low K^+ by the same regulators as AtHAK5, i.e., the CIPK23/CBL1/9 complex, supporting the putative role of Ca^{2+} as a secondary messenger involved in low-K^+ signaling (Li et al., 2006; Xu et al., 2006). Inactivation of the channel is achieved by the AIP1 phosphatase (Luan, 2009). It is worth to note that CBL proteins can also modify AKT1 activity in absence of CIPKs, as it is the case of CBL10 which is a negative regulator of AKT1 (Ren et al., 2013). Recently it has been shown that CIPK23 and AtKC1 act synergistically and balance K^+ uptake/leakage to modulate AKT1-mediated responses of *Arabidopsis* to low K^+ (Wang et al., 2016). Finally, nitric oxide has recently been shown to lower AKT1 activity by modulating vitamin B6 biosynthesis, constituting a new mechanism for the regulation of K^+ uptake (Xia et al., 2014).

The current model for the regulation of these two main systems involved in K^+ uptake, i.e., AtHAK5 and AKT1, is depicted in **Figure 2**.

It is worth mentioning that CIPK23/CBL is also involved in the regulation of NO_3^- uptake (Ho et al., 2009; Tsay et al., 2011; Léran et al., 2015), and that K^+ starvation significantly reduced the NO_3^- concentrations in tomato plants (Rubio et al., 2014) and induced several genes for NO_3^- uptake (Armengaud et al., 2004). This indicates that a cross-regulation between K^+ and NO_3^- nutrition exists and that the CIPK23/CBL complex may constitute one of the key elements for such regulation.

UPTAKE OF Na^+ AND CELL MECHANISMS INVOLVED

As for the identities of genes involved in Na^+ uptake from external solutions, the scenario is far less clear than that for K^+. With respect to high-affinity Na^+ uptake, despite this activity being widely observed in roots from several species (Garciadeblas et al., 2003; Haro et al., 2010), only a few transport systems belonging to the HKT and HAK transporter families have been shown to take up Na^+ within this range of concentrations. High-affinity K^+ transporters (HKT) are related to fungal and bacterial K^+ transporters from the Trk/Ktr families (Corratgé-Faillie et al., 2010). In plants, however, HKT transporters display varying

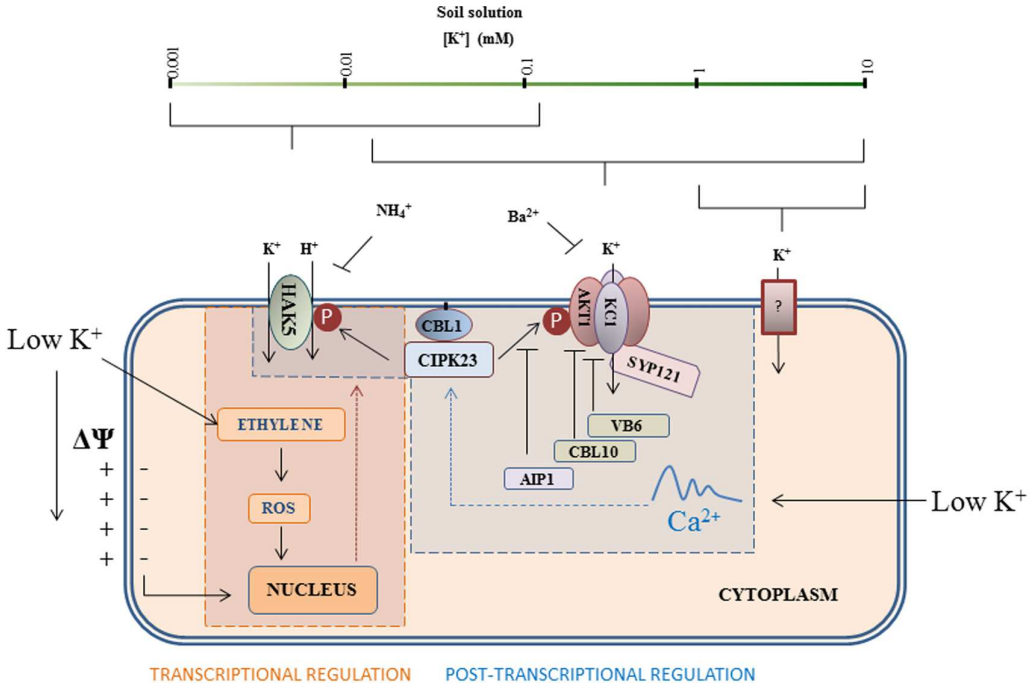

FIGURE 2 | Main pathways for root K^+ uptake and their regulatory mechanisms. HAK5-type transporters are high-affinity K^+ transporters involved in K^+ uptake at very low concentrations. When the external K^+ concentration increases, the inward-rectifier K^+ channel AKT1 together with HAK5, contributes to K^+ uptake. At K^+ concentrations above 200 μM, HAK5 is not present and AKT1 is the main system for low-affinity K^+ uptake. At very high concentrations, other unknown systems can secure K^+ supply if AKT1 is not functional. The HAK5 and AKT1 uptake systems are subjected to finely tuned regulation. At low K^+ concentrations, a hyperpolarization of the plasma membrane induces *HAK5* transcription. The signal cascade of HAK5 regulation is dependent on ethylene and ROS production. In addition, low external K^+ likely produces a specific cytoplasmic Ca^{2+} signal that is registered by the Ca^{2+} sensor CBL1, which induces CIPK23 recruitment to the plasma membrane resulting in the phosphorylation and subsequent activation of HAK5 and AKT1. The channel activity is downregulated through dephosphorylation by the AIP1 phosphatase, and interaction with CBL10 and vitamin B6. Other subunits such as KC1 and the SNARE protein SYP121 also cooperate in AKT1 regulation. It can be concluded that whereas HAK5 is subjected to transcriptional and post-transcriptional regulation, K^+ uptake through AKT1 is mainly regulated post-transcriptionally. The CIPK23/CBL1 complex emerges as a key regulator of K^+ nutrition.

Na^+/K^+ permeabilities. Phylogenetic and functional analyses have led to the identification of two HKT subfamilies (Platten et al., 2006): subfamily I, present in both monocotyledonous and dicotyledonous species, and subfamily II, identified only in monocotyledonous species so far. Subfamily II HKT transporters are expected to be all K^+-permeable and can operate as Na^+/K^+ symporters (Rubio et al., 1995; Jabnoune et al., 2009; Yao et al., 2010; Oomen et al., 2012) or K^+-selective uniporters (Horie et al., 2011; Sassi et al., 2012) when heterologously expressed in yeast and/or *Xenopus* oocytes. Subfamily I HKT transporters are Na^+-selective in *Arabidopsis* and rice and are mostly involved in Na^+ recirculation through vascular tissues (Maathuis, 2014; Véry et al., 2014), thus falling beyond the scope of the present review. In the rice cultivar Nipponbare, OsHKT2;1 provides a major pathway for root high-affinity Na^+ uptake that supports plant growth under limiting K^+ supply (Garciadeblas et al., 2003; Horie et al., 2007; **Figure 1**). Plants lacking a functional *OsHKT2;1* gene have shown reduced growth and lower Na^+ content when starved of K^+ in the presence of 0.5 mM Na^+, and under such conditions Na^+ can partially compensate K^+ demand (Horie et al., 2007). Besides Na^+, OsHKT2;1 can also transport K^+ when expressed in *Xenopus* oocytes (Jabnoune et al., 2009; Oomen et al., 2012), but K^+ transport is not detected when it was expressed in yeast or in tobacco BY2 cells (Horie et al., 2001; Yao et al., 2010). In OsHKT2;1 expressing oocytes, the shifts in reversal potentials induced by K^+ depended on the pre-treatment of oocytes. When the oocytes were pre-treated in low-Na^+ (0.5 mM Na^+) they showed smaller shifts that when pretreated with high-Na^+ (96 mM Na^+; Yao et al., 2010). Comparisons of Rb^+ influx between WT and *oshkt2;1* roots did not reveal significant differences between these genotypes (Horie et al., 2007). Thus, the possible involvement of OsHKT2;1 in root K^+ uptake remains to be verified. Another subfamily II HKT transporter, OsHKT2;2, is absent in the Nipponbare (japonica) cultivar but present in the indica cultivar Pokkali. The transporter obtained from the latter cultivar is permeable to both Na^+ and K^+ at low external concentrations when expressed in tobacco BY2 cells, yeast and *Xenopus* oocytes (Horie et al., 2001; Yao et al., 2010; Oomen et al., 2012). It is important to note that a natural chimera OsHKT2;2/1 present in the Nona Bokra (indica) cultivar maintains high-affinity K^+ uptake even at high Na^+ concentrations, something that is also observed for Pokkali OsHKT2;2 but not for Nipponbare OsHKT2;1 (Oomen et al., 2012). Despite the lack of data concerning *oshkt2;2*

knock-out mutants, it is tempting to speculate that OsHKT2;2 contributes to both K^+ and Na^+ high-affinity uptake in rice roots. As for HAK transporters, two members, none of them from higher plants, have been shown to mediate high-affinity Na^+ uptake: PpHAK13 from the moss *Physcomitrella patens* and YlHAK1 from the yeast *Yarrowia lipolytica* (Benito et al., 2012). PpHAK13, which belongs to cluster IV (Nieves-Cordones et al., 2016), transports Na^+, but not K^+, and high-affinity Na^+ uptake is abolished in *pphak13* mutants plants which evidences that PpHAK13 forms the major pathway for Na^+ entry at low external concentrations in *P. patens* plants. On the other hand, YlHAK1 is able to transport Na^+ and K^+ when expressed in yeast, but the latter cation is only transported when Na^+ is not added to the experimental solution. High-affinity Na^+ transporters from the HAK family in higher plants are still to be identified.

Concerning low-affinity Na^+ uptake, it is generally accepted that Na^+ can enter the plant through ion channels (Maathuis, 2014). Na^+-permeable channels include glutamate-like receptors (GLRs; Davenport, 2002) and cyclic nucleotide gated channels (CNGCs; Assmann, 1995; Bolwell, 1995; Trewavas, 1997; Newton and Smith, 2004) and possibly other, non-identified, non-selective cation channels (NSCCs; Maathuis and Sanders, 1993; Tyerman et al., 1997; Demidchik and Tester, 2002; Essah et al., 2003). Voltage-independent NSCCs (VI-NSCC) may constitute the main class of NSCCs involved in Na^+ entry since they are highly sensitive to Ca^{2+} as observed for Na^+ uptake in roots (Demidchik and Maathuis, 2007). Moreover, VI-NSCC blockers such as quinine or lanthanides also inhibited root Na^+ influx (Essah et al., 2003; Wang et al., 2006). Despite these encouraging observations linking VI-NSCCs and root Na^+ uptake, the molecular identity of these channels remains obscure at present. Several HAK and HKT transporters, which are expressed in roots, are also permeable at millimolar Na^+ concentrations (Santa-María et al., 1997; Horie et al., 2001; Takahashi et al., 2007; Mian et al., 2011; Oomen et al., 2012). It is worth to note that OsHKT2;1 and HvHKT2;1 contribute to Na^+ uptake in the millimolar range but they are downregulated in the presence of salt stress or K^+. Thus, when taking into account other experimental conditions and plant species, it remains unclear which other type/family of transport systems constitute the major pathway for low-affinity Na^+ uptake. It is likely that there is a large redundancy between the aforementioned channels and transporters. Insights into the identification of the contributing transport proteins would be of extraordinary biotechnological value since low-affinity Na^+ uptake allows for the massive entry of Na^+ within the plant that gives rise to toxicity. Interestingly, the secondary messengers cyclic AMP and GMP affect Na^+ influx. Studies on *Arabidopsis* seedlings (Maathuis and Sanders, 2001; Essah et al., 2003) and on pepper plants (Rubio et al., 2003) have shown that unidirectional Na^+ influx is reduced by cGMP addition. CNGCs have a cyclic-nucleotide binding domain and their activity is modulated by cyclic-nucleotides (Gao et al., 2014, 2016). It can be expected that the cyclic-nucleotide regulation of Na^+ fluxes occurs through direct cGMP (or cAMP) binding to this domain as it is the case of animal CNGCs (Craven and Zagotta, 2006).

Recently, it has been shown that salt stress triggers the formation of endocytic vesicles via a clathrin-independent mechanism (Baral et al., 2015). Such vesicles lead to the formation of vacuole-like structures that may help plants to better cope with salt stress. Endocytosis can modify the transporter complement of the plasma membrane (Sutter et al., 2007), thus affecting the Na^+ uptake pathways. But more interestingly, the endocytic process involves bulk-flow entry into root cells that may transport Na^+ ions from the apoplast to the vacuole-like structures. If this were true, it would constitute a parallel pathway for Na^+ uptake, independent from that mediated by transmembrane proteins. Moreover, this direct Na^+ transport into vacuoles would prevent Na^+ accumulation in the cytosol which leads to cell toxicity. Interestingly, vesicle trafficking has been recently suggested to play a role in plant adaptation to salt stress (Garcia de la Garma et al., 2015).

CONCLUDING REMARKS

K^+ is an essential macronutrient for plants while Na^+ may be beneficial or detrimental at low or high concentrations, respectively. Plant roots possess specific K^+ transport systems that can function under a wide range of concentrations to secure K^+ ions. The studies with knock-out mutants of the model plant *Arabidopsis* have led to the identification of two major pathways for K^+ uptake: the high-affinity K^+ transporter AtHAK5 and the inward-rectifying K^+ channel AKT1. These systems operate at low (micromolar) and high (millimolar) external K^+ concentrations, although an overlap in their operation is observed in the 10–200 μM K^+ range. Different mechanisms that include transcriptional and post-transcriptional regulation modulate the activity of these two systems in response to K^+ supply. Importantly, the CIPK23/CBL1 complex activates AtHAK5 as well as AKT1, pointing to its role as a central regulator of K^+ nutrition. Homologs of AtHAK5 and AKT1 have been found in many plant species, and in some of them, paralog genes exist which suggest function redundancy. This precludes assigning a function by only using sequence homology or heterologous expression studies. The recent characterization of rice knock-out plants has shed light on this matter. OsHAK1, OsHAK5, and OsAKT1 seem to contribute to root K^+ uptake as well as K^+ release into xylem, and they probably play additional unknown functions in the shoot. However, they play non-redundant roles: (i) OsHAK1 is mainly involved in root K^+ uptake at low concentrations, (ii) OsAKT1 mostly at high K^+ concentrations, and (iii) OsHAK5 is more relevant for K^+ translocation to the shoot. These systems may also play a role in salinity tolerance by maintaining the K^+/Na^+ homeostasis.

Regarding Na^+ transport systems, the information is scarcer. High-affinity Na^+ uptake and high-affinity Na^+ transporters have been described in some species, but they are lacking in many others. The pathways for low-affinity Na^+ uptake are not clearly identified yet, and several families of transporters contain members that could be good candidates. Recently, it has been

described that salt stress induced a new endocytic pathway that is clathrin-independent, non-discriminatory in its choice of cargo, and that operates across all layers of the root. This new pathway may contribute to the bulk Na^+ uptake and distribution across the root cells under saline stress conditions.

All of the above highlight the importance of characterizing the function of each transporter in each particular species. The studies with knock-out lines in *Arabidopsis* and rice evidence that the conclusions drawn in model species cannot be always fully extended to other, non-model species.

AUTHOR CONTRIBUTIONS

All authors listed, have made substantial, direct and intellectual contribution to the work, and approved it for publication.

FUNDING

This work was funded by the Ministerio de Economía y Competitividad, Spain (grant number AGL2015-66434-R).

REFERENCES

Alemán, F., Nieves-Cordones, M., Martínez, V., and Rubio, F. (2009). Differential regulation of the HAK5 genes encoding the high-affinity K^+ transporters of *Thellungiella halophila* and *Arabidopsis thaliana*. *Environ. Exp. Bot.* 65, 263–269. doi: 10.1016/j.envexpbot.2008.09.011

Alemán, F., Nieves-Cordones, M., Martínez, V., and Rubio, F. (2011). Root K^+ acquisition in plants: the *Arabidopsis thaliana* model. *Plant Cell Physiol.* 52, 1603–1612. doi: 10.1093/pcp/pcr096

Amtmann, A., and Blatt, M. R. (2009). Regulation of macronutrient transport. *New Phytol.* 181, 35–52. doi: 10.1111/j.1469-8137.2008.02666.x

Armengaud, P., Breitling, R., and Amtmann, A. (2004). The potassium-dependent transcriptome of *Arabidopsis* reveals a prominent role of jasmonic acid in nutrient signaling. *Plant Physiol.* 136, 2556–2576. doi: 10.1104/pp.104.046482

Armengaud, P., Breitling, R., and Amtmann, A. (2010). Coronatine-insensitive 1 (COI1) mediates transcriptional responses of *Arabidopsis thaliana* to external potassium supply. *Mol. Plant* 3, 390–405. doi: 10.1093/mp/ssq012

Ashley, M. K., Grant, M., and Grabov, A. (2006). Plant responses to potassium deficiencies: a role for potassium transport proteins. *J. Exp. Bot.* 57, 425–436. doi: 10.1093/jxb/erj034

Assmann, S. M. (1995). Cyclic AMP as a second messenger in higher plants (status and future prospects). *Plant Physiol.* 108, 885–889.

Baldwin, J. P., Nye, P. H., and Tinker, P. B. (1973). Uptake of solutes by multiple root systems from soil. 3. Model for calculating solute uptake by a randomly dispersed root system developing in a finite volume of soil. *Plant Soil* 38, 621–635. doi: 10.1007/BF00010701

Bañuelos, M. A., Garciadeblas, B., Cubero, B., and Rodríguez-Navarro, A. (2002). Inventory and functional characterization of the HAK potassium transporters of rice. *Plant Physiol.* 130, 784–795. doi: 10.1104/pp.007781

Baral, A., Irani, N. G., Fujimoto, M., Nakano, A., Mayor, S., and Mathew, M. K. (2015). Salt-induced remodeling of spatially restricted clathrin-independent endocytic pathways in *Arabidopsis* root. *Plant Cell* 27, 1297–1315. doi: 10.1105/tpc.15.00154

Barberon, M., and Geldner, N. (2014). Radial transport of nutrients: the plant root as a polarized epithelium. *Plant Physiol.* 166, 528–537. doi: 10.1104/pp.114.246124

Barraclough, P. B. (1989). Root-growth, macro-nutrient uptake dynamics and soil fertility requirements of a high-yielding winter oilseed rape crop. *Plant Soil* 119, 59–70. doi: 10.1007/BF02370269

Battie-Laclau, P., Laclau, J.-P., Piccolo, M. D. C., Arenque, B. C., Beri, C., Mietton, L., et al. (2013). Influence of potassium and sodium nutrition on leaf area components in *Eucalyptus grandis* trees. *Plant Soil* 371, 19–35. doi: 10.1007/s11104-013-1663-7

Bednarz, C. W., and Oosterhuis, D. M. (1999). Physiological changes associated with potassium deficiency in cotton. *J. Plant Nutr.* 22, 303–313. doi: 10.1016/j.jphotobiol.2012.02.002

Benito, B., Garciadeblas, B., and Rodriguez-Navarro, A. (2012). HAK transporters from *Physcomitrella patens* and *Yarrowia lipolytica* mediate sodium uptake. *Plant Cell Physiol.* 53, 1117–1123. doi: 10.1093/pcp/pcs056

Blatt, M. R. (1992). K^+ channels of stomatal guard cells. Characteristics of the inward rectifier and its control by pH. *J. Gen. Physiol.* 99, 615–644. doi: 10.1085/jgp.99.4.615

Bolwell, G. P. (1995). Cyclic AMP, the reluctant messenger in plants. *Trends Biochem. Sci.* 20, 492–495. doi: 10.1016/S0968-0004(00)89114-8

Burch-Smith, T. M., and Zambryski, P. C. (2012). Plasmodesmata paradigm shift: regulation from without versus within. *Annu. Rev. Plant Biol.* 63, 239–260. doi: 10.1146/annurev-arplant-042811-105453

Caballero, F., Botella, M. A., Rubio, L., Fernández, J. A., Martínez, V., and Rubio, F. (2012). A Ca^{2+}-sensitive system mediates low-affinity K^+ uptake in the absence of AKT1 in *Arabidopsis* plants. *Plant Cell Physiol.* 53, 2047–2059. doi: 10.1093/pcp/pcs140

Chen, G., Hu, Q., Luo, L., Yang, T., Zhang, S., Hu, Y., et al. (2015). Rice potassium transporter OsHAK1 is essential for maintaining potassium-mediated growth and functions in salt tolerance over low and high potassium concentration ranges. *Plant Cell Environ.* 38, 2747–2765. doi: 10.1111/pce.12585

Cheng, D., Wu, G., and Zheng, Y. (2015). Positive correlation between potassium uptake and salt tolerance in wheat. *Photosynthetica* 53, 447–454. doi: 10.1007/s11099-015-0124-3

Claassen, N., and Jungk, A. (1982). Potassium dynamics at the soil-root interface in relation to the uptake of potassium by maize plants. *Z. Pflanzenernahr. Bodenkd.* 145, 513–525. doi: 10.1002/jpln.19821450603

Corratgé-Faillie, C., Jabnoune, M., Zimmermann, S., Véry, A. A., Fizames, C., and Sentenac, H. (2010). Potassium and sodium transport in non-animal cells: the Trk/Ktr/HKT transporter family. *Cell. Mol. Life Sci.* 67, 2511–2532. doi: 10.1007/s00018-010-0317-7

Coskun, D., Britto, D. T., Kochian, L. V., and Kronzucker, H. J. (2016). How high do ion fluxes go? A re-evaluation of the two-mechanism model of K(+) transport in plant roots. *Plant Sci.* 243, 96–104. doi: 10.1016/j.plantsci.2015.12.003

Coskun, D., Britto, D. T., Li, M., Oh, S., and Kronzucker, H. J. (2013). Capacity and plasticity of potassium channels and high-affinity transporters in roots of barley and *Arabidopsis*. *Plant Physiol.* 162, 496–511. doi: 10.1104/pp.113.215913

Cramer, G., Epstein, E., and Lauchli, A. (1989). Na-Ca interactions in barley seedlings - relationship to ion-transport and growth. *Plant Cell Environ.* 12, 551–558. doi: 10.1111/j.1365-3040.1989.tb02128.x

Cramer, G. R., Lauchli, A., and Polito, V. S. (1985). Displacement of $Ca2^+$ by Na^+ from the plasmalemma of root-cells - A primary response to salt stress. *Plant Physiol.* 79, 207–211. doi: 10.1104/pp.79.1.207

Cramer, G. R., Lynch, J., Lauchli, A., and Epstein, E. (1987). Influx of Na^+, K^+ and Ca^{2+} into roots of alt-stressed cotton seedlings. *Plant Physiol.* 79, 207–211. doi: 10.1104/pp.79.1.207

Craven, K. B., and Zagotta, W. N. (2006). CNG and HCN channels: two peas, one pod. *Annu. Rev. Physiol.* 68, 375–401. doi: 10.1146/annurev.physiol.68.040104.134728

Cuin, T. A., Zhou, M., Parsons, D., and Shabala, S. (2012). Genetic behaviour of physiological traits conferring cytosolic K^+/Na^+ homeostasis in wheat. *Plant Biol. (Stuttg)* 14, 438–446. doi: 10.1111/j.1438-8677.2011.00526.x

Daram, P., Urbach, S., Gaymard, F., Sentenac, H., and Cherel, I. (1997). Tetramerization of the AKT1 plant potassium channel involves its C- terminal cytoplasmic domain. *EMBO J.* 16, 3455–3463. doi: 10.1093/emboj/16.12.3455

Davenport, R. (2002). Glutamate receptors in plants. *Ann. Bot.* 90, 549–557. doi: 10.1093/aob/mcf228

Deeken, R., Geiger, D., Fromm, J., Koroleva, O., Ache, P., Langenfeld-Heyser, R., et al. (2002). Loss of the AKT2/3 potassium channel affects sugar loading into the phloem of *Arabidopsis*. *Planta* 216, 334–344. doi: 10.1007/s00425-002-0895-1

Demidchik, V., and Maathuis, F. (2007). Physiological roles of nonselective cation channels in plants: from salt stress to signalling and development. *New Phytol.* 175, 387–404. doi: 10.1111/j.1469-8137.2007.02128.x

Demidchik, V., and Tester, M. (2002). Sodium fluxes through nonselective cation channels in the plasma membrane of protoplasts from *Arabidopsis* roots. *Plant Physiol.* 128, 379–387. doi: 10.1104/pp.010524

D'Onofrio, C., Kader, A., and Lindberg, S. (2005). Uptake of sodium in quince, sugar beet, and wheat protoplasts determined by the fluorescent sodium-binding dye benzofuran isophthalate. *J. Plant Physiol.* 162, 421–428. doi: 10.1016/j.jplph.2004.07.017

Drew, M. C. (1975). Comparison of effects of a localized supply of phosphate, nitrate, ammonium and potassium on growth of seminal root system, and shoot, in barley. *New Phytol.* 75, 479–490. doi: 10.1111/j.1469-8137.1975.tb01409.x

Duby, G., Hosy, E., Fizames, C., Alcon, C., Costa, A., Sentenac, H., et al. (2008). AtKC1, a conditionally targeted Shaker-type subunit, regulates the activity of plant K^+ channels. *Plant J.* 53, 115–123. doi: 10.1111/j.1365-313X.2007.03324.x

Engels, C., and Marschner, H. (1992). Adaptation of potassium translocation into the shoot of maize (*Zea mays*) to shoot demand: evidence for xylem loading as a regulating step. *Physiol. Plant.* 86, 263–268. doi: 10.1034/j.1399-3054.1992.860211.x

Epstein, E., and Hagen, C. E. (1952). A kinetic study of the absorption of alkali cations by barley roots. *Plant Pshyiol.* 27, 457–474. doi: 10.1104/pp.27.3.457

Epstein, E., Rains, D. W., and Elzam, O. E. (1963). Resolution of dual mechanisms of potassium absorption by barley roots. *Proc. Natl. Acad. Sci. U.S.A.* 49, 684–692. doi: 10.1073/pnas.49.5.684

Essah, P. A., Davenport, R., and Tester, M. (2003). Sodium influx and accumulation in *Arabidopsis*. *Plant Physiol.* 133, 307–318. doi: 10.1104/pp.103.022178

Eynard, A., Lal, R., and Wiebe, K. (2005). Crop response in salt-affected soils. *J. Sustain. Agric.* 27, 5–50. doi: 10.1007/BF00223914

Faiyue, B., Al-Azzawi, M. J., and Flowers, T. J. (2012). A new screening technique for salinity resistance in rice (*Oryza sativa* L.) seedlings using bypass flow. *Plant Cell Environ.* 35, 1099–1108. doi: 10.1111/j.1365-3040.2011.02475.x

Fernandez-Pozo, N., Menda, N., Edwards, J. D., Saha, S., Tecle, I. Y., Strickler, S. R., et al. (2015). The sol genomics network (SGN)–from genotype to phenotype to breeding. *Nucleic Acids Res.* 43, D1036–D1041. doi: 10.1093/nar/gku1195

Gao, Q. F., Fei, C. F., Dong, J. Y., Gu, L. L., and Wang, Y. F. (2014). *Arabidopsis* CNGC18 is a Ca^{2+}-permeable channel. *Mol. Plant* 7, 739–743. doi: 10.1093/mp/sst174

Gao, Q. F., Gu, L. L., Wang, H. Q., Fei, C. F., Fang, X., Hussain, J., et al. (2016). Cyclic nucleotide-gated channel 18 is an essential Ca^{2+} channel in pollen tube tips for pollen tube guidance to ovules in *Arabidopsis*. *Proc. Natl. Acad. Sci. U.S.A.* 113, 3096–3101. doi: 10.1073/pnas.1524629113

Garcia de la Garma, J., Fernandez-Garcia, N., Bardisi, E., Pallol, B., Asensio-Rubio, J. S., Bru, R., et al. (2015). New insights into plant salt acclimation: the roles of vesicle trafficking and reactive oxygen species signalling in mitochondria and the endomembrane system. *New Phytol.* 205, 216–239. doi: 10.1111/nph.12997

Garciadeblas, B., Benito, B., and Rodriguez-Navarro, A. (2002). Molecular cloning and functional expression in bacteria of the potassium transporters CnHAK1 and CnHAK2 of the seagrass *Cymodocea nodosa*. *Plant Mol. Biol.* 50, 623–633. doi: 10.1023/A:1019951023362

Garciadeblas, B., Senn, M. E., Bañuelos, M. A., and Rodriguez-Navarro, A. (2003). Sodium transport and HKT transporters: the rice model. *Plant J.* 34, 788–801. doi: 10.1046/j.1365-313X.2003.01764.x

Gattward, J. N., Almeida, A.-A. F., Souza, J. O. Jr., Gomes, F. P., and Kronzucker, H. J. (2012). Sodium-potassium synergism in *Theobroma cacao*: stimulation of photosynthesis, water-use efficiency and mineral nutrition. *Physiol. Plant.* 146, 350–362. doi: 10.1111/j.1399-3054.2012.01621.x

Gaymard, F., Cerutti, M., Horeau, C., Lemaillet, G., Urbach, S., Ravallec, M., et al. (1996). The baculovirus/insect cell system as an alternative to xenopus oocytes. *J. Biol. Chem.* 271, 22863–22870. doi: 10.1074/jbc.271.37.22863

Geiger, D., Becker, D., Vosloh, D., Gambale, F., Palme, K., Rehers, M., et al. (2009). Heteromeric AtKC1/AKT1 channels in *Arabidopsis* roots facilitate growth under K^+ limiting conditions. *J. Biol. Chem.* 284, 21288–21295. doi: 10.1074/jbc.M109.017574

Geldner, N. (2013). The endodermis. *Annu. Rev. Plant Biol.* 64, 531–558. doi: 10.1146/annurev-arplant-050312-120050

Gierth, M., Maser, P., and Schroeder, J. I. (2005). The potassium transporter AtHAK5 functions in K^+ deprivation-induced high-affinity K^+ uptake and AKT1 K^+ channel contribution to K^+ uptake kinetics in *Arabidopsis* roots. *Plant Physiol.* 137, 1105–1114. doi: 10.1104/pp.104.057216

Glass, A. (1976). Regulation of potassium absorption in barley roots. An allosteric model. *Plant Physiol.* 58, 33–37. doi: 10.1104/pp.58.1.33

Golldack, D., Quigley, F., Michalowski, C. B., Kamasani, U. R., and Bohnert, H. J. (2003). Salinity stress-tolerant and -sensitive rice (*Oryza sativa* L.) regulate AKT1-type potassium channel transcripts differently. *Plant Mol. Biol.* 51, 71–81. doi: 10.1023/A:1020763218045

Grabov, A. (2007). Plant KT/KUP/HAK potassium transporters: single family - multiple functions. *Anna. Bot.* 99, 1035–1041. doi: 10.1093/aob/mcm066

Hafsi, C., Debez, A., and Abdelly, C. (2014). Potassium deficiency in plants: effects and signaling cascades. *Acta Physiol. Plant.* 36, 1055–1070. doi: 10.1007/s00709-015-0845-y

Han, M., Wu, W., Wu, W.-H., and Wang, Y. (2016). Potassium transporter KUP7 is involved in K^+ acquisition and translocation in *Arabidopsis* root under K^+-limited conditions. *Mol. Plant* 9, 437–446. doi: 10.1016/j.molp.2016.01.012

Haro, R., Banuelos, M. A., and Rodriguez-Navarro, A. (2010). High-affinity sodium uptake in land plants. *Plant Cell Physiol.* 51, 68–79. doi: 10.1093/pcp/pcp168

Hernandez, M., Fernandez-Garcia, N., Garcia-Garma, J., Rubio-Asensio, J. S., Rubio, F., and Olmos, E. (2012). Potassium starvation induces oxidative stress in *Solanum lycopersicum* L. roots. *J. Plant Physiol.* 169, 1366–1374. doi: 10.1016/j.jplph.2012.05.015

Hille, B. (1992). *Ionic Channels of Excitable Membranes*. Sunderland, MA: Sinauer Associates, Inc.

Hirsch, R. E., Lewis, B. D., Spalding, E. P., and Sussman, M. R. (1998). A role for the AKT1 potassium channel in plant nutrition. *Science* 280, 918–921. doi: 10.1126/science.280.5365.918

Ho, C. H., Lin, S. H., Hu, H. C., and Tsay, Y. F. (2009). CHL1 functions as a nitrate sensor in plants. *Cell* 138, 1184–1194. doi: 10.1016/j.cell.2009.07.004

Hong, J. P., Takeshi, Y., Kondou, Y., Schachtman, D. P., Matsui, M., and Shin, R. (2013). Identification and characterization of transcription factors regulating *Arabidopsis* HAK5. *Plant Cell Physiol.* 54, 1478–1490. doi: 10.1093/pcp/pct094

Honsbein, A., Sokolovski, S., Grefen, C., Campanoni, P., Pratelli, R., Paneque, M., et al. (2009). A tripartite snare-K^+ channel complex mediates in channel-dependent K^+ nutrition in *Arabidopsis*. *Plant Cell* 21, 2859–2877. doi: 10.1105/tpc.109.066118

Hoopen, F. T., Cuin, T. A., Pedas, P., Hegelund, J. N., Shabala, S., Schjoerring, J. K., et al. (2010). Competition between uptake of ammonium and potassium in barley and *Arabidopsis* roots: molecular mechanisms and physiological consequences. *J. Exp. Bot.* 61, 2303–2315. doi: 10.1093/jxb/erq057

Horie, T., Costa, A., Kim, T. H., Han, M. J., Horie, R., Leung, H. Y., et al. (2007). Rice OsHKT2;1 transporter mediates large Na^+ influx component into K^+-starved roots for growth. *EMBO J.* 26, 3003–3014. doi: 10.1038/sj.emboj.7601732

Horie, T., Sugawara, M., Okada, T., Taira, K., Kaothien-Nakayama, P., Katsuhara, M., et al. (2011). Rice sodium-insensitive potassium transporter, OsHAK5, confers increased salt tolerance in tobacco BY2 cells. *J. Biosci. Bioeng.* 111, 346–356. doi: 10.1016/j.jbiosc.2010.10.014

Horie, T., Yoshida, K., Nakayama, H., Yamada, K., Oiki, S., and Shinmyo, A. (2001). Two types of HKT transporters with different properties of Na^+ and K^+ transport in *Oryza sativa*. *Plant J.* 27, 129–138. doi: 10.1046/j.1365-313x.2001.01077.x

Jabnoune, M., Espeout, S., Mieulet, D., Fizames, C., Verdeil, J. L., Conejero, G., et al. (2009). Diversity in expression patterns and functional properties in the rice HKT transporter family. *Plant Physiol.* 150, 1955–1971. doi: 10.1104/pp.109.138008

Jung, J. Y., Shin, R., and Schachtman, D. P. (2009). Ethylene mediates response and tolerance to potassium deprivation in *Arabidopsis*. *Plant Cell* 21, 607–621. doi: 10.1105/tpc.108.063099

Kellermeier, F., Armengaud, P., Seditas, T. J., Danku, J., Salt, D. E., and Amtmann, A. (2014). Analysis of the root system architecture of *Arabidopsis* provides a quantitative readout of crosstalk between nutritional signals. *Plant Cell* 26, 1480–1496. doi: 10.1105/tpc.113.122101

Ketchum, K. A., and Poole, R. J. (1991). Cytosolic calcium regulates a potassium current in corn (*Zea mays*) protoplasts. *J. Membr. Biol.* 119, 277–288. doi: 10.1007/BF01868732

Khayyat, M., Tafazoli, E., Rajaee, S., Vazifeshenas, M., Mahmoo- Dabadi, M. R., and Sajjadinia, A. (2009). Effects of NaCl and supple- mentary potassium on gas exchange, ionic content, and growth of salt-stressed strawberry plants. *J. Plant Nutr.* 32, 907–918. doi: 10.1080/01904160902870689

Kim, E. J., Kwak, J. M., Uozumi, N., and Schroeder, J. I. (1998). AtKUP1: an *Arabidopsis* gene encoding high-affinity potassium transport activity. *Plant Cell* 10, 51–62. doi: 10.2307/3870628

Kim, M. J., Ruzicka, D., Shin, R., and Schachtman, D. P. (2012). The *Arabidopsis* AP2/ERF transcription factor RAP2.11 modulates plant response to low-potassium conditions. *Mol. Plant* 5, 1042–1057. doi: 10.1093/mp/sss003

Kirkby, E., and Schubert, S. (2013). Management of potassium in plant and soil systems in China. *J. Plant Nutr. Soil Sci.* 176, 303–304. doi: 10.1002/jpln.201390018

Kochian, L. V., and Lucas, W. J. (1982). Potassium transport in corn roots: I. Resolution of kinetics into a saturable and linear component. *Plant Physiol.* 70, 1723–1731. doi: 10.1104/pp.70.6.1723

Krishnamurthy, P., Jyothi-Prakash, P. A., Qin, L., He, J., Lin, Q., Loh, C.-S., et al. (2014). Role of root hydrophobic barriers in salt exclusion of a mangrove plant *Avicennia officinalis*. *Plant Cell Environ.* 37, 1656–1671. doi: 10.1111/pce.12272

Kronzucker, H. J., and Britto, D. T. (2011). Sodium transport in plants: a critical review. *New Phytol.* 189, 54–81. doi: 10.1111/j.1469-8137.2010.03540.x

Kronzucker, H. J., Coskun, D., Schulze, L. M., Wong, J. R., and Britto, D. T. (2013). Sodium as nutrient and toxicant. *Plant Soil* 369, 1–23. doi: 10.1007/s11104-013-1801-2

Kronzucker, H. J., Szczerba, M. W., and Britto, D. T. (2003). Cytosolic potassium homeostasis revisited: K-42-tracer analysis in *Hordeum vulgare* L. reveals set-point variations in $[K^+]$. *Planta* 217, 540–546. doi: 10.1007/s00425-003-1032-5

Kronzucker, H. J., Szczerba, M. W., Moazami-Goudarzi, M., and Britto, D. T. (2006). The cytosolic Na^+:K^+ ratio does not explain salinity-induced growth impairment in barley: a dual-tracer study using $^{42}K^+$ and $^{24}Na^+$. *Plant Cell Environ.* 29, 2228–2237. doi: 10.1111/j.1365-3040.2006.01597.x

Kronzucker, H. J., Szczerba, M. W., Schulze, L. M., and Britto, D. T. (2008). Non-reciprocal interactions between K^+ and Na^+ ions in barley (*Hordeum vulgare* L.). *J. Exp. Bot.* 59, 2793–2801. doi: 10.1093/jxb/ern139

Lagarde, D., Basset, M., Lepetit, M., Conejero, G., Gaymard, F., Astruc, S., et al. (1996). Tissue-specific expression of *Arabidopsis* AKT1 gene is consistent with a role in K^+ nutrition. *Plant J.* 9, 195–203. doi: 10.1046/j.1365-313X.1996.09020195.x

Latz, A., Ivashikina, N., Fischer, S., Ache, P., Sano, T., Becker, D., et al. (2007). In planta AKT2 subunits constitute a pH- and Ca^{2+}-sensitive inward rectifying K^+ channel. *Planta* 225, 1179–1191. doi: 10.1007/s00425-006-0428-4

Lauchli, A. (1972). Translocation of inorganic solutes. *Ann. Rev. Plant Physiol.* 23, 197–218. doi: 10.1146/annurev.pp.23.060172.001213

Leigh, R. A., and Wyn Jones, R. G. (1984). A hypothesis relating critical potassium concentrations for growth to the distribution and functions of this ion in the plant-cell. *New Phytol.* 97, 1–13. doi: 10.1111/j.1469-8137.1984.tb04103.x

Léran, S., Edel, K. H., Pervent, M., Hashimoto, K., Corratgé-Faillie, C., Offenborn, J. N., et al. (2015). Nitrate sensing and uptake in *Arabidopsis* are enhanced by ABI2, a phosphatase inactivated by the stress hormone abscisic acid. *Sci. Signal.* 8:ra43. doi: 10.1126/scisignal.aaa4829

Li, J., Long, Y., Qi, G.-N., Li, J., Xu, Z.-J., Wu, W.-H., et al. (2014). The os-akt1 channel is critical for K^+ uptake in rice roots and is modulated by the rice CBL1-CIPK23 complex. *Plant Cell* 26, 3387–3402. doi: 10.1105/tpc.114.123455

Li, L., Kim, B. G., Cheong, Y. H., Pandey, G. K., and Luan, S. (2006). A Ca^{2+} signaling pathway regulates a K^+ channel for low-K^+ response in *Arabidopsis*. *Proc. Natl. Acad. Sci. U.S.A.* 103, 12625–12630. doi: 10.1073/pnas.0605129103

Luan, S. (2009). The CBL-CIPK network in plant calcium signaling. *Trends Plant Sci.* 14, 37–42. doi: 10.1016/j.tplants.2008.10.005

Maathuis, F. J., Ichida, A. M., Sanders, D., and Schroeder, J. I. (1997). Roles of higher plant K^+ channels. *Plant Physiol.* 114, 1141–1149. doi: 10.1104/pp.114.4.1141

Maathuis, F. J., and Sanders, D. (2001). Sodium uptake in *Arabidopsis* roots is regulated by cyclic nucleotides. *Plant Physiol.* 127, 1617–1625. doi: 10.1104/pp.010502

Maathuis, F. J. M. (2014). Sodium in plants: perception, signalling, and regulation of sodium fluxes. *J. Exp. Bot.* 65, 849–858. doi: 10.1093/jxb/ert326

Maathuis, F. J. M., and Amtmann, A. (1999). K^+ Nutrition and Na^+ toxicity: the basis of cellular K^+/Na^+ ratios. *Ann. Bot.* 84, 123–133. doi: 10.1006/anbo.1999.0912

Maathuis, F. J. M., and Sanders, D. (1993). Energization of potassium uptake in *Arabidopsis thaliana*. *Planta* 191, 302–307. doi: 10.1007/BF00195686

Maathuis, F. J. M., and Sanders, D. (1996a). Characterization of csi52, a Cs^+ resistant mutant of *Arabidopsis thaliana* altered in K^+ transport. *Plant J.* 10, 579–589. doi: 10.1046/j.1365-313X.1996.10040579.x

Maathuis, F. J. M., and Sanders, D. (1996b). Mechanisms of potassium absorption by higher plant roots. *Physiol. Plant.* 96, 158–168. doi: 10.1111/j.1399-3054.1996.tb00197.x

Malagoli, P., Britto, D. T., Schulze, L. M., and Kronzucker, H. J. (2008). Futile Na^+ cycling at the root plasma membrane in rice (*Oryza sativa* L.): kinetics, energetics, and relationship to salinity tolerance. *J. Exp. Bot.* 59, 4109–4117. doi: 10.1093/jxb/ern249

Marschner, P. (2012). *Marschner's Mineral Nutrition of Higher Plants* 3rd Edn. San Diego, CA: Academic Press.

Martínez-Cordero, M. A., Martinez, V., and Rubio, F. (2005). High-affinity K^+ uptake in pepper plants. *J. Exp. Bot.* 56, 1553–1562. doi: 10.1093/jxb/eri150

Mengel, K., Kirkby, E. A., Kosegarten, H., and Appel, T. (2001). *Principles on Plant Nutrition*. Dordrecht: Kluwer.

Mian, A., Oomen, R. J., Isayenkov, S., Sentenac, H., Maathuis, F. J. M., and Very, A.-A. (2011). Over-expression of an Na^+- and K^+-permeable HKT transporter in barley improves salt tolerance. *Plant J.* 68, 468–479. doi: 10.1111/j.1365-313X.2011.04701.x

Moody, P. W., and Bell, M. J. (2006). Availability of soil potassium and diagnostic soil tests. *Aust. J. Soil Res.* 44, 265–275. doi: 10.1071/SR05154

Morgan, S. H., Maity, P. J., Geilfus, C. M., Lindberg, S., and Muehling, K. H. (2014). Leaf ion homeostasis and plasma membrane H^+-ATPase activity in *Vicia faba* change after extra calcium and potassium supply under salinity. *Plant Physiol. Biochem.* 82, 244–253. doi: 10.1016/j.plaphy.2014.06.010

Munns, R., and Tester, M. (2008). Mechanisms of salinity tolerance. *Ann. Rev. Plant Biol.* 59, 651–681. doi: 10.1146/annurev.arplant.59.032607.092911

Nam, Y.-J., Tran, L.-S. P., Kojima, M., Sakakibara, H., Nishiyama, R., and Shin, R. (2012). Regulatory roles of cytokinins and cytokinin signaling in response to potassium deficiency in *Arabidopsis*. *PLoS ONE* 7:e47797. doi: 10.1371/journal.pone.0047797

Newton, R. P., and Smith, C. J. (2004). Cyclic nucleotides. *Phytochemistry* 65, 2423–2437. doi: 10.1016/j.phytochem.2004.07.026

Nieves-Cordones, M., Aleman, F., Martinez, V., and Rubio, F. (2010). The *Arabidopsis thaliana* HAK5 K^+ transporter is required for plant growth and K^+ acquisition from low K^+ solutions under saline conditions. *Mol. Plant* 3, 326–333. doi: 10.1093/mp/ssp102

Nieves-Cordones, M., Alemán, F., Martínez, V., and Rubio, F. (2014). K^+ uptake in plant roots. The systems involved, their regulation and parallels in other organisms. *J. Plant Physiol.* 171, 688–695. doi: 10.1016/j.jplph.2013.09.021

Nieves-Cordones, M., Martinez-Cordero, M. A., Martinez, V., and Rubio, F. (2007). An NH_4^+-sensitive component dominates high-affinity K^+ uptake in tomato plants. *Plant Sci.* 172, 273–280. doi: 10.1016/j.plantsci.2006.09.003

Nieves-Cordones, M., Miller, A., Alemán, F., Martínez, V., and Rubio, F. (2008). A putative role for the plasma membrane potential in the control of the expression of the gene encoding the tomato high-affinity potassium transporter HAK5. *Plant Mol. Biol.* 68, 521–532. doi: 10.1007/s11103-008-9388-3

Nieves-Cordones, M., Rodenas, R., Chavanieu, A., Rivero, R. M., Martinez, V., Gaillard, I., et al. (2016). Uneven HAK/KUP/KT protein diversity among angiosperms: species distribution and perspectives. *Front. Plant Sci.* 7:127. doi: 10.3389/fpls.2016.00127

Oomen, R. J., Benito, B., Sentenac, H., Rodriguez-Navarro, A., Talon, M., Very, A.-A., et al. (2012). HKT2;2/1, a K^+-permeable transporter identified in a salt-tolerant rice cultivar through surveys of natural genetic polymorphism. *Plant J.* 71, 750–762. doi: 10.1111/j.1365-313X.2012.05031.x

Osakabe, Y., Arinaga, N., Umezawa, T., Katsura, S., Nagamachi, K., Tanaka, H., et al. (2013). Osmotic stress responses and plant growth controlled by potassium transporters in *Arabidopsis*. *Plant Cell* 25, 609–624. doi: 10.1105/tpc.112.105700

Peterson, C. A., Emanuel, M. E., and Humphreys, G. B. (1981). Pathway of movement of apoplastic fluorescent dye tracers through the endodermis at the site of secondary root-formation in corn (*Zea mays*) and broad bean (*Vicia faba*). *Can. J. Bot.* 59:618. doi: 10.1139/b81-087

Pilot, G., Gaymard, F., Mouline, K., Cherel, I., and Sentenac, H. (2003). Regulated expression of *Arabidopsis* Shaker K^+ channel genes involved in

K^+ uptake and distribution in the plant. *Plant Mol. Biol.* 51, 773–787. doi: 10.1023/A:1022597102282

Platten, J. D., Cotsaftis, O., Berthomieu, P., Bohnert, H., Davenport, R. J., Fairbairn, D. J., et al. (2006). Nomenclature for HKT transporters, key determinants of plant salinity tolerance. *Trends Plant Sci.* 11, 372–374. doi: 10.1016/j.tplants.2006.06.001

Pyo, Y. J., Gierth, M., Schroeder, J. I., and Cho, M. H. (2010). High-affinity K^+ transport in *Arabidopsis*: AtHAK5 and AKT1 are vital for seedling establishment and postgermination growth under low-potassium conditions. *Plant Physiol.* 153, 863–875. doi: 10.1104/pp.110.154369

Qi, Z., Hampton, C. R., Shin, R., Barkla, B. J., White, P. J., and Schachtman, D. P. (2008). The high affinity K^+ transporter AtHAK5 plays a physiological role in planta at very low K^+ concentrations and provides a caesium uptake pathway in *Arabidopsis*. *J. Exp. Bot.* 59, 595–607. doi: 10.1093/jxb/erm330

Ragel, P., Rodenas, R., Garcia-Martin, E., Andres, Z., Villalta, I., Nieves-Cordones, M., et al. (2015). The CBL-interacting protein kinase CIPK23 regulates HAK5-mediated high-affinity K^+ uptake in *Arabidopsis* roots. *Plant Physiol.* 169, 2863–2873. doi: 10.1104/pp.15.01401

Rains, D. W., and Epstein, E. (1967a). Sodium absorption by barley roots: its mediation by mechanism 2 of alkali cation transport. *Plant Physiol.* 42, 319–323. doi: 10.1104/pp.42.3.314

Rains, D. W., and Epstein, E. (1967b). Sodium absorption by barley roots: role of the dual mechanisms of alkali cation transport. *Plant Physiol.* 42, 314–318. doi: 10.1104/pp.42.3.314

Reintanz, B., Szyroki, A., Ivashikina, N., Ache, P., Godde, M., Becker, D., et al. (2002). AtKC1, a silent *Arabidopsis* potassium channel alpha -subunit modulates root hair K^+ influx. *Proc. Natl. Acad. Sci. U.S.A.* 99, 4079–4084. doi: 10.1073/pnas.052677799

Ren, X.-L., Qi, G.-N., Feng, H.-Q., Zhao, S., Zhao, S.-S., Wang, Y., et al. (2013). Calcineurin B-like protein CBL10 directly interacts with AKT1 and modulates K^+ homeostasis in *Arabidopsis*. *Plant J.* 74, 258–266. doi: 10.1111/tpj.12123

Rodrigues, C. R. F., Silveira, J. A. G., Silva, E. N., Dutra, A. T. B., and Viegas, R. A. (2012). Potassium transport and partitioning alle- viates toxic effects of sodium on young physic nut plants. *Rev. Bras. Cien. Solo* 36, 223–232. doi: 10.1590/S0100-06832012000100023

Rodríguez-Navarro, A. (2000). Potassium transport in fungi and plants. *Biochim. Biophys. Acta* 1469, 1–30. doi: 10.1016/S0304-4157(99)00013-1

Römheld, V., and Kirkby, E. (2010). Research on potassium in agriculture: needs and prospects. *Plant Soil* 335, 155–180. doi: 10.1007/s11104-010-0520-1

Rubio, F., Alemán, F., Nieves-Cordones, M., and Martínez, V. (2010). Studies on *Arabidopsis* athak5, atakt1 double mutants disclose the range of concentrations at which AtHAK5, AtAKT1 and unknown systems mediate K^+ uptake. *Physiol. Plant.* 139, 220–228. doi: 10.1111/j.1399-3054.2010.01354.x

Rubio, F., Flores, P., Navarro, J. M., and Martinez, V. (2003). Effects of Ca^{2+}, K^+ and cGMP on Na^+ uptake in pepper plants. *Plant Sci.* 165, 1043–1049. doi: 10.1016/S0168-9452(03)00297-8

Rubio, F., Fon, M., Rodenas, R., Nieves-Cordones, M., Aleman, F., Rivero, R. M., et al. (2014). A low K^+ signal is required for functional high-affinity K^+ uptake through HAK5 transporters. *Physiol. Plant.* 152, 558–570. doi: 10.1111/ppl.12205

Rubio, F., Gassmann, W., and Schroeder, J. I. (1995). Sodium-driven potassium uptake by the plant potassium transporter HKT1 and mutations conferring salt tolerance. *Science* 270, 1660–1663. doi: 10.1126/science.270.5242.1660

Rubio, F., Nieves-Cordones, M., Alemán, F., and Martinez, V. (2008). Relative contribution of AtHAK5 and AtAKT1 to K^+ uptake in the high-affinity range of concentrations. *Physiol. Plant.* 134, 598–608. doi: 10.1111/j.1399-3054.2008.01168.x

Rubio, F., Santa-Maria, G. E., and Rodríguez-Navarro, A. (2000). Cloning of *Arabidopsis* and barley cDNAs encoding HAK potassium transporters in root and shoot cells. *Physiol. Plant.* 109, 34–43. doi: 10.1034/j.1399-3054.2000.100106.x

Salvador-Recatala, V. (2016). The AKT2 potassium channel mediates NaCl induced depolarization in the root of *Arabidopsis thaliana*. *Plant Signal. Behav.* 11:e1165381. doi: 10.1080/15592324.2016.1165381

Santa-María, G. E., Danna, C. H., and Czibener, C. (2000). High-affinity potassium transport in barley roots. Ammonium-sensitive and -insensitive pathways. *Plant Physiol.* 123, 297–306. doi: 10.1104/pp.123.1.297

Santa-María, G. E., Rubio, F., Dubcovsky, J., and Rodriguez-Navarro, A. (1997). The hak1 gene of barley is a member of a large gene family and encodes a high-affinity potassium transporter. *Plant Cell* 9, 2281–2289. doi: 10.2307/3870585

Sassi, A., Mieulet, D., Khan, I., Moreau, B., Gaillard, I., Sentenac, H., et al. (2012). The rice monovalent cation transporter OsHKT2;4: revisited ionic selectivity. *Plant Physiol.* 160, 498–510. doi: 10.1104/pp.112.194936

Sattelmacher, B., Muhling, K. H., and Pennewiss, K. (1998). The apoplast - its significance for the nutrition of higher plants. *Z. Pflanzen. Boden.* 161, 485–498. doi: 10.1002/jpln.1998.3581610502

Schachtman, D. P. (2015). The role of ethylene in plant response to K^+ deficiency. *Front. Plant Sci.* 6:1153. doi: 10.3389/fpls.2015.01153

Schreiber, L., Hartmann, K., Skrabs, M., and Zeier, J. (1999). Apoplastic barriers in roots: chemical composition of endodermal and hypodermal cell walls. *J. Exp. Bot.* 50, 1267–1280. doi: 10.1093/jexbot/50.337.1267

Sentenac, H., Bonneaud, N., Minet, M., Lacroute, F., Salmon, J. M., Gaymard, F., et al. (1992). Cloning and expression in yeast of a plant potassium ion transport system. *Science* 256, 663–665. doi: 10.1126/science.1585180

Shen, Y., Shen, L., Shen, Z., Jing, W., Ge, H., Zhao, J., et al. (2015). The potassium transporter OsHAK21 functions in the maintenance of ion homeostasis and tolerance to salt stress in rice. *Plant Cell Environ.* 38, 2766–2779. doi: 10.1111/pce.12586

Shin, R., Berg, R. H., and Schachtman, D. P. (2005). Reactive oxygen species and root hairs in *Arabidopsis* root response to nitrogen, phosphorus and potassium deficiency. *Plant Cell Physiol.* 46, 1350–1357. doi: 10.1093/pcp/pci145

Shin, R., and Schachtman, D. P. (2004). Hydrogen peroxide mediates plant root cell response to nutrient deprivation. *Proc. Natl. Acad. Sci. U.S.A.* 101, 8827–8832. doi: 10.1073/pnas.0401707101

Siddiqi, M. Y., and Glass, A. D. (1986). A model for the regulation of k influx, and tissue potassium concentrations by negative feedback effects upon plasmalemma influx. *Plant Physiol.* 81, 1–7. doi: 10.1104/pp.81.1.1

Spalding, E. P., Hirsch, R. E., Lewis, D. R., Qi, Z., Sussman, M. R., and Lewis, B. D. (1999). Potassium uptake supporting plant growth in the absence of AKT1 channel activity: inhibition by ammonium and stimulation by sodium. *J. Gen. Physiol.* 113, 909–918. doi: 10.1085/jgp.113.6.909

Stewart, W. M., Dibb, D. W., Johnston, A. E., and Smyth, T. J. (2005). The contribution of commercial fertilizer nutrients to food production. *Agron. J.* 97, 1–6. doi: 10.2134/agronj2005.0001

Subbarao, G. V., Ito, O., Berry, W. L., and Wheeler, R. M. (2003). Sodium - A functional plant nutrient. *Crit. Rev. Plant Sci.* 22, 391–416. doi: 10.1080/07352680390243495

Sutter, J.-U., Sieben, C., Hartel, A., Eisenach, C., Thiel, G., and Blatt, M. R. (2007). Abscisic acid triggers the endocytosis of the *Arabidopsis* KAT1 K^+ channel and its recycling to the plasma membrane. *Curr. Biol.* 17, 1396–1402. doi: 10.1016/j.cub.2007.07.020

Szczerba, M. W., Britto, D. T., and Kronzucker, H. J. (2006). Rapid, futile K^+ cycling and pool-size dynamics define low-affinity potassium transport in barley. *Plant Physiol.* 141, 1494–1507. doi: 10.1104/pp.106.082701

Taiz, L., and Zeiger, E. (1991). *Plant Physiology,* Chapters 8, 9, 10, 2nd Edn. Sunderland, MA: Sinauer.

Takahashi, R., Liu, S., and Takano, T. (2007). Cloning and functional comparison of a high-affinity K^+ transporter gene PhaHKT1 of salt-tolerant and salt-sensitive reed plants. *J. Exp. Bot.* 58, 4387–4395. doi: 10.1093/jxb/erm306

Takehisa, H., Sato, Y., Antonio, B., and Nagamura, Y. (2013). Global transcriptome profile of rice root in response to essential macronutrient deficiency. *Plant Signal. Behav.* 8:e24409. doi: 10.4161/psb.24409

Tester, M., and Leigh, R. A. (2001). Partitioning of nutrient transport processes in roots. *J. Exp. Bot.* 52, 445–457. doi: 10.1093/jexbot/52.356.653

Trewavas, A. J. (1997). Plant cyclic AMP comes in from the cold. *Nature* 390, 657–658. doi: 10.1038/37720

Tsay, Y.-F., Ho, C.-H., Chen, H.-Y., and Lin, S.-H. (2011). Integration of nitrogen and potassium signaling. *Ann. Rev. Plant Biol* 62, 207–226. doi: 10.1146/annurev-arplant-042110-103837

Tyerman, S. D., Skerrett, M., Garrill, A., Findlay, G. P., and Leigh, R. A. (1997). Pathways for the permeation of Na^+ and Cl- into protoplasts

derived from the cortex of wheat roots. *J. Exp. Bot.* 48, 459–480. doi: 10.1093/jxb/48.Special_Issue.459

Véry, A.-A., and Davies, J. M. (2000). Hyperpolarization-activated calcium channels at the tip of *Arabidopsis* root hairs. *Proc. Natl. Acad. Sci. U.S.A.* 97, 9801–9806. doi: 10.1073/pnas.160250397

Véry, A.-A., Nieves-Cordones, M., Daly, M., Khan, I., Fizames, C., and Sentenac, H. (2014). Molecular biology of K^+ transport across the plant cell membrane: what do we learn from comparison between plant species? *J. Plant Physiol.* 171, 748–769. doi: 10.1016/j.jplph.2014.01.011

Very, A. A., and Sentenac, H. (2002). Cation channels in the *Arabidopsis* plasma membrane. *Trends Plant Sci.* 7, 168–175. doi: 10.1016/S1360-1385(02)02262-8

Wakeel, A. (2013). Potassium-sodium interactions in soil and plant under saline-sodic conditions. *J. Plant Nutr. Soil Sci.* 176, 344–354. doi: 10.1002/jpln.201200417

Wakeel, A., Farooq, M., Qadir, M., and Schubert, S. (2011). Potassium substitution by sodium in plants. *Crit. Rev. Plant Sci.* 30, 401–413. doi: 10.1080/07352689.2011.587728

Wakeel, A., Steffens, D., and Schubert, S. (2010). Potassium substitution by sodium in sugar beet (*Beta vulgaris*) nutrition on K-fixing soils. *J. Plant Nutr. Soil Sci.* 173, 127–134. doi: 10.1002/jpln.200900270

Walker, D. J., Black, C. R., and Miller, A. J. (1998). The role of cytosolic potassium and ph in the growth of barley roots. *Plant Physiol.* 118, 957–964. doi: 10.1104/pp.118.3.957

Walker, D. J., Leigh, R. A., and Miller, A. J. (1996). Potassium homeostasis in vacuolate plant cells. *Proc. Natl. Acad. Sci. U.S.A.* 93, 10510–10514. doi: 10.1073/pnas.93.19.10510

Wang, B., Davenport, R. J., Volkov, V., and Amtmann, A. (2006). Low unidirectional sodium influx into root cells restricts net sodium accumulation in *Thellungiella halophila*, a salt-tolerant relative of *Arabidopsis thaliana*. *J. Exp. Bot.* 57, 1161–1170. doi: 10.1093/jxb/erj116

Wang, X. P., Chen, L. M., Liu, W. X., Shen, L., Wang, F. L., Zhou, Y., et al. (2016). AtKC1 and CIPK23 synergistically modulate AKT1-mediated low potassium stress responses in *Arabidopsis*. *Plant Physiol.* 170, 2264–2277. doi: 10.1104/pp.15.01493

Wang, Y., He, L., Li, H. D., Xu, J. A., and Wu, W. H. (2010). Potassium channel alpha-subunit AtKC1 negatively regulates AKT1-mediated K^+ uptake in *Arabidopsis* roots under low-K^+ stress. *Cell Res.* 20, 826–837. doi: 10.1038/cr.2010.74

White, P. J., and Broadley, M. R. (2000). Mechanisms of caesium uptake by plants. *New Phytol.* 147, 241–256. doi: 10.1046/j.1469-8137.2000.00704.x

Wyn Jones, R. G., and Pollard, A. (1983). "Proteins, enzymes and inorganic ions," in *Inorganic Plant Nutrition-Encyclopedia of Plant Physiology New Series 15*, eds A. Lauchli and R. L. Bieleski (Berlin: Springer-Verlag), 528–562.

Xia, J., Kong, D., Xue, S., Tian, W., Li, N., Bao, F., et al. (2014). Nitric oxide negatively regulates AKT1-mediated potassium uptake through modulating vitamin B6 homeostasis in *Arabidopsis*. *Proc. Natl. Acad. Sci. U.S.A.* 111, 16196–16201. doi: 10.1073/pnas.1417473111

Xu, J., Li, H. D., Chen, L. Q., Wang, Y., Liu, L. L., He, L., et al. (2006). A protein kinase, interacting with two calcineurin B-like proteins, regulates K^+ transporter AKT1 in *Arabidopsis*. *Cell* 125, 1347–1360. doi: 10.1016/j.cell.2006.06.011

Yang, T., Zhang, S., Hu, Y., Wu, F., Hu, Q., Chen, G., et al. (2014). The role of a potassium transporter oshak5 in potassium acquisition and transport from roots to shoots in rice at low potassium supply levels. *Plant Physiol.* 166, 945–959. doi: 10.1104/pp.114.246520

Yao, X., Horie, T., Xue, S., Leung, H. Y., Katsuhara, M., Brodsky, D. E., et al. (2010). Differential sodium and potassium transport selectivities of the rice OsHKT2;1 and OsHKT2;2 transporters in plant cells. *Plant Physiol.* 152, 341–355. doi: 10.1104/pp.109.145722

Yeo, A. R., Yeo, M. E., and Flowers, T. J. (1987). The contribution of an apoplastic pathway to sodium uptake by rice roots in saline conditions. *J. Exp. Bot.* 38, 1141–1153. doi: 10.1093/jxb/38.7.1141

Zhang, B., Karnik, R., Wang, Y., Wallmeroth, N., Blatt, M. R., and Grefen, C. (2015). The *Arabidopsis* R-SNARE VAMP721 Interacts with KAT1 and KC1 K^+ channels to moderate k^+ current at the plasma membrane. *Plant Cell* 27, 1697–1717. doi: 10.1105/tpc.15.00305

Zörb, C., Senbayram, M., and Peiter, E. (2014). Potassium in agriculture – Status and perspectives. *J. Plant Physiol.* 171, 656–669. doi: 10.1016/j.jplph.2013.08.008

Conflict of Interest Statement: The authors declare that the research was conducted in the absence of any commercial or financial relationships that could be construed as a potential conflict of interest.

frontiers in Plant Science

MINI REVIEW
published: 21 September 2016
doi: 10.3389/fpls.2016.01391

Transporters Involved in Root Nitrate Uptake and Sensing by *Arabidopsis*

*Mélanie Noguero and Benoît Lacombe**

Laboratoire de Biochimie et Physiologie Moléculaire des Plantes, Institut de Biologie Intégrative des Plantes "Claude Grignon", UMR CNRS/INRA/SupAgro/UM, Montpellier, France

Most plants use nitrate (NO_3^-) as their major nitrogen (N) source. The NO_3^- uptake capacity of a plant is determined by three interdependent factors that are sensitive to NO_3^- availability: (i) the functional properties of the transporters in roots that contribute to the acquisition of NO_3^- from the external medium, (ii) the density of functional transporters at the plasma membrane of root cells, and (iii) the surface and architecture of the root system. The identification of factors that regulate the NO_3^--sensing systems is important for both fundamental and applied science, because these factors control the capacity of plants to use the available NO_3^-, a process known as the "nitrate use efficiency." The molecular component of the transporters involved in uptake and sensing mechanism in *Arabidopsis* roots are presented and their relative contribution discussed.

Keywords: nutrient sensing, transporters, nitrates, development, plants

INTRODUCTION

Nitrate (NO_3^-) is an essential source of nitrogen for plant development and metabolism. With ammonium (NH_4^+) and urea ($CO(NH_2)_2$), it is the most used fertilizer in agriculture as a source of nitrogen (N) (Kiba and Krapp, 2016). But, beside its role as a nutrient, nitrate is also a signal molecule which is involved in the control of many physiological processes, plant growth and crop yield (Crawford, 1995; Krapp et al., 2014; Vidal et al., 2014). For example, as other nutrients like phosphate or ammonium (Drew et al., 1973; Drew and Saker, 1975), nitrate participates in the regulation of lateral roots development and architecture (Remans et al., 2006a; Walch-Liu et al., 2006b; Krouk et al., 2010a; Ruffel et al., 2011, 2014, 2016), leaf development (Chiu et al., 2004), flowering induction (Castro Marin et al., 2011) and seed dormancy (Alboresi et al., 2005). As a signal molecule, nitrate can induce the expression of a number of genes implicated in nitrate transport and assimilation (Wang et al., 2004; Bi et al., 2007; Krouk et al., 2011; Medici and Krouk, 2014).

Nitrate is often a limited resource and its accessibility is modified in both time and space, therefore plants must adapt nitrate inputs to the needs and availability in the soil. Nitrate can be assimilated in the roots or translocated to aerial organs *via* the xylem. Nitrate is then reduced to nitrite by nitrate reductase (NR) and further to ammonium by nitrite reductase (NiR) before incorporation in amino acids (Stitt, 1999). Otherwise, nitrate could also be stored, mainly in the vacuoles where concentration could vary from 5 mM to 75 mM (measured in roots of barley seedlings; Miller and Smith, 2008), in roots or shoots for further remobilization when nitrate availability became scarce.

To maximize uptake efficiency in a wide range of external nitrate concentration, plants own transport system with different properties to adjust nitrate uptake capacity (Miller et al., 2007); two

OPEN ACCESS

Edited by:
Janin Riedelsberger, University of Talca, Chile

Reviewed by:
Serge Delrot, University of Bordeaux, France
Zhenhua Zhang, Hunan Agricultural University, China

****Correspondence:***
Benoît Lacombe
benoit.lacombe@supagro.inra.fr

Received: *04 June 2016*
Accepted: *01 September 2016*
Published: *21 September 2016*

Citation:
Noguero M and Lacombe B (2016) Transporters Involved in Root Nitrate Uptake and Sensing by Arabidopsis. Front. Plant Sci. 7:1391. doi: 10.3389/fpls.2016.01391

types of transport systems known as Low Affinity Transport Systems (LATS) and High Affinity Transport Systems (HATS). The LATS allows transport in high (> 0.5 mM) external nitrate concentration whereas the HATS provide a capacity for nitrate absorption at low (< 0.5 mM) external nitrate concentrations. Within each of these transport systems both constitutive (c) and inducible (i) forms co-exist. Expression of these four kinds of transport systems is essential for an efficient uptake, and expression could be constitutive or inducible function of the external nitrate concentration perceived.

Four families of transporters participate in nitrate uptake, distribution or storage: NITRATE TRANSPORTER 2 (NRT2) transporters (Orsel et al., 2002; Krapp et al., 2014), NITRATE TRANSPORTER 1/PEPTIDE TRANSPORTER FAMILY (NPF) transporters (Léran et al., 2014), CHLORIDE CHANNEL FAMILY (CLC) transporters (Barbier-Brygoo et al., 2011) and SLOW ANION ASSOCIATED CHANNEL HOMOLOG (SLAC/SLAH) (Negi et al., 2008). Because roots constitute the main organ where exchange between plant and its environment take place, this review focuses on transporters identified in *Arabidopsis* root plasma membrane and contributing to nitrate uptake from the soil (**Figure 1**). Transporters from the NPF and NRT2 families are involved and interestingly some of these transporters are also involved in nitrate sensing.

HIGH-AFFINITY NITRATE TRANSPORTER: NRT2 FAMILY

Seven members have been described in the NRT2 family in *Arabidopsis* and characterized as high-affinity nitrate transporters (Krapp et al., 2014). The affinity for nitrate of these transporters is in the range of microM, saturable around 0.2–0.5 milliM. The role in nitrate influx in the root has been demonstrated for four of them: NRT2.1, NRT2.2, NRT2.4, and NRT2.5 (Orsel et al., 2002; Kiba et al., 2012; Lezhneva et al., 2014; Kiba and Krapp, 2016).

NRT2.1 expression is found in the epidermal and cortical cells of mature roots (**Figure 1**) (Wirth et al., 2007) and constitutes the most studied transporter in NRT2 family. *NRT2.1* expression is dependent to nitrate availability and seems to be regulated by different conditions: (i) induced by nitrate (Filleur and Daniel-Vedele, 1999) and as a consequence the representative of the iHATS (inducible high affinity transport system, see Introduction), (ii) repressed in high nitrate or nitrogen concentrations (Crawford, 1995), (iii) briefly expressed in response to nitrate deficiency (Crawford and Glass, 1998; Cerezo et al., 2001). Same regulation was observed in maize (Sorgona et al., 2011). *ZmNRT2.1* expression along the maize primary root increases after 4 h of nitrate treatment coordinated with elevation of nitrate uptake rate. These results reflect an important role of NRT2.1 transporter in the regulation of nitrate fluxes in roots. Water status is affected in *nrt2.1* mutant, suggesting that NRT2.1 also supports root hydraulic conductivity (Li et al., 2016).

Despite its low expression level, *NRT2.2* expression seems to follow the same regulation (i.e., in response to nitrate availability). Moreover, *NRT2.1* and *NRT2.2* genes are very close in genomic region of chromosome 1 (AGI NRT2.1: At1g08090 and NRT2.2: At1g08100). *atnrt2* KO mutants have been obtained for both transporters NRT2.1 and NRT2.2, and are affected in the high affinity nitrate transport activity, but not in the low affinity. However, in this *atnrt2* mutant, the deletion of both transporters did not result in the complete disappearance of the nitrate uptake ability in low nitrate concentration, and besides a low affinity transport activity, a residual high affinity nitrate transport response was observed, probably due to the presence of constitutive high affinity nitrate transporters (Cerezo et al., 2001; Miller et al., 2007). In maize, an analysis of several NRT2 genes expression in response to nitrate suggests that *ZmNRT2.1* and *ZmNRT2.2* are the main genes controlling high-affinity nitrate uptake (Garnett et al., 2013).

Another NRT2 family transporter, NRT2.4, has been identified to participate to nitrate transport in roots, additionally to its contribution to nitrate distribution to shoot. Although a low expression level compared to NRT2.1, NRT2.4 is expressed in the epidermis of the lateral root (**Figure 1**; also expressed in leaves) and is involved in nitrate uptake at very low nitrate concentration. Interestingly, nitrate perception could control expression of NRT2.4, induced in long-term starvation (Kiba et al., 2012). At low external nitrate concentration (25 μM), *nrt2.1/nrt2.2* double mutant is deficient for high affinity nitrate uptake and nitrate transport is severely affected but still occurs. NRT2.4 contribute to maintain a minimal transport activity in this mutant. Kiba et al. (2012) have demonstrated that overexpression of NRT2.4 in the *nrt2.1/nrt2.2* double mutant partially restore nitrate uptake activity. However NRT2.4 is not the only one to provide this transport activity because *nrt2.1/nrt2.2/nrt2.4* triple mutant keep its ability to transport nitrate (7% relative to WT) at very low concentration (20 μM nitrate), suggesting existence of others high affinity transporters. This role is partly shared by NRT2.5 as quadruple mutant *nrt2.1/nrt2.2/nrt2.4/nrt2.5* has a stronger reduced high affinity nitrate transport (3% relative to WT; Lezhneva et al., 2014). Interestingly, added NRT2.4 loss of function to *nrt2.1/nrt2.2* double mutant impact much more seedling growth under N deficiency than NRT2.5. Moreover, NRT2.4 and NRT2.5 transcripts increase during N limitation, suggesting significant implication of both in root nitrate uptake (Lezhneva et al., 2014).

Interaction with a small protein NAR2/NRT3 seems to be essential for nitrate uptake of some of the NRT2 (Orsel et al., 2006; Li et al., 2007). Two members constitute NAR2 family in *Arabidopsis*, but only NAR2.1/NRT3.1 is necessary for nitrate transport activity. Indeed, co-expression in oocytes of NAR2.1/NRT3.1 and all (expect NRT2.7) NRT2 members demonstrate the positive effect of NAR2.1 on NRT2 dependent nitrate uptake (Kotur et al., 2012). Moreover, these NRT2 family members interact with NAR2.1 in yeast two hybrids (Kotur et al., 2012). The effect of NAR2.1/NRT3.1 on NRT2.4 nitrate transport activity in xenopus oocyte is yet fully understood (Kiba et al., 2012). Besides contribution to nitrate transport, NAR2.1 seems to be implicated in NRT2.1 localization or stabilization at the plasma membrane (Wirth et al., 2007). NAR contribution to nitrate transport is also observed in others species, like barley, maize or rice. Measurements of

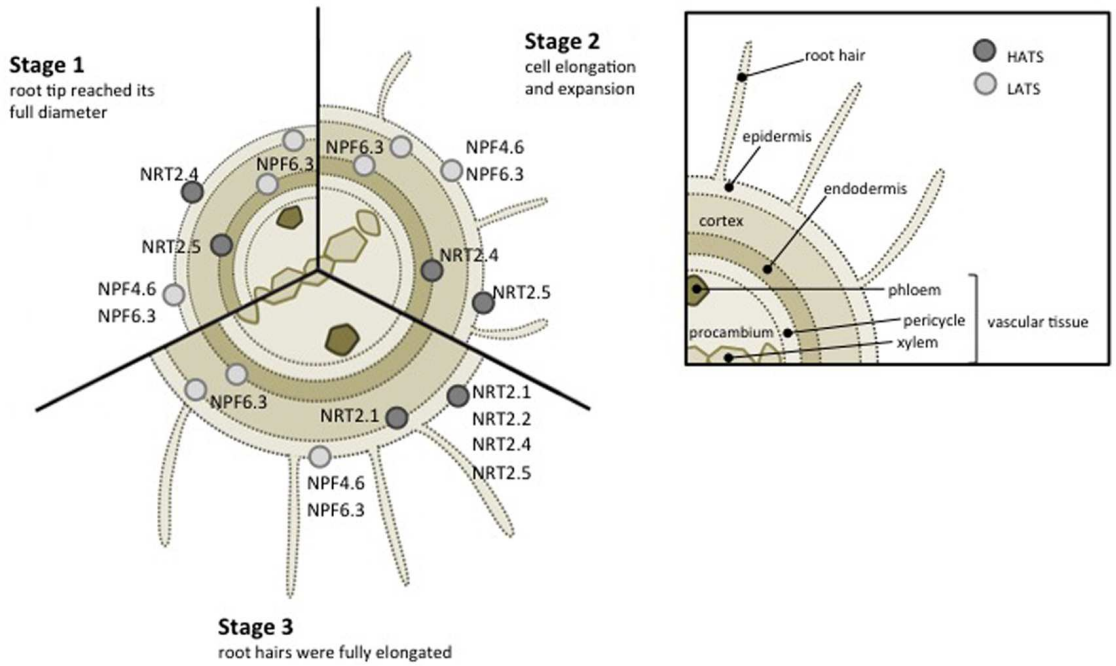

FIGURE 1 | Schematic representation of low- (light gray dots) and high- (dark gray dots) affinity nitrate transporters expressed in *Arabidopsis* root. Three stages of root developement have been represented according to Birnbaum et al. (2003).

the ^{15}N-nitrate enrichment in oocytes showed that co-injection of HvNRT2.1 and HvNAR2.3 was able to provide significant nitrate uptake (Tong et al., 2005). Lupini et al. (2016) show that ZmNAR2.1 has an important implication in ZmNRT2.1 expression and localization along root axis correlated with nitrate influxes (Lupini et al., 2016). In rice, the expression of the Os*NRT2.1, OsNRT2.2,* and *OsNRT2.3a* genes seems to be regulated by *OsNAR2.1*, itself transcriptionally induced by nitrate (Yan et al., 2011).

LOW-AFFINITY NITRATE TRANSPORTER: NPF FAMILY

In higher plants, NPF family includes a large number of genes, divided into eight subfamilies, and able to transport diversified substrates. However, no substrate selectivity correlates with sequence homology, and consequently with each subfamily (Léran et al., 2014). In *Arabidopsis*, NPF family consists of 53 members mainly characterized as low affinity transporters. Herein, NPF6.3/NRT1.1/CHL1 was firstly identified as low affinity nitrate transporter (Tsay et al., 1993). *NPF6.3* is expressed in several root tissues: epidermis, cortex and endodermis (**Figure 1**; also expressed in young leaf and flower buds) (Huang et al., 1996; Guo et al., 2002; Remans et al., 2006a). Consequently, NPF6.3 allows nitrate uptake from soil (Crawford, 1995; Munos et al., 2004) and is also implicated in nitrate translocation to aerials part (Boursiac et al., 2013; Léran et al., 2013). NPF6.3 reveals also an ability to switch to high-affinity activity in low nitrate conditions (Liu et al., 1999; Liu and Tsay, 2003; Ho et al., 2009). When phosphorylated, Thr 101 confers to NPF6.3 high affinity nitrate transport behavior whereas non-phosphorylated NPF6.3 acts as low-affinity transporter. The protein complex CIPK23-CBL9 (CIPK: CBL-Interacting Protein Kinase, CBL: Calcineurin-B like Protein) is implicated in the dual affinity transition changes thanks to its ability to phosphorylate Thr 101 residue. In low nitrate conditions, CIPK23-CBL9 phosphorylates NPF6.3 Thr 101 residue and promotes NPF6.3 high affinity nitrate transport (Liu and Tsay, 2003; Ho et al., 2009). Other proteins, namely ABI1 and ABI2 belonging to protein phosphatase 2C family from the clade A, contribute to NPF6.3 activity in xenopus oocytes (Léran et al., 2015). *In planta* experiments demonstrate that only ABI2 has a regulatory role on NPF6.3-dependent nitrate transport. This protein was able to modulate transport activity by preventing phosphorylation of CIPK23-CBL1 complex (Léran et al., 2015).

Functional characterization and regulation of NPF6.3 transporters is still ongoing and many residues seem to be implicated in nitrate transport ability. Recently, crystallization studies of NPF6.3 reveal a crucial role of His 356 residue in nitrate substrate binding and transport. In the presence of nitrate, authors show that NPF6.3 H356A variant loses its nitrate transport capacity compared to wild type NPF6.3 protein (Parker and Newstead, 2014; Sun et al., 2014).

NPF4.6/NRT1.2/AIT1, another nitrate transporter belonging to NPF family is involved in soil nitrate uptake. As for NPF6.3,

NPF4.6 is also expressed in root epidermis (**Figure 1**), however, NPF4.6 display a constitutive expression and activity is restricted to low affinity nitrate transport (Liu et al., 1999). NPF4.6 is also an ABA transporter implicated in seed dormancy and transpiration (Kanno et al., 2012).

NPF2.7/NAXT1 is another member of the NPF family expressed the cortex of mature roots (**Figure 1**) and implicated in root nitrate uptake in *Arabidopsis*. However, it seems to be mainly involved in nitrate efflux to the external media and consequently participate in nitrate homeostasis (Segonzac et al., 2007). As for others NPFs (i.e., NPF7.2, NPF7.3, and NPF2.3) expressed in *Arabidopsis* roots and characterized to date, their role consist mainly to nitrate translocation to xylem tissue for distribution to aerial parts (Lin et al., 2008, Li et al., 2010; Taochy et al., 2015).

NITRATE SENSING BY TRANSPORTERS

Although it constitutes an essential nutrient, nitrate is also known to be a signaling molecule involved in many physiological processes including gene regulation (Wang et al., 2004) and root development (Walch-Liu et al., 2006a). Within the different proteins involved in nitrate sensing (Medici and Krouk, 2014), two transporters described above, namely NRT2.1 and NPF6.3/NRT1.1, are key ones.

NRT2.1

Formation of lateral root is strongly affected by environmental condition and nutrient signals as nitrate are essential to influenced root architecture. Beside its role in high-affinity nitrate transport, NRT2.1 is involved in nitrate-dependent lateral root initiation (LRI). With genetic screen using the repression of LRI in seedlings growing on high sucrose/low nitrogen conditions, a *lin1* mutant has been isolated for its ability to initiate a large number of lateral roots (Malamy and Ryan, 2001). Further characterization of *lin1* mutant indicates a point mutation in NRT2.1 gene that leads to G119R substitution in the protein sequence is responsible for *lin1* phenotype (Little et al., 2005). Loss of function *lin1* mutant as well as three others *nrt2.1* mutants (*nrt2.1-1*, *nrt2.1-2,* and *nrt2.1-3*) exhibit nitrate-independent increases lateral root formation suggesting that NRT2.1 is implicated in LRI repression under specific conditions (i.e., high sucrose/low nitrate). Nitrate influx in *lin1* (as *nrt2.1* KO) mutant is significantly reduced compared to WT, indicating that nitrate uptake and/or accumulation could be correlated to inhibition of lateral root primordia (Little et al., 2005; Remans et al., 2006b). However, LRI is not only regulated by direct sensing of the external nitrate concentration and could be influenced by long-term nitrate growth condition. Thus, decrease in nitrate availability [seedling transferred from high (10 mM) to low (0.5 mM) nitrate media] seems to stimulate both lateral root length and LRI in WT plants (Remans et al., 2006b).

These results indicate that NRT2.1 deals with nitrate transporter activity independently from its nitrate sensors activity in the root development control. Nitrate effect on root development not only originates from current nitrate transport but also from nitrate already available from the plant.

NPF6.3/NRT1.1/CHL1

In addition to its nitrate transport activity (Tsay et al., 1993), NPF6.3/NRT1.1 functions as a nitrate sensor and is able to promote physiological response in the control of root system architecture and to modulate the expression level of many gens implicated in nitrate signaling pathway (Wang et al., 2004; Krouk et al., 2009, 2010b; Medici and Krouk, 2014; Medici et al., 2015). The NPF6.3 dependent regulation of NRT2.1 expression has been studied and is modulated according to nitrate concentration. Fast induction of NRT2.1 expression is observed in response to brief exposure to nitrate concentration (Ho et al., 2009; Bouguyon et al., 2015) whereas NRT2.1 is down regulated in long-term high nitrate supply (Munos et al., 2004; Krouk et al., 2006). Another nitrate dependent phenotype, lateral root development, is also NPF6.3/NRT1.1-dependent (Bouguyon et al., 2016). Thus in low nitrate condition, NPF6.3 acts as a repressor of lateral root primordia and it became an activator of root branching in response to nitrate supply (Remans et al., 2006a; Krouk et al., 2010a; Mounier et al., 2014).

The definitive proof of the role of NPF6.3/NRT1.1 in nitrate sensing has been given by the study of *chl1-9*, NPF6.3/NRT1.1-P492L (Ho et al., 2009). Although a normal level of transcript and protein expression, nitrate transport activity was suppressed in *chl1-9* knockout mutant, demonstrating that the Pro 492 residue is essential for nitrate uptake. Interestingly, this mutant is still able to induce NPF6.3/NRT1.1-dependent gene expression measured through NRT2.1 expression level, indicating that PNR is not affected in this mutant. This specific mutation demonstrates that the roles of NPF6.3 in transport and signaling belong to independent regulations (Ho et al., 2009; Bouguyon et al., 2015).

NPF6.3 ability to modulate lateral root development is mediated by its auxin transport capacity (Krouk et al., 2010a; Bouguyon et al., 2015). Correlations have been suggested between NPF6.3 auxin transport ability and nitrate sensing and signaling. Indeed, P492L and T101A point mutations decrease auxin transport capacity and plants expressing these mutants (i.e., *chl1-9* and NPF6.3-T101A) are affected in nitrate-dependent lateral root development, suggesting that phosphorylated form of NPF6.3 could be responsible for NPF6.3 dependent regulation of both nitrate and auxin transport and consequently for lateral root development (Bouguyon et al., 2015).

Finally, the NPF6.3/NRT1.1 regulators, the kinase CIPK23 and the phosphatase ABI2, are also involved in nitrate sensing (Ho et al., 2009; Léran et al., 2015): CIPK23 being a negative regulator of NPF6.3/NRT1.1 by phosphorylation, and then a repressor of PNR whereas ABI2 being a positive regulator of the negative regulator complex (CIPK23/CBL1). Recently, the *NRG2* (Nitrate Regulatory Gene) gene has been described to impact nitrate signaling *via* regulation of NPF6.3 in roots (and NPF7.2 in leaves). *nrg2* mutant grown in nitrate media supplemented with ammonium shows a lower expression of NPF6.3 expression in roots as well as down regulation of many nitrate responsive

genes. Consequently, theses mutants display a defect in nitrate accumulation on roots (Xu et al., 2016).

CONCLUSION

Two transporters, NRT2.1 and NPF6.3/NRT1.1, as well as their protein partners (NAR2, CBL1, CBL9, CIPK23, ABI2) are involved in nitrate transport and sensing. Although theses nitrate transporters are among the most studied, there are still some missing parts to better interpret the transport regulation and the modulation of root architecture, and as well the adjacent mechanisms responsible for optimization of nitrate use efficiency (NUE; O'Brien et al., 2016). Plant nitrate uptake constitutes an important trait to take into account to improve crop yield and NUE. Indeed in rice, plants overexpressing the high affinity nitrate transporter NRT2.3b have an increased nitrate uptake correlated to an improvement in growth capacity, yield and NUE (Fan et al., 2016), just like OsNRT1.1b also implicated in nitrate transport efficiency and NUE (Fan et al., 2015; Hu et al., 2015). Thus, the capacity of other NPF and NRT2 transporters to sense nitrate will be determined in further experiments and will help us to better understand how plant is able to cope with nitrate heterogeneity. Furthermore, identification of proteins belonging to the NRT2 and NPF6.3/NRT1.1 protein regulatory networks will give new insights in the nitrate sensing capacity of plants. This review deals with plasma membrane transporters, however, vacuolar transporters are involved in nitrate accumulation and consequently impacts on NUE, as observed in rapeseed for *BnNRT1.5* (Han et al., 2016). Thus, determination of molecular players and regulatory factors interacting with nitrate transporters, as well as others transporters like SLAH1 through which plants are able to balance between nitrate and chloride loading (Cubero-Font et al., 2016) constitutes a future challenge to better understand how nitrate influences plant growth and development.

AUTHOR CONTRIBUTIONS

All authors listed, have made substantial, direct and intellectual contribution to the work, and approved it for publication.

ACKNOWLEDGMENTS

BL is financially supported by the Agence Nationale de la Recherche (ANR-14-CE34-0007-01-HONIT with a post-doctoral fellowship to MN).

REFERENCES

Alboresi, A., Gestin, C., Leydecker, M. T., Bedu, M., Meyer, C., and Truong, H. N. (2005). Nitrate, a signal relieving seed dormancy in *Arabidopsis*. *Plant Cell Environ.* 28, 500–512. doi: 10.1111/j.1365-3040.2005.01292.x

Barbier-Brygoo, H., De Angeli, A., Filleur, S., Frachisse, J. M., Gambale, F., Thomine, S., et al. (2011). Anion channels/transporters in plants: from molecular bases to regulatory networks. *Annu. Rev. Plant Biol.* 62, 25–51. doi: 10.1146/annurev-arplant-042110-103741

Bi, Y. M., Wang, R. L., Zhu, T., and Rothstein, S. J. (2007). Global transcription profiling reveals differential responses to chronic nitrogen stress and putative nitrogen regulatory components in *Arabidopsis*. *BMC Genomics* 8:281. doi: 10.1186/1471-2164-8-281

Birnbaum, K., Shasha, D. E., Wang, J. Y., Jung, J. W., Lambert, G. M., Galbraith, D. W., et al. (2003). A gene expression map of the *Arabidopsis* root. *Science* 302, 1956–1960. doi: 10.1126/science.1090022

Bouguyon, E., Brun, F., Meynard, D., Kubes, M., Pervent, M., Léran, S., et al. (2015). Multiple mechanisms of nitrate sensing by *Arabidopsis* nitrate transceptor NRT1.1. *Nature Plants* 1:15015. doi: 10.1038/NPLANTS.2015.15

Bouguyon, E., Perrine-Walker, F., Pervent, M., Rochette, J., Cuesta, C., Benkova, E., et al. (2016). Nitrate controls root development through post-transcriptional regulation of the NRT1.1/*NPF*6.3 transporter/sensor. *Plant Physiol.* doi: 10.1104/pp.16.01047 [Epub ahead of print].

Boursiac, Y., Léran, S., Corratge-Faillie, C., Gojon, A., Krouk, G., and Lacombe, B. (2013). ABA transport and transporters. *Trends Plant Sci.* 18, 325–333. doi: 10.1016/j.tplants.2013.01.007

Castro Marin, I., Loef, I., Bartetzko, L., Searle, I., Coupland, G., Stitt, M., et al. (2011). Nitrate regulates floral induction in *Arabidopsis*, acting independently of light, gibberellin and autonomous pathways. *Planta* 233, 539–552. doi: 10.1007/s00425-010-1316-5

Cerezo, M., Tillard, P., Filleur, S., Munos, S., Daniel-Vedele, F., and Gojon, A. (2001). Major alterations of the regulation of root NO(3)(-) uptake are associated with the mutation of Nrt2.1 *and Nrt*2.2 genes in *Arabidopsis*. *Plant Physiol.* 127, 262–271. doi: 10.1104/pp.127.1.262

Chiu, C. C., Lin, C. S., Hsia, A. P., Su, R. C., Lin, H. L., and Tsay, Y. F. (2004). Mutation of a nitrate transporter, AtNRT1:4, results in a reduced petiole nitrate content and altered leaf development. *Plant Cell Physiol.* 45, 1139–1148. doi: 10.1093/pcp/pch143

Crawford, N. M. (1995). Nitrate: nutrient and signal for plant growth. *Plant Cell* 7, 859–868. doi: 10.1105/tpc.7.7.859

Crawford, N. M., and Glass, A. D. M. (1998). Molecular and physiological aspects of nitrate uptake in plants. *Trends Plant Sci.* 3, 389–395. doi: 10.1016/S1360-1385(98)01311-9

Cubero-Font, P., Maierhofer, T., Jaslan, J., Rosales, M. A., Espartero, J., Diaz-Rueda, P., et al. (2016). Silent S-Type anion channel subunit SLAH1 gates SLAH3 open for chloride root-to-shoot translocation. *Curr. Biol.* 26, 2213–2220. doi: 10.1016/j.cub.2016.06.045

Drew, M., Saker, L., and Ashley, T. (1973). Nutrient supply and the growth of the semicla root system in barley. I. The effect of nitrate concentration on the growth of axes and lateral. *J. Exp. Bot.* 24, 1189–1202. doi: 10.1093/jxb/24.6.1189

Drew, M. C., and Saker, L. R. (1975). Nutrient supply and the growth of the serninal root systern in barley. II. Localized cornpensatory increases in lateral root growth and rates of nitrate uptake when NO, is restricted to only part of the root system. *J. Exp. Bot.* 26, 79–80. doi: 10.1093/jxb/26.1.79

Fan, X., Feng, H., Tan, Y., Xu, Y., Miao, Q., and Xu, G. (2015). A putative 6-transmembrane nitrate transporter OsNRT1.1b plays a key role in rice under low nitrogen. *J. Integr. Plant Biol.* 58, 590–599. doi: 10.1111/jipb.12382

Fan, X., Tang, Z., Tan, Y., Zhang, Y., Luo, B., Yang, M., et al. (2016). Overexpression of a pH-sensitive nitrate transporter in rice increases crop yields. *Proc. Natl. Acad. Sci. U.S.A.* 113, 7118–7123. doi: 10.1073/pnas.1525184113

Filleur, S., and Daniel-Vedele, F. (1999). Expression analysis of a high-affinity nitrate transporter isolated from *Arabidopsis thaliana* by differential display. *Planta* 207, 461–469. doi: 10.1007/s004250050505

Garnett, T., Conn, V., Plett, D., Conn, S., Zanghellini, J., Mackenzie, N., et al. (2013). The response of the maize nitrate transport system to nitrogen demand and supply across the lifecycle. *New Phytol.* 198, 82–94. doi: 10.1111/nph.12166

Guo, F. Q., Wang, R., and Crawford, N. M. (2002). The *Arabidopsis* dual-affinity nitrate transporter gene AtNRT1.1 *(CHL*1) is regulated by auxin in both shoots and roots. *J. Exp. Bot.* 53, 835–844. doi: 10.1093/jexbot/53.370.835

Han, Y. L., Song, H. X., Liao, Q., Yu, Y., Jian, S. F., Lepo, J. E., et al. (2016). Nitrogen use efficiency is mediated by vacuolar nitrate sequestration capacity in roots of *Brassica napus*. *Plant Physiol.* 170, 1684–1698. doi: 10.1104/pp.15.01377

Ho, C. H., Lin, S. H., Hu, H. C., and Tsay, Y. F. (2009). CHL1 functions as a nitrate sensor in plants. *Cell* 138, 1184–1194. doi: 10.1016/j.cell.2009.07.004

Hu, B., Wang, W., Ou, S., Tang, J., Li, H., Che, R., et al. (2015). Variation in NRT1.1B contributes to nitrate-use divergence between rice subspecies. *Nat. Genet.* 47, 834–838. doi: 10.1038/ng.3337

Huang, N. C., Chiang, C. S., Crawford, N. M., and Tsay, Y. F. (1996). CHL1 encodes a component of the low-affinity nitrate uptake system in *Arabidopsis* and shows cell type-specific expression in roots. *Plant Cell* 8, 2183–2191. doi: 10.1105/tpc.8.12.2183

Kanno, Y., Hanada, A., Chiba, Y., Ichikawa, T., Nakazawa, M., Matsui, M., et al. (2012). Identification of an abscisic acid transporter by functional screening using the receptor complex as a sensor. *Proc. Natl. Acad. Sci. U.S.A.* 109, 9653–9658. doi: 10.1073/pnas.1203567109

Kiba, T., Feria-Bourrellier, A. B., Lafouge, F., Lezhneva, L., Boutet-Mercey, S., Orsel, M., et al. (2012). The *Arabidopsis* nitrate transporter NRT2.4 plays a double role in roots and shoots of nitrogen-starved plants. *Plant Cell* 24, 245–258. doi: 10.1105/tpc.111.092221

Kiba, T., and Krapp, A. (2016). Plant nitrogen acquisition under low availability: regulation of uptake and root architecture. *Plant Cell Physiol.* 57, 707–714. doi: 10.1093/pcp/pcw052

Kotur, Z., Mackenzie, N., Ramesh, S., Tyerman, S. D., Kaiser, B. N., and Glass, A. D. (2012). Nitrate transport capacity of the *Arabidopsis thaliana* NRT2 family members and their interactions with AtNAR2.1. *New Phytol.* 194, 724–731. doi: 10.1111/j.1469-8137.2012.04094.x

Krapp, A., David, L. C., Chardin, C., Girin, T., Marmagne, A., Leprince, A. S., et al. (2014). Nitrate transport and signalling in *Arabidopsis*. *J. Exp. Bot.* 65, 789–798. doi: 10.1093/jxb/eru001

Krouk, G., Lacombe, B., Bielach, A., Perrine-Walker, F., Malinska, K., Mounier, E., et al. (2010a). Nitrate-regulated auxin transport by NRT1.1 defines a mechanism for nutrient sensing in plants. *Dev. Cell* 18, 927–937. doi: 10.1016/j.devcel.2010.05.008

Krouk, G., Mirowski, P., LeCun, Y., Shasha, D. E., and Coruzzi, G. M. (2010b). Predictive network modeling of the high-resolution dynamic plant transcriptome in response to nitrate. *Genome Biol.* 11:R123. doi: 10.1186/gb-2010-11-12-r123

Krouk, G., Ruffel, S., Gutierrez, R. A., Gojon, A., Crawford, N. M., Coruzzi, G. M., et al. (2011). A framework integrating plant growth with hormones and nutrients. *Trends Plant Sci.* 16, 178–182. doi: 10.1016/j.tplants.2011.02.004

Krouk, G., Tillard, P., and Gojon, A. (2006). Regulation of the high-affinity NO3- uptake system by NRT1.1-*mediated NO*3- demand signaling in *Arabidopsis*. *Plant Physiol.* 142, 1075–1086. doi: 10.1104/pp.106.087510

Krouk, G., Tranchina, D., Lejay, L., Cruikshank, A. A., Shasha, D., Coruzzi, G. M., et al. (2009). A systems approach uncovers restrictions for signal interactions regulating genome-wide responses to nutritional cues in *Arabidopsis*. *PLoS Comput. Biol.* 5:e1000326. doi: 10.1371/journal.pcbi.1000326

Léran, S., Edel, K. H., Pervent, M., Hashimoto, K., Corratge-Faillie, C., Offenborn, J. N., et al. (2015). Nitrate sensing and uptake in *Arabidopsis* are enhanced by ABI2, a phosphatase inactivated by the stress hormone abscisic acid. *Sci. Signal.* 8:ra43. doi: 10.1126/scisignal.aaa4829

Léran, S., Muños, S., Brachet, C., Tillard, P., Gojon, A., and Lacombe, B. (2013). *Arabidopsis* NRT1.1 is a bidirectional transporter involved in root-to-shoot nitrate translocation. *Mol. Plant* 6, 1984–1987. doi: 10.1093/mp/sst068

Léran, S., Varala, K., Boyer, J. C., Chiurazzi, M., Crawford, N., Daniel-Vedele, F., et al. (2014). A unified nomenclature of NITRATE TRANSPORTER 1/PEPTIDE TRANSPORTER family members in plants. *Trends Plant Sci.* 19, 5–9. doi: 10.1016/j.tplants.2013.08.008

Lezhneva, L., Kiba, T., Feria-Bourrellier, A. B., Lafouge, F., Boutet-Mercey, S., Zoufan, P., et al. (2014). The *Arabidopsis* nitrate transporter NRT2.5 plays a role in nitrate acquisition and remobilization in nitrogen-starved plants. *Plant J.* 80, 230–241. doi: 10.1111/tpj.12626

Li, G., Tillard, P., Gojon, A., and Maurel, C. (2016). Dual regulation of root hydraulic conductivity and plasma membrane aquaporins by plant nitrate accumulation and high-affinity nitrate transporter NRT2.1. *Plant Cell Physiol.* 57, 733–742. doi: 10.1093/pcp/pcw022

Li, J. Y., Fu, Y. L., Pike, S. M., Bao, J., Tian, W., Zhang, Y., et al. (2010). The *Arabidopsis* nitrate transporter NRT1.8 functions in nitrate removal from the xylem sap and mediates cadmium tolerance. *Plant Cell* 22, 1633–1646. doi: 10.1105/tpc.110.075242

Li, W., Wang, Y., Okamoto, M., Crawford, N. M., Siddiqi, M. Y., and Glass, A. D. (2007). Dissection of the AtNRT2.1:*AtNRT*2.2 inducible high-affinity nitrate transporter gene cluster. *Plant Physiol.* 143, 425–433. doi: 10.1104/pp.106.091223

Lin, S. H., Kuo, H. F., Canivenc, G., Lin, C. S., Lepetit, M., Hsu, P. K., et al. (2008). Mutation of the *Arabidopsis* NRT1.5 nitrate transporter causes defective root-to-shoot nitrate transport. *Plant Cell* 20, 2514–2528. doi: 10.1105/tpc.108.060244

Little, D. Y., Rao, H., Oliva, S., Daniel-Vedele, F., Krapp, A., and Malamy, J. E. (2005). The putative high-affinity nitrate transporter NRT2.1 represses lateral root initiation in response to nutritional cues. *Proc. Natl. Acad. Sci. U.S.A.* 102, 13693–13698. doi: 10.1073/pnas.0504219102

Liu, K. H., Huang, C. Y., and Tsay, Y. F. (1999). CHL1 is a dual-affinity nitrate transporter of *Arabidopsis* involved in multiple phases of nitrate uptake. *Plant Cell* 11, 865–874. doi: 10.2307/3870820

Liu, K. H., and Tsay, Y. F. (2003). Switching between the two action modes of the dual-affinity nitrate transporter CHL1 by phosphorylation. *EMBO J.* 22, 1005–1013. doi: 10.1093/emboj/cdg118

Lupini, A., Mercati, F., Araniti, F., Miller, A. J., Sunseri, F., and Abenavoli, M. R. (2016). NAR2.1/*NRT*2.1 functional interaction with NO3(−) and H(+) fluxes in high-affinity nitrate transport in maize root regions. *Plant Physiol. Biochem.* 102, 107–114. doi: 10.1016/j.plaphy.2016.02.022

Malamy, J. E., and Ryan, K. S. (2001). Environmental regulation of lateral root initiation in *Arabidopsis*. *Plant Physiol.* 127, 899–909. doi: 10.1104/pp.010406

Medici, A., and Krouk, G. (2014). The primary nitrate response: a multifaceted signalling pathway. *J. Exp. Bot.* 65, 5567–5576. doi: 10.1093/jxb/eru245

Medici, A., Marshall-Colon, A., Ronzier, E., Szponarski, W., Wang, R., Gojon, A., et al. (2015). AtNIGT1/HRS1 integrates nitrate and phosphate signals at the *Arabidopsis* root tip. *Nat. Commun.* 6:6274. doi: 10.1038/ncomms7274

Miller, A. J., Fan, X., Orsel, M., Smith, S. J., and Wells, D. M. (2007). Nitrate transport and signalling. *J. Exp. Bot.* 58, 2297–2306. doi: 10.1093/jxb/erm066

Miller, A. J., and Smith, S. J. (2008). Cytosolic nitrate ion homeostasis: could it have a role in sensing nitrogen status? *Ann. Bot.* 101, 485–489. doi: 10.1093/aob/mcm313

Mounier, E., Pervent, M., Ljung, K., Gojon, A., and Nacry, P. (2014). Auxin-mediated nitrate signalling by NRT1.1 participates in the adaptive response of *Arabidopsis* root architecture to the spatial heterogeneity of nitrate availability. *Plant Cell Environ.* 37, 162–174. doi: 10.1111/pce.12143

Munos, S., Cazettes, C., Fizames, C., Gaymard, F., Tillard, P., Lepetit, M., et al. (2004). Transcript profiling in the chl1-5 mutant of *Arabidopsis* reveals a role of the nitrate transporter NRT1.1 in the regulation of another nitrate transporter, NRT2.1. *Plant Cell* 16, 2433–2447. doi: 10.1105/tpc.104.024380

Negi, J., Matsuda, O., Nagasawa, T., Oba, Y., Takahashi, H., Kawai-Yamada, M., et al. (2008). CO2 regulator SLAC1 and its homologues are essential for anion homeostasis in plant cells. *Nature* 452, 483–486. doi: 10.1038/nature06720

O'Brien, J. A., Vega, A., Bouguyon, E., Krouk, G., Gojon, A., Coruzzi, G., et al. (2016). Nitrate transport, sensing, and responses in plants. *Mol. Plant* 9, 837–856. doi: 10.1016/j.molp.2016.05.004

Orsel, M., Chopin, F., Leleu, O., Smith, S. J., Krapp, A., Daniel-Vedele, F., et al. (2006). Characterization of a two-component high-affinity nitrate uptake system in *Arabidopsis*. Physiology and protein-protein interaction. *Plant Physiol.* 142, 1304–1317.

Orsel, M., Krapp, A., and Daniel-Vedele, F. (2002). Analysis of the NRT2 nitrate transporter family in *Arabidopsis*. Structure and gene expression. *Plant Physiol.* 129, 886–896. doi: 10.1104/pp.005280

Parker, J. L., and Newstead, S. (2014). Molecular basis of nitrate uptake by the plant nitrate transporter NRT1.1. *Nature* 507, 68–72. doi: 10.1038/nature13116

Remans, T., Nacry, P., Pervent, M., Filleur, S., Diatloff, E., Mounier, E., et al. (2006a). The *Arabidopsis* NRT1.1 transporter participates in the signaling pathway triggering root colonization of nitrate-rich patches. *Proc. Natl. Acad. Sci. U.S.A.* 103, 19206–19211. doi: 10.1073/pnas.0605275103

Remans, T., Nacry, P., Pervent, M., Girin, T., Tillard, P., Lepetit, M., et al. (2006b). A central role for the nitrate transporter NRT2.1 in the integrated morphological and physiological responses of the root system to nitrogen limitation in *Arabidopsis*. *Plant Physiol.* 140, 909–921. doi: 10.1104/pp.105.075721

Ruffel, S., Gojon, A., and Lejay, L. (2014). Signal interactions in the regulation of root nitrate uptake. *J. Exp. Bot.* 65, 5509–5517. doi: 10.1093/jxb/eru321

Ruffel, S., Krouk, G., Ristova, D., Shasha, D., Birnbaum, K. D., and Coruzzi, G. M. (2011). Nitrogen economics of root foraging: transitive closure of the nitrate-cytokinin relay and distinct systemic signaling for N supply vs. *demand*. *Proc. Natl. Acad. Sci. U.S.A.* 108, 18524–18529. doi: 10.1073/pnas.1108684108

Ruffel, S., Poitout, A., Krouk, G., Coruzzi, G. M., and Lacombe, B. (2016). Long-distance nitrate signaling displays cytokinin dependent and independent branches. *J. Integr. Plant Biol.* 58, 226–229. doi: 10.1111/jipb.12453

Segonzac, C., Boyer, J. C., Ipotesi, E., Szponarski, W., Tillard, P., Touraine, B., et al. (2007). Nitrate efflux at the root plasma membrane: identification of an *Arabidopsis* excretion transporter. *Plant Cell* 19, 3760–3777. doi: 10.1105/tpc.106.048173

Sorgona, A., Lupini, A., Mercati, F., Di Dio, L., Sunseri, F., and Abenavoli, M. R. (2011). Nitrate uptake along the maize primary root: an integrated physiological and molecular approach. *Plant Cell Environ.* 34, 1127–1140. doi: 10.1111/j.1365-3040.2011.02311.x

Stitt, M. (1999). Nitrate regulation of metabolism and growth. *Curr. Opin. Plant Biol.* 2, 178–186. doi: 10.1016/S1369-5266(99)80033-8

Sun, J., Bankston, J. R., Payandeh, J., Hinds, T. R., Zagotta, W. N., and Zheng, N. (2014). Crystal structure of the plant dual-affinity nitrate transporter NRT1.1. *Nature* 507, 73–77. doi: 10.1038/nature13074

Taochy, C., Gaillard, I., Ipotesi, E., Oomen, R., Leonhardt, N., Zimmermann, S., et al. (2015). The *Arabidopsis* root stele transporter NPF2.3 contributes to nitrate translocation to shoots under salt stress. *Plant J.* 83, 466–479. doi: 10.1111/tpj.12901

Tong, Y., Zhou, J. J., Li, Z., and Miller, A. J. (2005). A two-component high-affinity nitrate uptake system in barley. *Plant J.* 41, 442–450. doi: 10.1111/j.1365-313X.2004.02310.x

Tsay, Y. F., Schroeder, J. I., Feldmann, K. A., and Crawford, N. M. (1993). The herbicide sensitivity gene CHL1 of *Arabidopsis* encodes a nitrate-inducible nitrate transporter. *Cell* 72, 705–713. doi: 10.1016/0092-8674(93)90399-B

Vidal, E. A., Moyano, T. C., Canales, J., and Gutierrez, R. A. (2014). Nitrogen control of developmental phase transitions in *Arabidopsis thaliana*. *J. Exp. Bot.* 65, 5611–5618. doi: 10.1093/jxb/eru326

Walch-Liu, P., Ivanov, I. I., Filleur, S., Gan, Y., Remans, T., and Forde, B. G. (2006a). Nitrogen regulation of root branching. *Ann. Bot.* 97, 875–881. doi: 10.1093/aob/mcj601

Walch-Liu, P., Liu, L. H., Remans, T., Tester, M., and Forde, B. G. (2006b). Evidence that L-glutamate can act as an exogenous signal to modulate root growth and branching in *Arabidopsis thaliana*. *Plant Cell Physiol.* 47, 1045–1057. doi: 10.1093/pcp/pcj075

Wang, R., Tischner, R., Gutierrez, R. A., Hoffman, M., Xing, X., Chen, M., et al. (2004). Genomic analysis of the nitrate response using a nitrate reductase-null mutant of *Arabidopsis*. *Plant Physiol.* 136, 2512–2522. doi: 10.1104/pp.104.044610

Wirth, J., Chopin, F., Santoni, V., Viennois, G., Tillard, P., Krapp, A., et al. (2007). Regulation of root nitrate uptake at the NRT2.1 protein level in *Arabidopsis thaliana*. *J. Biol. Chem.* 282, 23541–23552. doi: 10.1074/jbc.M700901200

Xu, N., Wang, R., Zhao, L., Zhang, C., Li, Z., Lei, Z., et al. (2016). The *Arabidopsis* NRG2 protein mediates nitrate signaling and interacts with and regulates key nitrate regulators. *Plant Cell* 28, 485–504. doi: 10.1105/tpc.15.00567

Yan, M., Fan, X., Feng, H., Miller, A. J., Shen, Q., and Xu, G. (2011). Rice OsNAR2.1 interacts with OsNRT2.1, OsNRT2.2 and OsNRT2.3a nitrate transporters to provide uptake over high and low concentration ranges. *Plant Cell Environ.* 34, 1360–1372. doi: 10.1111/j.1365-3040.2011.02335.x

Conflict of Interest Statement: The authors declare that the research was conducted in the absence of any commercial or financial relationships that could be construed as a potential conflict of interest.

frontiers in Plant Science

REVIEW
published: 29 August 2016
doi: 10.3389/fpls.2016.01296

Calcium-Mediated Abiotic Stress Signaling in Roots

*Katie A. Wilkins, Elsa Matthus, Stéphanie M. Swarbreck and Julia M. Davies**

Department of Plant Sciences, University of Cambridge, Cambridge, UK

Roots are subjected to a range of abiotic stresses as they forage for water and nutrients. Cytosolic free calcium is a common second messenger in the signaling of abiotic stress. In addition, roots take up calcium both as a nutrient and to stimulate exocytosis in growth. For calcium to fulfill its multiple roles must require strict spatio-temporal regulation of its uptake and efflux across the plasma membrane, its buffering in the cytosol and its sequestration or release from internal stores. This prompts the question of how specificity of signaling output can be achieved against the background of calcium's other uses. Threats to agriculture such as salinity, water availability and hypoxia are signaled through calcium. Nutrient deficiency is also emerging as a stress that is signaled through cytosolic free calcium, with progress in potassium, nitrate and boron deficiency signaling now being made. Heavy metals have the capacity to trigger or modulate root calcium signaling depending on their dose and their capacity to catalyze production of hydroxyl radicals. Mechanical stress and cold stress can both trigger an increase in root cytosolic free calcium, with the possibility of membrane deformation playing a part in initiating the calcium signal. This review addresses progress in identifying the calcium transporting proteins (particularly channels such as annexins and cyclic nucleotide-gated channels) that effect stress-induced calcium increases in roots and explores links to reactive oxygen species, lipid signaling, and the unfolded protein response.

Keywords: abiotic stress, calcium, heavy metal, hypoxia, nutrition, salinity, signaling

OPEN ACCESS

Edited by:
Janin Riedelsberger, University of Talca, Chile

Reviewed by:
Girdhar Kumar Pandey, University of Delhi, India
Joachim Krebs, Max Planck Institute for Biophysical Chemistry, Germany

****Correspondence:***
Julia M. Davies
jmd32@cam.ac.uk

Specialty section:
This article was submitted to Plant Physiology, a section of the journal Frontiers in Plant Science

Received: *24 May 2016*
Accepted: *12 August 2016*
Published: *29 August 2016*

Citation:
Wilkins KA, Matthus E, Swarbreck SM and Davies JM (2016) Calcium-Mediated Abiotic Stress Signaling in Roots. Front. Plant Sci. 7:1296. doi: 10.3389/fpls.2016.01296

INTRODUCTION

Plant roots are exposed to a variety of abiotic stresses as they navigate the soil, foraging for nutrients and water. Cytosolic free calcium ($[Ca^{2+}]_{cyt}$) is central to the response to these stresses, acting as a second messenger but also driving exocytosis (Carroll et al., 1998). Specificity of $[Ca^{2+}]_{cyt}$ signaling is determined by the amplitude and duration (and possible oscillation) of the $[Ca^{2+}]_{cyt}$ increase, often referred to as the "signature"' (McAinsh and Pittman, 2009), that is elicited by the stimulus. This signature would be driven by the opening of plasma membrane (PM) and endomembrane Ca^{2+}-permeable channels and terminated by the activity of Ca^{2+} efflux transporters in those membranes, plus Ca^{2+}-binding proteins, to restore the resting $[Ca^{2+}]_{cyt}$ of 100–200 nM. Use of organelle-targeted Ca^{2+} reporting proteins has shown that the Ca^{2+} content of the endoplasmic reticulum (ER) and Golgi increases after stress-induced transient increases in $[Ca^{2+}]_{cyt}$, strongly suggesting that Ca^{2+} is sequestered there to terminate the $[Ca^{2+}]_{cyt}$ signal (Ordenes et al., 2012; Bonza et al., 2013). Transport of Ca^{2+} into organelles is catalyzed by Ca^{2+}-ATPases. There are two distinct families: The Auto-inhibited Ca^{2+}-ATPases, ACA (that also

operate at the PM) and the ER Ca^{2+}-ATPases, ECA; reviewed by Bonza et al., 2016). The lower affinity CAX (Cation/H^+ Exchangers) appear to be restricted to endomembranes but also facilitate Ca^{2+} sequestration (Connorton et al., 2012). Changes in organelle free Ca^{2+} in roots could also play a part in signaling, most notably in the formation of symbioses and cell death (Stael et al., 2012; Zhao et al., 2013; Wagner et al., 2015). Decoding the $[Ca^{2+}]_{cyt}$ signature will be effected by specific Ca^{2+}-binding proteins. Calmodulins (CaMs) and Calmodulin-like proteins (CMLs) are encoded by multi-gene families in plants. They lack kinase domains, suggesting these proteins must target others with enzymatic activity. CaMs modulate transcription by binding to Calmodulin-binding Transcription Activators (CAMTAs) (Virdi et al., 2015). Other multi-gene families are also evident for Ca^{2+}-Dependent Protein Kinases (CPKs) and Calcineurin-B Like proteins (CBLs). The latter target CBL-Interacting Protein Kinases (CIPKs) to effect cellular responses (Thoday-Kennedy et al., 2015). Changes in $[Ca^{2+}]_{cyt}$ also have the potential to activate lipid signaling pathways. A somewhat forgotten aspect of Ca^{2+} signaling is the Ca^{2+} activation of members of the Phospholipase C and Phospholipase D families (Qin et al., 1997; Hunt et al., 2004; Dressler et al., 2014; Ruelland et al., 2015; Hou et al., 2016). Phospholipase C catalyses production of diacylglycerol and inositol trisphosphate ($InsP_3$) while Phospholipase D catalyses production of phosphatidic acid, thus $[Ca^{2+}]_{cyt}$ would have the capacity to trigger distinct lipid signals depending on the location and Ca^{2+}-sensitivity of the phospholipases. Targets of lipid signals have been reviewed recently by Hou et al. (2016).

The vast majority of $[Ca^{2+}]_{cyt}$ measurements are from *Arabidopsis thaliana* seedlings and guard cells, achieved using the luminescent Ca^{2+}-interacting aequorin protein. Far fewer studies have focused specifically on roots or utilized the greater sensitivity and spatial resolution of ratiometric fluorescent dyes. The genetically encoded YC3.6 Ca^{2+} reporter is now being used for both *Arabidopsis* and rice roots (Behera et al., 2015), holding much promise for the future. It is now clear that an identical stimulus can elicit markedly different root $[Ca^{2+}]_{cyt}$ signatures depending on genus. So far, rice root $[Ca^{2+}]_{cyt}$ signals have been found to be lower in amplitude but of longer duration than those of *Arabidopsis* (Behera et al., 2015).

Electrophysiological studies of root cell plasma membrane (PM) have advanced our understanding of the Ca^{2+} influx routes that could generate $[Ca^{2+}]_{cyt}$ signatures. There is a central role for PM voltage in $[Ca^{2+}]_{cyt}$ signaling, as individual stresses can hyperpolarize (render it more negative) or depolarize (render it less negative). Manipulating PM voltage elicits distinct $[Ca^{2+}]_{cyt}$ signatures and resultant transcriptional responses (Whalley et al., 2011; Whalley and Knight, 2013). Studies on root epidermal and root hair PM have shown that this membrane harbors channels that are activated by hyperpolarized voltage (Hyperpolarization-Activated Ca^{2+} Channels (HACCs); Véry and Davies, 2000; Demidchik et al., 2002, 2009; Ma et al., 2012), Depolarization-Activated Ca^{2+} Channels (DACCS); Demidchik et al., 2002; Miedema et al., 2008) and Voltage-Independent Ca^{2+} Channels (VICCs) (Demidchik et al., 2002). Thus changes in voltage would activate specific suites of channels to generate a signature. An additional tier of regulation of the PM Ca^{2+} influx routes is afforded by reactive oxygen species (ROS) that are produced during development and stress responses (**Figure 1**). This regulation depends on the specific ROS, its position, the cell type and the cell's developmental state. In *Arabidopsis* roots, sensitivity of PM Ca^{2+} channel activation by extracellular H_2O_2 decreases as epidermal cells mature but is still greater than that of the cortex (Demidchik et al., 2007). A similar picture emerges for extracellular hydroxyl radicals, which elicit greater PM Ca^{2+} influx currents in the epidermis and root hairs than the pericycle (Demidchik et al., 2003; Foreman et al., 2003). In epidermal PM of the elongation zone, extracellular hydroxyl radicals elicit different Ca^{2+} channel activity to extracellular H_2O_2 (Demidchik et al., 2003, 2007). Thus, ROS will play a significant part of generating cell-specific $[Ca^{2+}]_{cyt}$ signatures in response to stress.

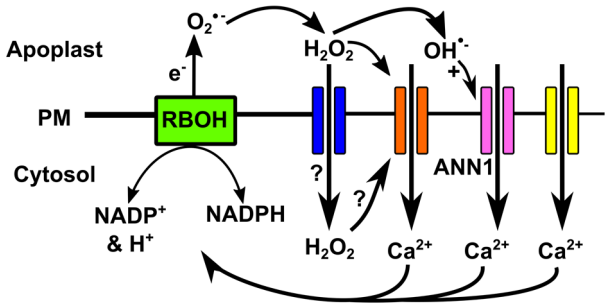

FIGURE 1 | Reactive oxygen species (ROS) regulation of PM Ca^{2+} channels in the *Arabidopsis* root elongation zone epidermis. NADPH oxidases (RBOH) generate extracellular superoxide anion that can undergo conversion to H_2O_2 and hydroxyl radicals ($OH^{\cdot}$) (Richards et al., 2015). H_2O_2 could activate HACC (orange) at the extracellular PM face or enter the cytosol through aquaporins (blue) to activate at the cytosolic face (directly or indirectly) (Demidchik et al., 2007). Extracellular hydroxyl radicals activate Annexin 1 (pink) (Demidchik et al., 2003; Foreman et al., 2003; Laohavisit et al., 2012). Ca^{2+} influx would depolarise the PM and if unopposed this could activate DACCs (yellow) (Demidchik et al., 2002). Increased $[Ca^{2+}]_{cyt}$ could further activate RBOH.

Stress-induced $[Ca^{2+}]_{cyt}$ elevation in roots remains poorly understood in terms of the genes encoding the PM or endo membrane Ca^{2+} channels involved. Plants have multi-gene families of Glutamate Receptor-Like channels (GLR; activated by a range of extracellular nitrogenous ligands) and Cyclic Nucleotide-Gated channels (CNGC; activated by intracellular cyclic nucleotides), with each gene encoding a potential subunit of a potentially tetrameric channel. Some members have been characterized as having Ca^{2+} channel forming ability (reviewed by Swarbreck et al., 2013 and Weiland et al., 2016). Membrane residency has yet to be determined for all proteins and while the majority tested are in the PM, in *Arabidopsis* GLR3.5 has been localized to both mitochondria and chloroplast, depending on its splicing variant (Teardo et al., 2015), CNGC19 to the vacuole (Yuen and Christopher, 2013) and CNGC20 potentially to both PM and vacuole (Fischer et al., 2013; Yuen and Christopher,

2013). Mechanosensitive Ca^{2+} channels of the PM have also been identified (Nakagawa et al., 2007; Hou et al., 2014; Yuan et al., 2014; Kamano et al., 2015), as has a vacuolar Ca^{2+} efflux channel TPC1 (Two Pore Channel1; Peiter et al., 2005). Root cells will express specific complements of these genes and their transcription can change under abiotic stress (Dinneny et al., 2008; Roy et al., 2008), with the implication that stress resets the $[Ca^{2+}]_{cyt}$ signaling system.

The threat of abiotic stress is global. Drought threatens plant productivity across continents, with water shortage not only imposing an osmotic challenge but also leading to soil hardness that roots must overcome. Changing weather patterns are bringing greater rainfalls to some areas (particularly Northern Europe) thus leading to the threat of hypoxic challenge from waterlogged soil (Shabala et al., 2014). Salinity stress arising from sodic soils is made worse by irrigation and counteracting nutritional deprivation by fertilizer application comes with an increasing economic and environmental cost. In this review, the effects of salinity, water availability (including soil hardness), nutritional deprivation, heavy metals and cold on root $[Ca^{2+}]_{cyt}$ will be addressed. The candidate channels for elevating $[Ca^{2+}]_{cyt}$ in roots will be introduced and the downstream consequences of the signal will be reviewed.

SALINITY STRESS FROM CHANNEL TO TRANSCRIPTION

The transporters for Na^+ influx into the root are not fully known but include the PM cyclic nucleotide-gated channels CNGC3 (Gobert et al., 2006) and CNGC10 (Guo et al., 2008; Jin et al., 2015) in *Arabidopsis*. Na^+ ingress is opposed by the Annexin1 protein and the AGB1 heterotrimeric G protein subunit in *Arabidopsis* roots (Laohavisit et al., 2013; Yu and Assmann, 2015). The mechanisms for sensing the increase in cytosolic Na^+ remain obscure (Maathuis, 2014; Shabala et al., 2015) however what *is* clear is that Na^+ entry depolarizes the root epidermal PM voltage (Maathuis, 2014). This is significant in that it implicates depolarization-activated and voltage-independent PM Ca^{2+}-permeable channels in generating the transient $[Ca^{2+}]_{cyt}$ increases observed in roots in response to NaCl (**Figure 2**). Both channels types are present in *Arabidopsis* root epidermal PM (Demidchik et al., 2002). However, involvement of hyperpolarization-activated PM Ca^{2+} channels should not be dismissed because increasing $[Ca^{2+}]_{cyt}$ shifts their activation voltage to more depolarized values (Véry and Davies, 2000; Demidchik et al., 2002) and they are implicated in the *Arabidopsis* root response to NaCl (Ma et al., 2012; Laohavisit et al., 2013).

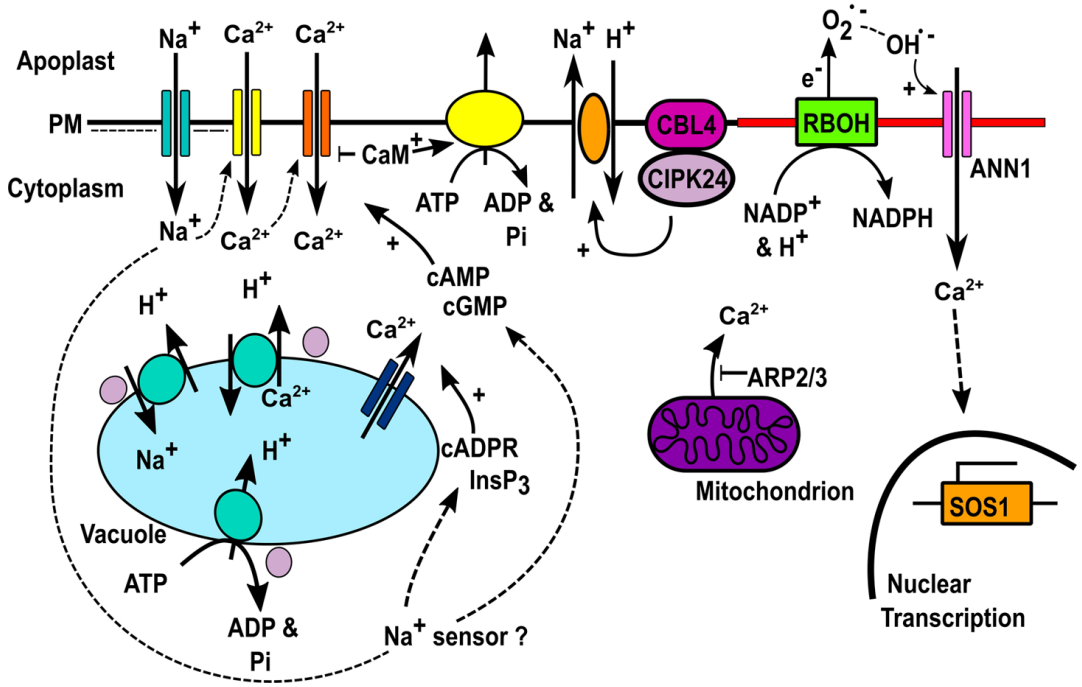

FIGURE 2 | Ca^{2+} transporters in salinity-stress signaling. Na^+ enters root epidermis and depolarises the PM, possibly activating DACCs (yellow) with the $[Ca^{2+}]_{cyt}$ increase also possibly activating HACCs (orange). Na^+ sensing results in cGMP/cAMP production that could activate CNGC HACCs (Shabala et al., 2015). $InsP_3$ and cADPR production causes Ca^{2+} release from stores by unknown channels (DeWald et al., 2001; Tracy et al., 2008; Zhang Y. et al., 2015; Zhang X. et al., 2015). ARP2/3 restricts mitochondrial Ca^{2+} efflux (Zhao et al., 2013). $[Ca^{2+}]_{cyt}$ activation of RBOH NADPH oxidase activity would promote extracellular hydroxyl radical formation and activation of Annexin1-mediated Ca^{2+} influx (pink) (Laohavisit et al., 2013). We hypothesize that these are held in a microdomain (red). This leads to *SOS1* transcription (Laohavisit et al., 2013). CaM activation would restrict CNGC-mediated Ca^{2+} influx and promote efflux by ACA Ca^{2+}-ATPase activation (Boursiac and Harper, 2007). $[Ca^{2+}]_{cyt}$ elevation activates CBL4 and CIPK24 (purple) leading to SOS1-mediated Na^+ extrusion (Liu et al., 2000). CIPK24 activates vacuolar V-ATPase to provide the driving force for NHX1 and CAX1 to sequester Na^+ and Ca^{2+} respectively, also activated by CIPK24 (Cheng et al., 2004; Batelli et al., 2007; Quintero et al., 2011).

Critically, hyperosmotic stress hyperpolarizes root epidermal PM voltage (Maathuis, 2014) and this would potentially be a basis for generating a component of the $[Ca^{2+}]_{cyt}$ signal specific to the hyperosmotic component of NaCl stress.

Ca^{2+} Influx across the PM

Application of NaCl can cause a heterogeneous increase in *Arabidopsis* and rice root $[Ca^{2+}]_{cyt}$ that depends on cell type, external $[Ca^{2+}]$, and the bathing medium's effect on PM voltage (Kiegle et al., 2000; Tracy et al., 2008; Laohavisit et al., 2013; Choi et al., 2014; Zhang Y. et al., 2015). Pericycle cells of *Arabidopsis* have a lower amplitude of $[Ca^{2+}]_{cyt}$ increase and a more variable recovery phase than the surrounding tissues (Kiegle et al., 2000), suggesting a cell-specific transporter complement. Block of NaCl-induced $[Ca^{2+}]_{cyt}$ increase by lanthanides implicates PM Ca^{2+} influx channels in the response of both *Arabidopsis* and rice roots (Tracy et al., 2008; Zhang Y. et al., 2015). The anti-apoptotic protein Bcl-2 mimics lanthanides in that its overexpression impairs the NaCl-induced $[Ca^{2+}]_{cyt}$ increase in rice roots (Kim et al., 2014). Clearly, the $[Ca^{2+}]_{cyt}$ increase could lead to cell death if it were great enough and Bcl-2 may interact directly with PM channels. The genetic identities of the PM Ca^{2+} influx channels initiating the NaCl-induced $[Ca^{2+}]_{cyt}$ increase remain unknown. It has been suggested that they may be Ca^{2+}-permeable CNGCs (Shabala et al., 2015) as salinity stress increased cytosolic cGMP in *Arabidopsis* seedlings within seconds (Donaldson et al., 2004). The source of cGMP may prove to be critical as only the $[Ca^{2+}]_{cyt}$ response to low NaCl (50 mM) was sensitive to inhibition of soluble guanylyl cyclase activity and the signal evoked by an equivalent osmotic stress was insensitive (Donaldson et al., 2004). It remains feasible that neither the ionic nor osmotic components of the $[Ca^{2+}]_{cyt}$ increase in response to high [NaCl] require cGMP. The osmotic component of NaCl stress could increase $[Ca^{2+}]_{cyt}$ in *Arabidopsis* roots through the PM mechanosensitive Ca^{2+}-permeable channel OSCA1 (Reduced Hyperosmolality-Induced $[Ca^{2+}]_I$ increase1). This channel mediates the $[Ca^{2+}]_{cyt}$ response to hyperosmotic stress (Yuan et al., 2014). Its discovery through a screen of aequorin-expressing mutants (Yuan et al., 2014) highlights the potential of this approach for identification of channels (and their families) involved in stress-induced $[Ca^{2+}]_{cyt}$ elevation.

The initial increase in $[Ca^{2+}]_{cyt}$ could be amplified by the production of ROS sourced ultimately by PM NADPH oxidases (encoded by *Respiratory Burst Oxidase Homolog* genes), with $[Ca^{2+}]_{cyt}$ activating these enzymes through their EF hands (**Figure 2**). In accordance with this, *Arabidopsis* root cortical cells lacking RBOHD and F have much lower PM hyperpolarization-activated Ca^{2+} activity in response to NaCl challenge than wild type (Ma et al., 2012). Mutant seedlings have an impaired $[Ca^{2+}]_{cyt}$ response. *Arabidopsis* RBOHD can be activated by CIPK26/CBL1/9 (Drerup et al., 2013) but a direct link to stress has not been shown. Extracellular hydroxyl radicals are likely to be the ROS involved in $[Ca^{2+}]_{cyt}$ elevation (Chung et al., 2008; Demidchik et al., 2010; Laohavisit et al., 2013; Richards et al., 2015). The extracellular superoxide anions produced by NADPH oxidases are readily converted to H_2O_2 and wall Fe/Cu act as Fenton catalysts to generate hydroxyl radicals (Richards et al., 2015). Their production by *Arabidopsis* roots is significantly increased under NaCl stress (Demidchik et al., 2010) and RBOHC is implicated as a driver for production (Chung et al., 2008). Extracellular hydroxyl radicals activate a PM Ca^{2+} influx in *Arabidopsis* root epidermis (Demidchik et al., 2003; Foreman et al., 2003) that has now been shown to be mediated by Annexin1 (Laohavisit et al., 2012).

Annexins are Ca^{2+}-binding proteins that can bind to or insert into membranes and are implicated in stress reactions (Laohavisit and Davies, 2011; Davies, 2014). Critically, when root epidermal protoplasts are challenged with NaCl, the resultant PM hyperpolarization-activated Ca^{2+} influx is lost in the *annexin1* loss of function mutant and the $[Ca^{2+}]_{cyt}$ signal is impaired (Laohavisit et al., 2013). Hydroxyl radicals are potent but short-lived so their effects must be close to the site of production (Richards et al., 2015). As NADPH oxidases can be held in lipid rafts it may be that hydroxyl radicals target co-resident channels. Finally, extracellular ATP levels of *Arabidopsis* roots increase in response to NaCl (Dark et al., 2011). Extracellular ATP activates root epidermal PM hyperpolarization-activated Ca^{2+} influx channels *via* RBOHC (Demidchik et al., 2009), suggesting the involvement of extracellular ROS in channel activation. Whether these channels involve Annexin1 remains to be determined but both the *annexin1* and *rbohc* loss of function mutants are impaired in $[Ca^{2+}]_{cyt}$-dependent transcriptional responses under NaCl stress (Chung et al., 2008; Laohavisit et al., 2013).

Calcium Release from Stores

Although not demonstrated in roots, the *Arabidopsis* Actin-Related Protein2/3 (ARP2/3) acts to limit NaCl-induced $[Ca^{2+}]_{cyt}$ increase, partly by limiting Ca^{2+} release from mitochondria. In the *arp2/3* mutant, the $[Ca^{2+}]_{cyt}$ increase is greater than wild type and so is the extent of mitochondrial-driven cell death (Zhao et al., 2013). Release of vacuolar Ca^{2+} to the cytosol in *Arabidopsis* roots may be by a Na^+/Ca^{2+} exchanger encoded by *AtNCL* (*Na*$^+$/*Ca*$^{2+}$ *Exchanger-Like*; Wang et al., 2012; Li P.H. et al., 2016). This tonoplast protein is thought to sequester Na^+ into the vacuole, coupled to the release of vacuolar Ca^{2+}. The concomitant increase in $[Ca^{2+}]_{cyt}$ could provide a negative feedback mechanism to limit further transport as Ca^{2+} binding to the exchanger's EF hands has been shown to be inhibitory *in vitro* (Li P.H. et al., 2016). Pharmacological approaches have also implicated internal stores in the NaCl-induced $[Ca^{2+}]_{cyt}$ increase in roots of both *Arabidopsis* and rice. Inhibitors of store release of Ca^{2+} by cADPR (cyclic ADP ribose) and inositol trisphosphate ($InsP_3$) suggested involvement of the $InsP_3$ pathway in *Arabidopsis* roots (Tracy et al., 2008). Moreover, salt and hyperosmotic stress in *Arabidopsis* roots caused an $InsP_3$ accumulation that correlated well with $[Ca^{2+}]_{cyt}$ increase (DeWald et al., 2001). The rice $[Ca^{2+}]_{cyt}$ signal was also sensitive to disruption of putative $InsP_3$-gated store release whilst impairment by thapsigargin implicated the ER as a participating store (Zhang Y. et al., 2015). However, using ER-targeted YC3.6, Bonza et al. (2013) detected an *increase* in *Arabidopsis* root ER $[Ca^{2+}]$ in response to salt stress. This followed the salt-induced $[Ca^{2+}]_{cyt}$ increase and critically, a drop in ER $[Ca^{2+}]$ prior to

the $[Ca^{2+}]_{cyt}$ increase was never observed. Therefore, with the level of resolution available, it appears that in this system the ER does not contribute to the $[Ca^{2+}]_{cyt}$ signal through store release but acts to return $[Ca^{2+}]_{cyt}$ to resting levels. Studies on *Populus euphratica* cultured cells identified the vacuole as the site of $InsP_3$ and cADPR action (Zhang X. et al., 2015). Certainly, Phospholipase C isoforms (as the source of $InsP_3$) are firmly implicated in salt stress responses (reviewed by Ruelland et al., 2015).

The genetic identities of the endomembrane Ca^{2+}-permeable channels implicated by pharmacological studies remain elusive. GLRs have recently been postulated to be involved in ER Ca^{2+} release (Weiland et al., 2016). The TPC1 vacuolar channel of *Arabidopsis* would be capable of releasing Ca^{2+} to the cytosol and recent analyses of its crystal structure has thrown greater light on its regulation by voltage and EF hands (Guo et al., 2016; Kintzer and Stroud, 2016). At current resolution afforded by YC3.6, its loss does not appear to have a significant impact on the magnitude of the *Arabidopsis* root $[Ca^{2+}]_{cyt}$ increase to salt, rather it slightly delays the response (Choi et al., 2014). However, TPC1 has a significant part to play in the propagation of a $[Ca^{2+}]_{cyt}$ wave that travels from the root apex through the cortical and endodermal tissue to signal the NaCl challenge to the shoots and elicit a transcriptional response. ROS also relay a salinity stress signal (reliant on RBOHD) in *Arabidopsis* leaves (Miller et al., 2009) but whether this occurs in roots and is involved in propagating the $[Ca^{2+}]_{cyt}$ wave remains to be tested.

Decoding, Na^+ Clearance, Transcription and the Unfolded Protein Response

Salinity-induced $[Ca^{2+}]_{cyt}$ elevation in roots drives a transcriptional response (Laohavisit et al., 2013; Zhang Y. et al., 2015) and post-translational modifications. The proteins sensing the NaCl-induced $[Ca^{2+}]_{cyt}$ increase are now being elucidated. For example, the *Arabidopsis* vacuolar Two Pore K^+ channel 1 (TPK1) would bind Ca^{2+}, and open to release K^+ to the cytosol to maintain a favorable Na^+/K^+ ratio (Latz et al., 2013). This could be further enhanced by phosphorylation by CPK3, which requires micromolar $[Ca^{2+}]$ for activity. CPK3 is present at both the PM and vacuole. It does not appear to contribute to a transcriptional response under salt stress but has a discrete set of protein targets to phosphorylate (Mehlmer et al., 2010). On prolonged salt stress, CPK29 expression is induced. This protein can phosphorylate TPK1 at sub-micromolar $[Ca^{2+}]$ and is envisaged to be part of longer-term K^+ homeostasis in adapted roots (Latz et al., 2013). Also in *Arabidopsis*, CPK27 (present at the root PM) acts to promote Na^+ efflux (Zhao et al., 2015). Intriguingly, CPK7 acts to limit water transport in *Arabidopsis* roots through lowering PIP1 aquaporin abundance (Li et al., 2015) but whether this is relevant to salinity or osmotic stress is not yet known. It can be readily envisaged that calmodulins will bind Ca^{2+} and as these are negative regulators of CNGC channels (Hua et al., 2003), would act to limit further Na^+ or Ca^{2+} influx at the PM. Further, CaM activation of ACAs (Autoinhibited Ca^{2+} ATPases) would restore $[Ca^{2+}]_{cyt}$ to pre-stimulus levels (Boursiac and Harper, 2007). Expression of ACAs varies with salt stress and, as shown by rice roots, can relate to salt tolerance (Yamada et al., 2014).

The Salt Overly Sensitive (SOS) pathway lies downstream of the root $[Ca^{2+}]_{cyt}$ increase. Delineated in *Arabidopsis* and now acknowledged as operating in crops and trees (Thoday-Kennedy et al., 2015), the SOS pathway leads to Na^+ efflux from the cytosol. Efflux across the PM is mediated by the SOS1 Na/H^+ antiporter. Salt stress induction of *SOS1* transcription lies downstream of Annexin1 in *Arabidopsis* roots and as SOS1 is required for adaptive adventitious root formation, the *annexin1* loss of function mutant accordingly produces fewer of these than wild type (Laohavisit et al., 2013). Additionally, the stability of salt stress-induced *SOS1* transcript requires RBOHC (Chung et al., 2008), further suggesting that this NADPH oxidase and Annexin1 may be in the same pathway. In *Arabidopsis* roots, increased $[Ca^{2+}]_{cyt}$ is sensed at the PM by CBL4 (SOS3) which can then react with the serine/threonine protein kinase CIPK24 (SOS2) (Liu et al., 2000). The resultant CBL/CIPK complex phosphorylates the PM Na/H^+ antiporter SOS1 at its auto-inhibitory C-terminus to achieve activation of Na^+ efflux (Quintero et al., 2011). Activation of SOS1 can also be achieved in *Arabidopsis* by Mitogen Activated Protein Kinase6 (MPK6) and loss of MPK6 function impairs root growth under salt stress (Yu et al., 2010). MPK6 is activated by a phosphatidic acid produced under salt stress by Phospholipase Dα1 (PLDα1) (Yu et al., 2010). As this PLD isoform contains a Ca^{2+}-binding C2 domain for its activation it is feasible that salt-induced $[Ca^{2+}]_{cyt}$ increase could activate SOS1 through this lipid-mediated pathway via MPK6 (Yu et al., 2015). This may help explain the importance of activation of PLDs in salt-stressed crop roots such as barley (Meringer et al., 2016). SOS2 may also promote activity of the vacuolar V-type H^+-ATPase to provide the driving force for Na^+ sequestration (Batelli et al., 2007). The NHX1 Na^+-H^+ exchanger may also be regulated by SOS2 to aid vacuolar Na^+ sequestration (Qiu et al., 2004) and SOS2 activation of the vacuolar CAX1 Ca^{2+}/H^+ antiporter would help terminate a $[Ca^{2+}]_{cyt}$ signature through Ca^{2+} sequestration (Cheng et al., 2004). Other CAX are involved in root tolerance of salt stress and the pathways to their induction and regulation now need to be identified (Yamada et al., 2014).

Salt exposure puts the plant's ER under stress, leading to an accumulation of unfolded or misfolded proteins that could lead to cell death (Liu et al., 2007, 2011). Such ER stress triggers upregulation of a suite of responses termed the "Unfolded Protein Response" (UPR), in which folding capacity is upregulated (including by Ca^{2+}-regulated chaperones), translation is curtailed and the ER-associated degradation pathway acts to lower the aberrant protein load (Deng et al., 2013; Ruberti et al., 2015; Hossain et al., 2016; Wan and Jiang, 2016). Expression of the ER Ca^{2+}-binding chaperones Calnexin and Calreticulin has been shown to upregulated in the *Arabidopsis* UPR (Christensen et al., 2008; Liu et al., 2011) and it would now be interesting to test whether these are involved in regulating levels of Ca^{2+} in the ER under stress. However, expression of rice's only calnexin gene is decreased under salt stress (Sarwat and Naqvi, 2013). It is not yet clear whether the salt-induced $[Ca^{2+}]_{cyt}$ signal in roots (or other parts

of the plant) helps initiate or regulate the UPR. It is feasible that the salt-induced $[Ca^{2+}]_{cyt}$ increase activates the root PM Phospholipase C2 (Hunt et al., 2004) because the *Arabidopsis* loss of function mutant is hypersensitive to tunicamycin, which can induce the UPR (Kanehara et al., 2015). With IP_3 as the product of Phospholipase C activity, this would implicate IP_3-mediated release of Ca^{2+} from stores. Indeed, for *Arabidopsis* seedlings the application of 2-aminoethoxydiphenyl borate as an inhibitor of IP_3-mediated Ca^{2+} release prevented salt stress-induced transcription of *BIP1/2* (encoding an ER chaperone) as a diagnostic of a UPR response (Liu et al., 2011). Intriguingly, application of La^{3+} as a blocker of PM Ca^{2+} influx prevented the upregulation of UPR gene expression which was produced by application of spermine to *Arabidopsis* seedlings (Sagor et al., 2015). Exogenous spermine (as with salt) can depolarise the root epidermal PM (Pottosin et al., 2014) and can also attenuate hydroxyl radical-induced cation fluxes at root epidermal PM (Zepeda-Jazo et al., 2011). Whether spermine and salt stress share a common pathway to the UPR response merits further investigation.

WATER AVAILABILITY IS SIGNALED THROUGH $[Ca^{2+}]_{cyt}$

The hyperosmotic challenge in $[Ca^{2+}]_{cyt}$ determinations is acute and does not mimic the chronic, progressive drought conditions that roots may face. Nevertheless, such studies have proved fruitful. As described above, the *Arabidopsis* OSCA1 PM Ca^{2+} influx channel drives the root's initial hyperosmotic stress $[Ca^{2+}]_{cyt}$ signal (Yuan et al., 2014). In an elegant study, heterologous expression of *Arabidopsis* genes in Chinese Hamster Ovary (CHO) cells containing the Fura-2 Ca^{2+}-reporting dye lead to the identification of Calcium-permeable Stress-gated cation Channel1 (CSC1; Hou et al., 2014), a close relative of OSCA1. CSC1 has been characterized in CHO cells as a PM Ca^{2+}-permeable channel that is activated by hyperosmotic stress. It is resident in plant PM (Hou et al., 2014) and is expressed in roots but to date an *in planta* role remains unreported. Targeting aequorin to the cytosolic face of the *Arabidopsis* vacuolar membrane has revealed the capacity of the vacuole to release Ca^{2+} in response to acute hyperosmotic stress, with pharmacological intervention suggesting an involvement of $InsP_3$ (Knight et al., 1997). As with salt stress, hyperosmotic stress-induced $[Ca^{2+}]_{cyt}$ increase could activate Phospholipases and initiate lipid signaling. Osmotic stress activates PLD in barley roots (Meringer et al., 2016). Although not tested directly, phosphatidic acid downstream of PLD could be involved in the activation of two sucrose non-fermenting-1 related protein kinase 2 proteins (SnRK2.4 and 2.10) in *Arabidopsis* roots under hyperosmotic stress. These SnRK2s are also activated under salt stress and relocate from the root epidermal cytosol to the PM; loss of function impairs root growth (McLoughlin et al., 2012). Work using Golgi-targeted aequorin in *Arabidopsis* seedlings has shown that an increase in Golgi $[Ca^{2+}]$ follows the $[Ca^{2+}]_{cyt}$ increase induced by hyperosmotic stress, suggesting that this organelle helps terminate the $[Ca^{2+}]_{cyt}$ signal (Ordenes et al., 2012).

The ABA produced under drought stress inhibits primary root growth and $[Ca^{2+}]_{cyt}$ is likely to play a role in the signaling pathway as exogenous ABA elevates root $[Ca^{2+}]_{cyt}$, which in *Arabidopsis* roots is controlled by the PM Proline-rich Extensin-like Receptor Kinase4 (PERK4) (Bai et al., 2009). PERK4's extracellular domain is wall associated and its intracellular domain has kinase activity. PM HACCs lie downstream of ABA and PERK4. The *perk4* mutant is not only impaired in ABA-induced HACC activity and $[Ca^{2+}]_{cyt}$ activation but also in ABA inhibition of primary root elongation (Bai et al., 2009). This implies that $[Ca^{2+}]_{cyt}$ elevation acts to arrest growth. RBOHD/F may lie downstream of PERK4 and upstream of HACCs in the root ABA pathway if the HACCs were ROS-activated. The *rbohd/f* mutant is impaired in both ABA-induced HACC activation and $[Ca^{2+}]_{cyt}$ elevation (Jiao et al., 2013). Another possibility is that CNGCs are involved as ABA can increase cGMP levels (Isner et al., 2012.). GLRs are firmly implicated in the drought response; overexpression of rice GLR1 and GLR2 enhances drought tolerance of both rice and *Arabidopsis* (Lu et al., 2014). The $[Ca^{2+}]_{cyt}$ increase is likely to lead to a transcriptional response as Ca^{2+}-sensing proteins are activated. ABA increases abundance and activity of *Arabidopsis* CPK4 and CPK11 leading to phosphorylation of the ABA-responsive transcription factors ABF1 and ABF4 and induction of drought stress genes (Zhu et al., 2007). Drought leads to CAMTA1 activity and the regulation of discrete gene sets including those for drought recovery (Pandey et al., 2013). In maize roots, drought stress triggers activity of CIPK8 (which interacts with CBL1, 4, and 9) and likely leads to adaptive transcription (Tai et al., 2016).

Hypoosmotic stress also elevates $[Ca^{2+}]_{cyt}$ and is relevant to waterlogged soils. In *Arabidopsis*, root PM harbors two mechanosensitive Ca^{2+}-permeable channels, MCA1 and MCA2 (Mid1-Complementing Activity; Kamano et al., 2015). MCA1 responds to hypoosmotic stress to elevate $[Ca^{2+}]_{cyt}$ (Nakagawa et al., 2007). Rice only harbors an MCA1 in the PM. It is present in the root and mediates hypoosmotic shock-induced $[Ca^{2+}]_{cyt}$ expression in cultured cells, probably lying upstream of NADPH oxidase activity (Kurusu et al., 2012). Abundant water not only exposes roots to potential hypoosmotic stress but also risks limiting their oxygen supply, the consequences of which are reviewed in the following section.

MECHANISTIC BASIS OF $[CA^{2+}]_{cyt}$ RESPONSE TO O_2 DEFICIENCY REMAINS POORLY UNDERSTOOD

Oxygen deficiency (hypoxia) or absence (anoxia) causes transient increases in root $[Ca^{2+}]_{cyt}$ but the signature is organ- and species-dependent (reviewed by Shabala et al., 2014). For example, when challenged by anoxia, root protoplasts from hypoxia-tolerant rice display a greater $[Ca^{2+}]_{cyt}$ signature than hypoxia-intolerant wheat root protoplasts (Yemelyanov et al., 2011). The location of the Ca^{2+} influx also varies; use of pharmacological blockers showed that the rice signature was generated by both PM influx and store release whilst wheat

appeared to rely solely on stores (Yemelyanov et al., 2011). The types of Ca^{2+} channels mediating the $[Ca^{2+}]_{cyt}$ increase have yet to be identified in any species. However, those activated by PM voltage depolarization are implicated. As O_2 deficiency lessens ATP production, activity of the PM H^+-ATPase can be compromised thus resulting in a less negative (depolarized) PM voltage as H^+ efflux is curtailed. The extent and duration of membrane depolarization varies with sensitivity to O_2 deprivation and cell type. Values of −70 to −80 mV have been reported for O_2-deprived barley root cells (Zeng et al., 2014) and theoretically these would be sufficient to activate PM depolarization-activated Ca^{2+} influx channels (Miedema et al., 2008) to contribute to an hypoxia/anoxia $[Ca^{2+}]_{cyt}$ signature. Downstream of the $[Ca^{2+}]_{cyt}$ signature, it is likely that CaM and ROPs (Rho GTPase) are activated (reviewed by Shabala et al., 2014). In *Arabidopsis* roots, hypoxia causes rapid upregulation of *CML38* expression and this protein appears to require Ca^{2+} to associate with the cytosolic stress granules that form and store messenger RNA ribonucleoproteins (Lokdarshi et al., 2016).

RBOH activity is firmly implicated in the response to low O_2. In *Arabidopsis*, *RBOHD* expression is induced by hypoxia and is required for transcription of hypoxia-induced genes (Yang and Hong, 2015). Hypoxia also induces ethylene production and in wheat roots this causes RBOH induction (Yamauchi et al., 2014). A further level of regulation has been found in *Arabidopsis*; the Hypoxia Responsive Universal Stress Protein 1 (HRU1) interacts with GTP-bound ROP2 and RBOHD (Gonzali et al., 2015). HRU1 is one of 44 putative universal stress proteins in *Arabidopsis*. It exists as a cytosolic dimer but anoxia promotes monomer formation and increased association with the PM. There it is thought to be part of a mobile complex with ROP2 and AtRBOHD leading to activation of that NADPH oxidase (Gonzali et al., 2015). Although RBOH activity has been linked to PM Ca^{2+} channel activation in several abiotic stress scenarios, hypoxia and anoxia have yet to be tested.

Ethylene has been shown to activate PM Ca^{2+}-permeable channels (with a weak voltage dependence) in tobacco suspension cells (Zhao et al., 2007) and it remains a possibility that these may play a part in the root hypoxia $[Ca^{2+}]_{cyt}$ signal with RBOH as an intermediary. Oxygen deprivation (and also sulfur and phosphate, Pi, deprivation) triggers programmed cell death (PCD) in mid-cortical cells for aerenchyma formation (Fagerstedt, 2010). This PCD is stimulated by ethylene and ROS and involves Ca^{2+} (Xu et al., 2013; Petrov et al., 2015). In wheat roots, anoxia causes mitochondria to release their Ca^{2+} and high $[Ca^{2+}]_{cyt}$ causes cytochrome c release (Virolainen et al., 2002). The abnormal mitochondrial ultrastructure in *Arabidopsis* caused by hypoxia is partially phenocopied by loss of GLR3.5 from the inner mitochondrial membrane, suggesting that this channel must be deactivated during PCD (Teardo et al., 2015). Further channels must now be identified to understand the hypoxic/anoxic response. Recent work on *Arabidopsis* roots has shown distinct, cell-specific levels of $[Ca^{2+}]_{cyt}$ after 24 h of hypoxia and highlighted the importance of CAX11 in controlling meristem $[Ca^{2+}]_{cyt}$ (Wang et al., 2016). Loss of CAX4 function resulted in lower tolerance of hypoxia thus further demonstrating the importance of Ca^{2+} sequestration in this stress response (Wang et al., 2016).

CA^{2+} SIGNALING IN NUTRIENT DEPRIVATION IS AN EMERGING AREA

Investigating $[Ca^{2+}]_{cyt}$ elevation in response to nutrient deprivation or resupply is technically challenging, particularly if using aequorin. Nevertheless it is now clear that nutrient levels can induce $[Ca^{2+}]_{cyt}$ changes and that downstream Ca^{2+} sensors regulate appropriate responses. The nutritional status of the root will have a part to play in determining the $[Ca^{2+}]_{cyt}$ signatures, particularly of the endodermis as the extent of suberization is set by nutrition (Barberon et al., 2016) and suberin lamellae determine endodermal $[Ca^{2+}]_{cyt}$ responses (Moore et al., 2002). To date, potassium, nitrate and boron have been studied.

Potassium

Plants must maintain cytosolic K^+ at around 80 mM for optimal growth even though soil concentration may be sub-millimolar and they deploy a multigene family of K^+ transporters in homeostatic control (Shabala and Pottosin, 2014). As extracellular K^+ decreases, the root epidermal PM hyperpolarizes and $[Ca^{2+}]_{cyt}$ increases (Demidchik et al., 2002). This increase can be abolished by gadolinium, implicating PM Ca^{2+} influx. The genetic identities of the PM Ca^{2+}-permeable channels that would effect the $[Ca^{2+}]_{cyt}$ increase remain unknown. The hyperpolarised PM correlates with induction of *HAK5* expression in tomato root (Nieves-Cordones et al., 2008). *HAK5* encodes the PM High Affinity K^+ transporter that facilitates K^+ uptake from low external concentrations that are thermodynamically unfavorable for channel-mediated influx. In *Arabidopsis* roots, low K^+-induction of *HAK5* expression (and other K^+-deprivation genes) has been shown to depend on RBOHC activity and ROS (Shin and Schachtman, 2004). At present it is unclear whether the hyperpolarization of the PM directly activates RBOHC (which as an electron exporter may be voltage-dependent) or whether ROS-activated PM Ca^{2+} channels are involved in the K^+-deprivation $[Ca^{2+}]_{cyt}$ signal. HAK5 activity in *Arabidopsis* roots is regulated by CIPK23-mediated phosphorylation, downstream of CBL1, CBL8, CBL9, and CBL10 (Ragel et al., 2015). The extent to which the transcriptional response to low K^+ availability is governed by $[Ca^{2+}]_{cyt}$ is unclear but deficiency does result in upregulation of transcripts of Ca^{2+} signaling proteins (CaM, CBL, CIPK) in *Arabidopsis* seedlings (Armengaud et al., 2004) and sugarcane roots (Zeng et al., 2015). At higher external $[K^+]$, the AKT1 channel (Arabidopsis K^+ Transporter1) facilitates uptake and its activity is promoted by CIPK23-mediated phosphorylation, downstream of CBL1 and CBL9 (Li et al., 2006; Cheong et al., 2007). This regulation is recapitulated in rice roots where CIPK23/CBL1 activate AKT1 (Li et al., 2014).

Nitrate

Nitrate is the most important form of nitrogen for agriculture and deprivation triggers significant transcriptional and

developmental responses. The effect of nitrate withdrawal on $[Ca^{2+}]_{cyt}$ has yet to be reported but recently it was shown that nitrate-starved *Arabidopsis* roots responded to nitrate resupply with a rapid, monophasic transient increase in $[Ca^{2+}]_{cyt}$ that was sensitive to lanthanides and phospholipase C (PLC) inhibition (Riveras et al., 2015). Lanthanum also blocked nitrate-induced $InsP_3$ production, suggesting that Ca^{2+} influx across the PM activated a PLC. The $[Ca^{2+}]_{cyt}$ and $InsP_3$ increases were entirely dependent on the PM nitrate influx transporter NRT1.1 (Nitrate Transporter1.1; Riveras et al., 2015). By using the *nrt1.1* mutant and pharmacological blockers, nitrate-induced gene transcription was also found to lie downstream of NRT1.1, and $[Ca^{2+}]_{cyt}$ elevation from PM influx and $InsP_3$-gated store release. Calcium is also key to the regulation of nitrate uptake capacity as CIPK23, which is activated by CBL9 and CBL1, and dephosphorylated by ABI2 (a member of the PP2C protein phosphatase family; Léran et al., 2015,), phosphorylates NRT1.1 under low nitrate condition, thus converting it from a low to high affinity transporter (Ho et al., 2009). By contrast CIPK8 positively regulates the low-affinity phase of the nitrate primary response which includes transcriptional regulation, but its regulation of primary root elongation is concentration independent in *Arabidopsis* (Hu et al., 2009). CBL7, which is upregulated under nitrate deprivation, positively regulates the nitrate-dependent induction of *NTR2.4* and *NTR2.5* gene expression (Ma Q. et al., 2015). Given the lack of a $[Ca^{2+}]_{cyt}$ reporter line available in crops up until recently for rice, little is known about nitrate deficiency-induced $[Ca^{2+}]_{cyt}$ signaling but CaM protein abundance of wheat roots declines under nitrate deficiency, suggesting a remodeling of signaling systems (Jiang et al., 2015).

Boron

Boron deficiency is widespread worldwide and particularly prevalent in China (Shorrocks, 1997). As B plays a dominant role in co-ordinating cell wall structure (Kobayashi et al., 1996), changes in cell wall stability are likely to influence the signal relayed into the cell upon B deprivation and indeed a rapid change in cell wall modulus has been observed (Goldbach et al., 2001). Early work in *Vicia faba* showed a release of membrane-bound Ca^{2+} into the apoplast (Mühling et al., 1998), raising the possibility of Ca^{2+} signaling during the early stages of B deficiency. Increased levels of both $[Ca^{2+}]_{cyt}$ and ROS have been suggested to lead to the increased root hair growth known to occur under B deprivation (González-Fontes et al., 2016). In cultured tobacco cells, transcriptional changes in response to short-term B deprivation (1 h) were abolished when withdrawing Ca^{2+} from the growth medium or upon treatment with the Ca^{2+} channel blocker lanthanum, thus implicating PM Ca^{2+} influx channels in generating a $[Ca^{2+}]_{cyt}$ signal (Koshiba et al., 2010). However, a transient $[Ca^{2+}]_{cyt}$ signal in direct response to B withdrawal has yet to be reported. Rather, work has focused on the possible remodeling of Ca^{2+} transport and signaling as a consequence of B deprivation.

Challenging cultured tobacco cells with Ca^{2+} resulted in a higher amplitude of $[Ca^{2+}]_{cyt}$ transient in B-deprived cells (1 h deprivation) than those grown under replete conditions (Koshiba et al., 2010). This suggests that B deprivation rapidly "resets" the PM's Ca^{2+} transport systems to generate altered $[Ca^{2+}]_{cyt}$ responses. The $[Ca^{2+}]_{cyt}$ response of B-deprived cells was sensitive to lanthanum and diphenyleneiodonium, pointing to the involvement of PM Ca^{2+} channels and NADPH oxidases respectively (Koshiba et al., 2010). *Arabidopsis* roots expressing the YC3.6 $[Ca^{2+}]_{cyt}$ reporter exhibited higher levels of $[Ca^{2+}]_{cyt}$ at the apex than controls after 6 and 24 h of B deprivation (Quiles-Pando et al., 2013). This time course of B deprivation also resulted in significant upregulation of *CNGC19* (encoding a vacuolar channel), four genes of the ACA family of P_{IIB}-type Ca^{2+}-ATPases (*ACA1,10,12,13*) and *CAX3* encoding a vacuolar cation-H^+ antiporter (Quiles-Pando et al., 2013). This suite of transporters could effect Ca^{2+} efflux from the vacuole (CNGC19) to increase $[Ca^{2+}]_{cyt}$ with clearance to the apoplast by ACA10-13 and sequestration to the vacuole by CAX3. How they are regulated remains to be determined, as does the involvement of the structurally compromised wall and the consequence of this higher level of apical $[Ca^{2+}]_{cyt}$. The area of higher $[Ca^{2+}]_{cyt}$ reported appears to correspond with the zone of inhibition of primary root elongation and the induction of cell death (Oiwa et al., 2013; Camacho-Cristobal et al., 2015). Once again, ethylene production appears to be upstream of NADPH oxidase-driven ROS production in growth arrest and death (Oiwa et al., 2013; Camacho-Cristobal et al., 2015).

Eight *CML* genes were also significantly upregulated after a day's B deprivation of *Arabidopsis roots* (*CML11,12,23,24, 30.37,45.47*), as were three *CPK* genes (*CPK1,28,29*) all suggesting a distinct change in intracellular Ca^{2+} signaling (Quiles-Pando et al., 2013). This B deprivation also caused upregulation of *WRKY* transcription factors (TF) (*WRKY38,40,46*), two three *MYB* family TF (*MYB14,15,78*) and downregulation of two *BZIP* family TFs (*bZIP34,61*) (González-Fontes et al., 2016). B deprivation has also been found to promote the senescence-associated *WRKY6* TF in the root tip (Kasajima et al., 2010). It has been suggested that the *CML*s and *CPK*s upregulated by B deprivation are part of the chain of events leading to TF activation in the nucleus (González-Fontes et al., 2016) and this now requires direct testing. CIPK8 also positively regulates nitrate induced up-regulation of BOR1, a gene encoding a boron transporter responsible for xylem loading (Hu et al., 2009), suggesting that root signaling results in preservation of shoot B supply.

HEAVY METAL STRESS HAS THE CAPACITY TO DISTORT Ca^{2+} SIGNALING

At the opposite end of nutritional deprivation is heavy metal stress. Industrial activity, mining and modern agricultural practices can lead to soil contamination by heavy metals (defined here as 7 g/cm^3 and above). Although some of these metals (such as Zn, Cu) are required as micronutrients they can be damaging in excess whilst others (such as Cd) have no physiological role and can be deleterious even at low concentrations, often impairing mineral nutrition. The consequences of heavy metal

exposure have been reviewed recently by Singh et al. (2016) and these authors explore signaling pathways (although not explicitly addressing Ca^{2+}), intersects with hormonal responses and detoxification.

Cadmium

Cadmium is a particular threat to Ca^{2+}-based processes because of its similar size. A recent review by Chmielowska-Bak et al. (2014) summarized the effects of Cd on ROS accumulation, NO accumulation, MAP kinase activation and downstream responses in a wide range of plant systems and, importantly, did this as a function of Cd exposure. With regards to Ca^{2+} a key question is whether Cd (as a Ca^{2+} "substitute") generates a signal in its own right or whether its impairment of Ca^{2+} homeostasis will be, in effect, the signal. Certainly Cd depolarises the rice root epidermal PM, which would impair Ca^{2+} influx and results in inhibition of root elongation (Li et al., 2012). Cd can permeate guard cell PM Ca^{2+} channels (Perfus-Barbeoch et al., 2002) and may compete with Ca^{2+} for entry into rice root hairs through PM HACC, thus limiting Ca^{2+} influx (Li et al., 2012). Competitive effects appear likely given the ability of exogenous Ca^{2+} addition to alleviate Cd inhibition of root growth of both terrestrial and aquatic plants, implying competition for uptake (Zhang et al., 2012; Rodriguez-Hernandez et al., 2015). Additionally, competitive inhibition by Cd of Ca^{2+} uptake through the wheat LCT1 transporter expressed in yeast has been observed (Clemens et al., 1998). Root hair growth in *Arabidopsis* is inhibited by Cd; it inhibits Ca^{2+} influx and so dissipates the apical $[Ca^{2+}]_{cyt}$ gradient needed for growth (Fan et al., 2011). This could reflect block of root hair Ca^{2+} influx channels or Cd outcompeting Ca^{2+} for that influx pathway. However, Yeh et al. (2007) observed an increase in rice root $[Ca^{2+}]_{cyt}$ following 15 min of Cd exposure, with a more tolerant variety sustaining a greater increase than a sensitive variety. In roots of the aquatic plant *Typha latifolia*, Cd exposure increases transcription of *TPC1* which suggests that vacuoles might release Ca^{2+} to the cytosol (Rodriguez-Hernandez et al., 2015). Inhibitor treatments indicated involvement of NADPH oxidases, hydroxyl radicals and CIPK upstream of a MAP kinase induction that linked to tolerance (Yeh et al., 2007). Cd stimulates expression and activity of NADPH oxidases in cucumber roots but it is not known if these responses are Ca^{2+}-dependent (Jakubowska et al., 2015). It is worth noting that it is not only an increase in $[Ca^{2+}]_{cyt}$ that could stimulate NADPH oxidase activity but that also the restriction of Ca^{2+} entry to the cytosol could cause stimulation (Mortimer et al., 2008). It seems likely that in *Arabidopsis* roots it would be CAXs predominating in terminating a Cd-induced increase in $[Ca^{2+}]_{cyt}$. CAX4 mediates Cd and Ca^{2+} transport into *Arabidopsis thaliana* vacuoles and is needed for correct growth under Cd stress (Mei et al., 2009). *CAX1* expression is higher in roots of the Cd-tolerant *A. halleri* compared to the sensitive *A. thaliana* (Baliardini et al., 2015).

A key point for future studies is the intersect between Cd and hormones in relation to $[Ca^{2+}]_{cyt}$. Exogenous Ca^{2+} can ameliorate Cd's inhibition of *Arabidopsis* root growth by counteracting effects of NO on auxin homeostasis (Hu et al., 2013; Li P. et al., 2016; Yuan and Huang, 2016). Cd also interferes with auxin homeostasis in barley roots (Zelinova et al., 2015). Auxin itself can increase *Arabidopsis* root $[Ca^{2+}]_{cyt}$ and this increase is mediated by CNGC14 at the PM, downstream of an unidentified auxin receptor (Shih et al., 2015). This begs the question of whether CNGC14 is an entry route for Cd and the pathway to disrupted auxin homeostasis. Additionally, Cd has been described as a "metallohormone" in that it triggers expression of brassinosteroid-regulated genes in *Arabidopsis* roots (Villiers et al., 2012). Brassinosteroids are themselves capable of transiently elevating $[Ca^{2+}]_{cyt}$ in *Arabidopsis* roots (through PM Ca^{2+} influx) and activate a possible DACC in wheat root PM (Straltsova et al., 2015). Again this raises the question of channel identity to help elucidate the relationship between Cd and brassinosteroid signaling and combat the effects of this potent soil contaminant.

Copper, Gadolinium and Lead

In contrast to Cd, transition heavy metals could be capable of generating ROS directly and so perturb $[Ca^{2+}]_{cyt}$ signaling. Transition metals can catalyze production of hydroxyl radicals from superoxide anion and hydrogen peroxide through the Haber-Weiss reaction, with Cu^{+} and Fe^{2+} catalyzing hydroxyl radical production from hydrogen peroxide through the Fenton reaction (Richards et al., 2015). Unless levels of these catalytic metals are tightly controlled, production of hydroxyl radicals (the most potent of the ROS) could inflict significant oxidative damage. Taking Cu as the exemplar, it plays a positive role in hydroxyl radical-activated cell wall loosening for root elongation (Fry et al., 2002) and this could be coupled in *Arabidopsis* roots to hydroxyl radical-activation of PM Annexin1-mediated Ca^{2+} influx to stimulate exocytosis and growth (Foreman et al., 2003; Laohavisit et al., 2012). This model proposes regulation by extracellular hydroxyl radicals while Rodrigo-Moreno et al. (2013) have proposed that Cu^{+} binding at the intracellular face of the PM in *Arabidopsis* root tips catalyzes hydroxyl radical production to regulate ion flux. This would allow coupling of Cu transport into the root to regulation of PM Ca^{2+} influx channels. Certainly, low levels of Cu can promote elongation of *Arabidopsis* primary root and this effect is diminished by blocking PM Ca^{2+} influx channels (Demidchik et al., 2003). The effects of extracellular Cu on PM Ca^{2+} channels and therefore on $[Ca^{2+}]_{cyt}$ signaling are likely to be complex. Electrophysiological analysis of *Arabidopsis* root epidermal PM has shown that Cu not only activates Ca^{2+} channels through ROS production (Annexin 1; Laohavisit et al., 2012) but also blocks channels, the molecular identity of which remains unknown (Demidchik et al., 2003).

Catalytic production of ROS by Cu is not the only route to modulating $[Ca^{2+}]_{cyt}$. Longer-term exposure to Cu can stimulate exocytosis-mediated ROS production. Lin et al. (2013) found that inhibiting vesicle traffic with brefeldin also inhibited Cu-stimulated ROS production in rice roots. Whether this involved NADPH oxidase or other ROS generators remains to be determined. Rice root $[Ca^{2+}]_{cyt}$ increases in response to Cu addition and could link to NADPH oxidases and CIPK activity leading to MAP kinase activation (Yeh et al., 2007). It triggers oxidative stress in *Populus* roots that leads to regulation of

CaM genes, implicating perturbation of $[Ca^{2+}]_{cyt}$ (Guerra et al., 2009).

In common with Cd, excess Cu also alters auxin homeostasis in roots and interferes with NO signaling (Lequeux et al., 2010; Kolbert et al., 2012). In excess, Cu stunts *Arabidopsis* root and root hair elongation and can inhibit lateral root outgrowth (Kolbert et al., 2012). Accumulation of lignin has been observed in both *Arabidopsis* and rice roots (Lequeux et al., 2010; Liu et al., 2015) and in the former accumulation is associated with the endodermis. It would now be interesting to ascertain whether such wall modification changes $[Ca^{2+}]_{cyt}$ signals in central cells or affects $[Ca^{2+}]_{cyt}$ propagative signaling to the shoot. Root tip cell death has also been observed (Huang et al., 2007; Lequeux et al., 2010; Rodrigo-Moreno et al., 2013). Cu-induced cell death in rice roots was attenuated by chelating extracellular Ca^{2+} thus implicating Ca^{2+} influx across the PM (Huang et al., 2007) while in *Arabidopsis* roots cell death was attenuated by addition of Gd^{3+} or verapamil as PM Ca^{2+} channel blockers (Rodrigo-Moreno et al., 2013).

Gd^{3+} is routinely used as a PM Ca^{2+} channel blocker, for example with proven efficacy against *Arabidopsis* root epidermal and root hair HACC, DACC and VICC (Véry and Davies, 2000; Demidchik et al., 2002; Miedema et al., 2008). It is also effective against the root PM hydroxyl radical-activated and H_2O_2-activated Ca^{2+} influx channels (Demidchik et al., 2003, 2007) and the Annexin1-mediated pathway (Laohavisit et al., 2012). As a consequence Gd^{3+} lowers Ca^{2+} influx (measured with ^{45}Ca; Demidchik et al., 2002). From this it can be anticipated that Gd^{3+} would have the capacity to dampen stress-induced $[Ca^{2+}]_{cyt}$ signaling in roots, including that mediated by oxidative stress (Demidchik et al., 2003, 2007) and elicited by NaCl (Laohavisit et al., 2013). Pb is less well studied in terms of $[Ca^{2+}]_{cyt}$. Exogenous Ca^{2+} can protect against root Pb accumulation, suggesting competitive uptake (Rodriguez-Hernandez et al., 2015). However, Pb was found to evoke Ca^{2+} accumulation and diphenyleneiodinium-sensitive ROS increase in rice roots, the latter leading to MAPK activation (Huang and Huang, 2008). Entry of Pb into *Arabidopsis* roots involves CNGC1 as its deletion confers greater tolerance but whether Pb permeates this channel is unknown (Sunkar et al., 2000). Pb has also been shown to increase expression of *TPC1* in *Typha* roots (Rodriguez-Hernandez et al., 2015) but whether this results in increased $[Ca^{2+}]_{cyt}$ in this or other roots is not known yet.

MECHANICAL STRESS

Roots experience a range of mechanical stimuli, induced as they encounter soil particles or neighboring roots. An increase in $[Ca^{2+}]_{cyt}$ together with an apoplastic alkanisation are early effects induced by mechanical stimuli. One of the known downstream events from the increase in $[Ca^{2+}]_{cyt}$ is the upregulation of touch-sensitive genes such as *CML12* and *CML24* (Braam, 1992). Mechanically triggered $[Ca^{2+}]_{cyt}$ changes are dependent on the type of stimulus and the responding tissue (Legue et al., 1997; Monshausen et al., 2009). For example, manually bending an *Arabidopsis* root induces a rapid, biphasic increase in $[Ca^{2+}]_{cyt}$ on the convex side of the roots where cells are stretched (Monshausen et al., 2009) while previously compressed cells on the concave side of the roots show a monophasic and less intense increase in $[Ca^{2+}]_{cyt}$ upon return to their resting position. The source of Ca^{2+} is likely to be extracellular (Monshausen et al., 2009; Richter et al., 2009; Kurusu et al., 2012); with internal stores being mobilized to amplify the response (Chehab et al., 2009; Toyota and Gilroy, 2013).

Over-expressing *MCA1* in *Arabidopsis* lead to an enhanced $[Ca^{2+}]_{cyt}$ transient post mechanical stimulation by the addition of a membrane crenator, however, the *mca1* mutant showed no difference from the wild type (Nakagawa et al., 2007). Accordingly, Shih et al. (2014) showed no change in *mca1* apoplastic alkalinisation following root bending, which is closely related to the $[Ca^{2+}]_{cyt}$ signature. Thus some levels of compensation occur in mutants deficient in mechanosensitive Ca^{2+} channels. In contrast to the MCAs, MSLs (MscS-Like) were identified in *Arabidopsis* due to their sequence similarity to the bacterial Mechanosensitive channels of small conductance (MscS) (Haswell et al., 2008). These are encoded by a multiple gene family of 10 members, with MSL9 and MSL10 found in the PM of root cells and required for a mechanosensitive channel activity. They are predominantly anion channels and their relationship to mechano-stimulated $[Ca^{2+}]_{cyt}$ increase has yet to be shown but may be through PM voltage regulation. At this point, it is unclear whether these channels represent mechano-sensors or act downstream of yet unknown mechano-sensors.

Recently, the PM receptor-like kinase FERONIA has been implicated in regulating the *Arabidopsis* mechano-stimulated $[Ca^{2+}]_{cyt}$ increase and downstream transcriptional regulation (Shih et al., 2014). *feronia* mutants lack the second peak of the biphasic increase in $[Ca^{2+}]_{cyt}$ elicited in stretched cells by manual bending. However, the mechanism by which FERONIA can regulate $[Ca^{2+}]_{cyt}$ remains unclear as its kinase activity is not essential and targets are unknown. As far as we know, this study was the first in which a mutant with an aberrant mechano-stimulated $[Ca^{2+}]_{cyt}$ increase also showed a root skewing phenotype. Root skewing (deviation from the vertical when grown on vertical or inclined agar) may be influenced by mechano-sensing. At this point, it is unclear whether FERONIA also plays a role in the mechanical induction of lateral root formation (Richter et al., 2009).

Cold Stress

Cold plays a key role in the regulation of physiology and development; the signaling processes relaying non-stressful temperatures (12°C and above) have been reviewed by Wigge (2013). The signaling cascades activated by cold stress (typically 4°C experimentally) and their relations with hormonal signaling have been reviewed by Knight and Knight (2012), Jeon and Kim (2013), Shi et al. (2015) and Eremina et al. (2016). Most studies on the effect of cold stress on $[Ca^{2+}]_{cyt}$ report on seedlings or leaves. From these it is well established that $[Ca^{2+}]_{cyt}$ elevation involves both Ca^{2+} influx across the PM and release from predominantly vacuolar stores (e.g., Knight et al., 1996; Mazars et al., 1997; Knight and Knight, 2000: Zhu et al., 2013). By

using an extracellular Ca^{2+}-reporting microelectrode, Sulaiman et al. (2012) confirmed that Ca^{2+} influx from the extracellular space is a component of the *Arabidopsis* root response to cold stress. For *Arabidopsis* roots, the $[Ca^{2+}]_{cyt}$ response to cold stress measured using aequorin is lower in amplitude and of much shorter duration than leaves (Zhu et al., 2013). Using aequorin Plieth et al. (1999) determined that the faster the rate of cooling *Arabidopsis* roots, the greater the $[Ca^{2+}]_{cyt}$ response. Sensitivity and magnitude of the $[Ca^{2+}]_{cyt}$ cooling response were enhanced by low temperature but repeated exposure to cold lead to desensitizing of the response. These results imply the existence of Ca^{2+} transport systems that could be regulated at the post-translational and possibly transcriptional levels. In *Arabidopsis*, cold-induced $[Ca^{2+}]_{cyt}$ elevation would activate a root PM calcium/calmodulin-regulated receptor-like kinase (CRLK1; Yang et al., 2010). This would then activate a specific mitogen-activated protein kinase kinase kinase (MEKK1) that then targets protein kinase kinase2 (MKK2; Furuya et al., 2013). This pathway leads to gene activation and freezing tolerance (Furuya et al., 2014). $[Ca^{2+}]_{cyt}$ elevation would also activate CIPK3, that acts an intersect with ABA signaling (Kim et al., 2003). Part of the transcriptional response to cold in *Arabidopsis* could be activated by increased $[Ca^{2+}]_{cyt}$ through CAMTA3 regulation of the transcriptional regulator CBF2 (C-Repeat/Dehydration Responsive Element Binding Factor2) (Doherty et al., 2009).

Cold stress has been found to depolarise the PM of root cells from cucumber and *Triana bogotensis* (Lyalin and Ktitorova, 1969; Minorsky and Spanswick, 1989), consistent with the effect of Ca^{2+} influx across the PM. A modeling exercise revealed the possible importance of a PM DACC in cold stress-induced $[Ca^{2+}]_{cyt}$ elevation of roots (White, 2009). Cold has been shown to activate a PM DACC in leaf protoplasts (Carpaneto et al., 2007) but this has not yet been shown for roots. As microtubule destabilization activates the *Arabidopsis* root PM DACC (Thion et al., 1998), this could link to the increased cold-induced $[Ca^{2+}]_{cyt}$ signal observed when microtubules are disrupted in *Nicotiana plumbaginifolia* leaf protoplasts (Mazars et al., 1997). Actin depolymerization is implicated in cold-induced Ca^{2+} influx across the PM into *Medicago sativa* suspension cells (Orvar et al., 2000). This in turn could relate to the cold-induced activation of pear pollen PM HACC that involves actin depolymerization (Wu et al., 2012). It would be timely therefore to investigate root PM for cold effects on HACC and DACC, exploring also the involvement of the cytoskeleton. In common with mechanical stress, cold stress could perturb the PM bilayer sufficiently to change Ca^{2+} channel activity. Work on *M. sativa* suspension cells showed that increasing membrane fluidity at 4°C prevented the Ca^{2+} influx across the PM that is necessary to trigger gene expression for freezing tolerance (Orvar et al., 2000). Conversely, imposing membrane rigidity at normal temperature triggers activation of the Ca^{2+}-dependent MEKK1-MKK2-MPK4 pathway in *Arabidopsis* seedlings (Furuya et al., 2014). The possibility that mechanosensitive channels are involved in cold-induced $[Ca^{2+}]_{cyt}$ signaling merits investigation. However, recent work on rice roots indicates another route to Ca^{2+} influx. COLD1 has been identified as a PM activator of the heterotrimeric G protein subunit α (Ma Y. et al., 2015). It is required for cold-activated Ca^{2+} influx to roots (measured using extracellular Ca^{2+}-reporting microelectrode) and elevation of root $[Ca^{2+}]_{cyt}$ (aequorin and cameleon determinations). This indicates that heterotrimeric G proteins lie upstream of PM Ca^{2+} channels in the cold response. In common with other stress responses, NADPH oxidase activity also appears in cold stress and needs to be placed in relation to Ca^{2+} channels. *Arabidopsis* roots exposed to cold stress use AtSRC2 (Soybean gene Regulated by Cold2) to enhance Ca^{2+} activation of the AtRBOHF NADPH Oxidase (Kawarazaki et al., 2013). This suggests that NADPH oxidase activity can lie downstream of Ca^{2+} channel activity. Curtailing cold-induced $[Ca^{2+}]_{cyt}$ elevation could involve vacuolar CAX1 activity in *Arabidopsis* (Catala et al., 2003).

CONCLUSION AND FUTURE PROSPECTS

A repeated message from this review is how incomplete our knowledge is of the channels mediating stress-induced $[Ca^{2+}]_{cyt}$ increases, and by extension those of organelles. Many members of channel gene families still await characterization. The identification of new families of channels is challenging and will require different approaches linking forward and reverse genetics to electrophysiology. Targets of Ca^{2+}-binding and interacting proteins also require further study. Components common to different abiotic stresses are emerging such as *Arabidopsis* CIPK23 in K^+ and nitrate deprivation. These common regulatory components are likely to represent critical steps where complex stress signals encountered in the soil are integrated in unified responses. Receptor like kinases such as FERONIA or PERK4 have emerged as new components in $[Ca^{2+}]_{cyt}$ signaling and perhaps other related proteins will be found to have a role in abiotic stress signaling. Remodeling of calcium signaling machinery after stress is also apparent with the possibility of components common to different stresses. For example, *Arabidopsis CNGC19* is upregulated under B limitation and salinity stress (Kugler et al., 2009). Finally, $[Ca^{2+}]_{cyt}$-dependent transcriptional responses can be delineated and future work could include the impact of stress-induced calcium signaling on epigenetic inheritance (Sani et al., 2013; Probst and Scheid, 2015).

AUTHOR CONTRIBUTIONS

All authors listed, have made substantial, direct and intellectual contribution to the work, and approved it for publication. KW, EM, SS, and JD wrote the review. KW produced the figures.

FUNDING

Funding for this work was from the BBSRC (BB/K009869/1 and Doctoral Training Programme) and the University of Cambridge Broodbank Trust.

REFERENCES

Armengaud, P., Beitling, R., and Amtmann, A. (2004). The potassium-dependent transcriptome of *Arabidopsis* reveals a prominent role of jasmonic acid in nutrient signaling. *Plant Physiol.* 136, 2556–2576. doi: 10.1104/pp.104.046482

Bai, L., Zhang, G., Zhou, Y., Zhang, Z., Wang, W., Du, Y., et al. (2009). Plasma membrane-associated proline-rich extension-like receptor kinase 4, a novel regulator of Ca^{2+} signaling, is required for abscisic acid responses in *Arabidopsis thaliana*. *Plant J.* 60, 314–327. doi: 10.1111/j.1365-313X.2009.03956.x

Baliardini, C., Meyer, C.-L., Salis, P., Saumitou-Laprade, P., and Verbruggen, N. (2015). CATION EXCHANGER1 cosegregates with cadmium tolerance in the metal hyperaccumulator *Arabidopsis halleri* and plays a role in limiting oxidative stress in *Arabidopsis* Spp. *Plant Physiol.* 169, 549–559. doi: 10.1104/pp.15.01037

Barberon, M., Vermeer, J. E. M., De Bellis, D., Wang, P., Naseer, S., Anderson, T. G., et al. (2016). Adaptation of root function by nutrient-induced plasticity of endodermal differentiation. *Cell* 164, 447–459. doi: 10.1016/j.cell.2015.12.021

Batelli, G., Verslues, P. R., Agius, F., Qiu, Q., Fujii, H., Pan, S., et al. (2007). SOS2 promotes salt tolerance in part by interacting with the vacuolar H^+-ATPase and upregulating its transport activity. *Mol. Cell Biol.* 27, 7781–7790. doi: 10.1128/MCB.00430-07

Behera, S., Wang, N., Zhang, C., Schmitz-Thom, I., Strohkamp, S., Schueltke, S., et al. (2015). Analyses of Ca^{2+} dynamics using a ubiquitin-10 promoter-driven Yellow Cameleon 3.6 indicator reveal reliable transgene expression and differences in cytoplasmic Ca^{2+} responses in *Arabidopsis* and rice (*Oryza sativa*) roots. *New Phytol.* 206, 751–760. doi: 10.1111/nph.13250

Bonza, M. C., Loro, G., Behera, S., Wong, A., Kudla, J., and Costa, A. (2013). Analyses of Ca^{2+} accumulation and dynamics in the endoplasmic reticulum of *Arabidopsis* root cells using a genetically encoded cameleon sensor. *Plant Physiol.* 163, 1230–1241. doi: 10.1104/pp.113.226050

Bonza, M. C., Luoni, L., Olivari, C., and DeMichelis, M. I. (2016). Plant type 2B Ca^{2+}-ATPases: the diversity of isoforms of the model plant *Arabidopsis thaliana*. *Adv. Biochem. Health Dis.* 14, 227–241.

Boursiac, Y., and Harper, J. F. (2007). The origin and function of calmodulin regulated Ca^{2+} pumps in plants. *J. Bioen. Biomem.* 39, 409–414. doi: 10.1007/s10863-007-9104-z

Braam, J. (1992). Regulated expression of the calmodulin-related TCH genes in cultured *Arabidopsis* cells – induction by calcium and heat shock. *Proc. Natl. Acad. Sci. U.S.A.* 89, 3213–3216. doi: 10.1073/pnas.89.8.3213

Camacho-Cristobal, J. J., Martin-Rejano, E. M., Begona Herrera-Rodriguez, M., Teresa Navarro-Gochicoa, M., Rexach, J., and Gonzalez-Fontes, A. (2015). Boron deficiency inhibits root cell elongation via an ethylene/auxin/ROS-dependent pathway in *Arabidopsis* seedlings. *J. Expt. Bot.* 66, 3831–3840. doi: 10.1093/jxb/erv186

Carpaneto, A., Ivashikina, N., Levchenko, V., Krol, E., Jeworutzki, E., Zhu, J.-K., et al. (2007). Cold transiently activates calcium-permeable channels in *Arabidopsis* mesophyll cells. *Plant Physiol.* 143, 487–494. doi: 10.1104/pp.106.090928

Carroll, A. D., Moyen, C., Van Kesteren, P., Tooke, F., Battey, N. H., and Brownlee, C. (1998). Ca^{2+}, annexins, and GTP modulate exocytosis from maize root cap protoplasts. *Plant Cell* 10, 1267–1276. doi: 10.1105/tpc.10.8.1267

Catala, R., Santos, E., Alonso, J. M., Ecker, J. R., Martinez-Zapater, J. M., and Salinas, J. (2003). Mutations in the Ca^{2+}/H^+ transporter CAX1 increase CBF/DREB1 expression and the cold-acclimation response in *Arabidopsis*. *Plant Cell* 15, 2940–2951. doi: 10.1105/tpc.015248

Chehab, E. W., Eich, E., and Braam, J. (2009). Thigmomorphogenesis: a complex plant response to mechanostimulation. *J. Expt. Bot.* 60, 43–56. doi: 10.1093/jxb/ern315

Cheng, N. H., Pittman, J. K., Zhu, J. K., and Hirschi, K. D. (2004). The protein kinase SOS2 activates the *Arabidopsis* H^+/Ca^{2+} antiporter CAX1 to integrate calcium transport and salt tolerance. *J. Biol. Chem.* 279, 2922–2926. doi: 10.1074/jbc.M309084200

Cheong, Y. H., Pandey, G. K., Grant, J. J., Batistic, O., Li, L., Kim, B.-G., et al. (2007). Two calcineurin B-like calcium sensors, interacting with protein kinase CIPK23, regulate leaf transcription and root potassium uptake in *Arabidopsis*. *Plant J.* 52, 223–239. doi: 10.1111/j.1365-313X.2007.03236.x

Chmielowska-Bak, J., Gryl, J., Rucinska-Sobkowiak, R., Arasimowicz-Jelonek, M., and Deckert, J. (2014). The new insights into cadmium sensing. *Front. Plant Sci.* 5:245. doi: 10.3389/fpls.2014.00245

Choi, W.-G., Toyota, M., Kim, S.-H., Hilleary, R., and Gilroy, S. (2014). Salt stress-induced Ca^{2+} waves are associated with rapid, long-distance root-to-shoot signaling in plants. *Proc. Natl. Acad. Sci. U.S.A.* 111, 6497–6502. doi: 10.1073/pnas.1319955111

Christensen, A., Svensson, K., Persson, S., Jung, J., Michalak, M., Widell, S., et al. (2008). Functional characterization of *Arabidopsis* calreticulin1a: A key alleviator of endoplasmic reticulum. *Plant Cell Physiol.* 49, 912–924. doi: 10.1093/pcp/pcn065

Chung, J. S., Zhu, J. K., Bressan, R. A., Hasagawa, P. M., and Shi, H. (2008). Reactive oxygen species mediate Na^+-induced SOS1 mRNA stability in *Arabidopsis*. *Plant J.* 53, 554–565. doi: 10.1111/j.1365-313X.2007.03364.x

Clemens, S., Antosiewicz, D. M., Ward, J. M., Schachtman, D. B., and Schroeder, J. I. (1998). The plant cDNA LCT1 mediates the uptake of calcium and cadmium in yeast. *Proc. Natl. Acad. Sci. U.S.A.* 95, 12043–12048. doi: 10.1073/pnas.95.20.12043

Connorton, J. M., Webster, R. E., Cheng, N. H., and Pittman, J. K. (2012). Knockout of multiple *Arabidopsis* cation/H^+ exchangers suggests isoform-specific roles in metal stress response, germination and see mineral nutrition. *PLoS ONE* 7:e47455. doi: 10.1371/journal.pone.0047455

Dark, A. M., Demidchik, V., Richards, S. L., Shabala, S. N., and Davies, J. M. (2011). Release of extracellular purines from plant roots and effect on ion fluxes. *Plant Signal. Behav.* 6, 1855–1857. doi: 10.4161/psb.6.11.17014

Davies, J. M. (2014). Annexin-mediated calcium signaling in plants. *Plants* 3, 128–140. doi: 10.3390/plants3010128

Demidchik, V., Bowen, H. C., Maathuis, F. J. M., Shabala, S. N., Tester, M. A., White, P. J., et al. (2002). *Arabidopsis thaliana* root non-selective cation channels mediate calcium uptake and are involved in growth. *Plant J.* 32, 799–808. doi: 10.1046/j.1365-313X.2002.01467.x

Demidchik, V., Cuin, T. A., Svistunenko, D., Smith, S. J., Miller, A. J., Shabala, S., et al. (2010). *Arabidopsis* root K^+-efflux conductance activated by hydroxyl radicals: single-channel properties, genetic basis and involvement in stress-induced death. *J. Cell Sci.* 123, 1468–1479. doi: 10.1242/jcs.064352

Demidchik, V., Shabala, S. N., Coutts, K. B., Tester, M. A., and Davies, J. M. (2003). Free oxygen radicals regulate plasma membrane Ca^{2+} and K^+-permeable channels in plant root cells. *J. Cell Sci.* 116, 81–88. doi: 10.1242/jcs.00201

Demidchik, V., Shabala, S. N., and Davies, J. M. (2007). Spatial variation in H_2O_2 response of *Arabidopsis thaliana* epidermal Ca^{2+} flux and plasma membrane Ca^{2+} channels. *Plant J.* 49, 377–386. doi: 10.1111/j.1365-313X.2006.02971.x

Demidchik, V., Shang, Z., Shin, R., Thompson, E. P., Rubio, L., Laohavisit, A., et al. (2009). Plant extracellular ATP signalling by plasma membrane NADPH oxidase and Ca^{2+} channels. *Plant J.* 58, 903–913. doi: 10.1111/j.1365-313X.2009.03830.x

Deng, Y., Srivatava, R., and Howell, S. H. (2013). Protein kinase and ribonuclease domians of IRE1 confer stress tolerance, vegetative growth and reproductive development. *Proc. Natl. Acad. Sci. U.S.A.* 110, 19633–19638. doi: 10.1073/pnas.1314749110

DeWald, D. B., Torabinejad, J., Jones, C. A., Shope, J. C., Cangelosi, A. R., Thompson, J. E., et al. (2001). Rapid accumulation of phosphatidylinositol 4,5-bisphosphate and inositol 1,4,5-trisphosphate correlates with calcium mobilization in salt-stressed *Arabidopsis*. *Plant Physiol.* 126, 759–769. doi: 10.1104/pp.126.2.759

Dinneny, J. R., Long, T. A., Wang, J. Y., Jung, J. W., Mace, D., Pointer, S., et al. (2008). Cell identity mediates the response of *Arabidopsis* roots to abiotic stress. *Science* 320, 942–945. doi: 10.1126/science.1153795

Doherty, C. J., Van Buskirk, H. A., Myers, S. J., and Thomashow, M. F. (2009). Roles for *Arabidopsis* CAMTA transcription factors in cold-regulated gene expression and freezing tolerance. *Plant Cell* 21, 972–984. doi: 10.1105/tpc.108.063958

Donaldson, L., Ludidi, N., Knight, M. R., Gehring, C., and Denby, K. (2004). Salt and osmotic stress cause rapid increases in *Arabidopsis thaliana* cGMP levels. *FEBS Letts.* 569, 317–320. doi: 10.1016/j.febslet.2004.06.016

Drerup, M. M., Schluecking, K., Hashimoto, K., Manishankar, P., Steinhorst, L., Kuchitsu, K., et al. (2013). The Calcineurin B-Like calcium sensors CBL1 and CBL9 together with their interacting protein kinase CIPK26 regulate the *Arabidopsis* NADPH oxidase RBOHF. *Mol. Plant* 6, 559–569. doi: 10.1093/mp/sst009

Dressler, L., Golbik, R., and Ulbrich-Hofmann, R. (2014). Lanthanides as substitutes for calcium ions in the activation of plant alpha-type phospholipase D. *Biol. Chem.* 395, 791–799. doi: 10.1515/hsz-2014-0112

Eremina, M., Rozhon, W., and Poppenberger, B. (2016). Hormonal control of cold stress responses in plants. *Cell. Mol. Life Sci.* 73, 797–810. doi: 10.1007/s00018-015-2089-6

Fagerstedt, K. V. (2010). "Programmed cell death and aerenchyma formation under hypoxia," in *Waterlogging Signalling and Tolerance in Plants*, eds S. Mancuso and S. Shabala (Berlin: Springer), 99–118.

Fan, J.-L., Wei, X.-Z., Wan, L.-C., Zhang, L.-Y., Zhao, X.-Q., Liu, W.-Z., et al. (2011). Disarrangement of actin filaments and Ca^{2+} gradient by $CdCl_2$ alters cell wall construction in *Arabidopsis thaliana* root hairs by inhibiting vesicular trafficking. *J. Plant Physiol.* 168, 1157–1167. doi: 10.1016/j.jplph.2011.01.031

Fischer, C., Kugler, A., Hoth, S., and Dietrich, P. (2013). An IQ domain mediates the interaction with calmodulin in a plant cyclic nucleotide-gated channel. *Plant Cell Physiol.* 54, 573–584. doi: 10.1093/pcp/pct021

Foreman, J., Demidchik, V., Bothwell, J. H. F., Mylona, P., Miedema, H., Torres, M. A., et al. (2003). Reactive oxygen species produced by NADPH oxidase regulate plant cell growth. *Nature* 422, 442–446. doi: 10.1038/nature01485

Fry, S. C., Miller, J. G., and Dumville, J. C. (2002). A proposed role for copper ions in cell wall loosening. *Plant Soil* 247, 57–67. doi: 10.1023/A:1021140022082

Furuya, T., Matsuoka, D., and Nanmori, T. (2013). Phosphorylation of *Arabidopsis thaliana* MEKK1 via Ca^{2+} signaling as a part of the cold stress response. *J. Plant Res.* 126, 833–840. doi: 10.1007/s10265-013-0576-0

Furuya, T., Matsuoka, D., and Nanmori, T. (2014). Membrane rigidification functions upstream of the MEKK1-MKK2-MPK4 cascade during cold acclimation in *Arabidopsis thaliana*. *FEBS Lett.* 588, 2025–2030. doi: 10.1016/j.febslet.2014.04.032

Gobert, A., Park, G., Amtmann, A., Sanders, D., and Maathuis, F. J. M. (2006). *Arabidopsis thaliana* cyclic nucleotide-gated channel 3 forms a non-selective ion transporter involved in germination and cation transport. *J. Expt. Bot.* 57, 791–800. doi: 10.1093/jxb/erj064

Goldbach, H. E., Yu, Q., Wingender, R., Schulz, M., Wimmer, M., Findeklee, P., et al. (2001). Rapid response reactions of roots to boron deprivation. *J. Plant Nutr. Soil Sci.* 164, 173–181. doi: 10.1002/1522-2624(200104)164:2<173::AID-JPLN173>3.3.CO;2-6

González-Fontes, A., Herrera-Rodriguez, M. B., Martin-Rejano, E. M., Navarro-Gochicoa, M. T., Rexach, J., and Camacho-Cristobal, J. J. (2016). Root responses to boron deficiency mediated by ethylene. *Front. Plant Sci.* 6:1103. doi: 10.3389/fpls.2015.01103

Gonzali, S., Loreti, E., Cardarelli, F., Novi, G., Parlanti, S., Pucciariello, C., et al. (2015). Universal stress protein HRU1 mediates ROS homeostasis under anoxia. *Nat. Plants* 1, 15151. doi: 10.1038/NPLANTS.2015.151

Guerra, F., Duplessis, S., Kohler, A., Martin, F., Tapia, J., Lebed, P., et al. (2009). Gene expression analysis of *Populus deltoides* roots subjected to copper stress. *Environ. Exp. Bot.* 67, 335–344. doi: 10.1016/j.envexpbot.2009.08.004

Guo, J., Zeng, W., Chen, Q., Lee, C., Chen, L., Yang, Y., et al. (2016). Structure of the voltage-gated two-pore channel TPC1 from *Arabidopsis thaliana*. *Nature* 531, 196–201. doi: 10.1038/nature16446

Guo, K.-M., Babourina, O., Christopher, D. A., Borsics, T., and Rengel, Z. (2008). The cyclic nucleotide-gated channel, AtCNGC10, influences salt tolerance in *Arabidopsis*. *Physiol. Plant.* 134, 499–507. doi: 10.1111/j.1399-3054.2008.01157.x

Haswell, E. S., Peyronnet, R., Barbier-Brygoo, H., Meyerowitz, E. M., and Frachisse, J. M. (2008). Two MscS homologs provide mechanosensitive channel activities in the *Arabidopsis* root. *Curr. Biol.* 18, 730–734. doi: 10.1016/j.cub.2008.04.039

Ho, C.-H., Lin, S.-H., Hu, H.-C., and Tsay, Y.-F. (2009). CHL1 functions as a nitrate sensor in plants. *Cell* 138, 1184–1194. doi: 10.1016/j.cell.2009.07.004

Hossain, M. A., Henriquez-Valencia, C., Gómez-Páez, M., Medina, J., Orellana, A., Vicente-Carbajosa, J., et al. (2016). Identification of novel components of the unfolded protein response in *Arabidopsis*. *Front. Plant Sci.* 7:650. doi: 10.3389/fpls.2016.00650

Hou, C. C., Tian, W., Kleist, T., He, K., Garcia, V., Bai, F., et al. (2014). DUF221 proteins are a family of osmosensitive calcium-permeable cation channels conserved across eukaryotes. *Cell Res.* 24, 632–635. doi: 10.1038/cr.2014.14

Hou, Q., Ufer, G., and Bartels, D. (2016). Lipid signalling in plant responses to abiotic stress. *Plant Cell Environ.* 39, 1029–1048. doi: 10.1111/pce.12666

Hu, H. C., Wang, Y. Y., and Tsay, Y. F. (2009). AtCIPK8, a CBL-interacting protein kinase, regulates the low-affinity phase of the primary nitrate response. *Plant J.* 57, 264–278. doi: 10.1111/j.1365-313X.2008.03685.x

Hu, Y. F., Zhou, G., Na, X. F., Yang, L., Nan, W. B., Liu, X., et al. (2013). Cadmium interferes with maintenance of auxin homeostasis in *Arabidopsis* seedlings. *J. Plant Physiol.* 170, 965–975. doi: 10.1016/j.jplph.2013.02.008

Hua, B. G., Mercier, R. W., and Zielinski, R. E. (2003). Functional interaction of calmodulin with a plant cyclic nucleotide gated cation channel. *Plant Physiol. Biochem.* 41, 945–954. doi: 10.1016/j.plaphy.2003.07.006

Huang, T.-L., and Huang, H.-J. (2008). ROS and CDPK-like kinase-mediated activation of MAP kinase in rice roots exposed to lead. *Chemosphere* 71, 1377–1385. doi: 10.1016/j.chemosphere.2007.11.031

Huang, W.-C., Huang, D.-D., Chien, P.-S., Yeh, C.-M., Chen, P.-Y., Chi, W.-C., et al. (2007). Protein tyrosine dephosphorylation during copper-induced cell death in rice roots. *Chemosphere* 69, 55–62. doi: 10.1016/j.chemosphere.2007.04.073

Hunt, L., Otterhag, L., Lee, J. C., Lasheen, T., Hunt, J., Seki, M., et al. (2004). Gene-specific expression and calcium activation of *Arabidopsis thaliana* phospholipase C isoforms. *New Phytol.* 162, 643–654. doi: 10.1111/j.1469-8137.2004.01069.x

Isner, J. C., Nühse, T., and Maathuis, F. J. M. (2012). The cyclic nucleotide cGMP is involved in plant hormone signalling and alters phosphorylation of *Arabidopsis thaliana* root proteins. *J. Expt. Bot.* 63, 3199–3205. doi: 10.1093/jxb/ers045

Jakubowska, D., Janicka-Russak, M., Kabala, K., Migocka, M., and Reda, M. (2015). Modification of plasma membrane NADPH oxidase activity in cucumber seedling roots in response to cadmium stress. *Plant Sci.* 234, 50–59. doi: 10.1016/j.plantsci.2015.02.005

Jeon, J., and Kim, J. (2013). Cold stress signaling networks in *Arabidopsis*. *J. Plant Biol.* 56, 69–76. doi: 10.1007/s12374-013-0903-y

Jiang, H. B., Wang, S. F., Yang, F., Zhang, Z. H., Qiu, H. C., Yi, Y., et al. (2015). Plant growth, nitrate content and Ca signaling in wheat (*Triticum aestivum* L.) roots under different nitrate supply. *Plant Sci. J.* 33, 362–368.

Jiao, Y., Sun, L., Song, Y., Wang, L., Liu, L., Zhang, L., et al. (2013). AtrbohD and AtrbohF positively regulate abscisic acid-inhibited primary root growth by affecting Ca^{2+} signalling and auxin response of roots in *Arabidopsis*. *J. Expt. Bot.* 64, 4183–4192. doi: 10.1093/jxb/ert228

Jin, Y. K., Jing, W., Zhang, Q., and Zhang, W. H. (2015). Cyclic nucleotide gated channel 10 negatively regulates salt tolerance by mediating Na^+ transport in *Arabidopsis*. *J. Plant Res.* 128, 211–220. doi: 10.1007/s10265-014-0679-2

Kamano, S., Kume, S., Iida, K., Lei, K.-J., Nakano, M., Nakayama, Y., et al. (2015). Transmembrane topologies of Ca^{2+}-permeable mechanosensitive channels MCA1 and MCA2 in *Arabidopsis thaliana*. *J. Biol. Chem.* 290, 30901–30909. doi: 10.1074/jbc.M115.692574

Kanehara, K., Yu, C.-Y., Cho, Y., Cheong, W.-F., Torta, F., Shui, G., et al. (2015). *Arabidopsis* AtPLC2 is a primary phosphoinositide-specific phospholipase C in phopshoinositide metabolism and the endoplasmic reticulum stress response. *PLOS Genet.* 11:e1005511. doi: 10.1371/journal.pgen.1005511

Kasajima, I., Ide, Y., Hirai, M. Y., and Fujiwara, T. (2010). WRKY6 is involved in the response to boron deficiency in *Arabidopsis thaliana*. *Physiol. Plant.* 139, 80–92. doi: 10.1111/j.1399-3054.2010.01349.x

Kawarazaki, T., Kimura, S., Iizuka, A., Hanamata, S., Nibori, H., Michikawa, M., et al. (2013). A low temperature-inducible protein AtSRC2 enhances the ROS-producing activity of NADPH oxidase AtRbohF. *Biochim. Biophys. Acta Mol. Cell Res.* 1833, 2775–2780. doi: 10.1016/j.bbamcr.2013.06.024

Kiegle, E., Moore, C. A., Haseloff, J., Tester, M. A., and Knight, M. R. (2000). Cell-type-specific calcium responses to drought, salt and cold in the *Arabidopsis* root. *Plant J.* 23, 267–278. doi: 10.1046/j.1365-313x.2000.00786.x

Kim, K. N., Cheong, Y. H., Grant, J. J., Pandey, G. K., and Luan, S. (2003). CIPK3, a calcium sensor-associated protein kinase that regulates abscisic acid and cold signal transduction in *Arabidopsis*. *Plant Cell* 15, 411–423. doi: 10.1105/tpc.006858

Kim, Y., Wang, M., Bai, Y., Zeng, Z., Guo, F., Han, N., et al. (2014). Bcl-2 suppresses activation of VPEs by inhibiting cytosolic Ca^{2+} level with elevated K^+ efflux in NaCl-induced PCD in rice. *Plant Physiol. Biochem.* 80, 168–175. doi: 10.1016/j.plaphy.2014.04.002

Kintzer, A. F., and Stroud, R. M. (2016). Structure, inhibition and regulation of two-pore channel TPC1 from *Arabidopsis thaliana*. *Nature* 531, 258–264. doi: 10.1038/nature17194

Knight, H., and Knight, M. R. (2000). Imaging spatial and cellular characteristics of low temperature calcium signature after cold acclimation in *Arabidopsis*. *J. Expt. Bot.* 51, 1679–1686. doi: 10.1093/jexbot/51.351.1679

Knight, H., Trewavas, A. J., and Knight, M. R. (1996). Cold calcium signaling in *Arabidopsis* involves two cellular pools and a change in calcium signature after acclimation. *Plant Cell* 8, 489–503. doi: 10.1105/tpc.8.3.489

Knight, H., Trewavas, A. J., and Knight, M. R. (1997). Calcium signalling in *Arabidopsis thaliana* responding to drought and salinity. *Plant J.* 12, 1067–1078. doi: 10.1046/j.1365-313X.1997.12051067.x

Knight, M. R., and Knight, H. (2012). Low-temperature perception leading to gene expression and cold tolerance in higher plants. *New Phytol.* 195, 737–751. doi: 10.1111/j.1469-8137.2012.04239.x

Kobayashi, B., Matoh, T., and Azuma, J. (1996). Two chains of rhamnogalacturonan II are cross-linked by borate-diol ester bonds in higher plant cell walls. *Plant Physiol.* 110, 1017–1020.

Kolbert, Z., Petö, A., Lehotai, N., Feigl, G., and Erdei, L. (2012). Long-term copper (Cu^{2+}) exposure impacts on auxin, nitric oxide (NO) metabolism and morphology of *Arabidopsis thaliana* L. *Plant Growth Regul.* 68, 151–159. doi: 10.1007/s10725-012-9701-7

Koshiba, T., Ishihara, A., and Matoh, T. (2010). Boron nutrition of cultured Tobacco BY-2 Cells. VI. Calcium is involved in early responses to boron deprivation. *Plant Cell Physiol.* 51, 323–327. doi: 10.1093/pcp/pcp179

Kugler, A., Koehler, B., Palme, K., Wolff, P., and Dietrich, P. (2009). Salt-dependent regulation of a CNG channel subfamily in *Arabidopsis*. *BMC Plant Biol.* 9:140. doi: 10.1186/1471-2229-9-140

Kurusu, T., Nishikawa, D., Yamazaki, Y., Gotoh, M., Nakano, M., Hamada, H., et al. (2012). Plasma membrane protein OsMCA1 is involved in regulation of hypo-osmotic shock-induced Ca^{2+} influx and modulates generation of reactive oxygen species in cultured rice cells. *BMC Plant Biol.* 12:11. doi: 10.1186/1471-2229-12-11

Laohavisit, A., and Davies, J. M. (2011). Annexins. *New Phytol.* 189, 40–53. doi: 10.1111/j.1469-8137.2010.03533.x

Laohavisit, A., Richards, S. L., Shabala, L., Chen, C., Colaço, R., Swarbreck, S. M., et al. (2013). Salinity-induced calcium signaling and root adaptation in *Arabidopsis* require the regulatory protein annexin1. *Plant Physiol.* 163, 253–262. doi: 10.1104/pp.113.217810

Laohavisit, A., Shang, Z.-L., Rubio, L., Cuin, T. A., Véry, A. A., Wang, A. H., et al. (2012). *Arabidopsis* annexin 1 mediates the radical-activated plasma membrane Ca^{2+} and K^+-permeable conductance in root cells. *Plant Cell* 24, 1522–1533. doi: 10.1105/tpc.112.097881

Latz, A., Mehlmer, N., Zapf, S., Mueller, T. D., Wurzinger, B., Pfister, B., et al. (2013). Salt stress triggers phosphorylation of the *Arabidopsis* vacuolar K^+ channel TPK1 by calcium-dependent protein kinases (CDPKs). *Mol. Plant* 6, 1274–1289. doi: 10.1093/mp/sss158

Legue, V., Blancaflor, E., Wymer, C., Perbal, G., Fahtin, D., and Gilroy, S. (1997). Cytoplasmic free calcium in *Arabidopsis* roots changes in response to touch but not gravity. *Plant Physiol.* 114, 789–800. doi: 10.1104/pp.114.3.789

Lequeux, H., Hermans, C., Lutts, S., and Verbruggen, N. (2010). Response to copper excess in *Arabidopsis thaliana*: impact on the root system architecture, hormone distribution, lignin accumulation and mineral profile. *Plant Physiol. Biochem.* 48, 673–682. doi: 10.1016/j.plaphy.2010.05.005

Léran, S., Edel, K. H., Pervent, M., Hashimoto, K., Corratge-Faillie, C., Offenborn, J. N., et al. (2015). Nitrate sensing and uptake in *Arabidopsis* are enhanced by ABI2, a phosphatase inactivated by the stress hormone abscisic acid. *Sci. Signal.* 8, ra43. doi: 10.1126/scisignal.aaa4829

Li, G., Boudsocq, M., Hem, S., Vialaret, J., Rossignol, M., Maurel, C., et al. (2015). The calcium-dependent protein kinase CPK7 acts on root hydraulic conductivity. *Plant Cell Environ.* 38, 1312–1320. doi: 10.1111/pce.12478

Li, J., Long, Y., Qi, G. N., Xu, Z. J., Wu, W. H., and Wang, Y. (2014). The OsAKT1 channel is critical for K^+ uptake in rice roots and is modulated by the rice CBL1-CIPK23 complex. *Plant Cell* 26, 3387–3402. doi: 10.1105/tpc.114.123455

Li, L., Kim, B.-G., Cheong, Y. H., Pandey, G. K., and Luan, S. (2006). A Ca^{2+} signalling pathway regulates a K^+ channel for low K^+ response in *Arabidopsis*. *Proc. Natl. Acad. Sci. U.S.A.* 103, 12625–12630. doi: 10.1073/pnas.0605129103

Li, P., Zhao, C. Z., Zhang, Y. Q., Wang, X. M., Wang, X. Y., Wang, J. F., et al. (2016). Calcium alleviates cadmium-induced inhibition on root growth by maintaining auxin homeostasis in *Arabidopsis* seedlings. *Protoplasma* 253, 185–200. doi: 10.1007/s00709-015-0810-9

Li, P. H., Zhang, G. Y., Gonzales, N., Guo, Y. Q., Hu, H. H., Park, S. H., et al. (2016). Ca^{2+}-regulated and diurnal rhythm-regulated Na^+/Ca^{2+} exchanger AtNCL affects flowering time and auxin signalling in *Arabidopsis*. *Plant Cell Environ.* 39, 377–392. doi: 10.1111/pce.12620

Li, S., Yu, J., Zhu, M., Zhao, F., and Luan, S. (2012). Cadmium impairs ion homeostasis by altering K^+ and Ca^{2+} channel activities in rice root hairs. *Plant Cell Environ.* 35, 1998–2013. doi: 10.1111/j.1365-3040.2012.02532.x

Lin, C. Y., Trinh, N. N., Fu, S. F., Hsiung, Y. C., Chia, L. C., Lin, C. W., et al. (2013). Comparison of early transcriptome responses to copper and cadmium in rice roots. *Plant Mol. Biol.* 81, 507–522. doi: 10.1007/s11103-013-0020-9

Liu, J. P., Ishitani, M., Halfter, U., Kim, C. S., and Zhu, J. K. (2000). The *Arabidopsis thaliana* SOS2 gene encodes a protein kinase that is required for salt tolerance. *Proc. Natl. Acad. Sci. U.S.A.* 97, 3730–3734. doi: 10.1073/pnas.97.7.3730

Liu, J.-X., Srivastava, R., Che, P., and Howell, S. H. (2007). Salt stress responses in *Arabidopsis* utilize a signal transduction pathway related to endoplasmic reticulum stress signaling. *Plant J.* 51, 897–909. doi: 10.1111/j.1365-313X.2007.03195.x

Liu, L., Li, Q., Yin, B., Zhang, H., Lin, B., Wu, Y., et al. (2011). The endoplasmic reticulum-associated degradation is necessary for plant salt tolerance. *Cell Res.* 21, 957–969. doi: 10.1038/cr.2010.181

Liu, Q., Zheng, L., He, F., Zhao, F.-J., Shen, Z., and Zheng, L. (2015). Transcriptional and physiological analyses identify a regulatory role for hydrogen peroxide in the lignin biosynthesis of copper-stressed rice roots. *Plant Soil* 387, 323–336. doi: 10.1007/s11104-014-2290-7

Lokdarshi, A., Conner, W. C., McClintock, C., Li, T., and Roberts, D. M. (2016). *Arabidopsis* CML38, a calcium sensor that localizes to ribonucleoprotein complexes under hypoxia stress. *Plant Physiol.* 170, 1046–1059. doi: 10.1104/pp.15.01407

Lu, G., Wang, X., Liu, J., Yu, K., Gao, Y., Liu, H., et al. (2014). Application of T-DNA activation tagging to identify glutamate receptor-like genes that enhance drought tolerance in plants. *Plant Cell Rep.* 33, 617–631. doi: 10.1007/s00299-014-1586-7

Lyalin, O. O., and Ktitorova, I. N. (1969). Resting potential of the root hair of *Trianea bogotensis*. *Sov. Plant Phys.* 16, 214–221.

Ma, L., Zhang, H., Sun, L., Jiao, Y., Zhang, G., Miao, C., et al. (2012). NADPH oxidase AtrbohD and AtrbohF function in ROS-dependent regulation of Na^+/K^+ homeostasis in *Arabidopsis* under salt stress. *J. Expt. Bot.* 63, 305–317. doi: 10.1093/jxb/err280

Ma, Q., Tang, R. J., Zheng, X. J., Wang, S. M., and Luan, S. (2015). The calcium sensor CBL7 modulates plant responses to low nitrate in *Arabidopsis*. *Biochem. Biophys. Res. Commun.* 468, 59–65. doi: 10.1016/j.bbrc.2015.10.164

Ma, Y., Dai, X. Y., Xu, Y. Y., Luo, W., Zheng, X. M., Zeng, D. L., et al. (2015). COLD1 confers chilling tolerance in rice. *Cell* 160, 1209–1221. doi: 10.1016/j.cell.2015.01.046

Maathuis, F. J. M. (2014). Sodium in plants: perception, signalling and regulation of sodium fluxes. *J. Expt. Bot.* 65, 849–858. doi: 10.1093/jxb/ert326

Mazars, C., Thion, L., Thuleau, P., Graziana, A., Knight, M. R., Moreau, M., et al. (1997). Organization of cytoskeleton controls the changes in cytosolic calcium of cold-shocked *Nicotiana plumbaginifolia* protoplasts. *Cell Calcium* 22, 413–420. doi: 10.1016/S0143-4160(97)90025-7

McAinsh, M. R., and Pittman, J. K. (2009). Shaping the calcium signature. *New Phytol.* 181, 275–294. doi: 10.1111/j.1469-8137.2008.02682.x

McLoughlin, F., Galvan-Ampudia, C. S., Julkowska, M. M., Caarls, L., van der Does, D., Lauriere, C., et al. (2012). The Snf1-related protein kinases SnRK2.4 and SnRK2.10 are involved in maintenance of root system architecture during salt stress. *Plant J.* 72, 436–449. doi: 10.1111/j.1365-313X.2012.05089.x

Mehlmer, N., Wurzinger, B., Stael, S., Hofmann-Rodrigues, D., Csaszar, E., Pfister, B., et al. (2010). The Ca^{2+}-dependent protein kinase CPK3 is required for MAPK-independent salt-stress acclimation in *Arabidopsis*. *Plant J.* 63, 484–498. doi: 10.1111/j.1365-313X.2010.04257.x

Mei, H., Cheng, N. H., Zhao, J., Park, S., Escareno, R. A., Pittman, J. K., et al. (2009). Root development under metal stress in *Arabidopsis thaliana* requires

the H^+/cation antiporter CAX4. *New Phytol.* 183, 95–105. doi: 10.1111/j.1469-8137.2009.02831.x

Meringer, M. V., Villasuso, A. L., Peppino, M. M., Usorach, J., Pasquare, S. J., Giusto, N. M., et al. (2016). Saline and osmotic stresses stimulate PLD/diacylglycerol kinase activities and increase the level of phosphatidic acid and proline in barley roots. *Environ. Expt. Bot.* 128, 69–78. doi: 10.1016/j.envexpbot.2016.03.011

Miedema, H., Demidchik, V., Véry, A.-A., Bothwell, J. H. F., Brownlee, C., and Davies, J. M. (2008). Two voltage-dependent calcium channels co-exist in the apical plasma membrane of *Arabidopsis thaliana* root hairs. *New Phytol.* 179, 378–385. doi: 10.1111/j.1469-8137.2008.02465.x

Miller, G., Schlauch, K., Tam, R., Cortes, D., Torres, M. A., Shulaev, V., et al. (2009). The plant NADPH oxidase RBOHD mediates rapid systemic signaling in response to diverse stimuli. *Sci. Signal.* 2, ra45. doi: 10.1126/scisignal.2000448

Minorsky, P. V., and Spanswick, R. M. (1989). Electrophysiological evidence for a role for calcium in temperature sensing by roots of cucumber seedlings. *Plant Cell Env.* 12, 137–143. doi: 10.1111/j.1365-3040.1989.tb01925.x

Monshausen, G. B., Bibikova, T. N., Weisenseel, M. H., and Gilroy, S. (2009). Ca^{2+} regulates reactive oxygen species production and pH during mechanosensing in *Arabidopsis* roots. *Plant Cell* 21, 2341–2356. doi: 10.1105/tpc.109.068395

Moore, C. A., Bowen, H. C., Scrase-Field, S., Knight, M. R., and White, P. J. (2002). The deposition of suberin lamellae determines the magnitude of cytosolic Ca^{2+} elevations in root endodermal cells subjected to cooling. *Plant J.* 30, 457–465. doi: 10.1046/j.1365-313X.2002.01306.x

Mortimer, J. C., Laohavisit, A., Miedema, H., and Davies, J. M. (2008). Voltage, reactive oxygen species and the influx of calcium. *Plant Sig. Behav.* 3, 698–699. doi: 10.4161/psb.3.9.6405

Mühling, K. H., Wimmer, M., and Goldbach, H. E. (1998). Apoplastic and membrane associated Ca^{2+} in leaves and roots as affected by boron deficiency. *Physiol. Plant.* 102, 179–184. doi: 10.1034/j.1399-3054.1998.1020204.x

Nakagawa, Y., Katagiri, T., Shinozaki, K., Qi, Z., Tatsumi, H., Furuichi, T., et al. (2007). *Arabidopsis* plasma membrane protein crucial for Ca^{2+} influx and touch sensing in roots. *Proc. Natl. Acad. Sci. U.S.A.* 104, 3639–3644. doi: 10.1073/pnas.0607703104

Nieves-Cordones, M., Miller, A. J., Aleman, F., Martinez, V., and Rubio, F. (2008). A putative role for the plasma membrane potential in the control of the expression of the gene encoding the tomato high-affinity potassium transporter HAK5. *Plant Mol. Biol.* 68, 521–532. doi: 10.1007/s11103-008-9388-3

Oiwa, Y., Kitayama, K., and Matoh, T. (2013). Boron deprivation immediately causes cell death in growing roots of *Arabidopsis thaliana* (L.) Heynh. *Soil Sci. Plant Nutr.* 59, 621–627. doi: 10.1080/00380768.2013.813382

Ordenes, V. R., Moreno, I., Maturana, D., Norambuena, L., Trewavas, A. J., and Orellana, A. (2012). In vivo analysis of the calcium signature in the plant Golgi apparatus reveals unique dynamics. *Cell Calcium* 52, 397–404. doi: 10.1016/j.ceca.2012.06.008

Orvar, B. L., Sangwan, V., Omann, F., and Dhindsa, R. S. (2000). Early steps in cold sensing by plant cells: the role of actin cytoskeleton and membrane fluidity. *Plant J.* 23, 785–794. doi: 10.1046/j.1365-313x.2000.00845.x

Pandey, N., Ranjan, A., Pant, P., Tripathi, R. K., Ateek, F., Pandey, H. P., et al. (2013). CAMTA 1 regulates drought responses in *Arabidopsis thaliana*. *BMC Genomics* 14:216. doi: 10.1186/1471-2164-14-216

Peiter, E., Maathuis, F. J. M., Mills, L. N., Knight, H., Pelloux, J., Hetherington, A. M., et al. (2005). The vacuolar Ca^{2+}-activated channel TPC1 regulates germination and stomatal movement. *Nature* 434, 404–408. doi: 10.1038/nature03381

Perfus-Barbeoch, L., Leonhardt, N., Vavasseur, A., and Forestier, C. (2002). Heavy metal toxicity: cadmium permeates through calcium channels and disturbs the plant water status. *Plant J.* 32, 539–548. doi: 10.1046/j.1365-313X.2002.01442.x

Petrov, V., Hille, J., Mueller-Roeber, B., and Gechev, T. S. (2015). ROS-mediated abiotic stress-induced programmed cell death in plants. *Front. Plant Sci.* 6:69. doi: 10.3389/fpls.2015.00069

Plieth, C., Hansen, U. P., Knight, H., and Knight, M. R. (1999). Temperature sensing by plants: the primary characteristics of signal perception and calcium response. *Plant J.* 18, 491–497. doi: 10.1046/j.1365-313X.1999.00471.x

Pottosin, I., Maria Velarde-Buendia, A., Bose, J., Fuglsang, A. T., and Shabala, S. (2014). Polyamines cause plasma membrane depolarization, activate Ca^{2+}-, and modulate H^+-ATPase pump activity in pea roots. *J. Expt. Bot.* 65, 2463–2472. doi: 10.1093/jxb/eru133

Probst, A. V., and Scheid, O. M. (2015). Stress-induced structural changes in plant chromatin. *Curr. Opin. Plant Biol.* 27, 8–16. doi: 10.1016/j.pbi.2015.05.011

Qin, W. S., Pappan, K., and Wang, X. M. (1997). Molecular heterogeneity of phospholipase D (PLD) – Cloning of PLD gamma and regulation of plant PLD gamma, -beta, and -alpha by polyphosphoinositides and calcium. *J. Biol. Chem.* 272, 28267–28273. doi: 10.1074/jbc.272.45.28267

Qiu, Q. S., Guo, Y., Quintero, F. J., Pardo, J. M., Schumaker, K. S., and Zhu, J. K. (2004). Regulation of vacuolar Na^+/H^+ exchange in *Arabidopsis thaliana* by the salt-overly-sensitive (SOS) pathway. *J. Biol. Chem.* 279, 207–215. doi: 10.1074/jbc.M307982200

Quiles-Pando, C., Rexach, J., Navarro-Gochicoa, M. T., Camacho-Cristóbal, J. J., Herrera-Rodríguez, M. B., and González-Fontes, A. (2013). Boron deficiency increases the level of cytosolic Ca^{2+} and expression of Ca^{2+}-related genes in *Arabidopsis thaliana* roots. *Plant Physiol. Biochem.* 65, 55–60. doi: 10.1016/j.plaphy.2013.01.004

Quintero, F. J., Martinez-Atienza, J., Villalta, I., Jiang, X., Kim, W. Y., Ali, Z., et al. (2011). Activation of the plasma membrane Na/H antiporter Salt-Overly-Sensitive 1 (SOS1) by phosphorylation of an auto-inhibitory C-terminal domain. *Proc. Natl. Acad. Sci. U.S.A.* 108, 2611–2616. doi: 10.1073/pnas.1018921108

Ragel, P., Rodenas, R., Garcia-Martin, E., Andres, Z., Villalta, I., Nieves-Cordones, M., et al. (2015). SOS the CBL-interacting protein kinase CIPK23 regulates HAK5-mediated high-affinity K^+ uptake in *Arabidopsis* roots. *Plant Physiol.* 169, 2863–2873. doi: 10.1104/pp.15.01401

Richards, S. L., Wilkins, K. A., Swarbreck, S. M., Anderson, A., Habib, N., McAinsh, M., et al. (2015). The hydroxyl radical; from seed to seed. *J. Expt. Bot.* 66, 37–46. doi: 10.1093/jxb/eru398

Richter, G. L., Monshausen, G. B., Krol, A., and Gilroy, S. (2009). Mechanical stimuli modulate lateral root organogenesis. *Plant Physiol.* 151, 1855–1866. doi: 10.1104/pp.109.142448

Riveras, E., Alvarez, J. M., Vidal, E. A., Oses, C., Vega, A., and Gutierrez, R. A. (2015). The calcium ion is a second messenger in the nitrate signaling pathway of *Arabidopsis*. *Plant Physiol.* 169, 1397–1404. doi: 10.1104/pp.15.00961

Rodrigo-Moreno, A., Andres-Colas, N., Poschenrieder, C., Gunse, B., Penarrubia, L., and Shabala, S. (2013). Calcium- and potassium-permeable plasma membrane transporters are activated by copper in *Arabidopsis* root tips: linking copper transport with cytosolic hydroxyl radical production. *Plant Cell Environ.* 36, 844–855. doi: 10.1111/pce.12020

Rodriguez-Hernandez, M. C., Bonifas, I., Alfaro-De la Torre, M. C., Flores-Flores, J. I., Bañuelos-Hernández, B., and Patiño-Rodríguez, O. (2015). Increased accumulation of cadmium and lead under Ca and Fe deficiency in *Typha latifolia*: a case study of two pore channel (TPC1) gene. *Environ. Exp. Bot.* 115, 38–48. doi: 10.1016/j.envexpbot.2015.02.009

Roy, S. J., Gilliham, M., Berger, B., Essah, P. A., Cheffings, C., Miller, A. J., et al. (2008). Investigating glutamate receptor-like gene co-expression in *Arabidopsis thaliana*. *Plant Cell Environ.* 31, 861–871. doi: 10.1111/j.1365-3040.2008.01801.x

Ruberti, C., Kim, S. J., Stefano, G., and Brandizzi, F. (2015). Unfolded protein responses in plants: one master, many questions. *Curr. Opin. Plant Biol.* 27, 59–66. doi: 10.1016/j.pbi.2015.05.016

Ruelland, E., Kravets, V., Derevyanchuk, M., Martinec, J., Zachowski, A., and Pokotylo, I. (2015). Role of phospholipid signalling in plant environmental responses. *Environ. Exp. Bot.* 114, 129143. doi: 10.1016/j.envexpbot.2014.08.009

Sagor, G. H. M., Chawla, P., Kim, D. W., Berberich, T., Kojima, S., Niitsu, M., et al. (2015). The polyamine spermine induces the unfolded protein response via the MAPK cascade in *Arabidopsis*. *Front. Plant Sci.* 6:687. doi: 10.3389/fpls.2015.00687

Sani, E., Herzyk, P., Perrella, G., Colot, V., and Amtmann, A. (2013). Hyperosmotic priming of *Arabidopsis* seedlings establishes a long-term somatic memory accompanied by specific changes of the epigenome. *Genome Biol.* 14, R59. doi: 10.1186/gb-2013-14-6-r59

Sarwat, M., and Naqvi, A. R. (2013). Heterologous expression of rice calnexin (OsCNX) confers drought tolerance. *Mol. Biol. Rep.* 40, 5451–5464. doi: 10.1007/s11033-013-2643-y

Shabala, S., and Pottosin, I. (2014). Regulation of potassium transport in plants under hostile conditions: implications for abiotic and biotic stress tolerance. *Physiol. Plant* 151, 257–279. doi: 10.1111/ppl.12165

Shabala, S., Shabala, L., Barcelo, J., and Poschenrieder, C. (2014). Membrane transporters mediating root signalling and adaptive responses to oxygen deprivation and soil flooding. *Plant Cell Environ.* 37, 2216–2233. doi: 10.1111/pce.12339

Shabala, S., Wu, H., and Bose, J. (2015). Salt stress sensing and early signalling in plant roots: current knowledge and hypothesis. *Plant Sci.* 241, 109–119. doi: 10.1016/j.plantsci.2015.10.003

Shi, Y. T., Ding, Y. L., and Yang, S. H. (2015). Cold signal transduction and its interplay with phytohormones during cold acclimation. *Plant Cell Physiol.* 56, 7–15. doi: 10.1093/pcp/pcu115

Shih, H. W., Depew, C. L., Miller, N. D., and Monshausen, G. B. (2015). The cyclic nucleotide-gated channel CNGC14 regulates root gravitropism in *Arabidopsis thaliana*. *Curr. Biol.* 25, 1–7. doi: 10.1016/j.cub.2015.10.025

Shih, H.-W., Miller, N. D., Dai, C., Spalding, E. P., and Monshausen, G. B. (2014). The receptor-like kinase FERONIA is required for mechanical signal transduction in *Arabidopsis* seedlings. *Curr. Biol.* 24, 1887–1892. doi: 10.1016/j.cub.2014.06.064

Shin, R., and Schachtman, D. P. (2004). Hydrogen peroxide mediates plant root cell response to nutrient deprivation. *Proc. Natl. Acad. Sci. U.S.A.* 101, 8827–8832. doi: 10.1073/pnas.0401707101

Shorrocks, V. M. (1997). The occurrence and correction of boron deficiency. *Plant Soil* 193, 121–148. doi: 10.1023/A:1004216126069

Singh, S., Parihar, P., Singh, R., Singh, V. P., and Prasad, S. M. (2016). Heavy metal tolerance in plants: role of transcriptomics, proteomics, metabolomics, and ionomics. *Front. Plant Sci.* 6:1143. doi: 10.3389/fpls.2015.01143

Stael, S., Wurzinger, B., Mair, A., Mehlmer, N., Vothknecht, U. C., and Teige, M. (2012). Plant organellar calcium signalling: an emerging field. *J. Expt. Bot.* 63, 1525–1542. doi: 10.1093/jxb/err394

Straltsova, D., Chykun, P., Subramaniam, S., Sosan, A., Kolbanov, D., Sokolik, A., et al. (2015). cation channels are involved in brassinosteroid signalling in higher plants. *Steroids* 97, 98–106. doi: 10.1016/j.steroids.2014.10.008

Sulaiman, Y., Knight, M. R., and Kataky, R. (2012). Non-invasive monitoring of temperature stress in *Arabidopsis thaliana* roots, using ion amperometry. *Anal. Meth.* 4, 1656–1661. doi: 10.1039/c2ay05747f

Sunkar, R., Kaplan, B., Bouche, N., Arazi, T., Dolev, D., Talke, I. N., et al. (2000). Expression of a truncated tobacco NtCBP4 channel in transgenic plants and disruption of the homologous *Arabidopsis* CNGC1 gene confer Pb^{2+} tolerance. *Plant J.* 24, 533–542. doi: 10.1046/j.1365-313x.2000.00901.x

Swarbreck, S. M., Colaço, R., and Davies, J. M. (2013). Update on plant calcium-permeable channels. *Plant Physiol.* 163, 1514–1522. doi: 10.1104/pp.113.220855

Tai, F., Yuan, Z., Li, S. P., Wang, Q., Liu, F., and Wang, W. (2016). ZmCIPK8, a CBL-interacting protein kinase, regulates maize response to drought stress. *Plant Cell Tiss. Org. Cul.* 124, 459–469. doi: 10.1007/s11240-015-0906-0

Teardo, E., Carraretto, L., De Bortoli, S., Costa, A., Behera, S., and Wagner, R. (2015). Alternative splicing-mediated targeting of the *Arabidopsis* GLUTAMATE RECEPTOR3.5 to mitochondria affects organelle morphology. *Plant Physiol.* 167, 216–227. doi: 10.1104/pp.114.242602

Thion, L., Mazars, C., Nacry, P., Bouchez, D., Moreau, M., Ranjeva, R., et al. (1998). Plasma membrane depolarization-activated calcium channels, stimulated by microtubule-depolymerizing drugs in wild-type *Arabidopsis thaliana* protoplasts, display constitutively large activities and a longer half-life in ton 2 mutant cells affected in the organization of cortical microtubules. *Plant J.* 13, 603–610.

Thoday-Kennedy, E. L., Jacobs, A. J., and Roy, S. J. (2015). The role of the CBL-CIPK calcium signalling network in regulating ion transport in response to abiotic stress. *Plant Growth Regul.* 76, 3–12. doi: 10.1007/s10725-015-0034-1

Toyota, M., and Gilroy, S. (2013). Gravitropism and mechanical signalling in plants. *Am. J. Bot.* 100, 111–125. doi: 10.3732/ajb.1200408

Tracy, F. E., Gilliham, M., Dodd, A. N., Webb, A. A. R., and Tester, M. (2008). NaCl-induced changes in cytosolic free Ca^{2+} in *Arabidopsis thaliana* are heterogeneous and modified by external ionic composition. *Plant Cell Environ.* 31, 1063–1073. doi: 10.1111/j.1365-3040.2008.01817.x

Véry, A. A., and Davies, J. M. (2000). Hyperpolarization-activated calcium channels at the tip of *Arabidopsis* root hairs. *Proc. Natl. Acad. Sci. U.S.A.* 97, 9801–9806. doi: 10.1073/pnas.160250397

Villiers, F., Jourdain, A., Bastien, O., Leonhardt, N., Fujioka, S., Tichtincky, G., et al. (2012). Evidence for functional interaction between brassinosteroids and cadmium response in *Arabidopsis thaliana*. *J. Expt. Bot.* 63, 1185–1200. doi: 10.1093/jxb/err335

Virdi, A. S., Singh, S., and Singh, P. (2015). Abiotic stress responses in plants: roles of calmodulin-regulated proteins. *Front. Plant Sci.* 6:809. doi: 10.3389/fpls.2015.00809

Virolainen, E., Blokhina, O., and Fagerstedt, K. (2002). Ca^{2+}-induced high amplitude swelling and cytochrome c release from wheat (*Triticum aestivum* L.) mitochondria under anoxic stress. *Ann. Bot.* 90, 509–516. doi: 10.1093/aob/mcf221

Wagner, S., Behera, S., De Bortoli, S., Logan, D. C., Fuchs, P., and Carraretto, L. (2015). The EF-Hand Ca^{2+}-binding protein MICU choreographs mitochondrial Ca^{2+} dynamics in *Arabidopsis*. *Plant Cell* 27, 3190–3212. doi: 10.1105/tpc.15.00509

Wan, S., and Jiang, L. (2016). Endoplasmic reticulum (ER) stress and the unfolded protein response (UPR) in plants. *Protoplasma* 273, 753–764. doi: 10.1007/s00709-015-0842-1

Wang, F. F., Chen, Z. H., Liu, X. H., Colmer, T. D., Zhou, M. X., and Shabala, S. (2016). Tissue-specific root ion profiling reveals essential roles of the CAX and ACA calcium transport systems in response to hypoxia in *Arabidopsis*. *J. Expt. Bot.* 67, 3747–3762. doi: 10.1093/jxb/erw034

Wang, P., Li, Z. W., Wei, J. S., Zhao, Z. L., Sun, D. Y., and Cui, S. J. (2012). A Na^{+}/Ca^{2+} exchanger-like protein (AtNCL) involved in salt stress in *Arabidopsis*. *J. Biol. Chem.* 287, 44062–44070. doi: 10.1074/jbc.M112.351643

Weiland, M., Mancuso, S., and Baluska, F. (2016). Signalling via glutamate and GLRs in *Arabidopsis thaliana*. *Funct. Plant Biol.* 43, 1–25.

Whalley, H. J., and Knight, M. R. (2013). Calcium signatures are decoded by plants to give specific gene responses. *New Phytol.* 197, 690–693. doi: 10.1111/nph.12087

Whalley, H. J., Sargeant, A. W., Steele, J. F., Lacoere, T., Lamb, R., Saunders, N. J., et al. (2011). Transcriptomic analysis reveals calcium regulation of specific promoter motifs in *Arabidopsis*. *Plant Cell* 23, 4079–4095. doi: 10.1105/tpc.111.090480

White, P. J. (2009). Depolarization-activated calcium channels shape the calcium signatures induced by low-temperature stress. *New Phytol.* 183, 7–8. doi: 10.1111/j.1469-8137.2009.02857.x

Wigge, P. A. (2013). Ambient temperature signalling in plants. *Curr. Opn. Plant Biol.* 16, 661–666. doi: 10.1016/j.pbi.2013.08.004

Wu, J. Y., Jin, C., Qu, H. Y., Tao, S. T., Xu, G. H., Wu, J., et al. (2012). Low temperature inhibits pollen viability by alteration of actin cytoskeleton and regulation of pollen plasma membrane ion channels in *Pyrus pyrifolia*. *Environ. Expt. Bot.* 78, 70–75. doi: 10.1016/j.envexpbot.2011.12.021

Xu, Q. T., Fan, H. Y., Jiang, Z., Zhou, Z. Q., Yang, L., Mei, F. Z., et al. (2013). Cell wall degradation and the dynamic changes of Ca^{2+} and related enzymes in the developing aerenchyma of wheat (*Triticum aestivum* L.) under waterlogging. *Acta Biol. Hung.* 64, 328–340. doi: 10.1556/ABiol.64.2013.3.6

Yamada, N., Theerawitaya, C., Ca-Um, S., Kirdmanee, C., and Takabe, T. (2014). Expression and functional analysis of putative vacuolar Ca^{2+}-transporters (CAXs and ACAs) in roots of salt tolerant and sensitive rice cultivars. *Protoplasma* 251, 1067–1075. doi: 10.1007/s00709-014-0615-2

Yamauchi, T., Watanabe, K., Fukazawa, A., Mori, H., Abe, F., Kawaguchi, K., et al. (2014). Ethylene and reactive oxygen species are involved in root aerenchyma formation and adaptation of wheat seedlings to oxygen-deficient conditions. *J. Expt. Bot.* 65, 261–273. doi: 10.1093/jxb/ert371

Yang, C.-Y., and Hong, C.-P. (2015). The NADPH oxidase RbohD is involved in primary hypoxia signalling and modulates expression of hypoxia-inducible genes under hypoxic stress. *Env. Expt. Bot.* 115, 63–72. doi: 10.1016/j.envexpbot.2015.02.008

Yang, T. B., Chaudhuri, S., Yang, L. H., Du, L. Q., and Poovaiah, B. W. (2010). A calcium/calmodulin-regulated member of the receptor-like kinase family confers cold tolerance in plants. *J. Biol. Chem.* 285, 7119–7126. doi: 10.1074/jbc.M109.035659

Yeh, C. M., Chien, P. S., and Huang, H. J. (2007). Distinct signalling pathways for induction of MAP kinase activities by cadmium and copper in rice roots. *J. Expt. Bot.* 58, 659–671. doi: 10.1093/jxb/erl240

Yemelyanov, V. V., Shishova, M. F., Chirkova, T. V., and Lindberg, S. M. (2011). Anoxia-induced elevation of cytosolic Ca^{2+} concentration depends on

different Ca^{2+} sources in rice and wheat protoplasts. *Planta* 234, 271–280. doi: 10.1007/s00425-011-1396-x

Yu, H. Q., Yong, T. M., Li, H. J., Liu, Y. P., Zhou, S. F., Fu, F. L., et al. (2015). Overexpression of a phospholipase D alpha gene from *Ammopiptanthus nanus* enhances salt tolerance of phospholipase D alpha 1-deficient *Arabidopsis* mutant. *Planta* 242, 1495–1509. doi: 10.1007/s00425-015-2390-5

Yu, L. J., Nie, J. N., Cao, C. Y., Jin, Y. K., Yan, M., Wang, F. Z., et al. (2010). Phosphatidic acid mediates salt stress response by regulation of MPK6 in *Arabidopsis thaliana*. *New Phytol.* 188, 762–773. doi: 10.1111/j.1469-8137.2010.03422.x

Yu, Y. Q., and Assmann, S. M. (2015). The heterotrimeric G-protein beta subunit, AGB1, plays multiple roles in the Arabidopsis salinity response. *Plant Cell Environ.* 38, 2143–2156. doi: 10.1111/pce.12542

Yuan, F., Yang, H., Xue, Y., Kong, D., Ye, R., Li, C., et al. (2014). OSCA1 mediates osmotic-stress-evoked Ca^{2+} increases vital for osmosensing in *Arabidopsis*. *Nature* 514, 367–371. doi: 10.1038/nature13593

Yuan, H.-M., and Huang, X. (2016). Inhibition of root meristem growth by cadmium involves nitric oxide-mediated repression of auxin accumulation and signalling in *Arabidopsis*. *Plant Cell Environ.* 39, 120–135. doi: 10.1111/pce.12597

Yuen, C. C. Y., and Christopher, D. A. (2013). The group IV-A cyclic nucleotide-gated channels, CNGC19 and CNGC 20, localize to the vacuole membrane in *Arabidopsis thaliana*. *AoB Plants* 5, plt012. doi: 10.1186/1471-2164-15-853

Zelinova, V., Alemayehu, A., Bocova, B., Huttova, J., and Tamas, L. (2015). Cadmium-induced reactive oxygen species generation, changes in morphogenic responses and activity of some enzymes in barley root tip are regulated by auxin. *Biologia* 70, 356–364. doi: 10.1515/biolog-2015-0035

Zeng, F., Konnerup, D., Shabala, L., Zhou, M., Colmer, T. D., Zhang, G., et al. (2014). Linking oxygen availability with membrane potential maintenance and K^+ retention of barley roots: implications for waterlogging stress tolerance. *Plant Cell Environ.* 37, 2325–2338. doi: 10.1111/pce.12422

Zeng, Q., Ling, Q., Fan, L., Li, Y., Hu, F., Chen, J., et al. (2015). Transcriptome profiling of sugarcane roots in response to potassium stress. *PLoS ONE* 10:e0126306. doi: 10.1371/journal.pone.0126306

Zepeda-Jazo, I., Maria Velarde-Buendia, A., Enriquez-Figueroa, R., Bose, J., Shabala, S., Muniz-Murguia, J., et al. (2011). Polyamines interact with hydroxyl radicals in activating Ca^{2+} and K^+ transport across the root epidermal plasma membranes. *Plant Physiol.* 157, 2167–2180. doi: 10.1016/j.plaphy.2012.09.002

Zhang, L., Chen, Z., and Zhu, C. (2012). Endogenous nitric oxide mediates alleviation of cadmium toxicity induced by calcium in rice seedlings. *J. Environ. Sci.* 24, 940–948. doi: 10.1016/S1001-0742(11)60978-9

Zhang, X., Shen, Z. D., Sun, J., Yu, Y. C., Deng, S. R., and Li, Z. Y. (2015). NaCl-elicited, vacuolar Ca^{2+} release facilitates prolonged cytosolic Ca^{2+} signaling in the salt response of *Populus euphratica* cells. *Cell Calcium* 57, 348–365. doi: 10.1016/j.ceca.2015.03.001

Zhang, Y., Wang, Y., Taylor, J. L., Jiang, Z., Zhang, S., Mei, F., et al. (2015). Aequorin-based luminescence imaging reveals differential calcium signalling responses to salt and reactive oxygen species in rice roots. *J. Expt. Bot.* 66, 2535–2545. doi: 10.1093/jxb/erv043

Zhao, M. G., Tian, Q. Y., and Zhang, W. H. (2007). Ethylene activates a plasma membrane Ca^{2+}-permeable channel in tobacco suspension cells. *New Phytol.* 174, 507–515. doi: 10.1111/j.1469-8137.2007.02037.x

Zhao, R., Sun, H. M., Zhao, N., Jing, X. S., Shen, X., and Chen, S. (2015). The *Arabidopsis* Ca^{2+}-dependent protein kinase CPK27 is required for plant response to salt-stress. *Gene* 563, 203–214. doi: 10.1016/j.gene.2015.03.024

Zhao, Y., Pan, Z., Zhang, Y., Qu, X. L., Zhang, Y. G., and Yang, Y. G. (2013). The Actin-Related Protein2/3 complex regulates mitochondrial-associated calcium signaling during salt stress in *Arabidopsis*. *Plant Cell* 25, 4544–4559. doi: 10.1105/tpc.113.117887

Zhu, S.-Y., Yu, X.-C., Wang, X.-J., Zhao, R., Li, Y., Fan, R.-C., et al. (2007). Two calcium-dependent protein kinases, CPK4 and CPK11, regulate abscisic acid signal transduction in *Arabidopsis*. *Plant Cell* 19, 3019–3036. doi: 10.1105/tpc.107.050666

Zhu, X. H., Feng, Y., Liang, G. M., Liu, N., and Zhu, J. K. (2013). Aequorin-based luminescence imaging reveals stimulus- and tissue-specific Ca^{2+} dynamics in *Arabidopsis* plants. *Mol. Plant* 6, 444–455. doi: 10.1093/mp/sst013

Conflict of Interest Statement: The authors declare that the research was conducted in the absence of any commercial or financial relationships that could be construed as a potential conflict of interest.

frontiers in Plant Science

ORIGINAL RESEARCH
published: 23 November 2016
doi: 10.3389/fpls.2016.01711

Accumulation and Secretion of Coumarinolignans and other Coumarins in *Arabidopsis thaliana* Roots in Response to Iron Deficiency at High pH

*Patricia Sisó-Terraza[1†], Adrián Luis-Villarroya[1†], Pierre Fourcroy[2‡], Jean-François Briat[2], Anunciación Abadía[1], Frédéric Gaymard[2], Javier Abadía[1] and Ana Álvarez-Fernández[1]**

[1] Plant Stress Physiology Group, Department of Plant Nutrition, Aula Dei Experimental Station, Consejo Superior de Investigaciones Científicas, Zaragoza, Spain, [2] Biochimie et Physiologie Moléculaire des Plantes, Centre National de la Recherche Scientifique, Institut National de la Recherche Agronomique, Université Montpellier, Montpellier, France

OPEN ACCESS

Edited by:
Janin Riedelsberger, University of Talca, Chile

Reviewed by:
Stefano Cesco, Free University of Bozen-Bolzano, Italy
Dierk Scheel, Leibniz Institute of Plant Biochemistry, Germany

***Correspondence:**
Ana Álvarez-Fernández
ana.alvarez@eead.csic.es

[†] These authors have contributed equally to this work.

[‡] This paper is dedicated to the Memory of Pierre Fourcroy, a CNRS researcher, to largely contributed to initiate this research.

Specialty section:
This article was submitted to Plant Physiology, a section of the journal Frontiers in Plant Science

Received: *29 July 2016*
Accepted: *31 October 2016*
Published: *23 November 2016*

Citation:
Sisó-Terraza P, Luis-Villarroya A, Fourcroy P, Briat J-F, Abadía A, Gaymard F, Abadía J and Álvarez-Fernández A (2016) Accumulation and Secretion of Coumarinolignans and other Coumarins in Arabidopsis thaliana Roots in Response to Iron Deficiency at High pH. Front. Plant Sci. 7:1711. doi: 10.3389/fpls.2016.01711

Root secretion of coumarin-phenolic type compounds has been recently shown to be related to *Arabidopsis thaliana* tolerance to Fe deficiency at high pH. Previous studies revealed the identity of a few simple coumarins occurring in roots and exudates of Fe-deficient *A. thaliana* plants, and left open the possible existence of other unknown phenolics. We used HPLC-UV/VIS/ESI-MS(TOF), HPLC/ESI-MS(ion trap) and HPLC/ESI-MS(Q-TOF) to characterize (identify and quantify) phenolic-type compounds accumulated in roots or secreted into the nutrient solution of *A. thaliana* plants in response to Fe deficiency. Plants grown with or without Fe and using nutrient solutions buffered at pH 5.5 or 7.5 enabled to identify an array of phenolics. These include several coumarinolignans not previously reported in *A. thaliana* (cleomiscosins A, B, C, and D and the 5′-hydroxycleomiscosins A and/or B), as well as some coumarin precursors (ferulic acid and coniferyl and sinapyl aldehydes), and previously reported cathecol (fraxetin) and non-cathecol coumarins (scopoletin, isofraxidin and fraxinol), some of them in hexoside forms not previously characterized. The production and secretion of phenolics were more intense when the plant accessibility to Fe was diminished and the plant Fe status deteriorated, as it occurs when plants are grown in the absence of Fe at pH 7.5. Aglycones and hexosides of the four coumarins were abundant in roots, whereas only the aglycone forms could be quantified in the nutrient solution. A comprehensive quantification of coumarins, first carried out in this study, revealed that the catechol coumarin fraxetin was predominant in exudates (but not in roots) of Fe-deficient *A. thaliana* plants grown at pH 7.5. Also, fraxetin was able to mobilize efficiently Fe from a Fe(III)-oxide at pH 5.5 and pH 7.5. On the other hand, non-catechol coumarins were much less efficient in mobilizing Fe and were present in much lower concentrations, making unlikely that they could play a role in Fe mobilization. The structural features of the array of coumarin type-compounds produced suggest some can mobilize Fe from the soil and others can be more efficient as allelochemicals.

Keywords: *Arabidopsis*, cleomiscosin, coumarin, fraxetin, iron nutrition, mass spectrometry, root secretion

INTRODUCTION

Iron (Fe) is required for many crucial biological processes, and is therefore essential for all living organisms. A sufficient supply of Fe is necessary for optimal plant productivity and agricultural produce quality (Briat et al., 2015). Iron is the fourth most abundant element in the earth's crust, but its availability for plants is influenced by pH and redox potential, as well as by the concentration of water-soluble Fe-complexes and the solubility of Fe(III)-oxides and oxyhydroxides (Lindsay, 1995). In calcareous soils, which cover more than 30% of the earth surface, the high soil pH and low soil organic matter content lead to Fe concentrations in the bulk soil solution far below those required for the optimal growth of plants and microbes (10^{-4}–10^{-9} and 10^{-5}–10^{-7} M, respectively; Guerinot and Ying, 1994). Since plants and microbiota have evolved in soils poor in available Fe, they have active mechanisms for Fe acquisition, often relying on the synthesis and secretion of an array of chemicals that modify the neighboring environment and reduce competition for Fe (Crumbliss and Harrington, 2009; Jin et al., 2014; Mimmo et al., 2014; Aznar et al., 2015). Some of these chemicals are capable to mine Fe from the soil *via* solubilization, chelation and reduction processes, whereas others can serve as repellants and/or attractants that inhibit or promote the growth of concomitant organisms.

In plants, two different Fe uptake mechanisms have been characterized (Kobayashi and Nishizawa, 2012). *Graminaceae* species use a chelation-type strategy (Strategy II) based on the synthesis of phytosiderophores (PS), metal-chelating substances of the mugineic acid family: PS are released by roots *via* specific transporters, mine Fe(III) from the soil by forming Fe(III)-PS complexes, and then complexes are taken up by transporters of the Yellow Stripe family. Non-graminaceous species such as *Arabidopsis thaliana* use a reduction-type strategy (Strategy I), based on the reduction of rhizospheric Fe(III) by a Fe(III) chelate reductase (FRO, ferric reduction oxidase) and the uptake of Fe(II) by root plasma membrane transporters (IRT, iron-regulated transporter). Other items of the Strategy I toolbox are an enhanced H^+-ATPase activity, an increased development of root hairs and transfer cells and the synthesis and secretion into the rhizosphere of a wide array of small molecules, including flavins, phenolic compounds and carboxylates (Cesco et al., 2010; Mimmo et al., 2014). Recent studies have unveiled direct roles in root Fe acquisition for flavin secretion in *Beta vulgaris* (Sisó-Terraza et al., 2016) and phenolics secretion in *Trifolium pratense* (Jin et al., 2006, 2007) and *A. thaliana* (Rodríguez-Celma et al., 2013; Fourcroy et al., 2014, 2016; Schmid et al., 2014; Schmidt et al., 2014).

The phenolic compounds category, including *ca.* 10,000 individual compounds in plants (Croteau et al., 2000), has been long considered to be one of the major components of the cocktail of small molecules secreted by roots of Fe-deficient plants (Cesco et al., 2010). In particular, the coumarin compounds class (O-containing heterocycles with a benzopyrone backbone; **Figure 1A**), which includes at least 1,300 compounds in plants (Borges et al., 2005) has been the focus of recent studies with *A. thaliana*. Upon Fe deficiency, there is a transcriptional up-regulation in roots both of the central phenylpropanoid pathway (from phenylalanine ammonia lyase, one of the upstream enzymes in the pathway, to the coumarate:CoA ligases 4CL1 and 4CL2 that mediate its last step) and of a crucial step of a phenylpropanoid biosynthetic branch, the 2-oxoglutarate-dependent dioxygenase enzyme feruloyl-CoA 6′-hydroxylase1 (F6′H1) (García et al., 2010; Yang et al., 2010; Lan et al., 2011; Rodríguez-Celma et al., 2013; Fourcroy et al., 2014; Schmid et al., 2014; Schmidt et al., 2014), which is responsible for the synthesis of the highly fluorescent coumarin scopoletin (Kai et al., 2008). Up to now, a total of five coumarins, esculetin, fraxetin, scopoletin, isofraxidin and an isofraxidin isomer have been described in Fe-deficient *A. thaliana* roots in both glycoside and aglycone forms (**Figure 1A**, Supplementary Table S1; Fourcroy et al., 2014; Schmid et al., 2014; Schmidt et al., 2014).

Root exudates from Fe-deficient *A. thaliana* plants contain the same coumarins that are found in root extracts, with the aglycone forms being more prevalent (Supplementary Table S1; Fourcroy et al., 2014; Schmid et al., 2014; Schmidt et al., 2014). These exudates have been shown to solubilize 17-fold more Fe from an Fe(III)-oxide (at pH 7.2) when compared to exudates from Fe-sufficient plants, and this was ascribed to the formation of Fe(III)-catechol complexes (Schmid et al., 2014). It is noteworthy that the catechol moiety in two of the five coumarins found to increase with Fe deficiency (esculetin and fraxetin) confers affinity for Fe(III) at high pH and therefore capability for Fe(III) chelation in alkaline soils. In the remaining three coumarins found so far (scopoletin, isofraxidin and its isomer), the catechol moiety is capped *via* hydroxyl (-OH) group methylation (**Figure 1A**), whereas in the glycoside forms of esculetin (esculetin 6-*O*-glucoside, known as esculin) and fraxetin (fraxetin 8-*O*-glucoside, known as fraxin) the catechol is capped *via* hydroxyl group glycosylation (**Figure 1A**). When coumarin synthesis is impaired, as in the *A. thaliana f6′h1* mutant, plants are unable to take up Fe from insoluble Fe sources at high pH (Rodríguez-Celma et al., 2013; Schmid et al., 2014; Schmidt et al., 2014), root exudates are unable to solubilize Fe from insoluble Fe sources, and supplementation of the agarose growth media with scopoletin, esculetin or esculin restores the Fe-sufficient phenotype (Schmid et al., 2014). However, in *in vitro* tests only esculetin (with a catechol moiety), was found to mobilize Fe(III) from an Fe(III) oxide source at high pH (Schmid et al., 2014).

The secretion of coumarins by Fe-deficient roots involves an ABC (ATP-binding cassette) transporter, ABCG37/PDR9, which is strongly over-expressed in plants grown in media deprived of Fe (Yang et al., 2010; Fourcroy et al., 2014, 2016) or containing insoluble Fe(III) at high pH (Rodríguez-Celma et al., 2013). The export of scopoletin, fraxetin, isofraxidin, and an isofraxidin isomer was greatly impaired in the mutant *abcg37* (Fourcroy et al., 2014), which, as it occurs with *f6′h1*, is inefficient in taking up Fe from insoluble Fe(III) at pH 7.0 (Rodríguez-Celma et al., 2013). The root secretion of fluorescent phenolic compounds in *A. thaliana* also requires the Fe deficiency-inducible β-glucosidase BGLU42 (Zamioudis et al., 2014). On the other hand, the IRT1/FRO2 high-affinity root Fe uptake system is necessary for the plant to take up Fe once mobilized, since *irt1* and *fro2* plants grown with unavailable Fe and in presence

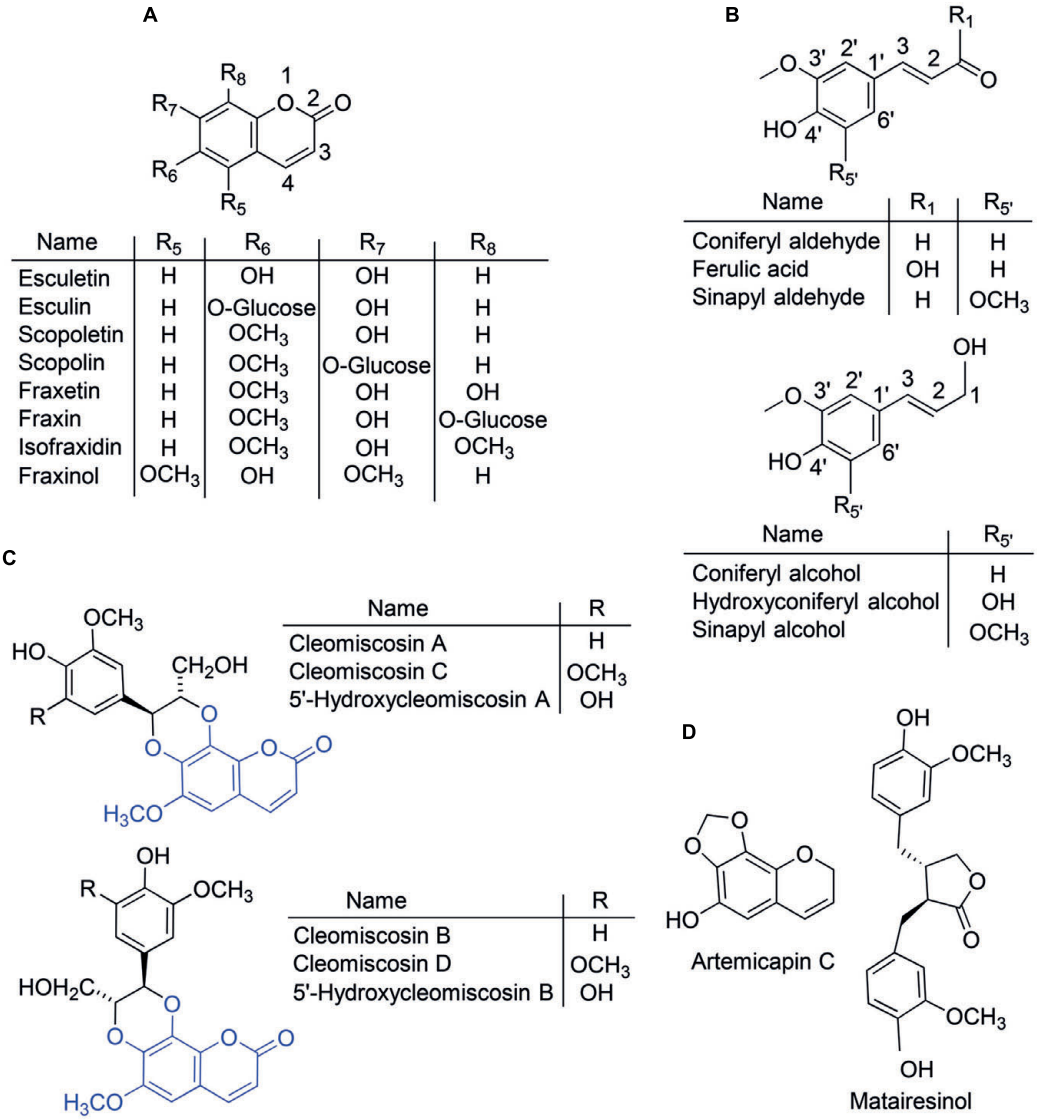

FIGURE 1 | Chemical structures of some of the phenolic compounds cited in this study. The plant compounds include coumarins and their glucosides **(A)**, coumarin precursors and monolignols **(B)** and coumarinolignans derived from the coumarin fraxetin **(C)**. The fraxetin moiety is highlighted in blue in the coumarinolignan structures. Compounds used as internal standards **(D)** include a methylenedioxy-coumarin and a lignan.

of phenolics develop chlorosis (Fourcroy et al., 2016). The co-regulation of *ABCG37* and coumarin synthesis genes with *FIT*, *IRT1*, *FRO2* and *AHA2* (Rodríguez-Celma et al., 2013) as well as the requirement of *FIT* for *F6'H1* up-regulation upon Fe deficiency (Schmid et al., 2014) support that all these components act in a coordinated mode.

Limitations inherent to the analytical procedures used and/or difficulties in compound structure elucidation have prevented the full characterization of the changes in coumarin composition promoted by Fe deficiency. First, HPLC coupled to fluorescence detection and mass spectrometry (MS and MS^n) identification was used, therefore focusing only on fluorescent coumarin compounds changing in response to Fe deficiency (Fourcroy et al., 2014); a similar approach was taken later on by Schmid et al. (2014). In a second approach, the use of full chromatographic MS profiles permitted the detection of dozens of compounds changing with Fe deficiency, but only the same coumarins already found with the fluorescence detection approach could be identified (Schmidt et al., 2014).

The aim of this study was to gain insight into the phenolic composition of *A. thaliana* root exudates in response to Fe deficiency, a necessary step for a thorough understanding of the function of phenolics in plant Fe acquisition. Root extracts and exudates from Fe-sufficient and Fe-deficient *A. thaliana* plants grown at pH 5.5 and 7.5 have been analyzed by HPLC coupled to five different detectors: fluorescence, photodiode array, MS-time of flight (TOF), MS-ion trap and MS-MS tandem quadrupole (Q)-TOF, and identification and quantification of phenolics was

carried out in roots and exudates. Up to now, quantification of coumarins in roots and exudates from Fe-deficient *A. thaliana* plants had been done only for the two fluorescent compounds esculetin and scopoletin (Schmid et al., 2014). We report herein the identification and quantification of coumarinolignans, coumarin precursors and additional coumarin glycosides, among an array of phenolics accumulated and/or secreted by *A. thaliana* roots in response to Fe deficiency. The root accumulation and secretion of coumarins and coumarinolignans was much higher in plants grown at pH 7.5 than those grown at pH 5.5, and the catechol coumarin fraxetin was predominant in nutrient solutions but not in root extracts. These findings demonstrate the inherent chemical complexity involved in the survival of *A. thaliana* in conditions of high competition for Fe, and give clues for the possible roles of some of the phenolic compounds found.

MATERIALS AND METHODS

Plant Culture and Experimental Design

Arabidopsis thaliana (L.) Heynh (ecotype Col0) seeds were germinated, pre-grown and grown as indicated in Fourcroy et al. (2014) with several modifications. Germination and plant growth took place in a controlled environment chamber (Fitoclima 10000 EHHF, Aralab, Albarraque, Portugal), at 21°C, 70% relative humidity and a photosynthetic photon flux density of 220 μmol m^{-2} s^{-1} photosynthetic active radiation with a photoperiod of 8 h light/16 h dark. Seeds were sown in 0.2 ml tubes containing 0.6% agar prepared in nutrient solution 1/4 Hoagland, pH 5.5. Iron was added as 45 μM Fe(III)-EDTA. After 10 d in the growth chamber, the bottom of the tubes containing seedlings was cut off and the tubes were placed in opaque 300-ml plastic boxes (pipette tip racks; Starlab, Hamburg, Germany), containing aerated nutrient solution 1/2 Hoagland, pH 5.5, supplemented with 20 μM Fe(III)-EDTA. Plants were grown for 11 d and nutrient solutions were renewed weekly. After that, plants (12 plants per rack) were grown for 14 days in nutrient solution 1/2 Hoagland with 0 or 20 μM Fe(III)-ethylendiaminedi(*o*-hydroxyphenylacetate) [Fe(III)-EDDHA; Sequestrene, Syngenta, Madrid, Spain]. Solutions were buffered at pH 5.5 (with 5 mM MES) or at 7.5 (with 5 mM HEPES) to maintain a stable pH during the whole treatment period. Nutrient solutions were renewed weekly. Two batches of plants were grown and analyzed. Pots without plants, containing only aerated nutrient solution (with and without Fe) were also placed in the growth chamber and the nutrient solutions sampled as in pots containing plants; these samples were later used as blanks for root exudate analyses.

Roots were sampled 3 days after the onset of Fe deficiency treatment, immediately frozen in liquid N_2, and stored at −80°C for RNA extraction. Nutrient solutions were sampled at days 7 and 14 after the onset of Fe deficiency treatment, and immediately stored at −20°C until extraction of phenolic compounds. Shoots and roots were sampled separately at the end of the experimental period. Leaf disks (0.1 cm × 0.1 cm) were taken from young leaves and stored at −20°C for photosynthetic pigment analysis. Roots were washed with tap water and then with type I water, dried with filter paper, and then frozen immediately (in aliquots of approximately 300 mg) in liquid N_2 and stored at −80°C until extraction of phenolic compounds. Roots and shoots from 12 plants per treatment and replication were processed for mineral analysis as in Fourcroy et al. (2014).

Photosynthetic Pigment Composition

Leaf pigments were extracted with acetone in the presence of Na ascorbate and stored as described previously (Abadía and Abadía, 1993). Pigment extracts were thawed on ice, filtered through a 0.45 μm filter and analyzed by HPLC-UV/visible as indicated in Larbi et al. (2004), using a HPLC apparatus (600 pump, Waters, Mildford, MA, USA) fitted with a photodiode array detector (996 PDA, Waters). Pigments determined were total chlorophyll (*Chl a* and *Chl b*), neoxanthin, violaxanthin, taraxanthin, antheraxanthin, lutein, zeaxanthin and β-carotene. All chemicals used were HPLC quality.

Mineral Analysis

Plant tissues were ground and digested as indicated in Fourcroy et al. (2014). Iron, Mn, Cu, and Zn were determined by flame atomic absorption spectrometry using a SOLAAR 969 apparatus (Thermo, Cambridge, UK).

Extraction of Phenolic Compounds from Roots and Nutrient Solutions

Phenolic compounds were extracted from roots and nutrient solutions as described in Fourcroy et al. (2014), with some modifications. First, extraction was carried out without adding internal standards (IS) to identify relevant compounds, including those increasing (or appearing) with Fe deficiency. This extract was also used to check for the presence of the compounds used as IS and other endogenous isobaric compounds that may co-elute with them, since in both cases there will be analytical interferences in the quantification process. The extraction was then carried out adding the following three IS compounds: artemicapin C (**Figure 1D**), a methylenedioxy-coumarin, for quantification of the coumarins scopoletin, fraxetin, isofraxidin and fraxinol; esculin (**Figure 1A**), the glucoside form of the coumarin esculetin, for quantification of coumarin glycosides; and the lignan matairesinol (**Figure 1D**), for quantification of coumarinolignans.

Frozen roots (*ca.* 100 mg) were ground in liquid N_2 using a Retsch M301 ball mill (Restch, Düsseldorf, Germany) for 3 min and then phenolic compounds were extracted with 1 ml of 100% LC-MS grade methanol, either alone or supplemented with 20 μl of a IS solution (37.5 μM artemicapin C, 50 μM esculin and 37.5 μM matairesinol) by homogenization in the same mill for 5 min. The supernatant was recovered by centrifugation (12,000 × *g* at 4°C and 5 min), and stored at −20°C. The pellet was re-suspended in 1 ml of 100% methanol, homogenized again for 5 min and the supernatant recovered. The two supernatant fractions were pooled, vacuum dried in a SpeedVac (SPD111V, Thermo-Savant, Thermo Fisher Scientific, Waltham, Massachusetts, MA, USA) and dissolved with 250 μl of a solution containing 15% methanol and 0.1% formic acid. Extracts

were filtered through poly-vinylidene fluoride (PVDF) 0.45 μm ultrafree-MC centrifugal filter devices (Millipore) and stored at −80°C until analysis.

Phenolic compounds in the nutrient solutions (300 ml of solution used for the growth of 12 plants) were retained in a SepPack C_{18} cartridge (Waters), eluted from the cartridge with 2 ml of 100% LC-MS grade methanol, and the eluates stored at −80°C. Samples were thawed and a 400 μl aliquot was dried under vacuum (SpeedVac) alone or supplemented with 10 μl of a IS solution (80 μM artemicapin C and 150 μM matairesinol). Dried samples were dissolved in 15% methanol and 0.1% formic acid to a final volume of 100 μl, and then analyzed by HPLC-MS. No determinations could be made in nutrient solutions of Fe-sufficient plants due to the presence of Fe(III)-EDDHA, that causes the overloading of C_{18} materials.

Extraction of Cleomiscosins from *Cleome viscosa* Seeds

Cleomiscosins were extracted from *Cleome viscosa* seeds (B & T World Seeds, Paguignan, France) as described by Chattopadhyay et al. (2008). Seeds were ground using a Retsch M400 ball mill and 25 g of the powder was defatted by homogenization with 50 ml petroleum ether at 25°C for 48 h. The defatting procedure was repeated three times. The solid residue was extracted with 50 ml methanol for 48 h at 25°C, and the extraction was repeated three times. The methanolic extracts were pooled, dried with a rotavapor device and the residue dissolved in 15% methanol and 0.1% formic acid.

Phenolic Compounds Analysis by HPLC-Fluorescence and HPLC-UV/VIS/ESI-MS(TOF)

HPLC-fluorescence analyses were carried out using a binary HPLC pump (Waters 125) coupled to a scanning fluorescence detector (Waters 474) as in Fourcroy et al. (2014). Separations were performed using an analytical HPLC column (Symmetry® C_{18}, 15 cm × 2.1 mm i.d., 5 μm spherical particle size, Waters) protected by a guard column (Symmetry® C_{18}, 10 mm × 2.1 mm i.d., 3.5 μm spherical particle size, Waters) and a gradient mobile phase built with 0.1% (v/v) formic acid in water and 0.1% (v/v) formic acid in methanol (Elution program 1; Supplementary Table S2). The flow rate and injection volume were 0.2 ml min^{-1} and 20 μl, respectively. Phenolic compounds were detected using λ_{exc} 365 and λ_{em} 460 nm.

HPLC-UV/VIS/ESI-MS(TOF) analysis was carried out with an Alliance 2795 HPLC system (Waters) coupled to a UV/VIS (Waters PDA 2996) detector and a time-of-flight mass spectrometer [MS(TOF); MicrOTOF, Bruker Daltonics, Bremen, Germany] equipped with an electrospray (ESI) source. Two HPLC protocols were used, the one described above and a second one with a different elution program (Elution program 2; Supplementary Table S2) designed to improve the separation of the phenolic compounds of interest. The ESI-MS(TOF) operating conditions and software used were as described in Fourcroy et al. (2014). Mass spectra were acquired in positive and negative ion mode in the range of 50–1000 mass-to-charge ratio (*m/z*) units. The mass axis was calibrated externally and internally using Li-formate adducts [10 mM LiOH, 0.2% (v/v) formic acid and 50% (v/v) 2-propanol]. The internal mass axis calibration was carried out by introducing the calibration solution with a divert valve at the first and last 3 min of each HPLC run. Molecular formulae were assigned based on exact molecular mass with errors <5 ppm (Bristow, 2006). Phenolic standards used are shown in Supplementary Table S3. Concentrations of phenolic compounds were quantified using external calibration with internal standardization with the exception of ferulic acid hexoside and the cleomiscosins. Ferulic acid hexoside was quantified as fraxin because there is no commercially available authenticated standard. The levels of the cleomiscosins are expressed in peak area ratio, relative to the lignan matairesinol used as IS. For quantification, analytes and IS peak areas were obtained from chromatograms extracted at the *m/z* (±0.05) ratios corresponding to $[M+H]^+$ ions, with the exception of glycosides, where the *m/z* ratios corresponding to $[M\text{-hexose}+H]^+$ ions were used.

Phenolic Compounds Analysis by HPLC/ESI-MS(Q-TOF) and by HPLC/ESI-MS(Ion Trap)

Phenolic compounds were also analyzed by HPLC/ESI-MS(Q-TOF) using a 1100 HPLC system (Agilent Technologies) coupled to a quadrupole time-of-flight mass spectrometer (Q-TOF; MicroTOF-Q, Bruker Daltonics) equipped with an ESI source. The HPLC conditions were described in Fourcroy et al. (2014) (see above and Supplementary Table S2). The ESI-MS(Q-TOF) operating conditions were optimized by direct injection of 50 μM solutions of phenolic compound standards at a flow rate of 250 μl h^{-1}. Mass spectra (50–1000 *m/z* range) were acquired in positive ion mode, with capillary and endplate offset voltages of 4.5 and −0.5 kV, respectively, and a collision cell energy of 100–2000 eV. The nebulizer (N_2) gas pressure, drying gas (N_2) flow rate and drying gas temperature were 1.0 bar, 4.0 L min^{-1} and 200°C, respectively. The mass axis was calibrated externally and internally as indicated above for the HPLC/ESI-MS(TOF) analysis. Molecular formulae for the product ions were assigned based on exact molecular mass with errors <5 ppm (Bristow, 2006).

HPLC/ESI-MS(ion trap) analysis was carried out with an Alliance 2795 HPLC system (Waters) coupled to an ion-trap mass spectrometer (HCT Ultra, BrukerDaltonics) equipped with an ESI source. The HPLC conditions were as described in Fourcroy et al. (2014) and Supplementary Table S2 (Elution program 2). ESI-ion trap-MS analysis was carried out in positive and/or negative ion mode, the MS spectra were acquired in the standard mass range mode and the mass axis was externally calibrated with a tuning mix (Agilent). The HCT Ultra was operated with settings shown in Supplementary Table S4. The ions of interest were subjected to collision induced dissociation (CID; using the He background gas present in the trap for 40 ms) to produce a first set of fragment ions, MS/MS or MS^2. Subsequently, some of the fragment ions were isolated and fragmented to give the next set of fragment ions, MS^3 and so on. For each precursor

ion, fragmentation steps were optimized by visualizing fragment intensity changes.

RNA Extraction and Quantitative RT-PCR Analysis

Total RNA was extracted from roots using the RNeasy Plant Mini Kit (Quiagen). One microgram RNA was treated with RQ1 DNase (Promega) before use for reverse transcription (Goscript reverse transcriptase; Promega) with oligo (dT)18 and 0.4 mM dNTPs (Promega). The cDNAs were diluted twice with water, and 1 μl of each cDNA sample was assayed by qRT-PCR in a LightCycler 480 (Roche Applied Science) using Lightcycler 480 SYBR Green master I (Roche Applied Science). Expression levels were calculated relative to the housekeeping gene PP2 (At1g13320) using the ΔΔCT method to determine the relative transcript level. The primers used for qRT-PCR were those described in Fourcroy et al. (2014) and indicated in Supplementary Table S5.

Dissolution of Fe(III)-oxide Using Coumarins

Ten milligrams of poorly crystalline Fe(III)-oxide was incubated (in the dark at 25°C and 300 ppm in a Eppendorf Thermomixer Comfort, Eppendorf AG, Hamburg, Germany) for 6 h with 1.5 ml of an assay solution containing appropriated concentrations (in the range of 0–100 μM) of different coumarins (fraxin, fraxetin, scopoletin, and isofraxidin) and 600 μM of bathophenanthrolinedisulphonate (BPDS) -as Fe(II) trapping agent- and buffered at pH 5.5 (with 5 mM MES-KOH) or pH 7.5 (with 5 mM HEPES-KOH). Afterward, the assay medium was filtered through PVDF 0.22 μm centrifugal filters (Millipore) at 10,000 *g* for 1 min. Absorbance was measured at 535 nm in the filtrates and then the Fe(II) concentration determined as Fe(II)-$BPDS_3$ using an extinction coefficient of 22.14 mM^{-1} cm^{-1}. The filtrates were also measured for total Fe by Inductively Coupled Plasma Mass Spectrometry (ICP-MS, Agilent 7500ce, Santa Clara, CA, USA) after diluting a 50 μl aliquot with 65% ultrapure HNO_3 (TraceSELECT Ultra, Sigma–Aldrich).

Statistical Analyses

Statistical analysis was carried out with SPSS for PC (v.23.0, IBM, Armonk, NY, USA), using ANOVA or non-parametric tests ($p \leq 0.05$), and a Levene test for checking homogeneity of variances. *Post hoc* multiple comparisons of means corresponding to each one the four different treatments were carried out ($p \leq 0.05$) using Duncan test when variances were equal and Games–Howell's test when variances were unequal.

RESULTS

Changes in Leaf Photosynthetic Pigment Concentrations, Fe Contents and Biomass with Fe Deficiency and High pH

Arabidopsis thaliana plants grown for 14 days in zero-Fe nutrient solution, buffered at either pH 5.5 or pH 7.5, had visible symptoms of leaf chlorosis (**Figure 2A**). The Chlorophyll (*Chl*) concentration in young leaves decreased by 56% in response to Fe deficiency, but was unaffected by the nutrient solution pH (**Figure 2B**). The concentrations of other photosynthetic pigments (neoxanthin, violaxanthin, lutein and β-carotene) in young leaves also decreased upon Fe deficiency (in the range of 48–60%) and were unaffected by the plant growth pH (Supplementary Table S6).

Iron deficiency decreased shoot biomass by 32% only when plants were grown at pH 7.5, whereas root biomass did not change significantly (**Figure 2C**). Shoot Fe content decreased significantly with Fe deficiency only in plants grown at pH 5.5 (by 61%; **Figure 2C**), whereas root Fe content was markedly decreased by 92% in plants grown at both pH values (**Figure 2C**). Iron deficiency also affected the contents of other micronutrients in plants, and this occurred mainly in shoots (Supplementary Table S7). The largest change found was a sixfold increase over the control value in the shoot Cu content of plants grown at pH 5.5.

Changes in the Expression of Genes Involved in Fe Root Uptake and the Phenylpropanoid Pathway with Fe Deficiency and High pH

The transcript levels of *IRT1*, *FRO2*, *ABCG37*, *F6'H1*, the caffeic acid/5-hydroxyferulic acid *O*-methyltransferase (*COMT*) and the trans-caffeoyl-CoA 3-*O*-methyltransferase (*CCoAMT*) were assessed by quantitative RT-PCR in control (Fe-sufficient) and Fe-deficient roots from both plants grown at pH 5.5 or at pH 7.5 3 days after treatment onset (**Figure 2D**). Under high Fe supply, the only pH effect observed was for *FRO2*, whose transcript abundance was 12-fold higher in plants grown at pH 7.5 than in those grown at pH 5.5. Under Fe deficiency conditions, *IRT1* and *FRO2* gene expression increased in plants grown both at pH 5.5 and pH 7.5; the increases were ninefold for *IRT1* and 15-fold for *FRO2* in plants grown at pH 5.5, and 20-fold for *IRT1* and 5-fold for *FRO2* in plants grown at pH 7.5. Other genes studied, *ABCG37* and *F6'H1*, also showed increases in their expression in response to Fe deficiency when compared to the Fe-sufficient controls, although they were smaller than those observed for *IRT1* and *FRO2*. The increases in *ABCG37* gene expression were 2- (although this change was not statistically significant) and 4-fold in plants grown at pH 5.5 and pH 7.5, respectively, whereas those of *F6'H1* were 4- and 8-fold in plants grown at pH 5.5 and pH 7.5. On the other hand, *COMT* and *CCoAMT* gene expression in roots was only increased by Fe deficiency at pH 7.5 (twofold).

Arabidopsis Roots Accumulate and Secrete an Array of Fluorescent and Non-fluorescent Phenolic-Type Compounds with Fe Deficiency and High pH

Methanolic extracts of roots of *A. thaliana* plants and their nutrient solutions were analyzed using the reverse phase C_{18} HPLC-based method used in Fourcroy et al. (2014) (Elution

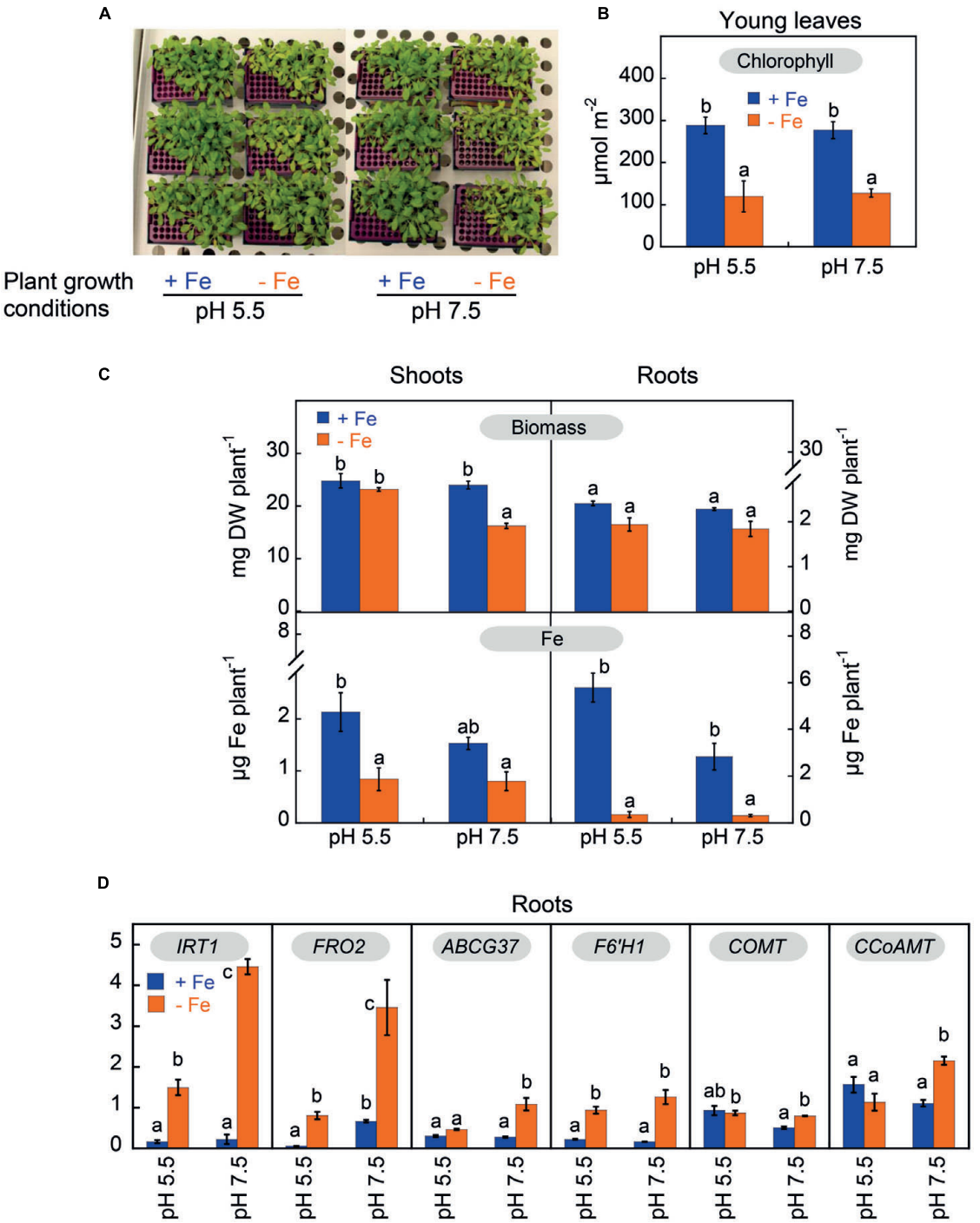

FIGURE 2 | Effects of Fe deficiency and high pH on plant Fe status, root Fe uptake machinery and phenylpropanoid pathway components in *Arabidopsis thaliana*. Plants were pre-grown for 11 days in the presence of 20 μM Fe (III)-EDTA at pH 5.5, and then grown for 14 days in a medium with 0 (−Fe) or 20 μM (+Fe) Fe(III)-EDDHA in nutrient solutions buffered at pH 5.5 (with 5 mM MES-NaOH) or 7.5 (with 5mM HEPES-NaOH). **(A)** Plants at day 14 after imposing treatments. **(B)** Leaf chlorophyll concentration in young leaves of plants at day 14 after imposing treatments; data are means ± SE ($n = 3$) and significant differences among treatments (at $p < 0.05$) are marked with different letters above the columns. **(C)** Dry weights and Fe contents in shoots and roots at day 14 after imposing treatments. Data are means ± SE for biomass ($n = 5$) and for Fe contents ($n = 2$–5), and significant differences among treatments (at $p < 0.05$) are marked with different letters above the columns. **(D)** Abundance of *IRT1*, *FRO2*, *ABCG37* (*PDR9*), *F6'H1*, *COMT* and *CCoAMT* transcripts in roots at day 3 after imposing treatments. RNAs were extracted from roots and analyzed by qRT-PCR, using PP2 (At1g13320) as housekeeping gene. The ΔΔCT method was used to determine the relative transcript level. Data are means ± SE ($n = 3$–5). For each gene, significant differences among treatments (at $p < 0.05$) are marked with different letters above the columns.

program 1), using both UV/VIS detection in the range 200–600 nm and fluorescence detection at λ_{exc} 365 and λ_{em} 460 nm (only the latter was used in the original study). Fluorescence alone cannot detect all phenolic compounds, since many of them emit little or no fluorescence. However, all phenolic compounds absorb light in the UV region; coumarins, their derivatives and precursors (e.g., ferulic and other cinnamic acids) have absorption maxima in the range 290–330 nm.

This is illustrated by the absorbance chromatograms of *A. thaliana* root extracts and growth media at 320 nm, which show many additional peaks to those found in fluorescence chromatograms obtained with the same samples (**Figure 3**). Each of the peaks in the chromatogram may contain one or more compounds (either fluorescent and/or non-fluorescent; see sections below for identification). In the control root extracts, fluorescence chromatograms showed only two peaks at approximately 10 and 15 min, whereas the absorbance chromatograms show several small peaks at two retention time (RT) ranges, 9–16 and 19–24 min, as well as a large peak at approximately 18 min (**Figure 3**). In the root extracts from Fe-deficient plants, increases were found in fluorescence in the area of the 15 min peak and in absorbance in the 18 min peak. In the control nutrient solution, the fluorescence chromatogram showed peaks at 10, 15, and 19 min, whereas the absorbance chromatogram showed peaks at 18 and 19 min (**Figure 3**). Iron deficiency caused large increases in the areas of all these peaks, with further absorbance ones appearing at 13, 14, 15, 16, and 17 min. This shows that Fe deficiency induces the synthesis, root accumulation and secretion to the growth media not only of fluorescent coumarins, as described by Fourcroy et al. (2014) and Schmid et al. (2014), but also of a number of previously unreported non-fluorescent phenolic compounds.

Identification of Phenolic Compounds Induced by Fe Deficiency as Coumarins, Coumarin Precursors and Coumarinolignans

To identify the compounds found in the *A. thaliana* root extracts and growth media, samples were analyzed using four different HPLC-UV/VIS/ESI-MS(TOF) protocols, including two Elution programs (1 and 2; Supplementary Table S2) and two electrospray (ESI) ionization modes (positive and negative). The newly designed Elution program 2 led to a better separation of phenolic compounds than that obtained with the original Elution program 1 used in Fourcroy et al. (2014). With the new elution program, RTs for a selected set of phenolics standards ranged from 8.4 (for esculin, the glucoside form of the coumarin esculetin) to 51.7 min (for the flavone apigenin) (Supplementary Figures S1 and S2). These HPLC/ESI-MS(TOF) analyses provided highly accurate (error below 5 ppm) measurements of the mass-to-charge (*m/z*) ratio of the detected ions, therefore allowing for accurate elemental formulae assignments (Bristow, 2006).

Raw MS(TOF) datasets (time, *m/z* and ion intensity) from the root extracts and nutrient solutions from Fe-deficient and Fe-sufficient plants were first analyzed with the DISSECT algorithm (Data Analysis 4.0; Bruker) to obtain mass spectral features attributable to individual compounds. From a total of approximately 180 possible mass spectral features analyzed per run and sample, only 18 complied with the following two requirements: (i) occurring at chromatographic RTs where absorbance at 320 nm was observed, and (ii) showing peak area increases (or appearing) with Fe-deficiency. Then, associated ions coming from adducts (with salts or solvents), dimers and trimers were discarded (with some exceptions, see below), and the ion chromatograms of all major remaining ions (including non-fragmented ones as well as fragment ions produced in the ESI source) were extracted with a precision of ±0.02 *m/z*. From these, we selected major ions showing large changes in peak areas in response to Fe deficiency, without considering fragments and minor ions. The localization in the chromatograms of the 18 selected compounds is depicted in **Figure 3**, and the RT, exact *m/z* and assigned elemental formulae are shown in **Table 1**. These 18 compounds were never detected in nutrient solutions of pots without plants, and include some coumarins already known to occur and others not previously reported, as explained in detail below.

Coumarins and Related Compounds Previously Reported in *A. thaliana* upon Fe-Deficiency

As expected, some compounds (five out of 18) have RTs and *m/z* values matching with those of coumarins previously found in roots and exudates from Fe-deficient *A. thaliana* plants (Fourcroy et al., 2014; Schmid et al., 2014; Schmidt et al., 2014). These include compounds *1, 7–9,* and *11* (**Figure 3**; **Table 1**), and were assigned to scopoletin hexoside, fraxetin, scopoletin, isofraxidin and fraxinol (an isofraxidin isomer), respectively (Supplementary Table S1). These annotations were further confirmed using the RT and *m/z* values of standards (**Table 1** vs. **Table 2**). A sixth compound, *2*, was assigned to ferulic acid hexoside based on the presence of a major ion at *m/z* 195.0656 in its positive MS(TOF) spectrum, which is consistent with the elemental formula of ferulic acid $[M+H]^+$ ion (**Table 2**) and with the neutral loss of a hexosyl moiety (162.0528 Da, $C_6H_{10}O_5$) from the $[M+H]^+$ ion (with an absolute error of 1.2 ppm). We could not confirm the identity using a ferulic acid hexoside standard because to the best of our knowledge no such standard is commercially available.

The remaining 12 compounds were subjected to further MS-based analyses to obtain structural information. First, low resolution HPLC/ESI-MS(ion trap) analyses were carried out, including MS^2 and/or MS^3 experiments with the $[M+H]^+$ or $[M-H]^-$ ions.

Coumarins and Coumarin-Precursor Hexosides Not Previously Reported in *Arabidopsis* upon Fe-Deficiency

Three of the compounds (*10*, *12,* and *13*) were identified as ferulic acid, coniferyl aldehyde and sinapyl aldehyde (three phenylpropanoid precursors; **Figure 1B**), respectively, by comparing the MS spectra of the analytes and those of standards: there was a good match of the RT values and exact *m/z* ratios of the $[M+H]^+$ and $[M-H]^-$ ions (**Tables 1** and **2**) as well as of the MS^2 spectra of the $[M+H]^+$ ions (**Tables 2** and **3**).

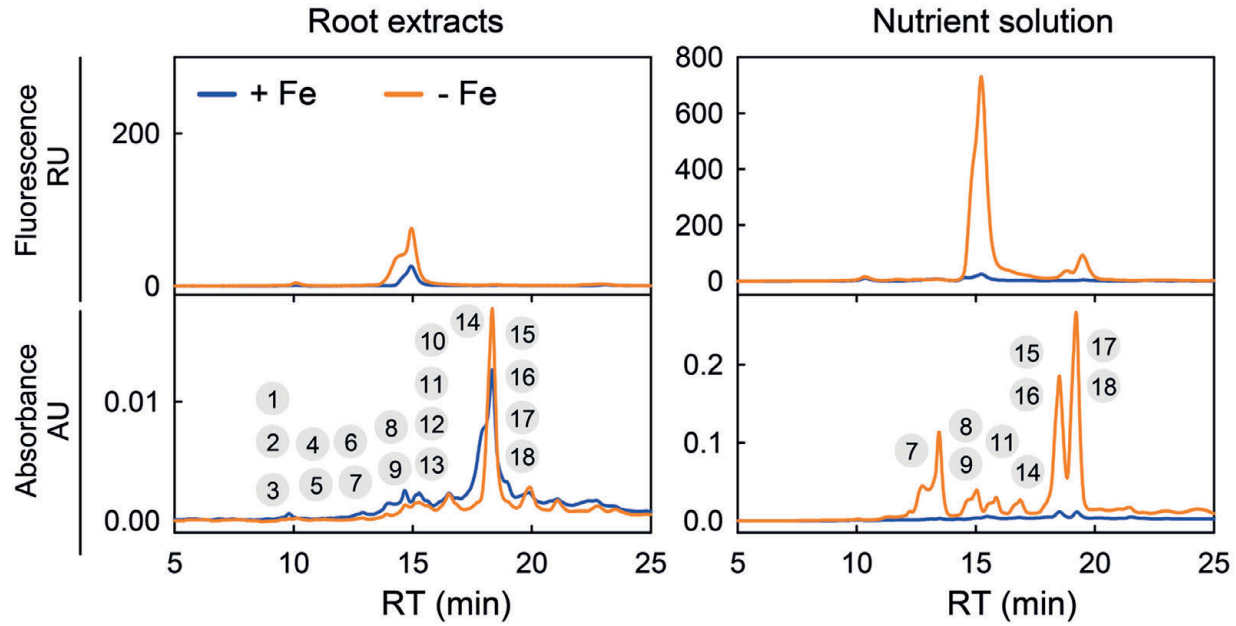

FIGURE 3 | Chromatographic separation of a range of phenolic-type compounds produced in response to Fe deficiency by *Arabidopsis thaliana* roots. Typical fluorescence (at λ_{exc} 365 and λ_{em} 460 nm) and absorbance (at 320 nm) chromatograms for root and growth media extracts from plants grown as described in Fourcroy et al. (2014): plants were pre-grown for 29 days in the presence of 45 μM Fe (III)-EDTA at pH 5.5, and then grown for 7 days in a medium with 0 (−Fe) or 45 μM Fe (III)-EDTA (+Fe) (the pH was not readjusted to 5.5, with the final pH being *c.* 7.0 in all pots). Chromatograms were obtained using Elution program 1. The encircled numbers above each peak correspond to the phenolic compounds listed in **Table 1**. RU, relative units, AU, absorbance units, and RT, retention time.

Four more compounds (*3–6*) were first confirmed to be hexoside-type compounds from the RT, exact *m/z* values and MS^2 spectra of the $[M\text{-}H]^-$ ions. The RT values of these compounds (12.3–14.9 min) were close to those of known coumarin glucosides (10.3 and 13.0 min for scopolin and fraxin, respectively), and lower than those of coumarin aglycones (16.4–25.1 min for fraxetin, scopoletin, isofraxidin and fraxinol), phenylpropanoids (e.g., 23.0 and 25.1 min for ferulic acid and sinapyl aldehyde), and glycoside and aglycone forms of other phenolics (e.g., 27–52 min for flavonoids, stilbenes and lignans) (Supplementary Figures S1 and S2). Therefore, the RTs indicate that compounds *3–6* are likely to be polar (i.e., hexoside) forms of coumarins and/or phenylpropanoids. Furthermore, in the MS(TOF) spectra, ions (positive/negative) at *m/z* 179.0707/177.0544, 209.0450/207.0289, 223.0600/221.0447 and 209.0801/207.0648 for *3*, *4*, *5*, and *6*, respectively, were consistent with the loss of a hexosyl moiety (162.05 Da) from their corresponding $[M+H]^+/[M\text{-}H]^-$ ions (see *m/z* values in **Table 1**). This was confirmed using the low resolution MS^2 spectra obtained with the ion trap: major fragment ions (100% relative intensity at *m/z* 177, 207, 221 and 207 in the MS^2 spectra of *3–6*, respectively; **Table 3**) corresponded to the $[M\text{-}H]^-$ ions (*m/z* 339, 369, 383 and 369 for *3*, *4*, *5*, and *6*, respectively) after a mass loss of 162 Da. The same mass loss was also observed in the MS^2 spectra of authenticated standards of the coumarin glucosides scopolin and fraxin described above, with major ions at *m/z* 193/191 (scopolin) and 209/207 (fraxin), corresponding with the *m/z* of their aglycones, scopoletin and fraxetin, respectively (**Table 2**). The rest of ions in the MS^2 spectra of compounds *3–6*, scopolin and fraxin showed significantly lower relative intensities (<40%), indicating the hexosyl loss is favored.

The aglycon moieties of compounds *3–6* were identified taking advantage of having the dehexosylated ions in the MS(TOF) spectra and also carrying out low resolution MS^3 experiments on the ion trap. First, from the positive and negative MS(TOF) spectra, the *m/z* values for dehexosylated ions (see above) of *3*, *4*, *5*, and *6* were assigned to the elemental formulae $C_{10}H_{10}O_3$, $C_{10}H_8O_5$, $C_{11}H_{10}O_5$ and $C_{11}H_{12}O_4$, respectively (with absolute errors <4 ppm). Two of these elemental formulae, $C_{10}H_{10}O_3$ and $C_{11}H_{12}O_4$, were consistent with coniferyl and sinapyl aldehydes, involved in coumarin synthesis (Kai et al., 2008) (**Table 2**), whereas the other two, $C_{10}H_8O_5$ and $C_{11}H_{10}O_5$, were consistent with two coumarins already identified in the samples (compounds *7* and *9*, respectively) (**Table 1**). Finally, compounds *3–6* were confirmed as the hexoside forms of coniferyl aldehyde, fraxetin, isofraxidin and sinapyl aldehyde, respectively (**Table 1**) from the good fit between the MS^3 ion trap spectra of *3-6* (339→177, 369→207, 383→221 and 369→207, respectively) (**Table 3**) and the MS^2 spectra of the corresponding aglycone standards (**Table 2**).

Coumarinolignans: Newly Identified Compounds Synthesized in Response to Fe-Deficiency

The last five compounds (*14–18* in **Table 1**) are very hydrophobic, since they elute later (RTs 31–39 min) than compounds *1–13* (RTs

TABLE 1 | Phenolic compounds secreted and accumulated by *Arabidopsis thaliana* roots in response to Fe deficiency: retention times (RT), exact mass-to-charge ratios (*m/z*), molecular formulae and error *m/z* (in ppm).

Compound #	RT (min) program 1	RT (min) program 2	Measured *m/z*	Molecular formula	Calculated *m/z*	Error *m/z* (ppm)	Annotation
1	9.8	10.3	355.1028	$C_{16}H_{19}O_9^+$	355.1024	1.1	7-hydroxy-6-methoxycoumarin hexoside (scopolin, scopoletin hexoside)
			353.0877	$C_{16}H_{17}O_9^-$	353.0867	2.8	
2	10.0	10.6	357.1182	$C_{16}H_{21}O_9^+$	357.1180	0.6	Ferulic acid hexoside
			355.1030	$C_{16}H_{19}O_9^-$	355.1024	1.7	
3	10.4	12.3	363.1055	$C_{16}H_{20}O_8Na^+$	363.1050	1.4	Coniferyl aldehyde hexoside
			339.1079	$C_{16}H_{19}O_8^-$	339.1074	−1.5	
4	11.3	13.0	371.0975	$C_{16}H_{19}O_{10}^+$	371.0973	0.5	7,8-dihydroxy-6-methoxycoumarin hexoside (fraxetin hexoside)
			369.0827	$C_{16}H_{17}O_{10}^-$	369.0816	3.0	
5	12.1	14.7	407.0949	$C_{17}H_{20}O_{10}Na^+$	407.0949	0.0	7-hydroxy-6,8-dimethoxycoumarin hexoside (isofraxidin hexoside)
			383.0992	$C_{17}H_{19}O_{10}^-$	383.0973	5.0	
6	12.3	14.9	409.0893	$C_{17}H_{22}O_9K^+$	409.0895	−0.5	Sinapyl aldehyde hexoside
			369.1194	$C_{17}H_{21}O_9^-$	369.1180	3.8	
7	13.0	16.4	209.0446	$C_{10}H_9O_5^+$	209.0445	0.5	7,8-dihydroxy-6-methoxycoumarin (fraxetin)
			207.0282	$C_{10}H_7O_5^-$	207.0288	−2.9	
8	14.5	20.0	193.0502	$C_{10}H_9O_4^+$	193.0495	3.6	7-hydroxy-6-methoxycoumarin (scopoletin)
			191.0341	$C_{10}H_7O_4^-$	191.0339	1.0	
9	14.8	21.6	223.0604	$C_{11}H_{11}O_5^+$	223.0601	1.3	7-hydroxy-6,8-dimethoxycoumarin (isofraxidin)
			221.0442	$C_{11}H_9O_5^-$	221.0445	−1.4	
10	15.6	23.0	195.0649	$C_{10}H_{11}O_4^+$	195.0652	−1.5	Ferulic acid
			193.0504	$C_{10}H_9O_4^-$	193.0495	4.7	
11	15.6	23.8	223.0604	$C_{11}H_{11}O_5^+$	223.0601	1.3	6-hydroxy-5,7-dimethoxycoumarin (fraxinol)
			221.0442	$C_{11}H_9O_5^-$	221.0445	−1.4	
12	16.1	24.6	179.0708	$C_{10}H_{11}O_3^+$	179.0703	2.7	Conyferyl aldehyde
			177.0551	$C_{10}H_9O_3^-$	177.0546	2.8	
13	16.5	25.1	209.0809	$C_{11}H_{13}O_4^+$	209.0808	0.5	Sinapyl aldehyde
			207.0660	$C_{11}H_{11}O_4^-$	207.0652	3.9	
14	16.5	30.7	403.1018	$C_{20}H_{19}O_9^+$	403.1024	−1.5	5′-hydroxycleomiscosins A and/or B
			401.0877	$C_{20}H_{17}O_9^-$	401.0867	2.5	
15	18.0	35.5	417.1175	$C_{21}H_{21}O_9^+$	417.1180	−1.2	Cleomiscosin D
			415.1022	$C_{21}H_{19}O_9^-$	415.1024	−0.5	
16	18.5	37.0	417.1173	$C_{21}H_{21}O_9^+$	417.1180	−1.7	Cleomiscosin C
			415.1022	$C_{21}H_{19}O_9^-$	415.1024	−0.5	
17	18.5	37.0	387.1073	$C_{20}H_{19}O_8^+$	387.1074	−0.3	Cleomiscosin B
			385.0930	$C_{20}H_{17}O_8^-$	385.0918	3.1	
18	19.0	38.6	387.1073	$C_{20}H_{19}O_8^+$	387.1074	−0.2	Cleomiscosin A
			385.0922	$C_{20}H_{17}O_8^-$	385.0918	1.0	

The m/z ratios for $[M+H]^+$ and $[M-H]^-$ were determined from the HPLC/ESI-MS(TOF) data obtained in positive and negative mode, respectively. For compounds 3, 5, and 6 in positive mode, the m/z shown are those measured for the Na ($[M+Na]^+$) or K ($[M+K]^+$) adducts, because they were more intense than those for $[M+H]^+$. Common names for coumarins are also indicated in brackets.

10–25 min), and have *m/z* values supporting elemental formulae with a high number of C atoms (20–21 vs. 10–17 for compounds *1–13*). In fact, the RTs of *14–18* are in line with those of phenolics bearing either C_{15} (C_6-C_3-C_6; as in flavonoids and stilbens) or C_{18} (C_6-C_3-C_3-C_6; as in lignans) skeletons (27–52 min; Supplementary Figures S1 and S2), whereas compounds *7–13* (coumarins and phenylpropanoids) share a C_9 (C_3–C_6) skeleton and compounds *1–6* (hexose conjugates of *7–13*) share a C_{15} (C_3-C_6-C_6) skeleton (**Table 1**).

The MS(TOF) spectra show that compounds *15–18* are two pairs of isomers, with elemental formulae $C_{21}H_{20}O_9$ for *15–16* and $C_{20}H_{18}O_8$ for *17–18*, with the difference between formulae being consistent with a single methoxy ($-OCH_3$) group. The elemental formula of compound *14*, $C_{20}H_{18}O_9$, is consistent with the addition of both a hydroxyl ($-OH$) group to *17–18* or the addition of a methyl ($-CH_3$) group to *15–16*. The presence of these structural differences are common among phenolics, since part of the phenylpropanoid biosynthesis proceeds *via* a series of ring hydroxylations and *O*-methylations. The low resolution MS^2 spectra from *14* to *18* (**Figure 4A**) indicate that these five compounds have highly related chemical structures: (i) the spectra of *15–16* show the same ions with only some differences in their relative intensity, and the same was also observed for *17–18*; (ii) most of the ions in the *15–18* spectra were either common (*m/z* 263, 233, 209, 161) or consistent with common mass losses from the $[M+H]^+$ ion (e.g., *m/z* 367 and 337 in the *15–16* and *17–18* MS^2 spectra, corresponding to a mass loss of 50 Da; Supplementary Table S8), and (iii) the spectrum of *14*

TABLE 2 | Phenolic compound standards used for identification purposes: retention times (RT), exact mass-to-charge ratios (*m/z*), molecular formulae and error *m/z* (in ppm).

Name	RT (min) program 2	Measured *m/z*	Molecular formula	Calculated *m/z*	Error *m/z* (ppm)	ESI-MS^n *m/z* (Relative intensity, in %)
7-hydroxy-6-methoxycoumarin 7-glucoside (scopolin, scopoletin 7-*O*-glucoside)	10.3	355.1021	$C_{16}H_{19}O_9^+$	355.1024	−0.8	MS^2 [355]: 337 (11), 245 (3), **193 (100)**, 149 (1), 165 (1), 133 (12), 105 (5) MS^3 [355→193]: 178 (16), 165 (21), 149 (11), 137 (6), **133 (100)**
		353.0876	$C_{16}H_{17}O_9^-$	353.0867	2.5	MS^2 [353]:**191 (100)**, 176 (9) MS^3 [353→191]: **176 (100)**
7,8-dihydroxy-6-methoxycoumarin 8-glucoside (fraxin)	13.0	371.0956	$C_{16}H_{19}O_{10}^+$	371.0973	−4.6	MS^2 [371]: 368 (11), 362 (13), 357 (12), 355 (66), 353 (35), 340 (13), 327 (23), 326 (25), 325 (195), 309 (15), 300 (17), 288 (10), 269 (19), 268 (11), 265 (11), 262 (14), 261 (17), 221 (12), **209 (100)**, 187 (19), 177 (14), 170 (19), 156 (15), 133 (24) MS^3 [371→209]: **194 (100)**
		369.0825	$C_{16}H_{17}O_{10}^-$	369.0816	2.4	MS^2 [369]: **207 (100)**, 192 (20) MS^3 [369→207]: **192 (100)**, 163 (0.2)
7,8-dihydroxy-6-methoxycoumarin (fraxetin)	16.4	209.0444	$C_{10}H_9O_5^+$	209.0445	−0.5	MS^2 [209]: 194 (31), 181 (52), 177 (15), 165 (7), 163 (80), 153(9), **149 (100)**, 135 (13), 107 (18)
		207.0291	$C_{10}H_7O_5^-$	207.0288	1.4	MS^2 [207]: **192 (100)**, 163 (0.3)
7-hydroxy-6-methoxycoumarin (scopoletin)	20.0	193.0494	$C_{10}H_9O_4^+$	193.0495	−0.5	MS^2 [193]: 178 (8), 165 (31), 149 (12), 137 (12), **133 (100)**, 117 (2), 105 (3), 89 (3), 63 (6)
		191.0346	$C_{10}H_7O_4^-$	191.0339	3.7	MS^2 [191]: **176 (100)**, 148 (0.4)
7-hydroxy-6,8-dimethoxycoumarin (isofraxidin)	21.6	223.0594	$C_{11}H_{11}O_5^+$	223.0601	−3.1	MS^2 [223]: **208 (100)**, 207 (7), 195 (14), 191 (8), 190 (49), 179 (7), 163 (72), 162 (6), 135 (19) 107 (45)
		221.0443	$C_{11}H_9O_5^-$	221.0445	−0.9	MS^2 [221]: **206 (100)**, 209 (0.5), 191 (5), 162 (0.8)
Ferulic acid	23.0	195.0657	$C_{10}H_{11}O_4^+$	195.0652	2.6	MS^2 [195]: **177 (100)**, 153 (4), 145 (3)
		193.0504	$C_{10}H_9O_4^-$	193.0495	4.7	MS^2 [193]: 178 (70), **149 (100)**, 139 (80)
6-hydroxy-5,7-dimethoxycoumarin (fraxinol)	23.8	223.0594	$C_{11}H_{11}O_5^+$	223.0601	−3.1	MS^2 [223]: **208 (100)**, 195 (11), 190 (40), 179 (6), 163 (54), 135 (19), 107 (39), 91 (4)
		221.0440	$C_{11}H_9O_5^-$	221.0444	−1.8	MS^2 [221]: **206 (100)**, 191 (5), 209 (0.5), 162 (0.2)
Coniferyl aldehyde	24.6	179.0706	$C_{10}H_{11}O_3^+$	179.0703	1.7	MS^2 [179]: **161 (100)**, 147 (97), 133 (18), 119 (7), 105 (10)
		177.0554	$C_{10}H_9O_3^-$	177.0546	4.5	MS^2 [177]: **162 (100)**, 163 (1), 158 (0.3)
Sinapyl aldehyde	25.1	209.0810	$C_{11}H_{13}O_4^+$	209.0808	1.0	MS^2 [209]: 191 (47), 181 (10), **177 (100)**, 153 (7), 149 (20), 145 (15), 131 (12), 121 (17), 103 (5)
		207.0662	$C_{11}H_{11}O_4^-$	207.0652	4.8	MS^2 [207]: **192 (100)**, 191 (0.3), 177 (2), 147 (0.2), 133 (0.2)

The m/z ratios of parent and fragment ions were determined from the data in the HPLC/ESI-MS(TOF) and HPLC/ESI-MS(ion trap) chromatograms, respectively, working in both positive and negative mode. Common names for coumarins and their glucosides are indicated in brackets. The parent ion m/z ratios correspond to $[M+H]^+$ and $[M-H]^-$. The major ion of the MS^2 and MS^3 spectra is indicated in bold.

also has some of these features, including an ion at *m/z* 209 and a mass loss of 30 Da from the $[M+H]^+$ ion (Supplementary Table S8). When the MS^2 spectra of *14–18* were obtained on a high resolution Q-TOF mass analyzer, which allows for an accurate mass determination of fragment ions, all spectra showed a common fragment ion at *m/z* 209.0435, consistent with the elemental formula $C_{10}H_9O_5^+$ (with an error of −4.7 ppm) (Supplementary Figure S3) of the dihydroxymethoxycoumarin fraxetin (compound *7*). The presence of a fraxetin moiety in compounds *14–18* was further confirmed by their MS^3 spectra (403→209, 417→209, 417→209, 387→209 and 387→209 for *14*, *15*, *16*, *17* and *18*, respectively; **Figure 4B**), which match perfectly with the fraxetin MS^2 spectrum.

Among the plant-derived fraxetin derivatives known so far (Begum et al., 2010; Zhang et al., 2014), six coumarinolignans have elemental formulae consistent with those of compounds *14–18*, including cleomiscosins A, B, C (also known as aquillochin) and D, first isolated and identified in seeds of *Cleome viscosa* (a common weed of the *Capparidaceae* family), and 5′-hydroxycleomiscosins A (also known as 5′-demethylaquillochin) and B, first isolated from *Mallotus apelta* roots and *Eurycorymbus cavaleriei* twigs, respectively. Cleomiscosins C and D (regioisomers -also called constitutional isomers- arising from the fusion of fraxetin and the monolignol sinapyl alcohol through a dioxane bridge; **Figure 1C**) have a formula identical to that of *15–16* ($C_{21}H_{20}O_9$), cleomiscosins A and B (regioisomers arising from the fusion of fraxetin and the monolignol coniferyl alcohol through a dioxane bridge; **Figure 1C**) have a formula identical to that of *17-18* ($C_{20}H_{18}O_8$), whereas 5′-hydroxycleomiscosins A and B (regioisomers arising

TABLE 3 | MS/MS data for some of the compounds secreted and accumulated by *Arabidopsis thaliana* roots in response to Fe deficiency: *m/z* ratios of the fragment ions and their relative intensity.

Compound #	Annotation	Parent ion *m/z*	Ion type	ESI-MS^n *m/z* (Relative intensity, in %)
3	Coniferylaldehyde hexoside	339.1	$[M-H]^-$	MS^2 [339]: 295 (6), 275 (8), 250 (6), 249 (3), 188 (3), **177 (100)**, 162 (3) MS^3 [339→177]: **162 (100)**
4	7,8-dihydroxy-6-methoxycoumarin hexoside (fraxetin hexoside)	369.1	$[M-H]^-$	MS^2 [369]: 325 (7), 323 (5), 223 (11), 215 (8), **207 (100)**, 193 (5), 192 (20) MS^3 [369→207]: **192 (100)**
5	7-hydroxy-6,8-dimethoxycoumarin hexoside (isofraxidin hexoside)	383.1	$[M-H]^-$	MS^2 [383]: 365 (13), 347 (24), 341 (12), 339 (10), 337 (22), 323 (24), 322 (18), 303 (14), 270 (20), 268 (25), 266 (18), 252 (9), 251 (30), **221 (100)**, 215 (38), 207 (7), 206 (11), 203 (11), 199 (15), 187 (8), 177 (20), 173(8), 156 (11), 131 (17), 129 (30), 125 (6), 114 (24) MS^3 [383→221]: **206 (100)**
6	Sinapyl aldehyde hexoside	369.1	$[M-H]^-$	MS^2 [369]: 351 (33), 325 (11), 289 (10), 254 (5), 253 (6), 246 (11), 245 (8), 239 (9), 237 (11), 217 (6), **207 (100)**, 192 (18), 159 (11), 128 (10) MS^3 [369→207]: **192 (100)**
10	Ferulic acid	193.1	$[M-H]^-$	MS^2 [193]: 178 (70), **149 (100)**, 134 (72)
12	Coniferyl aldehyde	179.1	$[M+H]^+$	MS^2 [179]: 161 (86), **147 (100)**, 133 (17), 119 (10), 105 (8)
13	Sinapyl aldehyde	209.1	$[M+H]^+$	MS^2 [209]: 191 (41), 181 (17), **177 (100)**, 149 (22), 145 (13), 131 (5), 121 (18)

*Numbers in italics (Compound #) refer to the labels used for each compound in **Table 1**. All data were taken from the HPLC-ESI-MS/MS(ion trap) analysis. The major ion of the MS^2 and MS^3 spectra is also indicated in bold.*

from the fusion of fraxetin and the monolignol hydroxyconiferyl alcohol, Cheng and Chen, 2000, **Figure 1C**), have a formula identical to that of compound *14* ($C_{20}H_{18}O_9$). The structural differences among these coumarinolignans -corresponding to the monolignol moiety (**Figure 1B**)- are identical to those found among the elemental formulae of *14–18*: (i) a methoxy group differentiates coniferyl from sinapyl alcohols and the elemental formula of *17–18* from that of *15–16*; (ii) a hydroxyl group differentiates hydroxyconiferyl from coniferyl alcohols and the elemental formula of *14* from that of *17–18*; and (iii) a methyl group differentiates hydroxyconiferyl and sinapyl alcohols and the formula of *14* from those of *15–16*.

To confirm the identification of *15–18* as cleomiscosins, we isolated coumarinolignans from *C. viscosa* seeds. The seed isolate was analyzed by both HPLC-UV/VIS/ESI-MS(TOF) and HPLC/ESI-MS(ion trap) using Elution program 2 and positive ESI ionization. The HPLC/ESI-MS(TOF) chromatogram for *m/z* 417.12 ± 0.02, corresponding to the cleomiscosins C and D $[M+H]^+$ ions, showed only two peaks, at 35.4 and 37.0 min, matching with the RTs of *15* and *16* (**Figure 4C**; **Table 1**). Similarly, the HPLC/ESI-MS(TOF) chromatogram for *m/z* 387.11 ± 0.02, corresponding to the cleomiscosins A and B $[M+H]^+$ ions, showed only two peaks, at 37.0 and 38.4 min, matching with the RTs of *17–18* (**Figure 4C**; **Table 1**). Peaks were assigned to cleomiscosin isomers according to the elution order reported in the literature (Chattopadhyay et al., 2008; Kaur et al., 2010). These annotations were confirmed by the full match between the MS^2 spectra of the cleomiscosins D, C, B, and A, and those of compounds *15*, *16*, *17* and *18*, respectively (**Figure 4C**). Compound *14* eluted at shorter times than the cleomiscosins (30.7 vs. 35.5–38.6 min), as expected from the structural differences between 5′-hydroxycleomiscosin A and B and cleomiscosins (see above). Furthermore, compound *14* shares elemental formula and the presence of a fraxetin moiety with 5′-hydroxycleomiscosins A and B, and its MS^2 spectrum showed a loss of 18 Da from the $[M+H]^+$ ion (**Figure 4B**; Supplementary Table S8), which was previously reported for 5′-hydroxycleomiscosin A (Cheng and Chen, 2000) but does not occur in cleomiscosins. Therefore, *14* was putatively annotated as 5′-hydroxycleomiscosin A and/or B (**Table 1**).

Coumarin and Coumarinolignan Concentrations in Root Extracts

Quantification of phenolic compounds was carried out using the $[M+H]^+$ and [M-hexoside+H]$^+$ signals in the HPLC/ESI-MS(TOF). Coumarins and their hexosides were quantified using authenticated standards, whereas coumarinolignan concentrations were estimated using peak/area ratios relative to that of the IS lignan matairesinol (**Figure 1D**), because of the lack of commercially available authenticated standards.

The phenolic compound profiles in root extracts included coumarins and coumarinolignans, and were markedly dependent on the plant growth pH (**Figure 5**); no phenolics of the flavonoid and stilbene families were found. Under sufficient Fe supply, root extracts from plants grown at pH 5.5 had mainly scopoletin hexoside (scopolin) and its aglycone (scopoletin) as well as the coumarin precursor hexoside of ferulic acid. When Fe-sufficient plants were grown at pH 7.5, no significant changes were found for ferulic acid hexoside, scopolin, scopoletin and fraxetin and isofraxidin hexosides, and the coumarinolignans cleomiscosins A, B, C, and D, whereas other coumarins increased (including fraxetin and isofraxidin).

Iron deficiency changed markedly the coumarin/-coumarinolignan profiles in root extracts (**Figure 5**). In plants grown at pH 5.5 the profiles were similar under Fe deficiency or sufficiency conditions, with moderate increases

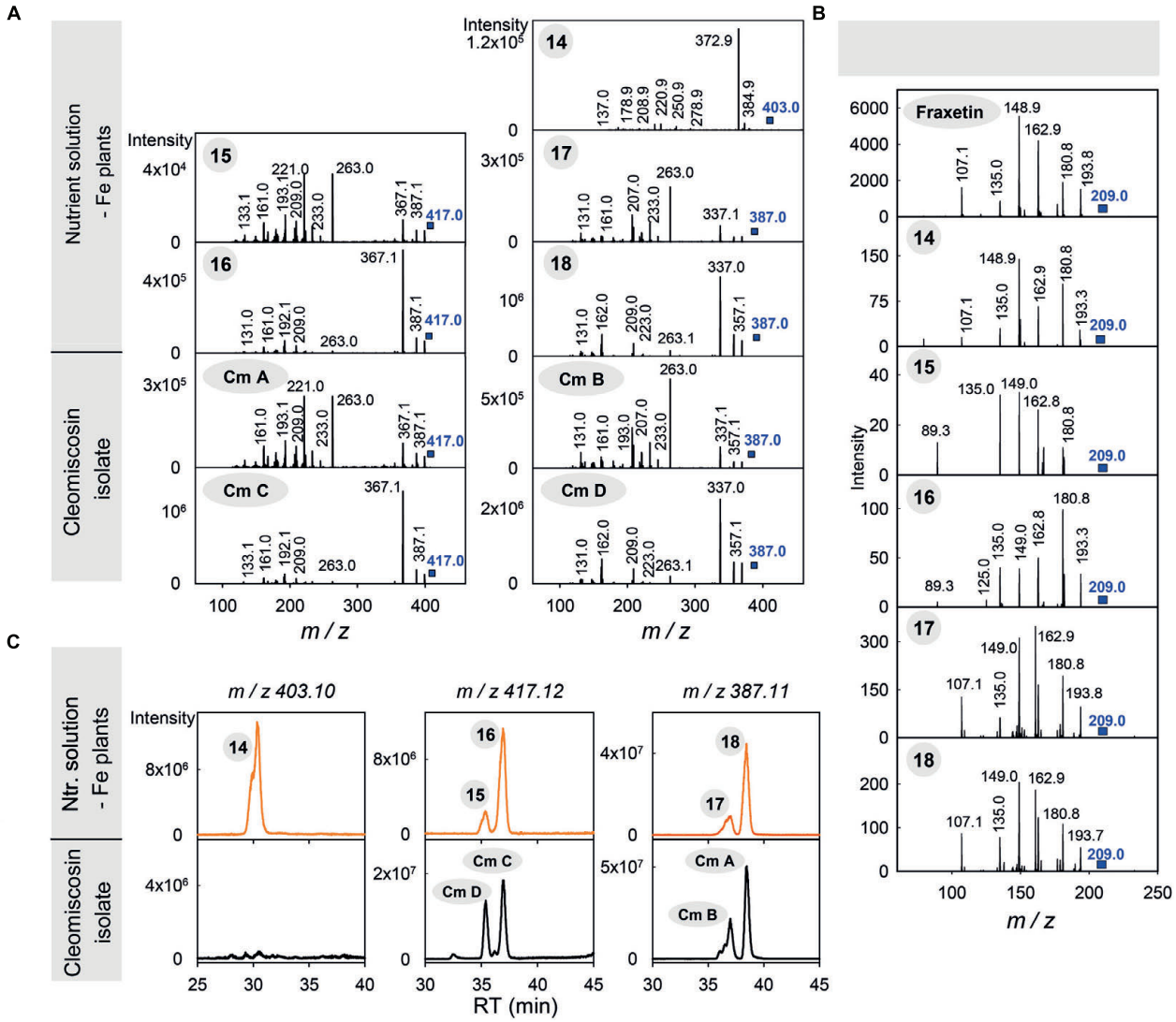

FIGURE 4 | Identification of compounds *14–18,* produced by Fe-deficient *Arabidopsis thaliana* roots, as coumarinolignans derived from fraxetin. **(A)** MS^2 spectra of compounds *14–18* and the cleomiscosins A (Cm A), B (Cm B), C (Cm C) and D (Cm D) isolated from *Cleome viscosa* seeds. **(B)** MS^2 spectra of fraxetin and MS^3 spectra of *m/z* 209 ion from the corresponding $[M+H]^+$ ions of compounds *14–18*. Spectra were obtained from the HPLC/ESI-MS(ion trap) analyses of growth media extracts from Fe-deficient plants and a cleomiscosin isolate. **(C)** Typical HPLC-ESI-MS(TOF) chromatograms for growth media extracts from Fe-deficient plants and for the cleomiscosin isolate, extracted at *m/z* 403.10, 417.12 and 387.11 and with a precision of ± 0.02 *m/z* units. The encircled numbers in the spectra and above each chromatographic peak correspond to the phenolic compounds listed in **Table 1**.

(not always significant) in fraxetin and isofraxidin hexosides and their aglycones (fraxetin, isofraxidin and fraxinol), as well as of the cleomiscosins A, B, C and D. However, in plants grown at pH 7.5 Fe deficiency caused a marked increase of all coumarin hexosides, their aglycones and all coumarinolignans. When compared to their concentration in Fe-sufficient plants at pH 7.5, the largest increase was 18-fold for cleomiscosin D, followed by 13-fold for isofraxidin, 12-fold for fraxinol and the cleomiscosins A, B, and C, 9-fold for the hexoside of isofraxidin, 7-fold for the hexoside of fraxetin and the aglycone fraxetin, 5-fold for scopoletin, and 2-fold for both scopolin and ferulic acid hexoside.

The most abundant coumarin in root extracts, irrespective of the growth conditions, was scopoletin (**Figure 6A**). Summing up the two forms detected, the hexoside and aglycone, scopoletin was 90–100% of the total coumarins, depending on the root conditions, with the aglycone form being always predominant (85–93%) (Supplementary Figure S4B). In the case of fraxetin, the aglycone was also the predominant form (at least 73–76%) in root extracts from plants grown at pH 7.5, whereas in plants grown in absence of Fe at pH 5.5, only 24% of the total fraxetin occurred in the aglycone form. In the case of isofraxidin the hexoside form was predominant, with the aglycone accounting for 23–46% of

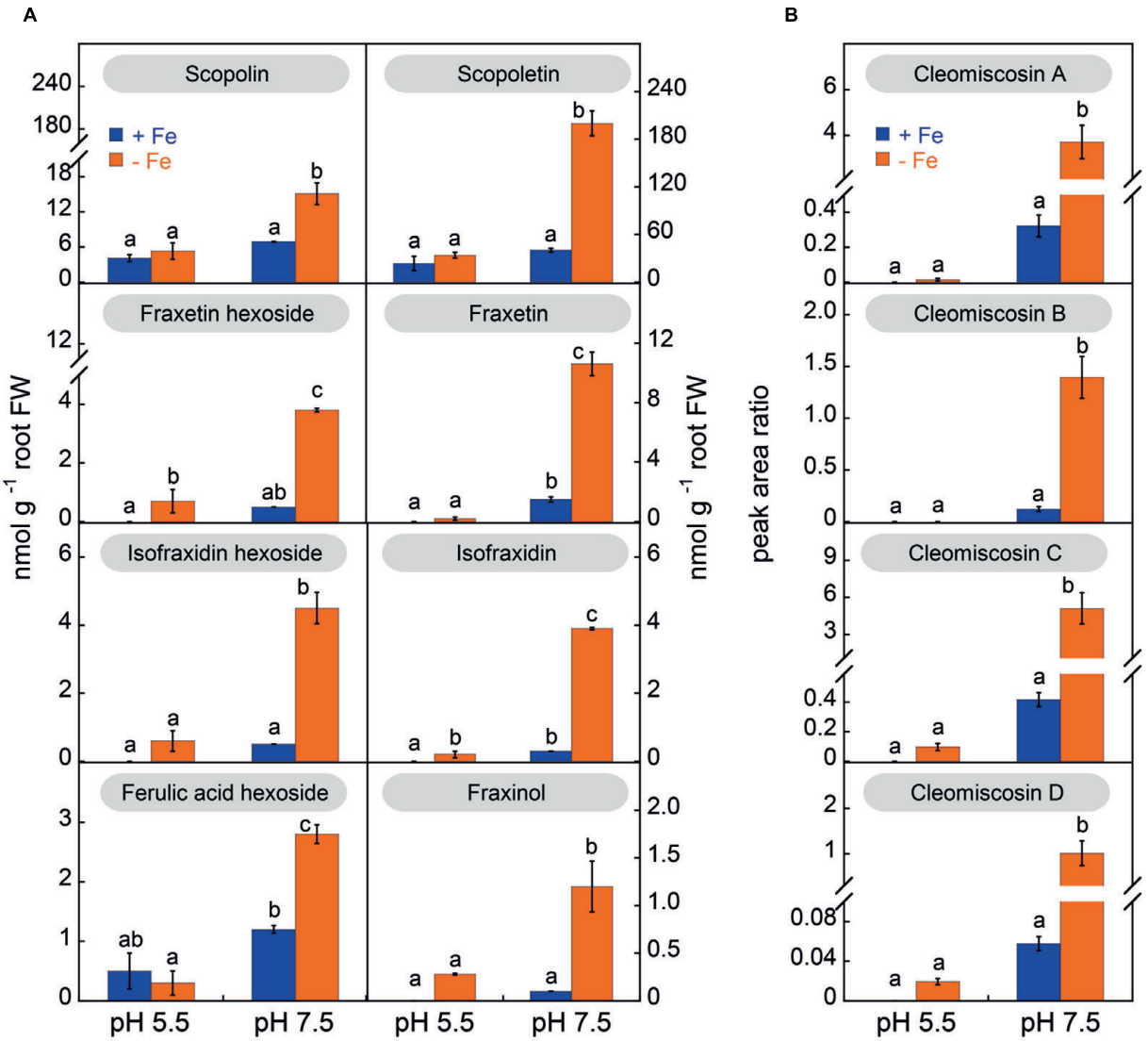

FIGURE 5 | Effects of Fe deficiency and high pH on the concentrations (in nmol g^{-1} root FW) of coumarins (A) and coumarinolignans (B) in *Arabidopsis thaliana* roots. Plants were pre-grown as indicated in **Figure 2** and grown for 14 days with 0 (−Fe) or 20 μM Fe (+Fe) in nutrient solution buffered at pH 5.5 (with 5 mM MES-NaOH) or 7.5 (with 5 mM HEPES-NaOH). Ferulic acid hexoside was quantified as fraxin. The levels of the cleomiscosins are expressed in peak area ratio, relative to the lignan matairesinol used as internal standard. Data are means ± SE (n = 3–5). For each compound, significant differences among treatments (at $p < 0.05$) are marked with different letters above the columns.

the total depending on the growth conditions (Supplementary Figure S4B).

Coumarin and Coumarinolignan Concentrations in the Nutrient Solution

The concentrations of coumarins and coumarinolignans were determined in the nutrient solution of Fe-deficient plants after 7 and 14 days after imposing Fe deficiency (nutrient solutions were renewed on day 7) (**Figure 7**). No determinations could be made in nutrient solutions of Fe-sufficient plants due to the presence of Fe(III)-EDDHA, which causes the overloading of C_{18} materials. Coumarin hexosides were only occasionally detected at trace levels (data not shown). When plants were grown at pH 5.5, the growth media at day 7 contained low concentrations of aglycones (scopoletin, fraxetin, isofraxidin, and fraxinol; **Figure 7**) and coumarinolignans (cleomiscosins A, C, and D as well as the putative 5′- hydroxycleomiscosin; **Figure 7**). After 14 days of Fe deficiency no significant changes were observed. In contrast, when plants were grown at pH 7.5, the concentration of coumarins and coumarinolignans in the nutrient solution were much higher than that found in the culture medium of plant grown at pH 5.5 (**Figure 7**). When compared to the concentrations found with Fe-deficient plants at pH 5.5, increases were large for scopoletin (6- and 12-fold at days 7 and 14, respectively) and very large for the rest of phenolics (in the range from 17- to 537-fold). In addition, when

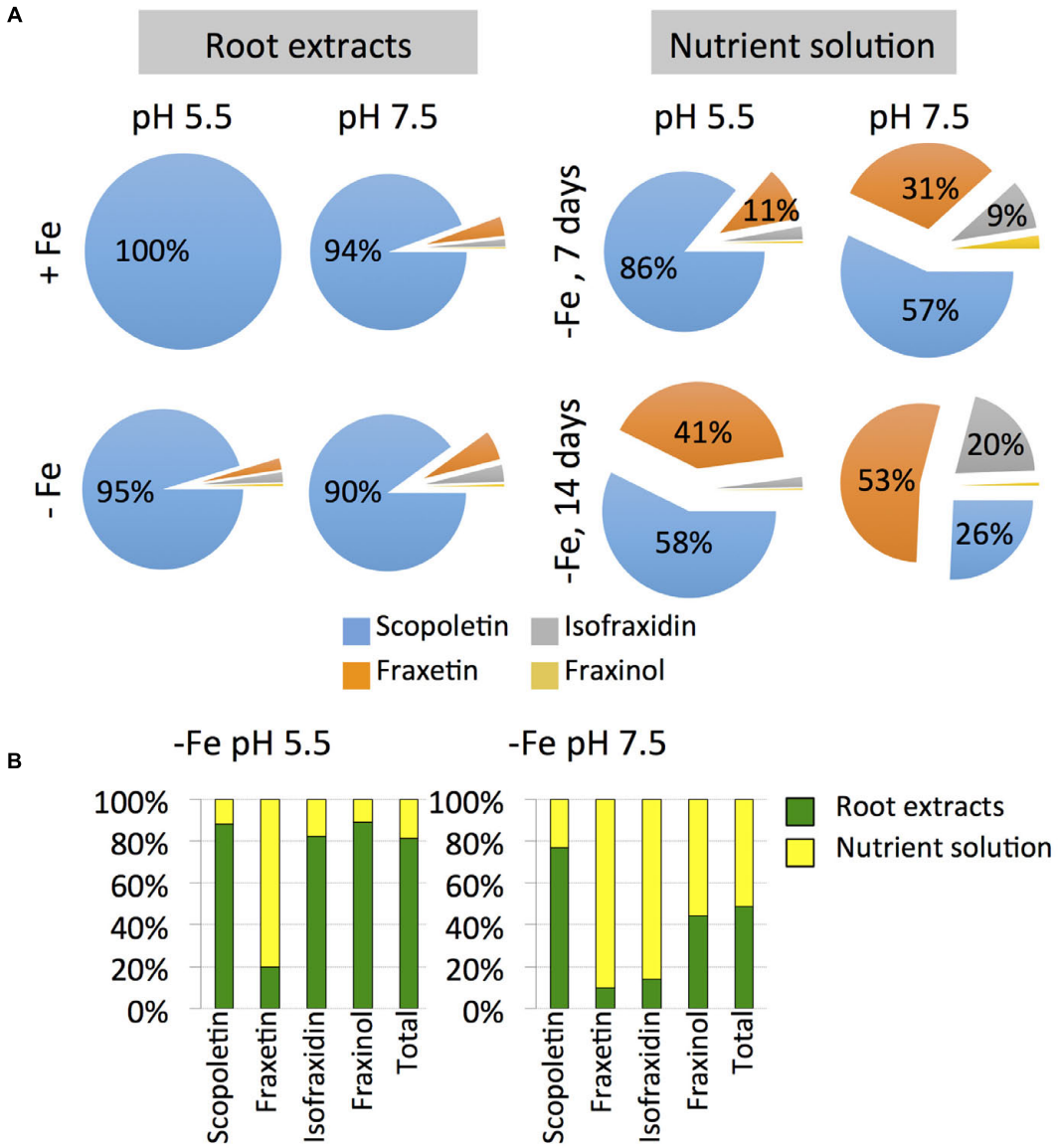

FIGURE 6 | Effects of Fe deficiency, high pH and/or time on the relative concentrations of coumarins (scopletin, fraxetin, isofraxidin, fraxinol and total coumarins) in root extracts and nutrient solution (A) and on the allocation of coumarins to the roots and the nutrient solutions of *Arabidopsis thaliana* (B). Plants were pre-grown as indicated in **Figure 2** and grown for 7 or 14 days with 0 (−Fe) or 20 μM Fe (+Fe) in nutrient solution buffered at pH 5.5 (with 5 mM MES-NaOH) or 7.5 (with 5 mM HEPES-NaOH). Data are means of $n = 3$–5. The absolute values are shown in **Figures 5** and **7**.

Fe-deficient plants were grown at pH 7.5, the concentrations of coumarins (with the exception of fraxinol) and coumarinolignans in the nutrient solution increased with time. When compared to the concentrations at day 7, increases at d 14 were 12-fold for isofraxidin, 9-fold for fraxetin, 5-fold for cleomiscosin A, 3-fold for 5′-hydroxycleomiscosins and the cleomiscosins B and D, and 2-fold for scopoletin and cleomiscosin C.

Scopoletin was the predominant coumarin only at pH 5.5 after 7 days of Fe deficiency (86% of the total coumarins), whereas at 14 days scopoletin and fraxetin accounted for 58 and 41% of the total, respectively (**Figure 6A**). At pH 7.5 scopoletin and fraxetin were the major coumarins at day 7 (57 and 31%, respectively), whereas at d 14 scopoletin, fraxetin and isofraxidin accounted for 26, 53, and 20% of the total, respectively.

Allocation of Coumarins to the Roots and the Nutrient Solutions

The allocation of coumarins produced by Fe-deficient plants was affected by the growth media pH. In plants grown at pH 5.5, only 19% of the total amount of coumarins was allocated to the nutrient solution, whereas for plants grown at pH 7.5 coumarins were allocated equally between nutrient solutions

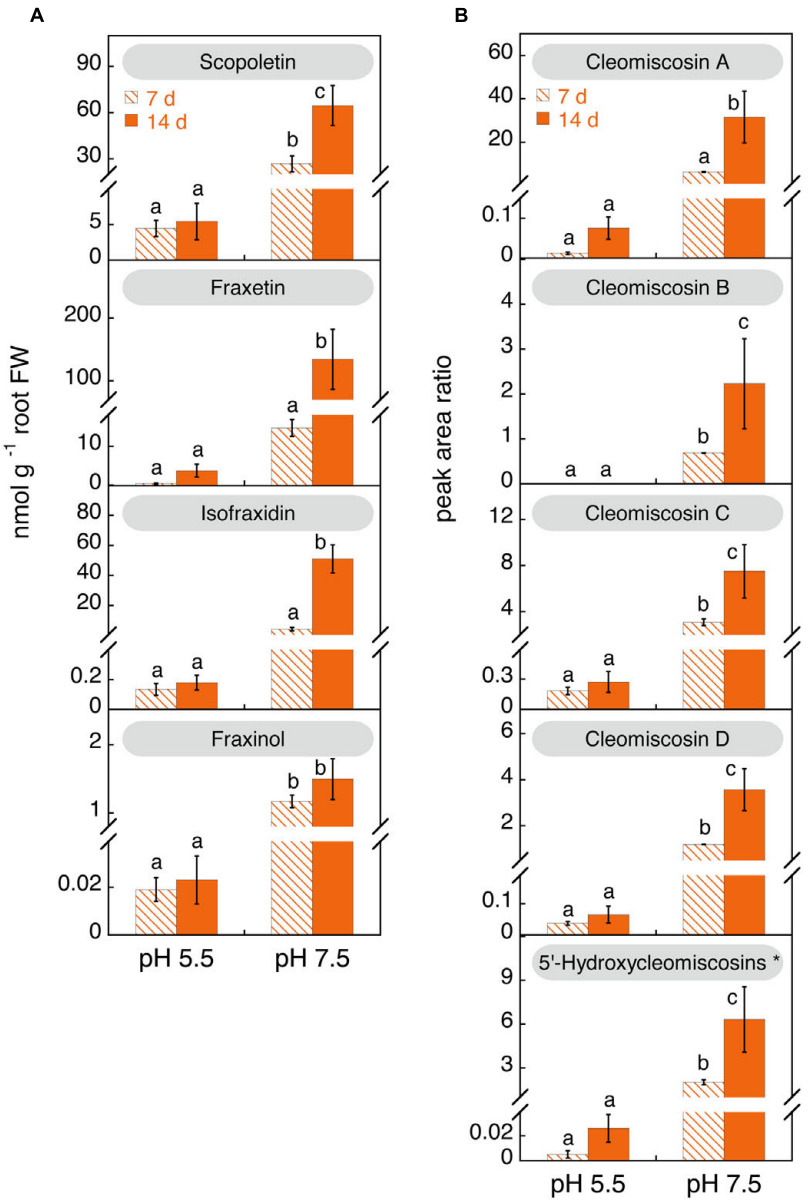

FIGURE 7 | Effects of time of Fe deficiency and high pH treatments on the concentrations (in nmol g^{-1} root FW) of coumarins (A) and coumarinolignans (B) in the nutrient solution of iron (Fe)-deficient *Arabidopsis thaliana*. Plants were pre-grown as indicated in **Figure 2** and grown for 7 or 14 days with 0 μM Fe in nutrient solution buffered at pH 5.5 (with 5 mM MES-NaOH) or 7.5 (with 5 mM HEPES-NaOH). The levels of the cleomiscosins are expressed in peak area ratio, relative to the lignan matairesinol used as internal standard. Data are means ± SE ($n = 3$–5). For each compound, significant differences among treatments (at $p < 0.05$) are marked with different letters above the columns. *5′-Hydroxycleomiscosins A and/or B should be considered since separation of these isomer compounds might have not been achieved.

(51% of the total per plant) and roots (49%) (**Figure 6B**). Fraxetin was preferentially allocated to the nutrient solution at both pH values, whereas isofraxidin and fraxinol did only so at pH 7.5.

Mobilization of Fe from Fe(III)-Oxide Promoted by Coumarins

In order to understand the role that coumarins could play in Fe plant nutrition, their ability to mobilize Fe from Fe(III)-oxide was measured in *in vitro* incubation assays. The experiments were carried out with a poorly crystaline Fe(III)-oxide and 1.5 ml of an assay medium containing 0 (blank) or 100 μM of coumarin and buffered at pH 5.5 or 7.5. Three out of the four coumarins assayed (scopoletin, isofraxidin and fraxin) have a catechol moiety capped *via* hydroxyl group methylation or hydroxyl group glucosylation, whereas the fourth coumarin, fraxetin, bears an available catechol moiety (see structures in **Figure 1A**). Coumarolignans could not be used in these

experiments because of the lack of commercial authenticated standards. Assays were run in the presence of the Fe(II) trapping agent BPDS to monitor the reductive dissolution of Fe(III)-oxide, and the concentration of Fe(II)-$BPDS_3$ was termed Fe(II). The overall mobilization of Fe was assessed by determining the total Fe in solution using ICP-MS (**Figure 8**). The Fe mobilized by the buffer solutions (blanks) was on the average 0.2 nmol Fe g^{-1} Fe(III)-oxide min^{-1}. When the assay medium contained the non-catechol coumarins fraxin, scopoletin and isofraxidin, the total Fe mobilized was in the range 0.9–1.2 nmol Fe g^{-1} Fe(III)-oxide min^{-1} (depending on the coumarins and the assay pH) and statistically significant differences were found when compared to the blank (**Figure 8A**). However, when the assay medium contained the catechol coumarin fraxetin, the amounts of Fe mobilized (5.8 and 9.4 nmol Fe g^{-1} Fe(III)-oxide min^{-1} for the assays at pH 5.5 and pH 7.5, respectively) were significantly higher than the rest (**Figure 8A**). Furthermore, the total mobilization of Fe promoted by fraxetin at pH 7.5 increased linearly when the concentration of fraxetin increased from 10 to 100 μM. A relevant fraction (40–44%) of the mobilized Fe was trapped by BPDS and this fraction also increased linearly when the concentration of fraxetin increased from 10 to 100 μM (**Figure 8B**).

DISCUSSION

Arabidopsis thaliana plants produce and secrete an array of phenolics in response to Fe deficiency when the pH of the nutrient solution is high. Phenolics found in this study include several coumarinolignans not previously reported in *A. thaliana* (cleomiscosins A, B, C, and D and the 5′-hydroxycleomiscosins A and/or B), as well as other previously reported coumarins (scopoletin, fraxetin, isofraxidin and fraxinol) and some coumarin precursors (ferulic acid and coniferyl and sinapyl aldehydes). The identification of all these phenolic compounds was achieved through an integrative interpretation of analytical data, including exact molecular mass-to-charge ratios (*m/z*), low and high-resolution MS^n spectra, chromatographic RTs and fluorescence/UV-VIS data. Furthermore, we report here for the first time on the quantification of all identified coumarins, revealing that Fe deficiency mainly induced the root accumulation and exudation of the non-catechol coumarin scopoletin and the catechol coumarin fraxetin, with the exudation of fraxetin being more prominent when Fe chlorosis was intense. Also, we show for the first time that fraxetin, but not scopoletin, was effective to mobilize Fe from an scarcely soluble Fe(III)-oxide.

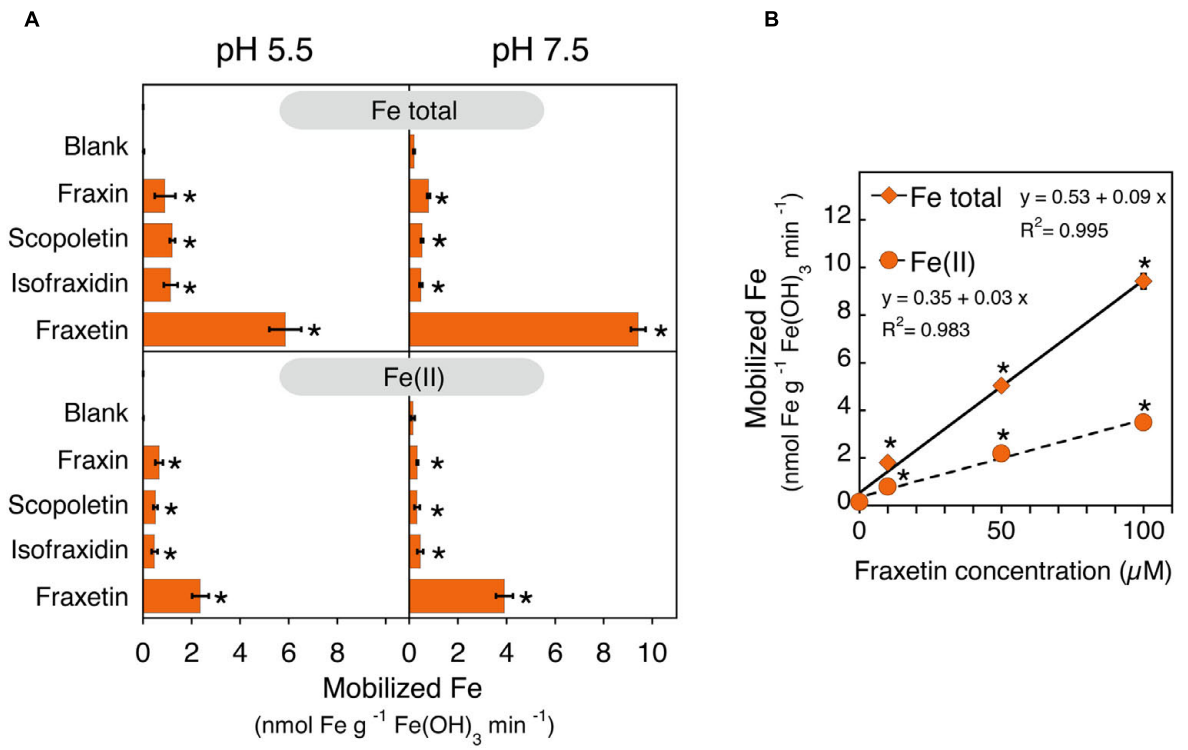

FIGURE 8 | Iron mobilization from an scarcely soluble Fe(III)-oxide as affected by coumarins. (A) Structure-activity relationship of coumarins on Fe mobilization activity. The assays consisted in the incubation of 10 mg of Fe(III)-oxide with a solution of 0 (blank) or 100 μM of the indicated coumarins and 600 μM BPDS at two different pH values, 5.5 and 7.5. Total Fe and Fe(II)-$(BPDS)_3$ in solution were determined by ICP-MS and spectrophotometry, respectively. **(B)** Effects of the fraxetin concentration on the Fe mobilization activity at pH 7.5. Scatter plot of the concentration of fraxetin vs. the total Fe mobilized and the Fe(II), with linear regression lines in black and their corresponding equations. In all cases **(A,B)**, data are means ± SE ($n = 3$–12) and asterisks denote a statistically significant difference between blank and a coumarin-containing assay medium as determined by Student's *t*- test ($p < 0.05$).

This is the first time cleomiscosins and 5′-hydroxycleomiscosins have been reported in *A. thaliana*. Cleomiscosins were found in both roots and nutrient solutions, whereas 5′-hydroxycleomiscosins were found only in nutrient solutions (**Figures 5B** and **7B**). All coumarinolignans found have a fraxetin moiety linked to different phenylpropanoid units (**Figure 1C**). Non-conventional lignans, including coumarinolignans and other hybrid ones, harbor a single phenylpropanoid unit, whereas conventional ones consist in phenylpropanoid dimers. The common coumarin moiety in the coumarinolignans found, fraxetin, has been consistently reported to increase with Fe deficiency in roots and growth media of *A. thaliana* (**Figures 5** and **7**; Fourcroy et al., 2014; Schmid et al., 2014; Schmidt et al., 2014). The phenylpropanoid units found are the primary lignin precursors coniferyl (in cleomiscosins A and B) and sinapyl alcohols (in cleomiscosins C and D), and the non-canonical monolignol 5-hydroxyconiferyl alcohol (in 5′-hydroxycleomiscosins A and B) (Begum et al., 2010) (**Figure 1C**). Previously, two other coumarinolignans, composed of esculetin and either coniferyl alcohol or sinapyl alcohol, were tentatively identified in *A. thaliana* root exudates (Strehmel et al., 2014). Until now, cleomiscosins have been only reported in seeds and stem wood and bark of various plant species, whereas 5′-hydroxycleomiscosins A and B were found in *Mallotus apelta* roots (Xu et al., 2008) and *Eurycorymbus cavaleriei* twigs (Ma et al., 2009), respectively. Cleomiscosin A has been reported in 22 plant species belonging to 12 families (e.g., Sapindaceae and Simaroubaceae), whereas cleomiscosins B, C, and D, although less common, have been found in 6–10 plant species belonging to 5–9 families (Begum et al., 2010).

Besides coumarinolignans, ferulic acid and other related metabolites were found to accumulate in roots of Fe-deficient *A. thaliana* plants when grown at high pH (**Table 1**; **Figure 5A**). This is consistent with Fe-deficient *A. thaliana* root transcriptomic (Rodríguez-Celma et al., 2013), proteomic (Lan et al., 2011) and metabolite data (Fourcroy et al., 2014): (i) ferulic acid can be converted to feruloyl-CoA by the action of 4-coumarate:CoA ligases (4CL1 and 4CL2), two enzymes that have been found to be robustly induced by Fe deficiency (Lan et al., 2011; Rodríguez-Celma et al., 2013), (ii) feruloyl-CoA is a key precursor in the biosynthesis of scopoletin (Kai et al., 2008), which accumulates in roots of Fe-deficient plants (**Figures 5A** and **7A**; Fourcroy et al., 2014; Schmid et al., 2014; Schmidt et al., 2014), and (iii) ferulic acid hexoside has been reported to occur in Fe-deficient roots (Fourcroy et al., 2014). Also, two other metabolites, coniferyl and sinapyl aldehydes, were occasionally found in Fe-deficient roots (in the aglycone and hexoside forms, **Tables 1** and **3**). Coniferyl aldehyde can either lead to scopoletin biosynthesis *via* oxidation to ferulic acid (Kai et al., 2008) or be reduced to coniferyl alcohol (Fraser and Chapple, 2011), a precursor of lignin and lignans (Barros et al., 2015), including cleomiscosins A and B. Sinapyl aldehyde is an intermediate metabolite in the synthesis of lignin and lignans such as cleomiscosins C and D (Barros et al., 2015), and may (assuming that isofraxidin synthesis is analogous to that of scopoletin, as proposed by Petersen et al., 1999) be a precursor of the coumarin isofraxidin, which accumulates consistently in Fe-deficient roots (**Figure 5A**).

Coumarins also accumulate in *A. thaliana* roots along with coumarinolignans and are secreted to the growth media in response to Fe deficiency, especially when pH was high. Four coumarins (scopoletin, fraxetin, isofraxidin and the isofraxidin isomer fraxinol) were found in both root extracts and nutrient solutions (**Tables 1** and **2**) confirming previous results (Fourcroy et al., 2014; Schmid et al., 2014; Schmidt et al., 2014) (Supplementary Table S1). We could identify fraxinol (annotated in a previous study as methoxyscopoletin; Fourcroy et al., 2014), using an authenticated standard. Aglycones and hexose conjugates of the four coumarins were found in roots (**Figure 5**; Supplementary Figure S4B), whereas only the aglycone forms were quantifiable in nutrient solutions, with hexoside forms being detected only occasionally and in low amounts (**Figure 7**). We did not detect three more coumarins, esculetin, isofraxetin and dihydroxyscopoletin, previously found as aglycones and/or glycoside forms by Schmid et al. (2014) and/or Schmidt et al. (2014) in roots or exudates of Fe-deficient *A. thaliana*. This could be due to differences in protocols for exudate collection and isolation of organic compounds from the growth/exudation media or plant growth conditions. In any case, from the published data it seems that the relative amount of these three coumarins was very low: in the only study where quantification of some coumarins was carried out, the amount of esculetin was 0.1% (roots) and <1% (exudates) when compared to those of scopoletin (Schmid et al., 2014). Assuming similar ratios in our study, the concentration of esculetin would be approximately 0.2–0.5 nmol g^{-1} root FW in roots and nutrient solutions, respectively, values still lower than those of fraxinol, the least abundant of the coumarins detected in this work (**Figures 5** and **7**). Regarding the other two coumarins not detected in this study, isofraxetin and dihydroxyscopoletin, they were only detected in Schmid et al. (2014) and Schmidt et al. (2014), respectively, indicating that their occurrence in Fe-deficient plants is not consistent.

High pH induces by itself a certain Fe stress that results in the synthesis of phenolics in roots. The increase in the production of some phenolic compounds was already observed in Fe-sufficient plants grown at high pH (**Figure 5**; Supplementary Figure S4A), along with decreases in root and shoot Fe contents (**Figure 2C**) and increases in *FRO2* expression (**Figure 2D**), even when leaf Chl and biomass were not affected (**Figures 2A–C**). It was already known that high pH compromises the root Fe acquisition from Fe(III)-chelates, with FCR activities being much lower at pH 7.5 than at the optimal pH range of 5.0-5.5 (in *A. thaliana* and other species; Moog et al., 1995; Susín et al., 1996), and FCR rates are known to be especially low with highly stable chelates such as Fe(III)-EDDHA (Lucena, 2006). When plants were grown in absence of Fe at pH 7.5 the Fe stress was much more intense and the synthesis of phenolics in roots was fully enhanced (when compared with Fe-sufficient plants grown either at high or low pH): concentrations of all phenolics in roots were much higher (**Figure 5**; Supplementary Figure S4A), the concentration of phenolics in the nutrient solution increased markedly with time (**Figure 7**; Supplementary

Figure S4A), and there were marked decreases in leaf Chl (**Figures 2A,B**), shoot biomass and shoot and root Fe contents (**Figure 2C**). The high pH/zero Fe effect is rapid, since only after 3 days roots already showed an increased expression of genes coding for root coumarin synthesis (*COMT*, *CCoAMT* and *F6′H1*) and Fe acquisition components (*IRT1* and *FRO2*) (when compared with Fe-sufficient plants grown either at high or low pH) (**Figure 2D**). In contrast, when plants were grown in absence of Fe at pH 5.5, there was no effect on biomass (**Figure 2C**) and the decreases in leaf Chl and shoot and root Fe contents (when compared with Fe-sufficient plants grown either at high or low pH) were as large as those found at high pH (**Figures 2A–C**), and only moderate effects were found with respect to phenolics, including: (i) increases of some phenolics in roots (fraxetin, isofraxidin, fraxinol, cleomiscosins A, C, and D) (**Figure 5**; Supplementary Figure S4A); (ii) time dependent increases in the concentration of all phenolics in the nutrient solution, although concentrations were always lower than those found at high pH (**Figure 7**; Supplementary Figure S4A), and (iii) a rapid (at 3 days) root increased expression of genes for Fe root uptake, although to a much lower extent than at high pH, without any change in the expression of genes involved in coumarin synthesis (**Figure 2D**).

Iron-supply and nutrient solution pH affect the relative coumarin concentrations in root extracts and growth media. Whereas the non-catechol coumarin scopoletin was initially the most abundant coumarin in root extracts and growth media, the catechol coumarin fraxetin was progressively more abundant with time in the growth media of plants grown with zero Fe (**Figure 6**). When other authors used HPLC-fluorescence for quantification, scopoletin was found to be the most abundant coumarin in the growth media of Fe-deficient *A. thaliana* (Schmid et al., 2014); fraxetin was not quantified in that study, possibly due to the very low fluorescence rate of this compound. The extremely low fluorescence of fraxetin in comparison with those of other coumarins (scopoletin, isofraxidin and esculetin) in the growth media of Fe-deficient *A. thaliana* plants is shown in Supplementary Figure S5. Interestingly, in the roots of Fe-deficient plants grown at pH 7.5 the coumarins that have a larger aglycone fraction (scopoletin and fraxetin; Supplementary Figure S4B), likely due to the action of a glucosidase, were also the prevalent ones in the growth media, supporting that the aglycone forms are likely to be the substrate for the plasma membrane transporter ABCG37. In this respect, the β-glucosidase BGLU42 is induced by Fe deficiency in roots (García et al., 2010; Yang et al., 2010; Lan et al., 2011; Rodríguez-Celma et al., 2013), and the roots of Fe-deficient *bglu42 A. thaliana* mutant plants apparently fail to secrete coumarins (Zamioudis et al., 2014). However, coumarin glucosides such as scopolin have been reported to occur in the exudates of Fe-deficient *A. thaliana* in other studies (Schmid et al., 2014; Schmidt et al., 2014).

The structural features of each coumarin-type compound may confer specific roles that contribute to the adaptation of *A. thaliana* to low Fe availability in alkaline conditions. The catechol moiety enable coumarins to mobilize efficiently Fe from an Fe(III)-oxide (**Figure 8A**). Fraxetin, a coumarin bearing a catechol moiety and a methoxy substituent, mobilized much more Fe than any of the non-catechol coumarins tested at the same concentration (100 μM; scopoletin, isofraxidin and fraxin) at physiologically relevant pH values (5.5 and 7.5). Specific structural features of the non-catechol coumarins tested, such as the *O*-glucosyl moiety (in fraxin) and one or two methoxy groups (in scopoletin/fraxin and ixofraxidin, respectively) do not appear to affect to the Fe mobilization ability of the coumarin, since these three coumarins mobilized similar amounts of Fe (**Figure 8A**). This confirms what has been reported previously (at pH 7.2) with the catechol coumarin esculetin (no methoxy substituent) and the non-catechol coumarins scopoletin (one methoxy and one hydroxy substituents) and esculin (one *O*-glucosyl and one hydroxy substituents) (Schmid et al., 2014). In addition, the present study revealed that the mobilization of Fe from Fe(III)-oxide promoted by fraxetin involves a significant reduction of Fe(III) to Fe(II) and appears to be controlled by the fraxetin concentration and the medium pH. Approximately 42% of the Fe mobilized by fraxetin was trapped by BPDS, regardless of the assay pH and the fraxetin concentration (**Figure 8**). The Fe(II) produced may be directly taken up by root cells, chelated by other natural ligands and/or re-oxidized to Fe(III). The amount of Fe mobilized by fraxetin was 1.6-fold higher at pH 7.5 -typical of calcareous soils- than at pH 5.5 (**Figure 8A**). Also, increases in fraxetin concentration (from 10 to 100 μM) led to a marked enhancement in Fe mobilization rates (**Figure 8B**). Most of the fraxetin produced by Fe-deficient plants (80–90%) was allocated to the nutrient solution regardless of the growth media pH, in contrast with the small amount of the non-catechol coumarin, scopoletin, allocated to the nutrient solution (12–23%) (**Figure 6B**). Taking also into account the concentrations estimated for scopoletin (21 μM), fraxetin (43 μM), isofraxidin (14 μM) and fraxinol (0.5 μM) in the soil solution surrounding the root (apex) of *A. thaliana* growing without Fe at pH 7.5 (calculated as in Römheld, 1991, for phytosiderophores), it seems likely that fraxetin could play a role as an Fe mobilizer in natural conditions. A catechol group is also present in the coumarinolignans 5′-hydroxycleomiscosins A and B (**Figure 1C**) that were found only in exudates (**Table 1**; **Figure 7**). Therefore, not only fraxetin but also 5-hydroxycleomiscosins A/B may have a role in mining Fe from soil Fe sources at high pH, providing soluble Fe for plant uptake. Unfortunately, no authenticated standards exist in the market for these compounds. On the other hand, coumarins, having or not catechol groups, play a well-established role in plant defense, serving as allelochemicals against a broad array of organisms (e.g., bacteria, fungi, nematodes, insects, etc), with their synthesis being activated in plants after infection (Weinmann, 1997; Bourgaud et al., 2006). Therefore, the array of coumarin-type compounds found in the growth media could play multiple roles, achieving different benefits for Fe-deficient plants.

Accumulating experimental evidences suggest that the Fe deficiency-elicited production of coumarin-type phenolics allows *A. thaliana* plants interacting with the rhizosphere microbiome, including beneficial and pathogen organisms. On one hand, Fe-deficient *A. thaliana* plants display reduced susceptibility

to infection with the necrotrophic fungus *Botrytis cinerea* and the bacterial plant pathogen *Dickeya dadantii*, with an Fe supplementation restoring symptoms severity (Kieu et al., 2012). On the other hand, the activation of immunity toward broadly diverse pathogens and even insects and herbivores in *A. thaliana* elicited by the beneficial rhizobacteria *Pseudomonas fluorescens* WCS417 and mediated by the root-specific transcription factor MYB72 (Van der Ent et al., 2008; Segarra et al., 2009), also required for the induction of Fe deficiency responses (Palmer et al., 2013), involves not only the production of F6'H1-dependent coumarins but also their secretion (Zamioudis et al., 2014). In fact, two *Arabidopsis* mutants failing in the production and/or secretion of coumarins, *myb72* and *bglu42*, did not show, when grown in the presence of WCS417, enhanced resistance against two biotrophic pathogens (the Gram-negative bacterium *Pseudomonas syringae* pv. tomato DC3000 and the pseudo-fungus *Hyaloperonospora arabidopsidis*; Zamioudis et al., 2014). Also, BGLU42 overexpression led to a significantly enhanced resistance against *B. cinerea*, *H. arabidopsidis* and *P. syringae* pv. tomato DC3000 (Zamioudis et al., 2014). The enhanced disease resistance of *A. thaliana* against different pathogens can be associated with the structure of the coumarin-type compounds produced, since different substituents in the backbone of coumarins and lignans can influence biological activity (Weinmann, 1997; Apers et al., 2003; Borges et al., 2005; Zhang et al., 2014; Pilkington and Barker, 2015).

Certain structural features of coumarins and coumarinolignans produced by roots of Fe-deficient *A. thaliana* plants may confer specific roles in shaping the rhizosphere microbiome. In fact, the existence of differences in inhibitory potential against specific microorganisms may be expected in Fe deficiency-induced coumarins. First, all coumarins detected in Fe-deficient *A. thaliana* root extracts and exudates are highly oxygenated and with hydroxyl/methoxy substituents: scopoletin and esculetin are di-oxygenated and fraxetin, fraxetin isomer, isofraxidin and fraxinol are tri-oxygenated (**Figure 1A**). A high number of oxygen-containing substituents in the benzopyrone coumarin backbone (**Figure 1A**) appears to be determinant for broadening the antibacterial spectrum (Kayser and Kolodziej, 1999), whereas the presence of simple substituents (e.g., hydroxy, methoxy) instead of bulkier chains may aid bacterial cell wall penetration. Second, an oxygenation pattern consisting in two methoxy substituents and at least one additional hydroxyl substituent is present in the minor tri-oxygenated coumarins isofraxidin and fraxinol produced by Fe-deficient *A. thaliana* roots. This oxygenation pattern seems to confer to tri-oxygenated coumarins a strong and wide inhibitory activity against Gram-positive and Gram-negative bacteria (Kayser and Kolodziej, 1999; Smyth et al., 2009). Furthermore, the estimated concentrations of scopoletin, fraxetin, isofraxidin and fraxinol in the soil solution surrounding the root (apex) of *A. thaliana* growing without Fe at pH 7.5 (see above) are close or above the minimum inhibitory concentration of di- and tri-oxygenated coumarins against Gram-positive and Gram-negative bacteria (1.3-11.2 and 0.9-4.5 μM, respectively; Kayser and Kolodziej, 1999).

Regarding plant coumarinolignans, the current knowledge on their biological activities is mostly pharmacological, derived from the ethno-medical utilization of some plant species (Begum et al., 2010; Zhang et al., 2014; Pilkington and Barker, 2015). Known activities of cleomiscosins include liver protection, cytotoxicity against lymphocytic leukemia cells, immunomodulation, and others. In plants, the defense roles for conventional lignans have been studied, and certain structural features appear to affect the activities against specific organisms. First, coumarinolignans are more aromatic than conventional lignans, suggesting they may have a higher effectiveness. For instance, increased antifungal activities were observed when the phenyl ring in a monomeric phenylpropanoid derivative was replaced by naphthyl or phenanthryl rings, whereas no or very low antifungal activity is associated to the monomeric phenylpropanoid moieties in conventional lignans (Apers et al., 2003). Second, the occurrence of methoxy substituents in lignans appear confer stronger insecticide and fungicide activities, whereas the presence of polar substituents, especially hydroxy or glycoside groups, sometimes reduced them (Harmatha and Nawrot, 2002; Harmatha and Dinan, 2003; Kawamura et al., 2004). Since cleomiscosin structures differ in the methoxy and hydroxy substituents (**Figure 1C**), their possible insecticide and fungicide activities is likely to be different.

Results presented here highlight that Fe deficiency elicits the accumulation in roots and secretion into the growth media of an array of coumarin-type compounds, including coumarinolignans (cleomiscosins A, B, C, and D and the 5′-hydroxycleomiscosins A and/or B) and simple coumarins (scopoletin, fraxetin, isofraxidin and fraxinol) in *A. thaliana*. The phenolics response was much more intense when the plant accessibility to Fe was decreased and Fe status deteriorated, as it occurs when plants are grown in the absence of Fe at pH 7.5. The structural features of the array of coumarins and lignans produced and their concentrations in roots and growth media suggest that they may play dual, complementary roles as Fe(III) mobilizers and allelochemicals. Fraxetin, a catechol coumarin, was the most prominent coumarin found in the growth media of Fe-deficient *A. thaliana* plants grown at high pH and was especially effective in mobilization of Fe from an Fe(III)-oxide. In contrast, the rest of coumarins were non-catechols and were present in much lower concentrations, and therefore their role in mobilizing Fe is unlikely, although they can still be efficient as allelochemicals. Therefore, the production and secretion of phenolics by roots in response to Fe deficiency would promote an overall decrease in the competition for Fe in the immediate vicinity of roots, resulting in improved plant Fe nutrition. Results also suggest that Fe deficiency could be a good experimental model to understand the ecological dynamics of the biotic interactions in the plant rhizosphere.

AUTHOR CONTRIBUTIONS

AA-F, PF, and AA conceived and designed the experiments, PS-T conducted experiments, collected data, and drafted the manuscript, AL-V quantified phenolics, carried out Fe mobilization studies and made figures, AA, FG, J-FB, JA, and

AA-F wrote, reviewed and edited the paper. All authors read and approved the final manuscript.

FUNDING

Work supported by the Spanish Ministry of Economy and Competitiveness (MINECO) (grant AGL2013-42175-R, co-financed with FEDER) and the Aragón Government (group A03). PS-T and AL-V were supported by MINECO-FPI contracts.

ACKNOWLEDGMENT

We thank Cristina Ortega and Gema Marco (Aula Dei Experimental Station-CSIC) for growing and harvesting plants.

SUPPLEMENTARY MATERIAL

The Supplementary Material for this article can be found online at: http://journal.frontiersin.org/article/10.3389/fpls.2016.01711/full#supplementary-material

REFERENCES

Abadía, J., and Abadía, A. (1993). "Iron and plant pigments," in *Iron Chelation in Plants and Soil Microorganisms*, eds L. L. Barton and B. C. Hemming (New York, NY: Academic Press), 327–343.

Apers, S., Vlietinck, A., and Pieters, L. (2003). Lignans and neolignans as lead compounds. *Phytochem. Rev.* 2, 201–217. doi: 10.1023/B:PHYT.0000045497.90158.d2

Aznar, A., Chen, N. W. G., Thomine, S., and Dellagi, A. (2015). Immunity to plant pathogens and iron homeostasis. *Plant Sci.* 240, 90–97. doi: 10.1016/j.plantsci.2015.08.022

Barros, J., Serk, H., Granlund, I., and Pesquet, E. (2015). The cell biology of lignification in higher plants. *Ann. Bot.* 115, 1053–1074. doi: 10.1093/aob/mcv046

Begum, S. A., Sahai, M., and Ray, A. B. (2010). Non-conventional lignans: coumarinolignans, flavonolignans, and stilbenolignans. *Fortschr. Chem. Org. Naturst.* 93, 1–70.

Borges, F., Roleira, F., Milhazes, N., Santana, L., and Uriarte, E. (2005). Simple coumarins and analogues in medicinal chemistry: occurrence, synthesis and biological activity. *Curr. Med. Chem.* 12, 887–916. doi: 10.2174/0929867053507315

Bourgaud, F., Hehn, A., Larbat, R., Doerper, S., Gontier, E., Kellner, S., et al. (2006). Biosynthesis of coumarins in plants: a major pathway still to be unravelled for cytochrome P450 enzymes. *Phytochem. Rev.* 5, 293–308. doi: 10.1007/s11101-006-9040-2

Briat, J. F., Dubos, C., and Gaymard, F. (2015). Iron nutrition, biomass production, and plant product quality. *Trends Plant Sci.* 20, 33–40. doi: 10.1016/j.tplants.2014.07.005

Bristow, A. W. T. (2006). Accurate mass measurement for the determination of elemental formula–A tutorial. *Mass Spectrom. Rev.* 25, 99–111. doi: 10.1002/mas.20058

Cesco, S., Neumann, G., Tomasi, N., Pinton, R., and Weisskopf, L. (2010). Release of plant-borne flavonoids into the rhizosphere and their role in plant nutrition. *Plant Soil* 329, 1–25. doi: 10.1007/s11104-009-0266-9

Chattopadhyay, S. K., Kumar, S., Tripathi, S., Kaur, R., Tandon, S., and Rane, S. (2008). High-performance liquid chromatography and LC-ESI-MS method for the identification and quantification of two biologically active isomeric coumarinolignoids cleomiscosin A and cleomiscosin B in different extracts of *Cleome viscosa*. *Biomed. Chromatogr.* 22, 1325–1345. doi: 10.1002/bmc.1062

Cheng, X. F., and Chen, Z. L. (2000). Coumarinolignoids of *Mallotus apelta*. *Fitoterapia* 71, 341–342. doi: 10.1016/S0367-326X(99)00160-4

Croteau, R., Kutchan, T. M., and Lewis, N. G. (2000). "Natural products (secondary metabolites)," in *Biochemistry and Molecular Biology of Plants*, eds B. Buchanan, W. Gruissem, and R. Jones (Rockville, MD: American Society of Plant Physiologists), 1250–1318.

Crumbliss, A. L., and Harrington, J. M. (2009). Iron sequestration by small molecules: thermodynamic and kinetic studies of natural siderophores and synthetic model compounds. *Adv. Inorg. Chem.* 61, 179–250. doi: 10.1016/S0898-8838(09)00204-9

Fourcroy, P., Sisó-Terraza, P., Sudre, D., Savirón, M., Reyt, G., Gaymard, F., et al. (2014). Involvement of the ABCG37 transporter in secretion of scopoletin and derivatives by *Arabidopsis* roots in response to iron deficiency. *New Phytol.* 201, 155–167. doi: 10.1111/nph.12471

Fourcroy, P., Tissot, N., Reyt, G., Gaymard, F., Briat, J. F., and Dubos, C. (2016). Facilitated Fe nutrition by phenolic compounds excreted by the *Arabidopsis* ABCG37/PDR9 transporter requires the IRT1/FRO2 high-affinity root Fe2+ transport system. *Mol. Plant* 9, 485–488. doi: 10.1016/j.molp.2015.09.010

Fraser, C. M., and Chapple, C. (2011). The phenylpropanoid pathway in *Arabidopsis*. *Arabidopsis Book* 9:e0152. doi: 10.1199/tab.0152

García, M. J., Lucena, C., Romera, F. J., Alcántara, E., and Pérez-Vicente, R. (2010). Ethylene and nitric oxide involvement in the up-regulation of key genes related to iron acquisition and homeostasis in *Arabidopsis*. *J. Exp. Bot.* 61, 3885–3899. doi: 10.1093/jxb/erq203

Guerinot, M. L., and Ying, Y. (1994). Iron: nutritious, noxious, and not readily available. *Plant Physiol.* 104, 815–820. doi: 10.1104/pp.104.3.815

Harmatha, J., and Dinan, L. (2003). Biological activities of lignans and stilbenoids associated with plant-insect chemical interaction. *Phytochem. Rev.* 2, 321–330. doi: 10.1023/B:PHYT.0000045494.98645.a3

Harmatha, J., and Nawrot, J. (2002). Insect feeding deterrent activity of lignans and related phenylpropanoids with a methylenedioxyphenyl (piperonyl) structure moiety. *Entomol. Exp. Appl.* 104, 51–60. doi: 10.1046/j.1570-7458.2002.00990.x

Jin, C. W., He, Y. F., Tang, C. X., Wu, P., and Zheng, S. J. (2006). Mechanisms of microbially enhanced Fe acquisition in red clover (*Trifolium pratense* L.). *Plant Cell Environ.* 29, 888–897. doi: 10.1111/j.1365-3040.2005.01468.x

Jin, C. W., Ye, Y. Q., and Zheng, S. J. (2014). An underground tale: contribution of microbial activity to plant iron acquisition via ecological processes. *Ann. Bot.* 113, 7–18. doi: 10.1093/aob/mct249

Jin, C. W., You, G. Y., He, Y. F., Tang, C. X., Wu, P., and Zheng, S. J. (2007). Iron deficiency-induced secretion of phenolics facilitates the reutilization of root apoplastic iron in red clover. *Plant Physiol.* 144, 278–285. doi: 10.1104/pp.107.095794

Kai, K., Mizutani, M., Kawamura, N., Yamamoto, R., Tamai, M., Yamaguchi, H., et al. (2008). Scopoletin is biosynthesized via ortho-hydroxylation of feruloyl CoA by a 2-oxoglutarate-dependent dioxygenase in *Arabidopsis thaliana*. *Plant J.* 55, 989–999. doi: 10.1111/j.1365-313X.2008.03568.x

Kaur, R., Kumar, S., Chatterjee, A., and Chattopadhyay, S. K. (2010). High-performance liquid chromatographic method for identification and quantification of three potent liver protective coumarinolignoids-cleomiscosin A, cleomiscosin B and cleomiscosin C-in extracts of *Cleome viscosa*. *Biomed. Chromatogr.* 24, 1000–1005. doi: 10.1002/bmc.1399

Kawamura, F., Ohara, S., and Nishida, A. (2004). Antifungal activity of constituents from the heartwood of *Gmelina arborea*: Part 1. Sensitive antifungal assay against Basidiomycetes. *Holzforschung* 58, 189–192.

Kayser, O., and Kolodziej, H. (1999). Antibacterial activity of simple coumarins: structural requirements for biological activity. *Z. Naturforsch. C* 54, 169–174. doi: 10.1515/znc-1999-3-405

Kieu, N. P., Aznar, A., Segond, D., Rigault, M., Simond-Côte, E., Kunz, C., et al. (2012). Iron deficiency affects plant defense responses and confers resistance to *Dickeya dadantii* and *Botrytis cinerea*. *Mol. Plant Pathol.* 13, 816–827. doi: 10.1111/j.1364-3703.2012.00790.x

Kobayashi, T., and Nishizawa, N. K. (2012). Iron uptake, translocation, and regulation in higher plants. *Annu. Rev. Plant Biol.* 63, 131–152. doi: 10.1146/annurev-arplant-042811-105522

Lan, P., Li, W. F., Wen, T. N., Shiau, J. Y., Wu, Y. C., Lin, W. D., et al. (2011). iTRAQ Protein profile analysis of *Arabidopsis* roots reveals new aspects critical for iron homeostasis. *Plant Physiol.* 155, 821–834. doi: 10.1104/pp.110.169508

Larbi, A., Abadía, A., Morales, F., and Abadía, J. (2004). Fe resupply to Fe-deficient sugar beet plants leads to rapid changes in the violaxanthin cycle and other photosynthetic characteristics without significant de novo chlorophyll synthesis. *Photosynth. Res.* 79, 59–69. doi: 10.1023/B:PRES.0000011919.35309.5e

Lindsay, W. L. (1995). "Chemical reactions in soils that affect iron availability to plants. A quantative approach," in *Iron Nutrition in Soils and Plants*, ed. J. Abadía (Dordrecht: Kluwer Academic Publishers), 7–14.

Lucena, J. J. (2006). "Synthetic iron chelates to correct iron deficiency in plants," in *Iron Nutrition in Plants and Rhizospheric Microorganisms*, eds L. L. Barton and J. Abadía (Dordrecht: Springer), 103–128.

Ma, Z., Zhang, X., Cheng, L., and Zhang, P. (2009). Three lignans and one coumarinolignoid with quinone reductase activity from *Eurycorymbus cavaleriei*. *Fitoterapia* 80, 320–326. doi: 10.1016/j.fitote.2009.04.003

Mimmo, T., Del Buono, D., Terzano, R., Tomasi, N., Vigani, G., Crecchio, C., et al. (2014). Rhizospheric organic compounds in the soil-microorganism-plant system: their role in iron availability. *Eur. J. Soil Sci.* 65, 629–642. doi: 10.1111/ejss.12158

Moog, P. R., van der Kooij, T. A. W., Brüggemann, W., Schiefelbein, J. W., and Kuiper, P. J. C. (1995). Responses to iron deficiency in *Arabidopsis thaliana*: the turbo iron reductase does not depend on the formation of root hairs and transfer cells. *Planta* 195, 505–513. doi: 10.1007/BF00195707

Palmer, C. M., Hindt, M. N., Schmidt, H., Clemens, S., and Guerinot, M. L. (2013). MYB10 and MYB72 are required for growth under iron-limiting conditions. *Plos Genet.* 9:e1003953. doi: 10.1371/journal.pgen.1003953

Petersen, M., Strack, D., and Matern, U. (1999). "Biosynthesis of phenylpropanoid and related compounds," in *Biochemistry of Plant Secondary Metabolism*, ed. M. Wink (Sheffield: Sheffield Academic Press Ltd), 151–221.

Pilkington, L. I., and Barker, D. (2015). Synthesis and biology of 1,4-benzodioxane lignan natural products. *Nat. Prod. Rep.* 32, 1369–1388. doi: 10.1039/c5np00048c

Rodríguez-Celma, J., Lin, W. D., Fu, G. M., Abadía, J., López-Millán, A. F., and Schmidt, W. (2013). Mutually exclusive alterations in secondary metabolism are critical for the uptake of insoluble iron compounds by *Arabidopsis* and *Medicago truncatula*. *Plant Physiol.* 162, 1473–1485. doi: 10.1104/pp.113.220426

Römheld, V. (1991). The role of phytosiderophores in acquisition of iron and other micronutrients in graminaceous species: an ecological approach. *Plant Soil* 130, 127–134. doi: 10.1007/BF00011867

Schmid, N. B., Giehl, R. F. H., Doll, S., Mock, H. P., Strehmel, N., Scheel, D., et al. (2014). Feruloyl-CoA 6'-hydroxylase1-dependent coumarins mediate iron acquisition from alkaline substrates in *Arabidopsis*. *Plant Physiol.* 164, 160–172. doi: 10.1104/pp.113.228544

Schmidt, H., Gunther, C., Weber, M., Sporlein, C., Loscher, S., Bottcher, C., et al. (2014). Metabolome analysis of *Arabidopsis thaliana* roots identifies a key metabolic pathway for iron acquisition. *PLoS ONE* 9:e102444. doi: 10.1371/journal.pone.0102444

Segarra, G., Van der Ent, S., Trillas, I., and Pieterse, C. M. J. (2009). MYB72, a node of convergence in induced systemic resistance triggered by a fungal and a bacterial beneficial microbe. *Plant Biol.* 11, 90–96. doi: 10.1111/j.1438-8677.2008.00162.x

Sisó-Terraza, P., Ríos, J. J., Abadía, J., Abadía, A., and Álvarez-Fernández, A. (2016). Flavins secreted by roots of iron-deficient *Beta vulgaris* enable mining of ferric oxide via reductive mechanisms. *New Phytol.* 209, 733–745. doi: 10.1111/nph.13633

Smyth, T., Ramachandran, V. N., and Smyth, W. F. (2009). A study of the antimicrobial activity of selected naturally occurring and synthetic coumarins. *Int. J. Antimicrob. Agents* 33, 421–426. doi: 10.1016/j.ijantimicag.2008.10.022

Strehmel, N., Böttcher, C., Schmidt, S., and Scheel, D. (2014). Profiling of secondary metabolites in root exudates of *Arabidopsis thaliana*. *Phytochemistry* 108, 35–46. doi: 10.1016/j.phytochem.2014.10.003

Susín, S., Abadía, A., González-Reyes, J. A., Lucena, J. J., and Abadía, J. (1996). The pH requirement for in vivo activity of the iron-deficiency-induced "Turbo" Ferric Chelate Reductase: a comparison of the iron-deficiency-induced iron reductase activities of intact plants and isolated plasma membrane fractions in sugar beet (*Beta vulgaris*). *Plant Physiol.* 110, 111–123.

Van der Ent, S., Verhagen, B. W. M., Van Doorn, R., Bakker, D., Verlaan, M. G., Pel, M. J. C., et al. (2008). MYB72 is required in early signaling steps of rhizobacteria-induced systemic resistance in *Arabidopsis*. *Plant Physiol.* 146, 1293–1304. doi: 10.1104/pp.107.113829

Weinmann, I. (1997). *Coumarins: Biology, Applications and Mode of Action*. Chichester: Wiley Press.

Xu, J. F., Feng, Z. M., Liu, J., and Zhang, P. C. (2008). New hepatoprotective coumarinolignoids from *Mallotus apelta*. *Chem. Biodivers.* 5, 591–597. doi: 10.1002/cbdv.200890055

Yang, T. J. W., Lin, W. D., and Schmidt, W. (2010). Transcriptional profiling of the *Arabidopsis* iron deficiency response reveals conserved transition metal homeostasis networks. *Plant Physiol.* 152, 2130–2141. doi: 10.1104/pp.109.152728

Zamioudis, C., Hanson, J., and Pieterse, C. M. J. (2014). β-Glucosidase BGLU42 is a MYB72-dependent key regulator of rhizobacteria-induced systemic resistance and modulates iron deficiency responses in *Arabidopsis* roots. *New Phytol.* 204, 368–379. doi: 10.1111/nph.12980

Zhang, J., Chen, J. J., Liang, Z. Z., and Zhao, C. Q. (2014). New Lignans and their biological activities. *Chem. Biodivers.* 11, 1–54. doi: 10.1002/cbdv.201100433

Conflict of Interest Statement: The authors declare that the research was conducted in the absence of any commercial or financial relationships that could be construed as a potential conflict of interest.

frontiers in Plant Science

REVIEW
published: 04 October 2016
doi: 10.3389/fpls.2016.01488

The ALMT Family of Organic Acid Transporters in Plants and Their Involvement in Detoxification and Nutrient Security

Tripti Sharma[1], Ingo Dreyer[1], Leon Kochian[2] and Miguel A. Piñeros[2]**

[1] Centro de Bioinformática y Simulación Molecular, Facultad de Ingeniería, Universidad de Talca, Talca, Chile, [2] Robert W. Holley Center for Agriculture and Health, United States Department of Agriculture–Agricultural Research Service, Cornell University, Ithaca, NY, USA

About a decade ago, members of a new protein family of anion channels were discovered on the basis of their ability to confer on plants the tolerance toward toxic aluminum ions in the soil. The efflux of Al^{3+}-chelating malate anions through these channels is stimulated by external Al^{3+} ions. This feature of a few proteins determined the name of the entire protein family as Aluminum-activated Malate Transporters (ALMT). Meanwhile, after several years of research, it is known that the physiological roles of ALMTs go far beyond Al-detoxification. In this review article we summarize the current knowledge on this transporter family and assess their involvement in diverse physiological processes.

Keywords: anion channel, ALMT, aluminum tolerance, nutrient transport, malate transport, citrate transport, review

OPEN ACCESS

Edited by:
Matthew Gilliham,
University of Adelaide, Australia

Reviewed by:
Enrico Martinoia,
University of Zurich, Switzerland
Thomas J. Bach,
University of Strasbourg, France

****Correspondence:***
Miguel A. Piñeros
map25@cornell.edu
Ingo Dreyer
idreyer@utalca.cl

Specialty section:
This article was submitted to Plant Physiology, a section of the journal Frontiers in Plant Science

Received: *31 July 2016*
Accepted: *20 September 2016*
Published: *04 October 2016*

Citation:
Sharma T, Dreyer I, Kochian L and Piñeros MA (2016) The ALMT Family of Organic Acid Transporters in Plants and Their Involvement in Detoxification and Nutrient Security. Front. Plant Sci. 7:1488. doi: 10.3389/fpls.2016.01488

INTRODUCTION

Organic Acids in Plants – Production, Importance, and Function

Organic acids play pivotal roles in plant primary metabolism. These acids are mainly produced and involved in central metabolic pathways, such as the tricarboxylic acid cycle, C3-, C4-, and CAM-photosynthesis and, to lesser extent, in the glyoxylate cycle in plants. Organic acids, such as malate, fumarate, lactate, and citrate, are of fundamental importance at the cellular level for several biochemical pathways, including energy production, formation of precursors for amino-acid biosynthesis, and at the whole plant level in modulating adaptation to the environment (Igamberdiev and Eprintsev, 2016). They are involved in stomatal function, phosphorous acquisition, aluminum tolerance, and temporary carbon storage, interchange of reductive power among subcellular compartments, pH regulation, and the response to biotic and abiotic stresses (Meyer et al., 2010a). Some organic molecules also function as signaling molecules, not only as allosteric regulators of many key enzymes, but also as modulators of gene expression (López-Bucio et al., 2000).

Research carried out in the past two decades revealed the importance of organic acid exudation for plants encountering/tolerating metal and nutritional stress at the root-soil interface. The roots

of rape (*Brassica napus*), for instance, excrete citric and malic acids into the rhizosphere and solubilize P from rock phosphate (Hoffland et al., 2006). Root exudation of citrate may play an important role in supplying Fe to dicotyledonous plants (Brown, 1978). Organic acids have also been found to modulate nitrate uptake. Malate moves down the phloem, accumulates in the root, and stimulates the uptake of nitrate by the roots of intact soybean plants (Touraine et al., 1992). Plants growing in alkaline soils, where calcium is abundant, often reduce the excess of cellular calcium by precipitating it in the form of calcium oxalate in vacuoles of roots, stems, leaves, flowers, fruits, and seeds (Webb, 1999). Likewise, the most ubiquitous tolerant mechanism in the plant kingdom is the exclusion of Al from the root apex via root exudation of organic acids.

Historical Perspective – Al Tolerance as a Gateway for the Discovery of a New Family of Anion Transporters

Electrophysiological approaches in the 1990's and early 2000 established the existence and early biophysical characterization of a variety of predominantly plasma membrane- and tonoplast-localized anion channels in plant cells (Tyerman, 1992; Roberts, 2006). Contrary to expectations, the molecular identity of most of these anion channels remained elusive, when the genome of *Arabidopsis thaliana* became accessible. This was predominantly due to the fact that the identified homologs of animal counterparts were mainly constituted by members of the CLC channel family (Hechenberger et al., 1996; Jentsch et al., 1999; Chen, 2005; Jentsch, 2008). Consequently, seven CLC homologs were identified in the *Arabidopsis* genome, and have been shown to localize to cellular endomembranes (tonoplast, golgi, and chloroplast). As some of their animal counterparts, they functionally encode H^+/Cl^- exchangers [reviewed by (Barbier-Brygoo et al., 2011)], but they are also involved as nitrate/proton antiporters in the nitrate accumulation in plant vacuoles (De Angeli et al., 2006). Paradoxically, the molecular identity of a new family of anion channels involved in a large variety of *in planta* roles, was revealed by studies in the field of Al-tolerance. Classical plant physiology studies provided evidence that several monocot and dicot plant species exclude phytotoxic Al^{3+} from entering the cells of the root tip by exuding di- and tri-carboxylic acids (e.g., citrate, malate, and/or oxalate), thereby chelating and immobilizing the soluble Al^{3+} at the root surface by forming stable, non-toxic complexes (Delhaize et al., 1993a,b; Ma et al., 1997). The thermodynamic nature of the transport, i.e., a large electrochemical gradient of organic acids from the cytosol to the apoplasm, suggested anion channels mediated the organic acid efflux. This prompted the implementation of electrophysiological techniques, the patch clamp technique for instance, to further characterize the transport process. With such an approach Ryan and coworkers (Ryan et al., 1997; Zhang et al., 2001) provided the first proof of an Al^{3+}-dependent plasma membrane anion (malate selective) conductance in wheat root protoplasts from an Al-tolerant line. Evidence for the existence of similar types of channels in protoplasts from Al-resistant maize roots was reported soon after (Kollmeier et al., 2001; Piñeros and Kochian, 2001; Piñeros et al., 2002), further indicating that these single anion channels could be activated by Al^{3+} in outside-out excised membrane patches in the absence of additional cytosolic factors. The similarities between the transport and activation properties reported in these electrophysiological studies and the Aluminum-activated organic acid exudation observed in intact wheat and maize roots provided the first indication that this novel type of anion channel was likely underlying the Al-activated organic acid release observed at the whole root level. Further elucidation of the molecular nature of these transporters came from a subtractive hybridization approach, using a pair of near-isogenic wheat lines differing at a single Al tolerance locus. This approach led to the identification of the *TaALMT1* gene (formerly named *ALMT1*), the founder of the so called ALMT (Aluminum-activated Malate Transporters) family (Sasaki et al., 2004). Heterologous expression of this gene in roots of transgenic rice seedlings and tobacco suspension cells conferred an Al-dependent exudation of malate. Consistently, functional analysis in *Xenopus* oocytes indicated that this transporter mediated an inward current caused by a malate efflux, which strongly depended on the presence of extracellular Al^{3+}. Transgenic barley (*Hordeum vulgare*) expressing TaALMT1 also showed an increase in Al-resistance in roots (Delhaize et al., 2004). Although TaALMT1 is functionally active in the absence of extracellular Al^{3+}, this unique functional property of Al-mediated enhancement of transport activity (awkwardly referred to as Al-activation) is responsible for the sometimes misleading historical name comprising all members of this transporter family as ALMT. To date 'Al activation' has only been reported in a small subset of ALMTs members, while *in planta* the functions of a large number of members have been shown to be highly diverse and transcend beyond root Al-resistance responses. Soon after its discovery in wheat, Al tolerance-related studies led to the identification of *AtALMT1*, the first out of 14 *Arabidopsis* ALMT members to be functionally characterized, as well as the homologs *BnALMT1* and *BnALMT2* from rape, *GmALMT1* in soybean, and *ScALMT1* in rye. They all shared similar functional characteristics consistent with their involvement in mediating the organic acid exudation in Al-tolerance response in these plant species (Hoekenga et al., 2006; Ligaba et al., 2006, 2007). Likewise, *MsALMT1* from *Medicago sativa* and *HlALMT1* from the grass *Holcus lanatus* have been described as crucial genes involved in Al resistance (**Figure 1**) (Chen Q. et al., 2013; Chen Z.C. et al., 2013). Subsequent studies in relation to the role of the novel and emerging ALMT family in mediating Al-resistance responses led to the identification of the maize homolog ZmALMT1. However, although ZmALMT1 was shown to function as a plasma membrane transporter capable of mediating a selective anion efflux and influx, the gene expression data as well as biophysical transport characteristics provided the first indication in the literature that the *in planta* function of some members of this ALMT family might extend beyond Al tolerance to a variety of physiological processes (Piñeros et al., 2008b). Since then an increasing number of studies have clearly indicated that ALMTs underlie a variety of processes, including metal toxicity avoidance, mineral nutrition,

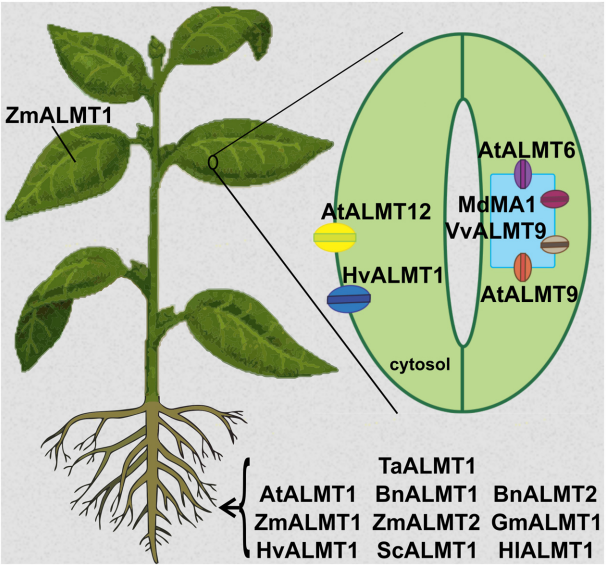

FIGURE 1 | Tissue localization of Aluminum-activated Malate Transporters (ALMTs) from different plant species. AtALMT1, BnALMT1, BnALMT2, GmALMT1, HlALMT1, ScALMT1, TaALMT1 are plasma membrane channels expressed in roots and are functionally involved in providing Al^{3+} tolerance to the plant. ZmALMT1 is found at the plasma membrane of cells throughout the plant, while ZmALMT2 is localized at the plasma membrane in root cells; both are also involved in anion homeostasis. In guard cells, AtALMT6 and AtALMT9 are targeted to the tonoplast, while AtALMT12 and HvALMT1 are localized at the plasma membrane; all play crucial roles in guard cell movement and thus stomatal opening and closure. HvALMT1 is expressed in guard cells and in root cells, where it is involved in turgor regulation in expanding cells. MdMA1 and VvALMT9 are tonoplast channels with expression in guard cells; they are involved in fruit flavor development in apple and grapes, respectively.

ion homeostasis, turgor regulation, fruit quality, and guard cell function.

PHYSIOLOGICAL ROLES

Root Abiotic Stress Responses – Adaptation to Acid Soils

Aluminum-activated Malate Transporters proteins play pivotal roles in the adaptation to acid soils. The main challenge of acid soils is the increased mobility of aluminum ions and their tendency to form highly stable complexes with phosphorus. Thus, a plant faces not only the toxicity of Al^{3+} ions but also a poor bioavailability of phosphate. By releasing organic acids both problems are tackled: The carboxylates chelate Al^{3+} ions and set phosphates free. However, the plant has to find a balance between the positive effects of organic acid release and the disadvantages of losing valuable carbon sources. Consequently, ALMT proteins are regulated at the transcriptional and functional level. The expression of *AtALMT1*, for instance, is under control of assorted signal inducers like abscisic acid (ABA) and indol-3-acetic acid (IAA) along with low pH and hydrogen peroxide (Kobayashi et al., 2013; Sukweenadhi et al., 2015). Elevated expression of AtALMT1 at low pH and in the presence of H_2O_2 coincides with the observation that Al treatment results in H_2O_2 accumulation in the root tips and in a reduction of the pH (Kobayashi et al., 2013). In soybean also phosphorus has been identified as signaling molecule (Liang et al., 2013). Root malate exudation appears to be critical for soybean adaptation to both Al toxicity and P deficiency on acid soils and the underlying channel GmALMT1 is coordinately regulated by pH, aluminum, and phosphorus.

Guard Cell Regulation

Regulation of CO_2 uptake and water loss in plants is achieved through the regulation of the stomatal aperture via osmotically driven guard cell movements (Kollist et al., 2014). Plasma membrane anion channels play an important role in stomatal movements by releasing anions and contributing to the depolarization of the guard cell plasma membrane (Barbier-Brygoo et al., 2011; Kollist et al., 2011; Roelfsema et al., 2012). Early electrophysiological studies in guard cells established the existence of two types of plasma membrane anion channels with distinct activation and deactivation kinetics, thereby named rapid (R)-type (QUAC) and slow (S)-type channels (SLAC; Hedrich et al., 1990; Linder and Raschke, 1992; Schroeder and Keller, 1992). Although less studied, malate permeable tonoplast channels were also identified in early studies (Pantoja et al., 1989).

Following the identification and characterization of the *Arabidopsis* root plasma membrane-targeted AtALMT1 channel (Hoekenga et al., 2006), studies evaluating the cellular localization of GFP-tagged AtALMT proteins, as well as promoter–GUS fusion experiments, indicated that two other channels of this protein family, AtALMT9 and AtALMT6, were localized to the tonoplast of guard cells, albeit not exclusively, proposing a role of these channels in vacuolar malate transport (**Figure 2**) (Kovermann et al., 2007; Meyer et al., 2011). Although *Atalmt9* KO plants were reported to show no visible phenotype, the malate flux across the membrane of vacuoles isolated from the *Atalmt9* KO appeared to be reduced compared to that recorded on wild type vacuoles (Kovermann et al., 2007). Consistently, heterologous expression of AtALMT9 in *Nicotiana benthamiana* leaves and *Xenopus* oocytes resulted in an enhancement of the malate current density across the mesophyll tonoplasts and oocyte plasma membrane, respectively. A more detailed analysis of AtALMT9 in its native environment, as well as after heterologous expression, however, has indicated that AtALMT9 is a chloride channel, which is activated by physiological concentrations of cytosolic malate (De Angeli et al., 2013b). Based on its functional characteristics it has been proposed that this channel plays an important role in fast and complete opening of stomata, while having no effect on stomatal closure. Consistently, *Atalmt9* KO plants showed a drought resistant phenotype, which is in line with the findings of impaired stomatal opening due to decreased uptake of chloride in guard cells.

Electrophysiological characterization of vacuoles isolated from AtALMT6-GFP over expressing *Arabidopsis* plants revealed in patch clamp experiments large, calcium-activated, inward-rectifying malate currents, i.e., a malate flux from the cytosol

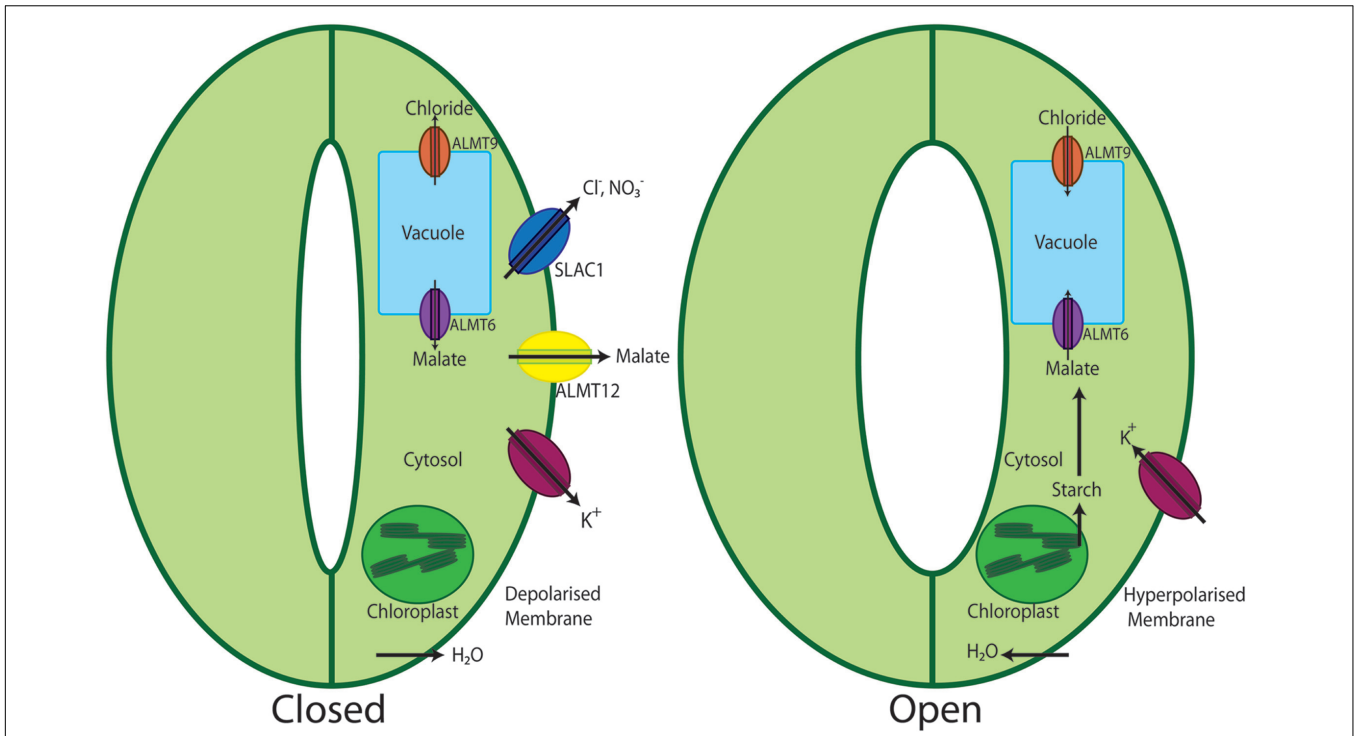

FIGURE 2 | Schematic representation of the role of ALMTs in stomatal opening and closure. During stomatal closure K^+ is released from the guard cell along with the release of malate via ALMT12 and Cl^- and NO_3^- ions via SLAC1 channels. This loss of osmolytes culminates in loss of water from the cell resulting in guard cell shrinking and stomatal closure. On the contrary, during stomatal opening, K^+ enters the cells, starch is degraded to malate balancing the charges. Upon increased malate concentrations it is transported to the vacuole by ALMT6. Besides, also ALMT9 is activated to facilitate the transport of Cl^- into the vacuole. This accumulation of solutes in the vacuole of guard cells decreases the water potential; water enters the cell causing the swelling of the guard cell, which finally results in stomatal opening.

to the vacuole. *Atalmt6* loss of function plants showed reduced malate currents in comparison to wild type *Arabidopsis* vacuoles. But presumably due to functional redundancy of malate transporters in guard cells, *Atalmt6* plants do not show phenotypic differences from the wild type (Meyer et al., 2011). AtALMT6 is regulated by changes in cytosolic Ca, being activated with increased levels in the micromolar range. Additionally, vacuolar pH and cytosolic malate are other key players of a regulatory mechanism imposing a threshold level for the activation of AtALMT6.

Expression analysis revealed also high expression of *AtALMT12* in guard cells. However, in contrast to AtALMT6 and AtALMT9, this protein is targeted to the guard cell plasma membrane. Comprehensive studies demonstrated AtALMT12 to function as a rapidly/quickly activating (R-type) anion channel (QUAC), which carries mainly chloride and nitrate currents (**Figure 1**) (Meyer et al., 2010b; Sasaki et al., 2010). The *Atalmt12* loss of function mutant showed impaired ABA, CO_2, and dark-induced stomatal closure. These results were further supported by patch clamp analyses of guard cell protoplasts from the knock out plant. There, a diminished R-type current in the presence of malate in the bath medium was observed, when compared with the wild type. Functional expression of the AtALMT12 protein in *Xenopus* oocytes further confirmed its role as an R-type channel.

Anion Homeostasis

The maize gene *ZmALMT1* encodes a plasma membrane-localized protein that, unlike its counterparts in wheat, *Arabidopsis*, and rape, is not involved in Al-activated organic acid exudation; it rather mediates anion influx and efflux. Transport of anions by ZmALMT1 is only feebly enhanced by Al and remains unchanged on changing internal citrate or malate concentrations (Piñeros et al., 2008b). Another member of the same family, ZmALMT2, is also localized on the plasma membrane and mediates large constitutive malate and citrate currents and is also permeable for the physiologically relevant anions Cl^- and NO_3^-. As ZmALMT1, it does not play a big role in Al tolerance response (Ligaba et al., 2012). Instead, both ZmALMT1 and ZmALMT2 are involved in plant nutrition and ion homeostasis (**Figure 1**). A similar role is played at the vacuolar level by AtALMT9 which mediates vacuolar malate uptake (Kovermann et al., 2007; Meyer et al., 2010a; Sasaki et al., 2010; De Angeli et al., 2013b).

Fruit Quality

Sequestration of organic acids in fruits has a major impact on their taste, smell, and flavor, thereby strongly influencing their agronomic value. In apples, the varieties in flavor/acidity are determined by differences in accumulation of malic acid in the mature fruit. Genetic studies indicated that variation in fruit

acidity is controlled by the major quantitative trait locus Ma (malic acid), which underlies an ALMT-like gene closely related to the *Arabidopsis* vacuolar AtALMT6 (Bai et al., 2012; Xu et al., 2012; Khan et al., 2013). Transient expression of Ma1::GFP in onion epidermal cells confirmed its vacuolar localization (**Figure 1**) (Ma et al., 2015). Likewise, the increased malic acid content in yeast cells overexpressing Ma1 is consistent with its putative role as an anion channel that mediates vacuolar malate accumulation *in planta*. Interestingly, the Ma locus consists of two different alleles, namely Ma1 and ma1, the latter coding for a truncated version of the protein due to a premature stop codon as a result of a single nucleotide substitution in the last exon. Further functional studies are required to figure out whether the allelic variants are functionally distinct, and thereby underlie the phenotypic differences in malic acid content.

In grapes, the sequestration of organic acids, in particular malic acid and tartaric acid, is a key determinant for berry development and a deciding factor for wine quality and production (Conde et al., 2007). Phylogenetic analyses indicate the *Vitis vinifera* genome to contain 12 members of the ALMT family (**Figure 3**). Based on cellular localization studies of ALMT:GFP chimeras transiently expressed in tobacco leaves, De Angeli et al. (2013a) identified the vacuolar VvALMT9::GFP as a suitable AtALMT9 homolog that could potentially underlie the unidirectional movement of organic acids into grape berry vacuoles (**Figure 1**). *VvALMT9* is constitutively expressed in berry mesocarp tissue, and its expression is upregulated during fruit maturation. Electrophysiological analyses of vacuoles isolated from tobacco leaves transiently expressing the VvALMT9::GFP protein indicated that VvALMT9 mediates

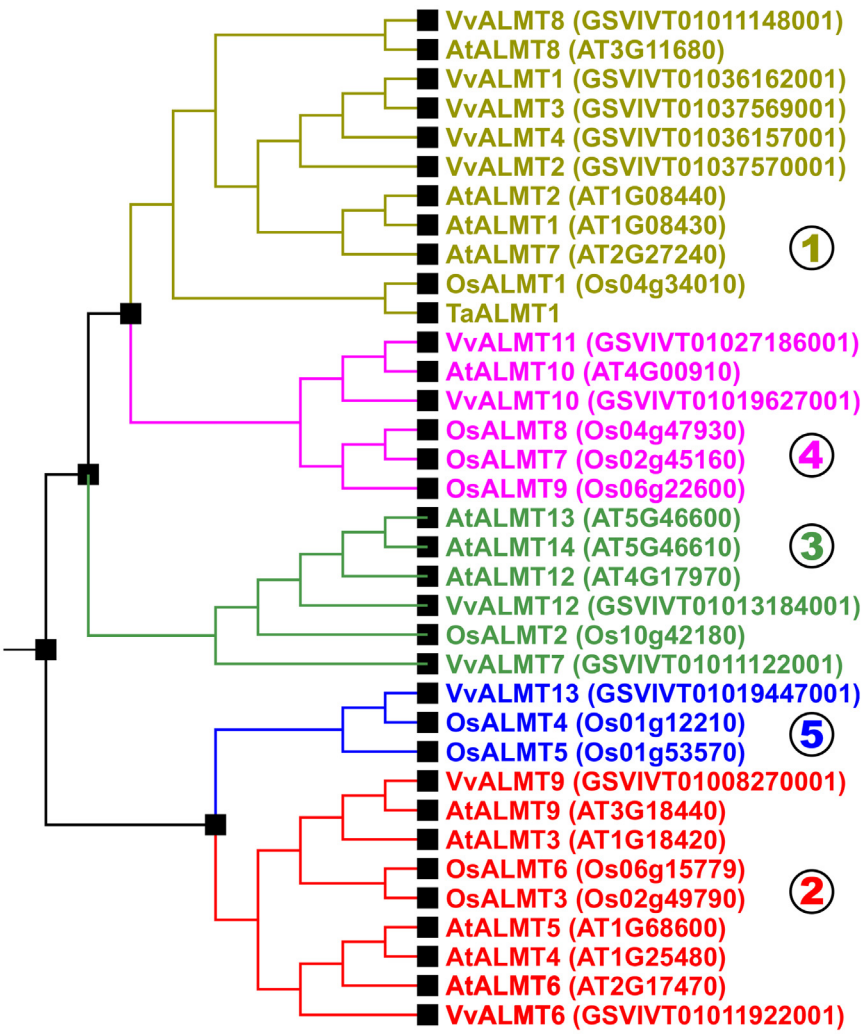

FIGURE 3 | Evolutionary relationship of ALMTs from *Arabidopsis thaliana*, *Oryza sativa* and *Vitis vinifera*. ALMTs of higher plants segregate into five different clades. Figure adapted from Dreyer et al. (2012). Nomenclature of ALMTs from *V. vinifera* according to De Angeli et al. (2013a). For better illustration, only TaALMT1 from *Triticum aestivum* was included in the tree as an example for functionally characterized ALMTs from species different from *A. thaliana, O. sativa*, and *V. vinifera*. ZmALMT1, ZmALMT2, HvALMT1, ScALMT1, and HlALMT1 cluster with TaALMT1 and OsALMT1 in clade 1; BnALMT1 and BnALMT2 cluster with AtALMT1 in clade 1; GmALMT1 clusters with AtALMT8 and VvALMT8 in clade 1; and MdMA1 clusters with AtALMT4, AtALMT5, AtALMT6, and VvALMT6 in clade 2.

the selective flux of malate and tartrate into the vacuole. This suggests that VvALMT9 facilitates the accumulation of malate and tartrate in the vacuole of grape berries.

Seed Development

HvALMT1 from barley shows large sequence similarity to TaALMT1 but it is not involved in Al tolerance. It is expressed in guard cells and mature root cells (Gruber et al., 2010). It is localized on the plasma membrane and unidentified motile vesicles in the cytosol mediating malate efflux and influx (**Figure 1**). Overexpression of HvALMT1 slows down the process of stomatal closure. These plants have a reduced growth rate in comparison to WT plants (Gruber et al., 2011). HvALMT1 helps in turgor regulations and balancing the osmoticum in expanding cells. Besides, it plays a crucial role in the acidification of the endosperm which is required for the activity of α-amylase, cysteine proteases, and ribonucleases that hydrolyze starch and storage proteins. HvALMT1 contributes to the release of malate in aleurone layers during seed germination (Xu et al., 2015).

GABA – Receptor

In an interesting study, Ramesh et al. (2015) showed that γ-aminobutyric acid (GABA) acts as negative regulator of TaALMT1, resulting in altered root growth and tolerance to Al, acidic, or alkaline pH. Stress conditions such as extreme pH, temperature, or salinity result in increased accumulation of GABA in plant tissues, which in turn prevents the release of malate from the root. This mechanism would help the plant to avoid excessive loss of reduced carbon which is crucial for plant growth and development under stress. Down-regulation of ALMT by GABA tends to hyperpolarize the membrane potential and therefore to decrease membrane excitability (Hedrich et al., 2016). Successful plant fertilization also needs a GABA gradient as it regulates growth of pollen tubes and directs it to the ovary. Upon analyzing other proteins of the ALMT family from different species, it was found that GABA also regulates anion-activated currents mediated by other members of this family. All ALMT proteins conserve a 12 aa long motif required for GABA regulation (**Figure 4**). This motif contains residues that have been associated with GABA binding in $GABA_A$ receptors (Boileau et al., 1999). However, GABA-induced inhibition of ALMT protein activities is not completely abrogated by site-directed mutagenesis in this motif, hinting toward the existence of multiple GABA-binding sites. GABA fluxes are observed in and out of wheat roots, which appears to be futile but might be legitimized if GABA is essential for cell-to-cell communication and biotropic interactions (Gilliham and Tyerman, 2016).

Microbe Interactions

Biotic factors, such as a pathogen attack, also regulate ALMT1 protein expression. In the study by Lakshmanan et al. (2012), a synthetic microbe-associated molecular pattern-peptide, flagellin 22 (flg 22) was found to induce AtALMT1 expression. A similar observation was made by Rudrappa et al. (2008), who showed increased release of malate via the induction of AtALMT1, when the aerial plant tissue was infected by pathogenic bacteria. As a consequence of the malate exudate, the plant defense mechanism strengthens by constituting a biofilm of beneficial bacteria at the root surface.

In *Lotus japonicus* the ALMT protein LjALMT4 is highly expressed in nitrogen fixing nodules. Heterologous expression of this protein in *Xenopus laevis* oocytes revealed that LjALMT4 mediates efflux of dicarboxylates. Since the protein is expressed in nodule vascular bundles, it is not involved in transport at the peribacteriod membrane, but is involved in efflux and influx of dicarboxylates and inorganic ions in Lotus nodule vasculatures (Takanashi et al., 2016).

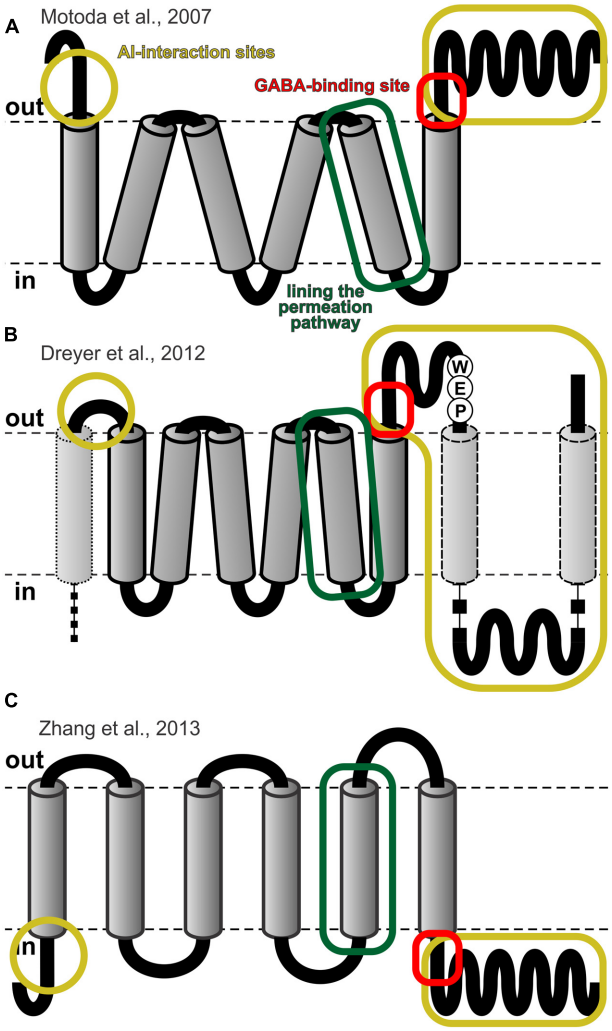

FIGURE 4 | Topological models for ALMTs. (A) Topological model proposed by Motoda et al. (2007) based on immunocytochemical data. **(B)** Reconciliation of Motoda's model with hydrophobicity analyses of the entire ALMT family and with experimental findings (Dreyer et al., 2012). **(C)** *Ad hoc* model proposed by Zhang et al. (2013) for vacuolar ALMTs by analogy with voltage-dependent K^+ channels. Figures adapted from (Dreyer et al., 2012; Zhang et al., 2013). The frames in yellow indicate regions that are involved in Al-sensing (Ligaba et al., 2013; Sasaki et al., 2014), the frames in red the conserved GABA-binding site (Ramesh et al., 2015), and the frames in green the fifth transmembrane domain that was found to contribute to the permeation pathway (Zhang et al., 2013).

STRUCTURE – FUNCTION

Molecular Evolution

The plant model organism *A. thaliana* has 14 genes that could be assigned to code for proteins belonging to the ALMT family. On the basis of amino acid sequence similarity these 14 members can be grouped into four different clades (**Figure 3**). Clade1 includes AtALMT1, 2, 7, and 8 (At1g08430, At1g08440, At2g27240, At3g11680), AtALMT10 (At4g00910) is member of clade 4, whereas clade 2 includes AtALMT3, 4, 5, 6, and 9 (At1g18420, At1g25480, At1g68600, At2g17470, and At3g18440). The protein family members AtALMT11, 12, 13, and 14 (At4g17585, At4g17970, At5g46600, At5g46610) belong to clade 3. It should be noted, however, that AtALMT11 is apparently not a full length protein. *AtALMT11* could be a truncated gene that does not encode a functional protein. In a larger evolutionary context, ALMTs are grouped into the Aromatic Acid Exporter (ArAE) family, which consists of bacterial and eukaryotic members from plants, yeast and protozoans (Transporter Classification Database 2.A.85[1]). The ALMTs, however, differ strongly from the non-plant members justifying the statement that ALMTs are unique to the plant kingdom. Systematic phylogenetic analyses showed that the ALMT family found today in higher plants can be subdivided into five clades (**Figure 3**) (Barbier-Brygoo et al., 2011; Dreyer et al., 2012). Clade 2/3 separated from clade 1/3/4 after the onset of bryophytes but before the appearance of lycophytes. After the emergence of lycophytes, first clade 3 separated from clade 1/4, then clade 1 and 4 diverged and finally clade 2 and 5 separated from each other (Dreyer et al., 2012). *Arabidopsis* does not have ALMTs that belong to clade 5.

Secondary Structure and Topology

In the absence of a crystal structure that is suitable for generating homology models of ALMTs, their structural and topological analyses remain challenging and controversial. Sequence alignments and secondary structure predictions indicate that all members of the ALMT family share a high degree of structural similarity within the N-terminal half of the proteins, while the C-terminal half is more variable. Hydrophobic analyses suggest that the N-terminal part builds the hydrophobic core with 6–7 transmembrane domains (TMDs). The C-terminal part is mostly hydrophilic but may contain additional two TMDs or membrane-anchored domains (**Figure 4B**) (Dreyer et al., 2012). An earlier immunocytochemical study probing the topology of TaALMT1 suggested the transport protein to consist of six transmembrane domains, such that the N- and C-terminus face the extracellular side of the plasma membrane (**Figure 4A**) (Motoda et al., 2007). However, inconsistencies of this topology with the functional characteristics reported for some of the ALMT members [e.g., compare (Motoda et al., 2007; Ryan et al., 2011) with (Meyer et al., 2010b; Dreyer et al., 2012; Ligaba et al., 2013; Mumm et al., 2013)], as well as measurements of the pH-dependent fluorescence intensity of N- or C-terminally tagged ALMT:YFP chimeras expressed in *Xenopus* oocytes (Mumm et al., 2013) argue in favor of an opposite topology, where the N- and C-terminus face the cytoplasmic environment (**Figure 4C**) (Zhang et al., 2013).

Function-structure analysis aimed at characterizing changes in ALMT functionality upon structural modifications, including protein truncation, domain swapping, and single point mutations start to provide insight into the functional role of the N- and C-terminal domains (Furuichi et al., 2010; Ligaba et al., 2013; Mumm et al., 2013; Zhang et al., 2013; Sasaki et al., 2014). For example, a structurally modified TaALMT1 lacking the entire C-terminal region is functionally resembling the transport/permeation properties of the unmodified wild type, but lacks the Al-responsiveness that is typical of this transporter (Ligaba et al., 2013). These observations indicate that the TMD-containing N-terminal domain comprises and assembles the permeation pathway, whilst the hydrophilic C-terminal domain underlies regulatory properties. The regulatory nature of the C-terminus of AtALMT12 (also named as QUAC) has been shown to be a key determinant of the voltage-dependent gating of this channel (Mumm et al., 2013). However, in contrast to the voltage-independent TaALMT1, removal of the C-terminus in AtALMT12 hindered its functionality. Although these types of mutagenesis studies have provided a useful tool to probe structure-function relations of ALMTs, the interpretation of the outcomes should be treated cautiously, and within a phylogenetic context. For example, single point mutations of a glutamate residue (position 276 in TaALMT1 and 284 in AtALMT12, respectively) that is part of the characteristic WEP fingerprint motif (Trp-Glu-Pro) present in all ALMTs (Dreyer et al., 2012), results in total loss of electrogenic transport (Ligaba et al., 2013; Mumm et al., 2013). As exemplified by these studies, significant functional changes might result from alterations of family-wide structural integrity, rather than modification of residues specifically associated with a particular functional characteristic. Finally, biochemical approaches on AtALMT9 have proven the multimeric nature of the ALMTs suggesting that AtALMT9 putatively assembles as a tetramer (Zhang et al., 2013).

Selectivity – Permeability

Functional analyses, for instance with electrophysiological techniques, have shown that members of the ALMT family are permeable to organic and inorganic anions and therefore mediate both their influx and their efflux. The malate permeability of TaALMT1 and the nomenclature (i.e., malate transporter) for this entire family of transporters was first established by two-electrode voltage-clamp experiments in *Xenopus* oocytes, whereby increasing the intracellular malate concentration experimentally by microinjecting malate resulted in an increase in inward current (i.e., anion efflux) in TaALMT1 expressing cells (Sasaki et al., 2004; Piñeros et al., 2008a). Various members of the ALMT family have also been shown to mediate efflux of inorganic anions when expressed in *Xenopus* oocytes, showing a general permeability sequence of $NO_3^- > Cl^-$, (Piñeros et al., 2008a,b; Ligaba et al., 2012;

[1]http://www.tcdb.org/

Sasaki et al., 2016). Patch clamp experiments, allowing access to ionic composition of both, the intracellular and extracellular environments of TaALMT1 expressed in tobacco protoplasts indicated that the inward current was highly selective to malate over nitrate and chloride, with a permeability sequence of $mal^{2-} >> NO_3^- >> Cl^-$ and a permeability ratio P_{mal}/P_{Cl} larger than 18 (Zhang et al., 2008). Likewise, ion substitution experiments in *Xenopus* oocytes indicated a P_{mal}/P_{Cl} between 10 and 30, depending on the external Cl^- concentration (Piñeros et al., 2008a). Noticeably, P_{mal}/P_{Cl} as low as one have also been reported for other ALMT members [e.g., ZmALMT2 (Ligaba et al., 2012)]. Although various permeability/selectivity sequences have been reported for some ALMTs [e.g., malate > fumarate > Cl^- for AtALMT9 (Kovermann et al., 2007) and fumarate > malate >> citrate > Cl^- > NO_3^- for ALMT6 (Meyer et al., 2011)], the relative permeability of a given anion (as well as the channel activity, see "Voltage-Dependence") is highly dependent on the ionic composition of permeating anions on both sides of the membrane, and should therefore be expected to represent only an approximation of those expected under physiologically relevant ionic concentrations.

Regulation

Enhancement by Extracellular Al^{3+}

Several members of the ALMT family, including the family founder TaALMT1, have been associated with *in planta* responses to Al-stress (**Figure 1**). Typically, exposure to Al results both in an upregulation of genes encoding these transporters and a so called "Al-induced" release of organic acids to the rhizosphere. This "Al-induced" release of organic acids *in planta* is the product of either increased protein levels and/or a direct regulatory effect of Al^{3+} on the transporter. Investigations of various members of the ALMT family in heterologous expression systems indicate that only a few of them, namely TaALMT1, AtALMT1, and BnALMT1 are not just functionally active in the absence of extracellular Al^{3+}, but also undergo conformational changes that lead to an enhancement of transport activity (i.e., malate release) upon exposure to extracellular Al^{3+}. This direct Al-activation occurs with high affinity within 3–5 min; it is specific to Al, suggesting that it involves direct interaction of Al^{3+} with the ALMT protein (Sasaki et al., 2004; Hoekenga et al., 2006; Piñeros et al., 2008a; Zhang et al., 2008). The latter functional fingerprint, ambiguously referred to Al-activation, is the unfortunate basis for the existing nomenclature (i.e., ALMT: Al-activated malate transporter) of the entire family of transporters, as only these three ALMTs (and HvALMT to a smaller degree) have been reported to undergo "Al activation," or rather Al^{3+}-induced enhanced transport activity upon exposure to Al^{3+}. These members are primarily localized on the plasma membrane of plant root cells; they are involved in the Al-regulated release of organic acids and underlie the far-reaching mechanism of Al-resistance in plant species. Along with Al, these proteins are also under tight regulation by different other factors. The current lack of suitable structural models has limited structural/functional and topological understanding of this transporter family (see "Secondary Structure and Topology"), hindering the understanding of the conformational changes undergone by the ALMTs upon interaction with Al^{3+}. Nonetheless, several studies have started to elucidate the nature of some of the potential molecular interactions underlying this process. Neutralization of negatively charged residues in the C-terminal domain has abolished the Al-enhancement of the TaALMT1 protein (Furuichi et al., 2010; Ligaba et al., 2013), originally suggesting that a subgroup of residues (particularly Glu274, Asp275, and Glu284) were the key determinants of the transport enhancement process. However, in light of the uncertainty and the controversy regarding the exact topology of ALMTs, the uniqueness of these residues remains questionable. A detailed structure-function study cross-referenced with a phylogenetic analysis of the ALMT proteins, re-assessed the role of protein domains and negatively charged residues in terms of overall conservation and structural integrity, as well as their potential role in the molecular mechanism leading to the Al-dependent response (Ligaba et al., 2013). In this study, neutralization of negative residues throughout the entire TaALMT1 protein weakened or even abolished transport enhancement by Al^{3+}. This study also highlighted the importance of integrating function-structure studies with a comprehensive phylogenetic analysis, as changes in protein functionality might result from alterations of residues involved in family-wide structural integrity, rather than the modification of residues specifically associated with a particular functional characteristic (e.g., transport enhancement by Al^{3+}). Overall, these studies suggest that not only potential domains in the C-terminus, but rather domains present throughout the protein are likely to be involved in Al-mediated enhancement of transport activity. Another report support this inference by functionally characterizing ALMT chimeras, where N-terminal and C-terminal domains of Al-responsive ALMTs have been swapped (Sasaki et al., 2014).

Transcriptional Regulation

The promoter of the *AtALMT1* gene contains several cis acting elements. One of these is recognized by the transcription factor AtSTOP1 that is crucial for Al-induced higher expression of AtALMT1 (Iuchi et al., 2007; Tokizawa et al., 2015). Likewise, the expression of the *H. lanatus HlALMT1* gene is also regulated through the number of cis-acting elements in its promoter region that are targeted by the Al responsive transcription factor HIART1 (Chen Z.C. et al., 2013). In contrast to these positive regulators, the WRKY46 transcription factor acts as a negative regulator or repressor of AtALMT1. *wrky46* loss of function mutants show higher ALMT1 expression along with increased malate exudation resulting in better Al tolerance in mutant plants (Ding et al., 2013).

Voltage-Dependence

In spite of structural similarity, the members of the ALMT family show diverse current-voltage (I-V) relationships. The voltage-dependent properties of ALMTs are best described so far for AtALMT12 (clade 3), and AtALMT6, AtALMT9, and VvALMT9 (all clade 2). AtALMT12 is open at positive voltages

and closes with hyperpolarization. Upon voltage steps, current amplitudes relax within ∼100 ms into a new voltage-dependent equilibrium (Meyer et al., 2010b; Imes et al., 2013; Mumm et al., 2013). The vacuolar channels AtALMT6, AtALMT9, and VvALMT9 are more active at negative voltages than at positive; they need several seconds to reach a new steady state after a voltage-step (Kovermann et al., 2007; Meyer et al., 2011; De Angeli et al., 2013a). Channels belonging to clade 1, in contrast, do not show pronounced signs of voltage-dependence. Upon voltage-steps, the current follows instantaneously the altered driving force (Sasaki et al., 2004; Hoekenga et al., 2006; Piñeros et al., 2008a,b; Ligaba et al., 2012). In some cases (e.g., ZmALMT1, TaALMT1, GmALMT1), a slight voltage-dependent inactivation of the currents is notable at sustained hyperpolarization. The reason for the voltage-dependence of some ALMTs is rather unclear; these channels do not comprise a region with clustered charges that may serve as a voltage-sensor. Instead, for AtALMT12 it was shown that the C-terminal end of the channel is involved in voltage-dependent gating. Fusion of GFP to the C-terminus rendered this channel voltage-insensitive. Therefore, it is speculated that a flexible C-terminus might block the channel in a "ball at a chain" manner (Mumm et al., 2013). Additionally, ALMTs react on intracellular and extracellular (or vacuolar) conditions. Detailed analysis of tonoplast-localized AtALMT6 showed regulation of channel activity through pH and cytosolic malate. These two factors determine whether ALMT6-conducted currents would be inwardly or outwardly rectifying depending on the vacuolar membrane potential (Meyer et al., 2011). In particular, the permeating ion malate increases channel activity from the cytosolic and from the extracellular (or vacuolar) site (De Angeli et al., 2013a,b). Also guard cell R-type anion channel activity is modulated by permeating anions on both sides of the membrane (Hedrich and Marten, 1993, Hedrich et al., 1994; Dietrich and Hedrich, 1998; Frachisse et al., 1999; Diatloff et al., 2004). It is thus speculated that ALMTs comprise two independent (so far not identified) malate-binding sites that contribute to the voltage-sensing process (Mumm et al., 2013).

Nucleotides/Phosphorylation

An apparent voltage-dependence of ALMTs can also be caused by cytosolic nucleotides that modulate/inhibit the channel activity by a reversible block of the pore region in a voltage-dependent manner (Zhang et al., 2014). Regulation of guard cell anion channels by cytosolic nucleotides has been reported previously (Hedrich et al., 1990; Schulz-Lessdorf et al., 1996; Thomine et al., 1997). Cytosolic nucleotides are centrally involved as substrates in phosphorylation processes that regulate channel activity. However, further analysis of R-type/QUAC channels proposed also a direct effect of cytosolic nucleotides as a 'voltage-dependent gate' that blocks the channel pore at hyperpolarized potentials (Colcombet et al., 2001). Thinking along the same line, the I-V relationship of AtALMT9 was studied and it was found that the channel is also regulated by cytosolic nucleotides. The block of AtALMT9 in the presence of ATP is voltage-dependent and it changes the monotonic I-V curve into a bell-shaped curve. The non-hydrolysable ATP analog AMPPNP was found to induce an even stronger inhibitory effect as compared to ATP confirming that the block of the channel activity is due to direct occlusion of the permeation pathway and not a secondary effect of phosphorylation. Mutation of Lys-193 in the putative pore region of the channel completely nullifies the effect of cytosolic nucleotides. The mechanism of voltage gating in plasma membrane and vacuolar channels based on the physical occlusion of the channel permeation pathway occurs at physiological ATP concentration at negative resting potentials and is orchestrated by the anion concentrations on both sides of the membrane (Zhang et al., 2014; De Angeli et al., 2016).

Cytosolic nucleotides appear to exert a bimodal regulation on ALMTs. Besides serving as voltage-dependent blockers they are essential as co-factors of kinases that phosphorylate and activate these channels (Ligaba et al., 2009; Imes et al., 2013). The activity of AtALMT12/QUAC1 is regulated by phosphorylation through the kinase Open Stomata 1 (OST1), which in turn is activated by ABA under stress conditions. Patch clamp studies on guard cells from the wild type and an *ost1* loss of function mutant show activation of R-type/ALMT12 currents in the wild type, which is considerably diminished in *ost1*. Co-expression of ALMT12 and OST1 in *Xenopus* oocytes resulted in a noticeable increase in R-type/ALMT12 activity (Imes et al., 2013). In the wheat channel TaALMT1 the amino acid S384 was identified as key residue for regulating channel activity via direct protein phosphorylation (Ligaba et al., 2009), a finding that fueled the discussion on the topology of ALMTs (**Figure 4**) (Motoda et al., 2007; Dreyer et al., 2012).

CONCLUSION

The historical protein family name "ALMT" could be largely misleading as meanwhile it is clear that many ALMTs are not involved in aluminum tolerance. Their physiological roles go far beyond, and up to now we have just got a small glimpse on this diversity. Future research will certainly be boosted when reliable structural data are available that allow to correlate structural motifs with functional properties. We should be prepared for more surprises from this protein family.

AUTHOR CONTRIBUTIONS

All authors conceived the project and had intellectual input on the project. TS, ID, and MP wrote the manuscript. All authors commented on the manuscript.

FUNDING

This work was supported by the FONDECYT grant N° 1150054 of the Comisión Nacional Científica y Tecnológica of Chile (ID and TS) and National Science Foundation award NSF/IOS-1444435 (MP and LK).

REFERENCES

Bai, Y., Dougherty, L., Li, M., Fazio, G., Cheng, L., and Xu, K. (2012). A natural mutation-led truncation in one of the two aluminum-activated malate transporter-like genes at the Ma locus is associated with low fruit acidity in apple. *Mol. Genet. Genomics* 287, 663–678. doi: 10.1007/s00438-012-0707-7

Barbier-Brygoo, H., De Angeli, A., Filleur, S., Frachisse, J.-M., Gambale, F., Thomine, S., et al. (2011). Anion channels/transporters in plants: from molecular bases to regulatory networks. *Annu. Rev. Plant Biol.* 62, 25–51. doi: 10.1146/annurev-arplant-042110-103741

Boileau, A. J., Evers, A. R., Davis, A. F., and Czajkowski, C. (1999). Mapping the agonist binding site of the GABAA receptor: evidence for a beta-strand. *J. Neurosci.* 19, 4847–4854.

Brown, J. C. (1978). Mechanism of iron uptake by plants. *Plant Cell Environ.* 1, 249–257. doi: 10.1111/j.1365-3040.1978.tb02037.x

Chen, Q., Wu, K.-H., Wang, P., Yi, J., Li, K.-Z., Yu, Y.-X., et al. (2013). Overexpression of MsALMT1, from the aluminum-sensitive *Medicago sativa* enhances malate exudation and aluminum resistance in tobacco. *Plant Mol. Biol. Rep.* 31, 769–774. doi: 10.1007/s11105-012-0543-2

Chen, T.-Y. (2005). Structure and function of clc channels. *Annu. Rev. Physiol.* 67, 809–839. doi: 10.1146/annurev.physiol.67.032003.153012

Chen, Z. C., Yokosho, K., Kashino, M., Zhao, F.-J., Yamaji, N., and Ma, J. F. (2013). Adaptation to acidic soil is achieved by increased numbers of cis -acting elements regulating ALMT1 expression in *Holcus lanatus*. *Plant J.* 76, 10–23. doi: 10.1111/tpj.12266

Colcombet, J., Thomine, S., Guern, J., Frachisse, J. M., and Barbier-Brygoo, H. (2001). Nucleotides provide a voltage-sensitive gate for the rapid anion channel of *arabidopsis* hypocotyl cells. *J. Biol. Chem.* 276, 36139–36145. doi: 10.1074/jbc.M103126200

Conde, C., Silva, P., Fontes, N., Dias, A. C. P., Tavares, R. M., Sousa, M. J., et al. (2007). Biochemical changes throughout grape berry development and fruit and wine quality. *Food* 1, 1–22. doi: 10.1186/s12864-016-2660-z

De Angeli, A., Baetz, U., Francisco, R., Zhang, J., Chaves, M. M., and Regalado, A. (2013a). The vacuolar channel VvALMT9 mediates malate and tartrate accumulation in berries of *Vitis vinifera*. *Planta* 238, 283–291. doi: 10.1007/s00425-013-1888-y

De Angeli, A., Monachello, D., Ephritikhine, G., Frachisse, J. M., Thomine, S., Gambale, F., et al. (2006). The nitrate/proton antiporter AtCLCa mediates nitrate accumulation in plant vacuoles. *Nature* 442, 939–942. doi: 10.1038/nature05013

De Angeli, A., Thomine, S., and Frachisse, J.-M. (2016). Anion channel blockage by ATP as a means for membranes to perceive the energy status of the cell. *Mol. Plant* 9, 320–322. doi: 10.1016/j.molp.2016.01.004

De Angeli, A., Zhang, J., Meyer, S., and Martinoia, E. (2013b). AtALMT9 is a malate-activated vacuolar chloride channel required for stomatal opening in *Arabidopsis*. *Nat. Commun.* 4:1804. doi: 10.1038/ncomms2815

Delhaize, E., Craig, S., Beaton, C. D., Bennet, R. J., Jagadish, V. C., and Randall, P. J. (1993a). Aluminum tolerance in wheat (*Triticum aestivum* L.) (I. uptake and distribution of aluminum in root apices). *Plant Physiol.* 103, 685–693. doi: 10.1104/pp.103.3.685

Delhaize, E., Ryan, P. R., and Randall, P. J. (1993b). Aluminum tolerance in wheat (*Triticum aestivum* L.) (II. aluminum-stimulated excretion of malic acid from root apices). *Plant Physiol.* 103, 695–702. doi: 10.1104/pp.103.3.695

Delhaize, E., Ryan, P. R., Hebb, D. M., Yamamoto, Y., Sasaki, T., and Matsumoto, H. (2004). Engineering high-level aluminum tolerance in barley with the ALMT1 gene. *Proc. Natl. Acad. Sci. U.S.A.* 101, 15249–15254. doi: 10.1073/pnas.0406258101

Diatloff, E., Roberts, M., Sanders, D., and Roberts, S. K. (2004). Characterization of anion channels in the plasma membrane of *Arabidopsis* epidermal root cells and the identification of a citrate-permeable channel induced by phosphate starvation. *Plant Physiol.* 136, 4136–4149. doi: 10.1104/pp.104.046995

Dietrich, P., and Hedrich, R. (1998). Anions permeate and gate GCAC1, a voltage-dependent guard cell anion channel. *Plant J.* 15, 479–487. doi: 10.1046/J.1365-313X.1998.00225.X

Ding, Z. J., Yan, J. Y., Xu, X. Y., Li, G. X., and Zheng, S. J. (2013). WRKY46 functions as a transcriptional repressor of ALMT1, regulating aluminum-induced malate secretion in *Arabidopsis*. *Plant J.* 76, 825–835. doi: 10.1111/tpj.12337

Dreyer, I., Gomez-Porras, J. L., Riaño-Pachón, D. M., Hedrich, R., and Geiger, D. (2012). Molecular evolution of slow and quick anion channels (SLACs and QUACs/ALMTs). *Front. Plant Sci.* 3:263. doi: 10.3389/fpls.2012.00263

Frachisse, J.-M., Thomine, S., Colcombet, J., Guern, J., and Barbier-Brygoo, H. (1999). Sulfate is both a substrate and an activator of the voltage-dependent anion channel of *Arabidopsis* hypocotyl cells. *Plant Physiol.* 121, 253–262. doi: 10.1104/PP.121.1.253

Furuichi, T., Sasaki, T., Tsuchiya, Y., Ryan, P. R., Delhaize, E., and Yamamoto, Y. (2010). An extracellular hydrophilic carboxy-terminal domain regulates the activity of TaALMT1, the aluminum-activated malate transport protein of wheat. *Plant J.* 64, 47–55. doi: 10.1111/j.1365-313X.2010.04309.x

Gilliham, M., and Tyerman, S. D. (2016). Linking metabolism to membrane signaling: the GABA-malate connection. *Trends Plant Sci.* 21, 295–301. doi: 10.1016/j.tplants.2015.11.011

Gruber, B. D., Delhaize, E., Richardson, A. E., Roessner, U., James, R. A., Howitt, S. M., et al. (2011). Characterisation of HvALMT1 function in transgenic barley plants. *Funct. Plant Biol.* 38, 163–175. doi: 10.1071/FP10140

Gruber, B. D., Ryan, P. R., Richardson, A. E., Tyerman, S. D., Ramesh, S., Hebb, D. M., et al. (2010). HvALMT1 from barley is involved in the transport of organic anions. *J. Exp. Bot.* 61, 1455–1467. doi: 10.1093/jxb/erq023

Hechenberger, M., Schwappach, B., Fischer, W. N., Frommer, W. B., Jentsch, T. J., and Steinmeyer, K. (1996). A family of putative chloride channels from *Arabidopsis* and functional complementation of a yeast strain with a CLC gene disruption. *J. Biol. Chem.* 271, 33632–33638. doi: 10.1074/jbc.271.52.33632

Hedrich, R., Busch, H., and Raschke, K. (1990). Ca2+ and nucleotide dependent regulation of voltage dependent anion channels in the plasma membrane of guard cells. *EMBO J.* 9, 3889–3892.

Hedrich, R., and Marten, I. (1993). Malate-induced feedback regulation of plasma membrane anion channels could provide a CO2 sensor to guard cells. *EMBO J.* 12, 897–901.

Hedrich, R., Marten, I., Lohse, G., Dietrich, P., Winter, H., Lohaus, G., et al. (1994). Malate-sensitive anion channels enable guard cells to sense changes in the ambient CO2 concentration. *Plant J.* 6, 741–748. doi: 10.1046/j.1365-313X.1994.6050741.x

Hedrich, R., Salvador-Recatalà, V., and Dreyer, I. (2016). Electrical wiring and long-distance plant communication. *Trends Plant Sci.* 21, 376–387. doi: 10.1016/j.tplants.2016.01.016

Hoekenga, O. A., Maron, L. G., Piñeros, M. A., Cançado, G. M. A., Shaff, J., Kobayashi, Y., et al. (2006). AtALMT1, which encodes a malate transporter, is identified as one of several genes critical for aluminum tolerance in *Arabidopsis*. *Proc. Natl. Acad. Sci. U.S.A.* 103, 9738–9743. doi: 10.1073/pnas.0602868103

Hoffland, E., Boogaard, R., Nelemans, J., and Findenegg, G. (2006). Biosynthesis and root exudation of citric and malic acids in phosphate-starved rape plants. *New Phytol.* 122, 675–680. doi: 10.1111/j.1469-8137.1992.tb00096.x

Igamberdiev, A. U., and Eprintsev, A. T. (2016). Organic acids: the pools of fixed carbon involved in redox regulation and energy balance in higher plants. *Front. Plant Sci.* 7:1042. doi: 10.3389/fpls.2016.01042

Imes, D., Mumm, P., Böhm, J., Al-Rasheid, K. A. S., Marten, I., Geiger, D., et al. (2013). Open stomata 1 (OST1) kinase controls R-type anion channel QUAC1 in *Arabidopsis* guard cells. *Plant J.* 74, 372–382. doi: 10.1111/tpj.12133

Iuchi, S., Koyama, H., Iuchi, A., Kobayashi, Y., Kitabayashi, S., Kobayashi, Y., et al. (2007). Zinc finger protein STOP1 is critical for proton tolerance in *Arabidopsis* and coregulates a key gene in aluminum tolerance. *Proc. Natl. Acad. Sci. U.S.A.* 104, 9900–9905. doi: 10.1073/pnas.0700117104

Jentsch, T. J. (2008). CLC chloride channels and transporters: from genes to protein structure, pathology and physiology. *Crit. Rev. Biochem. Mol. Biol.* 43, 3–36. doi: 10.1080/10409230701829110

Jentsch, T. J., Friedrich, T., Schriever, A., and Yamada, H. (1999). The CLC chloride channel family. *Pflügers Arch. Eur. J. Physiol.* 437, 783–795. doi: 10.1007/s004240050847

Khan, S. A., Beekwilder, J., Schaart, J. G., Mumm, R., Soriano, J. M., Jacobsen, E., et al. (2013). Differences in acidity of apples are probably mainly caused by a malic acid transporter gene on LG16. *Tree Genet. Genomes* 9, 475–487. doi: 10.1007/s11295-012-0571-y

Kobayashi, Y., Kobayashi, Y., Sugimoto, M., Lakshmanan, V., Iuchi, S., Kobayashi, M., et al. (2013). Characterization of the complex regulation of AtALMT1 expression in response to phytohormones and other inducers. *Plant Physiol.* 162, 732–740. doi: 10.1104/pp.113.218065

Kollist, H., Jossier, M., Laanemets, K., and Thomine, S. (2011). Anion channels in plant cells. *FEBS J.* 278, 4277–4292. doi: 10.1111/j.1742-4658.2011.08370.x

Kollist, H., Nuhkat, M., and Roelfsema, M. R. G. (2014). Closing gaps: linking elements that control stomatal movement. *New Phytol.* 203, 44–62. doi: 10.1111/nph.12832

Kollmeier, M., Dietrich, P., Bauer, C. S., Horst, W. J., and Hedrich, R. (2001). Aluminum activates a citrate-permeable anion channel in the aluminum-sensitive zone of the maize root apex. A comparison between an aluminum-sensitive and an aluminum-resistant cultivar. *Plant Physiol.* 126, 397–410. doi: 10.1104/pp.126.1.397

Kovermann, P., Meyer, S., Hörtensteiner, S., Picco, C., Scholz-Starke, J., Ravera, S., et al. (2007). The *Arabidopsis* vacuolar malate channel is a member of the ALMT family. *Plant J.* 52, 1169–1180. doi: 10.1111/j.1365-313X.2007.03367.x

Lakshmanan, V., Kitto, S. L., Caplan, J. L., Hsueh, Y.-H., Kearns, D. B., Wu, Y.-S., et al. (2012). Microbe-associated molecular patterns-triggered root responses mediate beneficial rhizobacterial recruitment in *Arabidopsis*. *Plant Physiol.* 160, 1642–1661. doi: 10.1104/pp.112.200386

Liang, C., Piñeros, M. A., Tian, J., Yao, Z., Sun, L., Liu, J., et al. (2013). Low pH, aluminum, and phosphorus coordinately regulate malate exudation through GmALMT1 to improve soybean adaptation to acid soils. *Plant Physiol.* 161, 1347–1361. doi: 10.1104/pp.112.208934

Ligaba, A., Dreyer, I., Margaryan, A., Schneider, D. J., Kochian, L., and Piñeros, M. (2013). Functional, structural and phylogenetic analysis of domains underlying the Al sensitivity of the aluminum-activated malate/anion transporter, TaALMT1. *Plant J.* 76, 766–780. doi: 10.1111/tpj.12332

Ligaba, A., Katsuhara, M., Ryan, P. R., Shibasaka, M., and Matsumoto, H. (2006). The BnALMT1 and BnALMT2 genes from rape encode aluminum-activated malate transporters that enhance the aluminum resistance of plant cells. *Plant Physiol.* 142, 1294–1303. doi: 10.1104/pp.106.085233

Ligaba, A., Katsuhara, M., Sakamoto, W., and Matsumoto, H. (2007). The BnALMT1 protein that is an aluminum-activated malate transporter is localized in the plasma membrane. *Plant Signal. Behav.* 2, 255–257. doi: 10.4161/psb.2.4.3868

Ligaba, A., Kochian, L., and Piñeros, M. (2009). Phosphorylation at S384 regulates the activity of the TaALMT1 malate transporter that underlies aluminum resistance in wheat. *Plant J.* 60, 411–423. doi: 10.1111/j.1365-313X.2009.03964.x

Ligaba, A., Maron, L., Shaff, J., Kochian, L., and Piñeros, M. (2012). Maize ZmALMT2 is a root anion transporter that mediates constitutive root malate efflux. *Plant Cell Environ.* 35, 1185–1200. doi: 10.1111/j.1365-3040.2011.02479.x

Linder, B., and Raschke, K. (1992). A slow anion channel in guard cells, activating at large hyperpolarization, may be principal for stomatal closing. *FEBS Lett.* 313, 27–30. doi: 10.1016/0014-5793(92)81176-M

López-Bucio, J., Nieto-Jacobo, M. F., Ramírez-Rodríguez, V., and Herrera-Estrella, L. (2000). Organic acid metabolism in plants: from adaptive physiology to transgenic varieties for cultivation in extreme soils. *Plant Sci.* 160, 1–13. doi: 10.1016/S0168-9452(00)00347-2

Ma, B., Liao, L., Zheng, H., Chen, J., Wu, B., Ogutu, C., et al. (2015). Genes encoding aluminum-activated malate transporter II and their association with fruit acidity in apple. *Plant Genome* 8. doi: 10.3835/plantgenome2015.03.0016

Ma, J. F., Zheng, S. J., and Matsumoto, H. (1997). Specific secretion of citric acid induced by Al stress in Cassia tora L. *Plant Cell Physiol.* 38, 1019–1025. doi: 10.1093/oxfordjournals.pcp.a029266

Meyer, S., De Angeli, A., Fernie, A. R., and Martinoia, E. (2010a). Intra- and extra-cellular excretion of carboxylates. *Trends Plant Sci.* 15, 40–47. doi: 10.1016/j.tplants.2009.10.002

Meyer, S., Mumm, P., Imes, D., Endler, A., Weder, B., Al-Rasheid, K. A. S., et al. (2010b). AtALMT12 represents an R-type anion channel required for stomatal movement in *Arabidopsis* guard cells. *Plant J.* 63, 1054–1062. doi: 10.1111/j.1365-313X.2010.04302.x

Meyer, S., Scholz-Starke, J., De Angeli, A., Kovermann, P., Burla, B., Gambale, F., et al. (2011). Malate transport by the vacuolar AtALMT6 channel in guard cells is subject to multiple regulation. *Plant J.* 67, 247–257. doi: 10.1111/j.1365-313X.2011.04587.x

Motoda, H., Sasaki, T., Kano, Y., Ryan, P. R., Delhaize, E., Matsumoto, H., et al. (2007). The membrane topology of ALMT1, an aluminum-activated malate transport protein in wheat (*Triticum aestivum*). *Plant Signal. Behav.* 2, 467–472. doi: 10.4161/psb.2.6.4801

Mumm, P., Imes, D., Martinoia, E., Al-Rasheid, K. A. S., Geiger, D., Marten, I., et al. (2013). C-terminus-mediated voltage gating of *Arabidopsis* guard cell anion channel QUAC1. *Mol. Plant* 6, 1550–1563. doi: 10.1093/mp/sst008

Pantoja, O., Dainty, J., and Blumwald, E. (1989). Ion channels in vacuoles from halophytes and glycophytes. *FEBS Lett.* 255, 92–96. doi: 10.1016/0014-5793(89)81067-1

Piñeros, M. A., Cançado, G. M. A., and Kochian, L. V. (2008a). Novel properties of the wheat aluminum tolerance organic acid transporter (TaALMT1) revealed by electrophysiological characterization in *Xenopus* oocytes: functional and structural implications. *Plant Physiol.* 147, 2131–2146. doi: 10.1104/pp.108.119636

Piñeros, M. A., Cançado, G. M. A., Maron, L. G., Lyi, S. M., Menossi, M., and Kochian, L. V. (2008b). Not all ALMT1-type transporters mediate aluminum-activated organic acid responses: the case of ZmALMT1 – an anion-selective transporter. *Plant J.* 53, 352–367. doi: 10.1111/j.1365-313X.2007.03344.x

Piñeros, M. A., and Kochian, L. V. (2001). A patch-clamp study on the physiology of aluminum toxicity and aluminum tolerance in maize. Identification and characterization of Al3+-induced anion channels. *Plant Physiol.* 125, 292–305. doi: 10.1104/pp.125.1.292

Piñeros, M. A., Magalhaes, J. V., Alves, V. M. C., and Kochian, L. V. (2002). The physiology and biophysics of an aluminum tolerance mechanism based on root citrate exudation in maize. *Plant Physiol.* 129, 1194–1206. doi: 10.1104/pp.002295

Ramesh, S. A., Tyerman, S. D., Xu, B., Bose, J., Kaur, S., Conn, V., et al. (2015). GABA signalling modulates plant growth by directly regulating the activity of plant-specific anion transporters. *Nat. Commun.* 6:7879. doi: 10.1038/ncomms8879

Roberts, S. K. (2006). Plasma membrane anion channels in higher plants and their putative functions in roots. *New Phytol.* 169, 647–666. doi: 10.1111/j.1469-8137.2006.01639.x

Roelfsema, M. R. G., Hedrich, R., and Geiger, D. (2012). Anion channels: master switches of stress responses. *Trends Plant Sci.* 17, 221–229. doi: 10.1016/j.tplants.2012.01.009

Rudrappa, T., Czymmek, K. J., Paré, P. W., and Bais, H. P. (2008). Root-secreted malic acid recruits beneficial soil bacteria. *Plant Physiol.* 148, 1547–1556. doi: 10.1104/pp.108.127613

Ryan, P. R., Skerrett, M., Findlay, G. P., Delhaize, E., and Tyerman, S. D. (1997). Aluminum activates an anion channel in the apical cells of wheat roots. *Proc. Natl. Acad. Sci. U.S.A.* 94, 6547–6552. doi: 10.1073/pnas.94.12.6547

Ryan, P. R., Tyerman, S. D., Sasaki, T., Furuichi, T., Yamamoto, Y., Zhang, W. H., et al. (2011). The identification of aluminium-resistance genes provides opportunities for enhancing crop production on acid soils. *J. Exp. Bot.* 62, 9–20. doi: 10.1093/jxb/erq272

Sasaki, T., Mori, I. C., Furuichi, T., Munemasa, S., Toyooka, K., Matsuoka, K., et al. (2010). Closing plant stomata requires a homolog of an aluminum-activated malate transporter. *Plant Cell Physiol.* 51, 354–365. doi: 10.1093/pcp/pcq016

Sasaki, T., Tsuchiya, Y., Ariyoshi, M., Ryan, P. R., Furuichi, T., and Yamamoto, Y. (2014). A domain-based approach for analyzing the function of aluminum-activated malate transporters from wheat (*Triticum aestivum*) and *Arabidopsis thaliana* in *Xenopus* oocytes. *Plant Cell Physiol.* 55, 2126–2138. doi: 10.1093/pcp/pcu143

Sasaki, T., Tsuchiya, Y., Ariyoshi, M., Ryan, P. R., and Yamamoto, Y. (2016). A chimeric protein of aluminum-activated malate transporter generated from wheat and *Arabidopsis* shows enhanced response to trivalent cations. *Biochim. Biophys. Acta* 1858, 1427–1435. doi: 10.1016/j.bbamem.2016.03.026

Sasaki, T., Yamamoto, Y., Ezaki, B., Katsuhara, M., Ahn, S. J., Ryan, P. R., et al. (2004). A wheat gene encoding an aluminum-activated malate transporter. *Plant J.* 37, 645–653. doi: 10.1111/j.1365-313X.2003.01991.x

Schroeder, J. I., and Keller, B. U. (1992). Two types of anion channel currents in guard cells with distinct voltage regulation. *Proc. Natl. Acad. Sci. U.S.A.* 89, 5025–5029. doi: 10.1073/pnas.89.15.7287-b

Schulz-Lessdorf, B., Lohse, G., and Hedrich, R. (1996). GCAC1 recognizes the pH gradient across the plasma membrane: a pH-sensitive and ATP-dependent anion channel links guard cell membrane potential to acid and energy metabolism. *Plant J.* 10, 993–1004. doi: 10.1046/j.1365-313X.1996.10060993.x

Sukweenadhi, J., Kim, Y.-J., Choi, E.-S., Koh, S.-C., Lee, S.-W., Kim, Y.-J., et al. (2015). *Paenibacillus yonginensis* DCY84(T) induces changes in *Arabidopsis*

thaliana gene expression against aluminum, drought, and salt stress. *Microbiol. Res.* 172, 7–15. doi: 10.1016/j.micres.2015.01.007

Takanashi, K., Sasaki, T., Kan, T., Saida, Y., Sugiyama, A., Yamamoto, Y., et al. (2016). A dicarboxylate transporter, LjALMT4, mainly expressed in nodules of *Lotus japonicus*. *Mol. Plant. Microbe Interact.* 29, 584–592. doi: 10.1094/MPMI-04-16-0071-R

Thomine, S., Guern, J., and Barbier-Brygoo, H. (1997). Voltage-dependent anion channel of *Arabidopsis* hypocotyls: nucleotide regulation and pharmacological properties. *J. Membr. Biol.* 159, 71–82. doi: 10.1007/s002329900270

Tokizawa, M., Kobayashi, Y., Saito, T., Kobayashi, M., Iuchi, S., Nomoto, M., et al. (2015). SENSITIVE TO PROTON RHIZOTOXICITY1, CALMODULIN BINDING TRANSCRIPTION ACTIVATOR2, and other transcription factors are involved in ALUMINUM-ACTIVATED MALATE TRANSPORTER1 expression. *Plant Physiol.* 167, 991–1003. doi: 10.1104/pp.114.256552

Touraine, B., Muller, B., and Grignon, C. (1992). Effect of phloem-translocated malate on NO3- uptake by roots of intact soybean plants. *Plant Physiol.* 99, 1118–1123. doi: 10.1104/pp.99.3.1118

Tyerman, S. D. (1992). Anion channels in plants. *Annu. Rev. Plant Physiol. Plant Mol. Biol.* 43, 351–373. doi: 10.1146/annurev.pp.43.060192.002031

Webb, M. A. (1999). Cell-mediated crystallization of calcium oxalate in plants. *Plant Cell* 11, 751–761. doi: 10.1105/tpc.11.4.751

Xu, K., Wang, A., and Brown, S. (2012). Genetic characterization of the Ma locus with pH and titratable acidity in apple. *Mol. Breed.* 30, 899–912. doi: 10.1007/s11032-011-9674-7

Xu, M., Gruber, B. D., Delhaize, E., White, R. G., James, R. A., You, J., et al. (2015). The barley anion channel, HvALMT1, has multiple roles in guard cell physiology and grain metabolism. *Physiol. Plant* 153, 183–193. doi: 10.1111/ppl.12234

Zhang, J., Baetz, U., Krügel, U., Martinoia, E., and De Angeli, A. (2013). Identification of a probable pore-forming domain in the multimeric vacuolar anion channel AtALMT9. *Plant Physiol.* 163, 830–843. doi: 10.1104/pp.113.219832

Zhang, J., Martinoia, E., and De Angeli, A. (2014). Cytosolic nucleotides block and regulate the *Arabidopsis* vacuolar anion channel AtALMT9. *J. Biol. Chem.* 289, 25581–25589. doi: 10.1074/jbc.M114.576108

Zhang, W.-H., Ryan, P. R., Sasaki, T., Yamamoto, Y., Sullivan, W., and Tyerman, S. D. (2008). Characterization of the TaALMT1 protein as an Al3+-activated anion channel in transformed tobacco (*Nicotiana tabacum* L.) cells. *Plant Cell Physiol.* 49, 1316–1330. doi: 10.1093/pcp/pcn107

Zhang, W.-H., Ryan, P. R., and Tyerman, S. D. (2001). Malate-permeable channels and cation channels activated by aluminum in the apical cells of wheat roots. *Plant Physiol.* 125, 1459–1472. doi: 10.1104/pp.125.3.1459

Conflict of Interest Statement: The authors declare that the research was conducted in the absence of any commercial or financial relationships that could be construed as a potential conflict of interest.

frontiers in Plant Science

ORIGINAL RESEARCH
published: 07 June 2016
doi: 10.3389/fpls.2016.00794

Nod Factor Effects on Root Hair-Specific Transcriptome of *Medicago truncatula*: Focus on Plasma Membrane Transport Systems and Reactive Oxygen Species Networks

Isabelle Damiani[1†], Alice Drain[2†], Marjorie Guichard[3], Sandrine Balzergue[4,5], Alexandre Boscari[1], Jean-Christophe Boyer[2], Véronique Brunaud[4,5], Sylvain Cottaz[6,7], Corinne Rancurel[1], Martine Da Rocha[1], Cécile Fizames[2], Sébastien Fort[6,7], Isabelle Gaillard[2], Vincent Maillol[6,8], Etienne G. J. Danchin[1], Hatem Rouached[2], Eric Samain[6,7], Yan-Hua Su[9], Julien Thouin[2], Bruno Touraine[2], Alain Puppo[1], Jean-Marie Frachisse[3], Nicolas Pauly[1] and Hervé Sentenac[2]**

[1] Centre National de la Recherche Scientifique, Institut National de la Recherche Agronomique, UMR 1355-7254 Institut Sophia Agrobiotech, Université Nice Sophia Antipolis, Sophia Antipolis, France, [2] Biochimie and Physiologie Moléculaire des Plantes, UMR 5004 Centre National de la Recherche Scientifique/386 Institut National de la Recherche Agronomique/SupAgro Montpellier/Université de Montpellier, Campus SupAgro-Institut National de la Recherche Agronomique, Montpellier, France, [3] Institute for Integrative Biology of the Cell, CEA, Centre National de la Recherche Scientifique, Université Paris-Sud, Université Paris-Saclay, Gif sur Yvette, France, [4] POPS Transcriptomic Platform, Centre National de la Recherche Scientifique, Institute of Plant Sciences Paris-Saclay, Institut National de la Recherche Agronomique, Université Paris-Sud, Université Evry, Université Paris-Saclay, Orsay, France, [5] POPS Transcriptomic Platform, Institute of Plant Sciences Paris-Saclay, Paris Diderot, Orsay, France, [6] Université Grenoble Alpes, CERMAV, Grenoble, France, [7] Centre National de la Recherche Scientifique, CERMAV, Grenoble, France, [8] Laboratoire d'Informatique, de Robotique et de Microélectronique de Montpellier and Institut de Biologie Computationnelle, Centre National de la Recherche Scientifique and Université Montpellier, Montpellier, France, [9] State Key Laboratory of Soil and Sustainable Agriculture, Institute of Soil Science, Chinese Academy of Sciences, Nanjing, China*

Root hairs are involved in water and nutrient uptake, and thereby in plant autotrophy. In legumes, they also play a crucial role in establishment of rhizobial symbiosis. To obtain a holistic view of *Medicago truncatula* genes expressed in root hairs and of their regulation during the first hours of the engagement in rhizobial symbiotic interaction, a high throughput RNA sequencing on isolated root hairs from roots challenged or not with lipochitooligosaccharides Nod factors (NF) for 4 or 20 h was carried out. This provided a repertoire of genes displaying expression in root hairs, responding or not to NF, and specific or not to legumes. In analyzing the transcriptome dataset, special attention was paid to pumps, transporters, or channels active at the plasma membrane, to other proteins likely to play a role in nutrient ion uptake, NF electrical and calcium signaling, control of the redox status or the dynamic reprogramming of root hair transcriptome induced by NF treatment, and to the identification of papilionoid legume-specific genes expressed in root hairs. About 10% of the root hair expressed genes were significantly up- or down-regulated by NF treatment, suggesting their involvement in remodeling

OPEN ACCESS

Edited by:
Janin Riedelsberger, University of Talca, Chile

Reviewed by:
Erik Limpens, Wageningen University, Netherlands
Jeremy Dale Murray, John Innes Centre, UK
Joachim Schulze, University Goettingen, Germany

***Correspondence:**
Nicolas Pauly
nicolas.pauly@sophia.inra.fr
Hervé Sentenac
hervé.sentenac@supagro.inra.fr

† These authors have contributed equally to this work.

Specialty section:
This article was submitted to Plant Physiology, a section of the journal Frontiers in Plant Science

Received: *31 March 2016*
Accepted: *22 May 2016*
Published: *07 June 2016*

Citation:
Damiani I, Drain A, Guichard M, Balzergue S, Boscari A, Boyer J-C, Brunaud V, Cottaz S, Rancurel C, Da Rocha M, Fizames C, Fort S, Gaillard I, Maillol V, Danchin EGJ, Rouached H, Samain E, Su Y-H, Thouin J, Touraine B, Puppo A, Frachisse J-M, Pauly N and Sentenac H (2016) Nod Factor Effects on Root Hair-Specific Transcriptome of Medicago truncatula: Focus on Plasma Membrane Transport Systems and Reactive Oxygen Species Networks. Front. Plant Sci. 7:794. doi: 10.3389/fpls.2016.00794

plant functions to allow establishment of the symbiotic relationship. For instance, NF-induced changes in expression of genes encoding plasma membrane transport systems or disease response proteins indicate that root hairs reduce their involvement in nutrient ion absorption and adapt their immune system in order to engage in the symbiotic interaction. It also appears that the redox status of root hair cells is tuned in response to NF perception. In addition, 1176 genes that could be considered as "papilionoid legume-specific" were identified in the *M. truncatula* root hair transcriptome, from which 141 were found to possess an ortholog in every of the six legume genomes that we considered, suggesting their involvement in essential functions specific to legumes. This transcriptome provides a valuable resource to investigate root hair biology in legumes and the roles that these cells play in rhizobial symbiosis establishment. These results could also contribute to the long-term objective of transferring this symbiotic capacity to non-legume plants.

Keywords: *Medicago truncatula*, root hairs, deep-RNA sequencing, Nod factors (lipochitooligosaccharides), legume-rhizobium symbiosis, plasma membrane transport systems, reactive oxygen species

INTRODUCTION

Root hairs are long tubular outgrowths that project into the soil from root epidermal cells named trichoblasts. Together with the pollen tube in plants, axons in animals, and hyphae in filamentous fungi, they provide one of the very rare models of cell types displaying polarized "tip" growth. Root hair elongation results in an increased area of the root-soil interface. At this interface, root hairs contribute to plant autotrophy by taking up nutrient ions and water from the soil solution.

Root hairs are also involved in beneficial interactions with soil microorganisms. They exudate compounds that act as a chemotactic signal or promote the growth of symbiotic fungi and bacteria (Bais et al., 2006). Moreover, they are directly involved in the formation of nitrogen-fixing nodules in legumes. The plant secretes signaling flavonoid compounds that are perceived by the rhizobial symbiont, which responds to this message by secreting specific lipochitooligosaccharides, named Nod factors (NF; Oldroyd and Downie, 2008). NF are signal molecules whose binding to root hair receptors triggers complex signaling events leading the root hair to curl and thereby to entrap rhizobia. Then, an infection thread develops, allowing rhizobia to migrate through the root cortex toward the nodule primordium.

With respect to the initial signals triggered by NF perception, the earliest events that have been reported so far involve reactive oxygen species (ROS) and ion fluxes across the cell membrane. ROS signals have been recorded within seconds after addition of NF on growing root hairs (Cardenas et al., 2008). In contrast, several minutes after NF perception, the production of hydrogen peroxide (H_2O_2) appears to be inhibited (Shaw and Long, 2003; Lohar et al., 2007). Several hours later, a gradual increase in ROS production occurs in root cortical cells of inoculated plants, which peaks at 24 h after rhizobial inoculation and remains high 48 h after inoculation (Ramu et al., 2002; Peleg-Grossman et al., 2007, 2012). Thus, ROS play a role in the early signaling leading to establishment of the symbiotic partnership (Montiel et al., 2012) as well as later on, when rhizobia invade the root hair via progression of the infection thread (for review, see Puppo et al., 2013).

Ions whose transport across the root hair plasma membrane has been shown to be rapidly modulated during the initial root hair response to NF are H^+, Ca^{2+}, Cl^-, and K^+ (Felle et al., 1996, 1998, 1999; Kurkdjian et al., 2000). In summary, the present model is that NF perception leads to a transient inhibition of plasma membrane H^+-ATPases (proton pumps), an activation of Ca^{2+} channels, allowing a depolarizing influx of Ca^{2+}, immediately followed by an activation of anion (Cl^- permeable) channels, mediating an efflux of anions that further depolarizes the cell membrane. In turn, this depolarization activates voltage-gated K^+ channels, giving rise to a repolarizing efflux of K^+. This series of events is thought to generate electrical and calcium signals that play a major role in the initial dialogue between root hairs and rhizobia (Felle et al., 1996, 1998, 1999; Kurkdjian et al., 2000). It might be connected to the first ROS signals triggered by NF perception since ROS production by NADPH oxidases has been shown to stimulate plasma membrane Ca^{2+} channel activity in Arabidopsis root hairs (Foreman et al., 2003). Also, based on results obtained in Arabidopsis, ROS could play a role in control of K^+ channel activity involved in electrical signaling (Garcia-Mata et al., 2010; Tran et al., 2013) as well as in control of annexins involved in Ca^{2+} signaling (Richards et al., 2014). The decision of the plant to engage in rhizobial symbiosis is strongly dependent on the availability of nutrient ions in the soil solution, in particular of nitrate and ammonium (Barbulova et al., 2007). Hence, by routing nutrient ions, transport systems are likely to impact the plant decision to establish symbiosis. ROS signals are likely to play a role in this process since nutrient ion deprivation has been shown to lead to altered levels of ROS in Arabidopsis and *M. truncatula* roots (Schachtman and Shin, 2007; Bonneau et al., 2013), and NADPH oxidases genes are necessary for up-regulation of genes in response to nutrient deficiency (Shin and Schachtman, 2004).

The multiple and essential functions of the root hair clearly establish this cell type as a system biology model to investigate

plant cell development, uptake of water and nutrients, and response to abiotic and biotic signals. Indeed, a number of genome-wide studies have been published using root hairs from several model and crop plants (Hossain et al., 2015; Wang et al., 2016). The present paper is conceived as a contribution to improved understanding of the molecular mechanisms underpinning the roles of root hairs in legumes. We used *M. truncatula* as a model legume. A detailed analysis of gene expression in *M. truncatula* root hairs from young seedlings (without lateral roots) and of their responses to NF treatments for 4 h (to get information on early NF signaling events) or 20 h has been carried out using a high throughput RNA sequencing strategy (RNA-seq). This is likely to provide the first RNA-seq dataset from *M. truncatula* root hairs, thereby the most exhaustive transcriptome available to date for this cell type, and thus a valuable resource to investigate root hair functions in legumes. Expert gene analyses have been focused in order to uncover ROS networks and pump, transporter and channel machineries likely to play a role in two major functions of root hairs, namely nutrient ion uptake and early molecular dialogue with rhizobia following NF perception. Moreover, using whole genome comparisons, we identified legume-specific genes expressed in root hairs, responding or not to NF. Altogether, these results constitute a promising dataset for researchers interested in plant mineral nutrition, rhizobial symbiosis, and legume specificities.

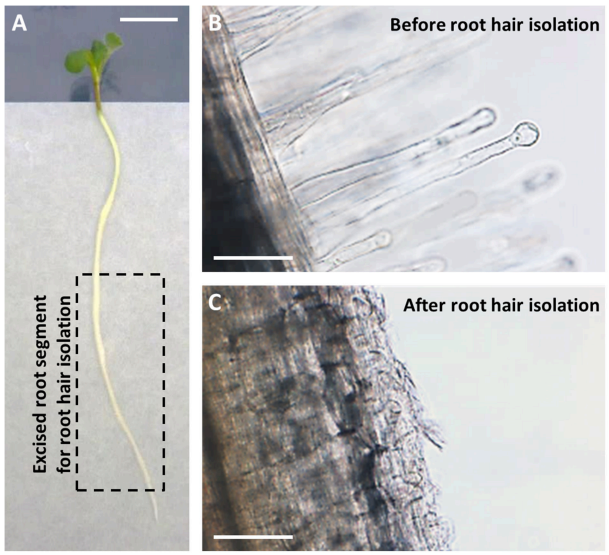

FIGURE 1 | Root hairs isolation from *Medicago truncatula*. (A) Five-day old seedling just before root hairs isolation (Scale bar = 1 cm). Root hairs were isolated by vortexing frozen excised root segments long of about 4 cm and free from the root tip (0.5 cm) as displayed by the dotted line rectangle. **(B,C)** Representative photographs of root material before **(B)** and after **(C)** root vortexing, showing the absence of root hairs in the remaining material at the end of the isolation procedure (Scale bar = 100 μm).

RESULTS

Preparation of Root Hair Libraries

Root hairs were obtained from excised root segments (**Figure 1**). Before excision, the root systems were treated with 10 nM NF solution for 4 or 20 h, or with pure H_2O as a control treatment (NF 4 h, NF 20 h, and control treatments, respectively). Microscopic observation of root segment samples before root hair isolation indicated that the two NF treatments had actually induced the expected root hair morphological changes, i.e., root hair tip swelling in the case of the NF 4 h treatment, and reoriented root hair growth and branching in the case of the NF 20 h treatment (**Figure 2A**). Root hairs in the H_2O treated control plants did not display such features (**Figure 2A**). RT-PCR analyses performed on root segments free from root hairs (material remaining after root hair isolation) provided further evidence that the NF treatments had been effective by showing a strong accumulation of *MtENOD11* transcripts (**Figure 2B**), one of the earliest markers induced by NF perception in root epidermal cells (Journet et al., 2001). Finally, absence of transcripts from the *MtSUNN* gene, which is known to be specifically expressed in root stele tissues (Schnabel et al., 2005), indicated that the root hair RNA pools were not substantially contaminated by RNA from inner root cells, and thus from whole root segments.

General Features of the *M. truncatula* Root Hair Transcriptome

RNA sequencing was carried out on two independent biological replicates for each of the three treatments (H_2O, NF 4 h, NF 20 h), yielding six root hair transcriptomic datasets. We generated ∼366 million high-quality paired-end reads, which were mapped to the *M. truncatula* predicted transcriptome (Mt4.0v1). About 266 million (ca. 73%) of paired-end reads were unambiguously mapped (Table S1). In order to assess the experimental variability, the two replicates obtained for a given treatment were compared by plotting the expression levels (expressed in Count per Million Reads) found in one dataset against those found in the second dataset (Figure S1). Linear regression analysis yielded R^2 coefficient of 0.99, 0.99, and 0.97 for the control, NF 4 h, and NF 20 h treatments, respectively. For a large majority of genes (≥65% whatever the treatment), the fold change in expression level between the two repetitions was lower than 1.5. As could be anticipated, we noticed that the biological variability in terms of expression level fold change was larger for genes displaying low expression levels. In order to further assess consistency among biological replicates for the transcriptome datasets, we subjected the expression data derived from the six datasets to principal component analysis (PCA; Figure S2). The first component (Dim1) clearly separated the control from the NF treated samples (Figure S2A) and the overall distribution confirmed that there was no biological repetition bias (Figure S2B).

To validate RNA-seq based differential gene expression in response to NF treatments, quantitative real-time RT-PCR (RT-qPCR) tests were also carried out. A set of 20 genes was selected (Table S11), amongst which receptors, pumps, and ion channels differing in their levels of expression. The expression level provided by the RT-qPCR experiments for the NF 4 h and

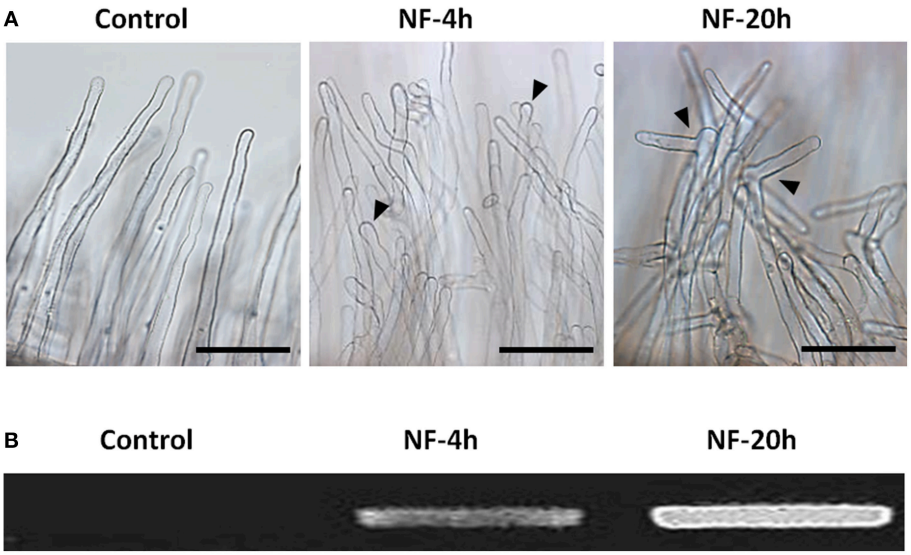

FIGURE 2 | Root responses to Nod factor treatments. (A) Root hair morphological responses. Representative photographs of root hairs from roots subjected to a control treatment with pure H_2O or treated with 10 nM Nod factors (NF) for 4 h or 20 h (left, middle, and right panel, respectively; Scale bar = 100 μm). **(B)** Gene expression response to NF highlighted by increased *MtENOD11* transcript accumulation. Differences in *MtENOD11* transcript levels were revealed by RT-PCR experiments performed in parallel on control roots or roots pretreated by Nod factors for 4 or 20 h (left, middle, and right lane of the electrophoresis gel, respectively).

NF 20 h treated samples were divided by the level of expression determined for the control samples, and the resulting ratios were compared to those obtained from the corresponding data derived from the RNA-seq experiments (from Table S2). The resulting plots (Figure S3) reveal some variability between the RNA-seq and RT-qPCR results, but no conflicting discrepancy.

To describe the *M. truncatula* root hair transcriptome and to explore the relative expression levels of the different genes, the expression level of each gene was calculated in FPKM (Fragments Per Kilobase of exons per Million fragments mapped) values, from alignment of the paired-end reads to the improved *M. truncatula* genome release (Tang et al., 2014). For these analyses, only the longest transcript isoform has been considered. The genes with a FPKM higher than or equal to 1 were considered as expressed in root hairs. Sorting these genes into three classes of expression level (1–10, 10–50, and >50 FPKM) resulted in a similar distribution for the three treatments (**Figure 3**). In absence of NF treatment, 16,069 transcripts were identified as expressed in root hairs (Table S2), representing 31.5% of the predicted genes in the Mt4.0v1 genome assembly. The total number of expressed genes was only slightly affected by the NF treatments (16,077 and 16,170 for NF 4 h and NF 20 h, respectively; Table S2). Compiling the data from the three different treatments leads to a total of 16,810 non-redundant genes identified as expressed in *M. truncatula* root hairs in at least one of the tested conditions (Table S2).

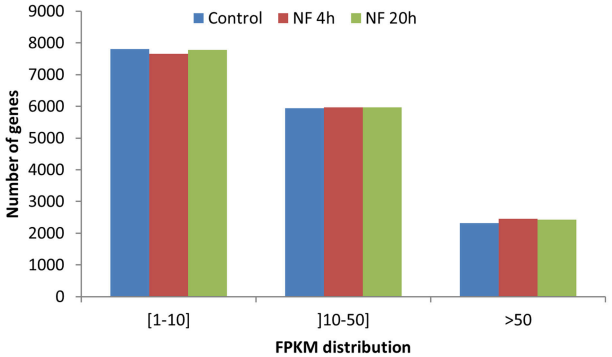

FIGURE 3 | Distribution of genes based on expression level in FPKM. Three classes have been defined from weakly expressed [(1–10) FPKM] to highly expressed (>50 FPKM).

Impact of the NF Treatments on Gene Expression

Transcriptional reprogramming in response to the NF 4 h and NF 20 h treatments was studied by assessing statistically significant differential gene expression between conditions, using EdgeR tool (Robinson et al., 2010). About 10% of the genes expressed in *M. truncatula* root hairs were thereby identified as significantly responding to NF, either being up- or down-regulated (with an adjusted $p < 0.05$; Table S3) 4 h and/or 20 h after the onset of the NF treatments. When compared with the expression data observed in the control root hairs, about 779 genes (614 up-regulated and 165 down-regulated) responded to the NF 4 h treatment, and 1525 genes (896 up-regulated and 629 down-regulated) to the NF 20 h treatment (Table S3). Among the genes identified as significantly responding to the 4 or 20 h NF treatments, 184 were specifically sensitive to the shorter treatment, 128 displaying up-regulation and 56 down-regulation, and 867 were specifically sensitive to the longer treatment, 349

displaying up-regulation and 518 down-regulation (Table S3). Thus, amongst the genes identified as responding to the NF 4 h treatment, a large majority (about 80%) displayed up-regulation. Amongst the genes identified as responsive to the NF 20 h treatment, up-regulation was again the more frequent case, but the corresponding percentage was then lower (60%). The Venn diagrams shown in **Figure 4** indicate that about 45% of the genes were significantly up-regulated at both time points, 4 and 20 h, and that there is less overlap (ca. 16%) for the down-regulated genes.

A Single Enrichment Analysis (SEA) of GO terms (Du et al., 2010) within the list of NF-responsive genes was performed (Table S4). Considering the "biological process" category (**Figure 5**), we noticed some common enriched terms in response to NF 4 h and NF 20 h treatments such as "oxidoreduction," "transmembrane transport," and "anion/inorganic anion transport." It is also worth to note that for both treatments (NF 4 h and NF 20 h), the analysis of the down-regulated gene list gave rise to about twice more significantly enriched GO terms than the up-regulated gene list. Over-represented semantic terms in the description of differentially expressed genes list was generated using the Gene Cloud software (Krouk et al., 2015). This analysis also identified the words "transporters" (or transport, uniport, symport) and "redox" (or oxydation, reduction, oxydoreductase) as amongst the enriched terms, especially in the description list of down-regulated genes at time 4 h with respect to the terms related to membrane transport (Figure S4).

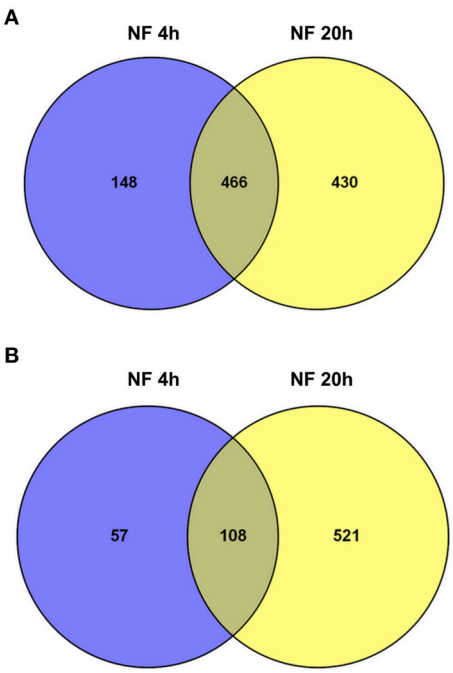

FIGURE 4 | Overview of significantly regulated genes identified in *Medicago truncatula* root hairs after Nod factor treatment. Venn diagram summarizing the number of differentially expressed genes in the two time points following NF treatment, and their respective overlaps. **(A)** Up-regulated genes (6.1% of the genes expressed in root hairs). **(B)** Down-regulated genes (3.9%).

Plasma Membrane Transport Systems Involved in Macro-Nutrients Uptake

Many homologs of genes identified in *Arabidopsis thaliana* or other species as playing a role in membrane transport of macronutrient ions were found to be expressed in *M. truncatula* root hairs. Candidate genes potentially involved in nitrate (NO_3^-), ammonium (NH_4^+), orthophosphate (Pi), sulfate (SO_4^{2-}), or potassium (K^+) transport are indicated in **Figure 6**. The *A. thaliana–M. truncatula* phylogenetic relationships of the corresponding gene families or subfamilies, named NPF (Nitrate transporter 1/Peptide transporter Family), NRT2, and NRT3 for NO_3^-, AMT (ammonium transporter) for NH_4^+, PHO1, and PHT1 for Pi, SULTR for SO_4^{2-}, HAK/KUP/KT, AKT1 (Shaker K^+ channel subfamily 1), and AtKC1 (Shaker subfamily 4) for K^+ are shown in Figures S5–S12, respectively. The expression level of these genes in the three conditions (control, NF 4 h and NF 20 h) are provided in Table S5. Interestingly almost half of the genes, expressed in root hair and potentially involved in nutrition functions, are regulated by NF 4 h or 20 h after NF treatment (17 up- and 10 down-regulated; Table S5). This proportion is significantly higher than that observed at the whole transcriptome level (ca. 10%; see above), indicating that the expression of the macronutrient transport machinery is especially reprogrammed following NF perception.

Ion Channels and Pumps Likely to Play a Role in Early Electrical and Calcium Signaling Following NF Perception

Early events triggered by NF perception are changes in ion fluxes through the root hair plasma membrane, resulting in electrical and calcium signals (Ehrhardt et al., 1992; Felle et al., 1998; Kurkdjian et al., 2000). The first events observed are an inhibition of H^+ secretion and an activation of Ca^{2+} influx and Cl^- efflux, resulting in plasma membrane depolarization. Candidate proton pumps, calcium channels, anion channels, and potassium channels that could play a role in these early signaling events (see Discussion) are indicated in **Figure 7**.

In *M. truncatula* as well as in Arabidopsis and probably in all plant species, the plasma membrane proton pumps (H^+-ATPase) are encoded by the AHA family (Falhof et al., 2016). Regarding the ion channel candidates, presently available information on gene families encoding such transport systems in plants, essentially gained in Arabidopsis, would lead to the following hypotheses: K^+ channels could be encoded by the Shaker family, anion channels by the SLAC (Slow Anion Channels), ALMT (ALuminium-induced Malate Transporter), and/or MSL (mechano-sensitive MscS-like channels) families, and calcium-permeable channels by the CNGC (Cyclic Nucleotide-Gated Channels), GLR (Glutamate Receptor-Like), ANN (Annexin), MCA (Mid1-Complementing Activity), and CSC/OSCA (reduced hyperosmolarity-induced Ca^{2+} increase/Calcium permeable Stress-gated cation Channel). Genes belonging to these families and displaying expression in *M. truncatula* root

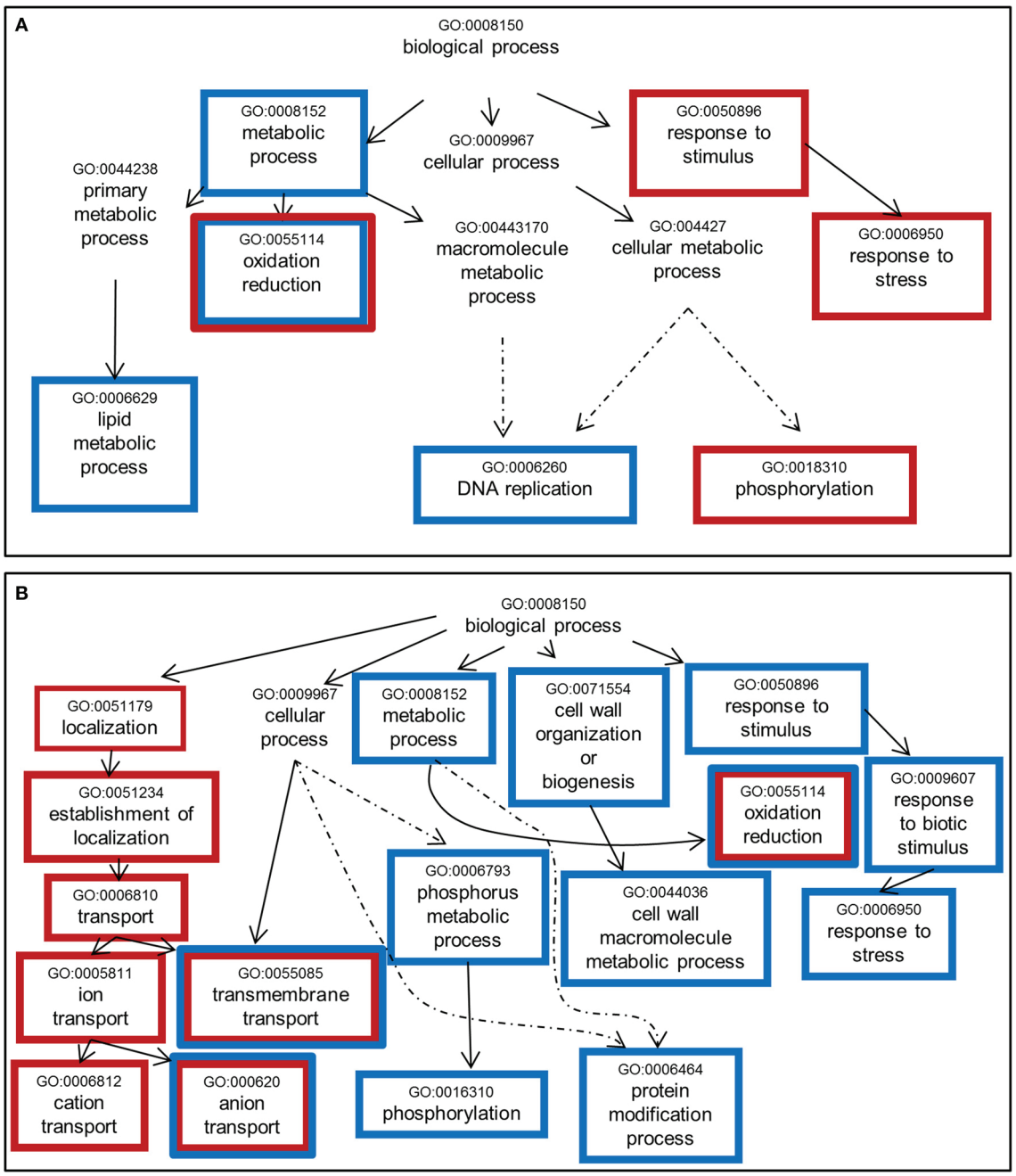

FIGURE 5 | Significantly enriched GO terms among genes whose expression is sensitive to Nod factor treatment. (A) Up-regulated genes. **(B)** Down-regulated genes. One thousand seventy genes were annotated using agriGO toolkit (http://bioinfo.cau.edu.cn/agriGO/index.php). GO terms identified with an adjusted $p < 0.05$ are enclosed into boxes. Red and blue boxes refer to the changes in expression levels induced by the NF 4 h and NF 20 h treatments, respectively. Dashed arrow indicates that all the GO levels have not been represented.

hairs are listed in Table S5. Arabidopsis–Medicago phylogenetic relationships obtained for the Shaker, AHA, SLAC, ALMT, MSL, MCA, CSC/OSCA, CNGC, GLR, and ANN families are displayed in panel A of Figures S12–S19, respectively. The expression levels (in FPKM, obtained from the control root hair dataset) of genes belonging to these families are provided in panel B of these figures. It is noteworthy that among the 60 candidate genes selected as likely to encode membrane transport systems playing a role in early electrical and calcium NF signaling in root hairs following NF perception, only a few of them are found to be induced (10) or repressed (5) by the NF treatments (Table S5). Thus, these 60 candidate proteins are already present

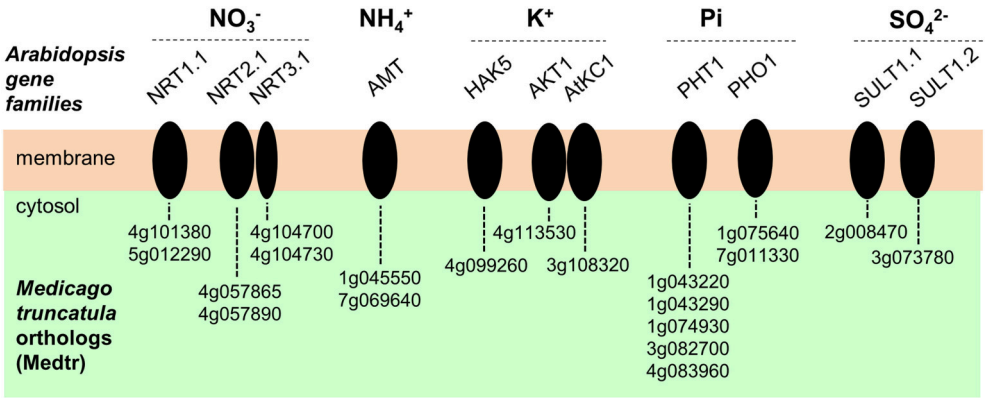

FIGURE 6 | Plasma membrane transport systems likely to play a role in transport of macronutrient ions in *Medicago truncatula* root hairs. Candidate genes potentially involved in nitrate (NO_3^-), ammonium (NH_4^+), orthophosphate (Pi), potassium (K^+) or sulfate (SO_4^{2-}) transport are represented. The corresponding acronyms in Arabidopsis are provided. NRT, NitRate Transporter. AMT, AMmonium Transporter. HAK, High Affinity K^+ transporter. AKT, Arabidopsis K^+ transport system (from the Shaker channel family). AtKC1, *Arabidopsis thaliana* K^+ channel 1 (member from the Shaker channel family). PHO1, PHOsphate 1. PHT1, PHosphate Transporter 1. SULT, SULfate Transporter.

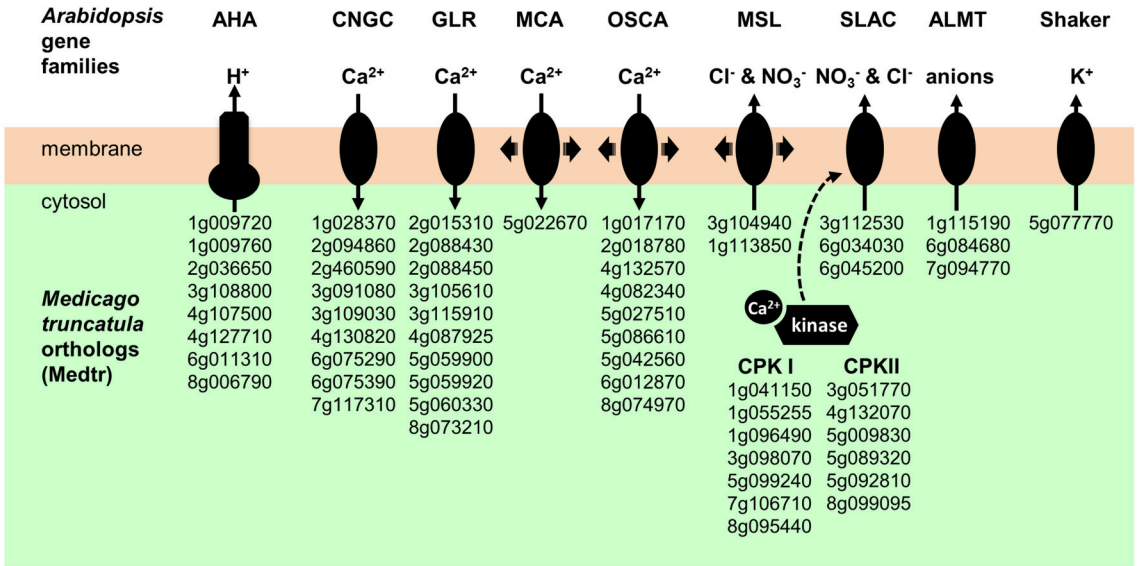

FIGURE 7 | Plasma membrane transport systems and regulatory kinases likely to play a role in early electrical and calcium signals triggered by NF perception. AHA, Autoinhibited H^+-ATPase. CNGC, Cyclic Nucleotide-Gated Channels. GLR, Glutamate Receptor-Like. MCA; Mid1-Complementing Activity. OSCA; Reduced hyperosmolarity-induced Ca^{2+} increase. MSL, Mechano-Sensitive MscS-Like channel. SLAC, Slow Anion Channel. ALMT, ALuminium-induced Malate Transporter. CPKI and CPKII, Calcium-dependant Protein Kinase I and II.

in root hairs before NF perception and their contribution (if any) to the signaling events triggered by NF perception would involve direct modifications of their transport activity rather than transcriptional responses.

A Repertoire of the Root Hair Redox Network

Genes involved in redox buffering or ROS synthesis/detoxification, according to the ROS network described by Mittler et al. (2004), were identified in the *M. truncatula* root hair transcriptome (Table S6; **Figure 8**). Among the well documented ROS producing systems, NADPH oxidases and peroxidases have been described as major sources of O_2^- and H_2O_2, respectively, during plant development and in response to biotic and abiotic stresses (Marino et al., 2012; O'brien et al., 2012. Plant NADPH oxidases are named Respiratory Burst Oxidase Homologs (*Rbohs*). In *M. truncatula*, the *Rboh* family comprises 10 genes, among which eight are expressed in root hairs (**Figure 8A**; Figure S20). The most highly expressed gene is RbohD (FPKM > 200; Table S6). One member of this family, *RbohG*, is slightly down-regulated following 20 h NF treatment.

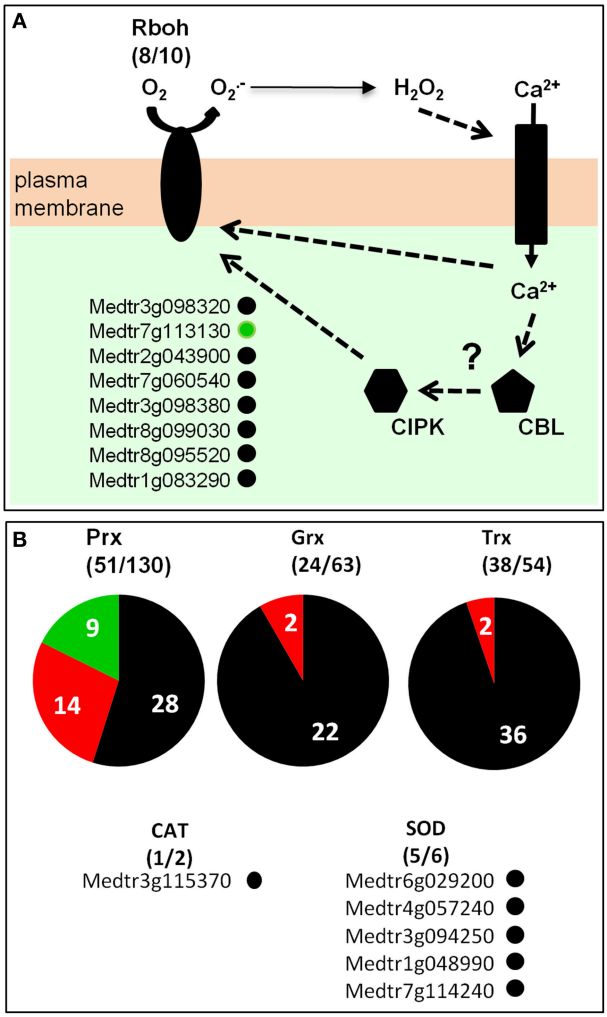

FIGURE 8 | *Medicago truncatula* ROS network in root-hairs. (A) RBOH (Respiratory Burst Oxidase Homolog) proteins catalyze the formation of superoxide anion, which is rapidly dismutated in hydrogen peroxide (H_2O_2) either spontaneously or by Superoxide Dismutase (SOD). H_2O_2 can regulate ion channels, which in turn modulate directly or indirectly RBOH activity possibly *via* calcineurin B-like-CBL-interacting protein kinase (CBL–CIPK)-mediated Ca^{2+} signaling. **(B)** Peroxidases (Prx), Glutaredoxins (Grx), Thioredoxins (Trx), catalases (CAT), and superoxide dismutases (SOD). For each gene family, the number of genes expressed in root hairs (over the total number of members of the corresponding family) is indicated. Dark gray, red, or green points or background: genes expressed in *M. truncatula* root hairs (FPKM value ≥ 1; see Table S6) that are insensitive, induced or repressed by NF treatment, respectively.

In the *M. truncatula* genome (Mt4.0v1), 130 genes have been annotated as peroxidases (**Figure 8B**), among which 54 are expressed in the root hair transcriptome including 14 (9 up and 5 down) and 20 (12 up and 8 down) responding to the 4 h and 20 h NF treatments, respectively (Table S6).

Enzymes involved in ROS detoxification, namely superoxide dismutases (SODs) and catalases, are also expressed in *M. truncatula* root hairs. Indeed, five out of the six *SOD* genes present in the *M. truncatula* genome, together with one of the two *catalase* genes (Table S6), are found as expressed in the control root hair transcriptome.

Legume Specific Genes Expressed in Root Hairs

We investigated whether part of the *ca.* 16,000 *M. truncatula* genes identified as expressed in root hairs were specific to legume plant species. We defined legume-specific genes as protein-coding genes that have no predicted ortholog in any of the 25 non-legume species considered in our comparative analysis (Table S7). It should be noted that all the legume species included in this comparative analysis belong to the papillionid subfamily, which is the largest and most widespread legume family (Wojciechowski et al., 2004). We used the OrthoMCL software (Li et al., 2003; Fischer et al., 2011) to define groups of orthologous proteins among the predicted whole protein sets from 31 plant genomes (Table S7), including six legume genomes (three from the Phaseoloid clade, i.e., tropical or warm season legumes, and three from the Galegoid clade, i.e., temperate or cool season legumes). We identified 1176 *M. truncatula* genes expressed in root hairs and specific to legume species (Table S8). Among them, 138 genes were conserved in all the six considered legume species genomes. Comparison of the control, NF 4 h and NF 20 h transcriptomes identifies 26 and 74 legume-specific root hair expressed genes as responsive to the 4 and 20 h NF treatments, respectively, with a fold change >2 and an adjusted $p < 0.05$ (Table S8). Up-regulation was observed in a large majority (84%) of the genes identified as displaying sensitivity to the NF 4 h treatment, and in only 43% of the genes displaying sensitivity to the NF 20 h treatment.

DISCUSSION

A Valuable Resource to Investigate Root Hair Functions in Legumes

Polarized tip growth, nutrient uptake, and communication with microsymbionts are three interconnected aspects of legume root hair biology. For instance, curling of the root hair upon NF perception involves re-orientation of polarized tip growth (Esseling et al., 2003). Also, root hair elongation can be stimulated by reduction in nutrient ion availability (Giehl and Von Wiren, 2014), inoculation with rhizobacteria (Vacheron et al., 2013) or addition of isolated lipochitooligosaccharides (Dazzo et al., 1996).

The present study has been mainly focused on the roles of legume root hairs in mineral nutrition and communication with symbiotic rhizobia. It is well-known that proteins likely to play a role in these functions, like ion channels, can be expressed at very low levels. In the case of ion channels, low expression levels are likely to result from the fact that such proteins mediate very high transport rates. In this context, our objective has been to get a deep description of the root hair transcriptome by carrying out RNA-seq analyses since this methodology allows detection of very lowly expressed transcripts (Wang et al., 2009). RNA-seq analyses have previously been reported for several *M. truncatula* tissues, including roots (Boscari et al., 2013; Camps

et al., 2015; Larrainzar et al., 2015) and nodules (Boscari et al., 2013; Cabeza R., et al., 2014; Cabeza R. A., et al., 2014; Roux et al., 2014; Avenhaus et al., 2015). To our knowledge, the present report is likely to provide the first RNA-seq transcriptome for *M. truncatula* root hairs and thereby the most exhaustive transcriptome available to date for this cell type. The effects of NF perception on root hair gene expression have been investigating at 4 and 20 h post-NF application.

We identify more than 16,000 genes expressed in *M. truncatula* root hairs (FPKM $\geq$1; Table S2), i.e., about 55 and 60% of the number of genes expressed in nodule tissues (ca. 30,000) or in whole root tissues (25,000–27,000; Boscari et al., 2013; Roux et al., 2014), respectively. Although, an FPKM cutoff value of one as a threshold to assess expression might be questionable, it is interesting to note that a similar proportion between the numbers of genes expressed in root hairs and in whole roots has been reported in Arabidopsis (Becker et al., 2014). About 10% of the ~16,000 genes expressed in root hairs were found to be significantly responsive to the NF treatments (787 and 1533 genes to the NF 4 h and NF 20 h treatments, respectively). In another legume model, *Glycine max*, Libault et al. (2010b) have investigated root hair responses to the symbiotic bacterium *Bradyrhizobium japonicum* using two complementary transcriptomic strategies (gene chip and RNAseq). This work led to the identification of 1973 genes that were differentially expressed in response to bacterial inoculation (Libault et al., 2010b). We also compared the present data with previous analyses of gene expression in *M. truncatula* roots (Czaja et al., 2012) or root hairs (Breakspear et al., 2014) carried out at 24 h post-NF application and performed using gene chip method (Table S10). From the 1050 and 849 genes identified as sensitive to NF treatment by Czaja et al. (2012) and Breakspear et al. (2014), respectively, about 35 and 42% display the same expression profile in our transcriptome analysis. Further, comparison with the single previous report on root hairs (Breakspear et al., 2014) is not straightforward since both the transcriptomic methods (gene chips vs. RNA-seq) and plant culture conditions were different. Indeed, Breakspear et al. (2014) used culture medium supplemented with aminoethoxyvinylglycine (AVG), an inhibitor of ethylene biosynthesis, probably leading to changes in hormone balance and root growth when compared with our experimental conditions. For instance, the two cytokinin response regulator genes *MtRR4* (*Medtr5g036480*) and *MtRR9* (*Medtr3g015490*) have been recently shown to be induced by NF treatment in presence of AVG, while only *MtRR9* is induced in absence of AVG (Van Zeijl et al., 2015). In agreement with this result, only *MtRR9* is identified as induced by NF in our transcriptome dataset (Table S2).

From the 1814 candidate genes proposed to play a role in polarized tip growth in Arabidopsis root hairs (Becker et al., 2014), we identified 1339 orthologous counterparts in the *M. truncatula* genome, among which 1089 are expressed in root hairs (Table S9). This suggests that the mechanisms underlying root hair tip growth are strongly conserved between *M. truncatula* and Arabidopsis. Providing further support to this hypothesis, 36 genes identified as crucial for root hair development and/or growth in Arabidopsis (Kwasniewski et al., 2013) are also found to be expressed in the present *M. truncatula* root hair transcriptomes. This includes genes involved in cell wall dynamics (e.g., expansin, pectate lyase, pectinesterase), in transcription regulation (bHLH) or in signaling (LRR-RLK, protein kinase; Table S10). It is also worth to note that *M. truncatula* root hairs expressed two homologs (*Medtr6g034030* and *Medtr6g045200*) of an Arabidopsis anion channel (AtSLAH3) known to play a role in pollen tube tip growth (Gutermuth et al., 2013). Altogether, these results provide evidence that the present transcriptome datasets constitute a valuable resource to further investigate major functions of root hair biology in *M. truncatula*.

A Panoply of Nutrient Ion Transporters that Includes Unexpected Systems

In silico mining of the transcriptome dataset in order to identify plasma membrane transport systems likely to play a role in plant mineral nutrition revealed candidate genes displaying significant expression levels in root hairs, whatever the nutrient ion we considered. The present results complete previous analyses establishing a genomic inventory of *M. truncatula* transporters (Benedito et al., 2010). Altogether, the results indicate that the *M. truncatula* root hair is a cell type particularly dedicated to plant mineral nutrition. Candidate genes likely to play a role in uptake from the soil solution of the macronutrients potassium, nitrate, ammonium, phosphate, and sulfate are listed in **Figure 7**; Table S5.

Two families of K^+ transport systems, named Shaker and HAK/KUP/KT, have been identified in Arabidopsis as playing a major role in K^+ uptake from the soil solution (Véry and Sentenac, 2003). The Shaker K^+ channel family is strongly conserved in plants, as well as its regulatory network that comprises protein kinase from the CIPK (CBL-Interacting Protein Kinase) family (Cuellar et al., 2013; Sharma et al., 2013; Véry et al., 2014). In Arabidopsis, two Shaker inward K^+ channel genes are expressed in root hairs, *AtAKT1* and *AtKC1*, giving rise to heteromeric K^+ channels involved in passive "low affinity" K^+ uptake from the soil solution (Sharma et al., 2013). The present transcriptome datasets indicate that only two inward Shaker channel genes are expressed in *M. truncatula* root hairs too, *Medtr4g113530* and *Medtr3g108320*, which are the closest relatives of the Arabidopsis *AtAKT1* and *AtKC1* (Figure S11). This suggests that these two genes encode Shaker subunits able to form heteromeric K^+ channels like in Arabidopsis. It has also been shown that phosphorylation of AtAKT1 channel subunits plays a crucial activating role in regulation of inward K^+ channel activity in roots (Sharma et al., 2013). The two calcineurin B-like calcium sensors CBL1 and CBL9 bind to the CBL-interacting protein kinase CIPK23, which then in turn phosphorylates AKT1 (Sharma et al., 2013). Interestingly, close homologs of these proteins (MtCIPK23: *Medtr2g049790*; MtCBL1: *Medtr3g091440*; MtCBL9: *Medtr4g099210*) are expressed in *M. truncatula* root hairs (Table S2). Regarding the HAK/KUP/KT transporter family, phylogenetic and transcriptome analyses (Figure S12) identify one gene, *Medtr4g099260*, that encodes a close homolog of the K^+ transporter AtHAK5, shown to be a major contributor to

active "high affinity" K^+ uptake in Arabidopsis roots (Gierth et al., 2005). Thus, in our experimental conditions (0.7 mM external K^+), *M. truncatula* root hairs seem to express both passive low affinity and active high affinity K^+ uptake systems. Last, regarding K^+ transport, *in silico* analyses reveal that *M. truncatula* root hairs express a transport system dedicated to K^+ secretion into the external medium, *Medtr5g077770*, which is, within the *M. truncatula* Shaker family, the single ortholog of the two Arabidopsis outwardly rectifying K^+ channels GORK and SKOR (Figure S12), the latter one being known as displaying activation by ROS (Garcia-Mata et al., 2010). Potential involvement of the Medtr5g077770 Shaker channel in establishment of nitrogen-fixing symbiosis will be discussed below.

Three families of membrane transport systems, named NPF (Nitrate transporter 1/Peptide transporter Family; Leran et al., 2014), NRT2 (Orsel et al., 2002), and NRT3 (Okamoto et al., 2006) in Arabidopsis, have been identified as playing a major role in nitrate uptake from the soil solution. The extensively studied AtNRT1.1/NPF6.3 "transceptor" is a dual affinity, bidirectional NO_3^- transporter (Liu et al., 1999; Leran et al., 2013) as well as a NO_3^- sensor mediating NO_3^- regulated auxin transport, which thereby plays an important role in root development (Krouk et al., 2010a). In the root stele, AtNRT1.1/NPF6.3 is also involved in NO_3^- secretion into the xylem sap toward the shoots (Leran et al., 2013), together with other NPF members (Lin et al., 2008; Taochy et al., 2015). A close homolog of AtNRT1.1/NPF6.3, *Medtr5g012290*, is the most highly expressed NPF member in *M. truncatula* root hair (**Figure 7**; Figure S5). Within the same NPF family, *Medtr5g093170* (MtNRT1.3/MtNPF6.8), which encodes a dual-affinity nitrate transporter similar to AtNRT1.1/NPF6.3 and demonstrated to play a role in control of root growth under N limitation (Morere-Le Paven et al., 2011), does not display expression in root hairs in our experimental conditions. NIP/LATD (*Medtr1g009200*), another NPF member from *M. truncatula*, is a high affinity NO_3^- transporter (Bagchi et al., 2012) involved in lateral root and nodule development as well as primary root meristem maintenance (Bright et al., 2005). NIP/LATD is required for ROS homeostasis and cell elongation in roots (Zhang et al., 2014). We found this gene expressed in *M. truncatula* root hairs, although at a level ∼6 times lower than that of *Medtr5g012290* (Figure S5B). *Medtr5g093170*/MtNRT1.3, which is a dual-affinity NO_3^- transporter able to transport ABA and to mediate NO_3^- inhibitory effects on primary root growth (Morere-Le Paven et al., 2011; Pellizzaro et al., 2014), was not expressed in root hairs in our experimental conditions.

In the NRT2 family, AtNRT2.1 is a NO_3^- inducible-, high affinity NO_3^- transporter (Li et al., 2007) and plays a key role in coordinating root development with NO_3^- availability (Remans et al., 2006). *Medtr4g057890* and *Medtr4g057865*, close homologs to AtNRT2.1 (Pellizzaro et al., 2014), are expressed in *M. truncatula* root hairs (**Figure 7**; Figure S6). Within the Arabidopsis NRT3 family, AtNRT3.1 has been shown to physically interact with AtNRT2.1 to form functional heteromeric transport systems that provide the major contribution to high affinity NO_3^- uptake from the soil (Yong et al., 2010). *Medtr4g104730*/MtNAR2.1 and *Medtr104700*/MtNAR2.2, the two Medicago homologs of AtNRT3.1, were by far most highly NO_3^- transport-related genes expressed in Medicago root hairs in our study, suggesting a major role for these genes in NO_3^- transport in *M. truncatula* root hairs.

Within the *M. truncatula* ammonium transporter family named AMT, the two members recently shown to have the highest levels of expression in roots as well as in shoots, *MtAMT1;1/Medtr1g045550* and *MtAMT2;1/Medtr7g069640* (Straub et al., 2014), are both expressed in root hairs (**Figure 6**; Figure S8). In contrast, the ammonium transporter *MtAMT2;3* (*Medtr8g074750*), which has been proposed to play a role in the uptake of NH_4^+ ions released by the fungus in plants engaged in arbuscular mycorrhizal (AM) symbiosis with *Glomus intraradices* (Breuillin-Sessoms et al., 2015), is not expressed in root hairs.

Evidence is available that root Pi uptake and transport is mainly mediated by transporters belonging to the PHT1 family (Nussaume et al., 2011). At least five members from the PHT1 family (out of 13) are expressed in *M. truncatula* root hairs (**Figure 6**; Table S5). This is in agreement with the hypothesis that root hairs play an essential role in plant Pi nutrition. It should also be noted that root hairs do not express *MtPT4*/*Medtr1g028600* and *MtPT8/Medtr5g068140*, two members from the PHT family shown to be induced upon AM symbiosis and then to contribute to the uptake of Pi ions released by the fungal membrane (Javot et al., 2011; Breuillin-Sessoms et al., 2015). Thus, it is tempting to speculate that, within large families of membrane transport systems such as the AMT and PHT families, some members have been specialized, maybe in terms of sensitivity to external pH, membrane polarization, or substrate concentration, in order to cope with the external conditions prevailing in either the soil solution or the apoplastic medium at the plant-microorganism interface.

M. truncatula root hairs can be assumed to also provide a major contribution to sulfate nutrition since they express *MtSULTR1.1/Medtr2g008470* and *MtSULTR1.2/Medtr3g073780*, which encode the closest homologs of the Arabidopsis *AtSult1;1* and *AtSult1;2* (**Figure 7**; Figure S10), the major contributors to high affinity sulfate uptake from the soil in Arabidopsis roots (Rouached et al., 2009). It is worth to note that while these genes are down-regulated in root hairs following NF treatment (Table S5), they are highly induced in mycorrhized *M. truncatula* roots as compared to non-mycorrhized roots whatever the growth medium S content (Gao et al., 2014; Wipf et al., 2014). In contrast, MtSULTR3.4b/*Medtr4g011970*, which has not been considered as expressed in control root hairs (FPKM < 1), is highly induced following NF treatment by almost 20 times. Thus, the route for sulfate nutrition appears different under normal condition or upon mycorrhiza or nitrogen-fixing symbiosis.

Two families of genes encoding membrane transporters, PHO1 and HKT, comprise members whose expression in *M. truncatula* root hairs could not be anticipated based on the present knowledge available in Arabidopsis or other plant species. The corresponding genes for the PHO1 family are *Medtr7g011330* and *Medtr1g075640* (**Figure 6**; Figure S9). Indeed, in Arabidopsis members from the PHO1 family (11

members), mainly PHO1 and PHO1; H1, are involved in Pi translocation into the xylem sap toward the shoots (Poirier et al., 1991; Hamburger et al., 2002; Stefanovic et al., 2007). Furthermore, direct evidence has been obtained that PHO1 is endowed with the capacity to mediate Pi secretion into the external (apoplasm) medium (Stefanovic et al., 2011; Arpat et al., 2012). It is thus tempting to speculate that the close homologs of PHO1 that are expressed in *M. truncatula* root hairs mediate secretion of Pi ions previously taken up by members from the PHT phosphate transporter family.

The HKT family comprises a single member in Arabidopsis, like in poplar and many dicots (Véry et al., 2014). Electrophysiological characterization of the Arabidopsis HKT, AtHKT1, the founder of plant HKT subfamily 1, has revealed a strong selectivity for Na^+ against K^+ and other cations, and no current rectification (Berthomieu et al., 2003). In other words, this transporter has the capacity to mediate Na^+ uptake as well as secretion. It has been shown to be expressed in the plant vasculature, where it plays a role in desalinization of the ascending xylem sap in roots and recirculation of Na^+ ions from shoots to roots via the phloem sap. Loss of function of this transporter results in increased plant sensitivity to salinity (Berthomieu et al., 2003). It is intriguing that the dicot *M. truncatula* possesses 4 HKT transporters, one of which displays expression in root hairs (*Medtr6g092840*; **Figure 6**; Figure S21). One may wonder whether such a number of HKT transporters contribute to *M. truncatula* tolerance to salt stress. This raises also the question of the actual roles of HKT transporters in root hairs and whether these roles involve Na^+ uptake or secretion.

Finally, regarding nutrient ion transport in *M. truncatula* root hairs, it is worth to note that the equipment of this cell type in plasma membrane transporters or channels is likely to confer on it the capacity to secrete all the above considered nutrient ions, including Pi. Secretion of K^+ and NO_3^- into the external medium could play a role in the control of transmembrane electrical gradient and/or of internal water potential or pH upon abiotic stresses (Ivashikina et al., 2001; Segonzac et al., 2007). The physiological meaning of Pi secretion toward the external medium is however more difficult to decipher. A hypothesis would be that such equipment in secretion systems plays a direct role in the overall process allowing translocation of nutrient ions toward the inner tissues. This would involve polarized localization (or polarized activity) of the systems dedicated to secretion of nutrient ions, allowing root hairs to secrete ions into the root apoplasm toward neighboring cortical cells and not toward the external solution. Such an apoplastic step in the migration of ions toward the stele and xylem sap would make sense if diffusion through root hair plasmodesmata toward the cortical cells was a limiting step in the overall radial transport process.

A Repertoire of Plasma Membrane Transport Systems Likely to Play a Role in Early NF Signaling

Early signaling events triggered by NF perception are changes in ion fluxes across the cell membrane, resulting in electrical and calcium signaling. The current model is that NF perception by root hair membrane receptors leads to an inhibition of the rate of H^+ excretion by plasma membrane proton pumps and to an activation of calcium and anion channels, allowing Ca^{2+} influx and anion efflux. These events induce a strong depolarization of the cell membrane. This depolarization activates voltage-sensitive K^+ channels, giving rise to an efflux of K^+ ions, which results in membrane repolarization (Felle et al., 1996, 1998, 1999; Bouteau et al., 1999; Kurkdjian et al., 2000; for review, Oldroyd, 2013). At the molecular level, the present knowledge about the systems involved in these early NF signaling events is very low. Candidate genes listed in **Figure 7** would however deserve to be tested by genetic and physiological analyses for a role in this signaling.

Plant plasma membrane proton pumps are encoded by the AHA gene family (Nguyen et al., 2015), which comprises five subfamilies in higher plants (Falhof et al., 2016). Eleven AHA genes are present in Arabidopsis and 13 in *M. truncatula*. Our data indicate that *M. truncatula* express five from these 13 genes in root hairs (Figure S13). Three genes, *Medtr4g127710*, *Medtr2g036650*, and *Medtr6g011310*, which have been recently named *MtAHA4*, *MtAHA5*, and *MtAHA6* (Nguyen et al., 2015), respectively, display much higher expression levels than the others. Interestingly, phosphoproteomic analyses of *M. truncatula* whole roots have revealed that 1 h treatment with NF leads to an increase in the phosphorylation status of the auto-inhibitory C-terminal domain of MtAHA5 pumps (Rose et al., 2012). Further, analyses have revealed that such a phosphorylation is likely to result in an increase in H^+ pumping activity of these proteins (Nguyen et al., 2015). This could play a role in repolarization of the cell membrane following the initial NF-induced depolarization. On the other hand, this report does not provide information about the molecular mechanisms underpinning the initial inhibition of H^+ secretion and membrane depolarization triggered by NF perception (Felle et al., 1996, 1998). Since the depolarization has been shown to occur very rapidly after NF perception, within a few minutes, it should essentially involve post-translational regulation. It is however worth to note that the present transcriptome data reveal a significant inhibition of *MtAHA5* expression (5 fold) as well as an increase in *MtAHA1* expression (80 fold) in response to NF treatment. *MtAHA1* had already been reported to be induced by both NFs and *S. meliloti* (Breakspear et al., 2014). *MtAHA1* has been shown to be specifically expressed in arbuscule-containing root cells and to be required for development of functional arbuscules (Krajinski et al., 2002, 2014; Wang et al., 2014). In our analyses, *MtAHA1* is not expressed in the control condition but strongly induced in the NF conditions (with a strongest induction at 4 h). Clearly, further genetic and biochemical analyses of the regulation and roles of the AHA pumps displaying expression in root hairs would be very useful. For instance, constitutively hyper-active AHA mutant pumps (genetically engineered based on the knowledge available in the Arabidopsis AHA family: Merlot et al., 2007) could be expressed in *M. truncatula* root hairs to assess the role of cell membrane depolarization in the early NF transduction pathway.

Regarding Ca^{2+}, several gene families, amongst which the CNGC, GLR, ANN, MCA, and CSC/OSCA families, might

encode channels involved in the initial Ca^{2+} influx and signals. The fact that, in animals, the CNGC, and GLR families play central roles in major signaling pathways has constituted a strong stimulus motivating extensive investigations of the roles of these systems in plants (Hedrich, 2012). Unfortunately, expression and functional characterization of plant CNGC and GLR has remained difficult or even unsuccessful in classical heterologous systems such as Xenopus oocytes, and the present knowledge about the transport activities of these systems is still quite unsatisfactory (Hedrich, 2012). It is thus very likely that progress in their functional characterization will essentially come from *in planta* investigations based on (electro) physiological and cell imaging analyses in mutant plants. Nonetheless, the fact that the plant CNGC and GLR families are relatively large, e.g., 20 CNGC and 20 GLR in Arabidopsis, 22 and 18 in *M. truncatula*, is likely to result in strong redundancy, at least in standard environmental conditions, and thus to render such analyses highly challenging. For instance, our present data identify 8 CNGC and 10 GLR (Table S5) genes as significantly expressed in *M. truncatula* root hairs. Interestingly however, for each of these two families, the expression levels of the genes expressed in this cell type vary within a very large range, by two orders of magnitude. It should also be mentioned that only few of them are regulated following 20 h NF treatment and none at the early time point. In this context, reverse genetics approaches to decipher the roles of these channels in early electrical signaling following NF treatment could be targeted to the genes displaying the highest levels of expression in root hairs. In plants, annexins are described as potential Ca^{2+}-permeable channels involved in Ca^{2+} and ROS signaling (Laohavisit et al., 2010, 2012). In addition, annexins displayed phospholipid and F-actin binding activity suggesting a role in cytoskeleton rearrangements, membrane trafficking processes, and cell expansion. The Medicago genome contains 20 *Ann* genes, and about half of them are expressed in root hairs (Figure S19). Our data indicate that four from these genes are up-regulated by NF and one (*Medtr8g038210/MtAnn1*) is specifically expressed under NF treatment (Table S5) as it has already been reported (Breakspear et al., 2014). Interestingly, a close association between ANN1 expression and rhizobial infection has been previously shown (De Carvalho Niebel et al., 1998). *MtAnn1* protein displays a cytoplasmic localization but preferentially accumulates at the nuclear periphery of rhizobia-activated outer cortical cells, suggesting a role in the induction of Ca^{2+} spiking observed in rhizobial symbiosis (De Carvalho-Niebel et al., 2002).

With respect to the depolarizing efflux of anions, two candidate gene families can be thought about, the SLAC (Figure S14) and ALMT (Figure S15) families (Hedrich, 2012). Two members from the SLAC family, *Medtr6g045200* and *Medtr6g034030*, display high levels of expression in *M. truncatula* root hairs (Figure S14B) and they both are close homologs of the Arabidopsis AtSLAH3, which has been proposed to mediate anion efflux in Arabidopsis pollen tubes (Gutermuth et al., 2013). It is worthy to note that the genes encoding their regulatory kinases CPKI and II are also expressed in the root hair (**Figure 7**). In Arabidopsis, SLAC anion channels are activated by kinases from CPK (Ca^{2+}-Dependent Protein Kinase) subfamilies I and II (Negi et al., 2008; Geiger et al., 2010). At least 13 CPK (7 from the CPK I subfamily and 6 from CPK II subfamily) potentially involved in SLAC channels activation are expressed in *M. truncatula* root hairs (**Figure 7**). Three ALMT genes are expressed in *M. truncatula* root hairs. In Arabidopsis, the ALMT family comprises 14 members, which are distributed into four clades, as also found in *M. truncatula* (Figure S15). ALMT are active either at the plasma membrane or at the vacuolar membrane (Barbier-Brygoo et al., 2011). In our study we found three ALMT genes expressed in root hairs, two of these, *Medtr7g094770* and *Medtr1g115190*, are up-regulated at 20 h post-NF application. They are homologous to AtALMT12 which is shown to encode a component of the R-type/QUAC anion current involved in guard cell signaling and requiring malate for activation (Meyer et al., 2010).

K^+ channel activity encoded by the Shaker family is thought to dominate the plasma membrane conductance to K^+ in most cell types in Arabidopsis (Lebaudy et al., 2007). Although this family is highly conserved in plants (Véry et al., 2014), the *M. truncatula* genome harbors a single outwardly rectifying Shaker K^+ channel gene, *Medtr5g077770*, while two channels of this functional type have been identified in Arabidopsis, GORK, and SKOR. GORK is expressed in guard cells, where it mediates K^+ efflux involved in stomatal closure (Hosy et al., 2003). It is also expressed in Arabidopsis root hairs, where its physiological role is still rather mysterious (Ivashikina et al., 2001). SKOR is expressed in root stele tissues where it contributes to K^+ secretion into the xylem sap toward the shoots (Gaymard et al., 1998). Thus, the K^+ channel encoded by *Medtr5g077770* is the single candidate from the Shaker family that can be proposed to play a role in cell membrane repolarization during the early electrical response to NF, besides being involved in stomatal movements and in K^+ secretion into the xylem sap.

The presence of mechanosensors (MS) channels in the root hair plasma membrane, able to rapidly transduce mechanical forces into ion fluxes and electrical signals, is worth considering since adhesion of the microsymbiont and curling of root hair might elicit local mechanical constraints. In plants, MS channels are encoded by at least four small gene families, MscS-like (MSL; Haswell and Meyerowitz, 2006), Mid1-Complementing Activity (MCA; Kurusu et al., 2013), Piezo (Coste et al., 2012), and one larger family, CSC/OSCA (Hou et al., 2014; Yuan et al., 2014). Arabidopsis displays 10 MSL genes, which are distributed into two clades. Clade I comprises genes encoding proteins localized in endomembranes while clade II comprises proteins predicted or shown to be targeted to the plasma membrane (Haswell and Meyerowitz, 2006; Haswell et al., 2008). Two *MtMSL* of clade II are expressed in *M. truncatula* root hairs (Figure S16), *Medtr3g104940* and *Medtr1g113850*. They encode close relatives of the well-described Arabidopsis AtMSL10 and AtMSL8, which have been shown to be gated by membrane stretching. AtMSL10 is more permeable to anions (Cl^- and NO_3^-) than to cations (Haswell et al., 2008; Maksaev and Haswell, 2012). The pollen-specific AtMSL8 channel has been proposed to be involved in sensing of mechanical stress induced by hypoosmotic shock (Hamilton et al., 2015).

MCA channels have been initially identified in Arabidopsis and exhibit 10% identity to yeast Mid1 (Nakagawa et al., 2007). *M. truncatula*, like Arabidopsis, possesses two MCA genes, and one of them (*Medtr5g022670*) is expressed in root hairs (Figure S16). Available information on plant MCA provides support to a model wherein these proteins either are themselves MS Ca^{2+} channels or are closely associated with the activity of an MS calcium channel (Nakagawa et al., 2007; Yamanaka et al., 2010; Kurusu et al., 2012). It is noteworthy that the Arabidopsis MCA1 is likely to play a role in root mechanosensing and growth as suggested by a defect in root entry into hard agar of *mca1* mutant plants (Nakagawa et al., 2007; Yamanaka et al., 2010).

The present knowledge on the CSC/OSCA family (Hou et al., 2014; Yuan et al., 2014), which comprises 15 members in Arabidopsis and 13 members in *M. truncatula*, is still rather low. The two members identified in Arabidopsis, AtCSC1 (Hou et al., 2014), and AtOSAC1 (Yuan et al., 2014), have been shown to be activated upon hyperosmotic shocks and then to behave as poorly selective cation channels permeable to Ca^{2+}. Among the 13 members of this family in *M. truncatula*, nine are expressed in root hairs (Figure S16; Table S5). Finally, the functional properties and physiological roles of Piezo family are still unknown in plant. The Piezo channel protein initially identified in mouse is an essential component of a cationic non-selective MS channel (Coste et al., 2012). *M. truncatula* has two homologs of the mouse Piezo, both expressed in root hairs (Figure S20) while only one homolog is present in Arabidopsis.

A Promising View of the ROS Network in Root-Hairs

NADPH oxidases (RBOHs) have been shown to be important actors involved in ROS production in plants (Marino et al., 2012; O'brien et al., 2012. In *M. truncatula*, 8 out of its 10 *Rboh* genes are expressed in root hairs (**Figure 8**; Figure S21; Table S6), including the highly expressed gene (FPKM > 200) *MtRbohD*, which is the closest ortholog of Arabidopsis *AtRbohC* (Foreman et al., 2003), and *MtRbohF*, whose expression in root hairs was already reported (Marino et al., 2011). *MtRbohF* is the closest homolog of the two Arabidopsis NADPH oxidases *AtRbohH* and *AtRbohJ*. In Arabidopsis tip-growing pollen tubes, these two NADPH oxidases generate pulsating tip-localized H_2O_2 production that functions, possibly through Ca^{2+} channel activation, to maintain a steady tip-focused Ca^{2+} gradient during growth (Boisson-Dernier et al., 2013). Loss of function of *AtRbohC* in Arabidopsis (Foreman et al., 2003) and of a monocot-specific *Rboh* gene in maize plants (Nestler et al., 2014) has been reported to result in root-hairless phenotype. In *M. truncatula*, none of the investigations performed so far into the effects of loss-of-function mutations in *Rboh* genes (*RbohA*, Marino et al., 2011; *RbohC*, Zhang et al., 2014; *RbohE*, Belmondo et al., 2016) has revealed any root hair phenotype, suggesting strong gene redundancy. However, such analyses have not yet targeted the two genes, *MtRbohD* and *MtRbohF*, which are identified by our transcriptome data as the most highly expressed in root hairs.

In addition to NADPH oxidases, other enzymes, namely class III peroxidases (PRXs), are involved in H_2O_2 production during plant-pathogen interaction (Kadota et al., 2015). PRXs that are mainly localized in cell wall have been shown to play a role in cell wall remodeling (Francoz et al., 2015). The present transcriptome data identify more than 50 PRX genes as displaying expression in root hairs (**Figure 8**; Table S6). Sensitivity of such peroxidases to NF treatment in our experimental conditions is discussed later.

Transcription factors regulating the expression of peroxidases have been identified (Tsukagoshi et al., 2010; Sundaravelpandian et al., 2013). UPBEAT1, a basic helix-loop-helix (bHLH) root transcription factor, has been shown to regulate the expression of several peroxidases that fine-tune ROS accumulation between the zone of cell proliferation and cell elongation where differentiation begins (Tsukagoshi et al., 2010). A putative ortholog of UPBEAT1 is found in *M. truncatula* (*Medtr1g096530*), and our transcriptome data reveal expression of this gene in root hairs (Table S2). More recently, mutations in the Mediator subunit *MED25/PFT1* gene, which encodes part of a complex that docks transcription factors bound to enhancers with core promoter components, have been shown to result in compromised root hair development, due to altered expression of a set of H_2O_2-producing class III peroxidases (Sundaravelpandian et al., 2013). An *M. truncatula* PFT1 ortholog, *Medtr5g054680*, is expressed in root hairs (Table S2). With *UPBEAT*/*Medtr1g096530*, *MtPFT1*/*Medtr5g054680* may be another transcription factor playing a role in controlling peroxidase expression, and thus ROS levels, in *M. truncatula* root hairs.

Many genes encoding enzymes involved in ROS detoxification, namely superoxide dismutases (SODs) and catalases, are expressed in *M. truncatula* root hairs (**Figure 8**; Table S6). The present data indicate that almost all SOD genes are expressed in root hairs. This result, together with the fact that the NADPH oxidases, which synthesize O_2^-, are also almost all expressed in root hairs, suggest that the management of O_2^- production and detoxification is of major importance and highly complex. Furthermore, it is now well established that ROS are important signals (Apel and Hirt, 2004) playing an essential role in Ca^{2+} channel activation in root hairs (Foreman et al., 2003; Takeda et al., 2008; Monshausen et al., 2009). Considering that the root hair is the entrance of the rhizobial symbiosis, these *M. truncatula* genes may be involved in steady state control of a tip-focused cytosolic Ca^{2+} gradient allowing fine tuning of calcium-regulated proteins, modification of the cytoskeleton, and localized vesicle exocytosis.

Finally, the presence in *M. truncatula* root hair transcriptome of sequences from at least 24 glutaredoxin (out of 63 in the genome) and 38 thioredoxin (out of 54) genes (Table S6) also provides evidence of the importance of redox control in root hair biology. Many Grxs and Trxs are present in plant genomes, but only a few of them have been shown to be expressed and characterized in root hairs among which the thioredoxin h5 (*At1g45145*) has been shown to be induced by pathogens and oxidative stress (Reichheld et al., 2002; Laloi et al., 2004).

NF Effects on Expression of Plasma Membrane Ion Transport Systems and ROS Network

As discussed above, it makes sense that NADPH oxidases and most transport systems listed in **Figure 7** as likely to play a role in the early electrical and calcium responses to NF are already significantly expressed in root hairs before NF arrival, *i.e.* that their expression in root hairs pre-exists to NF perception. However, enrichment analysis of GO terms indicates that, at a global level, NF treatments impact the transcription of genes belonging to categories related to membrane transport and redox activity (**Figures 7**, **8**).

Various candidate genes encoding transport systems likely to contribute to nutrient ion uptake from the soil solution by root hairs, as hypothesized in **Figure 6**, are rapidly down-regulated at the transcriptional level upon NF perception (Table S5). For instance, this is the case for the two high affinity sulfate transporter genes SULTR1;1 (*Medtr2g008470*) and SULTR1;2 (*Medtr3g073780*) as indicated above, and of the high affinity phosphate transporter genes MtPT1 (*Medtr1g043220*) and MtPT6 (*Medtr3g082700*). Such results suggest that the root hair rapidly reduces its contribution to plant mineral nutrition a few hours after NF perception, at least regarding the uptake of nutrient ions such as phosphate and sulfate.

In contrast, *M. truncatula* homologs of Arabidopsis major representatives from the three families of NO_3^- transport systems in Arabidopsis (NPF, NRT2, and NRT3) are not down-regulated upon NF treatments in *M. truncatula* root hairs, some of them being even up-regulated. This may suggest that nitrate fluxes are involved in plant response to NF. However, it is also worth to note that, in addition to their nitrate transport capacity, some Arabidopsis homologs of these *M. truncatula* transporters display other activities, leading to reprogramming of root architecture and modification of hormone fluxes or signaling events that may be of importance in the plant response to NF. For instance, both NO_3^- transporters AtNRT1.1 and AtNRT2.1 are involved in NO_3^- sensing and coordination of root development with NO_3^- availability (Little et al., 2005; Remans et al., 2006; Krouk et al., 2010b). Interestingly, AtNRT1.1, the closest homolog in Arabidopsis of the *Medtr5g012290* transporter, also transports auxin (Krouk et al., 2010b), and control of auxin transport and accumulation is known to be involved in early nodule development (Mathesius et al., 1998; De Billy et al., 2001). Data on *Pseudomonas syringae*/Arabidopsis interactions suggest that AtNRT2.1 also participates in down-regulating biotic stress (salicylic acid-dependent) defense mechanisms through modifications in hormone pathways and sensitivity to the bacterial effector (Camanes et al., 2012). In addition, AtNRT2.1 was recently found to play a major role in control of root hydraulic activity (Li et al., 2016), a function which, in *M. truncatula*, may facilitate root hair development upon NF perception. In this context, it is worth noting that the two *M. truncatula* AtNRT2.1 homologs (*Medtr4g057865*/MtNRT2.2 and *Medtr4g057890*/MtNRT2.1) are highly expressed in root hairs and significantly stimulated by NF treatments (Figure S6). Since *MtNRT2.2* was found hardly detectable in total roots even by RT-qPCR (Pellizzaro et al., 2015), it is likely that *M. truncatula* root hairs are particularly enriched in MtNRT2.2, suggesting a specific role of this transporter in this cell type.

Seven out of eight *Rboh* genes expressed in root hairs display no significant transcriptional regulation upon NF perception (**Figure 8**; Table S6). One root hair expressed *Rboh*, *MtRbohG*, is weakly repressed (**Figure 8**; Table S6). On the other hand, several RBOH proteins, including MtRBOHD, have been found to be phosphorylated after NF application (Rose et al., 2012). In Arabidopsis, RBOHD is controlled by Ca^{2+} via direct binding to EF-hand motifs and phosphorylation by Ca^{2+}-dependent protein kinases (Kadota et al., 2014, 2015; Li et al., 2014). Moreover, as mentioned above for AtAKT1 (Sharma et al., 2013), a direct interconnection between CBL–CIPK-mediated Ca^{2+} signaling and ROS signaling in plants provides evidence for a synergistic activation of the NADPH oxidase RBOHF. This activation would occur by direct Ca^{2+}-binding to its EF-hands and Ca^{2+}-induced phosphorylation by CBL1/9–CIPK26 complexes (Drerup et al., 2013). It is tempting to speculate that similar regulation mechanisms occur in *M. truncatula* root hairs too, giving rise to interactions between ROS and Ca^{2+} signaling pathways, since close homologs of Arabidopsis *CBL1/9* and *CIPK26* can be identified in the present transcriptome dataset (Table S2; **Figure 8A**). This would make sense with the fact that ROS signals and Ca^{2+} influx are very rapidly induced upon NF treatment, within a few seconds and then decreased (for review, see Felle et al., 1998; Puppo et al., 2013).

Except within the peroxidase family, only few genes involved in the ROS network as described by Mittler et al. (2004) are identified by the present data as sensitive to NF treatment (Table S6). The previous transcriptome data identified 10 "Rhizobially Induced Peroxidases" (*RIP1* to *RIP10*) genes, shown to be induced in root hairs by both *S. meliloti* and NF (Breakspear et al., 2014).One of these, *MtRip1*, was shown to be induced by H_2O_2 (Ramu et al., 2002). Interestingly, the expression patterns of these genes overlap with the sites of production of superoxide in infected root hairs, in nodules and roots (Chen et al., 2015). The present data (Table S6) reveal a set of 16 peroxidases genes displaying up-regulation upon NF perception, amongst which are 8 of the 10 previously identified RIP genes (Breakspear et al., 2014). All 16 of these peroxidases have a predicted secretion signal peptide, providing further support to the hypothesis of increased production of ROS in root hair apoplast during early NF signaling (Breakspear et al., 2014).

Papilionoid Legume Specific Genes Expressed in *Medicago truncatula* Root Hairs: Roles in Symbiosis Initiation?

We identified 1176 papilionoid legume-specific genes (LSGs) expressed in *M. truncatula* root hairs (Table S8). Previously, only 861 EST contigs had been identified as legume-specific in *M. truncatula* (Graham et al., 2004). Several classes of LSGs have been identified in *M. truncatula* including over 300 cysteine cluster proteins, 63 proline-rich proteins, and 21 glycine-rich

proteins (Benedito et al., 2008). Within the present list of LSGs expressed in root-hairs (Table S8), about 4% (i.e., 46 genes), encode putative disease resistance proteins. Furthermore, most of the papilionoid legume-specific genes displaying high levels of expression in root hairs (FPKM > 50) are putatively involved in defense mechanisms. It is noteworthy that many of these papilionoid legume-specific defense genes, such as *Medtr5g088770* and *Medtr7g093820*, which encode a cysteine protease inhibitor (cystatin) and a disease resistance response protein, respectively, are down-regulated following NF treatment (Table S8). Such a down-regulation of defense genes might be required to allow the initiation of symbiosis. With respect to this hypothesis, GO analysis indicates that the semantic categories "response to stimulus" and "response to stress" are over-represented within the set of genes displaying up-regulation in response to the 4 h NF treatment (**Figure 5**; Table S4). In contrast, later on, 20 h after NF application, these categories are over-represented within the set of down-regulated genes. Altogether, these results provide further support to the hypothesis that the plant cannot straightforwardly welcome rhizobia as beneficial partners and engage in symbiosis without rapidly altering and adapting its immune/defense system. Also supporting this hypothesis are transcriptomic and phosphoproteomic studies that have revealed rapid induction of defense related genes and phosphorylation of proteins known to be involved in plant immune system (Libault et al., 2010a; Rose et al., 2012; Nguyen et al., 2015). Interestingly, about 50% of the legume specific disease resistance genes expressed in *M. truncatula* root hairs possess orthologs in all the legume genomes selected for the present analysis. It is thus tempting to assume that such genes contribute to central root hair functions common to all legumes, and that some of them play a role in rhizobial symbiosis.

Actin nucleation facilitated by the ARP2/3 complex plays a central role in plant cell shape development where the SCAR/WAVE complex is shown to be an essential upstream activator of ARP2/3 function in plants (Jorgens et al., 2010). The Suppressor of cyclic AMP receptor/WASP family verprolin homologous (SCAR/WAVE) complex is conserved from animals to plants and, generally, is composed of the five subunits SCAR/WAVE, PIR121 (p53-inducible protein-121), NAP125 (NCK-associated protein-125), BRICK, and ABI (Abl-interacting protein). Recently, several studies have shown the importance of these proteins in legumes (NAP1: NCK-ASSOCIATED PROTEIN, (Miyahara et al., 2010); PIR1: 121F-SPECIFIC P53 INDUCIBLE RNA, Yokota et al., 2009; LjSCARN, Qiu et al., 2015). *Medtr7g116710* gene, encoding an ABl-like protein (ABlL1) is early induced by NF (Table S10). This gene has also been reported to be induced by rhizobia (Breakspear et al., 2014). Interestingly, this gene has also been shown to be regulated by H_2O_2 (Andrio et al., 2013) and was found to be specific to papilionoid legumes in our OrthoMCL comparative genomics analysis (Table S3). It may be speculated that this ABIL1-like protein could have a function in linking SCAR/WAVE-dependent actin nucleation with ROS during the establishment of the rhizobial symbiosis.

CONCLUSION

The present RNA-seq data provide the most exhaustive information available so far about gene expression in *M. truncatula* root hairs, before and after NF perception. These data have been analyzed by focusing mainly on genes likely to play a role in macronutrient ion transport across the root hair plasma membrane or in ROS signaling and early communication with rhizobia. These processes are of major importance for plant growth in natural ecosystems, when nutrient availability is limited. Hypotheses derived from the present transcriptome data identify candidate genes for reverse genetics investigation of a possible role in these processes and, more generally, provide a valuable resource for root hair systems biology.

MATERIALS AND METHODS

Plant Growth and Nod Factor Treatments

The whole experimental procedure was adapted from Sauviac et al. (2005). *M. truncatula* (ecotype Jemalong A17) seeds were scarified with sulfuric acid (99%) for 10 min and sterilized in 6% sodium hypochlorite solution for 3 min. After 3 h imbibition in sterile water, seed coats were removed and seeds were disposed on inverted 0.8% agar plates. The plates were kept for 48 h in the dark at 4°C. They were thereafter transferred at 21°C during 15 h for germination. Seedlings with a radicle long of about 2 cm were then transferred onto a sterile sheet (12 × 8.5 cm) of chromatography paper (Rogo-Sampaic, France) laid on solid Fahräeus medium in a Petri dish (12 × 12 cm, for 10 seedlings). Plantlets were grown in a growth chamber (70% humidity, 70 μE.m-2.s-1 light intensity) with a photoperiod of 16 h light (25°C) and 8 h dark (21°C) for 5 days in total before root hair isolation. Treatments with synthetic NF (Rasmussen et al., 2004) were performed either 4 or 20 h before root hair isolation (NF 4 h and NF 20 h treatments, respectively), by using 50 μl of 10 nM Nod factor solution per plant NodSm-IV(C16:2, Ac, S), gently deposited along of the root hair region (**Figure 1A**). Control roots were similarly treated with 50 μl of sterile water (Control Treatment). Root hairs were collected during the 7th hour of the light period on day 5. Two independent biological repeats were performed for all treatments, in each case with 100 plants.

Root Hairs Isolation and RNA Extraction

Root hairs were obtained from 4 cm-long root segments (**Figure 1A**) corresponding to the youngest part of the root hair zone. The root tip (ca. 0.5 cm) was excised to avoid contamination by root cap cells. Root hairs were isolated by freezing and vortexing the root segments in liquid nitrogen (Sauviac et al., 2005). About 60 mg of root hairs were obtained from 100 root segments.

RNA was extracted using the Qiagen RNeasy Plant Mini kit according to the supplier's instructions. DNA was removed using RNAse-free DNAse I (Qiagen) added directly onto the spin column. About 2.5–3 μg of RNA (measured using NanoDrop 1000 spectrophotometer, Thermo Scientific) were obtained from each root hair sample prepared from 100 plants. Total RNA were

checked for their integrity on RNANano chip, using Agilent 2100 bioanalyzer (Agilent Technologies, Waldbroon, Germany).

Transcriptome Studies

RNA-seq experiments were carried out at the POPS-transcriptomic platform (IPS2-Saclay, France) using an IG-CNS Illumina Hiseq2000 machine to perform paired-end 100 bp sequencing on cDNA libraries performed by TruSeq_Stranded_mRNA_SamplePrep_Guide_15031047_D protocol (Illumina®, California, USA). The 6 libraries have been sequenced in paired-end (PE) with a sizing of 260 bp and a read length of 100 bases. The multiplexing rate was three libraries per lane of Hiseq2000 machine (two lanes in total) to obtain around 50 million reads per sample.

RNA-seq Bioinformatic Treatment and Analysis

Each RNA-seq sample was subject to the same pipeline from trimming to count of transcript abundance as follows. The raw data (fastq) were trimmed to keep only bases with Phred Quality Score >20 and sequence read length >30 bases. Bowtie v2 was used to map reads to the *M. truncatula* transcriptome (Mt4.0v1 with—local option). The abundance of mRNAs was calculated by a local script which parses SAM files and counts only paired-end reads for which both reads map unambiguously to the same gene (i.e., reads mapping to multiple positions were discarded). According to these rules, around 73% of PE reads aligned to transcripts, in each RNA seq sample (Table S1). Differential gene expression across samples was analyzed using the EdgeR package (Version 2.4.6) in the statistical software "R" (Version 2.15.0). Raw read counts normalization was carried out with the EdgeR (v 2.4.6) software [with the Counts Per Million (CPM) function]. This method allows normalizing the data as a function of the size of the library. For each experimental treatment (control, NF 4 h, and NF 20 h) the libraries corresponding to the two replicates were normalized together, both libraries having the same normalization factor. For variability analyses, only genes with an average CPM >0 were considered. To control the false discovery rate, adjusted *p*-values were calculated using the Benjamini and Hochberg procedure (Storey and Tibshirani, 2003). Genes with an adjusted $p < 0.05$ were considered as being differentially expressed. In a complementary, we also wanted to explore the relative expression levels of the different genes with FPKM values. To achieve this, we aligned the quality checked reads to the *M. truncatula* annotated genome (Mt4.0v1) using TopHat (version tophat-2.0.10). Here again, reads mapping to multiple positions were discarded. As many as 85% of the read pairs aligned unambiguously to the genome. We then used Cufflinks (Trapnell et al., 2012) to estimate transcript abundance and generate FPKM values for all the corresponding genes (Table S2).

Assignment of Gene Ontology (GO) terms to differentially expressed genes was performed using agriGO (http://bioinfo.cau.edu.cn/agriGO/index.php) toolkit (Du et al., 2010). GO enrichment analysis of differentially expressed genes at 4 and 20 h following NF treatment was implemented using Singular Enrichment Analysis (SEA) with default parameters and *M. truncatula* genome locus (v4) as a background (Du et al., 2010). Briefly, a Fisher's exact test with a Benjamini-Yekutieli (FDR under dependency) adjustment method was used to classify the GO categories (Table S4). The significant GO terms were defined as having an adjusted $p < 0.05$.

Orthomcl Analyses

Predicted proteins from 31 fully sequenced plant genomes were collected from different sources (Table S7). This collection of plant proteomes included six legume species (*Medicago truncatula*, *Cicer arietinum* L., *Lotus japonicus*, *Glycine max*, *Phaseolus vulgaris*, and *Cajanus cajan*) as well as 23 other angiosperms (including monocots and dicots), one gymnosperm and a spikemoss (*Selaginella moellendorffii*) as an outgroup. An all against all comparison of all these 31 proteomes was performed using BLASTp (Altschul et al., 1997) with an *e*-value cutoff of 1e-5 and no SEG filter. The results of the all-against-all BLASTp analysis were fed to OrthoMCL v2.0 (Li et al., 2003; Fischer et al., 2011), which was run with a percentMatchCuttof of 50 and an inflation value of 1.5 for clustering granularity to create clusters of orthologous and in-paralogous plant proteins. Raw results of the OrthoMCL clustering analysis were parsed to identify clusters specific to legume species (clusters containing only legume genes). This list of legume-specific genes was crossed with the list of *M. truncatula* genes shown to be expressed in the root hairs. We then checked whether some of these legume-specific genes were conserved in all 6 legume species (included in our comparative proteome analysis).

Phylogeny Analyses

Except for the MSL family, polypeptide sequences were first aligned with Muscle (V3.8.31) and phylogenetic tree was generated with PhyML software (substitution model, LG matrix) using maximum-likelihood method and 1000 bootstrap replicates on Mobyle Pasteur website (http://mobyle.pasteur.fr/cgi-bin/portal.py#welcome). For MSL family, sequences were first aligned with Muscle using the conserved MscS domain as template to force the alignment around it (Jensen and Haswell, 2012). Phylogenetic trees were drawn with Dendroscope (http://ab.inf.uni-tuebingen.de/software/dendroscope/). Bootstrap values are indicated in gray at the corresponding nodes. The length of scale bar indicates the number of nucleotide substitutions per site.

Data Deposition

RNA-seq data from this article were deposited at Gene Expression Omnibus (http://www.ncbi.nlm.nih.gov/geo/, accession no. GSE67921) and at CATdb (http://urgv.evry.inra.fr/CATdb/; Project: NGS2013_04_POIL) according to the "Minimum Information About a Microarray Experiment" standards.

RT-qPCR Validation

For RT-qPCR validation, cDNA were obtained from root hair RNA extracted and treated as described above. The experiments were performed using three independent samples (biological replicates) for each treatment (control, NF 4 h,

and NF 20 h), different from the samples used for the RNA-seq analyses and obtained in another laboratory than the one having prepared the latter RNA samples. The integrity of RNA was checked on agarose gel and RNA quantity and quality was assessed using NanoDrop 1000 spectrophotometer (Thermo Scientific). Total RNA (500 ng) was reverse-transcribed by Superscript III reverse transcriptase (Invitrogen, Paisley, UK) according to the manufacturer's instructions. Real-time RT-qPCR was carried out using the GoTaq master mix (Promega; www.promega.com) according to the manufacturer's instructions. Reactions were run on the Chromo4 Real-Time PCR Detection System (Bio-Rad; www.qiagen.com), and quantification was performed with the Opticon Monitor analysis software version 3.1 (Bio-Rad). Data were analyzed with RqPCRBase, an R package working in the R computing environment (Hilliou and Tran, 2013). The mRNA levels were normalized against two constitutively expressed endogenous genes (a38: *Medtr4g109650*; a39: *Medtr4g046877*). PCR for each biological replicate was performed in three technical replicates. For each reaction, 5 µl of 60-fold-diluted cDNA and 0.3 µM primers were used. The initial denaturing time was 10 min, followed by 40 cycles at 95°C for 10 s and 60°C for 1 min. Specificity of amplification was confirmed by observing a single peak in the dissociation curves at the end of the PCR procedure. The gene-specific primers used are listed in Table S11.

AUTHOR CONTRIBUTIONS

ID, AD, MG, SB, VB carried out the experimental research. SC, SF, ER performed the chemo-enzymatic synthesis of NF. ID, AD, MG, IG, AB, AP, JMF, NP, HS evaluated the results, and contributed to writing the manuscript. MG, AB, SB, JCB, VB, ED, MD, VM, CF, CR, HR, YS, JT, BT contributed to RNA-seq analyses and biocomputing. ID, AD, AP, NP, HS wrote the paper. AP, JF, NP, HS conceived the project, participated in its design and coordination. All authors read and approved the final manuscript.

FUNDING

This work was funded by an Agence Nationale de la Recherche (ANR) project (CAROLS—Channels and Reactive Oxygen species in Legume root hair: role in Symbiosis with Rhizobium—ANR-11-BSV7-010-02). This work was supported by the "Institut National de la Recherche Agronomique," the "Centre National de la Recherche Scientifique," the University of Nice Sophia Antipolis and the French Government (National Research Agency, ANR) through the LABEX SIGNALIFE program (ANR-11-LABX-0028-01). ID was supported by a post-doctoral fellowship from the ANR (CAROLS: ANR-11-BSV7-010-02). AD was supported by doctoral fellowship (PER, Prix d'Encouragement à la Recherche) from the "Province Sud de la Nouvelle-Calédonie." SC, SF, ER are grateful to the Labex Arcane (ANR-11-LABX-0003-01) and the Carnot Polynat Institute for partial support of this study and the NMR and Mass Spectrometry Platforms of the ICMG (FR 2607).

ACKNOWLEDGMENTS

This study was supported by the ANR (Agence Nationale de la Recherche). We are grateful to Marie Le Gleuher-Pacoud for helpful lab assistance and Hugues Driguez for providing initial Nod factors preparation. We are grateful to the Genotoul bioinformatics platform Toulouse Midi-Pyrenees (Bioinfo Genotoul) for providing computing resources.

SUPPLEMENTARY MATERIAL

The Supplementary Material for this article can be found online at: http://journal.frontiersin.org/article/10.3389/fpls.2016.00794

REFERENCES

Altschul, S. F., Madden, T. L., Schaffer, A. A., Zhang, J., Zhang, Z., Miller, W., et al. (1997). Gapped BLAST and PSI-BLAST: a new generation of protein database search programs. *Nucleic Acids Res.* 25, 3389–3402. doi: 10.1093/nar/25.17.3389

Andrio, E., Marino, D., Marmeys, A., De Segonzac, M. D., Damiani, I., Genre, A., et al. (2013). Hydrogen peroxide-regulated genes in the *Medicago truncatula*-Sinorhizobium meliloti symbiosis. *New Phytol.* 198, 179–189. doi: 10.1111/nph.12120

Apel, K., and Hirt, H. (2004). REACTIVE OXYGEN SPECIES: metabolism, oxidative stress, and signal transduction. *Annu. Rev. Plant Biol.* 55, 373–399. doi: 10.1146/annurev.arplant.55.031903.141701

Arpat, A. B., Magliano, P., Wege, S., Rouached, H., Stefanovic, A., and Poirier, Y. (2012). Functional expression of PHO1 to the Golgi and trans-Golgi network and its role in export of inorganic phosphate. *Plant J.* 71, 479–491. doi: 10.1111/j.1365-313x.2012.05004.x

Avenhaus, U., Cabeza, R. A., Liese, R., Lingner, A., Dittert, K., Salinas-Riester, G., et al. (2015). Short-Term molecular acclimation processes of legume nodules to increased external oxygen concentration. *Front. Plant Sci.* 6:1133. doi: 10.3389/fpls.2015.01133

Bagchi, R., Salehin, M., Adeyemo, O. S., Salazar, C., Shulaev, V., Sherrier, D. J., et al. (2012). Functional assessment of the *Medicago truncatula* NIP/LATD protein demonstrates that it is a high-affinity nitrate transporter. *Plant Physiol.* 160, 906–916. doi: 10.1104/pp.112.196444

Bais, H. P., Weir, T. L., Perry, L. G., Gilroy, S., and Vivanco, J. M. (2006). The role of root exudates in rhizosphere interactions with plants and other organisms. *Annu. Rev. Plant Biol.* 57, 233–266. doi: 10.1146/annurev.arplant.57.032905.105159

Barbier-Brygoo, H., De Angeli, A., Filleur, S., Frachisse, J. M., Gambale, F., Thomine, S., et al. (2011). Anion channels/transporters in plants: from molecular bases to regulatory networks. *Annu. Rev. Plant Biol.* 62, 25–51. doi: 10.1146/annurev-arplant-042110-103741

Barbulova, A., Rogato, A., D'apuzzo, E., Omrane, S., and Chiurazzi, M. (2007). Differential effects of combined N sources on early steps of the Nod factor-dependent transduction pathway in *Lotus japonicus*. *Mol. Plant Microbe Interact.* 20, 994–1003. doi: 10.1094/MPMI-20-8-0994

Becker, J. D., Takeda, S., Borges, F., Dolan, L., and Feijo, J. A. (2014). Transcriptional profiling of Arabidopsis root hairs and pollen defines an apical cell growth signature. *BMC Plant Biol.* 14:197. doi: 10.1186/s12870-014-0197-3

Belmondo, S., Calcagno, C., Genre, A., Puppo, A., Pauly, N., and Lanfranco, L. (2016). The *Medicago truncatula* MtRbohE gene is activated in arbusculated cells and is involved in root cortex colonization. *Planta* 243, 251–262. doi: 10.1007/s00425-015-2407-0

Benedito, V. A., Li, H., Dai, X., Wandrey, M., He, J., Kaundal, R., et al. (2010). Genomic inventory and transcriptional analysis of *Medicago truncatula* transporters. *Plant Physiol.* 152, 1716–1730. doi: 10.1104/pp.109.148684

Benedito, V. A., Torres-Jerez, I., Murray, J. D., Andriankaja, A., Allen, S., Kakar, K., et al. (2008). A gene expression atlas of the model legume *Medicago truncatula*. *Plant J.* 55, 504–513. doi: 10.1111/j.1365-313X.2008.03519.x

Berthomieu, P., Conejero, G., Nublat, A., Brackenbury, W. J., Lambert, C., Savio, C., et al. (2003). Functional analysis of AtHKT1 in Arabidopsis shows that Na(+) recirculation by the phloem is crucial for salt tolerance. *EMBO J.* 22, 2004–2014. doi: 10.1093/emboj/cdg207

Boisson-Dernier, A., Lituiev, D. S., Nestorova, A., Franck, C. M., Thirugnanarajah, S., and Grossniklaus, U. (2013). ANXUR receptor-like kinases coordinate cell wall integrity with growth at the pollen tube tip via NADPH oxidases. *PLoS Biol.* 11:e1001719. doi: 10.1371/journal.pbio.1001719

Bonneau, L., Huguet, S., Wipf, D., Pauly, N., and Truong, H. N. (2013). Combined phosphate and nitrogen limitation generates a nutrient stress transcriptome favorable for arbuscular mycorrhizal symbiosis in *Medicago truncatula*. *New Phytol.* 199, 188–202. doi: 10.1111/nph.12234

Boscari, A., Del Giudice, J., Ferrarini, A., Venturini, L., Zaffini, A. L., Delledonne, M., et al. (2013). Expression dynamics of the *Medicago truncatula* transcriptome during the symbiotic interaction with Sinorhizobium meliloti: which role for nitric oxide? *Plant Physiol.* 161, 425–439. doi: 10.1104/pp.112.208538

Bouteau, F., Pennarun, A. M., Kurkdjian, A., Convert, M., Cornel, D., Monestiez, M., et al. (1999). Ion channels of intact young root hairs from Medicago sativa. *Plant Physiol. Biochem.* 37, 889–898. doi: 10.1016/S0981-9428(99)00101-1

Breakspear, A., Liu, C., Roy, S., Stacey, N., Rogers, C., Trick, M., et al. (2014). The root hair "infectome" of *Medicago truncatula* uncovers changes in cell cycle genes and reveals a requirement for Auxin signaling in rhizobial infection. *Plant Cell* 26, 4680–4701. doi: 10.1105/tpc.114.133496

Breuillin-Sessoms, F., Floss, D. S., Gomez, S. K., Pumplin, N., Ding, Y., Levesque-Tremblay, V., et al. (2015). Suppression of arbuscule degeneration in *Medicago truncatula* phosphate transporter4 mutants is dependent on the ammonium transporter 2 family protein AMT2;3. *Plant Cell* 27, 1352–1366. doi: 10.1105/tpc.114.131144

Bright, L. J., Liang, Y., Mitchell, D. M., and Harris, J. M. (2005). The LATD gene of *Medicago truncatula* is required for both nodule and root development. *Mol. Plant Microbe Interact.* 18, 521–532. doi: 10.1094/MPMI-18-0521

Cabeza, R. A., Liese, R., Lingner, A., Von Stieglitz, I., Neumann, J., Salinas-Riester, G., et al. (2014). RNA-seq transcriptome profiling reveals that *Medicago truncatula* nodules acclimate N(2) fixation before emerging P deficiency reaches the nodules. *J. Exp. Bot.* 65, 6035–6048. doi: 10.1093/jxb/eru341

Cabeza, R., Koester, B., Liese, R., Lingner, A., Baumgarten, V., Dirks, J., et al. (2014). An RNA sequencing transcriptome analysis reveals novel insights into molecular aspects of the nitrate impact on the nodule activity of *Medicago truncatula*. *Plant Physiol.* 164, 400–411. doi: 10.1104/pp.113.228312

Camanes, G., Pastor, V., Cerezo, M., Garcia-Andrade, J., Vicedo, B., Garcia-Agustin, P., et al. (2012). A deletion in NRT2.1 attenuates Pseudomonas syringae-induced hormonal perturbation, resulting in primed plant defenses. *Plant Physiol.* 158, 1054–1066. doi: 10.1104/pp.111.184424

Camps, C., Jardinaud, M. F., Rengel, D., Carrere, S., Herve, C., Debelle, F., et al. (2015). Combined genetic and transcriptomic analysis reveals three major signalling pathways activated by Myc-LCOs in *Medicago truncatula*. *New Phytol.* 208, 224–240. doi: 10.1111/nph.13427

Cardenas, L., Martinez, A., Sanchez, F., and Quinto, C. (2008). Fast, transient and specific intracellular ROS changes in living root hair cells responding to Nod factors (NFs). *Plant J.* 56, 802–813. doi: 10.1111/j.1365-313X.2008.03644.x

Chen, D. S., Liu, C. W., Roy, S., Cousins, D., Stacey, N., and Murray, J. D. (2015). Identification of a core set of rhizobial infection genes using data from single cell-types. *Front. Plant Sci.* 6:575. doi: 10.3389/fpls.2015.00575

Coste, B., Xiao, B., Santos, J. S., Syeda, R., Grandl, J., Spencer, K. S., et al. (2012). Piezo proteins are pore-forming subunits of mechanically activated channels. *Nature* 483, 176–181. doi: 10.1038/nature10812

Cuellar, T., Azeem, F., Andrianteranagna, M., Pascaud, F., Verdeil, J. L., Sentenac, H., et al. (2013). Potassium transport in developing fleshy fruits: the grapevine inward K(+) channel VvK1.2 is activated by CIPK-CBL complexes and induced in ripening berry flesh cells. *Plant J.* 73, 1006–1018. doi: 10.1111/tpj.12092

Czaja, L. F., Hogekamp, C., Lamm, P., Maillet, F., Martinez, E. A., Samain, E., et al. (2012). Transcriptional responses toward diffusible signals from symbiotic microbes reveal MtNFP- and MtDMI3-dependent reprogramming of host gene expression by arbuscular mycorrhizal fungal lipochitooligosaccharides. *Plant Physiol.* 159, 1671–1685. doi: 10.1104/pp.112.195990

Dazzo, F. B., Orgambide, G. G., Philip-Hollingsworth, S., Hollingsworth, R. I., Ninke, K. O., and Salzwedel, J. L. (1996). Modulation of development, growth dynamics, wall crystallinity, and infection sites in white clover root hairs by membrane chitolipooligosaccharides from Rhizobium leguminosarum biovar trifolii. *J. Bacteriol.* 178, 3621–3627.

De Billy, F., Grosjean, C., May, S., Bennett, M., and Cullimore, J. V. (2001). Expression studies on AUX1-like genes in *Medicago truncatula* suggest that auxin is required at two steps in early nodule development. *Mol. Plant Microbe Interact.* 14, 267–277. doi: 10.1094/MPMI.2001.14.3.267

De Carvalho Niebel, F., Lescure, N., Cullimore, J. V., and Gamas, P. (1998). The *Medicago truncatula MtAnn1* gene encoding an annexin is induced by Nod factors and during the symbiotic interaction with *Rhizobium meliloti*. *Mol. Plant Microbe Interact.* 11, 504–513. doi: 10.1094/MPMI.1998.11.6.504

De Carvalho-Niebel, F., Timmers, A. C., Chabaud, M., Defaux-Petras, A., and Barker, D. G. (2002). The Nod factor-elicited annexin MtAnn1 is preferentially localised at the nuclear periphery in symbiotically activated root tissues of *Medicago truncatula*. *Plant J.* 32, 343–352. doi: 10.1046/j.1365-313X.2002.01429.x

Drerup, M. M., Schlucking, K., Hashimoto, K., Manishankar, P., Steinhorst, L., Kuchitsu, K., et al. (2013). The Calcineurin B-like calcium sensors CBL1 and CBL9 together with their interacting protein kinase CIPK26 regulate the Arabidopsis NADPH oxidase RBOHF. *Mol. Plant* 6, 559–569. doi: 10.1093/mp/sst009

Du, Z., Zhou, X., Ling, Y., Zhang, Z., and Su, Z. (2010). agriGO: a GO analysis toolkit for the agricultural community. *Nucleic Acids Res.* 38, W64–W70. doi: 10.1093/nar/gkq310

Ehrhardt, D. W., Atkinson, E. M., and Long, S. R. (1992). Depolarization of alfalfa root hair membrane potential by Rhizobium meliloti Nod factors. *Science* 256, 998–1000. doi: 10.1126/science.10744524

Esseling, J. J., Lhuissier, F. G. P., and Emons, A. M. C. (2003). Nod factor-induced root hair curling: continuous polar growth towards the point of Nod factor application. *Plant Physiol.* 132, 1982–1988. doi: 10.1104/pp.103.021634

Falhof, J., Pedersen, J. T., Fuglsang, A. T., and Palmgren, M. (2016). Plasma membrane H(+)-ATPase regulation in the center of plant physiology. *Mol. Plant* 9, 323–337. doi: 10.1016/j.molp.2015.11.002

Felle, H. H., Kondorosi, E., Kondorosi, A., and Schultze, M. (1996). Rapid alkalinization in alfalfa root hairs in response to rhizobial lipochitooligosaccharide signals. *Plant J.* 10, 295–301. doi: 10.1046/j.1365-313x.1996.10020295.x

Felle, H. H., Kondorosi, E., Kondorosi, A., and Schultze, M. (1998). The role of ion fluxes in Nod factor signalling in *Medicago sativa*. *Plant J.* 13, 455–463. doi: 10.1046/j.1365-313x.1998.00041.x

Felle, H. H., Kondorosi, E., Kondorosi, A., and Schultze, M. (1999). Elevation of the cytosolic free [Ca2+] is indispensable for the transduction of the Nod factor signal in alfalfa. *Plant Physiol.* 121, 273–280. doi: 10.1104/pp.121.1.273

Fischer, S., Brunk, B. P., Chen, F., Gao, X., Harb, O. S., Iodice, J. B., et al. (2011). Using OrthoMCL to assign proteins to OrthoMCL-DB groups or to cluster proteomes into new ortholog groups. *Curr. Protoc. Bioinform. Chapter 6:Unit 6.*12.1–19. doi: 10.1002/0471250953.bi0612s35

Foreman, J., Demidchik, V., Bothwell, J. H., Mylona, P., Miedema, H., Torres, M. A., et al. (2003). Reactive oxygen species produced by NADPH oxidase regulate plant cell growth. *Nature* 422, 442–446. doi: 10.1038/nature01485

Francoz, E., Ranocha, P., Nguyen-Kim, H., Jamet, E., Burlat, V., and Dunand, C. (2015). Roles of cell wall peroxidases in plant development. *Phytochemistry* 112, 15–21. doi: 10.1016/j.phytochem.2014.07.020

Gao, Y., Tian, Q., and Zhang, W. H. (2014). Systemic regulation of sulfur homeostasis in *Medicago truncatula*. *Planta* 239, 79–96. doi: 10.1007/s00425-013-1958-1

Garcia-Mata, C., Wang, J., Gajdanowicz, P., Gonzalez, W., Hills, A., Donald, N., et al. (2010). A minimal cysteine motif required to activate the SKOR K+ channel of Arabidopsis by the reactive oxygen species H2O2. *J. Biol. Chem.* 285, 29286–29294. doi: 10.1074/jbc.M110.141176

Gaymard, F., Pilot, G., Lacombe, B., Bouchez, D., Bruneau, D., Boucherez, J., et al. (1998). Identification and disruption of a plant shaker-like outward channel involved in K+ release into the xylem sap. *Cell* 94, 647–655. doi: 10.1016/S0092-8674(00)81606-2

Geiger, D., Scherzer, S., Mumm, P., Marten, I., Ache, P., Matschi, S., et al. (2010). Guard cell anion channel SLAC1 is regulated by CDPK protein kinases with distinct Ca2+ affinities. *Proc. Natl. Acad. Sci. U.S.A.* 107, 8023–8028. doi: 10.1073/pnas.0912030107

Giehl, R. F. H., and Von Wiren, N. (2014). Root nutrient foraging. *Plant Physiol.* 166, 509–517. doi: 10.1104/pp.114.245225

Gierth, M., Maser, P., and Schroeder, J. I. (2005). The potassium transporter AtHAK5 functions in K(+) deprivation-induced high-affinity K(+) uptake and AKT1 K(+) channel contribution to K(+) uptake kinetics in Arabidopsis roots. *Plant Physiol.* 137, 1105–1114. doi: 10.1104/pp.104.057216

Graham, M. A., Silverstein, K. A., Cannon, S. B., and Vandenbosch, K. A. (2004). Computational identification and characterization of novel genes from legumes. *Plant Physiol.* 135, 1179–1197. doi: 10.1104/pp.104.037531

Gutermuth, T., Lassig, R., Portes, M. T., Maierhofer, T., Romeis, T., Borst, J. W., et al. (2013). Pollen tube growth regulation by free anions depends on the interaction between the anion channel SLAH3 and calcium-dependent protein kinases CPK2 and CPK20. *Plant Cell* 25, 4525–4543. doi: 10.1105/tpc.113.118463

Hamburger, D., Rezzonico, E., Macdonald-Comber Petetot, J., Somerville, C., and Poirier, Y. (2002). Identification and characterization of the Arabidopsis PHO1 gene involved in phosphate loading to the xylem. *Plant Cell* 14, 889–902. doi: 10.1105/tpc.000745

Hamilton, E. S., Jensen, G. S., Maksaev, G., Katims, A., Sherp, A. M., and Haswell, E. S. (2015). Mechanosensitive channel MSL8 regulates osmotic forces during pollen hydration and germination. *Science* 350, 438–441. doi: 10.1126/science.aac6014

Haswell, E. S., and Meyerowitz, E. M. (2006). MscS-like proteins control plastid size and shape in *Arabidopsis thaliana*. *Curr. Biol.* 16, 1–11. doi: 10.1016/j.cub.2005.11.044

Haswell, E. S., Peyronnet, R., Barbier-Brygoo, H., Meyerowitz, E. M., and Frachisse, J. M. (2008). Two MscS homologs provide mechanosensitive channel activities in the Arabidopsis root. *Curr. Biol.* 18, 730–734. doi: 10.1016/j.cub.2008.04.039

Hedrich, R. (2012). Ion channels in plants. *Physiol. Rev.* 92, 1777–1811. doi: 10.1152/physrev.00038.2011

Hilliou, F., and Tran, T. (2013). "RqPCRAnalysis: analysis of quantitative real-time PCR data," in *Bioinformatics 2013: Proceedings of the International Conference on Bioinformatics Models, Methods and Algorithms* (Barcelona), 202–211.

Hossain, M. S., Joshi, T., and Stacey, G. (2015). System approaches to study root hairs as a single cell plant model: current status and future perspectives. *Front. Plant Sci.* 6:363. doi: 10.3389/fpls.2015.00363

Hosy, E., Vavasseur, A., Mouline, K., Dreyer, I., Gaymard, F., Poree, F., et al. (2003). The Arabidopsis outward K+ channel GORK is involved in regulation of stomatal movements and plant transpiration. *Proc. Natl. Acad. Sci. U.S.A.* 100, 5549–5554. doi: 10.1073/pnas.0733970100

Hou, C., Tian, W., Kleist, T., He, K., Garcia, V., Bai, F., et al. (2014). DUF221 proteins are a family of osmosensitive calcium-permeable cation channels conserved across eukaryotes. *Cell Res.* 24, 632–635. doi: 10.1038/cr.2014.14

Ivashikina, N., Becker, D., Ache, P., Meyerhoff, O., Felle, H. H., and Hedrich, R. (2001). K(+) channel profile and electrical properties of Arabidopsis root hairs. *FEBS Lett.* 508, 463–469. doi: 10.1016/S0014-5793(01)03114-3

Javot, H., Penmetsa, R. V., Breuillin, F., Bhattarai, K. K., Noar, R. D., Gomez, S. K., et al. (2011). *Medicago truncatula* mtpt4 mutants reveal a role for nitrogen in the regulation of arbuscule degeneration in arbuscular mycorrhizal symbiosis. *Plant J.* 68, 954–965. doi: 10.1111/j.1365-313X.2011.04746.x

Jensen, G. S., and Haswell, E. S. (2012). Functional analysis of conserved motifs in the mechanosensitive channel homolog MscS-Like2 from *Arabidopsis thaliana*. *PLoS ONE* 7:e40336. doi: 10.1371/journal.pone.0040336

Jorgens, C. I., Grunewald, N., Hulskamp, M., and Uhrig, J. F. (2010). A role for ABIL3 in plant cell morphogenesis. *Plant J.* 62, 925–935. doi: 10.1111/j.1365-313x.2010.04210.x

Journet, E. P., El-Gachtouli, N., Vernoud, V., De Billy, F., Pichon, M., Dedieu, A., et al. (2001). *Medicago truncatula* ENOD11: a novel RPRP-encoding early nodulin gene expressed during mycorrhization in arbuscule-containing cells. *Mol. Plant Microbe Interact.* 14, 737–748. doi: 10.1094/MPMI.2001.14.6.737

Kadota, Y., Shirasu, K., and Zipfel, C. (2015). Regulation of the NADPH oxidase RBOHD during plant immunity. *Plant Cell Physiol.* 56, 1472–1480. doi: 10.1093/pcp/pcv063

Kadota, Y., Sklenar, J., Derbyshire, P., Stransfeld, L., Asai, S., Ntoukakis, V., et al. (2014). Direct regulation of the NADPH oxidase RBOHD by the PRR-associated kinase BIK1 during plant immunity. *Mol. Cell* 54, 43–55. doi: 10.1016/j.molcel.2014.02.021

Krajinski, F., Courty, P. E., Sieh, D., Franken, P., Zhang, H., Bucher, M., et al. (2014). The H+-ATPase HA1 of *Medicago truncatula* is essential for phosphate transport and plant growth during arbuscular mycorrhizal symbiosis. *Plant Cell* 26, 1808–1817. doi: 10.1105/tpc.113.120436

Krajinski, F., Hause, B., Gianinazzi-Pearson, V., and Franken, P. (2002). *Mtha1*, a plasma membrane H^+-ATPase gene from *Medicago truncatula*, shows arbuscule-specific induced expression in mycorrhizal tissue. *Plant Biol.* 4, 754–761. doi: 10.1055/s-2002-37407

Krouk, G., Carre, C., Fizames, C., Gojon, A., Ruffel, S., and Lacombe, B. (2015). GeneCloud reveals semantic enrichment in lists of gene descriptions. *Mol. Plant* 8, 971–973. doi: 10.1016/j.molp.2015.02.005

Krouk, G., Crawford, N. M., Coruzzi, G. M., and Tsay, Y. F. (2010a). Nitrate signaling: adaptation to fluctuating environments. *Curr. Opin. Plant Biol.* 13, 266–273. doi: 10.1016/j.pbi.2009.12.003

Krouk, G., Lacombe, B., Bielach, A., Perrine-Walker, F., Malinska, K., Mounier, E., et al. (2010b). Nitrate-regulated auxin transport by NRT1.1 defines a mechanism for nutrient sensing in plants. *Dev. Cell* 18, 927–937. doi: 10.1016/j.devcel.2010.05.008

Kurkdjian, A., Bouteau, F., Pennarun, A. M., Convert, M., Cornel, D., Rona, J. P., et al. (2000). Ion currents involved in early Nod factor response in Medicago sativa root hairs: a discontinuous single-electrode voltage-clamp study. *Plant J.* 22, 9–17. doi: 10.1046/j.1365-313x.2000.00714.x

Kurusu, T., Kuchitsu, K., Nakano, M., Nakayama, Y., and Iida, H. (2013). Plant mechanosensing and Ca2+ transport. *Trends Plant Sci.* 18, 227–233. doi: 10.1016/j.tplants.2012.12.002

Kurusu, T., Yamanaka, T., Nakano, M., Takiguchi, A., Ogasawara, Y., Hayashi, T., et al. (2012). Involvement of the putative Ca(2)(+)-permeable mechanosensitive channels, NtMCA1 and NtMCA2, in Ca(2)(+) uptake, Ca(2)(+)-dependent cell proliferation and mechanical stress-induced gene expression in tobacco (Nicotiana tabacum) BY-2 cells. *J. Plant Res.* 125, 555–568. doi: 10.1007/s10265-011-0462-6

Kwasniewski, M., Nowakowska, U., Szumera, J., Chwialkowska, K., and Szarejko, I. (2013). iRootHair: a comprehensive root hair genomics database. *Plant Physiol.* 161, 28–35. doi: 10.1104/pp.112.206441

Laloi, C., Mestres-Ortega, D., Marco, Y., Meyer, Y., and Reichheld, J. P. (2004). The Arabidopsis cytosolic thioredoxin h5 gene induction by oxidative stress and its W-box-mediated response to pathogen elicitor. *Plant Physiol.* 134, 1006–1016. doi: 10.1104/pp.103.035782

Laohavisit, A., Brown, A. T., Cicuta, P., and Davies, J. M. (2010). Annexins: components of the calcium and reactive oxygen signaling network. *Plant Physiol.* 152, 1824–1829. doi: 10.1104/pp.109.145458

Laohavisit, A., Shang, Z., Rubio, L., Cuin, T. A., Véry, A. A., Wang, A., et al. (2012). Arabidopsis annexin1 mediates the radical-activated plasma membrane Ca(2)+- and K+-permeable conductance in root cells. *Plant Cell* 24, 1522–1533. doi: 10.1105/tpc.112.097881

Larrainzar, E., Riely, B. K., Kim, S. C., Carrasquilla-Garcia, N., Yu, H. J., Hwang, H. J., et al. (2015). Deep sequencing of the *Medicago truncatula* root transcriptome reveals a massive and early interaction between nodulation factor and ethylene signals. *Plant Physiol.* 169, 233–265. doi: 10.1104/pp.15.00350

Lebaudy, A., Véry, A. A., and Sentenac, H. (2007). K+ channel activity in plants: genes, regulations and functions. *FEBS Lett.* 581, 2357–2366. doi: 10.1016/j.febslet.2007.03.058

Leran, S., Munos, S., Brachet, C., Tillard, P., Gojon, A., and Lacombe, B. (2013). Arabidopsis NRT1.1 is a bidirectional transporter involved in root-to-shoot nitrate translocation. *Mol. Plant* 6, 1984–1987. doi: 10.1093/mp/sst068

Leran, S., Varala, K., Boyer, J. C., Chiurazzi, M., Crawford, N., Daniel-Vedele, F., et al. (2014). A unified nomenclature of NITRATE TRANSPORTER 1/PEPTIDE TRANSPORTER family members in plants. *Trends Plant Sci.* 19, 5–9. doi: 10.1016/j.tplants.2013.08.008

Li, G., Tillard, P., Gojon, A., and Maurel, C. (2016). Dual regulation of root hydraulic conductivity and plasma membrane aquaporins by plant nitrate accumulation and high-affinity nitrate transporter NRT2.1. *Plant Cell Physiol.* 57, 733–742. doi: 10.1093/pcp/pcw022

Li, L., Li, M., Yu, L., Zhou, Z., Liang, X., Liu, Z., et al. (2014). The FLS2-associated kinase BIK1 directly phosphorylates the NADPH oxidase RbohD to control plant immunity. *Cell Host Microbe* 15, 329–338. doi: 10.1016/j.chom.2014.02.009

Li, L., Stoeckert, C. J. Jr., and Roos, D. S. (2003). OrthoMCL: identification of ortholog groups for eukaryotic genomes. *Genome Res.* 13, 2178–2189. doi: 10.1101/gr.1224503

Li, W., Wang, Y., Okamoto, M., Crawford, N. M., Siddiqi, M. Y., and Glass, A. D. (2007). Dissection of the AtNRT2.1:AtNRT2.2 inducible high-affinity nitrate transporter gene cluster. *Plant Physiol.* 143, 425–433. doi: 10.1104/pp.106.091223

Libault, M., Brechenmacher, L., Cheng, J., Xu, D., and Stacey, G. (2010a). Root hair systems biology. *Trends Plant Sci.* 15, 641–650. doi: 10.1016/j.tplants.2010.08.010

Libault, M., Farmer, A., Brechenmacher, L., Drnevich, J., Langley, R. J., Bilgin, D. D., et al. (2010b). Complete transcriptome of the soybean root hair cell, a single-cell model, and its alteration in response to Bradyrhizobium japonicum infection. *Plant Physiol.* 152, 541–552. doi: 10.1104/pp.109.148379

Lin, S. H., Kuo, H. F., Canivenc, G., Lin, C. S., Lepetit, M., Hsu, P. K., et al. (2008). Mutation of the Arabidopsis NRT1.5 nitrate transporter causes defective root-to-shoot nitrate transport. *Plant Cell* 20, 2514–2528. doi: 10.1105/tpc.108.060244

Little, D. Y., Rao, H., Oliva, S., Daniel-Vedele, F., Krapp, A., and Malamy, J. E. (2005). The putative high-affinity nitrate transporter NRT2.1 represses lateral root initiation in response to nutritional cues. *Proc. Natl. Acad. Sci. U.S.A.* 102, 13693–13698. doi: 10.1073/pnas.0504219102

Liu, K. H., Huang, C. Y., and Tsay, Y. F. (1999). CHL1 is a dual-affinity nitrate transporter of Arabidopsis involved in multiple phases of nitrate uptake. *Plant Cell* 11, 865–874. doi: 10.1105/tpc.11.5.865

Lohar, D. P., Haridas, S., Gantt, J. S., and Vandenbosch, K. A. (2007). A transient decrease in reactive oxygen species in roots leads to root hair deformation in the legume-rhizobia symbiosis. *New Phytol.* 173, 39–49. doi: 10.1111/j.1469-8137.2006.01901.x

Maksaev, G., and Haswell, E. S. (2012). MscS-Like10 is a stretch-activated ion channel from *Arabidopsis thaliana* with a preference for anions. *Proc. Natl. Acad. Sci. U.S.A.* 109, 19015–19020. doi: 10.1073/pnas.1213931109

Marino, D., Andrio, E., Danchin, E. G. J., Oger, E., Gucciardo, S., Lambert, A., et al. (2011). A *Medicago truncatula* NADPH oxidase is involved in symbiotic nodule functioning. *New Phytol.* 189, 580–592. doi: 10.1111/j.1469-8137.2010.03509.x

Marino, D., Dunand, C., Puppo, A., and Pauly, N. (2012). A burst of plant NADPH oxidases. *Trends Plant Sci.* 17, 9–15. doi: 10.1016/j.tplants.2011.10.001

Mathesius, U., Schlaman, H. R., Spaink, H. P., of Sautter, C., Rolfe, B. G., and Djordjevic, M. A. (1998). Auxin transport inhibition precedes root nodule formation in white clover roots and is regulated by flavonoids and derivatives of chitin oligosaccharides. *Plant J.* 14, 23–34. doi: 10.1046/j.1365-313X.1998.00090.x

Merlot, S., Leonhardt, N., Fenzi, F., Valon, C., Costa, M., Piette, L., et al. (2007). Constitutive activation of a plasma membrane H(+)-ATPase prevents abscisic acid-mediated stomatal closure. *EMBO J.* 26, 3216–3226. doi: 10.1038/sj.emboj.7601750

Meyer, S., Mumm, P., Imes, D., Endler, A., Weder, B., Al-Rasheid, K. A., et al. (2010). AtALMT12 represents an R-type anion channel required for stomatal movement in Arabidopsis guard cells. *Plant J.* 63, 1054–1062. doi: 10.1111/j.1365-313X.2010.04302.x

Mittler, R., Vanderauwera, S., Gollery, M., and Van Breusegem, F. (2004). Reactive oxygen gene network of plants. *Trends Plant Sci.* 9, 490–498. doi: 10.1016/j.tplants.2004.08.009

Miyahara, A., Richens, J., Starker, C., Morieri, G., Smith, L., Long, S., et al. (2010). Conservation in function of a SCAR/WAVE component during infection thread and root hair growth in *Medicago truncatula*. *Mol. Plant Microbe Interact.* 23, 1553–1562. doi: 10.1094/MPMI-06-10-0144

Monshausen, G. B., Bibikova, T. N., Weisenseel, M. H., and Gilroy, S. (2009). Ca2+ regulates reactive oxygen species production and pH during mechanosensing in Arabidopsis roots. *Plant Cell* 21, 2341–2356. doi: 10.1105/tpc.109.068395

Montiel, J., Nava, N., Cardenas, L., Sanchez-Lopez, R., Arthikala, M. K., Santana, O., et al. (2012). A *Phaseolus vulgaris* NADPH Oxidase gene is required for root infection by rhizobia. *Plant Cell Physiol.* 53, 1751–1767. doi: 10.1093/pcp/pcs120

Morere-Le Paven, M. C., Viau, L., Hamon, A., Vandecasteele, C., Pellizzaro, A., Bourdin, C., et al. (2011). Characterization of a dual-affinity nitrate transporter MtNRT1.3 in the model legume *Medicago truncatula*. *J. Exp. Bot.* 62, 5595–5605. doi: 10.1093/jxb/err243

Nakagawa, Y., Katagiri, T., Shinozaki, K., Qi, Z., Tatsumi, H., Furuichi, T., et al. (2007). Arabidopsis plasma membrane protein crucial for Ca^{2+} influx and touch sensing in roots. *Proc. Natl. Acad. Sci. U.S.A.* 104, 3639–3644. doi: 10.1073/pnas.0607703104

Negi, J., Matsuda, O., Nagasawa, T., Oba, Y., Takahashi, H., Kawai-Yamada, M., et al. (2008). CO2 regulator SLAC1 and its homologues are essential for anion homeostasis in plant cells. *Nature* 452, 483–486. doi: 10.1038/nature06720

Nestler, J., Liu, S., Wen, T. J., Paschold, A., Marcon, C., Tang, H. M., et al. (2014). Roothairless5, which functions in maize (*Zea mays* L.) root hair initiation and elongation encodes a monocot-specific NADPH oxidase. *Plant J.* 79, 729–740. doi: 10.1111/tpj.12578

Nguyen, T. T., Volkening, J. D., Rose, C. M., Venkateshwaran, M., Westphall, M. S., Coon, J. J., et al. (2015). Potential regulatory phosphorylation sites in a *Medicago truncatula* plasma membrane proton pump implicated during early symbiotic signaling in roots. *FEBS Lett.* 589, 2186–2193. doi: 10.1016/j.febslet.2015.06.035

Nussaume, L., Kanno, S., Javot, H., Marin, E., Pochon, N., Ayadi, A., et al. (2011). Phosphate Import in Plants: Focus on the PHT1 Transporters. *Front. Plant Sci.* 2:83. doi: 10.3389/fpls.2011.00083

O'brien, J. A., Daudi, A., Finch, P., Butt, V. S., Whitelegge, J. P., Souda, P., et al. (2012). A peroxidase-dependent apoplastic oxidative burst in cultured Arabidopsis cells functions in MAMP-elicited defense. *Plant Physiol.* 158, 2013–2027. doi: 10.1104/pp.111.190140

Okamoto, M., Kumar, A., Li, W., Wang, Y., Siddiqi, M. Y., Crawford, N. M., et al. (2006). High-affinity nitrate transport in roots of Arabidopsis depends on expression of the NAR2-like gene AtNRT3.1. *Plant Physiol.* 140, 1036–1046. doi: 10.1104/pp.105.074385

Oldroyd, G. E. (2013). Speak, friend, and enter: signalling systems that promote beneficial symbiotic associations in plants. *Nat. Rev. Microbiol.* 11, 252–263. doi: 10.1038/nrmicro2990

Oldroyd, G. E., and Downie, J. A. (2008). Coordinating nodule morphogenesis with rhizobial infection in legumes. *Annu. Rev. Plant Biol.* 59, 519–546. doi: 10.1146/annurev.arplant.59.032607.092839

Orsel, M., Krapp, A., and Daniel-Vedele, F. (2002). Analysis of the NRT2 nitrate transporter family in Arabidopsis. Structure and gene expression. *Plant Physiol.* 129, 886–896. doi: 10.1104/pp.005280

Peleg-Grossman, S., Melamed-Book, N., and Levine, A. (2012). ROS production during symbiotic infection suppresses pathogenesis-related gene expression. *Plant Signal. Behav.* 7, 409–415. doi: 10.4161/psb.19217

Peleg-Grossman, S., Volpin, H., and Levine, A. (2007). Root hair curling and *Rhizobium* infection in *Medicago truncatula* are mediated by phosphatidylinositide-regulated endocytosis and reactive oxygen species. *J. Exp. Bot.* 58, 1637–1649. doi: 10.1093/jxb/erm013

Pellizzaro, A., Clochard, T., Cukier, C., Bourdin, C., Juchaux, M., Montrichard, F., et al. (2014). The nitrate transporter MtNPF6.8 (MtNRT1.3) transports abscisic acid and mediates nitrate regulation of primary root growth in *Medicago truncatula*. *Plant Physiol.* 166, 2152–2165. doi: 10.1104/pp.114.250811

Pellizzaro, A., Clochard, T., Planchet, E., Limami, A. M., and Morere-Le Paven, M. C. (2015). Identification and molecular characterization of *Medicago truncatula* NRT2 and NAR2 families. *Physiol. Plant.* 154, 256–269. doi: 10.1111/ppl.12314

Poirier, Y., Thoma, S., Somerville, C., and Schiefelbein, J. (1991). Mutant of Arabidopsis deficient in xylem loading of phosphate. *Plant Physiol.* 97, 1087–1093. doi: 10.1104/pp.97.3.1087

Puppo, A., Pauly, N., Boscari, A., Mandon, K., and Brouquisse, R. (2013). Hydrogen peroxide and nitric oxide: key regulators of the Legume-Rhizobium and mycorrhizal symbioses. *Antioxid. Redox Signal.* 18, 2202–2219. doi: 10.1089/ars.2012.5136

Qiu, L., Lin, J. S., Xu, J., Sato, S., Parniske, M., Wang, T. L., et al. (2015). SCARN a novel class of SCAR Protein That Is Required for Root-Hair Infection during Legume nodulation. *PLoS Genet.* 11:e1005623. doi: 10.1371/journal.pgen.1005623

Ramu, S. K., Peng, H. M., and Cook, D. R. (2002). Nod factor induction of reactive oxygen species production is correlated with expression of the early nodulin gene rip1 in *Medicago truncatula*. *Mol. Plant Microbe Interact.* 15, 522–528. doi: 10.1094/MPMI.2002.15.6.522

Rasmussen, M. O., Hogg, B., Bono, J. J., Samain, E., and Driguez, H. (2004). New access to lipo-chitooligosaccharide nodulation factors. *Org. Biomol. Chem.* 2, 1908–1910. doi: 10.1039/b403575e

Reichheld, J. P., Mestres-Ortega, D., Laloi, C., and Meyer, Y. (2002). The multigenic family of thioredoxin h in *Arabidopsis thaliana*: specific expression and stress response. *Plant Physiol. Biochem.* 40, 685–690. doi: 10.1016/S0981-9428(02)01406-7

Remans, T., Nacry, P., Pervent, M., Girin, T., Tillard, P., Lepetit, M., et al. (2006). A central role for the nitrate transporter NRT2.1 in the integrated morphological and physiological responses of the root system to nitrogen limitation in Arabidopsis. *Plant Physiol.* 140, 909–921. doi: 10.1104/pp.105.075721

Richards, S. L., Laohavisit, A., Mortimer, J. C., Shabala, L., Swarbreck, S. M., Shabala, S., et al. (2014). Annexin 1 regulates the H2O2-induced calcium signature in *Arabidopsis thaliana* roots. *Plant J.* 77, 136–145. doi: 10.1111/tpj.12372

Robinson, M. D., Mccarthy, D. J., and Smyth, G. K. (2010). edgeR: a Bioconductor package for differential expression analysis of digital gene expression data. *Bioinformatics* 26, 139–140. doi: 10.1093/bioinformatics/btp616

Rose, C. M., Venkateshwaran, M., Volkening, J. D., Grimsrud, P. A., Maeda, J., Bailey, D. J., et al. (2012). Rapid phosphoproteomic and transcriptomic changes in the rhizobia-legume symbiosis. *Mol. Cell. Proteomics* 11, 724–744. doi: 10.1074/mcp.M112.019208

Rouached, H., Secco, D., and Arpat, A. B. (2009). Getting the most sulfate from soil: regulation of sulfate uptake transporters in Arabidopsis. *J. Plant Physiol.* 166, 893–902. doi: 10.1016/j.jplph.2009.02.016

Roux, B., Rodde, N., Jardinaud, M. F., Timmers, T., Sauviac, L., Cottret, L., et al. (2014). An integrated analysis of plant and bacterial gene expression in symbiotic root nodules using laser-capture microdissection coupled to RNA sequencing. *Plant J.* 77, 817–837. doi: 10.1111/tpj.12442

Sauviac, L., Niebel, A., Boisson-Dernier, A., Barker, D. G., and De Carvalho-Niebel, F. (2005). Transcript enrichment of Nod factor-elicited early nodulin genes in purified root hair fractions of the model legume *Medicago truncatula*. *J. Exp. Bot.* 56, 2507–2513. doi: 10.1093/jxb/eri244

Schachtman, D. P., and Shin, R. (2007). Nutrient sensing and signaling: NPKS. *Annu. Rev. Plant Biol.* 58, 47–69. doi: 10.1146/annurev.arplant.58.032806.103750

Schnabel, E., Journet, E. P., De Carvalho-Niebel, F., Duc, G., and Frugoli, J. (2005). The *Medicago truncatula* SUNN gene encodes a CLV1-like leucine-rich repeat receptor kinase that regulates nodule number and root length. *Plant Mol. Biol.* 58, 809–822. doi: 10.1007/s11103-005-8102-y

Segonzac, C., Boyer, J. C., Ipotesi, E., Szponarski, W., Tillard, P., Touraine, B., et al. (2007). Nitrate efflux at the root plasma membrane: identification of an Arabidopsis excretion transporter. *Plant Cell* 19, 3760–3777. doi: 10.1105/tpc.106.048173

Sharma, T., Dreyer, I., and Riedelsberger, J. (2013). The role of K(+) channels in uptake and redistribution of potassium in the model plant *Arabidopsis thaliana*. *Front. Plant Sci.* 4:224. doi: 10.3389/fpls.2013.00224

Shaw, S. L., and Long, S. R. (2003). Nod factor inhibition of reactive oxygen efflux in a host legume. *Plant Physiol.* 132, 2196–2204. doi: 10.1104/pp.103.021113

Shin, R., and Schachtman, D. P. (2004). Hydrogen peroxide mediates plant root cell response to nutrient deprivation. *Proc. Natl. Acad. Sci. U.S.A.* 101, 8827–8832. doi: 10.1073/pnas.0401707101

Stefanovic, A., Arpat, A. B., Bligny, R., Gout, E., Vidoudez, C., Bensimon, M., et al. (2011). Over-expression of PHO1 in Arabidopsis leaves reveals its role in mediating phosphate efflux. *Plant J.* 66, 689–699. doi: 10.1111/j.1365-313X.2011.04532.x

Stefanovic, A., Ribot, C., Rouached, H., Wang, Y., Chong, J., Belbahri, L., et al. (2007). Members of the PHO1 gene family show limited functional redundancy in phosphate transfer to the shoot, and are regulated by phosphate deficiency via distinct pathways. *Plant J.* 50, 982–994. doi: 10.1111/j.1365-313X.2007.03108.x

Storey, J. D., and Tibshirani, R. (2003). Statistical methods for identifying differentially expressed genes in DNA microarrays. *Methods Mol. Biol.* 224, 149–157. doi: 10.1385/1-59259-364-x:149

Straub, D., Ludewig, U., and Neuhauser, B. (2014). A nitrogen-dependent switch in the high affinity ammonium transport in *Medicago truncatula*. *Plant Mol. Biol.* 86, 485–494. doi: 10.1007/s11103-014-0243-4

Sundaravelpandian, K., Chandrika, N. N., and Schmidt, W. (2013). PFT1, a transcriptional Mediator complex subunit, controls root hair differentiation through reactive oxygen species (ROS) distribution in Arabidopsis. *New Phytol.* 197, 151–161. doi: 10.1111/nph.12000

Takeda, S., Gapper, C., Kaya, H., Bell, E., Kuchitsu, K., and Dolan, L. (2008). Local positive feedback regulation determines cell shape in root hair cells. *Science* 319, 1241–1244. doi: 10.1126/science.1152505

Tang, H., Krishnakumar, V., Bidwell, S., Rosen, B., Chan, A., Zhou, S., et al. (2014). An improved genome release (version Mt4.0) for the model legume *Medicago truncatula*. *BMC Genomics* 15:312. doi: 10.1186/1471-2164-15-312

Taochy, C., Gaillard, I., Ipotesi, E., Oomen, R., Leonhardt, N., Zimmermann, S., et al. (2015). The Arabidopsis root stele transporter NPF2.3 contributes to nitrate translocation to shoots under salt stress. *Plant J.* 83, 466–479. doi: 10.1111/tpj.12901

Tran, D., El-Maarouf-Bouteau, H., Rossi, M., Biligui, B., Briand, J., Kawano, T., et al. (2013). Post-transcriptional regulation of GORK channels by superoxide anion contributes to increases in outward-rectifying K(+) currents. *New Phytol.* 198, 1039–1048. doi: 10.1111/nph.12226

Trapnell, C., Roberts, A., Goff, L., Pertea, G., Kim, D., Kelley, D. R., et al. (2012). Differential gene and transcript expression analysis of RNA-seq experiments with TopHat and Cufflinks. *Nat. Protoc.* 7, 562–578. doi: 10.1038/nprot.2012.016

Tsukagoshi, H., Busch, W., and Benfey, P. N. (2010). Transcriptional regulation of ROS controls transition from proliferation to differentiation in the root. *Cell* 143, 606–616. doi: 10.1016/j.cell.2010.10.020

Vacheron, J., Desbrosses, G., Bouffaud, M. L., Touraine, B., Moenne-Loccoz, Y., Muller, D., et al. (2013). Plant growth-promoting rhizobacteria and root system functioning. *Front. Plant Sci.* 4:356. doi: 10.3389/fpls.2013.00356

Van Zeijl, A., Op Den Camp, R. H., Deinum, E. E., Charnikhova, T., Franssen, H., Op Den Camp, H. J., et al. (2015). Rhizobium lipo-chitooligosaccharide signaling triggers accumulation of cytokinins in *Medicago truncatula* roots. *Mol. Plant* 8, 1213–1226. doi: 10.1016/j.molp.2015.03.010

Véry, A. A., Nieves-Cordones, M., Daly, M., Khan, I., Fizames, C., and Sentenac, H. (2014). Molecular biology of K+ transport across the plant cell membrane: what do we learn from comparison between plant species? *J. Plant Physiol.* 171, 748–769. doi: 10.1016/j.jplph.2014.01.011

Véry, A. A., and Sentenac, H. (2003). Molecular mechanisms and regulation of K+ transport in higher plants. *Annu. Rev. Plant Biol.* 54, 575–603. doi: 10.1146/annurev.arplant.54.031902.134831

Wang, E., Yu, N., Bano, S. A., Liu, C., Miller, A. J., Cousins, D., et al. (2014). A H^+-ATPase that energizes nutrient uptake during mycorrhizal symbioses in rice and *Medicago truncatula*. *Plant Cell* 26, 1818–1830. doi: 10.1105/tpc.113.120527

Wang, H., Lan, P., and Shen, R. F. (2016). Integration of transcriptomic and proteomic analysis towards understanding the systems biology of root hairs. *Proteomics* 16, 877–893. doi: 10.1002/pmic.201500265

Wang, Z., Gerstein, M., and Snyder, M. (2009). RNA-Seq: a revolutionary tool for transcriptomics. *Nat. Rev. Genet.* 10, 57–63. doi: 10.1038/nrg2484

Wipf, D., Mongelard, G., Van Tuinen, D., Gutierrez, L., and Casieri, L. (2014). Transcriptional responses of *Medicago truncatula* upon sulfur deficiency stress and arbuscular mycorrhizal symbiosis. *Front. Plant Sci.* 5:680. doi: 10.3389/fpls.2014.00680

Wojciechowski, M. F., Lavin, M., and Sanderson, M. J. (2004). A phylogeny of legumes (Leguminosae) based on analysis of the plastid matK gene resolves

many well-supported subclades within the family. *Am. J. Bot.* 91, 1846–1862. doi: 10.3732/ajb.91.11.1846

Yamanaka, T., Nakagawa, Y., Mori, K., Nakano, M., Imamura, T., Kataoka, H., et al. (2010). MCA1 and MCA2 that mediate Ca2+ uptake have distinct and overlapping roles in *Arabidopsis*. *Plant Physiol.* 152, 1284–1296. doi: 10.1104/pp.109.147371

Yokota, K., Fukai, E., Madsen, L. H., Jurkiewicz, A., Rueda, P., Radutoiu, S., et al. (2009). Rearrangement of actin cytoskeleton mediates invasion of *Lotus japonicus* roots by *Mesorhizobium loti*. *Plant Cell* 21, 267–284. doi: 10.1105/tpc.108.063693

Yong, Z., Kotur, Z., and Glass, A. D. (2010). Characterization of an intact two-component high-affinity nitrate transporter from Arabidopsis roots. *Plant J.* 63, 739–748. doi: 10.1111/j.1365-313X.2010.04278.x

Yuan, F., Yang, H., Xue, Y., Kong, D., Ye, R., Li, C., et al. (2014). OSCA1 mediates osmotic-stress-evoked Ca2+ increases vital for osmosensing in Arabidopsis. *Nature* 514, 367–371. doi: 10.1038/nature13593

Zhang, C., Bousquet, A., and Harris, J. M. (2014). Abscisic acid and LATERAL ROOT ORGAN DEFECTIVE/NUMEROUS INFECTIONS AND POLYPHENOLICS modulate root elongation via reactive oxygen species in *Medicago truncatula*. *Plant Physiol.* 166, 644–658. doi: 10.1104/pp.114.248542

Conflict of Interest Statement: The authors declare that the research was conducted in the absence of any commercial or financial relationships that could be construed as a potential conflict of interest.

frontiers in Physiology

ORIGINAL RESEARCH
published: 13 September 2016
doi: 10.3389/fphys.2016.00402

Arabidopsis Mutant *bik1* Exhibits Strong Resistance to *Plasmodiophora brassicae*

Tao Chen[1,2], *Kai Bi*[1,2], *Zhangchao He*[1,2], *Zhixiao Gao*[1,2], *Ying Zhao*[1,2], *Yanping Fu*[1,2], *Jiasen Cheng*[1,2], *Jiatao Xie*[1,2] *and Daohong Jiang*[1,2]*

[1] State Key Laboratory of Agricultural Microbiology, Huazhong Agricultural University, Wuhan, China, [2] The Provincial Key Lab of Plant Pathology of Hubei Province, College of Plant Science and Technology, Huazhong Agricultural University, Wuhan, China

Botrytis-induced kinase1 (BIK1), a receptor-like cytoplasmic kinase, plays an important role in resistance against pathogens and insects in *Arabidopsis thaliana*. However, it remains unknown whether BIK1 functions against *Plasmodiophora brassicae*, an obligate biotrophic protist that attacks cruciferous plants and induces gall formation on roots. Here, we investigated the potential roles of receptors FLS2, BAK1, and BIK1 in the infection of *P. brassicae* cruciferous plants. Wild-type plants, *fls2,* and *bak1* mutants showed typical symptom on roots, and the galls were filled with large quantities of resting spores, while *bik1* mutant plants exhibited strong resistance to *P. brassicae*. Compared with that of the wild-type plants, the root hair and cortical infection rate of *bik1* mutant were significantly reduced by about 40–50%. A considerable portion of *bik1* roots failed to form typical galls. Even if some small galls were formed, they were filled with multinucleate secondary plasmodia. The *bik1* plants accumulated less reactive oxygen species (ROS) at infected roots than other mutants and wild-type plants. Exogenous salicylic acid (SA) treatment alleviated the clubroot symptoms in wild-type plants, and the expression of the SA signaling marker gene *PR1* was significantly increased in *bik1*. Both *sid2* (salicylic acid induction-deficient 2) and *npr1-1* [non-expresser of PR genes that regulate systemic acquired resistance (SAR)] mutants showed increased susceptibility to *P. brassicae* compared with wild-type plants. These results suggest that the resistance of *bik1* to *P. brassicae* is possibly mediated by SA inducible mechanisms.

Keywords: ***Arabidopsis thaliana***, ***Plasmodiophora brassicae***, **BIK1, SA, ROS, SAR, Clubroot**

OPEN ACCESS

Edited by:
Janin Riedelsberger, University of Talca, Chile

Reviewed by:
Jutta Ludwig-Müller, Dresden University of Technology, Germany
Maria J. Manzanares-Dauleux, Agrocampus Ouest, France

***Correspondence:**
Daohong Jiang
daohongjiang@mail.hzau.edu.cn

Specialty section:
This article was submitted to Plant Physiology, a section of the journal Frontiers in Physiology

Received: *26 May 2016*
Accepted: *29 August 2016*
Published: *13 September 2016*

Citation:
Chen T, Bi K, He Z, Gao Z, Zhao Y, Fu Y, Cheng J, Xie J and Jiang D (2016) Arabidopsis Mutant bik1 Exhibits Strong Resistance to Plasmodiophora brassicae. Front. Physiol. 7:402. doi: 10.3389/fphys.2016.00402

INTRODUCTION

The soil-borne obligate pathogen *Plasmodiophora brassicae* causes clubroot disease in species of *Brassicaceae*, including Arabidopsis. *P. brassicae* plunders nutrients from host roots to complete their life cycle, and causes the formation of root galls. Clubroot occurs in more than 60 countries and results in a 10–15% reduction in the yields of Cruciferae crops on a global scale (Dixon, 2009). *P. brassicae* has a complex but not completely understood infection process. A primary zoospore is released from each resting spore, which reaches the surface of a root hair and penetrates the cell wall, forming primary plasmodia in the root hair. After a number of nuclear divisions, the plasmodia cleave into zoosporangia, and the zoosporangia form clusters in the root hair or

penetrate root cortex cells, in which the pathogen develops into secondary plasmodia (Kageyama and Asano, 2009). Plasmodia provoke abnormal cell enlargement and uncontrolled cell division, leading to the development of club-shaped galls on the roots and the above-ground symptoms, such as wilting, stunting, yellowing, and premature senescence compared with healthy plants (Hwang et al., 2012). Each gall contains millions of resting spores that persist in the soil for up to 15 years even in the absence of a suitable host, making it difficult to manage clubroot diseases (Donald and Porter, 2009). The resting spores of *P. brassicae* are easily transmitted to elsewhere with contaminated soil, including farm machinery, boots, grazing animal hooves, infected transplants, and surface floodwater (Donald and Porter, 2009). Crop rotation, increased soil pH, improved drainage conditions, and fungicide application provide certain protection against the disease; however, under high clubroot pressure, these measures are generally not effective (Abbasi and Lazarovits, 2006). Besides, government policies concerning human health and environmental safety have led to the restriction or deregistration of a large number of previously useful active ingredients. Genetic resistance is the most effective and economical approach to clubroot management, and several resistant cultivars against clubroot have been previously reported (Hirai et al., 2004; Rocherieux et al., 2004; Chu et al., 2014). However, new races of the pathogen can rapidly appear (Fähling et al., 2003). Using *Arabidopsis thaliana* as a model system has facilitated the application of available genetic and molecular tools and has thus advanced our understanding of this economically important plant disease (Siemens et al., 2002). In clubroot-infected Arabidopsis, it is thought that perturbation in phytohormone content plays important roles in disease development (Malinowski et al., 2012), but little has been known about which genes are involved in the plant defense response.

Salicylic acid (SA) is an important secondary phenolic metabolite in a wide range of prokaryotic and eukaryotic organisms, including plants. SA regulates a multitude of developmental processes, such as plant cell growth, seed germination and development, thermo-tolerance, respiration, stomatal aperture, fruit yield, nodulation in legumes, and leaf senescence. More importantly, SA serves as a key signaling and regulatory molecule in plant defense responses, and it is regarded as the key plant immune hormone (Spoel and Dong, 2012; Liu et al., 2015). The biosynthesis of SA on pathogen detection is essential for local and systemic acquired resistance (SAR) and the accumulation of pathogenesis-related (PR) proteins (Boatwright and Pajerowska-Mukhtar, 2013). SA has long been recognized as a central component of defense in plants against a number of biotrophic pathogens and viruses (Vlot et al., 2009). The development of disease in a susceptible host and its molecular basis has been recently examined using an Arabidopsis model (Agarwal et al., 2011). In two Arabidopsis genotypes Col-0 (susceptible) and Bur-0 (partially resistant) which were infected with the virulent *P. brassicae*, clubroot development was partially inhibited by camalexin, SA and jasmonic acid (JA) signaling pathway (Lemarié et al., 2015a,b). Exogenous SA in *B. oleracea* enhances resistance to clubroot (Lovelock et al., 2013, 2016). SA methyltransferase gene *PbBSMT* was identified from *P. brassicae*, which can methylate SA in host cells (Ludwig-Muller et al., 2015).

Basal resistance, the first step in plant defense response, involves perception through surface-localized pattern recognition receptors (PRRs) of conserved molecules characterized by pathogen-associated molecular patterns (PAMPs) or microbe-associated molecular patterns (MAMPs) (Monaghan and Zipfel, 2012). A well-known PRR is Arabidopsis receptor kinase FLS2, which recognizes a conserved 22 amino acid N-terminal sequence of the bacterial flagellin protein (flg22) (Gomez-Gomez and Boller, 2000). FLS2 serves as an excellent model to understand plant innate immune signaling, and heterotrimeric G proteins are directly coupled to the FLS2 receptor complex to regulate immunity (Macho and Zipfel, 2014; Liang et al., 2016). The extracellular leucine-rich repeat domain of FLS2 perceives flg22 and rapidly recruits another LRR receptor-like kinase called BAK1, which plays a role in brassinolide signaling (Chinchilla et al., 2007; Schulze et al., 2010). BIK1, a receptor-like cytoplasmic kinase, is directly phosphorylated through BAK1 and is associated with the FLS2/BAK1 complex in modulating PAMP-mediated signaling (Lu et al., 2010; Zhang et al., 2010). The inactivation of BIK1 causes severe susceptibility to necrotrophic fungal pathogens but enhances the resistance against a virulent strain of the bacterial pathogen *Pseudomonas syringae* pv *tomato* (Veronese et al., 2006), and *bik1* plants displayed enhanced antibiosis and antixenosis toward aphids through inducing the up-regulation of *PAD4* expression (Lei et al., 2014).

In the present study, we investigated the potential roles of the receptors FLS2, BAK1 and BIK1, which have different levels of basal resistance to the compatible strain ZJ-1 of the clubroot pathogen *P. brassicae*. We challenged these loss-of-function mutants with *P. brassicae*. *bik1* exhibited strong resistance to *P. brassicae*, and the root hair and cortical infections were significantly decreased. Besides, the development of *P. brassicae* was inhibited in the infected *bik1* plants. We attempted to explain the mechanism underlying the resistance of *bik1* mutants against *P. brassicae*. *bik1* plants were reported to have a higher basal SA level than wild type plants (Veronese et al., 2006; Lei et al., 2014), and SA suppresses the formation of clubroots in broccoli (Lovelock et al., 2013, 2016). The obtained results showed that exogenous SA treatment could alleviate the symptoms of clubroot. In the mutant line *sid2* and *npr1-1* mutants, which had blocked SA biosynthesis and were SAR-deficient respectively, clubroot symptoms were found to be clearly more severe compared with in Col-0. These findings indicate that the Arabidopsis mutant *bik1* exhibits strong resistance to *P. brassicae* possibly because SA inducible mechanisms enhance the resistance to clubroot disease. However, the *bik1 sid2* double mutant showed strong resistance to *P. brassicae,* suggesting that this resistance is possibly attributable to SA pathway and other unknown pathways.

MATERIALS AND METHODS

Plant Materials, *P. brassicae* Inoculation and Growth Conditions

Arabidopsis thaliana ecotype Columbia (Col-0), which was used as the wild-type control in the present study, was kindly provided by Dr. Yangdou Wei at the University of Saskatchewan, and the mutants *fls2, bik1, bak1-4, bik1 sid2* were kindly donated by Dr. Libo Shan (Texas A & M university). *sid2* was bought from the Arabidopsis Biological Resource Center. The *bik1* mutant line was further identified as a homozygous mutant. The RT-PCR results showed that the *bik1* mRNA could not be detected in homozygous mutant plants (**Figure S1**), suggesting that these plants represent knockout mutants at the BIK1 locus. The *bik1 sid2* double mutant line was identified as a homozygous mutant. The RT-PCR results showed that the *bik1* and *sid2* mRNA could not be detected in homozygous mutant plants (**Figure S2**).

P. brassicae strain ZJ-1 was originally isolated from a diseased plant in a rapeseed field in Zhijiang County, Hubei Province, P R China. The virulence of single-spore isolated from *P. brassicae* strain ZJ-1 was tested on the differential hosts of Williams, showing the single-spore isolate derived from race 1 (Williams, 1966; Fähling et al., 2004). Resting spores of *P. brassicae* were extracted from clubroot galls (Asano et al., 1999), surface disinfested by freshly prepared 2% chloramine-T solution at room temperature for 20 min, washed twice with sterile water, adjusted to a concentration of 1.0×10^7 spores per mL, and were then stored at 4°C. *P. brassicae* was proliferated using the stored resting spores in greenhouse with rapeseed. Arabidopsis Col-0 and mutant seeds were germinated on the surface of vermiculite in small pots. The seedlings were transplanted to the soil at 14 days post-germination. After growing of 7 days in a growth chamber, plants were inoculated with 1 mL of the resting spore suspension (1×10^7 spores per mL) by injecting the soil around each plant. Arabidopsis and mutant plants grown in the 50 holes plate (54 cm × 28 cm × 5 cm), each seeding planted in one hole, the wild type and mutants Arabidopsis were planted in the same holes plate to reduce errors. The plants were grown in a plant growth chamber maintained at 70% humidity and 23°C with a 16/8-h day/night cycle. For all the mutants analyzed, gene expression was verified at 21 or 28 days post inoculation. Disease severity was assessed using a scoring system of 0–4 modified from Siemens reported (Siemens et al., 2002). A score of 0 indicated no disease; 1, very small galls mainly on lateral roots that did not impair the main root; 2, small galls covering the main root and few lateral roots; 3, medium to large galls, also on the main root; and 4, severe galls on lateral root, main root or rosette, with fine roots completely destroyed. Disease index (DI) was calculated using the five-grade scale according to the formula: $DI = (1n_1 + 2n_2 + 3n_3 + 4n_4) \times 100/4N_t$, where n_1–n_4 is the number of plants in the indicated class and N_t is the total number of plants tested.

ROS Determination

Reactive oxygen species (ROS) production was detected using the nitroblue tetrazolium (NBT) staining method (Montiel et al., 2012; Arthikala et al., 2014). The plants grown in the soil pot for 21 days after infection were used to determine O_2^- concentrations. The healthy roots and the galled roots were incubated for 5 h in dark at room temperature, and the roots were cleared in 90% ethanol.

DAB Staining

To estimate the produced H_2O_2 *in situ*, the roots were hand-sectioned using a double-edged razorblade. The sections were subsequently rapidly immersed in 1 mg/ml of 3′, 3′-diaminobenzidine (DAB) solution, vacuum infiltrated for 2 min, and incubated for 2–3 h at 25°C in darkness (Gorska-Czekaj and Borucki, 2013).

SA and MeSA Exogenous Treatment

A stock solution of SA (99.5%, Sigma Aldrich, dried substance) was prepared in ethanol/ddH_2O (v/v1:1), and diluted with sterile water at 2.5×10^{-5}mol/L concentration for spraying (Lovelock et al., 2013). MeSA (99%, VETEC) was diluted in 10% ethanol and was sprayed at the 2.5×10^{-5}mol/L concentration. SA and MeSA were used for three times of exogenous treatments. The first treatment was conducted 2 days prior to the inoculation, while the second treatment was carried out 2 days after inoculation, and the last was performed 10 days after inoculation. The total volume of each spraying was 2 L, and the remaining water was gently poured into the holding tray for slow absorption through the roots. Approximately 30 plants were treated for each sample (Lovelock et al., 2013).

Quantification of *P. brassicae* DNA Content in Infected Roots

DNA was extracted from root samples using the cetyl trimethyl ammonium bromide (CTAB) method (Allen et al., 2006). Quantitative PCR was performed on a CFX96 real-time PCR system (BioRad) using iTaq Universal SYBR Green supermix (BioRad) to quantify the *P. brassicae* target actin gene AY452179.1. Each reaction was performed with 2.5 ng of total DNA as template, and Arabidopsis actin gene AT3G18780 was used as an internal control for data normalization. Standard curves were constructed using serial dilutions of DNA extracted from the roots of Col-0 at 21 days after inoculation with *P. brassicae,* which was defined as a reference condition. Quantitative results were then expressed as the % of the *P. brassicae* mean DNA content in this reference condition (Lemarié et al., 2015a,b).

RNA Isolation and Quantitative Real-Time PCR

Total RNA was isolated from control roots, and the roots were inoculated with *P. brassicae* using TRIZOL reagent (Invitrogen). RNA samples were treated with DNase I to remove potential contaminating genomic DNA, followed by extraction with phenol:chloroform. First-strand cDNA was prepared using oligo (dT) primer. Quantitative PCR was performed on a CFX96 real-time PCR system (BioRad), using iTaq Universal SYBR Green supermix (BioRad). The following cycling conditions were used: 95°C for 30 s, 95°C for 5 s, 60°C for 15 s, and 72°C for 12 s. The reaction was performed for 40 cycles, followed by a step at 72°C

for 5 s. Each amplification used 3 technical replicates the results of which were averaged to give the value for a single biological replicate. The primer sequences are provided in **Table S1**. We tried using the two Arabiodopsis genes (actin and ubiquitin) for qRTPCR, and the results were similar. The data shown in this paper selected Arabidopsis ubiquitin10 (AT4G05320) served as an internal control for normalization.

Microscopic Analysis

Fluorescent and transmission electron microscopy (TEM) were performed using the following protocol. For fluorescent microscopy, the healthy roots or galled roots were treated with Nile red solution (10 μg/ml Nile red in acetone) for 3–5 s, and excess dye was removed after brief rinsing in H_2O. The root samples were subsequently observed using Nikon fluorescence microscopy. Nile red emits fluorescence over a broad range of wavelengths, but observation using a filter set for B excitation (used for FITC, Cy2, Alexa488, or GFP) generates the best images (Suzuki et al., 2013). For electron microscopy analysis, the roots were fixed in 2.5% glutaraldehyde for 4 h, and were subsequently postfixed in 1% osmium tetroxide for 3 h, washed, dehydrated through an ethanol series, and embedded in London resin white. Ultrathin sections were examined through TEM (HITACHI, H-7000).

Transverse Root Sectioning

Wild-type and mutant Arabidopsis were infected with *P. brassicae* for 21 days, and uninfected roots were used as the control. The healthy root tissues and galls were carefully washed with tap water and embedded in a frozen embedding medium (Sakura Finetek USA, Inc., Torrance, CA) at −23°C overnight. Transverse root sections (50 μm thick) were sliced using a freezing microtome (Leica CM1950, Germany) and attached to the slides. A drop of water was added, and the specimens were covered with cover glass. The plant cells and spores were observed using a Nikon light microscope.

Statistical Analysis

Statistical analysis was performed using SPSS (13.0) and a statistics package (Microsoft Excel 2010). In all experiments, One-way ANOVA, specifically Tukey's test with a $P = 0.05$, was used to analyze significant differences between treatment groups.

RESULTS

bik1 Exhibited Strong Resistance to *P. brassicae*

The symptoms of *P. brassicae*-infected plants included the formation of club-shaped galls on the roots, and the wilting, yellowing and premature senescence of the shoots. The plant defense response upon *P. brassicae* infection is often reflected by reduced gall size, root condition, and reduced resting spore production. To determine whether several known receptor-like kinases have function in clubroot-associated defense responses, we observed the infection and colonization of *P. brassicae* on the roots of the loss-of-function mutants (**Figure 1**). The roots of wild-type Arabidopsis infected by *P. brassicae* were formed of a typical galled, resulting in few rootlets; besides, the infected plants were yellowing (**Figure 1A** and **Figure S3**), and the ratio of gall formation was 100% (**Figure 1B**). The symptoms of *fls2* and *bak1* infected by clubroot-pathogen were similar to those of the wild type (**Figure 1A** and **Figure S3**), with a gall formation ratio of nearly 100% (**Figure 1B**). Interestingly, in *bik1*, the gall formation was inhibited as 79% of the plants that did not form a gall, and the root systems of *P. brassicae*-inoculated *bik1* plants still developed with plentiful lateral roots (**Figures 1A,B**). The *bik1* mutant line was identified as a homozygous mutant, and the RT-PCR results showed that the *bik1* mRNA could not be detected in homozygous mutant plants (**Figure S1**), suggesting that these plants were the knockout mutants at the BIK1 locus. To evaluate *P. brassicae* production in the galls, the actin gene expression levels of *P. brassicae* were measured using quantitative real-time PCR. For the phenotype of no gall formation on *bik1*-infected roots due to the largely reduced *P. brassicae* production (by 99.78%), and for the phenotype of mid gall formation, root spore production was reduced by approximately 92% (**Figure 1C**). The relative amount of *P. brassicae* DNA in total root-extracted DNA was evaluated through quantitative PCR (**Figure 1D**). The results indicated that root pathogen density was not reduced within the infected roots of *fls2* and *bak1* mutants compared with Col-0, suggesting that *fls2* and *bak1* mutants had no significant change of pathogen density within the root samples. However, the density of *P. brassicae* in the infected roots with and without the formation of small galls in *bik1* mutant was approximately 40 and 90% less than that in Col-0, respectively (**Figure 1D**). Taken together, the results showed that *bik1* plants exhibited strong resistance to *P. brassicae*.

To observe the *P. brassicae* development state in the galls of the infected roots, longitudinal sections of Arabidopsis control and loss-of-function mutant roots were observed. There was no zoospores in the negative control (uninfected wild type Arabidopsis root cells), and many resting spores were found in infected wild type, *fls2* and *bak1* root cells. No obvious zoospores were observed on the infected roots of *bik1*, which showed no gall formation phenotype (**Figure 2A**). TEM was used to clearly demonstrate the zoospore developmental stages in the very small galls on *bik1* root. The development of *P. brassicae* was in the state of multinucleate secondary plasmodium during cell division on *bik1* root (**Figure 2Bb**), while the wild-type root cells were filled with resting spores and the cell division was completed (**Figure 2Ba**). These observations suggested that *bik1* had inhibited development of *P. brassicae*, which explains the results that the wild-type roots showed severe galls with a high production of resting spores, while the *bik1* roots had fewer and smaller galls with less *P. brassicae*.

Suppression of Root Hair and Cortical Infections by the Loss of BIK1 Function

The life cycle of *P. brassicae* consists of three stages: survival in soil, root hair infection, and cortical infection (Schwelm et al., 2015). To investigate the potential involvement of BIK1 in the infection process, we compared the root hair and cortical infections between the wild-type and *bik1 mutant*

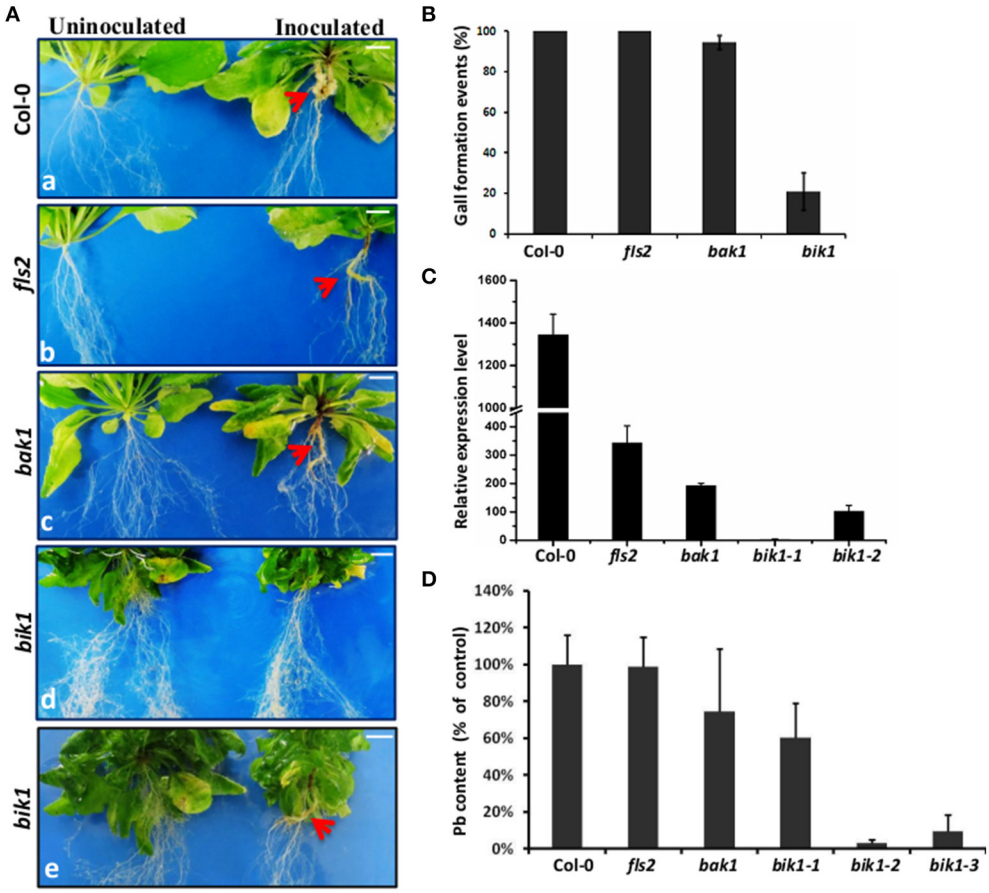

FIGURE 1 | Phenotypes and *P. brassicae* DNA contents in Arabidopsis control and several loss-of-function mutant roots. (A) Arabidopsis Col-0 roots **(a)** and several loss-of-function mutant RLKs, including FLS2 **(b)**, BAK1 **(c)**, and BIK1 **(d,e)** infected with *P. brassicae*; the root images were captured at 21 days after *P. brassicae* infection. The red arrows show the galls, and *bik1* showed two phenotypes: formation of small galls and no gall formation on the roots. Bar = 0.5 cm. **(B)** Disease symptoms of Arabidopsis control roots and several loss-of-function mutants for gall comparison. Clubroot symptoms were quantified for three biological replicates, each containing 30 plants per genotype. However, for some mutants especially the bik1 mutants several plants were excluded before statistics due to a poor growth (with very small shoots and roots). The error bars represent the SD of the experimental values obtained from three biological replicates. **(C)** Real-time PCR analysis was performed to assess the expression levels of *P. brassicae* at 21 days after inoculation. *bik1-1* showed no root gall formation, and *bik1-2* showed root gall formation. Root sample is a mixture of roots from different plants of the same mutant (over 3 plants). The error bars represent the SD of the experimental values obtained from three technical replicates. **(D)** Pathogen DNA quantification (Pb) by quantitative PCR, expressed the percentage of the mean Pb content in inoculated roots of Col-0, *fls2, bak1,* and *bik1* at 21 days after inoculation with *P. brassicae.* At least 3 plant roots were taken as mixed sample. *bik1-1* showed the formation of small galls on the roots, and *bik1-2* and *bik1-3* showed no formation of galls on the roots. Root sample is a mixture of roots from different plants of the same mutant (over 3 plants). The error bars represent the SD of the experimental values obtained from three technical replicates.

plants, including the colonization rate of primary plasmodia, zoosporangia, and secondary plasmodia (**Figures 3A,B**). Nile red was used to label *P. brassicae* for convenient and rapid detection of the stages of infection. The roots of more than 15 plants were selected for the control and *bik1* mutants and sliced into 1–2 cm segments. A total of approximately 100 root segments per sample were observed and counted to determine the presence of infection. Compared with root hair infection of the control (100% primary plasmodia and 87.17% zoosporangia, respectively), the root hair infection ratio of *bik1* mutant roots was reduced, showing 40.40% primary plasmodia and 54.47% zoosporangia, respectively (**Figure 3B**). Compared with the control roots (85.70% secondary plasmodia), the *bik1* mutant roots showed a reduced cortical infections ratio (43.17% secondary plasmodia) (**Figure 3B**). Thus, root hair and cortical infections appeared to be impaired by the knockout of BIK1 expression in the mutant.

High Level of ROS Accumulated in the Infected Roots of Arabidopsis

ROS plays dual roles in plants, both as toxic compounds and as the key regulators of many biological processes, such as growth, cell cycle, programmed cell death, hormone signaling, development, stress, and defense responses (Mittler et al., 2004). Pathogen infection may elicit ROS production. We used nitroblue tetrazolium (NBT), a reagent that allows the visualization of superoxide accumulation, to evaluate the ROS production in *P. brassicae*-infected roots of wild type

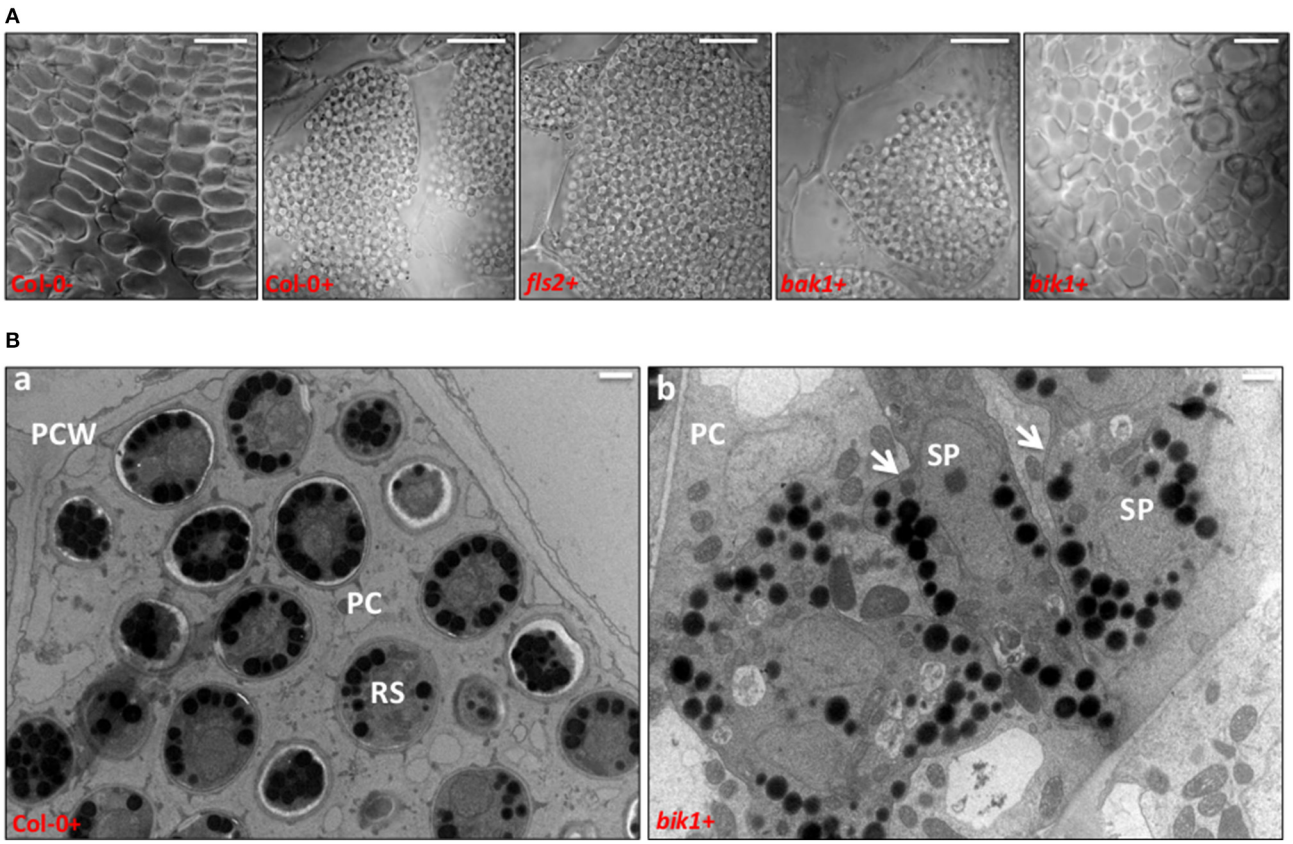

FIGURE 2 | Longitudinal sections and TEM of Arabidopsis control and loss-of-function mutant roots infected with *P. brassicae.* **(A)** Longitudinal sections of Arabidopsis control and loss-of-function mutant roots infected with *P. brassicae* after 21 days. Bar = 20 μm. **(B)** Transmission electron microscopy of Col-0 **(a)** and *bik1* **(b)** infected *with P. brassicae* for 21 days. Selected clearly visible clubs to section (− = uninoculated roots, + = inoculated roots). RS = resting spores; PC = plant cell; PCW = plant cell wall; SP = secondary plasmodium, white arrow. Bar = 1 μm.

Arabidopsis, *fls2*, *bak1,* and *bik1* mutants. NBT-formazan precipitates within the roots of all the mutants and control wild type were localized to the places of gall formation (**Figure 4**), and the NBT-formazan precipitates were much less abundant in the infected roots of *bik1* than in the roots of wild type or *fls2* and *bak1* mutant plants (**Figure 4**). We further observed the galls of *P. brassicae*-infected *Brassica rapa* through 3-3′-diaminobenzidine (DAB) staining. The results showed that the galled roots had much higher H_2O_2 accumulation than healthy roots in the cortex, which was filled with millions of *P. brassicae* resting spores (**Figure S4**). These results indicated that ROS might be an indicator of defense responses.

Treatment of Roots with SA Alleviated the Symptoms of Clubroot

SA is a central component of defense in plants against a number of biotrophic pathogens (Catinot et al., 2008; Vlot et al., 2009). Thus, we investigated the potential of SA to stimulate defense in Arabidopsis against *P. brassicae,* and methyl salicylate (MeSA) was used as the control. The formation of root galls was assessed at 3 weeks after three repeated treatments with SA or MeSA. SA treatment significantly reduced gall formation, and the proportion of galling was decreased by 90% (from 100 to 10%). MeSA treatment resulted in no reduction of gall formation (from 100 to 100%) (**Figures 5A–C**). The disease symptoms associated with *P. brassicae* were observed to be decreased in the roots treated with SA, but no observable change was found in shoot morphology (**Figure 5D**). Nile red staining clearly showed that a very small amount of spores were observed in SA-treated roots (**Figures 5E–G**). These results indicate that SA enhances the resistance against *P. brassicae.*

P. brassicae Altered the Expression of Defense Genes in *bik1*, Particularly *PR1*

P. brassicae-induced plant defense pathways are often regulated through certain plant hormones, JA pathway, and SA pathway (Lemarié et al., 2015b). The loss of BIK1 function resulted in higher basal SA levels and *PR1* gene expression than wild-type Col-0 Arabidopsis (Veronese et al., 2006; Lei et al., 2014). To determine whether the resistance to *P. brassicae* was conferred through the loss of BIK1 function involving defense-related plant hormones, we detected the expression levels of the SA-signaling marker gene *PR1* and the ET/JA marker genes

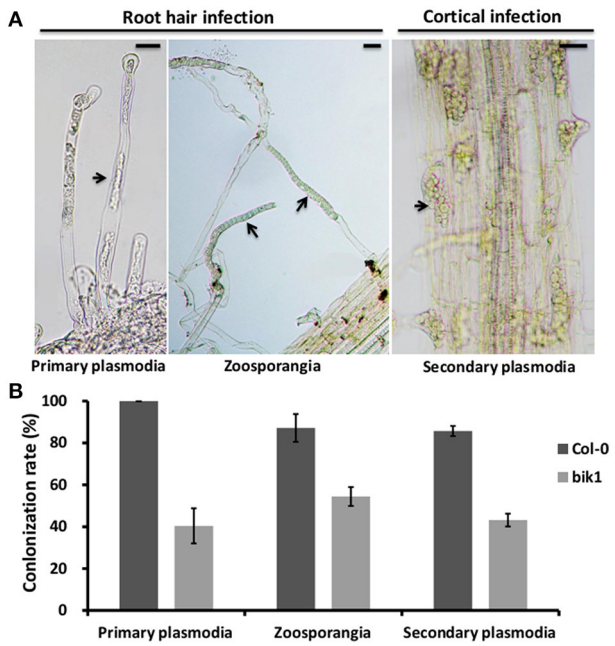

FIGURE 3 | Root hair and cortical infection stages in the roots of Arabidopsis control and *bik1* mutant plants. (A) The images show the key steps of *P. brassicae* infection in Arabidopsis control and *bik1* mutant plants, including root hair and cortical infections stages. Primary plasmodia of root hair infection were observed in the roots stained with Nile red for 3 days post inoculation. Zoosporangia of root hair infection and secondary plasmodia of cortical infection were observed in the roots stained with Nile red for 12 days post inoculation. The pictures were under light microscopy. Arrows indicate primary plasmodia, zoosporangia or secondary plasmodia. **(B)** Mean rate (100%) of primary plasmodia, zoosporangia and secondary plasmodia per root of the control and *bik1* mutant. The roots of more than 15 plants were selected for the control and *bik1* mutants and sliced into 1–2 cm segments. A total of approximately 100 root segments per sample were observed and counted to determine the presence of infection. The error bars represent the SD of the experimental values obtained from three biological replicates. Bar = 10 μm.

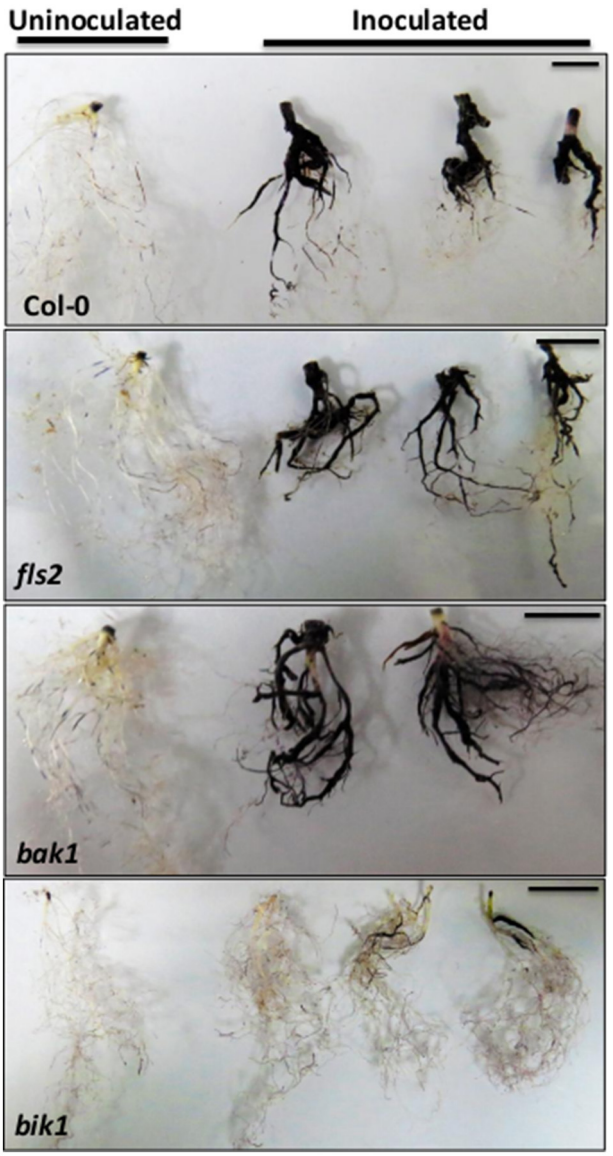

FIGURE 4 | Analysis of ROS production. Visualization of O_2^- production in representative NBT-stained control, and *fls2, bak1* and *bik1* mutant roots at 21 days post inoculation with *P. brassicae.* Dense blue forazan precipitates were observed at the site of H_2O_2 production. Bar = 1 cm.

ERF1 and *PDF1.2* at 21 days after infection of *P. brassicae* (**Figure 6**). In wild-type roots, the expression levels of *PR1, PDF1.2,* and *ERF1* were 6.5, 9.4, and 2.2-folds up-regulated after infection, respectively. Similar results were obtained for *fls2* mutant plants. However, the transcript level of the SA-responsive gene *PR1* in *bik1* mutant roots was 48.4-folds higher before *P. brassicae* infection and 11.5-folds higher after the infection compared with that in the wild type roots. These data implied that BIK1 might function as a negative regulator of SA accumulation both in the presence and absence of *P. brassicae* infection.

bik1 sid2 Double Mutant Failed to Restore the Susceptibility to *P. brassicae*

The loss of SID2 function blocks SA biosynthesis (Wildermuth et al., 2001). To assess the role of SA in *bik1* resistance to *P. brassicae*, *bik1, sid2,* and *bik1 sid2* double mutant plants were used for infection (**Figure 7**). The non-inoculated *sid2* mutant did not show any observable change in morphology compared with the wild type (**Figures 7A,D**, **Figure S5**). Besides, the severity of clubroot symptoms induced by *P. brassicae* was similar to that of wild-type plants: both of them showed yellowing leaves, severely galled and rotten taproots, and similar density of *P. brassicae* were detected (**Figures 7A–C,E**). These results are consistent with those reported previously (Lovelock et al., 2016). Apparently, *bik1* reduced the clubroot symptom and density of *P. brassicae* (**Figures 7A–E**). These results indicated that the elevation of SA accumulation was required for *bik1* resistance. Surprisingly, in the *bik1 sid2* double mutant with reduced SA accumulation (Laluk et al., 2011; Lei et al., 2014), the phenotypes were similar to those

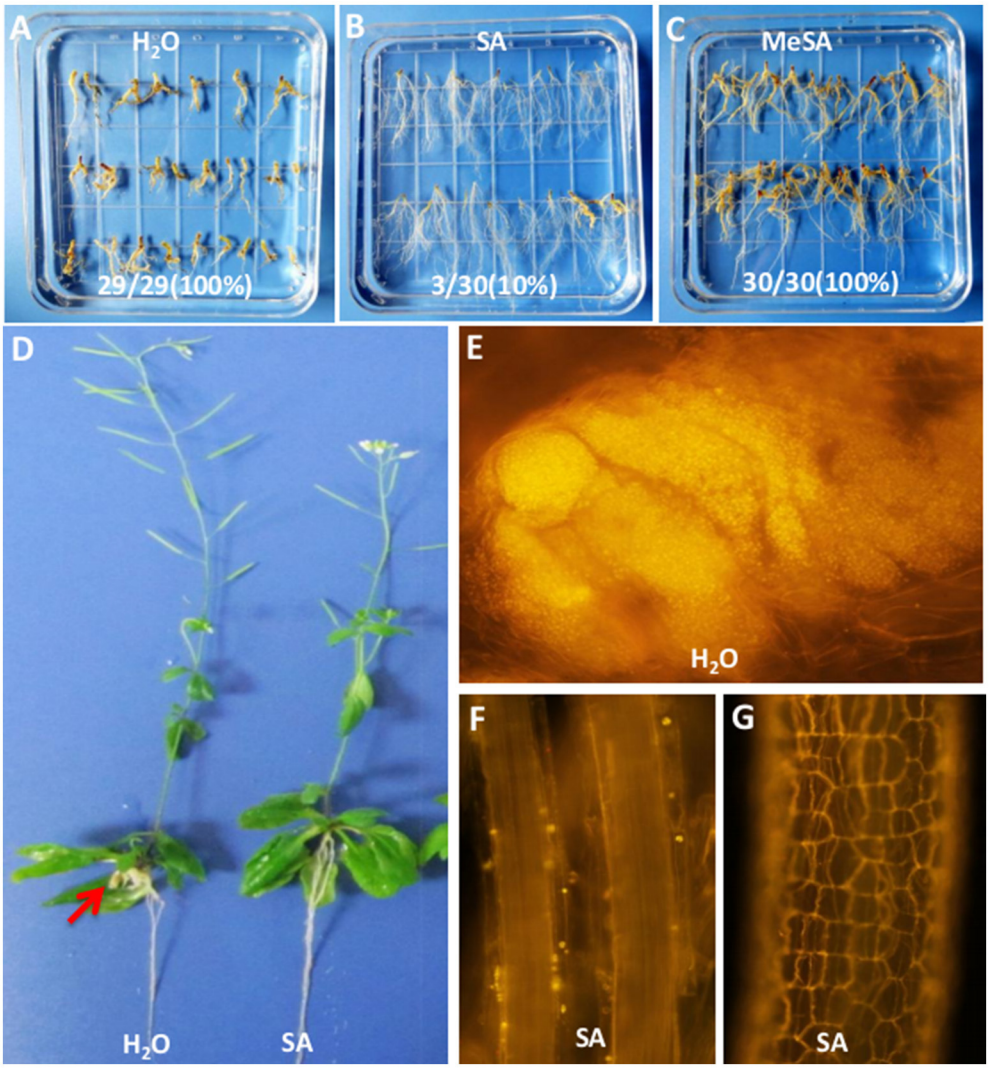

FIGURE 5 | Effect of SA treatment in the pot on gall reduction in 3-week-old infected plants. (A–C) Gall phenotype of Arabidopsis Col-0 infected with *P. brassicae* for 21 days in 3 different treatments, including H_2O (left), SA 2.5×10^{-5}mol/L for 3 times (middle), and 2.5×10^{-5}mol/L MeSA for 3 times (right). The number on the picture showed the gall formation events. **(D)** Images of whole plants of Arabidopsis Col-0 infected with *P. brassicae* for 21 days and treated with SA 2.5×10^{-5}mol/L for 3 times (right) or not (left). **(E)** Nile red staining for infected Col-0 clubroots. **(F,G)** Nile red staining for infected Col-0 clubroots treated with SA.

of *bik1* plants. These plants showed leaves with serrated margins and wrinkled surfaces, occasional curling, partial recovery to wild type, and strong resistance to *P. brassicae* similarly to *bik1* (**Figure 7** and **Figure S5**). The *bik1 sid2* double mutant line was identified as a homozygous mutant (**Figure S2**), which showed partial resistance to clubroot possibly due to an epistatic effect or some other unknown signal pathways that contribute to the resistance of *bik1* against *P. brassicae*.

SAR-Deficient Mutant *npr1-1* Was More Susceptible to *P. brassicae* than Col-0

SA and the SA-dependent signaling pathways play a major role in modulating SAR. In Arabidopsis plants defective in SA accumulation, SAR is significantly impaired, and in plants where SA is either over-expressed or externally supplied, enhanced SAR is typically observed (Fu and Dong, 2013). The *bik1* mutant plants showed higher SA level and up-regulated *PR1* gene expression compared with Col-0, indicating that the *bik1* mutant plants had enhanced SAR. To examine whether SAR is important for Arabidopsis to resist *P. brassicae*, the *npr1-1* mutant was inoculated with *P. brassicae*. The results showed that at 21 days post inoculation, the symptoms of *npr1-1* were more severe than those of Col-0 (**Figure 8**). The infected *npr1-1* leaves turned yellow and showed root rot, while the control plants showed galls on the roots (**Figures 8A–C**). We then evaluated the disease index in infected Col-0 and *npr1-1* plants (**Figure 8D**), and the index for Col-0 was 69.4, while

that for *npr1-1* was 88.1. These results indicated that *npr1-1* was more susceptible to *P. brassicae* than Col-0. Thus, the SAR of Arabidopsis also contributed to the resistance against *P. brassicae*.

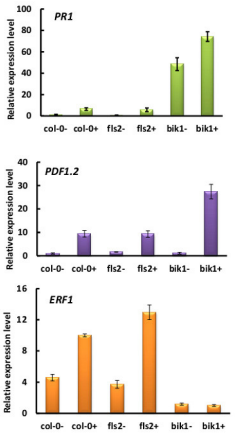

FIGURE 6 | Relative expression of SA, JA, and ET marker genes *PR1*, *ERF1,* and *PDF1.2* in response to infection with *P. brassicae* for 21 days (− = uninfection, + = infection). *P. brassicae* infection up-regulated the expression of these genes in both wild-type and mutant plants.

DISCUSSION

In the present study, we investigated the role of PAMP/MAMP signal receptors in the resistance of Arabidopsis against the infection of clubroot pathogen, and we found that Arabidposis mutant *fls2* and *bak1* were as susceptible to *P. brassicae* as wild-type plants; however, mutant *bik1* displayed strong resistance to *P. brassicae*, and exhibited suppressed root hair and cortical infections. The *bik1* mutant plants were reported to have a higher level of SA than wild-type plants (Veronese et al., 2006; Lei et al., 2014), and real-time PCR proved that the infection of *P. brassicae* induced *PR1* gene expression. *bik1* plants showed higher *PR1* gene expression than Col-0 both in the presence and absence of *P. brassicae* infection. Unsurprisingly, exogenous treatment with SA could enhance the resistance of wild type plants since similar findings were reported by other groups recently (Lovelock et al., 2013, 2016; Lemarié et al., 2015b). However, we found that *bik1 sid2* double mutant with reduced SA accumulation also had strong resistance to *P. brassica*. If it was not due to epistatic effect, the resistance of *bik1* could be attributed to both SA-mediated signal pathway and other unknown factors.

BIK1 is an immediate convergent substrate of several different pattern recognition receptors, including FLS2 (which binds bacterial flagellin), EFR (which binds bacterial elongation factor Tu), PEPR1 (which binds endogenous AtPep peptides), CERK1 (which binds fungal chitin), and BAK1 (which phosphorylates

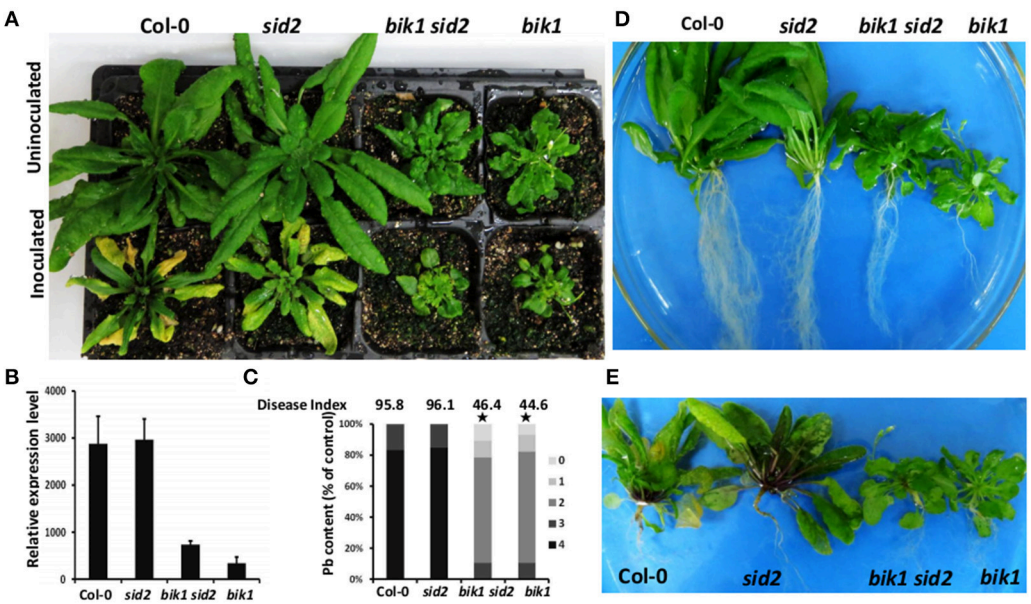

FIGURE 7 | Effect of *sid2* mutation on *bik1*-mediated resistance against *P. brassicae*. (A) Mature shoot phenotypes of wild type and mutant plants. The top of the picture shows uninoculated plants, while the bottom shows plants inoculated with *P. brassicae*. **(B)** Real-time PCR analysis was performed to assess the expression levels of *P. brassicae* at 28 days after inoculation with *P. brassicae*. **(C)** Phytopathological analysis of wild type and mutant plants. The percentages of plants in the individual disease classes are shown. 0, no symptoms; 1, very small galls mainly on lateral roots and that do not impair the main root; 2, small galls covering the main root and few lateral roots; 3, medium to large galls, also including the main root; and 4, severe galls on lateral root, main root or rosette; fine roots completely destroyed. For each treatment, 26–30 Arabidopsis plants were analyzed. The qualitative disease assessment data were initially analyzed using *spss* and subsequently further analyzed after comparing the mean rank differences. The asterisk indicates a significant difference at $P < 0.01$. The disease index for each sample is shown as a number above the respective histograms. **(D)** Images of the shoots without inoculation are shown in **(A)**. **(E)** Clubroot symptoms in plants. Images of the shoots with inoculation are shown in **(A)**.

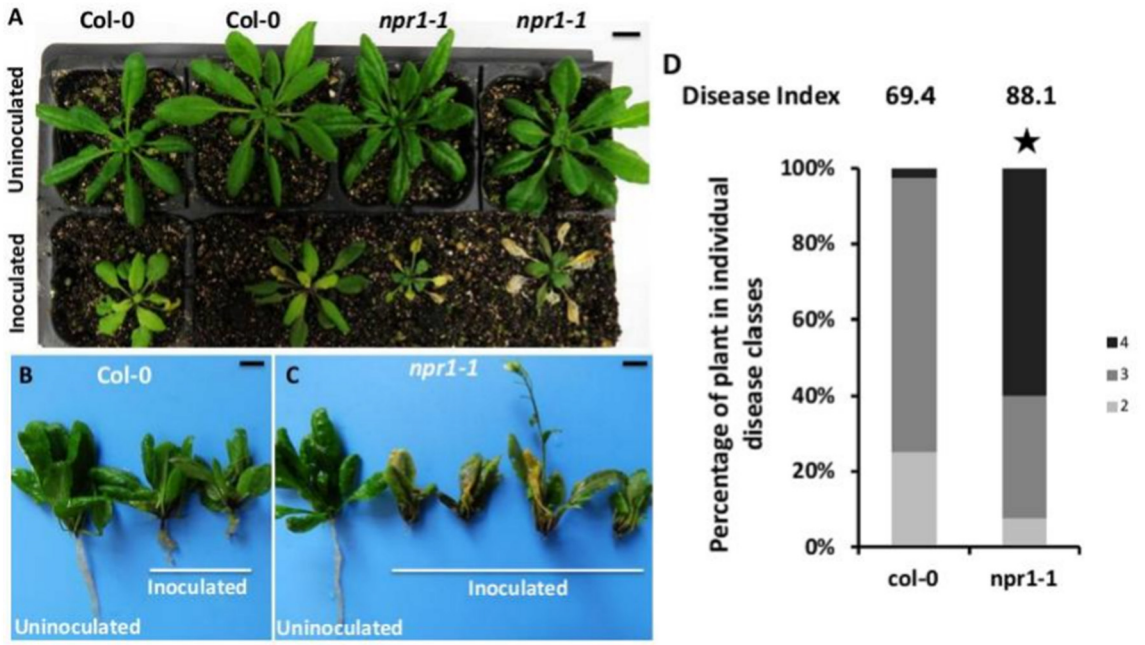

FIGURE 8 | Gall phenotype and phytopathological analysis of the wild type compared with *npr1-1* mutant plants at 21 days post inoculation with *P. brassicae*. (A) Mature shoot phenotypes of wild-type and mutant plants. The top of the picture shows uninoculated plants, and the bottom of the picture shows plants inoculated with *P. brassicae.* The left two panels show Arabidopsis Col-0 plants, while the right two panels show *npr1-1* mutant plants. **(B)** Gall phenotype of Arabidopsis Col-0. **(C)** Gall phenotype of *npr1-1* mutants. **(D)** Phytopathological analysis of wild type and mutant plants. The percentages of plants in the individual disease classes are shown. For each treatment, 40 Arabidopsis plants were analyzed. The qualitative disease assessment data were initially analyzed using *spss* and subsequently further analyzed after comparing the mean rank differences. The asterisk indicates a significant difference at $P < 0.01$. The disease index for each sample is shown as a number above the respective histogram.

several immune receptors), and is a key component of the plant immune system (Monaghan et al., 2015). Plants lacking functional BIK1 and related proteins such as PBL1 (*bik1 pbl1* mutants) are strongly impaired in PTI signaling and are more susceptible to bacterial and fungal pathogens (Veronese et al., 2006; Lu et al., 2010; Feng et al., 2012). Inactivation of *BIK1* causes severe susceptibility to necrotrophic fungal pathogens *B. cinerea* and *Alternaria brassicicola,* but enhances resistance to biotrophic bacterial pathogen *P. syringae* pv *tomato.* BIK1 acts as a negative regulator of basal resistance to virulent bacterial pathogens (Veronese et al., 2006). BIK1 is highly induced by *B. cinerea* and *P. syringae* (Veronese et al., 2006). Here, we did not detect any significant change in BIK1 (**Figure S6A**). The strong resistance mediated by *bik1* to aphids depends on the suppression of *PAD4* expression (Lei et al., 2014). *PAD4* was induced in response to aphid feeding, but was significantly reduced in response to clubroot infection (**Figure S6B**), Thus, BIK1 acts as a negative regulator of the defense response against the infection of *P. brassicae*, and the mechanism may be different from that of the resistance of BIK1 against biotrophic bacterial pathogens and phloem sap-feeding aphids. *P. brassicae* infection alters the phytohormone contents in Arabidopsis, and the plant hormone brassinosteroids (BR) plays a role during gall formation; besides, the BR synthesis inhibitor propiconazole and the BR receptor mutant *bri1-6* reduce gall formation (Schuller et al., 2014). However, phenotypic, molecular, and biochemical data suggested that BIK1 negatively regulates BR-mediated responses and signaling via the phosphorylation through BRI1, and the *bik1* mutant possesses enhanced BR signaling (Lin et al., 2013). These results suggest that resistance to *P. brassicae* in *bik1* mutant is unlikely to be caused by the plant defense-associated hormone BR; on the contrary, the mutant *bik1* needs partial compensation for the negative effect caused by the enhanced BR signaling.

SAR is one mechanism of induced defense that confers long-lasting protection against a broad spectrum of microorganisms (Durrant and Dong, 2004). SA and the SA-dependent signaling pathways play a major role in modulating SAR. In Arabidopsis plants defective in SA accumulation, SAR is significantly impaired, and in plants where SA is either over-expressed or externally supplied, enhanced SAR is typically observed (Fu and Dong, 2013). The Arabidopsis NPR1 is a key regulator in the signal transduction pathway that leads to SAR (Kinkema et al., 2000), and *npr1* mutant fails to respond to various SAR-inducing agents (SA, INA, and avirulent pathogens), displaying little expression of *PR* genes (*PR5* was 5-fold lower and *PR1* was 20-fold lower than the wild type), and exhibiting increased susceptibility to bacterial and fungal infections (Cao et al., 1994). We found that *npr1-1* mutant was more susceptible to *P. brassicae* than wild-type plants, suggesting that SAR might be involved in the defense of plants to deal with the infection and colonization of *P. brassicae.* In dicotyledonous plants, SA is necessary and

sufficient SA induces SAR (Vernooij et al., 1994). The *bik1* mutant plants showed higher SA levels and up-regulated *PR1* gene expression compared with Col-0, indicating that SAR was activated in *bik1* mutant plants, which is consistent with the results of Veronese et al. (2006). The *bik1* mutation affects the expression of defense-related genes *ERF1* and *PDF1.2* (**Figure 6**). These results indicate that *bik1* mutants had some changes in certain plant hormones, including SA, JA, and ET, which is consistent with the results of Veronese et al. (2006). Both the JA and the SA pathways contribute to the resistance against the biotrophic clubroot agent *P. brassicae* in Arabidopsis (Lemarié et al., 2015b). Further studies are needed to examine whether elevated JA and ET signaling in *bik1* plays a role in the resistance against *P. brassicae*.

Root hair infection is the first step for the colonization of *P. brassicae* on host roots. When we examined the infection of *P. brassicae* on *bik1* mutant, the root hair infection and cortical infection were reduced by nearly 50% compared with wild-type plants. This result suggests that the resistance of *bik1* mutant also occurred as early as at primary infection stage. The possible explanation is that BIK1 produces some unknown active compounds to inhibit the infection, or the structure of root hairs is likely to be slightly changed compared with that of the wild-type plants. A previous study showed that the root system of *bik1* was different from that of wild-type plants: *bik1* mutant was rich in root hairs, and its root hairs were longer than those of wild-type plants (Veronese et al., 2006). We also found that the developmental process of *P. brassicae* in cortical cells of *bik1* mutant was significantly suppressed. In the galls of wild-type plants, numerous resting spores were observed, while in the infected-roots of *bik1* mutant, only a few resting spores could be observed, and most of them were plasmodia. Furthermore, based on the quantity analysis of the expression of *P. brassicae* actin gene, the density of *P. brassicae* in *bik1* mutant was significantly reduced. Whether it is SA-meditated signal pathway or other factors that are involved in this suppression of primary infection and the development of *P. brassicae* in cortical cells needs further clarification.

ROS is important for counteracting against the invasion of other organisms. ROS is used to trigger cell death to prevent pathogens from establishing parasitic relationships with their hosts; besides, ROS also could kill pathogens directly. As a biotrophic pathogen, *P. brassicae* depends on host living cells for nutrients and proliferation. In this study, we found high level ROS accumulation at the place where *P. brassicae* colonized in the roots of wild-type plants, *fls2* and *bak1*, while relatively low level of ROS accumulation was observed in the roots of *P. brassicae*-inoculated *bik1*. These results suggest that oxidative stress induced by clubroots is an important immune response against invasion of pathogens. However, it is still largely unknown whether these ROS are generated by the host or by *P. brassicae*. NADPH oxidase (respiratory burst oxidase homologs) genes can be found in the P. *brassicae* genome; by analyzing the transcripts within specific life stages, NADPH oxidase genes were found to be expressed at every stage of development. We may use Arabidopsis knockout mutants without ROS production or with ROS overproduction to investigate the role of ROS during *P. brassicae* infection in th future.

AUTHOR CONTRIBUTIONS

TC and DJ designed research; TC, KB, ZH, ZG, and YZ performed research; TC, YF, JC, JX, and DJ analyzed data; TC and DJ wrote the paper. All authors read and approved the final manuscript.

FUNDING

This work was supported by the earmarked fund for China Agriculture Research System (CARS-13), the Fundamental Research Funds for the Central Universities (2013PY115), Natural Science Foundation of Hubei Province of China (2013CFB202) and the Specialized Research Fund for the Doctoral Program of Higher Education of China (20130146120032).

ACKNOWLEDGMENTS

We thank Dr. Libo Shan for *fls2, bik1, bak1-4, nahG, bik1 sid2* Arabidopsis mutant seeds and Dr. Yangdou Wei for Arabidopsis ecotype Columbia (Col-0) seeds.

SUPPLEMENTARY MATERIAL

The Supplementary Material for this article can be found online at: http://journal.frontiersin.org/article/10.3389/fphys.2016.00402

Figure S1 | Phenotype and identification of the homozygous *bik1* mutant. **(A)** Phenotype of 5- **(a,b)** and 10-week-old **(c)** Arabidopsis plants and *bik1* mutants. **(B)** Identification of the homozygous *bik1* mutant. **(a)** Diagram showing primer and T-DNA insertion sites. Genomic PCR **(b)** and RT-PCR **(c)** of homozygous *bik1* lines. Ubiquitin PCR product was used as an internal control.

Figure S2 | Identification of the homozygous *bik1 sid2* double mutant. Genomic PCR **(A)** and RT-PCR **(B)** of homozygous *bik1 sid2* lines. Ubiquitin PCR product was used as an internal control. Primer bik1(3) indicates the 3 primers used once, BIK1-LB, BIK1-LP, and BIK1-RP. Primer sid2 (3) indicates the 3 primers used once, SID2-LB, SID2-LP, and SID2-RP.

Figure S3 | Mature shoot phenotypes of various Arabidopsis genotypes used in the present study. Shoot images were acquired at 21 days after *P. brassicae* infection. Bar = 2 cm.

Figure S4 | DAB staining for production of H_2O_2 in *P. brassicae*-inoculated plants. Production of H_2O_2 in mock-inoculated **(A–C)** or *P. brassicae*-inoculated **(D–E)** plants at 21 days after infection. The roots were stained with DAB as described in the Methods section. **(A,D)** Were root phenotype, bar = 5 mm. **(B,E)** Were the root slices, the red arrows showed the resting spores, bar = 20 μm. **(C,F)** were the roots stained with DAB. The brown precipitate shows DAB polymerization at the site of H_2O_2 production, Bar = 20 μm. The experiments were repeated three times with similar results.

Figure S5 | Phenotypes of various Arabidopsis genotype mutants. Growth morphology of Arabidopsis wild type and mutant plants in the present study without infection with *P. brassicae*.

Figure S6 | Relative expression of *BIK1* (A) and *PAD4* (B) in wild type with or without *P. brassicae* inoculation for 21 days. (− = uninoculated roots, + = inoculated roots).

Table S1 | Primers used in this study.

REFERENCES

Abbasi, P. A., and Lazarovits, G. (2006). Effect of soil application of AG3 phosphonate on the severity of clubroot of bok choy and cabbage caused by *Plasmodiophora brassicae*. *Plant Dis.* 90, 1517–1522. doi: 10.1094/PD-90-1517

Agarwal, A., Kaul, V., Faggian, R., Rookes, J. E., Ludwig-Muller, J., and Cahill, D. M. (2011). Analysis of global host gene expression during the primary phase of the *Arabidopsis thaliana-Plasmodiophora brassicae* interaction. *Funct. Plant Biol.* 38, 462–478. doi: 10.1071/FP11026

Allen, G. C., Flores-Vergara, M. A., Krasnyanski, S., Kumar, S., and Thompson, W. F. (2006). A modified protocol for rapid DNA isolation from plant tissues using cetyltrimethylammonium bromide. *Nat. Protoc.* 1, 2320–2325. doi: 10.1038/nprot.2006.384

Arthikala, M. K., Sánchez-López, R., Nava, N., Santana, O., Cárdenas, L., and Quinto, C. (2014). RbohB, a *Phaseolus vulgaris* NADPH oxidase gene, enhances symbiosome number, bacteroid size, and nitrogen fixation in nodules and impairs mycorrhizal colonization. *New Phytol.* 202, 886–900. doi: 10.1111/nph.12714

Asano, T., Kageyama, K., and Hyakumachi, M. (1999). Surface disinfestation of resting spores of *Plasmodiophora brassicae* used to infect hairy roots of Brassica spp. *Phytopathology* 89, 314–319. doi: 10.1094/PHYTO.1999.89.4.314

Boatwright, J. L., and Pajerowska-Mukhtar, K. (2013). Salicylic acid: an old hormone up to new tricks. *Mol. Plant Pathol.* 14, 623–634. doi: 10.1111/mpp.12035

Cao, H., Bowling, S. A., Gordon, A. S., and Dong, X. (1994). Characterization of an arabidopsis mutant that is nonresponsive to inducers of systemic acquired resistance. *Plant Cell* 6, 1583–1592. doi: 10.1105/tpc.6.11.1583

Catinot, J., Buchala, A., Abou-Mansour, E., and Métraux, J. P. (2008). Salicylic acid production in response to biotic and abiotic stress depends on isochorismate in *Nicotiana benthamiana*. *FEBS Lett.* 582, 473–478. doi: 10.1016/j.febslet.2007.12.039

Chinchilla, D., Zipfel, C., Robatzek, S., Kemmerling, B., Nürnberger, T., Jones, J. D., et al. (2007). A flagellin-induced complex of the receptor FLS2 and BAK1 initiates plant defence. *Nature* 448, 497–500. doi: 10.1038/nature05999

Chu, M. G., Song, T., Falk, K. C., Zhang, X. G., Liu, X. J., Chang, A., et al. (2014). Fine mapping of Rcr1 and analyses of its effect on transcriptome patterns during infection by *Plasmodiophora brassicae*. *BMC Genomics* 15:1166. doi: 10.1186/1471-2164-15-1166

Dixon, G. R. (2009). The occurrence and economic impact of *Plasmodiophora brassicae* and clubroot disease. *J. Plant Growth Regul.* 28, 194–202. doi: 10.1007/s00344-009-9090-y

Donald, C., and Porter, I. (2009). Integrated control of clubroot. *J. Plant Growth Regul.* 28, 289–303. doi: 10.1007/s00344-009-9094-7

Durrant, W. E., and Dong, X. (2004). Systemic acquired resistance. *Annu. Rev. Phytopathol.* 42, 185–209. doi: 10.1146/annurev.phyto.42.040803.140421

Fähling, M., Graf, H., and Siemens, J. (2003). Pathotype separation of *Plasmodiophora brassicae* by the host plant. *J. Phytopathol.* 151, 425–430. doi: 10.1046/j.1439-0434.2003.00744.x

Fähling, M., Graf, H., and Siemens, J. (2004). Characterization of a single-spore isolate population of *Plasmodiophora brassicae* resulting from a single club. *J. Phytopathol.* 152, 438–444. doi: 10.1111/j.1439-0434.2004.00868.x

Feng, F., Yang, F., Rong, W., Wu, X. G., Zhang, J., Chen, S., et al. (2012). A Xanthomonas uridine 5′-monophosphate transferase inhibits plant immune kinases. *Nature* 485, U114–U149. doi: 10.1038/nature10962

Fu, Z. Q., and Dong, X. N. (2013). Systemic acquired resistance: turning local infection into global defense. *Annu. Rev. Plant Biol.* 64, 839–863. doi: 10.1146/annurev-arplant-042811-105606

Gómez-Gómez, L., and Boller, T. (2000). FLS2: an LRR receptor-like kinase involved in the perception of the bacterial elicitor flagellin in Arabidopsis. *Mol. Cell* 5, 1003–1011. doi: 10.1016/S1097-2765(00)80265-8

Górska-Czekaj, M., and Borucki, W. (2013). A correlative study of hydrogen peroxide accumulation after mercury or copper treatment observed in root nodules of *Medicago truncatula* under light, confocal and electron microscopy. *Micron* 52–53, 24–32. doi: 10.1016/j.micron.2013.07.007

Hirai, M., Harada, T., Kubo, N., Tsukada, M., Suwabe, K., and Matsumoto, S. (2004). A novel locus for clubroot resistance in *Brassica rapa* and its linkage markers. *Theor. Appl. Genet.* 108, 639–643. doi: 10.1007/s00122-003-1475-x

Hwang, S. F., Strelkov, S. E., Feng, J., Gossen, B. D., and Howard, R. J. (2012). *Plasmodiophora brassicae*: a review of an emerging pathogen of the Canadian canola (*Brassica napus*) crop. *Mol. Plant Pathol.* 13, 105–113. doi: 10.1111/j.1364-3703.2011.00729.x

Kageyama, K., and Asano, T. (2009). Life cycle of *Plasmodiophora brassicae*. *J. Plant Growth Regul.* 28, 203–211. doi: 10.1007/s00344-009-9101-z

Kinkema, M., Fan, W., and Dong, X. (2000). Nuclear localization of NPR1 is required for activation of PR gene expression. *Plant Cell* 12, 2339–2350. doi: 10.1105/tpc.12.12.2339

Laluk, K., Luo, H., Chai, M., Dhawan, R., Lai, Z., and Mengiste, T. (2011). Biochemical and genetic requirements for function of the immune response regulator BOTRYTIS-INDUCED KINASE1 in plant growth, ethylene signaling, and PAMP-triggered immunity in Arabidopsis. *Plant Cell* 23, 2831–2849. doi: 10.1105/tpc.111.087122

Lei, J., Finlayson, S. A., Salzman, R. A., Shan, L., and Zhu-Salzman, K. (2014). BOTRYTIS-INDUCED KINASE1 Modulates Arabidopsis Resistance to Green Peach Aphids via PHYTOALEXIN DEFICIENT4. *Plant Physiol.* 165, 1657–1670. doi: 10.1104/pp.114.242206

Lemarié, S., Robert-Seilaniantz, A., Lariagon, C., Lemoine, J., Marnet, N., Jubault, M., et al. (2015b). Both the jasmonic acid and the salicylic acid pathways contribute to resistance to the biotrophic clubroot agent Plasmodiophora brassicae in Arabidopsis. *Plant Cell Physiol.* 56, 2158–2168. doi: 10.1093/pcp/pcv127

Lemarié, S., Robert-Seilaniantz, A., Lariagon, C., Lemoine, J., Marnet, N., Levrel, A., et al. (2015a). Camalexin contributes to the partial resistance of *Arabidopsis thaliana* to the biotrophic soilborne protist *Plasmodiophora brassicae*. *Front. Plant Sci.* 6:539. doi: 10.3389/fpls.2015.00539

Liang, X., Ding, P., Lian, K., Wang, J., Ma, M., Li, L., et al. (2016). Arabidopsis heterotrimeric G proteins regulate immunity by directly coupling to the FLS2 receptor. *Elife* 5:e13568. doi: 10.7554/eLife.13568

Lin, W., Lu, D., Gao, X., Jiang, S., Ma, X., Wang, Z., et al. (2013). Inverse modulation of plant immune and brassinosteroid signaling pathways by the receptor-like cytoplasmic kinase BIK1. *Proc. Natl. Acad. Sci. U.S.A.* 110, 12114–12119. doi: 10.1073/pnas.1302154110

Liu, X., Rockett, K. S., Kørner, C. J., and Pajerowska-Mukhtar, K. M. (2015). Salicylic acid signalling: new insights and prospects at a quarter-century milestone. *Essays Biochem.* 58, 101–113. doi: 10.1042/bse0580101

Lovelock, D. A., Donald, C. E., Conlan, X. A., and Cahill, D. M. (2013). Salicylic acid suppression of clubroot in broccoli (*Brassicae oleracea* var. *italica)* caused by the obligate biotroph Plasmodiophora brassicae. *Australas. Plant Pathol.* 42, 141–153. doi: 10.1007/s13313-012-0167-x

Lovelock, D. A., Šola, I., Marschollek, S., Donald, C. E., Rusak, G., van Pée, K. H., et al. (2016). Analysis of salicylic acid-dependent pathways in *Arabidopsis thaliana* following infection with *Plasmodiophora brassicae* and the influence of salicylic acid on disease. *Mol. Plant Pathol.* 17, 1237–1251. doi: 10.1111/mpp.12361

Ludwig-Müller, J., Jülke, S., Geiss, K., Richter, F., Mithöfer, A., Šola, I., et al. (2015). A novel methyltransferase from the intracellular pathogen *Plasmodiophora brassicae* methylates salicylic acid. *Mol. Plant Pathol.* 16, 349–364. doi: 10.1111/mpp.12185

Lu, D., Wu, S., Gao, X., Zhang, Y., Shan, L., and He, P. (2010). A receptor-like cytoplasmic kinase, BIK1, associates with a flagellin receptor complex to initiate plant innate immunity. *Proc. Natl. Acad. Sci. U.S.A.* 107, 496–501. doi: 10.1073/pnas.0909705107

Macho, A. P., and Zipfel, C. (2014). Plant PRRs and the activation of innate immune signaling. *Mol. Cell* 54, 263–272. doi: 10.1016/j.molcel.2014.03.028

Malinowski, R., Smith, J. A., Fleming, A. J., Scholes, J. D., and Rolfe, S. A. (2012). Gall formation in clubroot-infected Arabidopsis results from an increase in existing meristematic activities of the host but is not essential for the completion of the pathogen life cycle. *Plant J.* 71, 226–238. doi: 10.1111/j.1365-313X.2012.04983.x

Mittler, R., Vanderauwera, S., Gollery, M., and Van Breusegem, F. (2004). Reactive oxygen gene network of plants. *Trends Plant Sci.* 9, 490–498. doi: 10.1016/j.tplants.2004.08.009

Monaghan, J., Matschi, S., Romeis, T., and Zipfel, C. (2015). The calcium-dependent protein kinase CPK28 negatively regulates the BIK1-mediated PAMP-induced calcium burst. *Plant Signal. Behav.* 10:e1018497. doi: 10.1080/15592324.2015.1018497

Monaghan, J., and Zipfel, C. (2012). Plant pattern recognition receptor complexes at the plasma membrane. *Curr. Opin. Plant Biol.* 15, 349–357. doi: 10.1016/j.pbi.2012.05.006

Montiel, J., Nava, N., Cárdenas, L., Sánchez-López, R., Arthikala, M. K., Sántana, O., et al. (2012). A *Phaseolus vulgaris* NADPH oxidase gene is required for root infection by Rhizobia. *Plant Cell Physiol.* 53, 1751–1767. doi: 10.1093/pcp/pcs120

Rocherieux, J., Glory, P., Giboulot, A., Boury, S., Barbeyron, G., Thomas, G., et al. (2004). Isolate-specific and broad-spectrum QTLs are involved in the control of clubroot in Brassica oleracea. *Theor. and Appl. Genet.* 108, 1555–1563. doi: 10.1007/s00122-003-1580-x

Schuller, A., Kehr, J., and Ludwig-Müller, J. (2014). Laser microdissection coupled to transcriptional profiling of Arabidopsis roots inoculated by *Plasmodiophora brassicae* indicates a role for brassinosteroids in clubroot formation. *Plant Cell Physiol.* 55, 392–411. doi: 10.1093/pcp/pct174

Schulze, B., Mentzel, T., Jehle, A. K., Mueller, K., Beeler, S., Boller, T., et al. (2010). Rapid heteromerization and phosphorylation of ligand-activated plant transmembrane receptors and their associated kinase BAK1. *J. Biol. Chem.* 285, 9444–9451. doi: 10.1074/jbc.M109.096842

Schwelm, A., Fogelqvist, J., Knaust, A., Jülke, S., Lilja, T., Bonilla-Rosso, G., et al. (2015). The *Plasmodiophora brassicae* genome reveals insights in its life cycle and ancestry of chitin synthases. *Sci. Rep.* 5:11153. doi: 10.1038/srep11153

Siemens, J., Nagel, M., Ludwig-Muller, J., and Sacristan, M. D. (2002). The interaction of *Plasmodiophora brassicae* and *Arabidopsis thaliana*: parameters for disease quantification and screening of mutant lines. *J. Phytopathol.* 150, 592–605. doi: 10.1046/j.1439-0434.2002.00818.x

Spoel, S. H., and Dong, X. N. (2012). How do plants achieve immunity? Defence without specialized immune cells. *Nat. Rev. Immunol.* 12, 89–100. doi: 10.1038/nri3141

Suzuki, M., Shinohara, Y., and Fujimoto, T. (2013). Histochemical detection of lipid droplets in cultured cells. *Methods Mol. Biol.* 931, 483–491. doi: 10.1007/978-1-62703-056-4_25

Vernooij, B., Friedrich, L., Morse, A., Reist, R., Kolditz-Jawhar, R., Ward, E., et al. (1994). Salicylic acid is not the translocated signal responsible for inducing systemic acquired resistance but is required in signal transduction. *Plant Cell* 6, 959–965. doi: 10.1105/tpc.6.7.959

Veronese, P., Nakagami, H., Bluhm, B., Abuqamar, S., Chen, X., Salmeron, J., et al. (2006). The membrane-anchored BOTRYTIS-INDUCED KINASE1 plays distinct roles in Arabidopsis resistance to necrotrophic and biotrophic pathogens. *Plant Cell* 18, 257–273. doi: 10.1105/tpc.105.035576

Vlot, A. C., Dempsey, D. A., and Klessig, D. F. (2009). Salicylic Acid, a multifaceted hormone to combat disease. *Annu. Rev. Phytopathol.* 47, 177–206. doi: 10.1146/annurev.phyto.050908.135202

Wildermuth, M. C., Dewdney, J., Wu, G., and Ausubel, F. M. (2001). Isochorismate synthase is required to synthesize salicylic acid for plant defence. *Nature* 414, 562–565. doi: 10.1038/35107108

Williams, P. H. (1966). A system for the determination of races of *Plasmodiophora brassicae* that infect Cabbage and Rutabaga. *Phytopathology* 56, 624–626.

Zhang, J., Li, W., Xiang, T., Liu, Z., Laluk, K., Ding, X., et al. (2010). Receptor-like cytoplasmic kinases integrate signaling from multiple plant immune receptors and are targeted by a Pseudomonas syringae effector. *Cell Host Microbe* 7, 290–301. doi: 10.1016/j.chom.2010.03.007

Conflict of Interest Statement: The authors declare that the research was conducted in the absence of any commercial or financial relationships that could be construed as a potential conflict of interest.

frontiers in Plant Science

REVIEW
published: 31 August 2016
doi: 10.3389/fpls.2016.01335

Roots Withstanding their Environment: Exploiting Root System Architecture Responses to Abiotic Stress to Improve Crop Tolerance

*Iko T. Koevoets[1], Jan Henk Venema[2], J. Theo. M. Elzenga[2] and Christa Testerink[1]**

[1] Swammerdam Institute for Life Sciences, Plant Cell Biology, University of Amsterdam, Amsterdam, Netherlands,
[2] Genomics Research in Ecology and Evolution in Nature – Plant Physiology, Groningen Institute for Evolutionary Life Sciences, University of Groningen, Groningen, Netherlands

To face future challenges in crop production dictated by global climate changes, breeders and plant researchers collaborate to develop productive crops that are able to withstand a wide range of biotic and abiotic stresses. However, crop selection is often focused on shoot performance alone, as observation of root properties is more complex and asks for artificial and extensive phenotyping platforms. In addition, most root research focuses on development, while a direct link to the functionality of plasticity in root development for tolerance is often lacking. In this paper we review the currently known root system architecture (RSA) responses in *Arabidopsis* and a number of crop species to a range of abiotic stresses, including nutrient limitation, drought, salinity, flooding, and extreme temperatures. For each of these stresses, the key molecular and cellular mechanisms underlying the RSA response are highlighted. To explore the relevance for crop selection, we especially review and discuss studies linking root architectural responses to stress tolerance. This will provide a first step toward understanding the relevance of adaptive root development for a plant's response to its environment. We suggest that functional evidence on the role of root plasticity will support breeders in their efforts to include root properties in their current selection pipeline for abiotic stress tolerance, aimed to improve the robustness of crops.

Keywords: abiotic stress tolerance, root system architecture (RSA), salinity, drought, nutrient limitation, flooding, temperature stress tolerance, crop breeding

OPEN ACCESS

Edited by:
Janin Riedelsberger, University of Talca, Chile

Reviewed by:
Rubén Rellán-Álvarez, CINVESTAV, Mexico
Vasileios Fotopoulos, Cyprus University of Technology, Cyprus

****Correspondence:***
Christa Testerink
c.s.testerink@uva.nl

Specialty section:
This article was submitted to Plant Physiology, a section of the journal Frontiers in Plant Science

Received: *20 June 2016*
Accepted: *18 August 2016*
Published: *31 August 2016*

Citation:
Koevoets IT, Venema JH, Elzenga JTM and Testerink C (2016) Roots Withstanding their Environment: Exploiting Root System Architecture Responses to Abiotic Stress to Improve Crop Tolerance. Front. Plant Sci. 7:1335. doi: 10.3389/fpls.2016.01335

INTRODUCTION

From Optimal to Suboptimal Conditions – Closing the Yield Gap

The world population is growing rapidly and this is accompanied by an increased food demand. In past decades, this growing food demand has been addressed by plant breeding consistent with optimal conditions for plant growth. In agricultural practices, the use of fertilizers, irrigation, pesticides, and other inputs can create these optimal conditions on the short-term. However, increasing evidence exists for the negative consequences of these practices on the long-term.

First of all, irrigation accounts for almost 70% of all freshwater usage in the world (FAO and ITPS, 2015). Freshwater scarcity is a big threat to the human population and the current water usage for agriculture is not sustainable (Rosegrant et al., 2009). Furthermore, irrigation causes

salinization of soils (Smedema and Shiati, 2002) and increases leaching of fertilizer. This leaching, together with excess use of fertilizer and deep tilling leads to higher greenhouse gas emissions (Snyder et al., 2009).

These problems illustrate the unsustainability of creating the optimal conditions our crops are selected for. In addition, climate change will further increase this challenge. Agriculture will have to deal with growing crops under suboptimal conditions, creating a gap between the yield potential and the currently reached yield – the so-called yield gap. An extensive research field tries to map the current yield gap (Lobell et al., 2009; Licker et al., 2010; Van Ittersum et al., 2013) with much focus on improving land management practices (Lobell et al., 2009; Mueller et al., 2012). In concert, plant breeding is shifting from creating "specialist" cultivars that require optimal conditions for their performance toward creating "robust" cultivars that can perform optimal in a broad range of suboptimal conditions, with the ultimate goal of closing the yield gap.

Crop yield is driven by the combination of climate, soil, management, and genetics. Under optimal circumstances the soil provides plants with stability, water, and nutrients. However, soils are heterogeneous environments, strongly influenced by outside factors. Nutrient deficiency, drought, salinity, flooding, and temperature are major drivers of the current and future yield gap. Researchers and breeders work together to develop crops that are able to withstand these stresses (as reviewed in Mickelbart et al., 2015). However, current crop selection is mainly focused on the shoot, whereas most major drivers of the yield gap affect soil properties, directly influencing the root system. This paper will therefore focus on the potential of optimizing root systems for improving crop abiotic stress tolerance.

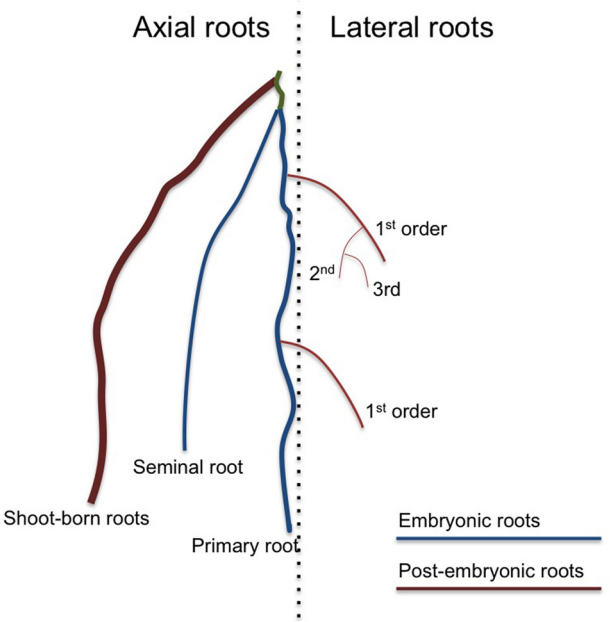

FIGURE 1 | An overview of the different root types that together form the root system. A dicot root system consists only of one primary root and several orders of lateral roots. In addition, dicots can produce special stress-induced shoot-born roots called adventitious roots. A monocot root system produces additional axial roots, which can be separated in embryonic seminal roots and non-embryonic shoot-born roots. There are several types of shoot-borne roots, such as nodal and crown roots, often distinguished by the exact place they develop and their increasing thickness. In monocots, the primary and seminal roots are especially important during early seedling establishment, but shoot-born roots soon take over and are responsible for most of the water and nutrient uptake. All axial root types can produce several orders of lateral roots.

Roots Bridging the Yield Gap

Breeding efforts to improve crop yield are in general focused on aboveground, shoot-related phenotypes, whereas the roots as 'hidden half' of the plant are still an under-utilized source of crop improvement (Den Herder et al., 2010; Wachsman et al., 2015). Trials aimed to select for new cultivars with improved crop yield are in general performed under optimal nutrient concentrations, which has often led to selection for smaller and less plastic roots (White et al., 2013). Moreover, modern cultivars develop in general faster and the earlier initiation of shoot sinks stimulates the investment of biomass into the shoots rather than into the roots. Modern wheat cultivars indeed have smaller root sizes and root:shoot ratios than older ones (Siddique et al., 1990; Waines and Ehdaie, 2007). Given the crucial role roots play in the establishment and performance of plants, researchers have started 'the second green revolution' to explore the possibility of yield improvements through optimization of root systems (Lynch, 2007).

Because water and nutrients are not evenly distributed in the soil, the spatial arrangement of the root system is crucial for optimal use of the available resources. This spatial arrangement of the root and its components is referred to as root system architecture (RSA). Length, number, positioning, and angle of root components (as described in **Figure 1**) together determine RSA (**Figure 2**). These traits determine the soil volume that is explored. In addition, the root surface area depends on root hair development and root diameter. The ability to adjust RSA is an important aspect of plant performance and its plasticity to a large variety of abiotic conditions (Smith and De Smet, 2012). Root development is guided by environmental information that is integrated into decisions regarding how fast and in which direction to grow, and where and when to develop new lateral roots (Malamy, 2005). The limits of root system plasticity are determined by intrinsic pathways governed by genetic components (Pigliucci, 2005; Smith and De Smet, 2012; Gifford et al., 2013; Jung and McCouch, 2013). Understanding the development and architecture of roots, as well its plasticity, holds thus great potential for stabilizing the productivity under suboptimal conditions in the root environment (de Dorlodot et al., 2007; Den Herder et al., 2010; Zhu et al., 2011). Although, plants are capable of adjusting a wide range of developmental and molecular processes in the root to cope with abiotic stress, this review will mainly focus on the plasticity of RSA, their proposed adaptive values, and its use in the selection and breeding of more robust crops.

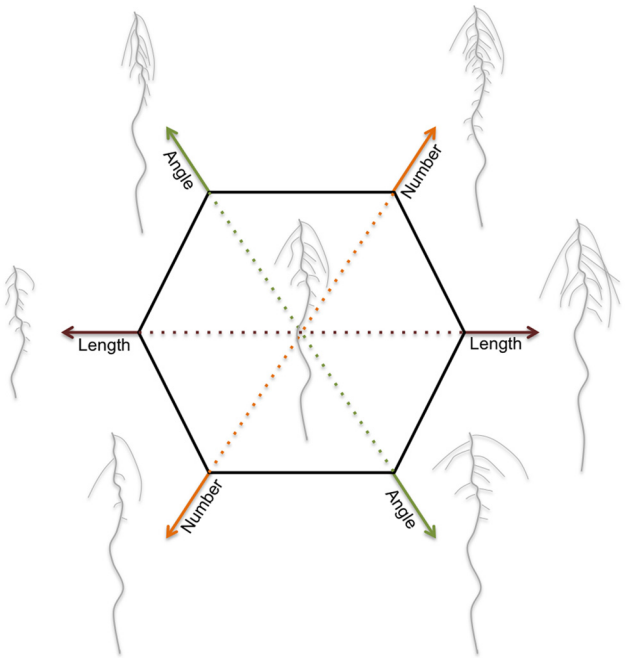

FIGURE 2 | RSA is defined as the spatial configuration of root components and determines the soil volume that can be explored by the roots. Dicot roots consist of a main root and several orders of lateral roots. Monocot roots contain in addition seminal roots and shoot-borne roots. Each plant species has genetically defined limits to its RSA. Within these limits, the RSA is plastic and external (abiotic stress) factors modulate the length, number, positioning and angle of root components. The RSA plasticity varies strongly among and within plant species. This figure illustrates the modulations in RSA for a typical dicot root system.

NUTRIENT LIMITATION: ADAPTING RSA FOR OPTIMAL FORAGING

Plants use macronutrients as the basis of proteins and nucleic acids. Especially the availability of phosphorus (P) and nitrogen (N) determine plant performance. Other nutrients are used as co-factors for enzymes or to drive membrane transport. Complications in nutrient acquisition can arise because of nutrient shortage in the soil, but other factors such as pH, the balance of different nutrients and soil composition also play a role. For examples, high salinity can decrease the solubility and thus availability of phosphate (Grattan and Grieve, 1998; Hu and Schmidhalter, 2005).

Nutrient deficiencies are responsible for the major part of currently observed yield gaps worldwide. Mueller et al. (2012) estimated that for 73% of the areas with a yield gap bigger than 25%, solely improving nutrient balances in the soil could close this gap. This illustrates the impact of nutrient imbalances and deficiencies on plant productivity. If we also consider the high use of fertilizer in agriculture, improving plants' capability of dealing with nutrient deficiencies and increasing their of nutrient acquisition is of major importance.

Nutrients are distributed heterogeneously and often have a strong vertical distribution pattern. Leaching on the one hand and plant cycling on the other hand influence the nutrient distribution pattern. Leaching is caused by vertical water flow and takes nutrients down to lower soil layers, were water flow decreases and nutrients accumulate. Plant cycling is based on nutrients taken up from and cycled back to the soil, which causes nutrients to deplete in the root zone and accumulate in the topsoil. Horizontal distribution of nutrients is mainly dependent on the plant distribution aboveground, leading to higher nutrient accumulation underneath canopies. Vertical distribution depends on the balance between leaching and plant cycling, which differs strongly between nutrients. Low mobile nutrients with a prominent role in plant growth, such as phosphate and potassium, undergo high plant cycling, leading to topsoil accumulation. In contrast, mobile nutrients, such as nitrate and chloride, are subject to leaching leading to accumulation in deeper soils (Jobbágy and Jackson, 2001, 2004). The challenge for plants is to cope with this heterogeneous and sometimes contrasting distribution of nutrients and other resources. In agriculture, plant cycling is often reduced, due to harvesting of plant material, increasing leaching and loss of nutrients. To cope with this heterogeneity, plants can adapt their RSA to specifically forage those parts of the soils where nutrient availability is high.

Recently, RSA changes upon a wide range of nutrient deficiencies have been mapped in *Arabidopsis* growing on agar plates (Gruber et al., 2013). Each deficiency led to a distinct response in RSA development, which is consistent with the fact that not all nutrients have the same accumulation pattern and thus ask for a different response. For example, the readily available forms of the two most limiting nutrients, nitrate (NO_3^-) and phosphate (PO_4^{3-}), have an almost opposite accumulation pattern in the soil (Jobbágy and Jackson, 2001). Whereas immobile phosphate accumulates in the topsoil, mobile nitrate quickly leaches to deeper soils. This challenges the plant to respond differently to a deficiency of these nutrients. Fortunately, the RSA responses to these deficiencies have been mapped extensively in both *Arabidopsis* and crop species, offering us many insights in functional RSA development.

Topsoil Foraging for Phosphate

Phosphate is a building block of, for example, nucleic acids and membrane phospholipids. Because of the high phosphate demand of plants, limitation in phosphate has a strong effect on plant growth (as reviewed in Péret et al., 2011; López-Arredondo et al., 2014). Efficient uptake of phosphate is therefore essential. High plant cycling, in combination with low mobility, leads to accumulation of phosphate in the topsoil. To optimally forage the soil for phosphate, plants need to develop a shallow root system (as reviewed in Lynch and Brown, 2001). The RSA response to phosphate deficiency in *Arabidopsis* is well-characterized (as reviewed by Péret et al., 2011). A strong shift from main root growth to lateral root growth is observed, which leads to a short root with a high number of long laterals (**Figure 3A**; Williamson, 2001; Linkohr et al., 2002; López-Bucio et al., 2002; Gruber et al., 2013). In addition, a strong proliferation of root hairs is observed.

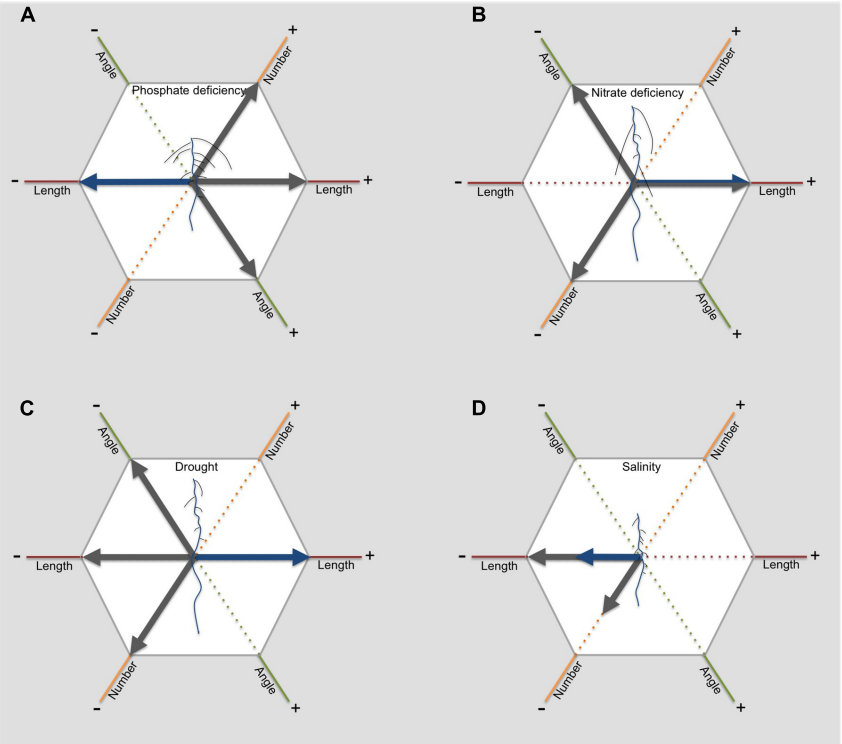

FIGURE 3 | The RSA responds to abiotic stress in different ways. This figure illustrates for dicots how length, angle and number of primary (blue) and lateral roots (grey) change in response to phosphate deficiency **(A)**, nitrate deficiency **(B)**, drought **(C)** and salinity **(D)**. The arrows indicate an either positive (to the right) or negative effect (to the left).

These changes result in a shallow root system, optimal for topsoil foraging.

For maize, a series of papers was published in which the value of certain root traits for phosphate acquisition was evaluated using a set of RILS distinctly different in these root traits. Shallow rooting maize varieties showed increased net phosphate acquisition, corrected for possible higher phosphate investments (Zhu et al., 2005b). A big screen of 242 accessions of maize on high and low phosphate availability confirmed the importance of root plasticity under low phosphate conditions (Bayuelo-Jiménez et al., 2011). Yield and biomass was increased for accessions with a higher number of nodal and lateral roots. In addition, dense root hair formation also correlated with higher biomass under low P conditions.

Shallow root system development is a result of strong investment in lateral root growth. Zhu and Lynch (2004) confirmed that in maize enhanced lateral root formation is beneficial for net phosphate acquisition. In comparison to the primary root and other components of the root system, lateral roots are cheap in terms of phosphate use. Similar results were found for enhanced seminal root growth, which is especially important for phosphate acquisition during early seedling development (Zhu et al., 2006). Several studies show that strigolactones are key regulators of both root and shoot responses to the level of available phosphate (Koltai, 2011; Ruyter-Spira et al., 2011; Mayzlish-Gati et al., 2012; Matthys et al., 2016). The effect of strigolactones on RSA depends on phosphate availability. Whereas strigolactones inhibit lateral root emergence and elongation and promote primary root elongation when phosphate is sufficient (Kapulnik et al., 2011a; Matthys et al., 2016), the opposite is observed when phosphate is depleted (Ruyter-Spira et al., 2011). Interestingly, a similar phosphate dependent effect of ABA on lateral root development has recently been observed (Kawa et al., 2016). The contrasting effect of strigolactones is a result of modulation of auxin distribution and sensitivity (Koltai et al., 2010; Ruyter-Spira et al., 2011; Mayzlish-Gati et al., 2012), both underlying the strong shift from primary to lateral root growth (López-Bucio et al., 2002; Nacry, 2005; Pérez-Torres et al., 2008a,b; Miura et al., 2011). Addition of the synthetic auxin NAA doubled expression levels of genes involved in the cell cycle specifically during phosphate starvation (Pérez-Torres et al., 2008b). Increased auxin sensitivity during phosphate starvation appears to be explained by increased expression of the auxin receptor TRANSPORT INHIBITOR RESPONSE1 (TIR1), leading to increased degradation of AUX/IAA and released repression on auxin response modules (Pérez-Torres et al., 2008a). Interestingly, strigolactones have been shown to be responsible for the increase of TIR1 expression during phosphate limitation (Mayzlish-Gati et al., 2012).

The inhibition of primary root growth in *Arabidopsis* (Col-0) in response to phosphate starvation has been shown to be strong and irreversible (Sánchez-Calderón et al., 2005).

During phosphate starvation, primary root development changes drastically, shifting from indeterminate growth to determinate growth (Sánchez-Calderón et al., 2005; Kawa et al., 2016). Preceding this drastic shift, changes in the quiescence center are observed, suggesting an important role during phosphate starvation. Consistently, Svistoonoff et al. (2007) show that specifically exposing the root cap to low phosphate is sufficient to induce growth arrest in the primary root. Mutants lacking determinate growth in low phosphate conditions show reduced activation of the phosphate starvation rescue system (Sánchez-Calderón et al., 2006). These findings suggest an important role for the root cap in sensing environmental conditions.

During phosphate limitation, *Arabidopsis* develops a high number of long root hairs (Bates and Lynch, 1996). Compared to mutants lacking root hairs, wild type plants have a higher phosphate uptake resulting in more plant growth (Bates and Lynch, 2000). Gahoonia and Nielsen (1998) measured phosphate uptake of root hairs by providing the radioisotope ^{32}P to root hairs of rye plants in the soil. The root hairs contributed to a substantial amount of 63% of total phosphate uptake. Consistently, a mutant of barley lacking root hairs took up half the amount of phosphate compared to the wild type (Gahoonia et al., 2001). Under low phosphate conditions, cultivars of barley with long root hairs are able to sustain high yields, whereas cultivars with short root hairs produce substantially less yield (Gahoonia and Nielsen, 2004). Interestingly, no disadvantage of root hair development under high phosphate availability is found for either *Arabidopsis* and Barley (Bates and Lynch, 2000, 2001; Gahoonia and Nielsen, 2004). As for other root traits, strigolactones seem to play a major role in the regulation of the number and length of root hairs (Koltai et al., 2010; Kapulnik et al., 2011a,b; Mayzlish-Gati et al., 2012).

Next to length and number of root components, the angle of the roots also determines whether a root system develops shallow or deep. Roots are able to sense gravity, allowing the main root to grow down into the soil, a response called gravitropism. Although lateral roots are also gravitropic, they typically show a gravitropic setpoint angle (GSA; Rosquete et al., 2013; Roychoudhry et al., 2013), resulting in non-vertical emergence from the main root (see also salinity and drought sections). Under low phosphate conditions, gravitropism could be expected to counteract development of a shallow root system ideal for topsoil foraging. In accordance, in common bean, development of a shallow root system depends on the ability to adjust the gravitropic offset angle. This ability indeed correlated with its ability to cope with low phosphate conditions (Bonser et al., 1995). Subsequent investigation of RILs with contrasting root gravitropic offset angles showed a strong correlation with phosphate acquisition and plant growth (Liao et al., 2004).

Deep Rooting and Selective Root Placement for Nitrate

In contrast to phosphate, nitrate is highly mobile in soils and is therefore prone to leaching. In environments where nitrate is limiting, deeper soil layers can often offer nitrogen supplies. Consistently, availability of phosphate and nitrate has contrasting effects on RSA. Low nitrate availability in general limits plant growth. However, low nitrate availability does not limit primary and lateral root elongation, enabling the root system to reach deeper layers of the soil (**Figure 3B**; Linkohr et al., 2002; Gruber et al., 2013). This shift in investment results in an increase in root:shoot ratio. For maize, a monocot species, reaching greater rooting depth requires the development of a lower number of crown roots. Maize genotypes with lower crown root number showed 45% greater rooting depth, which was accompanied with higher N acquisition (Saengwilai et al., 2014). The biggest difference in N acquisition was found in deeper layers, emphasizing the importance of a deep root system for nitrogen acquisition.

Lateral root density is not affected by homogeneous nitrate limitation. Interestingly, in a heterogeneous environment, a strong increase in lateral root density in nitrate patches is observed in both *Arabidopsis* and maize (Linkohr et al., 2002; Dina in 't Zandt et al., 2015). When plants are exposed to nitrate patches, lateral root elongation rates outside the patches were strongly decreased, indicating a shift of investment of resources. Plants are thus able to selectively place their roots to efficiently forage the soil. The mechanism of utilization of heterogeneously distributed nutrients by selective placement of lateral roots in or near nutrient enriched patches is best studied for nitrogen. However, selective root placement for a wide range of nutrients was already illustrated in 1975. A limited part of the root system of barley was exposed to high concentrations of phosphate, nitrate, ammonium, and potassium (Drew, 1975). For all of these nutrients a strong proliferation of lateral roots in the zone of high availability was observed. Growth of lateral roots in other zones was strongly limited. This emphasizes the importance of investigating this response for other nutrients.

The nitrate transporter NRT1.1 plays an important role in perceiving nitrate levels in the soil. The *nrt1.1* mutant displays no increase in lateral root proliferation in nitrate rich patches (Remans et al., 2006a), while the RSA response to homogeneous nitrate limitation is not affected in this mutant, indicating that this is not an effect of reduced nitrate uptake. Interestingly, NRT1.1 has the ability to transport auxin and this transport is inhibited by nitrate (Krouk et al., 2010). Mounier et al. (2014) showed that in nitrate patches, nitrate inhibits auxin transport by NRT1.1 out of lateral root tips and primordia, leading to auxin accumulation and stimulation of lateral root growth. Outside these patches, nitrate levels are low and NRT1.1 prevents accumulation and thus lateral root growth.

NRT1.1 has been shown to affect expression of several downstream genes involved in nitrate starvation responses, including NRT2.1 (Muños et al., 2004). NRT2.1 is a major component of high-affinity nitrate uptake in the root (Wirth et al., 2007). NRT1.1 and NRT2.1 seem to be responsible for repression of lateral root growth outside nitrate patches, based on their mutant phenotypes (Little et al., 2005; Remans et al., 2006b; Krouk et al., 2010). Nitrate starvation can trigger ethylene production, a phytohormone that influences root growth (Tian et al., 2009). NRT2.1, also induced by nitrate starvation, seems to stimulate ethylene production (Zheng et al., 2013). Conversely, ethylene inhibits NRT1.1 and NRT2.1 expression, possibly

providing a negative feedback loop important for fine tuning responses (Leblanc et al., 2008; Tian et al., 2009).

DROUGHT: SEARCHING FOR WATER SUPPLIES

Besides nutrient limitation, water limitation is the biggest driver of the yield gap. Mueller et al. (2012) have shown that in 16% of the areas with a current yield gap bigger then 25%, improving irrigation can solely close the gap. In addition, for all investigated areas improving irrigation would decrease the gap. This illustrates the importance of water availability for plants. Plants need water for transport, structure and photosynthesis among other processes. Most crops have high water requirements and are poorly drought resistant. However, irrigation is already responsible for 70% of the total use of available freshwater (FAO and ITPS, 2015). The present focus of plant breeders therefore is on improving water use efficiency of crops.

When water availability is limited, the soil osmotic potential decreases and plants are confronted with osmotic stress. Plants cannot take up water and sometimes even loose water to the soil. The high surrounding osmotic potential leads to loss of turgor, starting in the root. The combination of rapid sensing and signaling, followed by adjustments on both cellular and organ level, can enable the plant to limit water loss and survive drought stress (as reviewed in Robbins and Dinneny, 2015). Drought stress leads to distinct changes in RSA, both on whole-root system and sub-organ level.

Whole-Root Level: Deeper Rooting for Water

Water is generally stored in deeper soil layers, because the topsoil dries more quickly. Plants that develop deeper root systems will have access to water stored in these deeper layers. Among other traits, deeper rooting has been shown to be beneficial for plant production and survival under water limiting conditions (as reviewed in Comas et al., 2013). For example, the generally deeper rooting mutant *extremely drought tolerant1 (edt1)* in *Arabidopsis* shows high drought tolerance (Yu et al., 2008). This is explained by the ectopic overexpression of the HD-ZIP transcription factor *HDG11,* which directly promotes the transcription of genes encoding cell wall loosening proteins. These proteins promote cell elongation in the root, leading to an extended root system (Xu et al., 2014). Interestingly, expression of *HDG11* in other species such as rice, poplar and cotton, also confers drought tolerance (Yu et al., 2013, 2016).

Reaching deeper soils requires a shift from investment in lateral roots to investment in axile roots (**Figure 3C**). *Arabidopsis* shows a strong inhibition of lateral root emergence and elongation when grown on agar medium containing an osmoticum, such as sorbitol or mannitol, mimicking osmotic stress (Deak and Malamy, 2005; Xiong et al., 2006). Importantly, Xiong et al. (2006) showed a possible link between inhibition of lateral root growth on agar and drought tolerance in soil. Mutants performing well under drought conditions in soil, showed high sensitivity to ABA leading to strong inhibition of lateral root length on agar media. In comparison, less tolerant mutants showed no inhibition of lateral root length. ABSCISIC ACID INSENSITIVE4 (ABI4), enhanced by ABA during drought stress, can inhibit PIN1 expression, leading to decreased polar auxin transport and decreased lateral root formation (Shkolnik-Inbar and Bar-Zvi, 2010; Rowe et al., 2016). This mode of action of ABA provides a possible mechanistic explanation for the effect of ABA on lateral root formation.

Polar auxin transport by influx and efflux carriers determines auxin distribution in the root, which is not only important for LR formation, but also for bending of plant organs by differentially affecting cell elongation. This bending is essential for gravitropism of the main root. Positive gravitropism, growing in the direction of gravity, orientates the root downward and enables penetration of the soil. However, other root components, such as lateral, seminal and crown roots can display very different growth angles, partly suppressing gravitropism. The angle of these roots strongly determines whether RSA develops shallow or deep. In lateral roots PINs determine auxin distribution and thus the GSA (Rosquete et al., 2013). The magnitude of the difference in auxin concentration between the upper and lower side of the lateral root determines how strong a lateral root will bend (Roychoudhry et al., 2013). As previously described, auxin transport is inhibited during drought stress due to the inhibition of PIN1 expression (Liu et al., 2015), which might facilitate increased downward bending of the roots.

In several crop species increased downward bending of the roots is correlated with drought tolerance. In rice, a strong correlation between the angle of roots and drought tolerance is observed (Kato et al., 2006). High expression of the DEEPER ROOTING1 (DRO1) gene in rice, responsible for increased downward bending of the roots by altering the auxin distribution, results in maintained high yield under drought stress (Uga et al., 2013). This example indicates that adapting RSA, in this case both using genetic and transgenic approaches, can result in increased drought tolerance. Similar to rice, the angle of seminal roots in wheat cultivars also correlates with drought tolerance (Manschadi et al., 2008). Drought tolerant wheat cultivars develop seminal roots with a narrow angle, growing deeper into the soil.

Sub-organ Level: Hydrotropism and Hydropatterning

Although a strong vertical distribution pattern of water exists, soil heterogeneity in water content exists and sensing of available water is crucial for optimal water uptake. It has been shown that plants are able to partially repress gravitropism and grow toward water, the so-called hydrotropism response (as reviewed in Eapen et al., 2005; Takahashi et al., 2009; Cassab et al., 2013). To investigate hydrotropism in *Arabidopsis*, different growth systems have been used, in which either salt solutions or agar with sorbitol created a gradient in osmotic potential and thus a gradient in water availability. *Arabidopsis* was able to redirect growth of its main root away from a low osmotic potential and thus low water availability (Takahashi et al., 2002; Kaneyasu et al.,

2007; Moriwaki et al., 2013). This moisture-driven hydrotropic response has also been observed in other species including maize (Takahashi and Scott, 1991), cucumber (Mizuno et al., 2002), and pea (Takahashi and Suge, 1991; Takahashi et al., 1996).

As described previously, the distribution of auxin, driven by polar auxin transport, has a central role in regulating bending of plant organs and response to gravity. Interestingly, hydrotropism seems to be independent from polar auxin transport, as the repression of influx and efflux carriers of auxin do not inhibit the response (Kaneyasu et al., 2007). Recently, auxin distribution during hydrotropism was measured with the DII-VENUS SENSOR (Shkolnik et al., 2016). Indeed, during the first 2 h of hydrotropic response, no change in auxin distribution was observed. In the presence of NPA, an inhibitor of auxin transport, hydrotropic bending was not inhibited. The involvement of auxin through changes in auxin sensitivity or biosynthesis remains ellusive due to contrasting results showing either positive, negative or no effects of inhibition of auxin responses or sensitivity (Takahashi et al., 2002; Kaneyasu et al., 2007; Shkolnik et al., 2016).

It has been shown that *Arabidopsis* roots can distinguish a wet from a dry surface and selectively favor development of roots in these wet places over development in dry places (Bao et al., 2014). These wet surfaces determine where new lateral root founder cells are formed. Deak and Malamy (2005) have shown that under dry conditions lateral root primordia develop at similar rates as under control conditions. These primordia can subsequently be rapidly induced in zones with high water availability. The combination of formation and emergence of primordia leads to specific root proliferation at sites of high water availability, so-called hydropatterning. This process seems to be independent of the major drought stress hormone, ABA (Bao et al., 2014). Further research on this new topic is required to provide more knowledge on how plant roots sense moisture and adjust RSA accordingly.

SALINITY

Salinity is a major and increasing problem for agriculture (Rengasamy, 2006). Most crop species are salt sensitive and grow poorly on salinized soils (Sairam and Tyagi, 2004; Munns et al., 2006; Munns and Tester, 2008). In 1992, the extent of salinity-affected soils was estimated at 410 billion ha. Although an adequate mapping of the current extent of salinized soils is lacking, over 100 countries are confronted with soil salinization. On a yearly basis between 0.3 and 1.5 million ha of arable land are lost to salinization and another 20–40 million ha are strongly affected by salinity (FAO and ITPS, 2015). Although some of these are naturally occurring saline soils, current observed salinization is often the result of irrigation practices. Irrigation in arid zones, accounting for approximately 40% of irrigation worldwide, mobilizes salts stored in the deeper soil layers (Smedema and Shiati, 2002). In addition, due to freshwater scarcity, an increased use of brackish irrigation increases salt levels even further. The increasing losses of arable land due to salinization ask for the development of salt tolerant crops.

Similar to drought, salinity can cause problems due to the high osmotic potential in the soil, leading to osmotic stress. In addition, salinity affects plant growth due to the toxicity of high sodium Na^+ levels. Na^+ toxicity especially causes problems in the shoot by inhibiting photosynthesis among other processes (Munns, 2002). Na^+ is chemically similar to K^+ and can interfere with processes in which K^+ plays an essential role (Benito et al., 2014). The capacity to maintain a low Na^+/K^+ balance in the shoot has been shown to be closely linked to salt tolerance (Møller et al., 2009). Preventing Na^+ transport to the shoot is thus very important. The root system is responsible for water uptake, accompanied by dissolved ions including Na^+, and thus plays an essential role in preventing Na^+ from entering the vascular system and reaching the shoot.

Remodeling of the Root System during Salt Stress

Salt has a distinct effect on root growth (as reviewed in Galvan-Ampudia and Testerink, 2011). Although, low salt concentrations up to 50 mM can promote plant growth in *Arabidopsis* (Zolla et al., 2010; Zhao et al., 2011; Julkowska et al., 2014), higher salt concentrations have severe negative effects. Both primary and lateral root growth is inhibited during salt stress (**Figure 3D**; Julkowska et al., 2014). In addition, lateral root number specifically decreases in the root zone developed after exposure to salt stress (**Figure 3D**; Julkowska et al., 2014). Most studies show no effect of salt stress on lateral root density, indicating that the decrease in number of lateral roots is related to the inhibition of primary root growth (Julkowska et al., 2014).

Within seconds after exposure to salt stress, plant signaling is activated. This early signaling leads to adjustments in plant growth (as reviewed in Julkowska and Testerink, 2015), starting with a quiescence of growth in all plant organs. The quiescence phase is caused by a temporary inhibition of mitotic activity, leading to lower cell division rates (West et al., 2004). After the quiescence phase, growth recovers again. However, growth rates only recover to a certain extent, because the inhibition of the cell cycle during the quiescence phase results in fewer cells in the meristem (West et al., 2004). In addition, mature cell length is smaller in salt stressed roots.

Quiescence is induced by abscisic acid (ABA), which is rapidly up-regulated under salt stress due to the decrease in osmotic potential (Jia et al., 2002; Duan et al., 2013; Geng et al., 2013). ABA in general inhibits both gibberellin (GA) and brassinosteroid (BR) signaling (Achard et al., 2006; Gallego-Bartolome et al., 2012) and stress-induced reduction of growth has been shown to benefit the plant (Achard et al., 2006). It is thus proposed that the quiescence phase is essential to induce changes to cope with salt stress. The quiescence phase is followed by a partial growth recovery, that is mainly guided by an increase in GA and BR levels (Geng et al., 2013).

The length of the quiescence phase differs strongly between root components. Whereas quiescence in the main root takes approximately 8 h, this phase can take up to 2 days in lateral roots (Duan et al., 2013; Geng et al., 2013). In a similar way, the recovery extent of different organs differs. Although overall an

inhibition of root growth is observed, there is a distinct difference between the effects of salt on primary in comparison to lateral root growth. Julkowska et al. (2014) have shown that in Col-0 the relative growth rate of the primary root was more strongly affected than the growth rate of the lateral roots. This indicates that the RSA is remodeled during salt stress. The adaptive value of this remodeling with respect to salinity tolerance is still unclear and requires further research.

In a screen of 32 *Arabidopsis* accessions, a first indication for a relation between remodeling of RSA during salt stress and salt tolerance was found (Julkowska et al., 2014). The screen revealed four distinct growth strategies during salt stress, depending on the relative inhibition of the number of lateral roots, main root and lateral root growth rates. One of these strategies was correlated with a much lower Na^+/K^+ level in the shoot, indicating less Na^+ uptake and thus a higher tolerance. This strategy is characterized by a strong inhibition of lateral root growth rates, while main root growth rates and number of lateral roots are much less affected (**Figure 3D**).

Besides remodeling of the root system during salt stress, plants also show reduced gravitropism under saline conditions (Sun et al., 2007). Galvan-Ampudia et al. (2013) showed that plants can specifically redirect growth away from higher salt concentrations, a response called halotropism. This response was observed in *Arabidopsis*, tomato and sorghum seedlings, both on agar media and in soil. Similar to gravitropism, auxin redistribution is central in regulating halotropism. Endocytosis of PIN2, an auxin efflux carrier, at the side of high salt concentrations, redistributes auxin in the root (Galvan-Ampudia et al., 2013). The redistribution of auxin is supported by auxin-induced expression of AUX1, an auxin influx carrier (van den Berg et al., 2016). Both mathematical modeling and experimental data have shown that these processes, together with a transient PIN1 increase, are responsible for the root bending away from salt (Galvan-Ampudia et al., 2013; van den Berg et al., 2016).

Part of the salinity response is also triggered by osmotic stress and shows overlap with drought responses. However, the changes in RSA show distinct differences. For example, main root growth is strongly promoted during drought, whereas it is inhibited during salt stress. It is not well-known whether the above described quiescence phase is also displayed during drought stress. Because the osmotic component of salinity is believed to underlie this response, it is worth investigating. For halotropism and hydrotropism, although similar responses, the underlying mechanisms seem to differ. In contrast to halotropism, hydrotropism has shown to be independent of auxin transport (Kaneyasu et al., 2007). Halotropism is dependent on auxin distribution and occurs only in response to Na^+ ions, indicating it is a specific response to high salinity (Galvan-Ampudia et al., 2013; Pierik and Testerink, 2014). For drought stress, the function of changes in RSA has been studied extensively, whereas salinity research has been more focused on the underlying mechanistic principles. In future research, studying the overlaps and differences between these stresses can benefit knowledge in both areas.

Most crop species are highly sensitive to salinity. Tomato serves as a model crop that is widely used to study how salt tolerance can be enhanced in crop species. For a wide range of vegetables, including tomato, grafting is a very effective way to increase crop resistance to biotic and abiotic stresses, without affecting above ground characteristics (see also challenge 3 in section on crop selection). For several salt sensitive commercial tomato cultivars, grafting onto rootstocks of more tolerant cultivars has positive effects on productivity when exposed to high salinity (Estañ et al., 2005; Martinez-Rodriguez et al., 2008). The Na^+/K^+ levels in the shoot (scions) indicated that the tolerant rootstocks prevented Na^+ reaching the shoot, illustrating the importance of the root system for salt tolerance. Unfortunately, only little is known about RSA development of crops during salt stress. In rice, rye, and maize inhibition of root length has been observed under high salinity (Rodriguez et al., 1997; Rahman et al., 2001; Ogawa et al., 2006). Similar to *Arabidopsis*, maize shows a quiescence phase in response to exposure to high salinity, followed by recovery (Rodriguez et al., 1997). In rye, the reduction in root growth is related to a reduction in cell division and an increase in cell death (Ogawa et al., 2006). Further research on remodeling of the root system of crop species will be necessary to use our current knowledge in *Arabidopsis* to improve crop tolerance to salinity.

FLOODING: ANAEROBIC STRESS

Already 10% of cultivated land surface is so poorly drained that waterlogging, leading to anoxic conditions in the root zone, causes crop yield losses. Twenty percent of agricultural land in Eastern Europe and the Russian Federation and 16% in the USA are too wet for optimal plant functioning (Setter and Waters, 2003). As climate change is expected to lead to more frequent heavy precipitation during the plant growth season in some areas, these problems will increase. Flooding and hypoxia impose an immediate and dramatic limitation for root functioning. Limiting the oxygen supply to root cells causes an almost instantaneous arrest of root growth (as reviewed in Gibbs et al., 1998). Switching from aerobic respiration to the glycolytic generation of ATP leads to a severe reduction in energy available for maintenance, growth and ion uptake. Of these three different functions, growth takes 20–45% of ATP generated through respiration (Veen, 1981; van der Werf et al., 1988; Poorter et al., 1991; Scheurwater et al., 1998, 1999). Balancing the demand for energy with the reduced production through glycolysis could therefore also cause limiting root growth. Arrest of root growth could, however, also be caused by accumulation of products of anaerobic metabolism. A lethal drop in pH of the cytoplasm can occur when protons accumulate in the cytoplasm and the vacuole (Gerendás and Ratcliffe, 2002). In *Phragmites australis* addition of low molecular weight monocarboxylic acids, such as acetic acid, propionic acid, butyric acid and caproic acid, and sulfide, at concentration levels that have been measured *in situ*, arrested root elongation (Armstrong and Armstrong, 2001). As the rate of root elongation is one of the most important parameters determining nutrient uptake rate (Silberbush and Barber, 1983; Dunbabin, 2006),

flooding-induced inhibition of root growth ultimately would lead to nutrient limitation and negatively impact the survival of the whole plant.

One of the best-studied adaptations of plants to flooding conditions is the formation of aerenchymatic tissue in the root, which provides an alternative pathway for the supply of oxygen to the root tissue (Jackson and Armstrong, 1999; Gibberd et al., 2001; Rubinigg et al., 2002). This requires that new, well-adapted, adventitious roots are being formed (Visser et al., 1996). In these roots, axial oxygen loss can be kept to a minimum so that the root tip becomes a well-oxygenated micro-climate (Jackson and Armstrong, 1999). Most of the disadvantages for root metabolism imposed by the flooding-induced hypoxic conditions are thereby ameliorated. In monocot plants the formation of new nodal roots, replacing the old seminal roots and often containing aerenchyma, can be stimulated, leading to superficial rooting patterns (Rich and Watt, 2013). If plants are not capable of increasing their oxygen supply through aerenchymous conducts in the root or by placing new roots close to the soil surface where the oxygen level might be higher, survival of flooding is unlikely.

TEMPERATURE

Temperature is a key abiotic factor involved in seed germination and subsequent root system development during early seedling establishment. The temperature of the soil fluctuates by sinusoidal oscillations on a diurnal scale. However, depending on soil depth, changes in soil temperature are delayed and much lower in amplitude than variations in the atmospheric temperature (Walter et al., 2009). The root-zone temperature (RZT) thus fluctuates daily, seasonally, and with soil depth (Füllner et al., 2012). Depending on the season and the time of the day, the temperature of the root environment can be significantly different than the atmospheric temperature experienced by the shoots. The RZT directly affects root development, uptake and upward transport of water and nutrients (Aroca et al., 2001), phytohormone production (Ali et al., 1996; Veselova et al., 2005), which in turn affect water status (Bloom et al., 2004), stomatal conductance (Dodd et al., 2000), photosynthesis (Hurewitz and Janes, 1983), biomass partitioning (Delucia et al., 1992; Engels, 1994), leaf (Poiré et al., 2010), and shoot growth (Venema et al., 2008; Sakamoto and Suzuki, 2015). Plant species clearly differ in their optimal temperature range for root development; e.g., oat 4–7°C (Nielsen et al., 1960), wheat 14–18°C (Porter and Gawith, 1999), pea 15–20°C (Gladish and Rost, 1993), tomato 22–25°C (Gosselin and Trudel, 1984), sunflower 25–30°C (Seiler, 1998), and cotton 32–35°C (Mcmichael et al., 1993). Root:shoot ratios usually increase under unfavorable RZTs as long as temperature limits for root development are not reached (Engels, 1994; Venema et al., 2008; Füllner et al., 2012). This adaptation in root:shoot ratio may overcome restrictions in water and nutrient uptake due to increased water viscosity and/or decreased root hydraulic conductance (Equiza et al., 2001; Aroca et al., 2012). Global climate change is likely to exacerbate plant abiotic stress in coming decades by increasing fluctuations in soil temperature and (related) water availability (Lynch and Brown, 2012). Breeding crops with a broader root-zone temperature optimum is therefore of significant importance to improve future plant performance. Improved knowledge of the key regulators for RSA optimization would support these breeding efforts.

Temperature Effects on RSA

The exposure of both mono- and dicot plant roots to temperatures below or above their optimum temperature generally decreases (i) primary root length, (ii) lateral root density (numbers of lateral roots per unit primary root length) and (iii) the angle under which lateral roots emerge from the primary root, whereas the average lateral root length is unaffected (Mcmichael et al., 1993; Seiler, 1998; Nagel et al., 2009). In addition, roots suffering from supraoptimal temperature stress start to initiate second and third order laterals (Pardales et al., 1999) and are characterized by an increased average root diameter (Qin et al., 2007). In general, the modulating effect of sub- and supraoptimal RZTs on RSA development reduces the volume that roots may access for the uptake of water and nutrients. However, root temperature was kept spatially uniform in all these studies. Remarkably, monocot barley plants exposed to a vertical RZT gradient of 20–10°C showed increased shoot and root dry masses of 144 and 297%, respectively, and a 161% increase in root:shoot ratio compared with plants grown at a uniform RZT of 20°C (Füllner et al., 2012). Barley exposed to the vertical RZT revealed also accelerated tiller formation. The higher root biomass of plants grown at the vertical RZT gradient was not the result of longer roots but was associated with a higher proportion of thicker roots. Additionally, root systems developed under a vertical RZT gradient were much stronger concentrated in the upper 10 cm of the soil substrate gradient and their N and C concentrations were significantly lower than under uniform RZT conditions. These data clearly demonstrate that knowledge gained from experiments with uniform RZTs cannot simply be extrapolated to the field where roots experience vertical temperature gradients.

The temperature dependence of RSA development shows strong inter- (Mcmichael et al., 1993; Lee et al., 2009) and intraspecific variation (Seiler, 1998; Hund et al., 2007, 2008). The temperature plasticity of the RSA is most extensively studied in maize. In this monocot species, the total lateral root length correlated significantly with improved photosynthesis-related traits and dry matter accumulation at suboptimal growth temperature (Hund et al., 2007). A high density of long lateral roots was therefore regarded as a promising trait to improve early seedling vigor at suboptimal soil temperatures (Hund et al., 2008). Nevertheless, breeding has to focus on optimizing RSA over a broad range of RZTs as roots also experience temperatures in the optimal- or even supraoptimal range during the entire growth season. At high (root-zone) temperatures the development of long axile roots is of greater importance than lateral roots to facilitate appropriate water uptake from the lower soil layers in times of drought stress (Hund et al., 2008). A schematic overview of general observed effects of non-optimal temperatures on RSA and its adaptations to broaden the RZT range for optimal plant performance are presented in **Figure 4**.

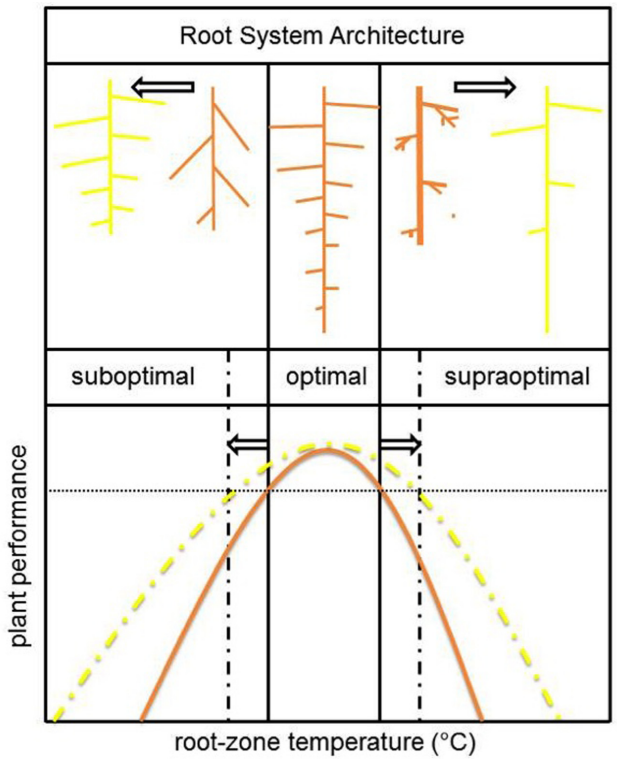

FIGURE 4 | Schematic overview of the effect of root-zone temperature on plant performance and underlying general changes in RSA (brown). To broaden the temperature range for optimal plant performance (yellow), plants should invest in lateral root formation (suboptimal temperature range) and/or axile root length (supraoptimal temperature range). The adaptive value of these RSA changes are, respectively, an increased root surface area to improve resource uptake capacity and drought adaptation by penetration to lower soil layers.

To optimize RSA over a broader temperature range, Hund et al. (2012) provided the prove-of-concept that hybrids of southern dent and northern flint maize inbred lines, which contrast in temperature dependence of axile and lateral root elongation rates, showed improved rooting potential across the sum of all temperatures. Application of this heterosis effect can lead to hybrids that can perform well in a broader range of temperature conditions, thereby improving the robustness of whole-plant performance.

Temperature Modulation of Root Elongation

The primary stunting effect of sub- and supraoptimal temperatures on RSA is caused by inhibition of root elongation (Pahlavanian and Silk, 1988; Pritchard et al., 1990; Pardales et al., 1992; Gladish and Rost, 1993; Nagel et al., 2009). In *Arabidopsis* accessions, the relative decrease in root elongation rates after transfer from 21 to 10°C were not significantly correlated with the average temperature during the growing season of the specific ecotype, suggesting that primary root growth at 10°C is not a key factor in adaptation to colder habitats (Lee et al., 2009). Within tomato, however, the relative inhibition of root elongation and root growth rates at low temperatures were indicative for the difference in chilling tolerance between domestic cultivars and high-altitude accessions of the wild tomato *Solanum habrochaites* (Zamir and Gadish, 1987; Venema et al., 2008). Dynamic changes in temperature severely affect the elongation rate of root cells rather than the length of the elongation zone (Nagel et al., 2009). In the short-term (hours), inhibition in root cell elongation by low temperature is related to a decrease in the *in vivo* extensibility of the cell wall (Pritchard et al., 1990). Gravitropism experiments with *Arabidopsis* roots demonstrated that acute cold stress (4°C) selectively inhibits the basipetal auxin transport due to blocking the intracellular trafficking of a subset of proteins that include auxin efflux carriers (*PIN2* and *PIN3*). As a consequence, auxin accumulates to a level at which root cell elongation is inhibited (Shibasaki et al., 2009). When plant roots have enough time to acclimate to a constant low RZT (weeks), cell elongation rates increase again and the length of the elongation zone expands (Pahlavanian and Silk, 1988). This may explain the strong linear relationship between temperature and elongation rates of both primary and later roots directly after germination and its disappearance later on during seedling establishment (Aguirrezabal and Tardieu, 1996).

Variation in root elongation rates among *Arabidopsis* accessions correlated at optimal temperature with the production rate of cells within the root meristem (Beemster et al., 2002). Cell production, in turn, was determined by variation in cell cycle duration and, to a lesser extent, by differences in the number of dividing cells. Cell production rates strongly correlated with the activity of the cyclin-dependent kinase (CDKA). Low temperature decreased the division potential of the root meristem in *Arabidopsis* by reducing both the meristem size and cell number (Zhu et al., 2015). The repression of the division potential of root meristematic cells at a suboptimal temperature of 16°C could be ascribed to a reduced accumulation of auxin in the root apex. Long-term (7 days) exposure to 16°C inhibited the expression of *PIN1/3/7* and auxin biosynthesis-related genes suggesting that auxin transport and biosynthesis both contribute to the low-temperature mediated reduction of auxin accumulation in roots tips. Root length and meristem cell number of ARABIDOPSIS RESPONSE REGULATOR 1 (*arr1-3*) and 12 (*arr12-1*) cytokinin signaling mutants were much less susceptible to low temperature than wild-type roots. This difference was related to higher *PIN1/3* expression in the mutants, which in turn resulted in a less pronounced reduction in auxin accumulation. These data, together with the results obtained with the cytokinin signaling mutant *ahp1-1 ahp2-1 ahp3*, strongly suggest the involvement of cytokinin signaling in the modulation of RSA development at low temperature (Zhu et al., 2015).

High RZT (40°C) reduced the elongation and cell production rate of Sorghum seminal roots with 14 and 26%, respectively, for every 2 days of exposure (Pardales et al., 1992). In contrast to low temperatures, the underlying inhibitory effects of high temperatures and heat stress on root elongation are poorly studied. The limited information that is available in the literature excludes the involvement of altered IAA transport

or levels (Gladish et al., 2000), but supports the involvement of increased ethylene levels (Qin et al., 2007). Inhibitors of ethylene biosynthesis partly alleviated the effect of high RZT on root elongation, stomatal conductance and shoot water status, however, they failed in ameliorating the negative effects on photosynthesis and biomass accumulation. This points to a non-stomatal limitation of photosynthesis mediated by high temperature-induced changes in nutrient uptake (Qin et al., 2007).

CROP SELECTION ON RSA: THE CHALLENGES

This review presents a number of examples in which plasticity of RSA traits considerably impact a plant's capability to cope with one or more abiotic stresses. These examples emphasize the great potential that selection on RSA traits holds for crop improvement. However, the aboveground focus of crop selection is not without reason. In this concluding section we will discuss three major challenges breeders face when applying selection for RSA in their crop improvement programs and possible ways to tackle these.

Challenge 1: High Throughput Belowground Screening

The most prominent challenge for crop selection on RSA is uncovering the hidden world of plant roots. Whether crops are grown in fields or in greenhouses, roots are usually grown in a substrate, which prevents easily screening their properties. The growth substrate also greatly affects how roots develop. The currently most common method to investigate RSA, growth on agar medium, is very artificial. Most often roots grow in light, with an excess of sucrose, in 2D and the humidity inside the Petri dish is almost saturated. Effort is taken to improve this system, for example by shielding the roots from light (Silva-Navas et al., 2015). Although agar media provide an easy, adequate and cheap method that can be used for research on *Arabidopsis* in the lab, its use in crop selection is not straightforward.

In the last decade a wide range of new and improved methods to research roots in a more natural environment have been developed (as reviewed in Zhu et al., 2011; Downie et al., 2015; Judd et al., 2015; Kuijken et al., 2015). Most systems are based on either a transparent growth medium or a medium from which the roots can easily be removed without damage. Agar and other gel-like mediums are suited for imaging during growth, although the resistance of the medium influences root growth and the humidity in these substances is very high. A good alternative is hydroponics, in which the root is growing inside a nutrient solution (Tocquin et al., 2003; Chen et al., 2011; Le Marié et al., 2014; Mathieu et al., 2015). Hydroponics is also used in greenhouse culture, making it highly relevant for crop selection. This system also eases harvesting roots for different purposes and measuring exudates of roots. However, roots develop very differently, because resistance is lacking and humidity and nutrients are dispersed homogeneously. In addition, a good supply of oxygen is essential to prevent oxidative stress. A third alternative which is also very promising for automated imaging is aeroponics (Zobel et al., 1976; Ritter et al., 2001). In this system roots are grown in water-saturated air created by for example spraying with water and nutrients. This system lacks any material to grow in, which eases imaging. However, without much resistance, roots grow very vast and can have problems extending their root system to the sides against gravity. Last, root systems can be grown inside soil, which is of course most realistic for field crops and many greenhouse crops. However, non-destructive imaging inside soil asks for imaging methods that reach further than a simple camera. Several groups have recently reported the use of X-ray and MRI scans to image roots inside the soil (Mooney et al., 2012; Mairhofer et al., 2013; Metzner et al., 2015; Wang et al., 2015). Although these methods are more expensive, they offer great opportunities for automated imaging. An alternative method is GLO-Roots, based on luminescence genes expressed inside roots (Rellán-Álvarez et al., 2015). This system visualizes the root system through a thin layer of soil. For fundamental research labs, this is more feasible and also offers the opportunities to image the expression of certain genes in the root system. For root breeding, this is less interesting, because the plants are genetically modified and grown in 2D systems.

As more methods come available to study the root system and also methods are developed suitable for high-throughput screening of root systems, the need for good root image analysis software is growing. A wide range of root image analysis software exists (as reviewed in Lobet et al., 2013; Spalding and Miller, 2013; Kuijken et al., 2015). These tools range from automated to non-automated. For a limited amount of data, non-automated software prevents mistakes and gives the user a lot of freedom. However, the analysis is very time consuming and is therefore not suited for large datasets. Automated software can analyze a large dataset rapidly, but especially in complex root systems the analysis is limited to global data such as rooting depth and width. In semi-automated software, such as SmartRoot (Lobet et al., 2011) and EZ-rhizo (Armengaud et al., 2009), the level of user interactions is greater to ensure a lesser degree of analysis errors. Again, this will be more time consuming for larger root systems. In addition, when observing very large root systems, it is even hard to separate roots by eye. Therefore, the development of improved methods of root image analysis has high priority for the field.

Above described methods are all suited for 2D images of root systems. When simplifying root growth to a 2D system, spatial orientation of roots gets lost. Therefore, new methods such as growing roots in gel cylinders (Iyer-Pascuzzi et al., 2010) and using X-ray to image through soil will offer sophisticated opportunities to grow and image roots in 3D (as reviewed in Piñeros et al., 2016). Although only limited options for reconstructing and analyzing 3D images are currently available, it might eventually be easier to analyze 3D than 2D images, because overlapping and clumping together of roots will be much less common. Developing a good automated imaging analysis set-up of root systems can offer great advancements in crop selection and would be an entirely feasible investment for breeding companies.

Challenge 2: Dealing with the Complexity of Interacting Stresses

Although the complexity of the combination of different biotic and abiotic stresses is not restricted to the root system, it does make selecting on RSA more challenging. The described RSA responses are mostly known for single stresses and some of the responses are very contrasting. A good example for this is that in drought-tolerant cultivars with a deep-rooting water-conserving phenotype, less root mass is available to forage for phosphorous at shallow depths (Lynch and Wojciechowski, 2015). Certain stresses tend to occur together often and therefore it might be useful to further investigate the specific RSA response to these conditions. A good example is salt stress and phosphate starvation, as phosphate ions tend to precipitate in saline soils and become unavailable to plants (Naidu and Rengasamy, 1993; Grattan and Grieve, 1998). Both stresses have contrasting effects on several RSA traits and the inhibiting effect of salt on lateral root development might even further limit phosphate uptake. Crucial in crop breeding aimed to optimize RSA is the availability of variation and plasticity in RSA, as observed among *Arabidopsis* accessions (Mouchel et al., 2004; Rosas et al., 2013; Ristova and Busch, 2014), related tomato species (Ron et al., 2013) and wheat varieties (Pound et al., 2013). Recently, Kawa et al. (2016) studied the natural variation in the response of 330 *Arabidopsis* accessions to the combination of salinity and phosphate starvation. In general, responses to salt stress were favored and especially lateral root growth was strongly inhibited. However, not all accessions showed the same response and this natural variation was associated with 13 genetic candidate loci for integrating the plants' response to combined stress (Kawa et al., 2016). For many crops, however, the natural variation in RSA is currently still underexploited. Moreover, we need to advance our understanding of the adaptive value of genetically determined differences in RSA on the level of crop performance, marketable yield and fruit quality in targeted root environments and growth conditions.

Because the complexity of experiments and screenings increases with every additional variable, modeling can provide very useful tools to support research and breeding. A wide range of plant models on different scales is available to the community. These models should now be integrated with a multiscale modeling approach (Band et al., 2012; Rellán-Álvarez et al., 2016) in which developmental processes, RSA, outside environmental factors and plant performance are connected. Current models, however, are often not easy to integrate. When developing a model, the general challenge is to make it comprehensive, widely applicable and simple. For models describing RSA, most are falling short in one of these requirements. Some are only applicable for a certain species or stage of life, which limits the use for crop systems. As soon as models tend to be more widely applicable or incorporate more conditions, they tend to become more complex and the number of parameters increases. This decreases the ease of interpretation and especially the ease of integration into a larger model (including soil and plant performance models). The last few years, a range of more simple models have been published. These models are often based on a few simple rules. For example, ArchiSimple bases root system development on the fact that the growth rate of a root depends on the thickness of the root (Pagès and Picon-Cochard, 2014; Pagés et al., 2014). By using a simple and widely applicable model, it will be possible to implement models of soil behavior and of plant productivity. Some of the root models have already been integrated with models for changes in the soil (as reviewed in Pedersen et al., 2010; Dunbabin et al., 2013; Van der Putten et al., 2013) and show to be very promising in predicting the responses of the root system. One example is the ROOTMAP model, which integrates soil-water-nutrient dynamics with root growth responses in a three dimensional system (Dunbabin et al., 2002). Simulations are based on a simple external supply/internal demand principle. The model has shown its use in simulating the efficiency of different RSA types in both heterogeneous phosphate and nitrate supplies (Dunbabin et al., 2004; Chen et al., 2008). A good example of how such a model can provide valuable information is given by Chen et al. (2008), who show how the model can guide the efficient placement of phosphorus fertilizer. In a similar way, this kind of model could guide in selecting a preferred RSA and potentially even predicting possibly involved processes.

A model that integrates soil behavior, RSA and plant performance will offer a lot of information to breeders. To confirm whether a root system is advantageous under certain stresses as predicted by the model, RILS with contrasting root systems could be exploited (as illustrated in Liao et al., 2004; Zhu and Lynch, 2004; Zhu et al., 2005a). If indeed the predicted root system is advantageous, breeders could screen for this type of root system in a high throughput phenotyping system as described in the previous section. This screen can then be used for determining genes that are associated with this trait and can be used as targets for further selection. The model could also predict whether changing certain root system characteristics would negatively influence productivity. Of course, developing such a model is a major challenge still, but investments in developing a good model will be able to speed up crop selection and could model complex combinations of stresses.

Challenge 3: Improving RSA without Compromising Yields

Crop selection on aboveground traits has lead to high-yielding cultivars and crop selection for a certain RSA may come with costs. The root:shoot ratio is known to increase during almost every abiotic stress that has been discussed in this review. On the other hand, selection on RSA does not equal selection for a bigger root system. Our examples show shifts between different root organs, rather than shifts in biomass partitioning between the shoot and the root. In this way, deeper rooting in rice, caused by expression of *HDG11*, confers drought tolerance without any yield penalty (Yu et al., 2013, 2016). However, unwanted side effects of selection are not uncommon. An excellent tool to address this problem is to make use of grafting.

Grafting is the process in which the root system (rootstock) of one plant is connected to the shoot (scion) of another (as reviewed in Warschefsky et al., 2016). This process naturally

occurs in some tree species (Mudge et al., 2009) and this phenomenon may have triggered the development of grafting in Asia where it is now used in agriculture for over 2000 years to improve plant production (Kubota et al., 2008). In woody perennial crops (Albacete et al., 2015; Warschefsky et al., 2016) as well as in annual vegetable crops (Schwarz et al., 2010; Albacete et al., 2015), the selection and breeding of suitable rootstocks offers a powerful tool to sustain and expand the cultivation under suboptimal growth conditions (Gregory et al., 2013). Grafting has the advantage that not every cultivar needs RSA optimization separately, allowing improvement of rooting and (a)biotic stress tolerance of already existing elite cultivars. As such, grafting is considered as a surgical and fast alternative to breeding. Designing rootstocks for specific environments is becoming a feasible target to face future cultivation problems all around the world associated with global climate change (drought, salinization, occurrence of temperature extremes; Gregory et al., 2013). Important in this respect is to gain more knowledge of (i) the natural variation in RSA that exists within crops, and (ii) by what communication mechanisms the root(stock) modulates the shoot (scion) phenotype and performance, and visa versa (Warschefsky et al., 2016). In this way, grafting can rapidly advance our understanding of the adaptive value of differences in RSA on the level of shoot performance, marketable yield and fruit quality under targeted growth conditions.

THE VALUE OF MODEL SPECIES

A key aspect for engineering better performing crops via RSA optimization is improved understanding of the regulatory processes and underlying genetic components that regulate root growth. Root growth regulation, and its response to changing environmental conditions, is a highly complicated process that is controlled at many different levels by complex actions of gene networks in both time and space. Advances in this area are merely derived from work in *Arabidopsis* (as reviewed in Wachsman et al., 2015; Slovak et al., 2016). It is expected that due to the increasing number of highly efficient root phenotyping platforms, the use of GWAS for root traits, the increasing available functional genomics resources for roots, and the development of smart root model systems, much progress in our understanding of control mechanisms involved in root development will be achieved over the next 5–10 years.

Although *Arabidopsis* is often studied under artificial conditions, it is these conditions that make it possible to investigate the partly discussed mechanistic and cellular base behind the observed RSA responses. For crop species only limited information on these processes is available. Interestingly, most plasticity in RSA responses overlaps between our model species and crops, even independent of differences between monocots and dicots. Sparsely investigated functionality of RSA in *Arabidopsis* supports the results found in crops and conversely sparsely investigated molecular insights in crops confirmed results already established in *Arabidopsis*. Of course, not all mechanisms, responses and genes can be transferred from *Arabidopsis* to crops, but taken together the reviewed research, *Arabidopsis* proves to provide very valuable information for the development of crops able to withstand a wide range of abiotic stresses. This review stresses the importance of incorporating RSA into current crop selection, but we should not forget the wonderful tools we already have. Incorporating RSA into current crop selection also means incorporating *Arabidopsis* research into the current breeding pipeline, possibly even more then for aboveground traits.

AUTHOR CONTRIBUTIONS

All authors listed, have made substantial, direct and intellectual contribution to the work, and approved it for publication.

FUNDING

This work was supported by the Netherlands Organization for Scientific Research (NWO) ALW Graduate Program grant 831.15.004 to IK and CT.

REFERENCES

Achard, P., Cheng, H., De Grauwe, L., Decat, J., Schoutteten, H., Moritz, T., et al. (2006). Integration of plant responses to environmentally activated phytohormonal signals. *Science* 311, 91–94. doi: 10.1126/science.1118642

Aguirrezabal, L. A. N., and Tardieu, F. (1996). An architectural analysis of the elongation of field-grown sunflower root systems. Elements for modelling the effects of temperature and intercepted radiation. *J. Exp. Bot.* 47, 411–420. doi: 10.1093/jxb/47.3.411

Albacete, A., Martínez-Andújar, C., Martínez-Pérez, A., Thompson, A. J., Dodd, I. C., and Pérez-Alfocea, F. (2015). Unravelling rootstock × scion interactions to improve food security. *J. Exp. Bot.* 66, 2211–2226. doi: 10.1093/jxb/erv027

Ali, I., Kafkafi, U., Yamaguchi, I., Sugimoto, Y., and Inanaga, S. (1996). Effects of low root temperature on sap flow rate, soluble carbohydrates, nitrate contents and on cytokinin and gibberellin levels in root xylem exudate of sand-grown tomato. *J. Plant Nutr.* 19, 619–634.

Armengaud, P., Zambaux, K., Hills, A., Sulpice, R., Pattison, R. J., Blatt, M. R., et al. (2009). EZ-Rhizo: integrated software for the fast and accurate measurement of root system architecture. *Plant J.* 57, 945–956. doi: 10.1111/j.1365-313X.2008.03739.x

Armstrong, J., and Armstrong, W. (2001). An overview of the effects of phytotoxins on Pragmites australis in relation to die-back. *Aquat. Bot.* 69, 251–268. doi: 10.1016/S0304-3770(01)00142-5

Aroca, R., Porcel, R., and Ruiz-Lozano, J. M. (2012). Regulation of root water uptake under abiotic stress conditions. *J. Exp. Bot.* 63, 43–57. doi: 10.1093/jxb/err266

Aroca, R., Tognoni, F., Irigoyen, J. J., Sánchez-Díaz, M., and Pardossi, A. (2001). Different root low temperature response of two maize genotypes differing in chilling sensitivity. *Plant Physiol. Biochem.* 39, 1067–1073. doi: 10.1016/S0981-9428(01)01335-3

Band, L. R., Fozard, J. A., Godin, C., Jensen, O. E., Pridmore, T., Bennett, M. J., et al. (2012). Multiscale systems analysis of root growth and development: modeling beyond the network and cellular scales. *Plant Cell* 24, 3892–3906. doi: 10.1105/tpc.112.101550

Bao, Y., Aggarwal, P., Robbins, N. E., Sturrock, C. J., Thompson, M. C., Tan, H. Q., et al. (2014). Plant roots use a patterning mechanism to position lateral root branches toward available water. *Proc. Natl. Acad. Sci. U.S.A.* 111, 9319–9324. doi: 10.1073/pnas.1400966111

Bates, T. R., and Lynch, J. P. (1996). Stimulation of root hair elongation in *Arabidopsis thaliana* by low phosphorus availability. *Plant. Cell Environ.* 19, 529–538. doi: 10.1111/j.1365-3040.1996.tb00386.x

Bates, T. R., and Lynch, J. P. (2000). The efficiency of *Arabidopsis thaliana* (Brassicaceae) root hairs in phosphorus acquisition. *Am. J. Bot.* 87, 964–970. doi: 10.2307/2656995

Bates, T. R., and Lynch, J. P. (2001). Root hairs confer a competitive advantage under low phosphorus availability. *Plant Soil* 236, 243–250. doi: 10.1023/A:1012791706800

Bayuelo-Jiménez, J. S., Gallardo-Valdéz, M., Perez-Decelis, V. A., Magdaleno-Armas, L., Ochoa, I., and Lynch, J. P. (2011). Genotypic variation for root traits of maize (*Zea mays* L.) from the Purhepecha Plateau under contrasting phosphorus availability. *Field Crops Res.* 121, 350–362. doi: 10.1016/j.fcr.2011.01.001

Beemster, G. T., De Vusser, K., De Tavernier, E., De Bock, K., and Inzé, D. (2002). Variation in growth rate between *Arabidopsis* ecotypes is correlated with cell division and A-type cyclin-dependent kinase activity. *Plant Physiol.* 129, 854–864. doi: 10.1104/pp.002923

Benito, B., Haro, R., Amtmann, A., Cuin, T. A., and Dreyer, I. (2014). The twins K^+ and Na^+ in plants. *J. Plant Physiol.* 171, 723–731. doi: 10.1016/j.jplph.2013.10.014

Bloom, A. J., Zwieniecki, M. A., Passioura, J. B., Randall, L. B., Holbrook, N. M., and St. Clair, D. A. (2004). Water relations under root chilling in a sensitive and tolerant tomato species. *Plant Cell Environ.* 27, 971–979. doi: 10.1111/j.1365-3040.2004.01200.x

Bonser, A. M., Lynch, J., and Snapp, S. (1995). Effect of phosphorus availability on basal root-growth angle in bean. *Plant Physiol.* 108:112.

Cassab, G. I., Eapen, D., and Campos, M. E. (2013). Root hydrotropism: an update. *Am. J. Bot.* 100, 14–24. doi: 10.3732/ajb.1200306

Chen, W., Dunbabin, V., Bell, R., Brennan, R., and Bowden, B. (2008). "Simulating and understanding root growth using ROOTMAP to guide phosphorus fertiliser placement in wide row lupin cropping systems," in *Proceedings of the 12th International Lupin conference: "Lupins for Health and Wealth,"* Canterbury.

Chen, Y. L., Dunbabin, V. M., Diggle, A. J., Siddique, K. H. M., and Rengel, Z. (2011). Development of a novel semi-hydroponic phenotyping system for studying root architecture. *Funct. Plant Biol.* 38, 355–363. doi: 10.1071/FP10241

Comas, L. H., Becker, S. R., Cruz, V. M. V., Byrne, P. F., and Dierig, D. A. (2013). Root traits contributing to plant productivity under drought. *Front. Plant Sci.* 4:442. doi: 10.3389/fpls.2013.00442

de Dorlodot, S., Forster, B., Pagès, L., Price, A., Tuberosa, R., and Draye, X. (2007). Root system architecture: opportunities and constraints for genetic improvement of crops. *Trends Plant Sci.* 12, 474–481. doi: 10.1016/j.tplants.2007.08.012

Deak, K. I., and Malamy, J. (2005). Osmotic regulation of root system architecture. *Plant J.* 43, 17–28. doi: 10.1111/j.1365-313X.2005.02425.x

Delucia, E. H., Heckathorn, S. A., and Day, T. A. (1992). Effects of soil-temperature on growth, biomass allocation and resource acquisition of andropogon-gerardii vitman. *New Phytol.* 120, 543–549. doi: 10.1111/j.1469-8137.1992.tb01804.x

Den Herder, G., Van Isterdael, G., Beeckman, T., and De Smet, I. (2010). The roots of a new green revolution. *Trends Plant Sci.* 15, 600–607. doi: 10.1016/j.tplants.2010.08.009

Dina in 't Zandt, D., Marié, C., Kirchgessner, N., Visser, E. J. W., and Hund, A. (2015). High-resolution quantification of root dynamics in split-nutrient rhizoslides reveals rapid and strong proliferation of maize roots in response to local high nitrogen. *J. Exp. Bot.* 66, 5507–5517. doi: 10.1093/jxb/erv307

Dodd, I. C., He, J., Turnbull, C. G., Lee, S. K., and Critchley, C. (2000). The influence of supra-optimal root-zone temperatures on growth and stomatal conductance in *Capsicum annuum* L. *J. Exp. Bot.* 51, 239–248. doi: 10.1093/jexbot/51.343.239

Downie, H. F. F., Adu, M. O. O., Schmidt, S., Otten, W., Dupuy, L. X. X., White, P. J. J., et al. (2015). Challenges and opportunities for quantifying roots and rhizosphere interactions through imaging and image analysis. *Plant. Cell Environ.* 38, 1213–1232. doi: 10.1111/pce.12448

Drew, M. C. (1975). Comparison of the effects of a localised supply of phosphate, nitrate, ammonium and potassium on the growth of the seminal root system, and the shoot, in barley. *New Phytol.* 75, 479–490. doi: 10.1111/j.1469-8137.1975.tb01409.x

Duan, L., Dietrich, D., Ng, C. H., Chan, P. M. Y., Bhalerao, R., Bennett, M. J., et al. (2013). Endodermal ABA signaling promotes lateral root quiescence during salt stress in *Arabidopsis* seedlings. *Plant Cell* 25, 324–341. doi: 10.1105/tpc.112.107227

Dunbabin, V. (2006). "Using the ROOTMAP model of crop root growth to investigate root-soil interactions," in *Proceedings of the 13th Australian Agronomy Conference: "Ground-breaking stuff,"* Perth, WA, eds N. C. Turner, T. Acuna, and R. C. Johnson (Parkville, VIC: Australian Society of Agronomy), 10–14.

Dunbabin, V., Diggle, A. J., and Rengel, Z. (2002). Modeling the interactions between water and nutrient uptake and root growth. *Plant Soil* 239, 29–38.

Dunbabin, V., Rengel, Z., and Diggle, A. J. (2004). Simulating form and function of root systems: efficiency of nitrate uptake is dependent on root system architecture and the spatial and temporal variability of nitrate supply. *Funct. Ecol.* 18(2), 204–211.

Dunbabin, V. M., Postma, J. A., Schnepf, A., Pagès, L., Javaux, M., Wu, L., et al. (2013). Modelling root-soil interactions using three-dimensional models of root growth, architecture and function. *Plant Soil* 372, 93–124. doi: 10.1007/s11104-013-1769-y

Eapen, D., Barroso, M. L., Ponce, G., Campos, M. E., and Cassab, G. I. (2005). Hydrotropism: root growth responses to water. *Trends Plant Sci.* 10, 44–50. doi: 10.1016/j.tplants.2004.11.004

Engels, C. (1994). Effect of root and shoot meristem temperature on shoot to root dry matter partitioning and the internal concentrations of nitrogen and carbohydrates in maize and wheat. *Ann. Bot.* 73, 211–219. doi: 10.1006/anbo.1994.1025

Equiza, M. A., Miravea, J. P., and Tognetti, J. A. (2001). Morphological, anatomical and physiological responses related to differential shoot vs. root growth inhibition at low temperature in spring and winter wheat. *Ann. Bot.* 87, 67–76. doi: 10.1006/anbo.2000.1301

Estañ, M. T., Martinez-Rodriguez, M. M., Perez-Alfocea, F., Flowers, T. J., and Bolarin, M. C. (2005). Grafting raises the salt tolerance of tomato through limiting the transport of sodium and chloride to the shoot. *J. Exp. Bot.* 56, 703–712. doi: 10.1093/jxb/eri027

FAO and ITPS (2015). *Status of the World's Soil Resources (SWSR) – Main Report*. Rome: Food and Agriculture Organization of the United Nations.

Füllner, K., Temperton, V. M., Rascher, U., Jahnke, S., Rist, R., Schurr, U., et al. (2012). Vertical gradient in soil temperature stimulates development and increases biomass accumulation in barley. *Plant Cell Environ.* 35, 884–892. doi: 10.1111/j.1365-3040.2011.02460.x

Gahoonia, T. S., and Nielsen, N. E. (1998). Direct evidence on participation of root hairs in phosphorus (32P) uptake from soil. *Plant Soil* 198, 147–152. doi: 10.1023/A:1004346412006

Gahoonia, T. S., and Nielsen, N. E. (2004). Barley genotypes with long root hairs sustain high grain yields in low-P field. *Plant Soil* 262, 55–62. doi: 10.1023/B:PLSO.0000037020.58002.ac

Gahoonia, T. S., Nielsen, N. E., Joshi, P. A., and Jahoor, A. (2001). A root hairless barley mutant for elucidating genetic of root hairs and phosphorus uptake. *Plant Soil* 235, 211–219. doi: 10.1023/A:1011993322286

Gallego-Bartolome, J., Minguet, E. G., Grau-Enguix, F., Abbas, M., Locascio, A., Thomas, S. G., et al. (2012). Molecular mechanism for the interaction between gibberellin and brassinosteroid signaling pathways in *Arabidopsis*. *Proc. Natl. Acad. Sci. U.S.A.* 109, 13446–13451. doi: 10.1073/pnas.1119992109

Galvan-Ampudia, C. S., Julkowska, M. M., Darwish, E., Gandullo, J., Korver, R. A., Brunoud, G., et al. (2013). Halotropism is a response of plant roots to avoid a saline environment. *Curr. Biol.* 23, 2044–2050. doi: 10.1016/j.cub.2013.08.042

Galvan-Ampudia, C. S., and Testerink, C. (2011). Salt stress signals shape the plant root. *Curr. Opin. Plant Biol.* 14, 296–302. doi: 10.1016/j.pbi.2011.03.019

Geng, Y., Wu, R., Wee, C. W., Xie, F., Wei, X., Chan, P. M. Y., et al. (2013). A spatio-temporal understanding of growth regulation during the salt stress response in *Arabidopsis*. *Plant Cell* 25, 2132–2154. doi: 10.1105/tpc.113.112896

Gerendás, J., and Ratcliffe, R. (2002). "Root pH regulation," in *Plant Roots: The Hidden Half*, eds Y. Waisel, A. Eshel, and U. Kafkafi (New York, NY: Marcel Dekker), 23-1–23-18. doi: 10.1201/9780203909423.ch33

Gibberd, M. R., Gray, J. D., Cocks, P. S., and Colmer, T. D. (2001). Waterlogging tolerance among a diverse range of trifolium accessions is related to root porosity, lateral root formation and 'aerotropic rooting.' *Ann. Bot.* 88, 579–589. doi: 10.1006/anbo.2001.1506

Gibbs, J., Turner, D. W., Armstrong, W., Sivasithamparam, K., and Greenway, H. (1998). Response to oxygen deficiency in primary maize roots. II. Development of oxygen deficiency in the stele has limited short-term impact on radial hydraulic conductivity. *Aust. J. Plant Physiol.* 25:759–763. doi: 10.1071/PP98087

Gifford, M. L., Banta, J. A., Katari, M. S., Hulsmans, J., Chen, L., Ristova, D., et al. (2013). Plasticity regulators modulate specific root traits in discrete nitrogen environments. *PLoS Genet.* 9:e1003760. doi: 10.1371/journal.pgen.1003760

Gladish, D. K., and Rost, T. L. (1993). The effects of temperature on primary root growth dynamics and lateral root distribution in garden pea (*Pisum sativum* L., cv. "Alaska"). *Environ. Exp. Bot.* 33, 243–258. doi: 10.1016/0098-8472(93)90070-V

Gladish, D. K., Sutter, E. G., and Rost, T. L. (2000). The role of free indole-3-acetic acid (IAA) levels, IAA transport, and sucrose transport in the high temperature inhibition of primary root development in pea (*Pisum sativum* L. cv. Alaska). *J. Plant Growth Regul.* 19, 347–358. doi: 10.1007/s003440000017

Gosselin, A., and Trudel, M. J. (1984). Interactions between root-zone temperature and light levels on growth, development and photosynthesis of *Lycopersicon esculentum* Mill. cultivar "Vendor." *Sci. Hortic. (Amsterdam)* 23, 313–321. doi: 10.1016/0304-4238(84)90027-X

Grattan, S. R., and Grieve, C. M. (1998). Salinity-mineral nutrient relations in horticultural crops. *Sci. Hortic. (Amsterdam)* 78, 127–157. doi: 10.1016/S0304-4238(98)00192-7

Gregory, P. J., Atkinson, C. J., Bengough, A. G., Else, M. A., Fernández-Fernández, F., Harrison, R. J., et al. (2013). Contributions of roots and rootstocks to sustainable, intensified crop production. *J. Exp. Bot.* 64, 1209–1222. doi: 10.1093/jxb/ers385

Gruber, B. D., Giehl, R. F. H., Friedel, S., and von Wirén, N. (2013). Plasticity of the *Arabidopsis* root system under nutrient deficiencies. *Plant Physiol.* 163, 161–179. doi: 10.1104/pp.113.218453

Hu, Y., and Schmidhalter, U. (2005). Drought and salinity: a comparison of their effects on mineral nutrition of plants. *J. Plant Nutr. Soil Sci.* 168, 541–549. doi: 10.1002/jpln.200420516

Hund, A., Fracheboud, Y., Soldati, A., and Stamp, P. (2008). Cold tolerance of maize seedlings as determined by root morphology and photosynthetic traits. *Eur. J. Agron.* 28, 178–185. doi: 10.1016/j.eja.2007.07.003

Hund, A., Reimer, R., Stamp, P., and Walter, A. (2012). Can we improve heterosis for root growth of maize by selecting parental inbred lines with different temperature behaviour? *Philos. Trans. R. Soc. Lond. B Biol. Sci.* 367, 1580–1588. doi: 10.1098/rstb.2011.0242

Hund, A., Richner, W., Soldati, A., Fracheboud, Y., and Stamp, P. (2007). Root morphology and photosynthetic performance of maize inbred lines at low temperature. *Eur. J. Agron.* 27, 52–61. doi: 10.1016/j.eja.2007.01.003

Hurewitz, J., and Janes, H. W. (1983). Effect of altering the root-zone temperature, carbon exchange rate, and leaf starch accumulation in the tomato. *Plant Physiol.* 73, 46–50. doi: 10.1104/pp.73.1.46

Iyer-Pascuzzi, A. S., Symonova, O., Mileyko, Y., Hao, Y., Belcher, H., Harer, J., et al. (2010). Imaging and analysis platform for automatic phenotyping and trait ranking of plant root systems. *Plant Physiol.* 152, 1148–1157. doi: 10.1104/pp.109.150748

Jackson, M. B., and Armstrong, W. (1999). Formation of aerenchyma and the processes of plant ventilation in relation to soil flooding and submergence. *Plant Biol.* 1, 274–287. doi: 10.1111/j.1438-8677.1999.tb00253.x

Jia, W., Wang, Y., Zhang, S., and Zhang, J. (2002). Salt-stress-induced ABA accumulation is more sensitively triggered in roots than in shoots. *J. Exp. Bot.* 53, 2201–2206. doi: 10.1093/jxb/erf079

Jobbágy, E. G., and Jackson, R. B. (2001). The distribution of soil nutrients with depth: global patterns and the imprint of plants. *Biogeochemistry* 53, 51–77. doi: 10.1023/A:1010760720215

Jobbágy, E. G., and Jackson, R. B. (2004). The uplift of soil nutrients by plants: biogeochemical consequences across scales. *Ecology* 85, 2380–2389. doi: 10.1890/03-0245

Judd, L., Jackson, B., and Fonteno, W. (2015). Advancements in root growth measurement technologies and observation capabilities for container-grown plants. *Plants* 4, 369–392. doi: 10.3390/plants4030369

Julkowska, M. M., Hoefsloot, H. C. J., Mol, S., Feron, R., de Boer, G.-J., Haring, M. A., et al. (2014). Capturing *Arabidopsis* root architecture dynamics with ROOT-FIT reveals diversity in responses to salinity. *Plant Physiol.* 166, 1387–1402. doi: 10.1104/pp.114.248963

Julkowska, M. M., and Testerink, C. (2015). Tuning plant signaling and growth to survive salt. *Trends Plant Sci.* 20, 586–594. doi: 10.1016/j.tplants.2015.06.008

Jung, J. K., and McCouch, S. (2013). Getting to the roots of it: genetic and hormonal control of root architecture. *Front. Plant Sci.* 4:186. doi: 10.3389/fpls.2013.00186

Kaneyasu, T., Kobayashi, A., Nakayama, M., Fujii, N., Takahashi, H., and Miyazawa, Y. (2007). Auxin response, but not its polar transport, plays a role in hydrotropism of *Arabidopsis* roots. *J. Exp. Bot.* 58, 1143–1150. doi: 10.1093/jxb/erl274

Kapulnik, Y., Delaux, P. M., Resnick, N., Mayzlish-Gati, E., Wininger, S., Bhattacharya, C., et al. (2011a). Strigolactones affect lateral root formation and root-hair elongation in *Arabidopsis*. *Planta* 233, 209–216. doi: 10.1007/s00425-010-1310-y

Kapulnik, Y., Resnick, N., Mayzlish-Gati, E., Kaplan, Y., Wininger, S., Hershenhorn, J., et al. (2011b). Strigolactones interact with ethylene and auxin in regulating root-hair elongation in *Arabidopsis*. *J. Exp. Bot.* 62, 2915–2924. doi: 10.1093/jxb/erq464

Kato, Y., Abe, J., Kamoshita, A., and Yamagishi, J. (2006). Genotypic variation in root growth angle in rice (*Oryza sativa* L.) and its association with deep root development in upland fields with different water regimes. *Plant Soil* 287, 117–129. doi: 10.1007/s11104-006-9008-4

Kawa, D., Julkowska, M., Montero Sommerfeld, H., Horst, A. T., Haring, M. A., and Testerink, C. (2016). Phosphate-dependent root system architecture responses to salt stress. *Plant Physiol.* doi: 10.1104/pp.16.00712 [Epub ahead of print].

Koltai, H. (2011). Strigolactones are regulators of root development. *New Phytol.* 190, 545–549. doi: 10.1111/j.1469-8137.2011.03678.x

Koltai, H., Dor, E., Hershenhorn, J., Joel, D. M., Weininger, S., Lekalla, S., et al. (2010). Strigolactones' effect on root growth and root-hair elongation may be mediated by auxin-efflux carriers. *J. Plant Growth Regul.* 29, 129–136. doi: 10.1007/s00344-009-9122-7

Krouk, G., Lacombe, B., Bielach, A., Perrine-Walker, F., Malinska, K., Mounier, E., et al. (2010). Nitrate-regulated auxin transport by NRT1.1 defines a mechanism for nutrient sensing in plants. *Dev. Cell* 18, 927–937. doi: 10.1016/j.devcel.2010.05.008

Kubota, C., McClure, M. A., Kokalis-Burelle, N., Bausher, M. G., and Rosskopf, E. N. (2008). Vegetable grafting: history, use, and current technology status in North America. *HortScience* 43, 1664–1669.

Kuijken, R. C. P., Van Eeuwijk, F. A., Marcelis, L. F. M., and Bouwmeester, H. J. (2015). Root phenotyping: from component trait in the lab to breeding. *J. Exp. Bot.* 66, 5389–5401. doi: 10.1093/jxb/erv239

Le Marié, C., Kirchgessner, N., Marschall, D., Walter, A., and Hund, A. (2014). Rhizoslides: paper-based growth system for non-destructive, high throughput phenotyping of root development by means of image analysis. 10:13. doi: 10.1186/1746-4811-10-13

Leblanc, A., Renault, H., Lecourt, J., Etienne, P., Deleu, C., and Le Deunff, E. (2008). Elongation changes of exploratory and root hair systems induced by aminocyclopropane carboxylic acid and aminoethoxyvinylglycine affect nitrate uptake and BnNrt2.1 and BnNrt1.1 transporter gene expression in oilseed rape. *Plant Physiol.* 146, 1928–1940. doi: 10.1104/pp.107.109363

Lee, Y. P., Fleming, A. J., Körner, C., and Meins, F. (2009). Differential expression of the CBF pathway and cell cycle-related genes in *Arabidopsis* accessions in response to chronic low-temperature exposure. *Plant Biol.* 11, 273–283. doi: 10.1111/j.1438-8677.2008.00122.x

Liao, H., Yan, X., Rubio, G., Beebe, S. E., Blair, M. W., and Lynch, J. P. (2004). Genetic mapping of basal root gravitropism and phosphorus acquisition efficiency in common bean. *Funct. Plant Biol.* 31, 959–970. doi: 10.1071/FP03255

Licker, R., Johnston, M., Foley, J. A., Barford, C., Kucharik, C. J., Monfreda, C., et al. (2010). Mind the gap: how do climate and agricultural management explain the "yield gap" of croplands around the world? *Glob. Ecol. Biogeogr.* 19, 769–782. doi: 10.1111/j.1466-8238.2010.00563.x

Linkohr, B. I., Williamson, L. C., Fitter, A. H., and Leyser, H. M. O. (2002). Nitrate and phosphate availability and distribution have different effects on root system architecture of *Arabidopsis*. *Plant J.* 29, 751–760. doi: 10.1046/j.1365-313X.2002.01251.x

Little, D. Y., Rao, H., Oliva, S., Daniel-Vedele, F., Krapp, A., and Malamy, J. E. (2005). The putative high-affinity nitrate transporter NRT2.1 represses lateral root initiation in response to nutritional cues. *Proc. Natl. Acad. Sci. U.S.A.* 102, 13693–13698. doi: 10.1073/pnas.0504219102

Liu, W., Li, R.-J., Han, T.-T., Cai, W., Fu, Z.-W., and Lu, Y.-T. (2015). Salt stress reduces root meristem size by nitric oxide-mediated modulation of auxin accumulation and signaling in *Arabidopsis*. *Plant Physiol.* 168, 00030.2015. doi: 10.1104/pp.15.00030

Lobell, D. B., Cassman, K. G., and Field, C. B. (2009). Crop yield gaps: their importance, magnitudes, and causes. *Annu. Rev. Environ. Resour.* 34, 179–204. doi: 10.1146/annurev.environ.041008.093740

Lobet, G., Draye, X., and Perilleux, C. (2013). An online database for plant image analysis software tools. *Plant Methods* 9:38. doi: 10.1186/1746-4811-9-38

Lobet, G., Pagès, L., and Draye, X. (2011). A novel image analysis toolbox enabling quantitative analysis of root system architecture. *Plant Physiol.* 157, 29–39. doi: 10.1104/pp.111.179895

López-Arredondo, D. L., Leyva-González, M. A., González-Morales, S. I., López-Bucio, J., and Herrera-Estrella, L. (2014). Phosphate nutrition: improving low-phosphate tolerance in crops. *Annu. Rev. Plant Biol.* 65, 95–123. doi: 10.1146/annurev-arplant-050213-035949

López-Bucio, J., Hernández-Abreu, E., Sánchez-Calderón, L., Nieto-Jacobo, M. F., Simpson, J., and Herrera-Estrella, L. (2002). Phosphate availability alters architecture and causes changes in hormone sensitivity in the *Arabidopsis* root system. *Plant Physiol.* 129, 244–256. doi: 10.1104/pp.010934

Lynch, J. P. (2007). Turner review no. 14. Roots of the second green revolution. *Aust. J. Bot.* 55, 493–512. doi: 10.1071/BT06118

Lynch, J. P., and Brown, K. M. (2001). Topsoil foraging - An architectural adaptation of plants to low phosphorus availability. *Plant Soil* 237, 225–237. doi: 10.1023/A:1013324727040

Lynch, J. P., and Brown, K. M. (2012). New roots for agriculture: exploiting the root phenome. *Philos. Trans. R. Soc. Lond. B Biol. Sci.* 367, 1598–1604. doi: 10.1098/rstb.2011.0243

Lynch, J. P., and Wojciechowski, T. (2015). Opportunities and challenges in the subsoil: pathways to deeper rooted crops. *J. Exp. Bot.* 66, 2199–2210. doi: 10.1093/jxb/eru508

Mairhofer, S., Zappala, S., Tracy, S., Sturrock, C., Bennett, M. J., Mooney, S. J., et al. (2013). Recovering complete plant root system architectures from soil via X-ray μ-Computed Tomography. *Plant Methods* 9:8. doi: 10.1186/1746-4811-9-8

Malamy, J. E. (2005). Intrinsic and environmental response pathways that regulate root system architecture. *Plant Cell Environ.* 28, 67–77. doi: 10.1111/j.1365-3040.2005.01306.x

Manschadi, A. M., Hammer, G. L., Christopher, J. T., and DeVoil, P. (2008). Genotypic variation in seedling root architectural traits and implications for drought adaptation in wheat (*Triticum aestivum* L.). *Plant Soil* 303, 115–129. doi: 10.1007/s11104-007-9492-1

Martinez-Rodriguez, M. M., Estañ, M. T., Moyano, E., Garcia-Abellan, J. O., Flores, F. B., Campos, J. F., et al. (2008). The effectiveness of grafting to improve salt tolerance in tomato when an "excluder" genotype is used as scion. *Environ. Exp. Bot.* 63, 392–401. doi: 10.1016/j.envexpbot.2007.12.007

Mathieu, L., Lobet, G., Tocquin, P., and Périlleux, C. (2015). "Rhizoponics": a novel hydroponic rhizotron for root system analyses on mature *Arabidopsis thaliana* plants. *Plant Methods* 11:3. doi: 10.1186/s13007-015-0046-x

Matthys, C., Walton, A., Struk, S., Stes, E., Boyer, F.-D., Gevaert, K., et al. (2016). The Whats, the Wheres and the Hows of strigolactone action in the roots. *Planta* 243, 1327–1337. doi: 10.1007/s00425-016-2483-9

Mayzlish-Gati, E., De-Cuyper, C., Goormachtig, S., Beeckman, T., Vuylsteke, M., Brewer, P. B., et al. (2012). Strigolactones are involved in root response to low phosphate conditions in *Arabidopsis*. *Plant Physiol.* 160, 1329–1341. doi: 10.1104/pp.112.202358

Mcmichael, B. L., Quisenberry, E., Systems, C., Stress, P., and Conservation, W. (1993). The impact of the soil environment on the growth of root systems. *Environ. Exp. Bot.* 33, 53–61. doi: 10.1016/0098-8472(93)90055-K

Metzner, R., Eggert, A., van Dusschoten, D., Pflugfelder, D., Gerth, S., Schurr, U., et al. (2015). Direct comparison of MRI and X-ray CT technologies for 3D imaging of root systems in soil: potential and challenges for root trait quantification. *Plant Methods* 11, 1–11. doi: 10.1186/s13007-015-0060-z

Mickelbart, M. V., Hasegawa, P. M., and Bailey-Serres, J. (2015). Genetic mechanisms of abiotic stress tolerance that translate to crop yield stability. *Nat. Rev. Genet.* 16, 237–251. doi: 10.1038/nrg3901

Miura, K., Lee, J., Gong, Q., Ma, S., Jin, J. B., Yoo, C. Y., et al. (2011). SIZ1 regulation of phosphate starvation-induced root architecture remodeling involves the control of auxin accumulation. *Plant Physiol.* 155, 1000–1012. doi: 10.1104/pp.110.165191

Mizuno, H., Kobayashi, A., Fujii, N., Yamashita, M., and Takahashi, H. (2002). Hydrotropic response and expression pattern of auxin-inducible gene, CS-IAA1, in the primary roots of clinorotated cucumber seedlings. *Plant Cell Physiol.* 43, 793–801. doi: 10.1093/Pcp/Pcf093

Møller, I. S., Gilliham, M., Jha, D., Mayo, G. M., Roy, S. J., Coates, J. C., et al. (2009). Shoot Na+ exclusion and increased salinity tolerance engineered by cell type-specific alteration of Na+ transport in *Arabidopsis*. *Plant Cell* 21, 2163–2178. doi: 10.1105/tpc.108.064568

Mooney, S. J., Pridmore, T. P., Helliwell, J., and Bennett, M. J. (2012). Developing X-ray computed tomography to non-invasively image 3-D root systems architecture in soil. *Plant Soil* 352, 1–22. doi: 10.1007/s11104-011-1039-9

Moriwaki, T., Miyazawa, Y., Kobayashi, A., and Takahashi, H. (2013). Molecular mechanisms of hydrotropism in seedling roots of *Arabidopsis thaliana* (Brassicaceae). *Am. J. Bot.* 100, 25–34. doi: 10.3732/ajb.1200419

Mouchel, C. F., Briggs, G. C., and Hardtke, C. S. (2004). Natural genetic variation in *Arabidopsis* identifies BREVIS RADIX, a novel regulator of cell proliferation and elongation in the root. *Genes Dev.* 18, 700–714. doi: 10.1101/gad.1187704

Mounier, E., Pervent, M., Ljung, K., Gojon, A., and Nacry, P. (2014). Auxin-mediated nitrate signalling by NRT1.1 participates in the adaptive response of *Arabidopsis* root architecture to the spatial heterogeneity of nitrate availability. *Plant Cell Environ.* 37, 162–174. doi: 10.1111/pce.12143

Mudge, K., Janick, J., Scofield, S., and Goldschmidt, E. (2009). "A history of grafting," in *Horticultural Reviews* Vol. 35, ed. J. Janick (Hoboken, NJ: John Wiley & Sons, Inc.).

Mueller, N. D., Gerber, J. S., Johnston, M., Ray, D. K., Ramankutty, N., and Foley, J. A. (2012). Closing yield gaps through nutrient and water management. *Nature* 490, 254–257. doi: 10.1038/nature11420

Munns, R. (2002). Comparative physiology of salt and water stress. *Plant Cell Environ.* 25, 239–250. doi: 10.1046/j.0016-8025.2001.00808.x

Munns, R., James, R. A., and Läuchli, A. (2006). Approaches to increasing the salt tolerance of wheat and other cereals. *J. Exp. Bot.* 57, 1025–1043. doi: 10.1093/jxb/erj100

Munns, R., and Tester, M. (2008). Mechanisms of salinity tolerance. *Annu. Rev. Plant Biol.* 59, 651–681. doi: 10.1146/annurev.arplant.59.032607.092911

Muños, S., Cazettes, C., Fizames, C., Gaymard, F., Tillard, P., Lepetit, M., et al. (2004). Transcript profiling in the chl1-5 mutant of *Arabidopsis* reveals a role of the nitrate transporter NRT1. 1 in the regulation of another nitrate transporter, NRT2. 1. *Plant Cell* 16, 2433–2447. doi: 10.1105/tpc.104.024380.tration

Nacry, P. (2005). A role for auxin redistribution in the responses of the root system architecture to phosphate starvation in *Arabidopsis*. *Plant Physiol.* 138, 2061–2074. doi: 10.1104/pp.105.060061

Nagel, K., Kastenholz, B., Jahnke, S., van Dusschoten, D., Aach, T., Muhlich, M., et al. (2009). Temperature responses of roots: impact on growth, root system archetecture and implications for phenotyping. *Funct. Plant Biol.* 36, 947–959. doi: 10.1071/FP09184

Naidu, R., and Rengasamy, P. (1993). Ion interactions and constraints to plant nutrition in Australian sodic soils. *Aust. J. Soil Res.* 31, 801–819. doi: 10.1071/Sr9930801

Nielsen, K. F., Halstead, R. L., MacLean, A. J., Holmes, R. M., and Bourget, S. J. (1960). The influence of soil temperature on the growth and mineral composition of oats. *Can. J. Soil Sci.* 40, 255–263. doi: 10.4141/cjss60-032

Ogawa, A., Kitamichi, K., Toyofuku, K., and Kawashima, C. (2006). Quantitative analysis of cell division and cell death in seminal root of rye under salt stress. *Plant Prod. Sci.* 9, 56–64. doi: 10.1626/pps.9.56

Pagés, L., Bécel, C., Boukcim, H., Moreau, D., Nguyen, C., and Voisin, A. S. (2014). Calibration and evaluation of ArchiSimple, a simple model of root system architecture. *Ecol. Modell.* 290, 76–84. doi: 10.1016/j.ecolmodel.2013.11.014

Pagès, L., and Picon-Cochard, C. (2014). Modelling the root system architecture of Poaceae. Can we simulate integrated traits from morphological parameters of growth and branching? *New Phytol.* 204, 149–158. doi: 10.1111/nph.12904

Pahlavanian, A. L. I. M., and Silk, W. K. (1988). Effect of temperature on spatial and temporal aspects of growth in the primary maize root. *Plant Physiol.* 87, 529–532.

Pardales, J. R., Kono, Y., and Yamauchi, A. (1992). Epidermal cell elongation in sorghum seminal roots exposed to high root-zone temperature. *Plant Sci.* 81, 143–146. doi: 10.1016/0168-9452(92)90035-K

Pardales, J. R. J., Banoc, D. M., Yamauchi, A., Iijima, M., and Kono, Y. (1999). Root System Development of Cassava and Sweetpotato during Early Growth Stage as Affected by High Root Zone Temperature. *Plant Prod. Sci.* 2, 247–251. doi: 10.1626/pps.2.247

Pedersen, A., Zhang, K., Thorup-Kristensen, K., and Jensen, L. S. (2010). Modelling diverse root density dynamics and deep nitrogen uptake-a simple approach. *Plant Soil* 326, 493–510. doi: 10.1007/s11104-009-0028-8

Péret, B., Clément, M., Nussaume, L., and Desnos, T. (2011). Root developmental adaptation to phosphate starvation: better safe than sorry. *Trends Plant Sci.* 16, 442–450. doi: 10.1016/j.tplants.2011.05.006

Pérez-Torres, C. A., López-Bucio, J., Cruz-Ramírez, A., Ibarra-Laclette, E., Dharmasiri, S., Estelle, M., et al. (2008a). Phosphate availability alters lateral root development in *Arabidopsis* by modulating auxin sensitivity via a mechanism involving the TIR1 auxin receptor. *Plant Cell* 20, 3258–3272. doi: 10.1105/tpc.108.058719

Pérez-Torres, C. A., López-Bucio, J., and Herrera-Estrella, L. (2008b). Phosphate availability alters lateral root development in *Arabidopsis* by modulating auxin sensitivity via a mechanism involving the TIR1 auxin receptor. *Plant Cell* 20, 3258–3272. doi: 10.1105/tpc.108.058719

Pierik, R., and Testerink, C. (2014). The art of being flexible: how to escape from shade, salt, and drought. *Plant Physiol.* 166, 5–22. doi: 10.1104/pp.114.239160

Pigliucci, M. (2005). Evolution of phenotypic plasticity: where are we going now? *Trends Ecol. Evol.* 20, 481–486. doi: 10.1016/j.tree.2005.06.001

Piñeros, M. A., Larson, B. G., Shaff, J. E., Schneider, D. J., Falcão, A. X., Yuan, L., et al. (2016). Evolving technologies for growing, imaging and analyzing 3D root system architecture of crop plants. *J. Integr. Plant Biol.* 58, 230–241. doi: 10.1111/jipb.12456

Poiré, R., Wiese-Klinkenberg, A., Parent, B., Mielewczik, M., Schurr, U., Tardieu, F., et al. (2010). Diel time-courses of leaf growth in monocot and dicot species: endogenous rhythms and temperature effects. *J. Exp. Bot.* 61, 1751–1759. doi: 10.1093/jxb/erq049

Poorter, H., van der Werf, A., Atkin, O. K., and Lambers, H. (1991). Respiratory energy requirements of roots vary with the potential growth rate of a plant species. *Physiol. Plant.* 83, 469–475. doi: 10.1034/j.1399-3054.1991.830321.x

Porter, J. R., and Gawith, M. (1999). Temperatures and the growth and development of wheat: a review. *Eur. J. Agron.* 10, 23–36. doi: 10.1016/S1161-0301(98)00047-1

Pound, M. P., French, A. P., Atkinson, J. A., Wells, D. M., Bennett, M. J., and Pridmore, T. (2013). RootNav: navigating images of complex root architectures. *Plant Physiol.* 162, 1802–1814. doi: 10.1104/pp.113.221531

Pritchard, J., Barlow, P. W., Adam, J. S., and Tomos, A. D. (1990). Biophysics of the inhibition of the growth of maize roots by lowered temperature. *Plant Physiol.* 93, 222–230. doi: 10.1104/pp.93.1.222

Qin, L., He, J., Lee, S. K., and Dodd, I. C. (2007). An assessment of the role of ethylene in mediating lettuce (*Lactuca sativa*) root growth at high temperatures. *J. Exp. Bot.* 58, 3017–3024. doi: 10.1093/jxb/erm156

Rahman, M. S., Matsumuro, T., Miyake, H., and Takeoka, Y. (2001). Effects of salinity stress on the seminal root tip ultrastructures of rice seedlings (*Oryza sativa* L.). *Plant Prod. Sci.* 4, 103–111. doi: 10.1626/pps.4.103

Rellán-Álvarez, R., Lobet, G., and Dinneny, J. R. (2016). Environmental control of root system biology. *Annu. Rev. Plant Biol.* 67, 1–26. doi: 10.1146/annurev-arplant-043015-111848

Rellán-Álvarez, R., Lobet, G., Lindner, H., Pradier, P. L., Sebastian, J., Yee, M. C., et al. (2015). GLO-Roots: an imaging platform enabling multidimensional characterization of soil-grown root systems. *Elife* 4:e07597. doi: 10.7554/eLife.07597

Remans, T., Nacry, P., Pervent, M., Filleur, S., Diatloff, E., Mounier, E., et al. (2006a). The *Arabidopsis* NRT1.1 transporter participates in the signaling pathway triggering root colonization of nitrate-rich patches. *Proc. Natl. Acad. Sci. U.S.A.* 103, 19206–19211. doi: 10.1073/pnas.0605275103

Remans, T., Nacry, P., Pervent, M., Girin, T., Tillard, P., Lepetit, M., et al. (2006b). A central role for the nitrate transporter NRT2.1 in the integrated morphological and physiological responses of the root system to nitrogen limitation in *Arabidopsis*. *Plant Physiol.* 140, 909–921. doi: 10.1104/pp.105.075721

Rengasamy, P. (2006). World salinization with emphasis on Australia. *J. Exp. Bot.* 57, 1017–1023. doi: 10.1093/jxb/erj108

Rich, S. M., and Watt, M. (2013). Soil conditions and cereal root system architecture: review and considerations for linking Darwin and Weaver. *J. Exp. Bot.* 64, 1193–1208. doi: 10.1093/jxb/ert043

Ristova, D., and Busch, W. (2014). Natural variation of root traits: from development to nutrient uptake. *Plant Physiol.* 166, 518–527. doi: 10.1104/pp.114.244749

Ritter, E., Angulo, B., Riga, P., Herrán, C., Relloso, J., and San Jose, M. (2001). Comparison of hydroponic and aeroponic cultivation systems for the production of potato minitubers. *Potato Res.* 44, 127–135. doi: 10.1007/BF02410099

Robbins, N. E., and Dinneny, J. R. (2015). The divining root: moisture-driven responses of roots at the micro- and macro-scale. *J. Exp. Bot.* 66, 2145–2154. doi: 10.1093/jxb/eru496

Rodriguez, H. G., Roberts, J. K. M., Jordan, W. R., and Drew, M. C. (1997). Growth, water relations, and accumulation of organic and inorganic solutes in roots of maize seedlings during salt stress. *Plant Physiol.* 113, 881–893. doi: 10.1104/pp.113.3.881

Ron, M., Dorrity, M. W., de Lucas, M., Toal, T., Hernandez, R. I., Little, S. A., et al. (2013). Identification of novel loci regulating interspecific variation in root morphology and cellular development in tomato. *Plant Physiol.* 162, 755–768. doi: 10.1104/pp.113.217802

Rosas, U., Cibrian-Jaramillo, A., Ristova, D., Banta, J. A., Gifford, M. L., Fan, A. H., et al. (2013). Integration of responses within and across *Arabidopsis* natural accessions uncovers loci controlling root systems architecture. *Proc. Natl. Acad. Sci. U.S.A.* 110, 15133–15138. doi: 10.1073/pnas.1305883110

Rosegrant, M. W., Ringler, C., and Zhu, T. (2009). Water for agriculture: maintaining food security under growing scarcity. *Annu. Rev. Environ. Resour.* 34, 205–222. doi: 10.1146/annurev.environ.030308.090351

Rosquete, M. R., Von Wangenheim, D., Marhavý, P., Barbez, E., Stelzer, E. H. K., Benková, E., et al. (2013). An auxin transport mechanism restricts positive orthogravitropism in lateral roots. *Curr. Biol.* 23, 817–822. doi: 10.1016/j.cub.2013.03.064

Rowe, J. H., Topping, J. F., Liu, J., and Lindsey, K. (2016). Abscisic acid regulates root growth under osmotic stress conditions via an interacting hormonal network with cytokinin, ethylene and auxin. *New Phytol.* 211, 225–239. doi: 10.1111/nph.13882

Roychoudhry, S., Del Bianco, M., Kieffer, M., and Kepinski, S. (2013). Auxin controls gravitropic setpoint angle in higher plant lateral branches. *Curr. Biol.* 23, 1497–1504. doi: 10.1016/j.cub.2013.06.034

Rubinigg, M., Stulen, I., Theo, M. E. J., and Colmer, T. D. (2002). Spatial patterns of radial oxygen loss and nitrate net flux along adventitious roots of rice raised in aerated or stagnant solution. *Funct. Plant Biol.* 29, 1475–1481. doi: 10.1071/FP02081

Ruyter-Spira, C., Kohlen, W., Charnikhova, T., van Zeijl, A., van Bezouwen, L., de Ruijter, N., et al. (2011). Physiological effects of the synthetic strigolactone analog GR24 on root system architecture in *Arabidopsis*: another belowground role for strigolactones? *Plant* 155, 721–734. doi: 10.1104/pp.110.166645

Saengwilai, P., Tian, X., and Lynch, J. P. (2014). Low crown root number enhances nitrogen acquisition from low-nitrogen soils in maize. *Plant Physiol.* 166, 581–589. doi: 10.1104/pp.113.232603

Sairam, R. K., and Tyagi, A. (2004). Physiology and molecular biology of salinity stress tolerance in plants. *Curr. Sci.* 86, 407–421. doi: 10.1016/j.tplants.2005.10.002

Sakamoto, M., and Suzuki, T. (2015). Effect of root-zone temperature on growth and quality of hydroponically grown red leaf lettuce (*Lactuca sativa* L. cv. Red Wave). *Am. J. Plant. Sci.* 6, 2350–2360. doi: 10.4236/ajps.2015.614238

Sánchez-Calderón, L., López-Bucio, J., Chacón-López, A., Cruz-Ramírez, A., Nieto-Jacobo, F., Dubrovsky, J. G., et al. (2005). Phosphate starvation induces a

determinate developmental program in the roots of *Arabidopsis thaliana*. *Plant Cell Physiol.* 46, 174–184. doi: 10.1093/pcp/pci011

Sánchez-Calderón, L., López-Bucio, J., Chacón-López, A., Gutiérrez-Ortega, A., Hernández-Abreu, E., and Herrera-Estrella, L. (2006). Characterization of low phosphorus insensitive mutants reveals a crosstalk between low phosphorus-induced determinate root development and the activation of genes involved in the adaptation of *Arabidopsis* to phosphorus deficiency. *Plant Physiol.* 140, 879–889. doi: 10.1104/pp.105.073825

Scheurwater, I., Clarkson, D. T., Purves, J. V., Van Rijt, G., Saker, L. R., Welschen, R., et al. (1999). Relatively large nitrate efflux can account for the high specific respiratory costs for nitrate transport in slow-growing grass species. *Plant Soil* 215, 123–134. doi: 10.1023/A:1004559628401

Scheurwater, I., Cornelissen, C., Dictus, F., Welschen, R., and Lambers, H. (1998). Why do fast- and slow-growing grass species differ so little in their rate of root respiration, considering the large differences in rate of growth and ion uptake? *Plant Cell Environ.* 21, 995–1005. doi: 10.1046/j.1365-3040.1998.00341.x

Schwarz, D., Rouphael, Y., Colla, G., and Venema, J. H. (2010). Grafting as a tool to improve tolerance of vegetables to abiotic stresses: thermal stress, water stress and organic pollutants. *Sci. Hortic. (Amsterdam)* 127, 162–171. doi: 10.1016/j.scienta.2010.09.016

Seiler, G. J. (1998). Influence of temperature on primary and lateral root growth of sunflower seedlings. *Environ. Exp. Bot.* 40, 135–146. doi: 10.1016/S0098-8472(98)00027-6

Setter, T. L., and Waters, I. (2003). Review of prospects for germplasm improvement for waterlogging tolerance in wheat, barley and oats. *Plant Soil* 253, 1–34. doi: 10.1023/A:1024573305997

Shibasaki, K., Uemura, M., Tsurumi, S., and Rahman, A. (2009). Auxin response in *Arabidopsis* under cold stress: underlying molecular mechanisms. *Plant Cell* 21, 3823–3838. doi: 10.1105/tpc.109.069906

Shkolnik, D., Krieger, G., Nuriel, R., and Fromm, H. (2016). Hydrotropism: root bending does not require auxin redistribution. *Mol. Plant* 9, 757–759. doi: 10.1016/j.molp.2016.02.001

Shkolnik-Inbar, D., and Bar-Zvi, D. (2010). ABI4 mediates abscisic acid and cytokinin inhibition of lateral root formation by reducing polar auxin transport in *Arabidopsis*. *Plant Cell* 22, 3560–3573. doi: 10.1105/tpc.110.074641

Siddique, K. H. M., Belford, R. K., and Tennant, D. (1990). Root: shoot ratios of old and modern, tall and semi-dwarf wheats in a mediterranean environment. *Plant Soil* 121, 89–98. doi: 10.1007/BF00013101

Silberbush, M., and Barber, S. (1983). Sensitivity of simulated phosphorus uptake to parameters used by a mechanistic-mathematical model. *Plant Soil* 74, 93–100. doi: 10.1007/BF02178744

Silva-Navas, J., Moreno-Risueno, M. A., Manzano, C., Pallero-Baena, M., Navarro-Neila, S., Téllez-Robledo, B., et al. (2015). D-Root: a system for cultivating plants with the roots in darkness or under different light conditions. *Plant J.* 84, 244–255. doi: 10.1111/tpj.12998

Slovak, R., Ogura, T., Satbhai, S. B., Ristova, D., and Busch, W. (2016). Genetic control of root growth: from genes to networks. *Ann. Bot.* 117, 9–24. doi: 10.1093/aob/mcv160

Smedema, L. K., and Shiati, K. (2002). Irrigation and salinity: a perspective review of the salinity hazards of irrigation development in the arid zone. *Irrig. Drain. Syst.* 16, 161–174. doi: 10.1023/A:1016008417327

Smith, S., and De Smet, I. (2012). Root system architecture: insights from *Arabidopsis* and cereal crops. *Philos. Trans. R. Soc. B Biol. Sci.* 367, 1441–1452. doi: 10.1098/rstb.2011.0234

Snyder, C. S., Bruulsema, T. W., Jensen, T. L., and Fixen, P. E. (2009). Review of greenhouse gas emissions from crop production systems and fertilizer management effects. *Agric. Ecosyst. Environ.* 133, 247–266. doi: 10.1016/j.agee.2009.04.021

Spalding, E. P., and Miller, N. D. (2013). Image analysis is driving a renaissance in growth measurement. *Curr. Opin. Plant Biol.* 16, 100–104. doi: 10.1016/j.pbi.2013.01.001

Sun, F., Zhang, W., Hu, H., Li, B., Wang, Y., Zhao, Y., et al. (2007). Salt modulates gravity signaling pathway to regulate growth direction of primary roots in *Arabidopsis*. *Plant Physiol.* 146, 178–188. doi: 10.1104/pp.107.109413

Svistoonoff, S., Creff, A., Reymond, M., Sigoillot-Claude, C., Ricaud, L., Blanchet, A., et al. (2007). Root tip contact with low-phosphate media reprograms plant root architecture. *Nat. Genet.* 39, 792–796. doi: 10.1038/ng2041

Takahashi, H., Miyazawa, Y., and Fujii, N. (2009). Hormonal interactions during root tropic growth: hydrotropism versus gravitropism. *Plant Mol. Biol.* 69, 489–502. doi: 10.1007/s11103-008-9438-x

Takahashi, H., and Scott, T. K. (1991). Hydrotropism and its interactions with gravitropism in maize roots. *Plant Physiol.* 96, 558–564. doi: 10.1104/pp.96.2.558

Takahashi, H., and Suge, H. (1991). Root hydrotropism of an agravitropic pea mutant, ageotropum. *Physiol. Plant.* 82, 24–31. doi: 10.1111/j.1399-3054.1991.tb02898.x

Takahashi, H., Takano, M., Fujii, N., Yamashita, M., and Suge, H. (1996). Induction of hydrotropism in clinorotated seedling roots of Alaska pea, *Pisum sativum* L. *J. Plant Res.* 109, 335–337. doi: 10.1007/Bf02344481

Takahashi, N., Goto, N., Okada, K., and Takahashi, H. (2002). Hydrotropism in abscisic acid, wavy, and gravitropic mutants of *Arabidopsis thaliana*. *Planta* 216, 203–211. doi: 10.1007/s00425-002-0840-3

Tian, Q. Y., Sun, P., and Zhang, W. H. (2009). Ethylene is involved in nitrate-dependent root growth and branching in *Arabidopsis thaliana*. *New Phytol.* 184, 918–931. doi: 10.1111/j.1469-8137.2009.03004.x

Tocquin, P., Corbesier, L., Havelange, A., Pieltain, A., Kurtem, E., Bernier, G., et al. (2003). A novel high efficiency, low maintenance, hydroponic system for synchronous growth and flowering of *Arabidopsis thaliana*. *BMC Plant Biol.* 3:2. doi: 10.1186/1471-2229-3-2

Uga, Y., Sugimoto, K., Ogawa, S., Rane, J., Ishitani, M., Hara, N., et al. (2013). Control of root system architecture by DEEPER ROOTING 1 increases rice yield under drought conditions. *Nat. Genet.* 45, 1097–1102. doi: 10.1038/ng.2725

van den Berg, T., Korver, R. A., Testerink, C., and ten Tusscher, K. H. W. J. (2016). Modeling halotropism: a key role for root tip architecture and reflux loop remodeling in redistributing auxin. *Development* doi: 10.1242/dev.135111 [Epub ahead of print].

Van der Putten, W. H., Bardgett, R. D., Bever, J. D., Bezemer, T. M., Casper, B. B., Fukami, T., et al. (2013). Plant-soil feedbacks: the past, the present and future challenges. *J. Ecol.* 101, 265–276. doi: 10.1111/1365-2745.12054

van der Werf, A., Kooijman, A., Welschen, R., and Lambers, H. (1988). Respiratory energy costs for the maintenance of biomass, for growth and for ion uptake in roots of *Carex diandra* and *Carex acutiformis*. *Physiol. Plant.* 72, 483–491. doi: 10.1111/j.1399-3054.1988.tb09155.x

Van Ittersum, M. K., Cassman, K. G., Grassini, P., Wolf, J., Tittonell, P., and Hochman, Z. (2013). Yield gap analysis with local to global relevance-A review. *Field Crops Res.* 143, 4–17. doi: 10.1016/j.fcr.2012.09.009

Veen, B. (1981). Relation between root respiration and root activity. *Plant Soil* 63, 73–76. doi: 10.1007/BF02374259

Venema, J. H., Dijk, B. E., Bax, J. M., van Hasselt, P. R., and Elzenga, J. T. M. (2008). Grafting tomato (*Solanum lycopersicum*) onto the rootstock of a high-altitude accession of *Solanum habrochaites* improves suboptimal-temperature tolerance. *Environ. Exp. Bot.* 63, 359–367. doi: 10.1016/j.envexpbot.2007.12.015

Veselova, S. V., Farhutdinov, R. G., Veselov, S. Y., Kudoyarova, G. R., Veselov, D. S., and Hartung, W. (2005). The effect of root cooling on hormone content, leaf conductance and root hydraulic conductivity of durum wheat seedlings (*Triticum durum* L.). *J. Plant Physiol.* 162, 21–26. doi: 10.1016/j.jplph.2004.06.001

Visser, E. J. W., Bogemann, G. M., Blom, C. W. P. M., and Voesenek, L. A. C. J. (1996). Ethylene accumulation in waterlogged Rumex plants promotes formation of adventitious roots. *J. Exp. Bot.* 47, 403–410. doi: 10.1093/jxb/47.3.403

Wachsman, G., Sparks, E. E., and Benfey, P. N. (2015). Genes and networks regulating root anatomy and architecture. *New Phytol.* 208, 26–38. doi: 10.1111/nph.13469

Waines, J. G., and Ehdaie, B. (2007). Domestication and crop physiology: roots of green-revolution wheat. *Ann. Bot.* 100, 991–998. doi: 10.1093/aob/mcm180

Walter, A., Silk, W. K., and Schurr, U. (2009). Environmental effects on spatial and temporal patterns of leaf and root growth. *Annu. Rev. Plant Biol.* 60, 279–304. doi: 10.1146/annurev.arplant.59.032607.092819

Wang, Q., Komarov, S., Mathews, A., and Li, K. (2015). *Combined 3D PET and Optical Projection Tomography Techniques for Plant Root Phenotyping. arXiv Preprint arXiv:1501.00242*. Available at: http://arxiv.org/abs/1501.0242\T1\textbackslash nhttp://arxiv.org/abs/1501.00242

Warschefsky, E. J., Klein, L. L., Frank, M. H., Chitwood, D. H., Londo, J. P., von Wettberg, E. J. B., et al. (2016). Rootstocks: diversity, domestication, and impacts on shoot phenotypes. *Trends Plant Sci.* 21, 418–437. doi: 10.1016/j.tplants.2015.11.008

West, G., Inze, D., Inzé, D., Beemster, G., and Inze, D. (2004). Cell cycle modulation in the response of the primary root of *Arabidopsis* to salt stress. *Plant Physiol.* 135, 1050–1058. doi: 10.1104/pp.104.040022.termining

White, P. J., George, T. S., Gregory, P. J., Bengough, A. G., Hallett, P. D., and McKenzie, B. M. (2013). Matching roots to their environment. *Ann. Bot.* 112, 207–222. doi: 10.1093/aob/mct123

Williamson, L. C. (2001). Phosphate availability regulates root system architecture in *Arabidopsis*. *Plant Physiol.* 126, 875–882. doi: 10.1104/pp.126.2.875

Wirth, J., Chopin, F., Santoni, V., Viennois, G., Tillard, P., Krapp, A., et al. (2007). Regulation of root nitrate uptake at the NRT2.1 protein level in *Arabidopsis thaliana*. *J. Biol. Chem.* 282, 23541–23552. doi: 10.1074/jbc.M700901200

Xiong, L., Wang, R.-G., Mao, G., and Koczan, J. M. (2006). Identification of drought tolerance determinants by genetic analysis of root response to drought stress and abscisic acid. *Plant Physiol.* 142, 1065–1074. doi: 10.1104/pp.106.084632

Xu, P., Cai, X. T., Wang, Y., Xing, L., Chen, Q., and Xiang, C. B. (2014). HDG11 upregulates cell-wall-loosening protein genes to promote root elongation in *Arabidopsis*. *J. Exp. Bot.* 65, 4285–4295. doi: 10.1093/jxb/eru202

Yu, H., Chen, X., Hong, Y.-Y., Wang, Y., Xu, P., Ke, S.-D., et al. (2008). Activated expression of an *Arabidopsis* HD-START protein confers drought tolerance with improved root system and reduced stomatal density. *Plant Cell* 20, 1134–1151. doi: 10.1105/tpc.108.058263

Yu, L., Chen, X., Wang, Z., Wang, S., Wang, Y., Zhu, Q., et al. (2013). *Arabidopsis* enhanced drought tolerance1/HOMEODOMAIN GLABROUS11 confers drought tolerance in transgenic rice without yield penalty. *Plant Physiol.* 162, 1378–1391. doi: 10.1104/pp.113.217596

Yu, L. H., Wu, S. J., Peng, Y. S., Liu, R. N., Chen, X., Zhao, P., et al. (2016). *Arabidopsis* EDT1/HDG11 improves drought and salt tolerance in cotton and poplar and increases cotton yield in the field. *Plant Biotechnol. J.* 14, 72–84. doi: 10.1111/pbi.12358

Zamir, D., and Gadish, I. (1987). Pollen selection for low temperature adaptation in tomato. *Theor. Appl. Genet.* 74, 545–548. doi: 10.1007/BF00288849

Zhao, Y., Wang, T., Zhang, W., and Li, X. (2011). SOS3 mediates lateral root development under low salt stress through regulation of auxin redistribution and maxima in *Arabidopsis*. *New Phytol.* 189, 1122–1134. doi: 10.1111/j.1469-8137.2010.03545.x

Zheng, D., Han, X., An, Y., Guo, H., Xia, X., and Yin, W. (2013). The nitrate transporter NRT2.1 functions in the ethylene response to nitrate deficiency in *Arabidopsis*. *Plant Cell Environ.* 36, 1328–1337. doi: 10.1111/pce.12062

Zhu, J., Ingram, P. A., Benfey, P. N., and Elich, T. (2011). From lab to field, new approaches to phenotyping root system architecture. *Curr. Opin. Plant. Biol.* 14, 310–317. doi: 10.1016/j.pbi.2011.03.020

Zhu, J., Kaeppler, S. M., and Lynch, J. P. (2005a). Mapping of QTLs for lateral root branching and length in maize (*Zea mays* L.) under differential phosphorus supply. *Theor. Appl. Genet.* 111, 688–695. doi: 10.1007/s00122-005-2051-3

Zhu, J., Kaeppler, S. M., and Lynch, J. P. (2005b). Topsoil foraging and phosphorus acquisition efficiency in maize (*Zea mays*). *Funct. Plant Biol.* 32, 749–762. doi: 10.1071/FP05005

Zhu, J., and Lynch, J. P. (2004). The contribution of lateral rooting to phosphorus acquisition efficiency in maize (*Zea mays*) seedlings. *Funct. Plant Biol.* 31, 949–958. doi: 10.1071/FP04046

Zhu, J., Mickelson, S. M., Kaeppler, S. M., and Lynch, J. P. (2006). Detection of quantitative trait loci for seminal root traits in maize (*Zea mays* L.) seedlings grown under differential phosphorus levels. *Theor. Appl. Genet.* 113, 1–10. doi: 10.1007/s00122-006-0260-z

Zhu, J., Zhang, K. X., Wang, W. S., Gong, W., Liu, W. C., Chen, H. G., et al. (2015). Low temperature inhibits root growth by reducing auxin accumulation via ARR1/12. *Plant Cell Physiol.* 56, 727–736. doi: 10.1093/pcp/pcu217

Zobel, R. W., Del Tredici, P., and Torrey, J. G. (1976). Method for growing plants aeroponically. *Plant Physiol.* 57, 344–346. doi: 10.1104/pp.57.3.344

Zolla, G., Heimer, Y. M., and Barak, S. (2010). Mild salinity stimulates a stress-induced morphogenic response in *Arabidopsis thaliana* roots. *J. Exp. Bot.* 61, 211–224. doi: 10.1093/jxb/erp290

Conflict of Interest Statement: The authors declare that the research was conducted in the absence of any commercial or financial relationships that could be construed as a potential conflict of interest.

frontiers in Plant Science

ORIGINAL RESEARCH
published: 09 January 2017
doi: 10.3389/fpls.2016.02035

Durum Wheat Roots Adapt to Salinity Remodeling the Cellular Content of Nitrogen Metabolites and Sucrose

Maria Grazia Annunziata[1†], *Loredana F. Ciarmiello*[2†], *Pasqualina Woodrow*[2†], *Eugenia Maximova*[1], *Amodio Fuggi*[2] *and Petronia Carillo*[2*†]

[1] *Department of Metabolic Networks, Max Planck Institute of Molecular Plant Physiology, Potsdam, Germany,* [2] *Dipartimento di Scienze e Tecnologie Ambientali, Biologiche e Farmaceutiche, Università degli Studi della Campania "Luigi Vanvitelli", Caserta, Italy*

Plants are currently experiencing increasing salinity problems due to irrigation with brackish water. Moreover, in fields, roots can grow in soils which show spatial variation in water content and salt concentration, also because of the type of irrigation. Salinity impairs crop growth and productivity by inhibiting many physiological and metabolic processes, in particular nitrate uptake, translocation, and assimilation. Salinity determines an increase of sap osmolality from about 305 mOsmol kg^{-1} in control roots to about 530 mOsmol kg^{-1} in roots under salinity. Root cells adapt to salinity by sequestering sodium in the vacuole, as a cheap osmoticum, and showing a rearrangement of few nitrogen-containing metabolites and sucrose in the cytosol, both for osmotic adjustment and oxidative stress protection, thus providing plant viability even at low nitrate levels. Mainly glycine betaine and sucrose at low nitrate concentration, and glycine betaine, asparagine and proline at high nitrate levels can be assumed responsible for the osmotic adjustment of the cytosol, the assimilation of the excess of ammonium and the scavenging of ROS under salinity. High nitrate plants with half of the root system under salinity accumulate proline and glutamine in both control and salt stressed split roots, revealing that osmotic adjustment is not a regional effect in plants. The expression level and enzymatic activities of asparagine synthetase and Δ1-pyrroline-5-carboxylate synthetase, as well as other enzymatic activities of nitrogen and carbon metabolism, are analyzed.

Keywords: osmotic adjustment, glycine betaine, asparagine, asparagine synthetase, P5CS, nitrate reductase

OPEN ACCESS

Edited by:
Janin Riedelsberger, University of Talca, Chile

Reviewed by:
Sergey Shabala, University of Tasmania, Australia
Anna Maria Mastrangelo, Centro di Ricerca per l'Orticoltura (CRA), Italy

***Correspondence:**
Petronia Carillo
petronia.carillo@unina2.it

[†] *These authors have contributed equally to this work.*

Specialty section:
This article was submitted to Plant Physiology, a section of the journal Frontiers in Plant Science

Received: *23 September 2016*
Accepted: *20 December 2016*
Published: *09 January 2017*

Citation:
Annunziata MG, Ciarmiello LF, Woodrow P, Maximova E, Fuggi A and Carillo P (2017) Durum Wheat Roots Adapt to Salinity Remodeling the Cellular Content of Nitrogen Metabolites and Sucrose. Front. Plant Sci. 7:2035. doi: 10.3389/fpls.2016.02035

INTRODUCTION

Salinity affects more than 40% of soils in the Mediterranean basin (Nedjimi, 2014). In this area seawater intrusion into freshwater aquifers and irrigation with brackish water highly contribute to soil salinization (Rana and Katerji, 2000). Indeed, irrigation with salinized water and scarce winter rainfall contribute to further increase the salt stress problems with a significant decrease in crops productivity. In these conditions, crops have to cope with daily exposure to hyperosmotic stress and seasonal effects due to salt accumulation in the roots (Maggio et al., 2011).

Soil salinity inhibits plant growth mainly due to osmotic stress and ion toxicity (Munns and Tester, 2008; Gorham et al., 2010). High salinity decreases the capacity of roots to extract water from soil, and high concentrations of salts within the plant itself can be toxic, resulting in plant

nutritional imbalance and oxidative stress (Hasegawa et al., 2000; Munns, 2002; Munns and Tester, 2008). This dual effect reduces plant growth, development, and survival. However, the extent of the damage to crops depends on the concurrent salt toxicity levels and phenological stage sensitivity to salt stress (Lutts et al., 1995; Hasegawa et al., 2000). Seedling stage, for example, is the more vulnerable phase of durum wheat growth under salinity (Carillo et al., 2008). This species, which is mainly cropped in Mediterranean type climate, is more sensitive to salinity than bread wheat (Gorham et al., 1990; James et al., 2006) and yields poorly on saline soil (Munns et al., 2006; Rahnama et al., 2011) partly due to the scarce ability of durum wheat to exclude sodium (Colmer et al., 2006; James et al., 2011). Sodium has, in fact, a damaging effect on cytosol and organelles metabolism because it tends to replace potassium in key enzymatic reactions. For this reason, the potassium to sodium ratio is more critical than the absolute amount of sodium for the cell performance under salinity (Maathuis and Amtmann, 1999; Shabala and Cuin, 2008; Cuin et al., 2009). However, exposure to salinity triggers specific strategies for cell osmotic adjustment and control of ion and water homeostasis to minimize stress damage and to re-establish growth (Hasegawa et al., 2000; Puniran-Hartley et al., 2014; Gao et al., 2016; Woodrow et al., 2016). A ubiquitous mechanism that plants have evolved to adapt to salinity involves sodium sequestration in the vacuole, as a cheap osmoticum, and synthesis and accumulation of compatible compounds, which have a much higher cost in terms of energy needed for their synthesis (50–70 moles ATP for mole), both for osmotic adjustment and oxidative stress protection in the cytosol (Raven, 1985; Cuin et al., 2009; Shabala, 2013). Most of compatible solutes are N-containing metabolites, such as amino acids, amines, and betaines (Mansour, 2000). Therefore, nitrogen availability is of pivotal importance in plants under salinity. This is true not only for growth, but also for the synthesis of these organic solutes involved in osmoprotection (Krishna Rao and Gnanam, 1990; Silveira et al., 2001). Nevertheless, salinity affects root nitrate influx and loading of nitrate into the root xylem (Peuke and Jeschke, 1999), nitrate reductase activity (Abd-El-Baki et al., 2000; Carillo et al., 2005), amino acid metabolism (Silveira et al., 2012), and protein synthesis (Aslam et al., 1996). The imbalance between nitrogen assimilation and protein synthesis under salinity could be responsible for the increase of free amino acids in roots and shoots of plants under salinity (Silveira et al., 2001). In particular, salinity greatly increases the levels of proline and glycine betaine in durum wheat (Munns, 2002; Carillo et al., 2008), as in other Poaceae (Sairam and Tyagi, 2004; Carillo et al., 2005; Ashraf and Foolad, 2007). In many halophytes, leaf concentration of proline, GB or both contributes to the osmotic pressure in the cell as a whole (Flowers et al., 1977). In glycophytes, proline and GB have lower concentrations but, being partitioned exclusively to the cytoplasm, which makes up about <10% of the volume of the cell, they are able to determine significant osmotic pressure and balance the vacuolar osmotic potential (Cuin et al., 2009).

Notwithstanding several studies have already been carried out on durum wheat under salinity, most of them were performed on leaves. Only few data concern the effects of salinity on root metabolic profile, and how metabolite changes are related to the physiology of cells and root tissues (Zubaidi et al., 1999; Maggio et al., 2003; Carillo et al., 2005; Cuin and Shabala, 2007; Cuin et al., 2008). Moreover, plant metabolic response to salt stress can greatly differ depending on environmental factors in the soil. One of these factors is that salinity in the fields is normally distributed in patches (Richards, 1983) and therefore heterogeneous (Sonneveld and de Kreij, 1999; Kong et al., 2012). Experiments carried out in hydroponics, a homogenous environment, and in soils have given contrasting results. It has been argued, thus, that it is more realistic to study the effects of salinity in heterogeneous split root systems than by exposing whole roots to specific levels of NaCl or at least comparing the salt effect in the two different situations (Rahnama et al., 2011; Bazihizina et al., 2012; Kong et al., 2012).

Since it is unquestionable that the elucidation of fundamental molecular and physiological responses to salinity is instrumental to improving crops salt tolerance, in the present study uniform and non-uniform salinity have been simulated with a split-root system in which the root system was divided into two equal portions and each portion irrigated with 0 mM (control) or 100 mM NaCl (salt stress) solution and 10 mM KNO_3. Moreover, for the uniform salinity treatment (with the entire root system grown at 0 or 100 mM NaCl), low and high nitrate concentrations (0.1 and 10 mM KNO_3, respectively) are applied.

These conditions are used to study physiological root responses to salinity focusing on: (i) root ions accumulation and effect on some physiological parameters; (ii) osmolytes accumulation and contribution with ions to the osmotic balance of the root cells; (iii) expression and activity of the main enzymes involved in the synthesis of nitrogen-containing osmolytes; (iv) antioxidant response.

MATERIALS AND METHODS

Plant Material and Growth Conditions

Seeds of durum wheat (*Triticum durum* Desf. cv. Ofanto) were supplied from the Center for Cereal Research of Foggia (Italy) and germinated in the dark on filter paper moistened with deionized water at 21°C. Thereafter, individual seedlings were transferred to 4.5 L pots placed into a phytotron under controlled conditions (16 h photoperiod, 350 μmol m^{-2} s^{-1} PAR, thermoperiod 25:20°C day:night, 65% relative humidity). Initially the pots contained distilled water, that was replaced after 3 days with a modified (nitrogen-free) Hoagland medium (Carillo et al., 2005), and then after other 3 days with Hoagland medium containing 0.1 or 10 mM KNO_3. The nutrient solution was continually aerated and replaced every 3 days.

Starting from day 10 of hydroponic culture, the medium was supplemented with 50 mM NaCl, increased to 100 mM NaCl 1 day later. The gradual exposure of plants to the increasing NaCl reflected that of field growing conditions, and prevented salt shock (Woodrow et al., 2016). A subgroup of 10 mM KNO_3 grown plants was cultured in a split-root system with half of their roots treated with or without 100 mM NaCl. The control plants in the other pot from each group were grown without supplemented NaCl. The root length of six replicate plants of each treatment on days 5, 10, 15, and 20 of hydroponic culture was measured.

The roots of 20-day-old plants were immediately used for the determination of physiological and morphological parameters or stored at −80°C.

Physiological and Morphological Measurements

Roots were immediately weighed to obtain the fresh weight and re-weighted after floating on deionized water for 24 h at 4°C in the dark and after being dried at 70°C for 48 h. The relative water content (RWC) was obtained as [(root fresh weight − root dry weight)/(root turgor weight − root dry weight)] × 100. Water potential was measured by using a pressure bomb (Scholander et al., 1965). The root vigor index (RVI) was calculated as: RVI = percentage germination (∼88%) × average roots dry weight (in mg) (Woodrow et al., 2016).

For light microscopy fresh root were cut in 2 mm or smaller size pieces with a razor blade with the aid of a stereomicroscope. Samples were placed on a glass slide in water, covered with a cover slip and immediately examined. Microscopy was performed on an Olympus BX51 microscope (Olympus Optical Co., Hamburg, Germany) equipped with differential interference contrast (DIC). Roots were examined at 20, 40, and 100 magnification; for this latter a 100 oil-immersion objective was used. Images were captured using a digital camera and CellPrism software.

Ions, Osmolality, Hydrogen Peroxide, and Metabolites Analysis

Ions were assayed according to Carillo et al. (2011). Root sap osmolality was measured according to Cuin et al. (2009). The amounts of hydrogen peroxide (H_2O_2) were determined according to Baptista et al. (2007). Total proteins, starch and sugars were evaluated according to Carillo et al. (2012). Total fructans were measured according to Morcuende et al. (2004). Fructan classes were determined according to Cimini et al. (2015). Starch and total fructans were expressed as glucose equivalents.

Primary amino acids, proline, and glycine betaine were extracted and assayed according to Woodrow et al. (2016). Ascorbic acid (ASCAc), dehydroascorbic acid (DHA), reduced and oxidized glutathione (GSH and GSSG) were extracted as described by Annunziata et al. (2012) and Woodrow et al. (2012) and determined according to Queval and Noctor (2007). Malondialdehyde was assayed according to Carillo et al. (2011). Contribution of metabolites and ions to osmolality was calculated according to Cuin et al. (2009) and Puniran-Hartley et al. (2014).

Enzyme Extractions and Assays

All the procedures for root enzyme extractions and assays were carried out at 4°C. Enzymes were extracted according to Gibon et al. (2004), except where differently indicated. Asparagine synthetase (AS; EC 6.3.5.4) was extracted in roots of 20-day-old plants and immediately desalted and assayed in a solution containing 1 mM aspartate semialdehyde (an inhibitor of asparaginase) and 1 mM amino(oxy)acetic acid (an inhibitor of aspartate aminotransferase) according to Duff et al. (2011). NADH-dependent glutamate synthase (Fd-GOGAT; EC 1.4.1.14), glutamine synthetase (GS; EC 6.3.1.2), and nitrate reductase (NR; EC 1.6.6.1) were assayed according to Gibon et al. (2004). Phosphoenolpyruvate carboxylase (PEPC; EC 4.1.1.31) was assayed according to Esposito et al. (1998). Deaminating glutamate dehydrogenase activities (GDH; EC 1.4.1.2) was determined according to Skopelitis et al. (2007). Δ1-pyrroline-5-carboxylate synthetase activity (P5CS; EC 2.7.2.11) was determined according to Parre et al. (2010). For all assayed enzyme activities, parallel control experiments were performed after desalting the extracts via centrifugal filtration through Sephadex G-25 PD-10 columns (Amersham Biosciences) equilibrated with Hepes-KOH 50 mM pH 7.5, $MgCl_2$ 10 mM, dithiothreitol 1 mM and eluted by spinning at 1800 g for 1 min. The enzyme activities were expressed as μmol h^{-1} g^{-1} FW.

RNA Extraction and cDNA Synthesis

Total RNA was isolated from powdered roots according to Woodrow et al. (2016). RNA quantity and quality were determined spectrophotometrically using the NanoDrop ND-1000 UV-VIS (Thermo Scientific, Wilmington, MA) and separated on 1.5% agarose gel stained with SYBR safe (Invitrogen). mRNA was purified from ∼500 μg of total RNA using a mRNA Isolation Kit (Roche) following manufacturer's instructions. First strand cDNA was synthesized from 1 μg of mRNA by reverse transcriptase with both random hexamer primers and anchored oligo dT according to the instructions of the SensiFAST™ cDNA Synthesis Kit (Bioline).

RT-PCR and Gene Expression

Asparagine synthetase (*Asn1*, *Asn2*, *Asn3*), Δ-pyrroline-5-carboxylate synthetase (*P5CS*), and nitrate reductase (*NR*) gene expression analysis was carried out by semiquantitative RT-PCR reactions, using Transcriptor High Fidelity cDNA Synthesis Sample Kit (Roche). RT-PCR was performed in a total volume of 50 μl containing 300 ng of the first strand cDNA reaction products, 5 μl of FastStart Buffer with 20 mM $MgCl_2$, 0.2 mM deoxynucleotides, 50 pmol of primers (Table S1), and 2 U of FastStart Taq DNA polymerase (Roche). RT-PCR analysis was performed using gene-specific primers for *Asn1*, *Asn2*, and *Asn3* isoforms (Wang et al., 2005; Gao et al., 2016), *NR* (Carillo et al., 2005; Wang et al., 2005), and degenerate primers for *P5CS* (Woodrow et al., 2016) (Table S1). The amount of *TdAsn1*, *TdAsn2*, *TdAsn3*, *TdNR*, and *TdP5CS* templates mRNA levels were based on the comparison with the level of the 190 bp mRNA for actin (Woodrow et al., 2010), a constitutively expressed "house-keeping" gene. The semi-quantitative PCR was used to estimate the transcript levels. All PCR reactions included an initial denaturation step of 2 min at 95°C. Afterwards, in order to prevent amplifications reaching the plateau phase, several dilution tests (1:5; 1:10; 1:15) were performed combined with various numbers of cycles (30–35) with a denaturation step (30 s at 95°C), an annealing step (30 s at 40–70°C), an extension step (2 min at 72°C), and a final extension for 7 min at 72°C. Finally the experiments with a 1:5 dilution and 35 cycles were carried out. Amplification products were visualized on 1.5% (w/v)

agarose gels, using a UV light. Densitometric evaluation of DNA bands was performed with the Imager 1D/2D software (Image Lab v. 3.0, Bio-Rad). Band intensity was expressed as relative absorbance units. Band signals were normalized using the actin signals.

Cloning and Sequencing of P5CS cDNA

The 0.5 kb *P5CS* cDNA amplification products were purified from agarose gel and cloned into a pGEM-T Easy Vector system II (Promega) by mixing 2 μL of amplified product with 25 ng of pGEM-T Easy Vector, 3 U T4 ligase, and 1 μL ligation buffer in 10 μL volume. The ligation product was cleaned with sec-butanol and precipitated with ethanol. The sample was resuspended in 10 μL of 0.5 M Tris-EDTA and transformed into *Escherichia coli* cells. Twenty clones were sequenced by BMR Genomics (Padova).

Statistical Analysis

Roots from six plants for each treatment were used for determination of length, measurements of fresh and dry weight, and water potential. The other analyses were performed on four biological replicates for each treatment. The analysis of variance (ANOVA) and the Pearson correlation analysis were performed by SigmaPlot 12 software (Systat Software Inc., Richmond, CA, USA). The mean differences were compared to their corresponding Least Significant Differences (LSD) at 0.05 and 0.01 confidence levels. A heat map generated in Excel (Carillo et al., 2008) was used to summarize the plant responses to the salt and light stresses. Results were calculated as $\log_2$ (salt stress or HL values/average of controls) and were visualized using a false color scale, with blue indicating an increase and red a decrease of values relative to those in control condition. No differences were visualized by white squares. Principal component analysis (PCA) on the different analyzed parameters was carried out using Multibase 2015, an Excel add-in program for Windows (http://www.numericaldynamics.com) according to Ciarmiello et al. (2015).

RESULTS

Root Growth and Physiological Parameters

The extension rate of roots of wheat seedlings at low nitrate (LNR) was higher than that of high nitrate roots (HNR) and high nitrate split roots (HNSR) between day 10 and 15 either in control and salt stressed plants (**Figures 1A–C**). Between day 15 and 20 in plants under salinity the extension rate of HNR and HNSR strongly increased compared to LNR, and in particular in HNSR it was significantly higher ($P < 0.01$) than in the other two treatments (**Figure 1C**). Nonetheless, at day 20 the length of HNR and HNSR was significantly lower ($P < 0.05$) than LNR either under control or salinity treatment (**Table 1**). The fresh weight of HNR was 1.4-fold higher than that of LNR, independently of salinity. The fresh weight of HNSR in control conditions did not differ significantly from HNR one, while that of HNSR under salinity was about 3-fold smaller than that of salt stressed HNR (**Table 1**). The root dry weight, showed a different pattern, being similar in control and in salt stressed treatments (on average 48.8 or 45.6 mg per plant, respectively), independently of nitrogen treatment, with the exception of HNSR under salinity that showed the lowest weight (14.6 mg per plant) (**Table 1**).

The RWC of control LNR and HNR and HNSR was about 92, 97, and 94%, respectively. Salinity halved the RWC in LNR and decreased of about 8% that of HNR and HNSR (**Table 1**).

The root vigor index (RVI) was, on average, 43 in control roots both at low and high nitrate. The RVI decreased by 22, 30, and 70% of controls in LNR, HNR, and HNSR under salinity, respectively (**Table 1**).

The root water potential (Y_w) was higher in control than in salt stressed plants. Salinity reduced it from −0.40 and −0.25 MPa of control LNR and HNR, respectively, to values of about −0.58 and −0.39. HNSR showed root Y_w similar to that of LNR either in control and salt stress treatment (**Table 1**).

Ions and Hydrogen Peroxide Content

The concentration of chloride (Cl^-) and sodium (Na^+) in roots of either control and salt stressed plants decreased when

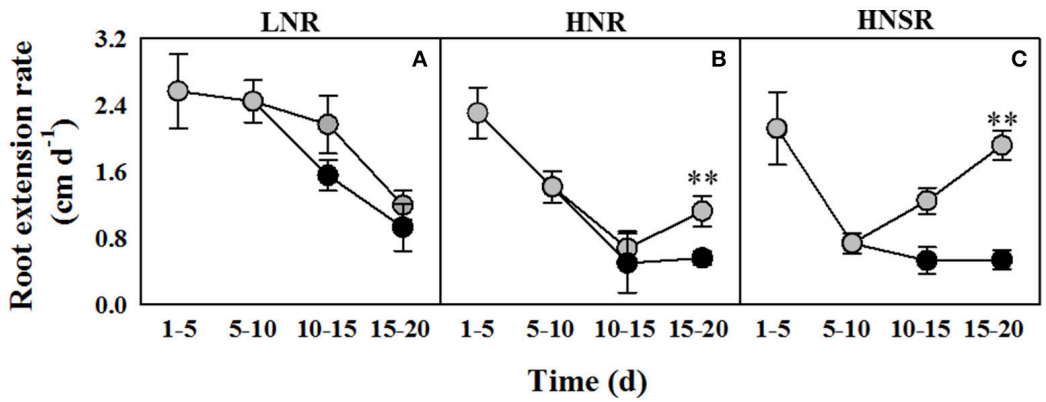

FIGURE 1 | Root extension rate of durum wheat roots cultured in 0.1 (LNR, A) and 10 mM KNO_3^- with (HNR, **B**) or without (HNSR, **C**) split root system, under control (○) or salt (100 mM NaCl, ●) conditions. Six replicate plants of each treatment were measured on days 5, 10, 15, and 20 of hydroponic culture. KNO_3^- was added on day 5 and 100 mM NaCl was added from day 10. The values are means ± *SD* ($n = 6$). Significant differences between treatments are indicated by asterisks (**$p < 0.01$; LSD-test).

TABLE 1 | Physiological parameters, ions and hydrogen peroxide, carbohydrates, MDA, ascorbic acid, and glutathione expressed per g fresh weight in roots of durum wheat seedlings grown with 0.1 or 10 mM NO_3^- (with or without root split system), under 0 or 100 mM NaCl.

	0.1 mM NO_3^-		10 mM NO_3^-		10 mM NO_3^- split	
	0 mM NaCl	100 mM NaCl	0 mM NaCl	100 mM NaCl	0 mM NaCl	100 mM NaCl
PHYSIOLOGICAL PARAMETERS						
Lenght (cm)	66.1 ± 9.4^{a}	41.5 ± 3.7^{b}	28.3 ± 5.3^{cd}	22.8 ± 2.5^{c}	34.0 ± 1.4^{d}	24.0 ± 3.0^{c}
Fresh weight (mg/plant)	544 ± 64^{a}	402 ± 34^{b}	750 ± 63^{c}	544 ± 31^{a}	639 ± 98^{c}	139 ± 16^{d}
Dry weight (mg/plant)	49.3 ± 3.7^{a}	42.8 ± 1.6^{b}	51.1 ± 4.3^{a}	48.1 ± 4.6^{ab}	46.0 ± 4.4^{ab}	14.6 ± 1.0^{c}
RWC	92.0 ± 4.2^{ac}	43.4 ± 8.2^{b}	96.9 ± 3.4^{a}	88.9 ± 1.3^{c}	94.0 ± 0.5^{a}	85.8 ± 5.5^{c}
Root vigor index	43.4 ± 3.0^{ac}	37.7 ± 1.04^{b}	45.0 ± 2.2^{a}	42.3 ± 1.7^{ac}	40.5 ± 1.2^{c}	13 ± 0.7^{d}
Root water potential (MPa)	−0.40 ± 0.09^{a}	−0.58 ± 0.08^{b}	−0.25 ± 0.04^{c}	−0.39 ± 0.03^{a}	−0.30 ± 0.06^{ac}	−0.56 ± 0.05^{b}
Sap osmolality (mOsmol kg^{-1})	343 ± 36^{a}	575 ± 55^{b}	284 ± 47^{c}	543 ± 61^{b}	289 ± 33^{ac}	470 ± 55^{b}
Root/Shoot DW ratio	1.06 ± 0.13^{a}	1.45 ± 0.16^{b}	0.55 ± 0.04^{c}	0.59 ± 0.07^{c}		
IONS AND HYDROGEN PEROXIDE (μmol g^{-1} FW)						
Chloride	30.3 ± 2.7^{a}	111.8 ± 13^{b}	23.6 ± 2.0^{c}	62.7 ± 7.5^{d}	20.9 ± 3.1^{c}	59.7 ± 1.6^{c}
Nitrate	0.05 ± 0.01^{a}	0.10 ± 0.01^{a}	34.5 ± 4.8^{b}	23.4 ± 4.9^{c}	35.4 ± 0.6^{d}	19.3 ± 0.5^{c}
Potassium	119 ± 13^{a}	87.3 ± 6.4^{b}	79.1 ± 15.8^{b}	113 ± 9.1^{a}	86.0 ± 8.3^{b}	98.0 ± 10.0^{b}
Sodium	19.2 ± 1.72^{a}	101.3 ± 14^{b}	10.5 ± 1.1^{c}	84.7 ± 16.1^{b}	14.1 ± 2.6^{c}	77.9 ± 15.0^{b}
Potassium:Sodium	6.22 ± 0.70^{a}	0.86 ± 0.11^{b}	7.51 ± 0.62^{a}	1.33 ± 0.14^{c}	6.10 ± 0.80^{a}	1.26 ± 0.15^{c}
Hydrogen peroxide	1.79 ± 0.21^{a}	4.76 ± 0.61^{b}	1.18 ± 0.24^{c}	3.16 ± 0.35^{d}	1.99 ± 0.31^{a}	3.26 ± 0.84^{d}
CARBOHYDRATES (μmol g^{-1} FW)						
Starch (Geq)	15.6 ± 2.6^{a}	14.4 ± 3.5^{a}	13.0 ± 1.7^{a}	14.0 ± 1.54^{a}	13.0 ± 1.4^{a}	14.3 ± 1.6^{a}
Hexoses	8.83 ± 0.72^{a}	5.60 ± 0.41^{b}	6.06 ± 0.87^{b}	5.55 ± 0.20^{b}	6.04 ± 0.61^{b}	4.66 ± 0.32^{c}
Sucrose	5.11 ± 0.31^{a}	8.60 ± 0.91^{b}	4.33 ± 0.83^{a}	4.90 ± 0.36^{a}	6.17 ± 0.70^{a}	5.86 ± 0.84^{a}
Total fructans (G_{eq})	44.1 ± 5.3^{a}	30.9 ± 1.7^{b}	9.13 ± 3.27^{c}	18.6 ± 2.8^{d}	11.9 ± 2.5^{c}	14.5 ± 1.7^{cd}
1-Kestose	5.69 ± 0.27^{a}	4.85 ± 0.32^{b}	0.36 ± 0.03^{c}	0.89 ± 0.12^{d}	0.46 ± 0.07^{c}	0.72 ± 0.09^{d}
Inulin	0.38 ± 0.06^{a}	0.63 ± 0.10^{b}	0.20 ± 0.03^{c}	0.158 ± 0.02^{c}	0.28 ± 0.02^{d}	0.10 ± 0.02^{e}
Nystose	1.216 ± 0.088^{a}	6.024 ± 1.253^{b}	0.533 ± 0.045^{c}	1.341 ± 0.10^{a}	0.67 ± 0.09^{c}	1.10 ± 0.14^{a}
1-Fructofuranosylnystose	2.925 ± 0.36^{a}	4.948 ± 0.292^{b}	1.652 ± 0.269^{ac}	2.013 ± 0.40^{a}	2.04 ± 0.19^{a}	1.52 ± 0.18^{c}
Total fructans:Starch	2.83 ± 0.33^{a}	2.14 ± 0.24^{b}	0.70 ± 0.09^{c}	1.33 ± 0.11^{d}	0.92 ± 0.13^{c}	1.01 ± 0.16^{c}
MDA, ASCORBIC ACID, AND GLUTATHIONE (nmol g^{-1} FW)						
MDA	6.51 ± 1.58^{a}	12.43 ± 0.89^{b}	18.2 ± 1.8^{c}	11.7 ± 1.3^{b}	16.6 ± 1.2^{c}	14.5 ± 2.9^{bc}
AsAc	0.66 ± 0.11^{a}	0.63 ± 0.12^{a}	0.64 ± 0.1^{a}	0.77 ± 0.17^{a}	0.53 ± 0.08^{a}	0.85 ± 0.13^{b}
DHA	0.62 ± 0.04^{a}	0.29 ± 0.05^{b}	0.64 ± 0.08^{a}	2.45 ± 0.36^{c}	0.69 ± 0.09^{a}	1.91 ± 0.24^{c}
AsAc +DHA	1.27 ± 0.10^{a}	0.92 ± 0.14^{b}	1.29 ± 0.20^{a}	3.22 ± 0.42^{c}	1.22 ± 0.15^{a}	2.76 ± 0.31^{b}
DHA:AsAc	0.96 ± 0.22^{a}	0.49 ± 0.12^{b}	1.00 ± 0.15^{a}	3.17 ± 0.41^{c}	1.30 ± 0.22^{a}	2.25 ± 0.35^{d}
GSH	20.2 ± 1.6^{a}	4.0 ± 0.3^{b}	67.8 ± 5.4^{c}	70.3 ± 5.6^{c}	44.7 ± 3.6^{d}	86.6 ± 8.9^{e}
GSSG	40.8 ± 3.5^{ad}	9.5 ± 2.0^{b}	21.3 ± 1.7^{c}	50.2 ± 6.2^{a}	38.4 ± 3.7^{d}	14.6 ± 1.3^{e}
GSH + GSSG	60.9 ± 4.9^{a}	13.5 ± 1.1^{b}	89.1 ± 7.1^{c}	120 ± 11^{d}	83.1 ± 6.7^{c}	101 ± 8^{d}
GSSG:GSH	2.02 ± 0.11^{a}	2.39 ± 0.26^{a}	0.31 ± 0.07^{b}	0.71 ± 0.06^{c}	0.86 ± 0.10^{c}	0.17 ± 0.01^{d}

Values are mean ± SD (n = 4). Means in the same row with different letters are significantly different (p < 0.05, LSD-test). On the right a heat map summarizes the differences between samples.

nitrate (NO_3^-) concentration in the culture medium increased, even though not significantly for Na^+ under salinity, while significantly for Cl^-. This latter was about 30 and 22 μmol g^{-1} FW in control LNR and HNR and HNSR and 112 and 61 μmol g^{-1} FW in salt stressed LNR and HNR and HNSR, respectively (**Table 1**).

The Na^+ content was 19.2 ± 1.7 and 101 ± 14 μmol g^{-1} FW in control and salt stressed LNR, and 10.5 ± 1.1 and 84.7 ± 16.1 μmol g^{-1} FW in control and salt stressed oHNR, respectively. The Na^+ content of HNSR was similar to that of HNR (**Table 1**).

The NO_3^- concentration of roots at low nitrate was similar to that of the nutrient solution, while in HNR and HNSR at 10 mM KNO_3 it exceeded that of the nutrient solution by about 3.5- and 2.1-fold in control and salt stressed plants, respectively (**Table 1**).

Potassium (K^+) content ranged between about 87 and 110 μmol g^{-1} FW and was not significantly dependent on NO_3^- or salt treatment (**Table 1**). The K^+ to Na^+ content ratio, which provides information about the potential of the plants to discriminate the two ions (Gorham et al., 1990), was, on average, 6.7 in all control roots. This value was significantly decreased

($p < 0.01$) by the salt treatment to 0.86 and about 1.3 in salt treated LNR and HNR, respectively (**Table 1**).

The hydrogen peroxide concentration of roots was 1.9 μmol g–1 FW in control LNR and HNSR and 1.2 μmol g–1 FW in control HNR. In response to salinity, its content increased 2.7-fold in LNR and HNR and 1.6-fold in HNSR (**Table 1**).

N-Containing Compounds

The total proteins of control roots of LNR and HNR and HNSR were, on average, 3.3 mg g^{-1} FW. Salinity did not significantly change their content (**Table 2**).

The total free amino acid concentration of roots of control plants depended on nitrate nutrition, and was 3.6-fold higher in HNR than in LNR (**Table 2**). Glutamate, proline, glutamine, aspartate, and asparagine were quantitatively the major amino acids representing about 58, 74, and 77% of total free amino acids in LN, HN, and HNs control roots, respectively (**Table 2**). Salinity significantly increased the free amino acid concentration in LNR and HNR (1.5- and 1.4-fold, respectively, $p < 0.01$), but not in HNSR. This result was mostly due to alanine, asparagine, and aspartate which increased 2.8-, 2.8- and 2.5-fold, respectively, in LNR, and to asparagine and proline which

TABLE 2 | Total proteins, free amino acids, glycine betaine (GB), and enzyme activities in durum wheat roots under 0.1 and 10 mM NO_3^- (with or without root split system), under 0 and 100 mM NaCl.

	0.1 mM NO_3^-		10 mM NO_3^-		10 mM NO_3^- split	
	0 mM NaCl	100 mM NaCl	0 mM NaCl	100 mM NaCl	0 mM NaCl	100 mM NaCl
Total proteins (mg g^{-1} FW)	2.93 ± 0.42^{a}	3.11 ± 0.52^{ab}	3.45 ± 0.36^{b}	2.90 ± 0.21^{a}	3.62 ± 0.29^{b}	3.11 ± 0.44^{ab}
AMINO ACIDS AND GB (μmol g^{-1} FW)						
Total free amino acids	2.57 ± 0.14^{a}	3.85 ± 0.22^{b}	8.14 ± 0.86^{c}	11.3 ± 0.8^{d}	10.1 ± 0.9^{cd}	9.22 ± 0.66^{c}
Alanine	0.11 ± 0.01^{a}	0.31 ± 0.01^{b}	0.75 ± 0.06^{c}	0.77 ± 0.08^{c}	0.59 ± 0.00^{d}	0.63 ± 0.06^{cd}
Arginine	0.04 ± 0.00^{a}	0.06 ± 0.00^{b}	0.06 ± 0.01^{b}	0.09 ± 0.01^{c}	0.07 ± 0.01^{b}	0.06 ± 0.01^{b}
Asparagine	0.11 ± 0.01^{a}	0.31 ± 0.02^{b}	0.27 ± 0.05^{b}	2.45 ± 0.23^{c}	0.72 ± 0.06^{d}	0.75 ± 0.11^{d}
Aspartate	0.13 ± 0.01^{a}	0.32 ± 0.01^{b}	1.23 ± 0.13^{c}	1.32 ± 0.12^{c}	1.48 ± 0.03^{d}	0.96 ± 0.08^{e}
Cysteine	0.03 ± 0.00^{a}	0.04 ± 0.00^{b}	0.04 ± 0.00^{b}	0.05 ± 0.00^{c}	0.06 ± 0.01^{cd}	0.07 ± 0.01^{d}
Glutamine	0.28 ± 0.06^{a}	0.27 ± 0.03^{a}	0.71 ± 0.13^{b}	1.05 ± 0.08^{c}	1.51 ± 0.01^{d}	1.69 ± 0.06^{e}
Glutamate	0.56 ± 0.03^{a}	0.94 ± 0.07^{b}	3.26 ± 0.48^{c}	2.22 ± 0.23^{d}	3.20 ± 0.02^{c}	2.45 ± 0.19^{d}
Glycine	0.04 ± 0.00^{a}	0.04 ± 0.00^{a}	0.06 ± 0.01^{b}	0.06 ± 0.00^{b}	0.07 ± 0.01^{bc}	0.09 ± 0.01^{c}
Histidine	0.08 ± 0.01^{a}	0.09 ± 0.01^{a}	0.13 ± 0.02^{b}	0.24 ± 0.02^{c}	0.16 ± 0.00^{d}	0.13 ± 0.01^{b}
Isoleucine	0.11 ± 0.01^{a}	0.10 ± 0.01^{a}	0.07 ± 0.00^{b}	0.13 ± 0.01^{c}	0.08 ± 0.00^{b}	0.06 ± 0.00^{d}
Leucine	0.13 ± 0.01^{a}	0.11 ± 0.01^{ab}	0.10 ± 0.01^{b}	0.13 ± 0.01^{a}	0.10 ± 0.00^{b}	0.07 ± 0.01^{c}
Lysine	0.07 ± 0.00^{a}	0.09 ± 0.01^{b}	0.03 ± 0.01^{c}	0.07 ± 0.01^{a}	0.05 ± 0.01^{d}	0.08 ± 0.01^{b}
Metionine	0.03 ± 0.00^{a}	0.04 ± 0.00^{a}	0.05 ± 0.00^{b}	0.05 ± 0.00^{b}	0.06 ± 0.00^{b}	0.05 ± 0.00^{b}
Phenilalanine	0.03 ± 0.00^{a}	0.09 ± 0.00^{b}	0.19 ± 0.06^{c}	0.07 ± 0.01^{bc}	0.08 ± 0.01^{b}	0.06 ± 0.00^{c}
Proline	0.41 ± 0.03^{a}	0.54 ± 0.02^{b}	0.55 ± 0.06^{b}	1.50 ± 0.10^{c}	0.83 ± 0.11^{d}	1.10 ± 0.06^{e}
Serine	0.13 ± 0.01^{a}	0.18 ± 0.00^{b}	0.28 ± 0.02^{c}	0.39 ± 0.04^{d}	0.32 ± 0.01^{c}	0.41 ± 0.03^{d}
Threonine	0.09 ± 0.02^{a}	0.09 ± 0.01^{a}	0.16 ± 0.03^{b}	0.20 ± 0.02^{b}	0.20 ± 0.02^{b}	0.17 ± 0.01^{b}
Triptophane	0.06 ± 0.00^{a}	0.07 ± 0.02^{a}	0.03 ± 0.00^{b}	0.05 ± 0.00^{a}	0.03 ± 0.00^{b}	0.02 ± 0.00^{b}
Tyrosine	0.02 ± 0.00^{a}	0.02 ± 0.00^{a}	0.05 ± 0.01^{b}	0.26 ± 0.02^{c}	0.28 ± 0.04^{c}	0.24 ± 0.02^{c}
Valine	0.11 ± 0.01^{a}	0.13 ± 0.01^{a}	0.13 ± 0.02^{a}	0.21 ± 0.02^{b}	0.17 ± 0.01^{c}	0.13 ± 0.01^{a}
Glutamine:Glutamate	0.50 ± 0.01^{a}	0.29 ± 0.03^{b}	0.22 ± 0.03^{c}	0.47 ± 0.07^{a}	0.47 ± 0.04^{a}	0.69 ± 0.09^{d}
Amides	0.39 ± 0.02^{a}	0.58 ± 0.04^{b}	0.98 ± 0.07^{c}	3.50 ± 0.18^{d}	2.24 ± 0.18^{e}	2.44 ± 0.03^{e}
Minor amino acids	0.69 ± 0.06^{a}	0.80 ± 0.10^{a}	0.83 ± 0.08^{a}	1.29 ± 0.11^{b}	1.10 ± 0.08^{bc}	0.90 ± 0.09^{c}
BCAAs	0.36 ± 0.04^{a}	0.34 ± 0.03^{a}	0.30 ± 0.02^{a}	0.47 ± 0.04^{b}	0.35 ± 0.03^{a}	0.25 ± 0.02^{c}
GB	0.86 ± 0.13^{a}	2.58 ± 0.30^{b}	0.67 ± 0.05^{a}	2.43 ± 0.36^{b}	0.70 ± 0.11^{a}	0.64 ± 0.19^{a}
ENZYME ACTIVITIES (μmol h^{-1} mg^{-1} PROT)						
AS	0.38 ± 0.02^{a}	0.66 ± 0.10^{b}	0.73 ± 0.04^{b}	1.67 ± 0.20^{c}	1.02 ± 0.15^{d}	0.96 ± 0.12^{d}
GDH	6.54 ± 0.82^{a}	5.54 ± 0.29^{a}	4.50 ± 0.48^{a}	4.79 ± 0.32^{a}	4.03 ± 0.58^{a}	4.41 ± 0.36^{a}
GOGAT	2.99 ± 0.30^{a}	1.04 ± 0.11^{b}	2.38 ± 0.36^{a}	4.71 ± 0.65^{d}	2.58 ± 0.18^{a}	2.53 ± 0.29^{a}
GS	18.1 ± 1.7^{ac}	19.6 ± 1.1^{a}	9.82 ± 0.75^{b}	15.5 ± 1.4^{c}	9.49 ± 1.05^{b}	11.1 ± 1.3^{b}
NR	5.81 ± 0.61^{a}	3.77 ± 0.36^{b}	11.2 ± 1.87^{c}	9.43 ± 1.56^{c}	9.40 ± 1.51^{c}	8.57 ± 0.66^{c}
NiR	55.2 ± 4.7^{a}	31.9 ± 4.7^{b}	63.6 ± 2.8^{c}	46.9 ± 4.5^{ad}	53.6 ± 4.4^{a}	41.1 ± 2.7^{d}
P5CS	1.99 ± 0.31^{a}	2.06 ± 0.19^{a}	2.16 ± 0.23^{a}	4.50 ± 0.33^{b}	3.35 ± 0.42^{c}	3.46 ± 0.27^{c}
PEPC	1.45 ± 0.22^{a}	0.64 ± 0.09^{b}	2.08 ± 0.17^{c}	1.39 ± 0.13^{a}	1.59 ± 0.15^{a}	1.26 ± 0.18^{a}

Values are mean ± SD (n = 4). Means in the same row with different letters are significantly different ($p < 0.05$, LSD-test).

increased 9- and 2.7-fold, respectively, in HNR (**Table 2**). While the slight decrease of free amino acids in HNSR under salinity was mostly due to aspartate and glutamate which decreased by 35 and 24%, respectively (**Table 2**). Glutamate content was decreased by salinity by 32% in HNR, while increased by it (1.7-fold) in LNR (**Table 2**, $p < 0.01$).

Salinity increased the glutamine to glutamate ratio by 2.2- and 1.5-fold in HNR and HNSR, but reduced it by 42% in LNR compared to respective controls (**Table 2**).

Salinity increased the minor amino acids content in HNR by 1.6-fold compared to respective control, and this increase was mainly due to tyrosine and branched chain amino acids (BCCAs) which increased 5.7- and 1.6-fold, respectively (**Table 2**).

The glycine betaine (GB) concentration in roots was highly dependent on salinity except for HNSR, being, on average, 0.8 and 2.5 μmol g^{-1} FW in control and salt stressed treatments of LNR and HNR, independently of nitrogen nutrition. HNSR showed a constant value of GB similar to that of LNR and HNR control plants either in control and salt treated plants (**Table 2**).

Carbohydrates Content

Starch content, not significantly affected by nitrate nutrition and salinity in roots, was, on average, 14 μmol G g^{-1} FW (**Table 1**).

Sucrose concentration was, on average, 5.2 μmol g^{-1} FW in all control roots and in salt treated HNR and HNSR, while salinity increased its content by 1.7-fold in LNR (**Table 1**). Root hexose content (glucose and fructose) was 8.83 ± 14 μmol g^{-1} FW in control LNR, while it significantly decreased ($p < 0.05$) in all other treatments (on average, −37%) and in particular in HNSR in which it almost halved (**Table 1**). Fructans content was 44.1 and 10.5 μmol g^{-1} FW in control LNR and HNR and HNSR, respectively (**Table 3**). Salinity significantly decreased total fructans (−30%, $p < 0.01$) in LNR, while doubled them in HNR. The total fructans to starch ratio had a similar trend to fructans (**Table 1**). Among root fructans, nystose (GF_4), 1-Fructofuranosylnystose (GF_4), and inulin (GF29 dahlia type) increased under salinity of 5-, 1.7-, and 1.7-fold in control LNR, respectively; while under salt stress only nystose was significantly increased ($p > 0.05$) of 2.5- and 1.6- in HNR and HNSR, respectively, but remaining at a concentration about 5-fold lower than that found in LNR under salinity (**Table 1**).

Malondialdehyde, Ascorbic Acid, and Glutathione

Malondialdehyde (MDA) levels were significantly higher ($p < 0.01$) in salt stress LNR compared to control ones. In HNR MDA content was higher in control roots than in salt treated ones, while HNSR shower a similar value that was, on average, 15.5 nmol g^{-1} FW (**Table 1**).

Ascorbic acid (AsAc) level (**Table 1**) was, on average, 0.6 nmol g^{-1} FW in LNR and HNR, independently of salinity, and in control HNSR. Salt stress HNSR showed an AsAc content 1.3-fold higher than in the all other treatments. Dehydroascorbic acid (DHA) was at the same concentration as GSH in control roots. Salinity almost halved DHA in LNR, but strongly increased it in HNR and HNSR by 3.8- and 2.8-fold, respectively. The ratio of DHA/AsAc showed a similar trend to DHA (**Table 1**).

TABLE 3 | Relative contribution (%) of inorganic ions, amino acids, glycine betaine, sucrose, fructans, and other metabolites toward the total osmolality.

	cLNR	sLNR	cHNR	sHNR	cHNRS	sHNSR
Chloride	8.84	19.43	8.33	11.5	7.24	12.7
Nitrate	0.01	0.02	12.2	4.32	12.2	4.12
Potassium	34.7	15.2	27.9	20.8	29.8	20.9
Sodium	5.59	17.6	3.71	15.6	4.88	16.6
Ions contribution	49.2	52.3	52.0	52.3	54.1	54.2
Total amino acids	0.75	0.67	2.87	2.08	3.49	1.96
Asparagine	0.03	0.05	0.10	0.45	0.25	0.16
Glutamine	0.08	0.05	0.25	0.19	0.52	0.36
Minor AA	0.10	0.06	0.11	0.09	0.12	0.05
Proline	0.12	0.09	0.19	0.28	0.29	0.23
Glycine betaine	0.25	0.45	0.24	0.45	0.24	0.14
Hexoses	2.57	0.97	2.13	1.02	2.09	0.99
Sucrose	1.49	1.50	1.52	0.90	2.14	1.25
Kestose	1.66	0.84	0.13	0.16	0.16	0.15
Inulin	0.11	0.11	0.07	0.03	0.10	0.02
Nistose	0.35	1.05	0.19	0.25	0.23	0.23
Fructofuranosyl nystose	0.85	0.86	0.58	0.37	0.71	0.32
Organic osmolytes	8.04	6.45	7.73	5.26	9.15	5.07
Other metabolites	42.8	41.3	40.2	42.5	36.7	40.7

Values are mean ± SD (n = 4). The SD was lower than 13% of the average value.

Reduced glutathione (GSH) content was dependent on nitrogen nutrition and salinity. In LNR, the GSH in control plants was at the highest concentration in the HNR (67.8 nmol g^{-1} FW) compared with LNR (20.2 nmol g^{-1} FW) and HNSR (44.7 nmol g^{-1} FW). GSH content was decreased by salt treatment in LNR (−80%) while almost doubled in HNSR. Oxidized GSH (GSSG) had a concentration of about 40 nmol g^{-1} FW in LNR and HNSR and of 21.3 nmol g^{-1} FW in HNR under control conditions. Salinity increased GSSG in HNR by 2.4-fold ($p < 0.01$), but it strongly decreased its content in the other treatments. The GSSG/GSH ratio was significantly higher ($p < 0.01$) in control LNR, independently of salinity, compared to the other treatments (**Table 1**).

Ions and Metabolites Contribution to the Root Osmolality

Durum wheat sap osmolality was, on average, 305 mOsmol kg^{-1} in all control roots, while it significantly increased ($P < 0.01$) after salinity treatment, reaching a value about 1.7-fold higher than that of the respective controls (**Table 1**). The relative contribution of the inorganic ions to osmolality was on average 51.8 and 52.9% for control and salt stressed roots, respectively (**Table 3**). In particular, the relative ion contribution toward osmolality increased from 8.8 to 19.4% for chloride and from 5.6 to 17.6% for sodium in LNR; while it varied from about 7.8–21.1% for chloride and from 4.3 to 16.1% for sodium in HNR and HNSR. On the contrary, the potassium contribution toward osmolality decreased under salinity from 34.7 to 15.2% in LNR, and from about 28.8–20.8% in HNR and HNSR. Only in HNR and HNSR,

nitrate contribution toward osmolality decreased under salinity from 12.2 to about 4.2%. It is interesting to note that the contribution of nitrate and potassium together to osmolality was of about 40% in controls while it decreased to 15 and 25% in LNR and HN(S)R under salinity, respectively (**Table 3**).

The contribution of the measured organic osmolytes to osmolality was, on average, 8.3 and 5.6% in control and salt stressed roots, respectively. It was due for about 85 and 55% to sugars in LNR and HN(S)R, respectively (**Table 3**).

According to Puniran-Hartley et al. (2014), it is possible to speculate that other metabolites present in the cell can contribute to osmolality, and their relative contribution can be calculated as difference between the total sap osmolality (**Table 1**) and the contribution of the measured major inorganic ions and organic osmolytes shown in **Table 3**. The calculated organic osmolytes contribution was therefore 50.8 and 48% in control LNR and HNR, 47.7% in salt stressed LNR and HNR, and 45.8% for HNSR, independently of salinity (**Table 3**).

Ions and Metabolites Expressed in Terms of Dry Weight

Given the salt stress induced-reduction of RWC in LNR and of dry weight in HNSR, ions and metabolites results were also expressed in terms of dry weight (Tables S2, S3). However, while the data about LNR and HNR were in agreement with those reported in literature, keeping almost unchanged the salt stressed values to control values ratio (with fluctuations of <10%), the amount of metabolites and ions in the salt stressed HNSR samples were so concentrated to appear unlikely (about 3-fold higher than other data previously reported). This finding made difficult to carry out a proper effective comparison between the concentrations of ions and metabolites when values were expressed on a dry weight basis. In particular, the increase of ions and metabolites concentrations coincided with a 4.6- and 3.1-fold decrease of salt-treated HNSR fresh and dry weight compared with the respective controls (Tables S2, S3).

Gene Expression

Nitrate reductase (*NR*), asparagine synthetase (*Asn1*, *Asn2*, *Asn3*) and Δ1-pyrroline-5-carboxylate synthase (*P5CS*) genes showed differential expression levels (**Figure 2** and Figure S1).

Nitrogen increased the expression level of *TdNR,* being the highest expression level found in HNSR independently of salinity (Figure S1).

Three out of four isoforms of *Asn* present in wheat (Gao et al., 2016) were considered (*TdAsn1*, *TdAsn2*, *and TdAsn3*), using three different primer pairs, because they can be up-regulated by nitrogen and/or salt stress (Wang et al., 2005; Antunes et al., 2008; Gao et al., 2016). The three isoforms were expressed in all treatments. *TdAsn1* and *TdAsn3* expression was highly inducible by nitrogen and salinity; it was detected at higher extent in HNR and HNSR. While *TdAsn2* was expressed at very low level in all treatments (**Figures 2A,C** and Figure S1).

Using degenerate primers (formed of a mix of four different combinations) we found an unique *TdP5CS* transcript significantly up-regulated by salt stress independently of nitrogen treatment ($p < 0.01$), even mainly expressed in HNR and HNSR.

In order to understand if also for *P5CS* different isoforms are present in durum wheat, the PCR products were cloned and the sequenced cDNA clones were used as a query in a BLASTN search for all wheat A and B chromosomes with the GrainGenes 2.0 database (http://wheat.pw.usda.gov/GG2/index.shtml) and URGI database (https://wheat-urgi.versailles.inra.fr/) (Barabaschi et al., 2015). *T. durum* is, in fact, an allotetraploid plant with a AABB genome ($2n = 4x = 28$) formed through hybridization between two separate but related diploid species, *T. monococcum* or *T. urartu* (AA, $2n = 14$) and *T. searsii* or *T. speltoides* (BB, $2n = 14$). Search results showed an identity of 98–100% with the *P5CS* transcripts belonging to *T. durum* cv. Strongfield, *T. durum* Cappelli, *T. urartu*, and *A. speltoideas* plants. The alignment of the 20 *P5CS* transcript sequences obtained (Figure S4) revealed two or three single point mutations among clones, generating six different fragments of similar size. These latter showed a high homology with four nucleotide sequences identified on chromosomes 1B, 3A, 3B (in two different locus) and 7A, according to Mayer et al. (2014) which found that A and B sub-genomes contain very similar proportions of genes (60.1–61.3%). The six different transcripts were *P5CS* orthologs and paralogs (Wang et al., 2014).

Enzyme Activities

Nitrate reductase (NR) activity was dependent on nitrate nutrition (**Table 2**). The NR activity was 5.8 ± 0.6 and 11.2 ± 1.9 μmol NO_2^- h^{-1} mg^{-1} protein, respectively. Salt treatment significantly reduced the NR activity only in LNR (−35%, $p < 0.01$). The activation state of NR in control roots was about 90%, independently of nitrogen nutrition and salt treatment (Carillo et al., 2005).

Nitrite reductase (NiR) activity was between 4.8- and 9.5-fold higher than the NR activity in the same treatments. In particular NiR activity was about 54 μmol h^{-1} mg^{-1} protein in LNR and HNR and HNSR and 64 μmol h^{-1} mg^{-1} protein in HNR. Salinity decreased it by 42% in LNR and by about 23% in HNR and HNSR (**Table 2**).

Glutamine synthetase (GS) activity, due only to the cytosolic GS isoforms in durum wheat roots (Nigro et al., 2016), was, on average, 18.9 μmol h^{-1} mg^{-1} protein in control and salt stressed LNR. GS activity significantly decreased in control HNR and control and salt treated HNSR (−46%, $p < 0.01$), while it remained unvaried in salt treated HNR (**Table 2**).

Glutamate synthase (GOGAT) showed a similar activity in control LNR and HNR and HNSR, that was, on average, 2.6 μmol h^{-1} mg^{-1} protein. Salinity significantly increased GOGAT activity by 2-fold ($p < 0.01$) only in HNR, while significantly decreased it in LNR (–65%, $p < 0.01$; **Table 2**).

Deaminating glutamate dehydrogenase (GDH) activity was, on average, 6.0 and 4.4 μmol h^{-1} mg^{1} protein in LNR and HNR and HNSR, respectively, independently of salinity (**Table 2**).

In response to salinity, AS activity increased of 1.8 and 2.3 in LNR and HNR compared to the respective controls, reaching 0.66 and 1.67 μmol h^{-1} mg^{-1} protein, while it did not significantly vary ($p > 0.05$) in HNSR independently of salinity (**Table 2**; **Figure 2E**).

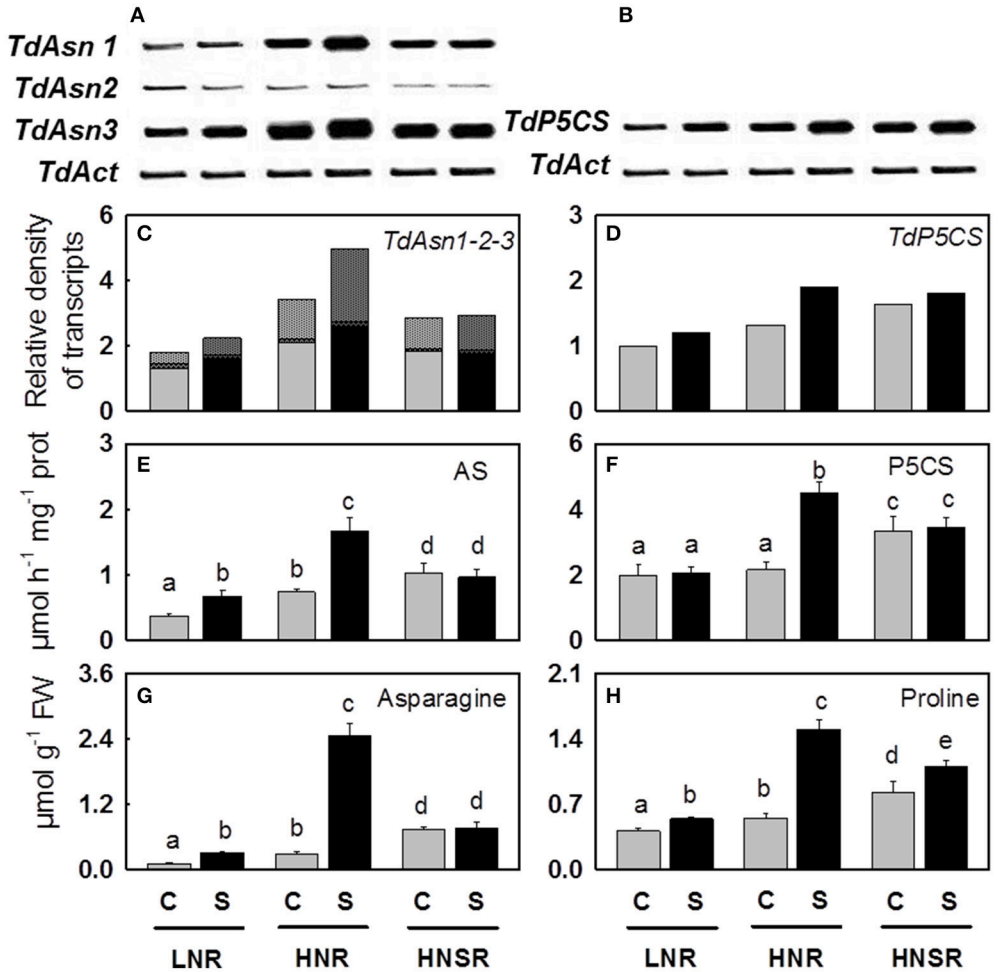

FIGURE 2 | Asparagine synthetase (*Asn1*, *Asn2*, *and Asn3*) (A) and Δ1-pyrroline-5-carboxylate synthase (*P5CS*) **(B)** genes and their relative densitometric quantification normalized using the actin signals **(C,D)**, the AS **(E)** and P5CS **(F)** enzymatic activities, the content of asparagine **(G)**, and proline **(H)** in roots of control (■) and salt stressed (■) plants. Plants were subjected to salt stress starting from day 10 of culture. Control plants were grown without NaCl addition. Plants were harvested after 20 days of hydroponic culture. The values are mean ± *SD* ($n = 4$). Different letters above bars indicate significant difference between treatments ($p < 0.05$, LSD-test).

Phosphoenolpyruvate carboxylase (PEPC) activity was about 1.5 μmol h^{-1} mg^{-1} protein in LNR and HNSR and 2.1 μmol h^{-1} mg^{-1} protein in HNR. Salinity significantly decreased it in LNR (−56%) and HNR (−33%) ($p < 0.01$; **Table 2**).

Δ1-pyrroline-5-carboxylate synthetase (P5CS) activity was, on average, 2.9 μmol h^{-1} mg^{-1} protein in control and salt stressed LNR and control HNR, and 4.8 μmol h^{-1} mg^{-1} protein in HNSR. Salinity increased significantly HNR activity by 2.1-fold (**Table 2**, $p < 0.01$).

Microscopy of Root Tips

Root tips of durum wheat plants were observed by DIC microscopy (**Figure 4**). In **Figure 1A**, a salt stressed root tip was divided in three zones pointing out the meristem (1), elongation (2), and mature cells (3). The root tips from control plants were characterized by densely packed tissues with small intercellular spaces (**Figure 4B**). Root tips from salt stressed plants showed extensive vacuolization and lack of typical organization of apical tissue; moreover a slight plasmolysis due to a lack of continuity and adherence between cells was present with a tendency to the arrest of growth and differentiation (**Figure 4C**). At higher magnification the presence of salt crystals between the wall and the cell membrane, and in vacuoles (though smaller) and plastids were observed (**Figure 4D**). The lack of cuticle in the roots allowed to exclude the silicon nature of these aggregates. These latter were not visible in control root tips (not shown).

Statistical Analysis

The principal component analysis (PCA) of all analyzed parameters expressed for fresh weight showed a well-defined separation among samples from the different treatments. The first two principal components accounted for 63.5% of the variation. The PCA scatter-plot split the samples into five main groups. Nitrogen nutrition contributed to the clear separation

on component 1 (PC1), which described 42% of the variability, while salinity contributed to separation on PC2, which described 21.5% of the variability (Figure S2A). In the Figure S2B only the top 10 contributors were highlighted. In particular, asparagine, proline and minor amino acids highly influenced the salt stressed HNR and HNSR samples grouped in the first quadrant. GB, fructans to starch ratio and sucrose influenced the salt stressed LNR samples in the second quadrant. While potassium to sodium ratio and root Y_w influenced control HNR, and nitrate and MDA influenced control HNSR both present in the fourth quadrant.

In the Figure S3, the PCA of all analyzed parameters expressed for dry weight showed an unforeseen separation among salt stressed HNSR samples from all other different treatments. The first two principal components accounted for 82.7% of the variation. The PCA scatter-plot split the samples into three main groups. Salt stressed HNSR clustered on the border between the fourth and the first quadrant, fully separated from all other HN(S)R samples grouped in the second quadrant, and the LNR samples present in the third quadrant (Figure S3).

A heat map representing the changes in metabolite levels in shoots under different treatments provided an integrated view of the effect of nitrogen nutrition and salinity on durum wheat roots (**Figure 3**). The most interesting result was the strong increase induced by salinity of GB and sucrose in LNR and of GB, asparagine and proline in HNR. While no differences were found between control and salt stressed HNSR.

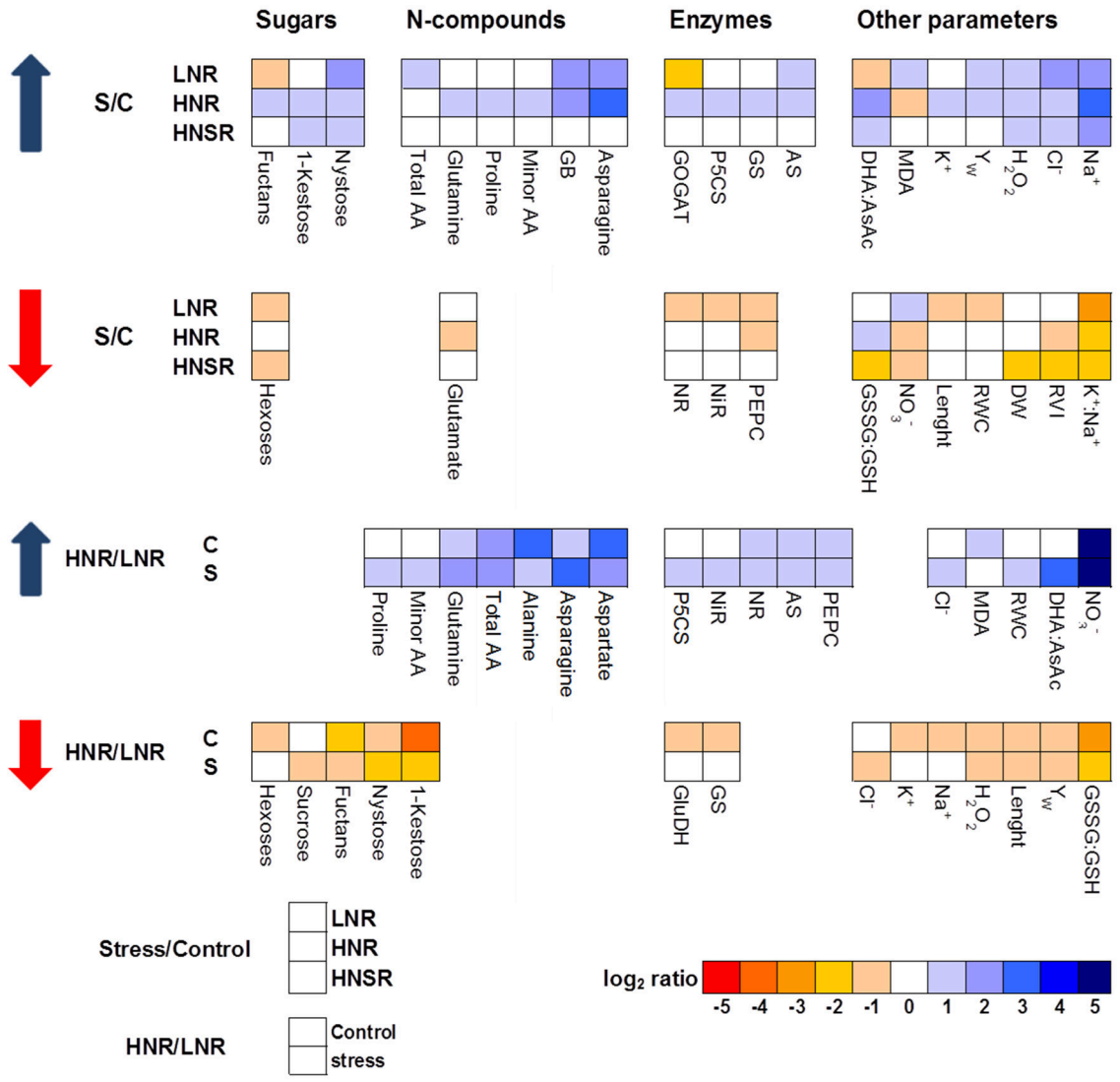

FIGURE 3 | Heat map analysis summarizing the plant responses to nitrogen nutrition and salinity. Results were calculated as Logarithm base 2 (Log_2) of salt stressed values/control values (S/C) or high nitrogen/low nitrogen (HN/LN) for all the treatments, LN, HN, and HN_{split} (LNR, HNR, and HNSR). Results were visualized using a false color scale, with blue indicating an increase and red a decrease of values relative to those in control condition. No differences were visualized by white squares.

DISCUSSION

Durum wheat, as other plants, displays elaborate root plastic responses to a heterogeneous environment such as soil, in which nutrients and salts concentration in the circulating solution can be extremely spatially and temporally variable, actively prioritizing growth toward nutrients, or trying to limit its exposure to salinity (Bazihizina et al., 2012; Galvan-Ampudia et al., 2013; Nacry et al., 2013; Kiba and Krapp, 2016; Koevoets et al., 2016).

Durum wheat root extension was, in fact, highly induced by N limitation (**Table 1**) as already found in a wide range of species, including maize and Arabidopsis (Roycewicz and Malamy, 2012). Moreover, nitrogen affects the distribution of sugars across plant organs (Lemoine et al., 2013), and in particular N-limitation determined an accumulation of carbohydrates in LNR which was correlated with higher root growth rate and root/shoot ratio (Marschner, 1986; Stitt et al., 2002; Remans et al., 2006).

Since nitrogen is acquired entirely by the root system, the increase in the root/shoot ratio allows plants to have more chances to obtain nitrogen to sustain growth (Roycewicz and Malamy, 2012). This is in agreement with the fact that plants, in response to a shortage in mineral nutrition, allocate more resources to the organs involved in mineral acquisition, for increasing root surface and allowing a more efficient exploitation of nutrients in relation to their spatial distribution in the soil (Stitt, 1999; Stitt et al., 2002; Zhang and Pilbeam, 2011). Moreover, high level of nitrate in the medium resulted in a higher root weight but a decrease of root length and root/shoot ratio, probably dependent on the accumulation of nitrate itself in the plant (Stitt, 1999; Roycewicz and Malamy, 2012) (**Table 1**). On the contrary, salinity and, even more, N-limitation and salinity reduced not only durum wheat extension rate and consequently root length, but also fresh and dry weight as well as root vigor index in agreement with earlier studies (Neumann et al., 1994). Reduction in root extension rates might come from the marked lowering of root turgor and water potential (Rodriguez et al., 1997), as also reported in other species (Qin et al., 2010). However, Neumann et al. (1994) reported that lower root extension in maize could be related to hardening of cell walls and not to changes in water potential. Indeed, in wheat roots the apical zone showed signs of wall hardening, with a tendency to the arrest of growth and differentiation (**Figure 4**).

Partial salt stress applied through split-root system affected at the highest extent the part of the root exposed to salt. The strong reduction of HNSR length and weight in the fraction of root treated with salinity vs. the significant increase of control HNSR ones is in agreement with the compensatory growth described in non-stressed areas of root systems under stress (Schumacher and Smucker, 1984). Plants with split roots probably make the salt stressed part stop growing because there is the other root part that can work for the uptake of water and nutrients. This allows the salt stressed HNSR to accumulate large amounts of organic compounds by spending all the available energy (also that needed for growth) without jeopardizing shoot growth and survival.

Whereas, the better conditions of salt stressed HNR compared to LNR ones can be explained by the ability of these plants to realize an osmotic adjustment that maintains a high RWC even at low root water potential, resulting in maintenance of turgor and prevention of tissue desiccation (Morgan, 1984). Osmotic adjustment helps cells to withstand salt stress by maintaining sufficient turgor for growth and metabolism to proceed and involve transport, accumulation, and compartmentation of inorganic ions and compatible solutes (Munns, 2002; Carillo et al., 2008, 2011; Wu et al., 2015).

The increase of salinity not only increased the absolute value for chloride and sodium in the sap, but also the relative contribution of these ions to osmolality (Puniran-Hartley et al., 2014), being the total contribution almost stable. In fact, since the synthesis of osmolytes has a huge cost (50–70 moles ATP for mole; Raven, 1985; Shabala, 2013), it is highly unlikely that the cell could adjust the ion balance only by increasing *de novo* synthesis of compatible metabolites (Shabala, 2013). On the contrary, the increase in root sodium and chloride content suggested that durum wheat cells could use these ions as a cheap osmoticum for turgor maintenance by sequestering them in vacuoles (Puniran-Hartley et al., 2014). At the same time the osmolarity of cytosol was matched with that of vacuole by the reshaping of few classes of metabolites (N-containing ones and sugars) used for multiple purposes, that is as osmolytes and for protection against oxidative stress. Indeed, an ∼100 mOsm increase in organic osmolytes level between control and salt stressed roots (**Table 1**) is enough to osmotic balance the root cell, assuming most of them are located in the cytosol and that the cytosol represents <10% of the root cell total volume fraction (Cuin et al., 2009), while vacuoles and apoplast occupy almost 85 and 5% of it, respectively (Munnich and Zoglauer, 1979; Lee et al., 1990; Patel et al., 1990; Rodriguez et al., 1997).

GB, one of the main nitrogen-containing compatible osmolytes found in durum wheat under salt stress (Carillo et al., 2005; Ashraf and Foolad, 2007; Carillo et al., 2008), was accumulated at the same extent in LNR and HNR under salinity being independent of nitrate treatment, but dependent on salinity (**Figure 1A**). The lack of an influence of N nutrition on GB accumulation in roots suggests that organic N reserves within the plant can be mobilized to satisfy the demand resulting from salt stress (Carillo et al., 2008). GB and sucrose, but not proline, played a major role during osmotic adjustment of LNR under salinity (**Figure 3** and Figure S2).

In HNR proline contribution to the osmotic adjustment increased while that of sucrose decreased (**Table 3**). A strong correlation was found among proline content, P5CS activity, *TdP5CS* transcript ($r \geq 0.94$; $P < 0.001$). This result suggested that at high nitrate salt stress can induce *TdP5CS* gene expression and activity causing a *de novo* synthesis and accumulation of proline according to (Strizhov et al., 1997; Carillo et al., 2008). Moreover, the presence of *P5CS* orthologs and paralogs could satisfy the need for high amounts of proline or provide an efficient means for a differential transcriptional regulation in response to stress (Long and Dawid, 1980; Rai and Penna, 2013).

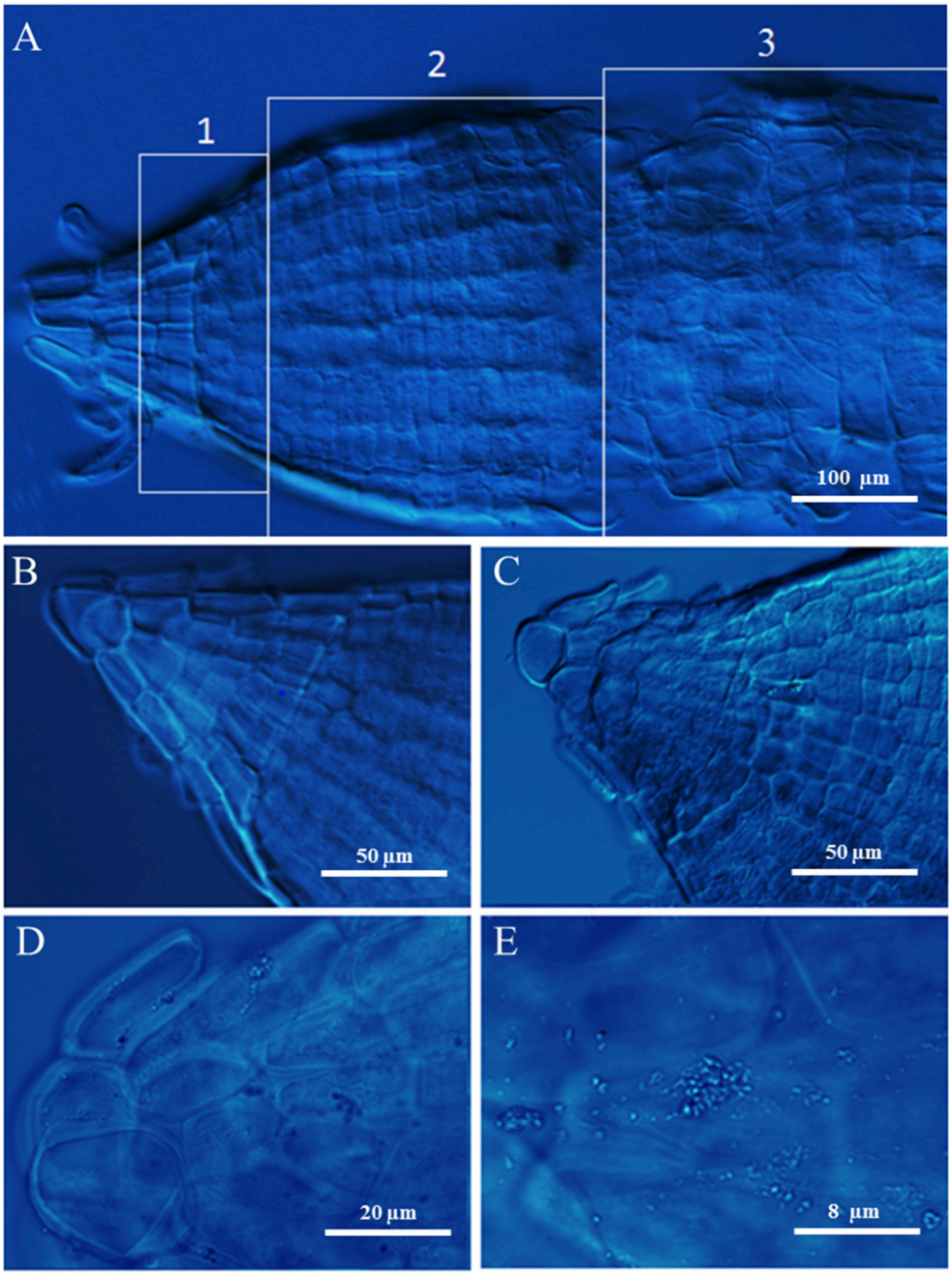

FIGURE 4 | Root tips of durum wheat grown in absence (B) or presence of 100 mM NaCl **(A,C–E)** observed using DIC microscopy. In A the numbers 1, 2, and 3 point out the meristem, elongation, and mature root zones, respectively.

Fructans, which were highly concentrated in low nitrate treatment independently of salinity, increased in HNR under salinity compared to the respective control while the other carbohydrates remained constant (**Table 1**). One of the advantages of accumulation of fructans in the protection against abiotic stress is the high water solubility of these carbohydrates (Livingston et al., 2009). Accumulation of fructans can contribute to membrane stabilization (Valluru and Van den Ende, 2008) and, even indirectly, to the release of sugars which can take part in osmotic adjustment reducing the cytosol water potential and allowing root cell expansion under salt stress (Krasensky and Jonak, 2012).

Glutamate and glutamine highly increased in control HNR. Their increase in roots in presence of nitrate as nitrogen source is supported by several studies and explained by the nitrate induction of the GS-GOGAT pathway specifically localized in

the proplastids of roots. This latter is a pathway not available for ammonium assimilation in the absence of nitrate (Britto and Kronzucker, 2002). Glutamate decreased in HNR under salinity according to Woodrow et al. (2016) (**Table 2**). The decrease of glutamate could depend on its use as nitrogen donor in biosynthetic transamination for the production of amides, in particular asparagine which strongly increased in salt stressed HNR (Forde and Lea, 2007) (**Table 2**, **Figures 2G**, **3**). The increase of asparagine was probably due to a *de novo* synthesis catalyzed by the isoforms of asparagine synthetase *TdAsn1* and *TdAsn3*, which were strongly induced by simultaneous salinity and high levels of nitrogen metabolites (e.g., glutamine and glutamate; Lam et al., 1994; Wang et al., 2005; Lea et al., 2007; Gao et al., 2016). In particular, a very strong correlation was found between *TdAsn1*, AS, and asparagine ($r \geq 0.92$; $P < 0.001$). The up-regulation of AS genes by salt and other abiotic stresses were also reported in maize and Arabidopsis (Chevalier et al., 1996; Wong et al., 2004).

The increase of asparagine, as well as glutamine, has been previously reported in wheat leaves (Carillo et al., 2005; Wang et al., 2005), as well as its possible role in osmotic adjustment, macromolecule protection and ammonium detoxification (Herrera-Rodríguez et al., 2004). Minor amino acids significantly increased only in salt treated HNR, potentially functioning both as compatible compounds and antioxidant (Woodrow et al., 2016). Their variations can depend on an increase of carbohydrates and/or amides (Noctor et al., 2002; Fritz et al., 2006) or on changes of glutamine to glutamate ratio (**Table 2**).

The significant increase of total amino acids in salt stressed HNR was not replicated in HNSR in the same conditions (**Table 2**).

However, the total contribution of GB, amino acids and soluble sugars to osmolality in root tissues was quite low, about 5.6% in all roots under salinity. This means that different compounds accounting for about 41.5% of total osmolality, were accumulated in roots and participated to the osmotic balance and oxidative stress protection of root cells under salt stress.

Total ascorbate (AsAc) and glutathione (GSH), which are of paramount importance in the prevention or repair of damages deriving from ROS (Noctor and Foyer, 1998), increased only in salt stressed HNR and HNSR, as well as GSSG to GSH ratio and DHA to AscAc ratio, with the exception of GSSG to GSH ratio in salt treated HNSR (**Table 1**). This indicates that the ASC–GSH cycle did not play a crucial role for scavenging ROS especially under simultaneous high nitrate and salinity condition.

In LNR, MDA, a marker of lipid peroxidation and therefore, indirectly, of cell damage, was significantly increased under salt stress treatments and was well-correlated with hydrogen peroxide accumulation (**Table 1**). Unexpectedly, high levels of MDA were found in control HNR and HNSR where low levels of hydrogen peroxide were present. Schmid-Siegert et al. (2012) has reported that MDA in roots cannot derive from lipid peroxidation of polyunsaturated fatty acids. The aldehyde is pathogen-inducible in these regions and its level can be increased by cellular mediators that are involved both in defense and growth.

CONCLUSIONS

Durum wheat roots under salinity showed few changes in selected metabolites which allowed the plant viability even at low nitrate. This metabolic rearrangement was necessary to meet the demand for anti-stress agents including compatible solutes and antioxidants (Obata and Fernie, 2012). Thus, while the sodium was used as osmoticum in the vacuole, mainly glycine betaine, sucrose, nystose, and 1-fructofuranosylnystose at low nitrate, and glycine betaine, asparagine and proline at high nitrate were responsible for the osmotic adjustment, the assimilation of the excess of ammonium and the scavenging of ROS under salinity in the cytosol. The strong increase of the sole asparagine and glutamine in HNSR, either in control and salt stress conditions, suggests that the stress-induced adjustment is not a regional effect. On the contrary, the plant operates as an integrated system in which metabolic stress-induced signals spread in the plant and change the metabolism even in areas in which the stress conditions are not present. Notwithstanding this, different parts of plant root systems may behave as physiologically autonomous units, differing their responses to environmental signals (Gašparíková et al., 2002), and preserving their own capability to supply the shoots with water, nutrients or assimilates (Shani et al., 1993). In this way one part of the root system can compensate the plant for a decreased supply or a loss of functionality by the other part, optimizing plant viability under heterogeneous water, nutrients or stressing conditions (Shani et al., 1993).

AUTHOR CONTRIBUTIONS

PC designed the research; MA, LC, PW, EM, and PC performed the research; PC and AF analyzed the data; PC wrote the paper. All authors read and approved the final manuscript.

FUNDING

MA and EM thank Max Planck Society for funding. LC, PW, AF, and PC thank Seconda Universitá degli Studi di Napoli and Campania Region (Italy) PSR 214-f2 action within the project "Network for the protection and management of genetic resources, agrofood (AGRIGENET)."

SUPPLEMENTARY MATERIAL

The Supplementary Material for this article can be found online at: http://journal.frontiersin.org/article/10.3389/fpls.2016.02035/full#supplementary-material

REFERENCES

Abd-El-Baki, G. K., Siefritz, F., Man, H. M., Weiner, H., Kaldenhoff, R., and Kaiser, W. M. (2000). Nitrate reductase in *Zea mays* L. under salinity. *Plant Cell Environ.* 23, 515–521. doi: 10.1046/j.1365-3040.2000.00568.x

Annunziata, M. G., Attico, A., Woodrow, P., Oliva, M. A., Fuggi, A., and Carillo, P. (2012). An improved fluorimetric HPLC method for quantifying tocopherols in *Brassica rapa* L. subsp. *sylvestris* after harvest. *J. Food Composition Anal.* 27, 145–150. doi: 10.1016/j.jfca.2012.05.006

Antunes, F., Aguilar, M., Pineda, M., and Sodek, L. (2008). Nitrogen stress and the expression of asparagine synthetase in roots and nodules of soybean (Glycine max). *Physiol. Plant.* 133, 736–743. doi: 10.1111/j.1399-3054.2008.01092.x

Ashraf, M., and Foolad, M. R. (2007). Roles of glycine betaine and proline in improving plant abiotic stress resistance. *Environ. Exp. Bot.* 59, 206–216. doi: 10.1016/j.envexpbot.2005.12.006

Aslam, M., Travis, R. L., and Rains, D. W. (1996). Evidence for substrate induction of a nitrate efflux system in barley roots. *Plant physiology* 112, 1167–1175.

Baptista, P., Martins, A., Pais, M., Tavares, R., and Lino-Neto, T. (2007). Involvement of reactive oxygen species during early stages of ectomycorrhiza establishment between Castanea sativa and Pisolithus tinctorius. *Mycorrhiza* 17, 185–193. doi: 10.1007/s00572-006-0091-4

Barabaschi, D., Magni, F., Volante, A., Gadaleta, A., Šimková, H., Scalabrin, S., et al. (2015). Physical mapping of bread wheat chromosome 5A: an integrated approach. *Plant Genome* 8. doi: 10.3835/plantgenome2015.03.0011

Bazihizina, N., Barrett-Lennard, E. G., and Colmer, T. D. (2012). Plant responses to heterogeneous salinity: growth of the halophyte *Atriplex nummularia* is determined by the root-weighted mean salinity of the root zone. *J. Exp. Bot.* 63, 6347–6358. doi: 10.1093/jxb/ers302

Britto, D. T., and Kronzucker, H. J. (2002). NH_4^+ toxicity in higher plants: a critical review. *J. Plant Physiol.* 159, 567–584. doi: 10.1078/0176-1617-0774

Carillo, P., Cacace, D., De Pascale, S., Rapacciuolo, M., and Fuggi, A. (2012). Organic vs. traditional potato powder. *Food Chem.* 133, 1264–1273. doi: 10.1016/j.foodchem.2011.08.088

Carillo, P., Mastrolonardo, G., Nacca, F., and Fuggi, A. (2005). Nitrate reductase in durum wheat seedlings as affected by nitrate nutrition and salinity. *Funct. Plant Biol.* 32, 209–219. doi: 10.1071/FP04184

Carillo, P., Mastrolonardo, G., Nacca, F., Parisi, D., Verlotta, A., and Fuggi, A. (2008). Nitrogen metabolism in durum wheat under salinity: accumulation of proline and glycine betaine. *Funct. Plant Biol.* 35, 412–426. doi: 10.1071/FP08108

Carillo, P., Parisi, D., Woodrow, P., Pontecorvo, G., Massaro, G., Annunziata, M. G., et al. (2011). Salt-induced accumulation of glycine betaine is inhibited by high light in durum wheat. *Funct. Plant Biol.* 38, 139–150. doi: 10.1071/FP10177

Chevalier, C., Bourgeois, E., Just, D., and Raymond, P. (1996). Metabolic regulation of asparagine synthetase gene expression in maize (*Zea mays* L.) root tips. *Plant J.* 9, 1–11.

Ciarmiello, L. F., Piccirillo, P., Carillo, P., De Luca, A., and Woodrow, P. (2015). Determination of the genetic relatedness of fig (*Ficus carica* L.) accessions using RAPD fingerprint and their agro-morphological characterization. *South Afr. J. Bot.* 97, 40–47. doi: 10.1016/j.sajb.2014.11.012

Cimini, S., Locato, V., Vergauwen, R., Paradiso, A., Cecchini, C., Vandenpoel, L., et al. (2015). Fructan biosynthesis and degradation as part of plant metabolism controlling sugar fluxes during durum wheat kernel maturation. *Front. Plant Sci.* 6:89. doi: 10.3389/fpls.2015.00089

Colmer, T. D., Flowers, T. J., and Munns, R. (2006). Use of wild relatives to improve salt tolerance in wheat. *J. Exp. Bot.* 57, 1059–1078. doi: 10.1093/jxb/erj124

Cuin, T. A., Betts, S. A., Chalmandrier, R., and Shabala, S. (2008). A root's ability to retain K^+ correlates with salt tolerance in wheat. *J. Exp. Bot.* 59, 2697–2706. doi: 10.1093/jxb/ern128

Cuin, T. A., and Shabala, S. (2007). Compatible solutes reduce ROS-induced potassium efflux in *Arabidopsis* roots. *Plant Cell Environ.* 30, 875–885. doi: 10.1111/j.1365-3040.2007.01674.x

Cuin, T. A., Tian, Y., Betts, S. A., Chalmandrier, R., and Shabala, S. (2009). Ionic relations and osmotic adjustment in durum and bread wheat under saline conditions. *Funct. Plant Biol.* 36, 110–119. doi: 10.1071/FP09051

Duff, S. M. G., Qi, Q., Reich, T., Wu, X., Brown, T., Crowley, J. H., et al. (2011). A kinetic comparison of asparagine synthetase isozymes from higher plants. *Plant Physiol. Biochem.* 49, 251–256. doi: 10.1016/j.plaphy.2010.12.006

Esposito, S., Carillo, P., and Carfagna, S. (1998). Ammonium metabolism stimulation of glucose-6P dehydrogenase and phosphoenolpyruvate carboxylase in young barley roots. *J. Plant Physiol.* 153, 61–66. doi: 10.1016/S0176-1617(98)80045-X

Flowers, T. J., Troke, P. F., and Yeo, A. R. (1977). The mechanism of salt tolerance in halophytes. *Annu. Rev. Plant Physiol.* 28, 89–121.

Forde, B. G., and Lea, P. J. (2007). Glutamate in plants: metabolism, regulation, and signalling. *J. Exp. Bot.* 58, 2339–2358. doi: 10.1093/jxb/erm121

Fritz, C., Palacios-Rojas, N., Feil, R., and Stitt, M. (2006). Regulation of secondary metabolism by the carbon–nitrogen status in tobacco: nitrate inhibits large sectors of phenylpropanoid metabolism. *Plant J.* 46, 533–548. doi: 10.1111/j.1365-313X.2006.02715.x

Galvan-Ampudia, C. S., Julkowska, M. M., Darwish, E., Gandullo, J., Korver, R. A., Brunoud, G., et al. (2013). Halotropism is a response of plant roots to avoid a saline environment. *Curr. Biol.* 23, 2044–2050. doi: 10.1016/j.cub.2013.08.042

Gao, R., Curtis, T. Y., Powers, S. J., Xu, H., Huang, J., and Halford, N. G. (2016). Food safety: structure and expression of the asparagine synthetase gene family of wheat. *J. Cereal Sci.* 68, 122–131. doi: 10.1016/j.jcs.2016.01.010

Gašparíková, O., Mistrík, I., and Čiamporová, M. (2002). Waisel, Y., Eshel, A., Kafkafi, U., eds. Plant roots – the hidden half. *Ann. Bot.* 90, 775–776. doi: 10.1093/aob/mcf252

Gibon, Y., Blaesing, O. E., Hannemann, J., Carillo, P., Hohne, M., Hendriks, J. H., et al. (2004). A robot-based platform to measure multiple enzyme activities in Arabidopsis using a set of cycling assays: comparison of changes of enzyme activities and transcript levels during diurnal cycles and in prolonged darkness. *Plant Cell* 16, 3304–3325. doi: 10.1105/tpc.104.025973

Gorham, J., Jones, R. G. W., and Bristol, A. (1990). Partial characterization of the trait for enhanced K^+–Na^+ discrimination in the D genome of wheat. *Planta* 180, 590–597. doi: 10.1007/BF02411458

Gorham, J., Läuchli, A., and Leidi, E. O. (2010). "Plant responses to salinity," in *Physiology of Cotton*, eds J. M. Stewart, D. M. Oosterhuis, J. J. Heitholt and J. R. Mauney (Dordrecht: Springer Netherlands), 129–141.

Hasegawa, P. M., Bressan, R. A., Zhu, J. K., and Bohnert, H. J. (2000). Plant cellular and molecular responses to high salinity. *Annu. Rev. Plant Physiol. Plant Mol. Biol.* 51, 463–499. doi: 10.1146/annurev.arplant.51.1.463

Herrera-Rodríguez, M. B., Maldonado, J. M., and Pérez-Vicente, R. (2004). Light and metabolic regulation of *HAS1, HAS1.1* and *HAS2*, three asparagine synthetase genes in *Helianthus annuus*. *Plant Physiol. Biochem.* 42, 511–518. doi: 10.1016/j.plaphy.2004.05.001

James, R. A., Blake, C., Byrt, C. S., and Munns, R. (2011). Major genes for Na^+ exclusion, *Nax1* and *Nax2* (wheat *HKT1;4* and *HKT1;5*), decrease Na^+ accumulation in bread wheat leaves under saline and waterlogged conditions. *J. Exp. Bot.* 62, 2939–2947. doi: 10.1093/jxb/err003

James, R., Davenport, R., and Munns, R. (2006). Physiological characterization of two genes for Na^+ exclusion in durum wheat, *Nax1* and *Nax2*. *Plant Physiol.* 142, 1537–1547. doi: 10.1104/pp.106.086538

Kiba, T., and Krapp, A. (2016). Plant nitrogen acquisition under low availability: regulation of uptake and root architecture. *Plant Cell Physiol.* 57, 707–714. doi: 10.1093/pcp/pcw052

Koevoets, I. T., Venema, J. H., Elzenga, J. T. M., and Testerink, C. (2016). Roots withstanding their environment: exploiting root system architecture responses to abiotic stress to improve crop tolerance. *Front. Plant Sci.* 7:1335. doi: 10.3389/fpls.2016.01335

Kong, X., Luo, Z., Dong, H., Eneji, A. E., and Li, W. (2012). Effects of non-uniform root zone salinity on water use, Na^+ recirculation, and Na^+ and H^+ flux in cotton. *J. Exp. Bot.* 63, 2105–2116. doi: 10.1093/jxb/err420

Krasensky, J., and Jonak, C. (2012). Drought, salt, and temperature stress-induced metabolic rearrangements and regulatory networks. *J. Exp. Bot.* 63, 1593–1608. doi: 10.1093/jxb/err460

Krishna Rao, R., and Gnanam, A. (1990). Inhibition of nitrate and nitrite reductase activities by salinity stress in *Sorghum vulgare*. *Phytochemistry* 29, 1047–1049. doi: 10.1016/0031-9422(90)85400-A

Lam, H. M., Peng, S., and Coruzzi, G. M. (1994). Metabolic regulation of the gene encoding glutamine-dependent asparagine synthetase in *Arabidopsis thaliana*. *Plant Physiol.* 106, 1347–1357.

Lea, P. J., Sodek, L., Parry, M. A. J., Shewry, P. R., and Halford, N. G. (2007). Asparagine in plants. *Ann. Appl. Biol.* 150, 1–26. doi: 10.1111/j.1744-7348.2006.00104.x

Lee, R. B., Rarcliffe, R. G., and Southon, T. E. (1990). 31P NMR measurements of the cytoplasmic and vacuolar Pi content of mature maize roots: relationships with phosphorus status and phosphate fluxes. *J. Exp. Bot.* 41, 1063–1078. doi: 10.1093/jxb/41.9.1063

Lemoine, R., La Camera, S., Atanassova, R., Dédaldéchamp, F., Allario, T., Pourtau, N., et al. (2013). Source-to-sink transport of sugar and regulation by environmental factors. *Front. Plant Sci.* 4:272. doi: 10.3389/fpls.2013.00272

Livingston, D. P., Hincha, D. K., and Heyer, A. G. (2009). Fructan and its relationship to abiotic stress tolerance in plants. *Cell. Mol. Life Sci.* 66, 2007–2023. doi: 10.1007/s00018-009-0002-x

Long, E. O., and Dawid, I. B. (1980). Repeated genes in eukaryotes. *Annu. Rev. Biochem.* 49, 727–764. doi: 10.1146/annurev.bi.49.070180.003455

Lutts, S., Kinet, J. M., and Bouharmont, J. (1995). Changes in plant response to NaCl during development of rice (*Oryza sativa* L.) varieties differing in salinity resistance. *J. Exp. Bot.* 46, 1843–1852. doi: 10.1093/jxb/46.12.1843

Maathuis, F. J. M., and Amtmann, A. (1999). K^+nutrition and Na^+toxicity: the basis of cellular K^+/Na^+ratios. *Ann. Bot.* 84, 123–133. doi: 10.1006/anbo.1999.0912

Maggio, A., Bressan, R. A., Ruggiero, C., Xiong, L., and Grillo, S. (2003). "Salt tolerance: placing advances in molecular genetics into a physiological and agronomic context," in *Abiotic Stresses in Plants*, eds L. S. di Toppi and B. Pawlik-Skowrońska (Dordrecht: Springer Netherlands), 53–69.

Maggio, A., De Pascale, S., Fagnano, M., and Barbieri, G. (2011). Saline agriculture in Mediterranean environments. *Ital. J. Agron.* 6, 36–43. doi: 10.4081/ija.2011.e7

Mansour, M. M. F. (2000). Nitrogen containing compounds and adaptation of plants to salinity stress. *Biol. Plant.* 43, 491–500. doi: 10.1023/A:1002873531707

Marschner, H. (1986). *Mineral Nutrition of Higher Plants*. London: Academic Press Inc.

Mayer, K. F., Rogers, J., Doležel, J., Pozniak, C., Eversole, K., Feuillet, C., et al. (2014). A chromosome-based draft sequence of the hexaploid bread wheat (*Triticum aestivum*) genome. *Science* 345. doi: 10.1126/science.1251788

Morcuende, R., Kostadinova, S., Pérez, P., Martín del Molino, I. M., and Martínez-Carrasco, R. (2004). Nitrate is a negative signal for fructan synthesis, and the fructosyltransferase-inducing trehalose inhibits nitrogen and carbon assimilation in excised barley leaves. *New Phytol.* 161, 749–759. doi: 10.1046/j.1469-8137.2004.00990.x

Morgan, J. M. (1984). Osmoregulation and water stress in higher plants. *Annu. Rev. Plant Physiol.* 35, 299–319. doi: 10.1146/annurev.pp.35.060184.001503

Munnich, H., and Zoglauer, M. (1979). Bestimmung des Volumenanteils der Vakuolen in Zellen der Wurzelspitze von *Zea mays* L. *Biol. Rundschau* 17, 119–123.

Munns, R. (2002). Comparative physiology of salt and water stress. *Plant Cell Environ.* 25, 239–250. doi: 10.1046/j.0016-8025.2001.00808.x

Munns, R., James, R. A., and Läuchli, A. (2006). Approaches to increasing the salt tolerance of wheat and other cereals. *J. Exp. Bot.* 57, 1025–1043. doi: 10.1093/jxb/erj100

Munns, R., and Tester, M. (2008). Mechanisms of salinity tolerance. *Annu. Rev. Plant Biol.* 59, 651–681. doi: 10.1146/annurev.arplant.59.032607.092911

Nacry, P., Bouguyon, E., and Gojon, A. (2013). Nitrogen acquisition by roots: physiological and developmental mechanisms ensuring plant adaptation to a fluctuating resource. *Plant Soil* 370, 1–29. doi: 10.1007/s11104-013-1645-9

Nedjimi, B. (2014). Effects of salinity on growth, membrane permeability and root hydraulic conductivity in three saltbush species. *Biochem. Syst. Ecol.* 52, 4–13. doi: 10.1016/j.bse.2013.10.007

Neumann, P. M., Azaizeh, H., and Leon, D. (1994). Hardening of root cell walls: a growth inhibitory response to salinity stress. *Plant Cell Environ.* 17, 303–309. doi: 10.1111/j.1365-3040.1994.tb00296.x

Nigro, D., Fortunato, S., Giove, S. L., Paradiso, A., Gu, Y. Q., Blanco, A., et al. (2016). Glutamine synthetase in durum wheat: genotypic variation and relationship with grain protein content. *Front. Plant Sci.* 7:971. doi: 10.3389/fpls.2016.00971

Noctor, G., and Foyer, C. H. (1998). Ascorbate and glutathione: keeping active oxygen under control. *Annu. Rev. Plant Physiol. Plant Mol. Biol.* 49, 249–279. doi: 10.1146/annurev.arplant.49.1.249

Noctor, G., Novitskaya, L., Lea, P. J., and Foyer, C. H. (2002). Co-ordination of leaf minor amino acid contents in crop species: significance and interpretation. *J. Exp. Bot.* 53, 939–945. doi: 10.1093/jexbot/53.370.939

Obata, T., and Fernie, A. R. (2012). The use of metabolomics to dissect plant responses to abiotic stresses. *Cell. Mol. Life Sci.* 69, 3225–3243. doi: 10.1007/s00018-012-1091-5

Parre, E., de Virville, J., Cochet, F., Leprince, A.-S., Richard, L., Lefebvre-De Vos, D., et al. (2010). "A new method for accurately measuring Δ1-pyrroline-5-carboxylate synthetase activity," in *Plant Stress Tolerance: Methods and Protocols*, ed R. Sunkar (Totowa, NJ: Humana Press), 333–340.

Patel, D. D., Barlow, P. W., and Lee, R. B. (1990). Development of vacuolar volume in the root tips of pea. *Ann. Bot.* 65, 159–169.

Peuke, A. D., and Jeschke, W. D. (1999). The characterization of inhibition of net nitrate uptake by salt in salt-tolerant barley (*Hordeum vulgare* L. cv. California Mariout). *J. Exp. Bot.* 50, 1365–1372. doi: 10.1093/jxb/50.337.1365

Puniran-Hartley, N., Hartley, J., Shabala, L., and Shabala, S. (2014). Salinity-induced accumulation of organic osmolytes in barley and wheat leaves correlates with increased oxidative stress tolerance: in planta evidence for cross-tolerance. *Plant Physiol. Biochem.* 83, 32–39. doi: 10.1016/j.plaphy.2014.07.005

Qin, J., Dong, W. Y., He, K. N., Yu, Y., Tan, G. D., Han, L., et al. (2010). NaCl salinity-induced changes in water status, ion contents and photosynthetic properties of *Shepherdia argentea* (Pursh) Nutt. seedlings. *Plant Soil Environ.* 56, 325–332.

Queval, G., and Noctor, G. (2007). A plate reader method for the measurement of NAD, NADP, glutathione, and ascorbate in tissue extracts: application to redox profiling during Arabidopsis rosette development. *Anal. Biochem.* 363, 58–69. doi: 10.1016/j.ab.2007.01.005

Rahnama, A., Munns, R., Poustini, K., and Watt, M. (2011). A screening method to identify genetic variation in root growth response to a salinity gradient. *J. Exp. Bot.* 62, 69–77. doi: 10.1093/jxb/erq359

Rai, A. N., and Penna, S. (2013). Molecular evolution of plant P5CS gene involved in proline biosynthesis. *Mol. Biol. Rep.* 40, 6429–6435. doi: 10.1007/s11033-013-2757-2

Rana, G., and Katerji, N. (2000). Measurement and estimation of actual evapotranspiration in the field under Mediterranean climate: a review. *Eur. J. Agron.* 13, 125–153. doi: 10.1016/S1161-0301(00)00070-8

Raven, J. A. (1985). Tansley review no. 2. Regulation of pH and generation of osmolarity in vascular plants: a cost-benefit analysis in relation to efficiency of use of energy, nitrogen and water. *New Phytol.* 101, 25–77. doi: 10.1111/j.1469-8137.1985.tb02816.x

Remans, T., Nacry, P., Pervent, M., Girin, T., Tillard, P., Lepetit, M., et al. (2006). A central role for the nitrate transporter NRT2.1 in the integrated morphological and physiological responses of the root system to nitrogen limitation in Arabidopsis. *Plant Physiol.* 140, 909–921. doi: 10.1104/pp.105.075721

Richards, R. A. (1983). Should selection for yield in saline regions be made on saline or non-saline soils? *Euphytica* 32, 431–438. doi: 10.1007/BF00021452

Rodriguez, H. G., Roberts, J., Jordan, W. R., and Drew, M. C. (1997). Growth, water relations, and accumulation of organic and inorganic solutes in roots of maize seedlings during salt stress. *Plant Physiol.* 113, 881–893. doi: 10.1104/pp.113.3.881

Roycewicz, P., and Malamy, J. E. (2012). Dissecting the effects of nitrate, sucrose and osmotic potential on Arabidopsis root and shoot system growth in laboratory assays. *Philos. Trans. R. Soc. B Biol. Sci.* 367, 1489–1500. doi: 10.1098/rstb.2011.0230

Sairam, R., and Tyagi, A. (2004). Physiology and molecular biology of salinity stress tolerance in plants. *Curr. Sci.* 86, 407–421. doi: 10.1007/1-4020-4225-6

Schmid-Siegert, E., Loscos, J., and Farmer, E. E. (2012). Inducible malondialdehyde pools in zones of cell proliferation and developing tissues in Arabidopsis. *J. Biol. Chem.* 287, 8954–8962. doi: 10.1074/jbc.M111.322842

Scholander, P. F., Bradstreet, E. D., Hemmingsen, E. A., and Hammel, H. T. (1965). Sap pressure in vascular plants: negative hydrostatic pressure can be measured in plants. *Science* 148, 339–346. doi: 10.1126/science.148.3668.339

Schumacher, T. E., and Smucker, A. J. M. (1984). Effect of localized anoxia on *Phaseolus vulgaris* L. root growth. *J. Exp. Bot.* 35, 1039–1047. doi: 10.1093/jxb/35.7.1039

Shabala, S. (2013). Learning from halophytes:physiological basis and strategies to improve abiotic stress tolerance in crops. *Ann. Bot.* 112, 1209–1221. doi: 10.1093/aob/mct205

Shabala, S., and Cuin, T. A. (2008). Potassium transport and plant salt tolerance. *Physiol. Plant.* 133, 651–669. doi: 10.1111/j.1399-3054.2007.01008.x

Shani, U., Waisel, Y., Eshel, A., Xue, S., and Ziv, G. (1993). Responses to salinity of grapevine plants with split root systems. *New Phytol.* 124, 695–701.

Silveira, J. A. G., Melo, A. R. B., Martins, M. O., Ferreira-Silva, S. L., Aragão, R. M., Silva, E. N., et al. (2012). Salinity affects indirectly nitrate acquisition associated with glutamine accumulation in cowpea roots. *Biol. Plant.* 56, 575–580. doi: 10.1007/s10535-012-0065-7

Silveira, J. A. G., Melo, A. R. B., Viégas, R. A., and Oliveira, J. T. A. (2001). Salinity-induced effects on nitrogen assimilation related to growth in cowpea plants. *Environ. Exp. Bot.* 46, 171–179. doi: 10.1016/S0098-8472(01)00095-8

Skopelitis, D. S., Paranychianakis, N. V., Kouvarakis, A., Spyros, A., Stephanou, E. G., and Roubelakis-Angelakis, K. A. (2007). The isoenzyme 7 of tobacco NAD(H)-dependent glutamate dehydrogenase exhibits high deaminating and low aminating activities *in vivo*. *Plant Physiol.* 145, 1726–1734. doi: 10.1104/pp.107.107813

Sonneveld, C., and de Kreij, C. (1999). Response of cucumber (*Cucumis sativus* L.) to an unequal distribution of salts in the root environment. *Plant Soil* 209, 47–56. doi: 10.1023/A:1004563102358

Stitt, M. (1999). Nitrate regulation of metabolism and growth. *Curr. Opin. Plant Biol.* 2, 178–186. doi: 10.1016/S1369-5266(99)80033-8

Stitt, M., Muller, C., Matt, P., Gibon, Y., Carillo, P., Morcuende, R., et al. (2002). Steps towards an integrated view of nitrogen metabolism. *J. Exp. Bot.* 53, 959–970. doi: 10.1093/jexbot/53.370.959

Strizhov, N., Ábrahám, E., Ökrész, L., Blickling, S., Zilberstein, A., Schell, J., et al. (1997). Differential expression of two P5CS genes controlling proline accumulation during salt-stress requires ABA and is regulated by ABA1, ABI1 and AXR2 in Arabidopsis. *Plant J.* 12, 557–569. doi: 10.1046/j.1365-313X.1997.00557.x

Valluru, R., and Van den Ende, W. (2008). Plant fructans in stress environments: emerging concepts and future prospects. *J. Exp. Bot.* 59, 2905–2916. doi: 10.1093/jxb/ern164

Wang, H., Liu, D., Sun, J., and Zhang, A. (2005). Asparagine synthetase gene TaASN1 from wheat is up-regulated by salt stress, osmotic stress and ABA. *J. Plant Physiol.* 162, 81–89. doi: 10.1016/j.jplph.2004.07.006

Wang, S., Wong, D., Forrest, K., Allen, A., Chao, S., Huang, B. E., et al. (2014). Characterization of polyploid wheat genomic diversity using a high-density 90 000 single nucleotide polymorphism array. *Plant Biotechnol. J.* 12, 787–796. doi: 10.1111/pbi.12183

Wong, H.-K., Chan, H.-K., Coruzzi, G. M., and Lam, H.-M. (2004). Correlation of ASN2 gene expression with ammonium metabolism in Arabidopsis. *Plant Physiol.* 134, 332–338. doi: 10.1104/pp.103.033126

Woodrow, P., Ciarmiello, L. F., Annunziata, M. G., Pacifico, S., Iannuzzi, F., Mirto, A., et al. (2016). Durum wheat seedling responses to simultaneous high light and salinity involve a fine reconfiguration of amino acids and carbohydrate metabolism. *Physiol. Plant.* doi: 10.1111/ppl.12513. [Epub ahead of print].

Woodrow, P., Fuggi, A., Pontecorvo, G., Kafantaris, I., Annunziata, M. G., Massaro, G., et al. (2012). cDNA cloning and differential expression patterns of ascorbate peroxidase during post-harvest in *Brassica rapa* L. *Mol. Biol. Rep.* 39, 7843–7853. doi: 10.1007/s11033-012-1627-7

Woodrow, P., Pontecorvo, G., Fantaccione, S., Fuggi, A., Kafantaris, I., Parisi, D., et al. (2010). Polymorphism of a new Ty1-copia retrotransposon in durum wheat under salt and light stresses. *Theor. Appl. Genet.* 121, 311–322. doi: 10.1007/s00122-010-1311-z

Wu, H., Shabala, L., Liu, X., Azzarello, E., Zhou, M., Pandolfi, C., et al. (2015). Linking salinity stress tolerance with tissue-specific Na^+ sequestration in wheat roots. *Front. Plant Sci.* 6:71. doi: 10.3389/fpls.2015.00071

Zhang, H., and Pilbeam, D. J. (2011). "Morphological adaptations of Arabidopsis roots to nitrogen supply," in *Nitrogen Metabolism in Plants in the Post-genomic Era*, eds C. H. Foyer and H. Zhang (West Sussex: Wiley-Blackwell), 269–283.

Zubaidi, A., McDonald, G. K., and Hollamby, G. J. (1999). Shoot growth, root growth and grain yield of bread and durum wheat in South Australia. *Aust. J. Exp. Agric.* 39, 709–720.

Conflict of Interest Statement: The authors declare that the research was conducted in the absence of any commercial or financial relationships that could be construed as a potential conflict of interest.

frontiers in Plant Science

ORIGINAL RESEARCH
published: 08 February 2016
doi: 10.3389/fpls.2016.00081

Salt Stress Affects the Redox Status of Arabidopsis Root Meristems

*Keni Jiang[1], Jacob Moe-Lange[2], Lauriane Hennet[1] and Lewis J. Feldman[1]**

[1] Department of Plant and Microbial Biology, University of California, Berkeley, Berkeley, CA, USA, [2] Department of Biology, Stanford University, Stanford, CA, USA

We report the redox status (profiles) for specific populations of cells that comprise the Arabidopsis root tip. For recently germinated, 3–5-day-old seedlings we show that the region of the root tip with the most reduced redox status includes the root cap initials, the quiescent center and the most distal portion of the proximal meristem, and coincides with (overlays) the region of the auxin maximum. As one moves basally, further into the proximal meristem, and depending on the growth conditions, the redox status becomes more oxidized, with a 5–10 mV difference in redox potential between the two borders delimiting the proximal meristem. At the point on the root axis at which cells of the proximal meristem cease division and enter the transition zone, the redox potential levels off, and remains more or less unchanged throughout the transition zone. As cells leave the transition zone and enter the zone of elongation the redox potentials become more oxidized. Treating roots with salt (50, 100, and 150 mM NaCl) results in marked changes in root meristem structure and development, and is preceded by changes in the redox profile, which flattens, and initially becomes more oxidized, with pronounced changes in the redox potentials of the root cap, the root cap initials and the quiescent center. Roots exposed to relatively mild levels of salt (<100 mM) are able to re-establish a normal, pre-salt treatment redox profile 3–6 days after exposure to salt. Coincident with the salt-associated changes in redox profiles are changes in the distribution of auxin transporters (AUX1, PIN1/2), which become more diffuse in their localization. We conclude that salt stress affects root meristem maintenance, in part, through changes in redox and auxin transport.

Keywords: redox, auxin, root, meristem, Arabidopsis, salt-stress

OPEN ACCESS

Edited by:
Janin Riedelsberger, University of Talca, Chile

Reviewed by:
Laurent Laplaze, Institut de Recherche pour le Développement, France
Teva Vernoux, Centre National de la Recherche Scientifique, France
Romy Schmidt, RWTH Aachen Univeristy, Germany

****Correspondence:***
Lewis J. Feldman
ljfeldman@berkeley.edu

Specialty section:
This article was submitted to Plant Physiology, a section of the journal Frontiers in Plant Science

Received: *01 November 2015*
Accepted: *16 January 2016*
Published: *08 February 2016*

Citation:
Jiang K, Moe-Lange J, Hennet L and Feldman LJ (2016) Salt Stress Affects the Redox Status of Arabidopsis Root Meristems. Front. Plant Sci. 7:81. doi: 10.3389/fpls.2016.00081

INTRODUCTION

Increases in soil salinity present a notable challenge to agriculture. As a consequence of human activities, many once fertile lands are becoming less productive due to increased salts. Additionally, alterations in rainfall patterns, often associated with climate change, result in less rainfall and hence less leaching from soils of accumulated salts and minerals. As well, the increasing use of more marginal lands for farming often means that growers have to contend with naturally occurring high levels of salts. In total, the FAO estimates that the accumulation of salts impacts on the agricultural production of over 397 million hectares (FAO, 2005). The effects of salts on plant growth and development are numerous, with the severity dependent on the concentration(s) of the salts, the sensitivity of the crop to the salts, and on the capacity of the plants to tolerate or mitigate the effects of the salts (Munns, 2005). Focusing specifically on the influences of salts on

roots, typical salt-related effects include decreases in root elongation (Potters et al., 2007; Bernstein, 2013), changes in root architecture (Julkowska et al., 2014), changes in the root gravity response ("halotropism"; Sun et al., 2008), and changes in root anatomy, including decreases in cell size, a reduction in cell division, and alterations in patterns of differentiation, as, for example, the differentiation of the Casparian strip unusually close to the root meristem (Hajibagheri et al., 1989). The inhibition of root elongation by salt is most often linked to a decrease in the amount of cell expansion in the root elongation zone (Zhong and Läuchli, 1993; West et al., 2004; Bustos et al., 2008). But the final length of a root is not only dependent on cell elongation but also on how many cells are available to elongate. In this regard West et al. (2004) show that the response of roots to salt stress also involves an inhibition of the cell cycle, so that cells comprising the meristem stop dividing at a smaller size, resulting in cells elongating closer to the root tip. As a consequence, root meristems in salt-stressed roots are generally reduced in size and therefore produce fewer cells to elongate (Kurth et al., 1986; Zidan et al., 1990; Azaizeh and Steudle, 1991). In summary, as noted by Bernstein (2013) and others (West et al., 2004), the available evidence suggests that salinity inhibits root growth through a combination of the effects of salts on both cell division and cell elongation.

Much of the work investigating the physiological, biochemical and molecular bases for salt-associated changes in roots has focused on the root meristem (Bernstein, 2013). Evidence points to salinity, in part, affecting meristem structure and function as a consequence of salt-induced changes in the distribution of auxin transport proteins (members of the PIN protein family; Chávez-Avilés et al., 2013), resulting in changes in the patterns of auxin distribution at the root meristem. Recently, Iglesias et al. (2014) advanced the notion that suppression in auxin signaling may be a way in which plants modify (increase) their tolerance to salinity, and these workers showed that this mechanism involved a repression by NaCl of the Aux/IAA repressors. A more general physiological response of roots to salinity is the onset of oxidative stress, characterized by an increase in, and accumulation of various reactive oxygen species (ROS), such as OH- and H_2O_2. Toxicity is generally associated with the induction by ROS of a cascade of reactions resulting in the initiation of a variety of physiologically detrimental processes (Bernstein, 2010; Hernandez et al., 2010). With regard to ROS toxicity, much effort has been directed to understanding the antioxidant mechanisms that plants use to mitigate the effects of salinity-induced ROS, with a focus on the salt-stress-induced changes in the activities of antioxidant (ROS-detoxifying) enzymes (Dat et al., 2000; Mittler, 2002; Apel and Hirt, 2004). Not surprisingly, salt-stress-induced changes in the root's antioxidant response are reported to be spatially and temporally variable, and likely also linked to the developmental stage of the root tissues and cell types (Hernandez et al., 2010).

Although ROS production is generally considered to be detrimental, there is convincing evidence that ROS may also have a dual role, and function positively to promote many developmental processes, such as signaling and cell expansion (Rodríguez et al., 2002; Foreman et al., 2003; Rubio et al., 2009; Shoresh et al., 2011). Therefore, maintaining a balance, or homeostasis in ROS is considered central to normal development, as suggested earlier by Kerk and Feldman (1995) and Jiang et al. (2003) for the organization of the root meristem. Thus, based on an appreciation of this dual role for ROS, and on the hypothesis that salt stress causes changes in root ROS homeostasis, an important question to ask is, how is ROS status affected in roots treated with varying levels/periods of exposure to salinity? Surprisingly, little information addresses this central question. Not only are data lacking on the redox status of salt-stressed roots, but as well, little is known of the redox status for non-stressed roots. Using redox sensitive dyes investigators have demonstrated *relative* levels of particular species of reactive oxygen, but these results are mostly qualitative, often specific for one type of reactive oxygen species, and thus not a measure of the overall redox state of the tissue (Shin et al., 2005). Here, we report on the overall redox status in Arabidopsis roots in non-stressed and also in saline environments. We focus on the root meristem (terminal mm of the root) because it is here where many salt-sensitive processes (e.g., cell division and elongation) predominately occur. We report, for the first time, the redox potentials for various regions of the root meristem in relation to imposed salt stress. We show that different regions of the root respond uniquely to salt stress, not only spatially, but temporally as well. Moreover, the differing responses to varying levels of salt point to mechanisms, and to limitations used by roots to adjust (or not), to saline soils. For this effort we employ Arabidopsis seedlings which express a redox-sensitive reporter (roGFP) (Hanson et al., 2004) that we have previously described (Jiang et al., 2006), and which has also been used recently for a determination of redox status in plants exposed to drought stress (Brossa et al., 2013).

MATERIALS AND METHODS

Plant Material

For measuring and monitoring redox potentials seed of *Arabidopsis thaliana* transgenic line c-roGFP (Jiang et al., 2006) were used. For auxin-related experiments the following Arabidopsis transgenic marker lines were used: *DR5:GUS* (Ulmasov et al., 1997), PIN1:GFP (Friml et al., 2002); PIN2:GFP (Xu and Scheres, 2005), AUX1:YFP (Swarup et al., 2004). The expression patterns of each of these promoter lines were visualized using a Zeiss LSM710 confocal microscope. For GUS staining, seedlings were placed in the GUS solution (Ulmasov et al., 1997) for 1 h at 37°C, after which time the roots were fixed (ethanol:acetic acid, 3:1) and then mounted in chloral hydrate.

Salt-Stress Treatment

Seeds expressing the c-roGFP (Jiang et al., 2006) were surface sterilized and plated on 0.5x MS agar (+1% sucrose) supplemented with varying concentrations of NaCl (0, 50, 100, and 150 mM) and then incubated for 3 days at 4°C, following which the plates were transferred to a growth chamber (16 h photoperiod, 23.5°C). After varying periods of time (3–9 days) on the NaCl-supplemented agar media, the vertically-oriented Petri dishes on which the seedlings were growing were re-oriented to the horizontal and placed directly on the stage of the microscope. A coverslip was affixed and measurements made of the redox

status of the root meristem. For each time point (i.e., 3, 6, and 9 days) $n = 16$. The controls for all three time points ($n = 48$) are averaged to give an overall control plot as seen in **Figure 1**. (**Supplementary Figure 1A** shows the three individual plots used to obtain the average shown in **Figure 1**). In order to assess the effects of short periods of exposure to salt (3, 6, 12, and 24 h), the experimental set-up had to be modified so that roots could reach a developmental stage suitable for observation (at least 3–5 days after germination). For these short time-exposures, salt-stress experiments seeds were sterilized and plated on salt-free 0.5x MS medium supplemented with 1% sucrose, incubated in cold for 3 days, and allowed to germinate with the Petri plate oriented vertically for an additional 5 days (16 h photoperiod) at 23.5°C. Subsequently the vertically-oriented plates were immersed in 150 mM NaCl in 0.5x MS (no sugar) so that only the roots were submerged in the salt-supplemented liquid medium. After a 3 h exposure to salt the redox status of the root, which remained attached to the agar medium, was measured. After each measurement the Petri dish was returned to the vertical position and re-immersed in the same liquid salt solution, as before. Redox measurements were again made on the *same* roots after 6, 12, and 24 h additional exposure to salt. After the final measurement (at 24 h) the roots were treated with H_2O_2 followed by DTT, in order to normalize for calculating redox potential (as described in Jiang et al., 2006). A control curve, for short-term exposure to salt (**Figure 1**) was obtained by averaging the four individual control plots (immersion in 0.5x MS only) for 3, 6, 12, and 24 h ($n = 8$ for each time point; **Supplementary Figure 1B**).

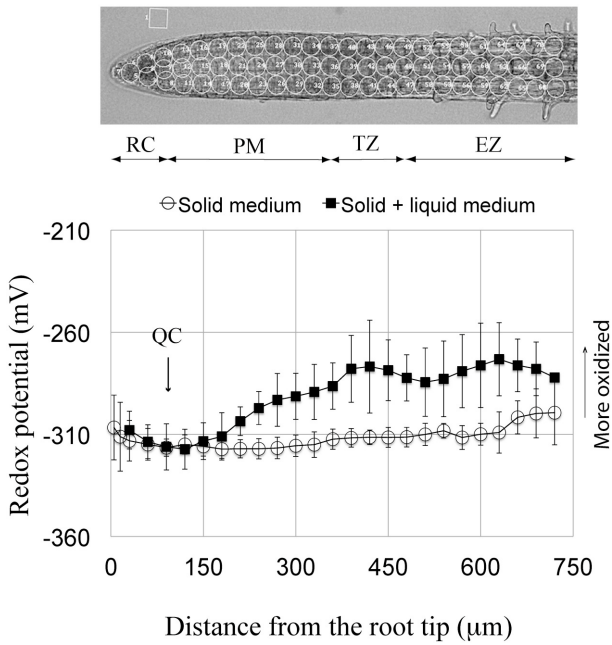

FIGURE 1 | Redox potential profile of the primary root tip of Arabidopsis. Circled regions in the root above the profiles indicate areas of the redox measurements. Two profile curves are shown; one from roots grown continuously on solid 0.5x MS agar medium (open circles) and the other (solid squares) shows the redox profile from roots grown for 5 days on 0.5x MS agar and then immersed in 0.5x MS liquid medium for 3–24 h. Each curve is a summation obtained by averaging the measurements from the individual, corresponding curves shown in **Supplementary Figure 1** (i.e., for immersion, averaging control curves from 3, 6, 12, and 24 h, and for growth on solid medium only, averaging the control curves from 3, 6, and 9 days). Standard deviations are shown for the 48 roots used to obtain the redox profile for roots grown continuously on agar, and for the eight roots used to obtain the redox profile for roots grown on agar with subsequent immersion. The more negative the potential, the more reduced is the redox status. Note that the two curves overlap in the distal-most 180 μm of the root. RC, root cap; QC, quiescent center; PM, proximal meristem; TZ, transition zone; EZ, elongation zone.

Ratiometric Measurements of Redox Status

Ratiometric measurements were made as described previously (Jubany-Mari et al., 2010). Briefly, a Nikon Diaphot FN600 microscope fitted with Plan Fluor 10x/0.30NA dry objective and a Chroma Technology Phluorin filter set (exciters D410/30 and D470/20, dichroic mirror 500DCXR, emitter HQ535/50) microscope was used. Images were captured of the entire terminal mm of the root using a Hamamatsu Orca-100 cooled CCD camera (Hamamatsu Corp.). Emission data (fluorescence) were collected over time and processed using MetaFluor 6.1 image analysis software (Molecular Devices), which controlled both filters and the data collection, as detailed by Jiang et al. (2006).

Measurements of redox status were performed by focusing on the median plane of intact roots, which raises the question of whether the redox values measured in this manner provides accurate readings of median plane redox status. By acquiring a "z" stack of optical sections using a Zeiss LSM710 confocal microscope, equipped with a 20x objective, we were able to confirm that redox potentials measured using the aforementioned Nikon microscope set-up accurately reflects redox status as measured using a confocal microscope focused on the median plane (data not shown).

Root Anatomy; Measurements of Internal Cellular Characteristics

After various times on the salt-supplemented media root lengths were measured (distance between the hypocotyl junction and the root tip). Subsequently, roots were fixed for microscopy (3:1, ethanol:acetic acid) at 4°C, for 1 week, and for observations mounted in chloral hydrate. Cell counts and cell length measurements were obtained from cortical files in reference to landmarks (quiescent center [QC], elongation zone [EZ]; Perilli and Sabatini, 2010). The length of the proximal meristem (PM), defined by Verbelen et al. (2006) as the "root meristem," included cells between the QC and the first isodiametric cell, which marked the distal end of the transition zone (TZ region). The TZ includes all isodiametric cortical cells between the PM and the EZ (the EZ is defined as originating at the point [location] in the root at which cells lose their isodiametric shape and begin to elongate). After mounting in chloral hydrate roots were photographed and cell shapes and lengths analyzed using ImageJ software. At least six roots were used for each measurement and data were analyzed using the Student's *t*-test and *p*-values determined. For our work, results were considered to be statistically significant with a $p < 0.05$.

RESULTS

Redox Profiles of Control Root Tips

Here we characterize, for the first time, the overall redox status of specific zones comprising the terminal mm of the Arabidopsis primary root. We report that the redox status/profile can vary, depending on whether seedlings are grown on agar only, or on agar plus short-term immersion in liquid culture medium. But irrespective how seedlings were grown, the root cap (RC) shows a relatively oxidized redox status (−308 to −312 mV), and that as one moves in a proximal direction, the overall redox level gradually becomes more negative (more reduced), so that the redox state of the QC is at, or nearly at, the most reduced redox level of any cells at the root tip (−317 mV; **Figure 1**, **Supplementary Figure 1**). Just proximal to the QC begins the zone of maximum cell divisions (the proximal meristem [PM]). Cells of the PM directly adjacent to the QC show a similar or slightly more reduced redox status compared to their neighboring QC cells. Moving more proximally in the PM, and focusing on seedlings grown long-term on agar, we observe a rise in the overall redox state, indicating a more oxidized status, which is reflected by a change in redox potential between the distal and proximal boundaries of the PM. Moving further proximally into the TZ, the redox status plateaus and levels off at an average redox potential of about −312 mV. Continuing to move basally from the TZ into the EZ the redox potential initially is little changed and fluctuates somewhat around −310 mV. With further movement proximally the redox potential of the EZ becomes markedly more positive (more oxidized) reaching a value of about −300 mV at a distance of about 750 μm from the root tip. This very reproducible redox profile, for different-aged roots grown on plain agar, contrasts markedly with the profile of roots grown 5 days on agar, and subsequently immersed in a bathing solution (**Figure 1**). Short-term immersion of roots results in a remarkably different, reproducible redox profile, compared to roots grown solely on agar. For roots immersed 3–24 h the redox status of the PM becomes markedly more oxidized, beginning ∼100 μm proximal to the QC/PM border, reaching a value of about −280 mV at the PM/TZ interface. As the only difference in environments leading to these contrasting profiles is, whether or not seedling roots are or are not immersed, we attribute the more oxidized status of immersed roots as due to the onset of immersion-induced oxidative stress in the portion of the terminal mm beyond the most-distal 180 μm, a point to which we will return in the Discussion.

Redox Profiles in Tips of Salt-Treated Roots

Roots were exposed to varying concentrations of salt (50, 100, and 150 mM NaCl) for different lengths of time and the redox status of the root tip characterized. Following short-term treatments (immersion) for 3, 6, and 12 h with 150 mM salt, the overall redox status of the terminal 180 μm (RC, QC, and distal PM) has become more oxidized (**Figure 2**, **Supplementary Figure 2**). After a 24 h salt treatment the redox status has begun to shift to a more negative (reduced) redox state. With increasing periods of exposure (6 and 9 days) to salt, the redox potentials move to more negative (reduced) redox potentials, shifting from values between −270 and −290 mV, to values between −280 to −310 mV (**Figures 3A–C**, **Supplementary Figure 3**). With the exception of the QC, exposing roots for 3 days to 100 mM salt, results in a more oxidized redox state compared to controls. However, extending the salt treatment to 6 days, again with the exception of the QC, results in an overall redox pattern matching that of control roots. But after a 9-day, 100 mM salt treatment the overall redox status of the root becomes slightly more oxidized compared to the control. Interestingly, the region of the QC shows little change from a 6-day salt treatment and remains as the most oxidized zone of the 9 day, 100 mM salt-treated roots. Treating roots with 50 mM salt, the lowest NaCl concentration used, showed a 3 and 6 day redox response pattern quite similar to exposure of roots to 100 mM salt, with an initial rise (indicating a more oxidized status), and by day 6 a return to a more reduced redox status, closely matching the control. However, after 9 days of exposure to 50 mM salt, unlike a 9-day exposure to 100 and 150 mM salt, the redox status becomes even more reduced and overall, the redox profile becomes even more negative (more reduced) than the control (**Figure 3C**, **Supplementary Figures 3C,F,H**).

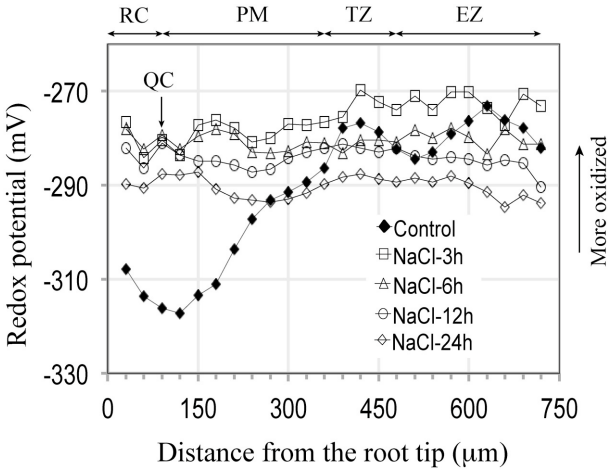

FIGURE 2 | Redox potential profiles of Arabidopsis primary roots grown 5 days on soild agar and then immersed in 100 mM NaCl for varying periods of time (3–24 h). For all periods of exposure the redox status of the entire root becomes more oxidized, with the greatest change occurring in the terminal 300 μm (Compared to control curve from **Figure 1**). Each salt treatment redox profile curve represents an average from 7 to 8 roots, for which the standard deviations are shown in **Supplementary Figure 2**.

Effects of Salt Treatments on Overall Root Length, Cell Number, and Cell Length

Salt treatments affect root length (**Figure 4A**). After a 3-day treatment (50, 100, and 150 mM NaCl) roots are statistically ($p < 0.05$; $n = 19$) shorter than the control. Focusing specifically on the terminal half mm region in 100 mM salt treatments, we report that all reduction in length is due to a statistically significant ($p < 0.05$; $n = 6$) reduction in the length of the PM (**Figures 4B–D**), which is linked to a reduction in cell

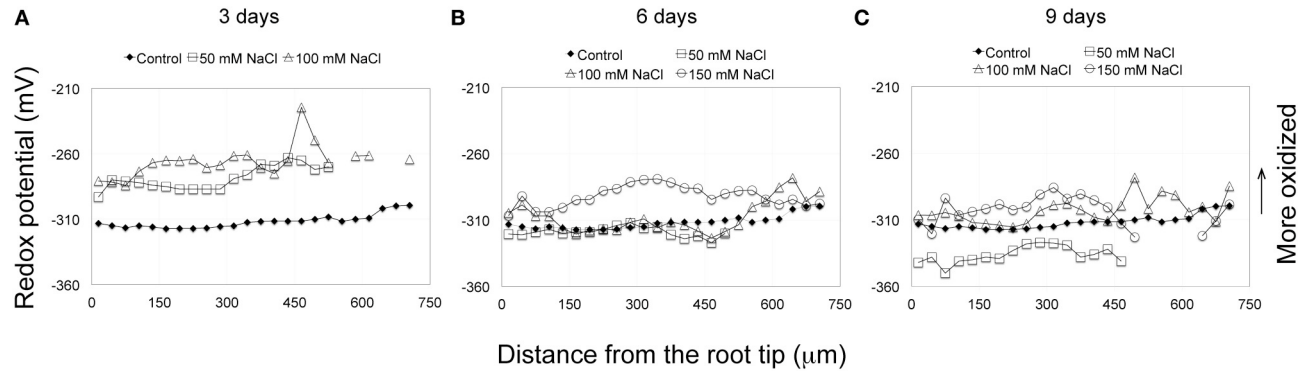

FIGURE 3 | (A–C) Redox profiles of Arabidopsis primary roots, grown on solid medium, and treated for extended periods (3–9 days) with various concentrations of NaCl (50–150 mM). After 6 days treatment with 50 mM NaCl the redox profile more or less matches the redox values and profiles of the control, whereas by day 9 the overall redox status of 50 mM salt-treated roots has become more reduced than the control. Except for the terminal 180 μm, the redox profile of 100 mM salt-treated roots matches the control, but by day 9 becomes, overall, more oxidized. The redox profiles of roots treated continuously with 150 mM NaCl, in general, remain at values more positive (more oxidized) than the control. The control curve (solid squares) is obtained as described in **Figure 1**. Each salt treatment redox profile curve represents an average from eight roots, for which the standard deviations are shown in **Supplementary Figure 3**.

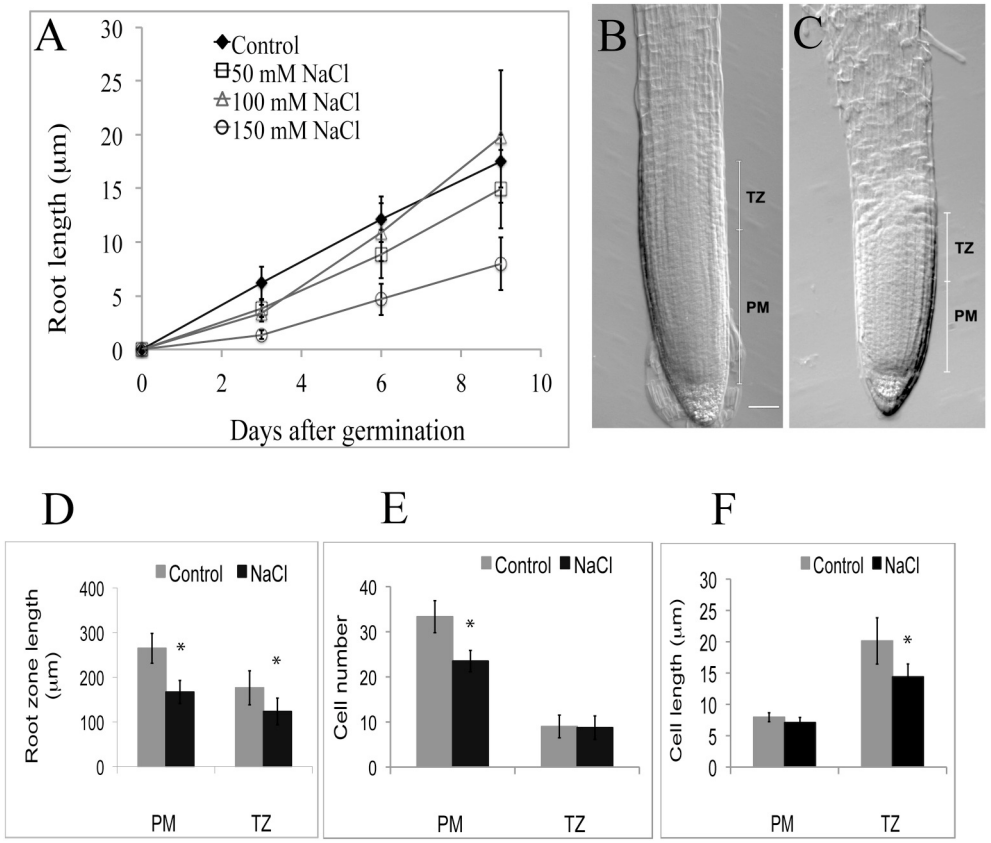

FIGURE 4 | (A–F) Growth parameters of the proximal meristem and transition zone in Arabidopsis primary roots, ± salt treatments. **(A)** Root length after varying periods of treatment with NaCl (50–150 mM). **(B)** Intact 3-day-old control root tip. **(C)** Intact tip from root treated 3 days with 100 mM NaCl. Note the shortening of the PM in the salt-treated root (scale bar = 20 μm). **(D–F)** Comparison of cellular characteristics of the PM and TZ in roots treated with 100 mM salt for 3 days: D, overall lengths; E, number of cells; F, cell length. PM, proximal meristem, TZ, transition zone, $n = 6$; *indicates a statistical significance of $p < 0.05$.

number in the PM of salt-treated roots, compared to controls (**Figure 4E**), and to a slight, but statistically significant reduction in cell length in the TZ (**Figure 4F**). On average, cell numbers in the PM of salt-treated roots declined by 29%, with no effect of salt (100 mM) on cell length (**Figures 4E,F**), whereas for the TZ, only cell length, but not cell number was affected by the salt treatment

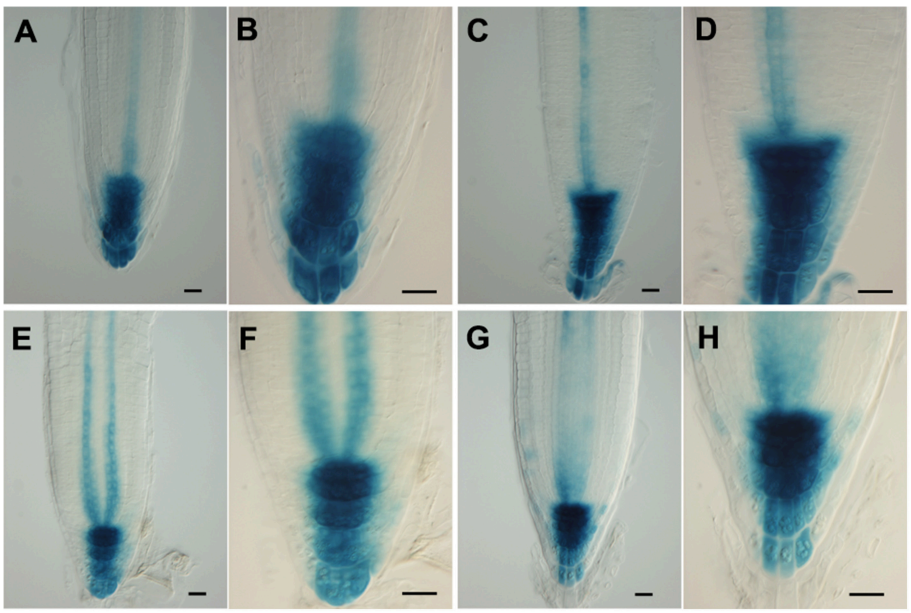

FIGURE 5 | (A–H) Patterns of expression of an auxin-responsive promoter (DR5) in Arabidopsis root tips, ± salt treatment. Using the DR5GUS reporter in roots treated with 150 mM salt for 3 h **(A–D)** or 24 h **(E–H)** in order to reveal auxin distribution. **(A,B,E,F)** control; **(C,D,G,H)** plus salt. Scale bar = 20 μm. $n = 10$ roots for control and for each treatment.

(**Figures 4E,F**). Thus, salt-treatment affected the functioning of both the PM and the TZ, but in different ways.

Effects of Salt Treatments on Auxin Distribution and on the Localization of Auxin Transporters

As proposed earlier (Chávez-Avilés et al., 2013), we also observe a modest increase in the expression of an auxin-regulated promoter (*DR5GUS*) following salt treatments, suggesting an increase in the accumulation of auxin at the root tip, with greater staining (higher levels) of auxin found in the regions basal (proximal) to the QC in the root tip in 3 h, 150 mM salt-treated roots, as compared to controls (**Figures 5A–H**). Salt treatment of roots perturbs the localization of auxin transporters. Following a 6 h salt treatment, AUX1, an auxin influx carrier (Kleine-Vehn et al., 2006), becomes more restricted in its distribution and is no longer expressed in the cells of the vascular tissues, and also shows a diminished level of expression in the RC (**Figures 6A,B**). Likewise, for both PIN1 and PIN2, auxin efflux carriers (Zazímalová et al., 2007), salt treatment perturbs the distribution of these carriers. For PIN1, a 24 h salt treatment almost completely abolishes any association of the protein with membranes (**Figures 7A–D**), whereas for PIN2, salt treatment results in a disappearance of the protein from the cortical layer directly to the inside of the epidermis, and as well, in a diminishment (12–24 h after beginning the salt treatment) in the localization of the PIN2 to membranes in the epidermis (**Figures 8A–D**). But unlike for AUX1 whose pattern is changed by 6 h after beginning the salt treatment, for PIN1/2 a change in pattern is not observed until 10–12 h after beginning salt treatment, considerably after the salt-induced change in redox (at about 3 h).

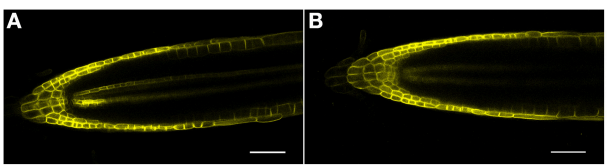

FIGURE 6 | (A,B) AUX1 (AUX1-YFP) confocal microscopic localization in roots, ± salt. **(A)** Control root; note reporter expression in both the epidermis and vascular tissue. **(B)** Root treated with 150 mM salt for 6 h. Note the loss of AUX1 expression in the central vascular tissue as well as a diminishment in expression in both the QC and RC. Scale bar = 50 μm, $n = 4$ roots for control and eight roots for each treatment.

DISCUSSION

The Redox Profile of the Arabidopsis Root Tip

Arabidopsis root tips display a complex pattern of redox potentials, with the region of the QC and the adjacent cells of the PM showing the most reduced potentials (**Figure 1**). In comparison, the adjacent RC bordering directly on the distal face of the QC shows a more oxidized status. The complexity in the redox state and pattern at the root tip are influenced by the immediate environment surrounding the roots, as can seen by comparing the redox profiles from control roots grown continuously on solid medium, with the profiles from roots grown initially on solid medium, but then subsequently

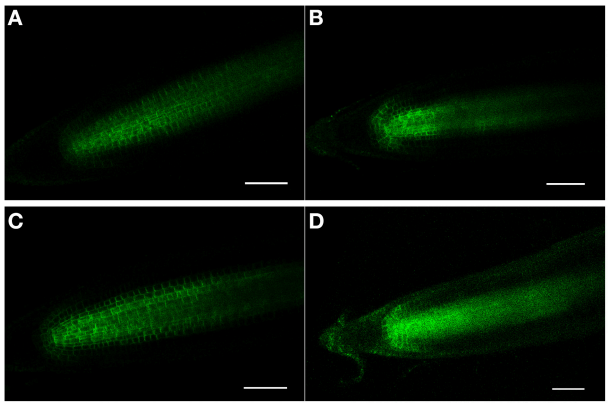

FIGURE 7 | (A–D) PIN1 (PIN1-GFP) confocal localization in Arabidopsis roots, ± salt. **(A,C)** Control roots (no salt treatment) after 12 and 24 h, respectively. **(B,D)** Roots treated for 12 and 24 h, respectively, with 150 mM salt. Note that after 24 h of salt treatment that PIN1-GFP expression has become diffuse and is no longer specifically associated with the membranes. Scale bar = 50 μm, $n = 6$ roots for the control and seven roots for each treatment.

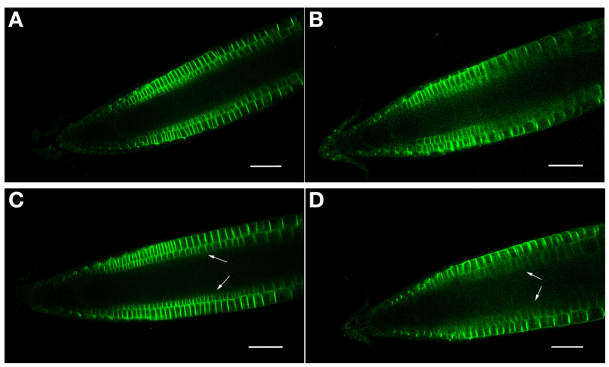

FIGURE 8 | (A–D) PIN2 (PIN2-GFP) confocal localization in Arabidopsis roots, ± salt. **(A,C)** Control roots (no salt treatment) after 12 and 24 h, respectively. **(B,D)** Roots treated for 12 and 24 h, respectively, with 150 mM salt. Note that a 24 h salt treatment results in a diminishment of PIN2-GFP expression in the cortical layer directly beneath the epidermis (arrows). Scale bar = 50 μm, $n = 6$ roots for the control and seven for each treatment.

immersed in the same, but now liquid medium for 3–24 h (**Figure 1**). For both treatments the redox profiles are identical for the most distal, terminal 180 μm of the root, which includes the RC, the QC and the most distal region of the PM. However, proximal to the most distal 180 μm region of the root the redox profiles diverge, with more oxidized values observed for roots immersed in liquid, as compared to the profiles from roots grown continuously on agar. While the shapes of the two curves are similar (e.g., both show the development of more negative redox potentials as one moves through the PM to the TZ), the magnitude of the response differs between the two treatments. We conclude that immersion, even for short periods (3 h), may induce a level of stress that results in relatively oxidized values for regions of *control* roots proximal to the most distal 180 μm, and that this immersion-related stress masks or overlays possible salt-induced changes in redox potentials. For this reason, possible salt-associated changes in the redox profiles in the regions beyond distal-most 180 μm region of the root tip cannot be determined using immersed roots. But since, immersion does not result in changes of the redox profile within the first 180 μm of the tip, this allows us to explore the effects of short-term exposure to salt on the distal-most region of the root tip (the RC, QC, and distal PM). This also suggests that with regard to redox status that the tip-most region of Arabidopsis roots is either unaffected by immersion stress, or has unique mechanisms to buffer oxidative stress, and therefore to retain a pre-immersion redox profile.

In non-immersed, control roots the PM (the region of highest mitoses) initially exhibits a stable, reduced redox potential (−317 mV) which rises to −312 mV (a more oxidized potential) at the proximal border of the PM, at which point cell divisions have ceased (at the PM/TZ boundary). Redox status has been linked to cell division activity. As early as 1931 Rapkine demonstrated in sea urchin eggs that the oscillating patterns in thiol accumulation could be linked to the cell cycle (Rapkine, 1931). Since this observation, considerable evidence has accumulated pointing to reactive oxygen species (ROS) functioning as second messengers regulating cell proliferation. Thus, it is now generally accepted that oscillations in redox metabolism represent a fundamental mechanism linking oxidative metabolism to the regulation of the cell cycle, and to subsequent differentiation (Sauer et al., 2001; Menon and Goswami, 2007; Fehér et al., 2008; Sarsour et al., 2009). Tsukagoshi et al. (2010) have recently explored the transition from proliferation to differentiation in roots and conclude that there is a "clear correlation between growth rate, location of the TZ, and the relative distribution of different ROS species" in the meristem and in the zone of elongation. At this point it is probably fair to conclude that for Arabidopsis roots, that as the redox status of the main zone of cell division (the PM) becomes more oxidized, that this is associated with a decrease in mitoses and with the onset of differentiation. However, it is also clear that redox status by itself does not determine whether a cell will divide, as demonstrated by the infrequent divisions of cells of the QC, which exhibit redox potentials more reduced than found in the dividing cells of the PM. A consideration of other factors affecting cellular proliferation, besides redox status, will be discussed subsequently.

Effects of Salt Treatments on the Root Redox Profile

Being cognizant of the possible effects of immersion on redox profiles, we can, nevertheless conclude that for the most distal 180 μm of the root tip, that salt treatments (3 h, 150 mM) result in marked changes in redox status, shifting the redox potentials of the RC, QC and distal PM by 32, 38, and 30 mV, respectively, to more oxidized values (**Figure 2**). Increasing the exposure period to salt to 24 h does not result in more oxidized redox potentials within the terminal 180 μm region, compared to a 3 h salt treatment. Thus, we conclude that an initial, short-term (3 h) exposure to salt is sufficient to trigger the maximal change in redox; even prolonging the salt treatments to 3 days does not move the redox profile (values) in a more oxidized direction. With increasing periods of exposure to salt the redox

profiles begin to shift from maximum oxidized values (−280 to −270 mV) to more reduced values (−300 to −290 mV) after 6 days of salt treatment, and to even more reduced values after 9 days of salt exposure (−310 to −300 mV), thereby suggesting that in such roots, processes have been initiated to buffer and ameliorate salt-induced changes in redox. Of particular note are the long-term redox responses of roots treated with 50 mM salt, for which we find that after 9 days exposure to salt that the redox profile has, overall, shifted to a level that is about 20 mV *more* reduced than control roots. Fifty mM salt-treated roots, therefore, appear to have overcompensated in the readjustment of their redox profiles in response to salt stress. Our results further suggest that Arabidopsis roots are unable to restore their redox values to control profiles when exposed to salt concentrations between, or exceeding 100 to 150 mM NaCl.

Considerable research now points to plants responding to increased ROS via a variety of mechanisms, most often involving antioxidant enzymes (Bernstein, 2013). Although, beyond the scope of this research, our work suggests that there must be a complex balancing of the redox status along the length of the root, reflecting the roles of ROS in both promoting (e.g., for cell elongation), as well as inhibiting many cellular activities. Perturbing this balance, either chemically of genetically, can affect cell size, as recently demonstrated by Lu et al. (2014) with mutants of Arabidopsis in which the expression of peroxidase genes is upset. For our work treating roots with salt, initially all levels of salt cause a decrease in root length. In this regard it is worth noting that as with unusually oxidized redox levels, unusually reduced levels may also negatively impact on root physiology, as suggested by a reduction in length of 50 mM salt-treated, compared to controls (**Figure 4A**). After 9 days of salt treatment roots exposed to 100 mM salt exceed the length of control roots, whereas roots treated with either 50 or 150 mM salt are shorter than control roots, suggesting that there is an optimal redox value, neither too reduced (as in 50 mM treatments), nor too oxidized (as in 150 mM treatments) at which root elongation is optimal (**Figure 4A**). West et al. (2004) explored the cellular basis of these differences in lengths in salt-treated Arabidopsis roots and concluded that salt did not affect the length of the cell cycle, but rather that salt reduced overall root length by affecting meristem size and final cell length. Our results support the conclusion that high levels of salt (>100 mM) cause a decrease in the size (number of cells) in the PM (**Figures 4A–F**), the primary region of production of new cells for the root. Here we suggest that the size of the PM, and its functioning, are related to an overlaying of the redox gradient, so that maximum cell divisions occur within a region of the PM that is neither too oxidized, nor too reduced in redox potential. It is, we suggest, no coincidence that the PM/TZ boundary is marked by a reduction/cessation in cell division that is associated with a concomitant flattening of the redox curve at a relatively oxidized redox potential.

Redox/Auxin Signaling and Root Development

While our work points to a central role for redox gradients in the structure and functioning of the root meristem, exactly how redox signaling affects root meristem development and maintenance is not known. Kerk and Feldman (1995) suggested that the redox status of the maize QC was central to root meristem structure and activity, and proposed a model linking auxin and redox status at the root meristem. Here, we show that a salt-associated change in redox status at the root tip is paralleled by a change in the distribution of auxin transport proteins, thereby supporting a possible link between redox signaling and auxin, and in agreement with earlier work of Pasternak et al. (2002) and Bashandy et al. (2010). Using Arabidopsis mutated in key redox-regulating enzymes these workers showed a decrease in polar auxin transport and thereby concluded that redox status (specifically, glutathione homeostasis) plays a role in root development by affecting auxin signaling, a conclusion supported and extended by Yu et al. (2013) who proposed that glutathione redox status affects the root apical meristem, in part, through an auxin/PLETHORA (PLT)- dependent pathway. More recently, Iglesias et al. (2014) showed that salinity leads to a suppression of auxin signaling by triggering "the stabilization of Aux/IAA repressors," leading these workers to propose that salt stress signals are integrated into plant development by an "ROS-auxin crosstalk." In this context, the salt-induced alterations to auxin transporters, which we have observed, might be part of a mechanism to suppress auxin signaling and thereby enhance tolerance to salinity. In this regard too the observations of Sun et al. (2008) that salt treatment (150 mM) results in a decrease in PIN2 abundance, and the recent work of Liu et al. (2015) that salt stress downregulates the expression of *PIN* genes, provides added evidence that salt may affect auxin distribution in the root by affecting the levels/operation of auxin transporters. This downregulation in *PIN* gene expression may be related to the modest increase in the expression of an auxin-responsive promoter (*DR5GUS*) in the QC, which both we and Chávez-Avilés et al. (2013) have observed. Interestingly, Liu et al. (2015) also report that salt treatment affects the level of expression of DR5 in the root tip, but they link salt treatment to a modest decrease, rather than an increase, as we report, in DR5-GFP expression. So while we do not yet know many of the specifics of the manner in which redox influences auxin status in the root (and likely, vice versa as well), evidence suggests that salt-induced changes in redox status in roots can influence root meristem maintenance, at least in part, by affecting auxin transport. Worth mentioning with regard to the work of Kerk and Feldman (1995) and Jiang et al. (2003) are their observations that the QC was the *most* oxidized population of cells (in maize roots), a result which differs from what we here report for Arabidopsis, in which the QC maintains a relatively reduced status. The resolution of this apparent contradiction may rest on the fact that Jiang et al. (2003) used a redox-reporter sensitive to a rather narrow range of redox species, whereas for the current effort the roGFP has a broader range and therefore likely provides a more complete picture of overall redox status (Jiang et al., 2006).

In summary, we report the redox status of specific populations of cells which comprise the Arabidopsis root tip, and as well explore the effects of salt (NaCl) on redox profiles. From the complex redox responses of roots to salt, a number

of general observations can be made. First, roots respond rapidly to exposure to salts by shifting their overall redox status to more oxidized values, which initially come to be more or less the same along the entire length of the root tip, thereby eliminating any differences in redox potentials between the different regions (i.e., RC, QC, PM, TZ, EZ). Secondly, depending on the salt concentration (<100 mM), Arabidopsis roots are able to restore redox levels and patterns to control values. However, as salt levels increase (between 100 and 150 mM), Arabidopsis roots are less able to moderate their redox status to more reduced, control values. Finally, we provide evidence that salt stress affects root development and maintenance, in part, through changes in redox/auxin transport.

AUTHOR CONTRIBUTIONS

All authors contributed equally to the research. The paper was written by LF and KJ.

SUPPLEMENTARY MATERIAL

The Supplementary Material for this article can be found online at: http://journal.frontiersin.org/article/10.3389/fpls.2016.00081

Supplementary Figure 1 | (A,B) Redox profiles for control roots grown continuously on agar **(A)** for 3, 6, or 9 days or on agar plus immersion **(B)** for 3, 6, 12, or 24 h. Each curve in **(A)** represents the average of 16 roots, with accompanying standard deviations, and for **(B)** each curve is the average of eight roots, with accompanying standard deviations. For each treatment the control curve is an average of 16 roots at the same time point.

Supplementary Figure 2 | (A–D) Redox profiles for immersed, salt-treated (150 mM NaCl) roots. **(A)** 3 h salt treatment; **(B)** 6 h salt treatment; **(C)** 12 h salt treatment; **(D)** 24 h salt treatment. Each curve represents the average of eight roots, with accompanying standard deviations. For each treatment the control curve is an average of eight roots at the same time point.

Supplementary Figure 3 | (A–H) Individual Redox profiles of Arabidopsis primary roots grown on solid medium and treated for extended periods (3–9 days) with various concentrations of NaCl (50–150 mM). This figure shows the individual curves, with standard deviations, used to generate the summary redox profiles in **Figures 3A–C.**

REFERENCES

Apel, K., and Hirt, H. (2004). Reactive oxygen species: metabolism, oxidative stress and signal transduction. *Annu. Rev. Plant Biol.* 55, 373–399. doi: 10.1146/annurev.arplant.55.031903.141701

Azaizeh, H., and Steudle, H. (1991). Effects of salinity on water transport of excised maize (Zea mays L.) roots. *Plant Physiol.* 97, 1136–1145. doi: 10.1104/pp.97.3.1136

Bashandy, T., Guilleminot, J., Vernoux, T., Caparros-Ruiz, D., Ljung, K., Meyer, Y., et al. (2010). Interplay betweenthe NADP-linked thioredoxin and glutathione systems in Arabidopsis auxin signaling. *Plant Cell* 22, 376–391. doi: 10.1105/tpc.109.071225

Bernstein, N. (2010). Involvement of the plant antioxidative response in the differential growth sensitivity to salinity of leaves vs. roots during cell development. *Free Radic. Biol. Med.* 49, 1161–1171. doi: 10.1016/j.freeradbiomed.2010.06.032

Bernstein, N. (2013). "Effects of salinity on root growth plant roots," in *Plant Roots: The Hidden Half, 4th Edn.,* Vol. 36, eds A. Eshel and T. Beeckman (Boca Raton, FL: CRC Press), 1–18.

Brossa, R., Pintó-Marijuan, M., Jiang, K., Alegre, L., and Feldman, L. J. (2013). Assessing the regulation of leaf redox status under water stress conditions in *Arabidopsis thaliana*. *Plant Signal Behav.* 8:e24781. doi: 10.4161/psb.24781

Bustos, D., Lascano, R., Villasuso, A. L., Machado, E., Senn, M. E., Cordoba, A., et al. (2008). Reductions in maize root-tip elongation by salt and osmotic stress do not correlate with apoplastic O2 levels. *Ann. Bot.* 102, 551–559. doi: 10.1093/aob/mcn141

Chávez-Avilés, M. N., Andrade-Pérez, C. L., and de la Cruz, H. R. (2013). PP2A mediates lateral root development under NaCl-induced osmotic stress throughout auxin redistribution in *Arabidopsis thaliana*. *Plant Soil* 368, 591–602. doi: 10.1007/s11104-012-1540-9

Dat, J., Vandenabeele, S., Vranová, E., Van Montagu, M., Inze, D., and Van., Breusegen, F. (2000). Dual action of the active oxygen species during plant stress responses. *Cell Mol. Life Sci.* 57, 779–995. doi: 10.1007/s000180050041

FAO (2005). *Global Network on Integrated Soil Management for Sustainable Use of Salt-affected Soils.* Rome: FAO Land and Plant Nutrition Management Service. Available online at: http://www.fao.org/ag/agl/agll/spush

Fehér, A., Ötvös, K., and Pasternak, T. P., Szandtner, A. P. (2008). The involvement of reactive oxygen species (ROS) in the cell cycle activation (G0-to-G1 transition) of plant cells. *Plant Signal. Behav.* 3, 823–826. doi: 10.4161/psb.3.10.5908

Foreman, J., Demidchik, V., Bothwell, J. H., Mylona, P., Miedema, H., Torres, M. A., et al. (2003). Reactive oxygen species produced by NADPH oxidase regulate plant cell growth. *Nature* 422, 442–446. doi: 10.1038/nature01485

Friml, J., Benkova, E., Blilou, I., Wisniewska, J., Hamann, T., Ljung, K., et al. (2002). AtPIN4 mediates sink-driven auxin gradients and root patterning in Arabidopsis. *Cell* 108, 661–673. doi: 10.1016/S0092-8674(02)00656-6

Hajibagheri, M. A., Yeo, A. R., Flowers, T. J., and Collins, J. C. (1989). Salinity resistance in Zea mays: fluxes of potassium, sodium and chloride, cytoplasmic concentrations and microsomal membrane lipids. *Plant Cell Environ.* 12, 753–757.

Hanson, G. T., Aggeler, R., Oglesbee, D., Cannon, M., Capaldi, R. A., Tsien, R. Y., et al. (2004). Investigating mitochondrial redox potential with redox-sensitive green fluorescent protein. *J. Biol. Chem.* 279, 13044–13053. doi: 10.1074/jbc.M312846200

Hernandez, M., Fernandez-Garcia, N., Diaz-Vivancos, P., and Olmos, E. (2010). A different role for hydrogen peroxide and the antioxidative system under short and long salt stress in Brassica oleracea roots. *J. Exp. Bot.* 61, 521–535. doi: 10.1093/jxb/erp321

Iglesias, M. J., Terrile, M. C., Windels, D., Lombardo, M. C., Bartoli, C. G., et al. (2014). MiR393 Regulation of auxin signaling and redox-related components during acclimation to salinity in Arabidopsis. *PLoS ONE* 9:e107678. doi: 10.1371/journal.pone.0107678

Jiang, K., Meng, Y. L., and Feldman, L. J. (2003). Quiescent center formation in maize roots is associated with an auxin-regulated oxidizing environment. *Development* 130, 1429–1438. doi: 10.1242/dev.00359

Jiang, K., Schwartzer, C., Lally, E., Zhang, S., Ruzin, S., Machen, T., et al. (2006). Expression and characterization of a redox-sensing green fluorescent protein (reduction-oxidation sensitive green fluorescent protein) in Arabidopsis. *Plant Physiol.* 141, 397–403. doi: 10.1104/ pp.106.078246

Jubany-Mari, T., Alegre-Batlle, L., Jiang, K., and Feldman, L. J. (2010). Use of a redox-sensing GFP (c-roGFP1) for real-time monitoring of cytosol redox status in *Arabidopsis thaliana* water-stressed plants. *FEBS Lett.* 584, 889–97. doi: 10.1016/j. febslet.2010.01.014

Julkowska, M. M., Hoefsloot, H. C. J., Mol, S., Feron, R., de Boer, G. J., Haring, M. A., et al. (2014). Capturing Arabidopsis root architecture dynamics with ROOT-FIT reveals diversity in responses to salinity. *Plant Physiol.* 16, 1388–1402. doi: 10.1104/pp.114.248963

Kerk, N. M., and Feldman, L. J. (1995). A biochemical model for the initiation and maintenance of the quiescent center: implications for organization of root meristems. *Development* 121, 2825–2833.

Kleine-Vehn, J., Dhonukshe, P., Swarup, R., Bennett, M., and Friml, J. (2006). Subcellular trafficking of the *Arabidopsis* auxin influx carrier AUX1 uses

a novel pathway distinct from PIN1. *Plant Cell* 18, 3171–3181. doi: 10.1105/tpc.106.042770

Kurth, E., Cramer, G. R., Läuchli, A., and Epstein, E. (1986). Effects of NaCl and $CaCl_2$ on cell enlargement and cell production in cotton roots. *Plant Physiol.* 82, 1102–1106. doi: 10.1104/pp.82.4.1102

Liu, W., Li, R.-J., Han, T.-T., Cai, W., Fu, Z.-W., and Lu, Y.-T. (2015). Salt stress reduces root meristem size by nitric-oxide mediated modulation of auxin accumulation and signaling in Arabidopsis. *Plant Physiol.* 168, 343–356. doi: 10.1104/pp.15.00030

Lu, D., Wang, T., Persson, S., Mueller-Roeber, B., and Schippers, J. H. M. (2014). Transcriptional control of ROS homeostasis by KUODA1 regulates cell expansion during leaf development. *Nat. Commun.* 5, 3767 doi: 10.1038/ncomms4767

Menon, S. G., and Goswami, P. C. (2007). A redox cycle within the cell cycle: ring in the old with the new. *Oncogene* 26, 1101–1109. doi: 10.1038/sj.onc.1209895

Mittler, R. (2002). Oxidative stress, antioxidants and stress tolerance. *Trends Plant Sci.* 7, 406–410. doi: 10.1016/S1360-1385(02)02312-9

Munns, R. (2005). Genes and salt tolerance: bringing them together. *New Phytol.* 167, 645–663. doi: 10.1111/j.1469-8137.2005.01487.x

Pasternak, T. P., Prinsen, E., Ferhan, A., Pal, M., Potters, G., Asard, H., et al. (2002). The role of auxin, pH, and stress in the activation of embryogenic cell division in leaf protoplast-derived cells of alfalfa. *Plant Physiol.* 129, 1807–1819. doi: 10.1104/pp.000810

Perilli, S., and Sabatini, S. (2010). "Analysis of root meristem size and development," in *Plant Developmental Biology, Methods in Molecular Biology,* eds L. Henning and C. Köhler (New York, NY: Springer), 177–187.

Potters, G., Pasternak, T. P., Guisez, Y., Palme, K. J., and Jansen, M. A. (2007). Stress-induced morphogenic responses: growing out of trouble? *Trends Plant Sci.* 12, 98–105. doi: 10.1016/j.tplants.2007.01.004

Rapkine, L. (1931). Su les processus chimiques au cours de la division cellulaire. *Ann. Physiol. Physiochem Biol.* 7, 382–418.

Rodríguez, A. A., Grunberg, K. A., and Taleisnik, E. L. (2002). Reactive oxygen species in the elongation zone of maize leaves are necessary for leaf extension. *Plant Physiol.* 129, 1627–1632. doi: 10.1104/pp.001222

Rubio, M. C., Bustos-Sammamed, P., Clemente, M. R., and Becana, M. (2009). Effects of salt stress on expression of antioxidant genes and proteins in the model legume Lotus japonicus. *New Phytol.* 181, 851–859. doi: 10.1111/j.1469-8137.2008.02718.x

Sarsour, E. H., Kumar, M. G., Chaudhuri, L., Kalen, A. L., and Goswami, P. C. (2009). Redox control of the cell cycle in health and disease *Antoioxid. Redox Signal.* 11, 2985–3011. doi: 10.1089/ars.2009.2513

Sauer, H., Wartenberg, M., and Hescheler, J. (2001). Reactive oxygen species as intracellular messengers during cell growth and differentiation. *Cell Physiol. Biochem.* 11, 173–186. doi: 10.1159/000047804

Shin, R., Berg, H., and Schachtman, D. P. (2005). Reactive oxygen species in root hairs in Arabidopsis root response to nitrogen, phosphorous and potassium deficiency. *Plant Cell Physiol.* 46, 1350–1357. doi: 10.1093/pcp/pci145

Shoresh, M., Spivak, M., and Bernstein, N. (2011). Involvement of calcium- mediated effects on ROS metabolism in regulation of growth improvement under salinity. *Free Radic. Biol. Med.* 51, 1221–1234. doi: 10.1016/j.freeradbiomed.2011.03.036

Sun, F., Zhang, W., Hu, H., Li, B., Wang, Y., Zhao, Y., et al. (2008). Salt modulates gravity signaling pathway to regulate growth direction of primary roots in Arabidopsis. *Plant Physiol.* 146, 178–188. doi: 10.1104/pp.107.109413

Swarup, R., Kargul, J., Marchant, A., Zadik, D., Rahman, A., Mills, R., et al. (2004). Structure-function analysis of the presumptive Arabidopsis auxin permease AUX1. *Plant Cell* 16, 3069–3083. doi: 10.1105/tpc.104.024737

Tsukagoshi, H., Busch, W., and Benfey, P. N. (2010). Transcriptional regulation of ROS controls transition from proliferation to differentiation in the root. *Cell* 12, 606–616. doi: 10.1016/j.cell.2010.10.020

Ulmasov, T., Murfett, J., Hagen, G., and Guilfoyle, T. J. (1997). Aux/IAA proteins repress expression of reporter genes containing natural and highly active synthetic auxin response elements. *Plant Cell* 9, 1963–1971. doi: 10.1105/tpc.9.11.1963

Verbelen, J. P., Condder, T. D., Le, J., Vissenberg, K., and Baluska, F. (2006). The root apex of *Arabidopsis thaliana* consists of four distinct zones of growth activities -meristematic zone, transition zone, fast elongation zone and growth terminating zone. *Plant Signal. Behav.* 1, 296–304. doi: 10.4161/psb.1.6.3511

West, G., Inzé, D., and Beemster, G. T. S. (2004). Cell Cycle Modulation in the response of the primary root of Arabidopsis to salt stress. *Plant Physiol.* 135, 1050–1058. doi: 10.1104/pp.104.040022

Xu, J., and Scheres, B. (2005). Dissection of Arabidopsis ADP-RIBOSYLATION FACTOR 1 function in epidermal cell polarity. *Plant Cell* 17, 525–536. doi: 10.1105/tpc.104.028449

Yu, X., Pasternak, T., Eiblmeier, M., Ditengou, F., Kochersperger, P., Sun, J., et al. (2013). Plastid-localized glutathione reductase2–regulated glutathione redox status is essential for Arabidopsis root apical meristem maintenance. *Plant Cell* 25, 4451–4468. doi: 10.1105/tpc.113.117028

Zazímalová, R. E., Kreceka, P., Skuoa, P., Hoyerová, K., and Pastrasek, J. (2007). Polar transport of the plant hormone auxin – the role of PIN-FORMED (PIN) proteins. *Cell. Mol. Life Sci.* 64, 1621–1637. doi: 10.1007/s00018-007-6566-4

Zhong, H., and Läuchli, A. (1993). Spatial and temporal aspects of growth in the primary root of cotton seedlings: effect of NaCl and $CaCl_2$. *J. Exp. Bot.* 44, 763–771. doi: 10.1093/jxb/44.4.763

Zidan, I., Azaizeh, H., and Neumann, P. M. (1990). Does salinity reduce growth of maize root epidermal cells by inhibiting their capacity for cell wall acidification? *Plant Physiol.* 93, 7–11. doi: 10.1104/pp.93.1.7

Conflict of Interest Statement: The authors declare that the research was conducted in the absence of any commercial or financial relationships that could be construed as a potential conflict of interest.

frontiers in Plant Science

REVIEW
published: 21 October 2016
doi: 10.3389/fpls.2016.01457

Grafting: A Technique to Modify Ion Accumulation in Horticultural Crops

Muhammad A. Nawaz[1,2], Muhammad Imtiaz[3], Qiusheng Kong[1], Fei Cheng[1], Waqar Ahmed[4], Yuan Huang[1] and Zhilong Bie[1]**

[1] College of Horticulture and Forestry Sciences, Huazhong Agricultural University/Key Laboratory of Horticultural Plant Biology, Ministry of Education, Wuhan, China, [2] Department of Horticulture, University College of Agriculture, University of Sargodha, Sargodha, Pakistan, [3] Microelement Research Center, College of Resources and Environment, Huazhong Agricultural University, Wuhan, China, [4] United States Agency for International Development (USDA) and Cultivating New Frontiers in Agriculture (CNFA), Lahore, Pakistan

Grafting is a centuries-old technique used in plants to obtain economic benefits. Grafting increases nutrient uptake and utilization efficiency in a number of plant species, including fruits, vegetables, and ornamentals. Selected rootstocks of the same species or close relatives are utilized in grafting. Rootstocks absorb more water and ions than self-rooted plants and transport these water and ions to the aboveground scion. Ion uptake is regulated by a complex communication mechanism between the scion and rootstock. Sugars, hormones, and miRNAs function as long-distance signaling molecules and regulate ion uptake and ion homeostasis by affecting the activity of ion transporters. This review summarizes available information on the effect of rootstock on nutrient uptake and utilization and the mechanisms involved. Information on specific nutrient-efficient rootstocks for different crops of commercial importance is also provided. Several other important approaches, such as interstocking (during double grafting), inarching, use of plant-growth-promoting rhizobacteria, use of arbuscular mycorrhizal fungi, use of plant growth substances (e.g., auxin and melatonin), and use of genetically engineered rootstocks and scions (transgrafting), are highlighted; these approaches can be combined with grafting to enhance nutrient uptake and utilization in commercially important plant species. Whether the rootstock and scion affect each other's soil microbiota and their effect on the nutrient absorption of rootstocks remain largely unknown. Similarly, the physiological and molecular bases of grafting, crease formation, and incompatibility are not fully identified and require investigation. Grafting in horticultural crops can help reveal the basic biology of grafting, the reasons for incompatibility, sensing, and signaling of nutrients, ion uptake and transport, and the mechanism of heavy metal accumulation and restriction in rootstocks. Ion transporter and miRNA-regulated nutrient studies have focused on model and non-grafted plants, and information on grafted plants is limited. Such information will improve the development of nutrient-efficient rootstocks.

Keywords: grafting, rootstock, scion, root growth, ion uptake, miRNAs, utilization efficiency, transgrafting

OPEN ACCESS

Edited by:
Janin Riedelsberger, University of Talca, Chile

Reviewed by:
Serge Delrot, University of Bordeaux, France
Francisco Perez-Alfocea, Spanish National Research Council, Spain

***Correspondence:**
Yuan Huang
huangyuan@mail.hzau.edu.cn
Zhilong Bie
biezhilong@hotmail.com

Specialty section:
This article was submitted to Plant Physiology, a section of the journal Frontiers in Plant Science

Received: *24 July 2016*
Accepted: *12 September 2016*
Published: *21 October 2016*

Citation:
Nawaz MA, Imtiaz M, Kong Q, Cheng F, Ahmed W, Huang Y and Bie Z (2016) Grafting: A Technique to Modify Ion Accumulation in Horticultural Crops. Front. Plant Sci. 7:1457. doi: 10.3389/fpls.2016.01457

INTRODUCTION

Grafting is a special type of plant propagation, in which a part of a plant (scion) is joined to another plant (rootstock) for the two parts to grow together and form a new plant. Grafting commonly occurs in nature, and the occurrence of natural grafts might have inspired humans to use grafting in the agriculture sector a thousand years ago (Mudge et al., 2009). The rootstocks used for a specific crop are the crop's close relatives or wild selections (mostly within the *genera*), but natural grafts between different families have also been observed (Warschefsky et al., 2016). Grafting has been practiced in fruit trees for a long time; however, its application in vegetables is relatively new. Various fruit grafting references that appear in the Bibble and ancient Greek and Chinese literature suggest that grafting was utilized in Asia, Europe, and the Middle East in fifth century BC (Melnyk and Meyerowitz, 2015). Similarly, a Chinese book written in first century BC and a Korean book written in seventeenth century AD indicate that grafting was utilized in these periods to produce large gourd fruits (Lee and Oda, 2003). Grafting enhances plant vigor, extends the harvesting period (Lee et al., 2010), improves yield and fruit quality (Huang et al., 2009; Rouphael et al., 2010; Tsaballa et al., 2013), prolongs postharvest life (Zhao et al., 2011), tolerates low and high temperatures (López-Marín et al., 2013; Li et al., 2016b), deals with salinity and heavy metal stress (Santa-Cruz et al., 2002; Estañ et al., 2005; Albacete et al., 2009; Schwarz et al., 2010; Huang et al., 2013a; Wahb-Allah, 2014; Penella et al., 2015, 2016), increases drought and flooding stress endurance (Schwarz et al., 2010; Bhatt et al., 2015), improves water use efficiency (Cantero-Navarro et al., 2016), manages soil-borne and foliar pathogens (Louws et al., 2010; Arwiyanto et al., 2015; Miles et al., 2015; Suchoff et al., 2015), manages root knot nematodes (Lee et al., 2010), controls weeds (Dor et al., 2010; Louws et al., 2010), and produces new plant species (Fuentes et al., 2014). Commercial grafting is currently practiced in a number of plant species, including fruits (citrus, apple, mango, grape, peach, plum, apricot, almond, and cherry), vegetables (watermelon, melon, cucumber, tomato, pepper, eggplant, and bitter gourd), and ornamentals (rose, chrysanthemum, bougainvillea, and bonsai), to obtain economic benefits.

In addition to these commercially important benefits, grafting increases nutrient uptake and utilization efficiency in a number of plant species (Pulgar et al., 2000; Zen et al., 2004; Ahmed et al., 2006, 2007; Albacete et al., 2009, 2015a,b; Lee et al., 2010; Schwarz et al., 2013; Huang et al., 2013b; Esmaeili et al., 2015). The world's nutrient resources are finite (Venema et al., 2011) and thus require justified utilization; moreover, inorganic fertilizers are expensive. Scientists are working to modify the root architecture of cereal crops (monocots) to enhance nutrient uptake and utilization efficiency (Meister et al., 2014; Rogers and Benfey, 2015; Wissuwa et al., 2016). Rootstock grafting is used as an alternative for horticultural crops; appropriate and compatible rootstocks are utilized to improve water and nutrient acquisition and nutrient utilization efficiency (Gregory et al., 2013; Albacete et al., 2015a,b). Nutrient efficiency is a general term that refers to the capacity of a plant to acquire and use nutrients. It is measured by plant dry weight produced per unit of nutrient supplied (g DW/g nutrient supplied). This parameter includes nutrient uptake efficiency and nutrient use efficiency (Gerendás et al., 2008). Although other efficiency indicators, such as nutrient harvest index, nutrient influx rate, and nutrient partitioning, have been proposed (Rengel and Damon, 2008), measurement of plant growth and harvestable yield per unit input of applied fertilizer remains reliable (Venema et al., 2011; Santa-Maria et al., 2015).

Several reviews have been conducted on grafting history, grafting methods, breeding and selection of rootstocks, biotic and abiotic stresses, pathogens, amelioration of heavy metals, and hormonal signaling (Lee, 1994; Lee and Oda, 2003; Davis et al., 2008; Kubota and McClure, 2008; Aloni et al., 2010; Lee et al., 2010; Louws et al., 2010; Pérez-Alfocea et al., 2010; Rouphael et al., 2010; Savvas et al., 2010; Schwarz et al., 2013; Edelstein et al., 2016), but none of these reviews sufficiently elucidated the role of grafting in modifying ion uptake and accumulation. Therefore, the current review summarizes available information on the effects of rootstocks on enhancing nutrient uptake, accumulation, and utilization as well as the mechanism involved. Additionally, other important approaches are presented; these approaches can be combined with grafting to further enhance nutrient acquisition and utilization efficiency.

FRUIT CROPS

The use of rootstocks in fruit plants affects tree vigor and size, precocity, fruit quality and taste, harvestable yield, resistance to pests, and tolerance against edaphic and environmental conditions by invigorating the scions and increasing nutrient uptake, transport, and utilization efficiency (Albrigo, 1977; Ahmed et al., 2006, 2007; Castle, 2010; Habran et al., 2016). In a previous study, the grafting of kinnow (*Citrus reticulata* Blanco) onto nine different rootstocks increased the concentration of nitrogen (4–18%), phosphorous (11–77%), and potassium (3–43%) in the leaves of the grafted plants; the number of fruits per plant increased to 0.12–5.63 times that of poorly performing rootstock (Ahmed et al., 2007). In another study, total nitrogen accumulation and utilization efficiency differed in various citrus rootstocks; rough lemon (*Citrus jambhiri* Lush.) accumulated a total nitrogen value of 22.1 mg/g DW, whereas Cleopatra mandarin (*Citrus reshni* hort. ex Tanaka) accumulated only 6.1 mg/g DW (Sorgona et al., 2006). Boron concentration in the leaves, stems, and roots of different citrus rootstocks is significantly affected in normal and boron-deficient conditions (Mei et al., 2011). Citrange rootstock [*C. sinensis* (L.) Osb. × *P. trifoliata* (L.) Raf.] is superior to trifoliate orange [*Poncirus trifoliata* (L.) Raf.] under both low and high levels of boron supply. Although the level of boron in different plant parts grafted onto citrange is lower than that grafted onto trifoliate orange, the ratio of semi-bound boron to free boron is much higher in citrange grafted plants; this higher ratio increases boron use efficiency (Liu et al., 2011, 2013). Evidently, uptake capacity is not the only important factor; the transport and reallocation of cellular boron to cell walls also affect rootstock responses to nutrient deficiency. Wang et al. (2016a) recently applied inarching (a special type of grafting) of Carrizo citrange

[*C. sinensis* (L.) Osb. × *P. trifoliate* (L.) Raf.] to enhance boron uptake in Newhall navel orange [*C. sinensis* (L.) Osb. cv. Newhall] budded onto trifoliate orange [*P. trifoliata* (L.) Raf.]. Inarching significantly increased the levels of boron in the new leaves, new twigs, scion stem, and new rootstock stem under boron-adequate and boron-deficient conditions. This technique can improve nutrient supply in already growing grafted or self-rooted fruit plants under field conditions.

In apples, Cong et al. (2014) found that rootstocks have different potassium uptakes and accumulation efficiencies; these differences become increasingly pronounced under potassium-deficient conditions. Zarrouk et al. (2005) discovered that the concentrations of macro and micronutrients (N, P, K, Ca, Mg, Fe, Mn, Zn, Na, and Cu) in the leaves and flowers of peach are significantly affected by different rootstocks. Similarly, Amiri et al. (2014) reported that apple rootstocks (M9, MM106, and MM111) increase the concentration of N (5–34%), Mg (5–68%), Zn (10–39%), Fe (4–34%), and Mn (11–70%) and reduce the uptake of K (6–19%), and Ca (10–28%). Trees grafted onto M9 are efficient in N, Mn, and Fe uptake but perform poorly in K and Ca uptake. MM106 rootstock possesses the highest efficiency in P uptake and transport. In this study, the fruit yield of plants grafted onto MM111 increased by 44% compared with plants grafted onto M9 rootstock. Mestre et al. (2015) observed that the concentrations of all macro and micronutrients differ significantly in the leaves of Big Top nectarine (*Prunus persica* var. *nectarina*) grafted onto 12 *Prunus* rootstocks. The rootstocks demonstrate a selective behavior for different elements, such as K, Ca, and Cu.

Rootstocks significantly alter the concentration of nutrients in sweet cherry leaves. The GiSelA 6 rootstock (*Prunus cerasus* × *Prunus canescens*, Gi 148/1) performs well in N, P, K, Zn, B, and Mn uptake and transport, but trees grafted onto it tend to develop Ca, Mg, and Cu deficiencies. Similarly, the *Prunus mahaleb* rootstock performs efficiently in N, P, K, Ca, Mg, Fe, and Cu uptake and transport but performs poorly in Zn, B, and Mn absorption and translocation in plants. The leaves of plants grafted onto *Prunus fruticosa* Prob. show deficiencies in several nutrients (N, P, Ca, Mg, and Cu) and are thus unfit for use (Hrotko et al., 2014). Slowik et al. (1979) studied the avocado (*Persea americana* Mill.) cultivar Hass by using Duke and Topa Topa (avocado rootstocks of Mexican origin) and concluded that only the concentrations of N, P, Mg, Cu, Mn, and Fe are affected by the rootstocks; no significant differences were observed for K, Ca, Na, Cl, and Zn. Sherafati et al. (2011) found that in pistachio (*Pistacia vera* L.), the K, Zn, and Fe contents of the leaves are affected by rootstock and scion combinations. Akbari scion (*Pistacia vera* L.) budded onto Badami rootstock (*P. vera* L.) efficiently absorbed K and Zn (1.56% and 11.05 ppm, respectively), whereas minimal amounts of K and Zn (0.80% and 7.33 ppm, respectively) were found in Akbari scion budded onto Daneshmandi rootstock (*P. vera* L.). Barg-seyah scion (*P. vera* L.) budded onto Kalle-ghouchi rootstock (*P. vera* L.) absorbed the largest amount of Fe (241 ppm) and Cu (12.15 ppm) among all rootstock and scion combinations.

Ibacache and Sierra (2009) demonstrated that rootstocks significantly affect grapevine nutrition. They studied the effect of 10 rootstocks on grapevines and found significant differences in nutrient concentration in the petioles of four scion cultivars. The petiole P levels doubled in all scion cultivars when Salt Creek rootstock (*Vitis vinifera* L.) was used. Potassium was also increased by up to 5–155% by rootstocks in all scion cultivars. Similarly, N levels increased to 67% in Flame Seedless (*V. vinifera* L.), 77% in Red Globe (*V. vinifera* L.), 33% in Thompson Seedless (*V. vinifera* L.), and 8.5% in Superior Seedless (*V. vinifera* L.) scions compared with self-rooted vines. Bavaresco et al. (2003) utilized two rootstocks for grapevines and observed that the hybrid rootstock 41 B (*V. vinifera* × *V. berlandieri*) significantly increased the nutrient uptake and whole plant dry mass (24%) compared with 3309 C (*V. riparia* × *V. rupestris*). The total N, P, K, Ca, and Mg contents of the plant increased by 38, 21.5, 18, 35, and 12%, respectively. Additionally, the concentrations of micronutrients (Zn, Mn, and B) increased by 16, 94, and 18%, respectively, whereas Cu slightly decreased (1%). Lecourt et al. (2015) observed that rootstocks significantly affect the plant growth (dry matter) and concentration of macro and micronutrients in the leaves and root tissues of grapevine (V. *vinifera* L.). Cabernet Sauvignon (*V. vinifera* L.) grafted onto Riparia Gloire de Montpellier (*V. riparia* L.) increased the leaf N (3%), K (44%), S (70%), Ca (27%), Mg (58%), Fe (65%), Zn (57%), B (93%), Mn (83%), and Al (46%) concentrations compared with Cabernet Sauvignon grafted onto 1103 Paulsen (*V. rupestris* × *V. berlandieri*) irrigated with 2.45 mmol N supply. Habran et al. (2016) investigated the effect of N and rootstock on N uptake and their effect on secondary metabolism in grapes. Cabernet Sauvignon (*V. vinifera* L.) grafted onto 110 Richter increased the leaf and petiole N concentration by up to 14% and 1%, and 9% and 30% under low and optimum levels of N supply, respectively, compared with Cabernet Sauvignon grafted onto Riparia Gloire de Montpellier (*V. riparia*). Rootstocks also affected vine growth (14–16%), berry weight, and composition at the time of harvest. Zamboni et al. (2016) recently declared M1 rootstock [106-8 (*V. riparia* × *V. cordifolia* × *V. rupestris*) × Resseguier n.4 (*V. berlandieri*)] as superior over M3 [R 27 (*V. berlandieri* × *V. riparia*) × Teleki 5C (*V. berlandieri* × *V. riparia*)], 1103P (*V. berlandieri* × *V. rupestris*), and 101–14 (*V. riparia* × *V. rupestris*) rootstocks because of its balanced leaf nutrient profile, nitrogen use efficiency, and improved vine growth (30%). Various rootstocks behave differently in terms of yield, physiological responses, and severity of Fe deficiency; proper rootstock selection can mitigate nutrient deficiency symptoms and responses in grapevines (Covarrubias et al., 2016).

VEGETABLE CROPS

Grafting in vegetable crops is a relatively new procedure that has gained popularity in the last few decades (Lee et al., 2010). Similar to fruit crops, melon (*Cucumis melo* L.) cultivars Yuma and Gallicum grafted onto three *Cucurbita maxima* (Shintoza, RS-841, and Kamel) rootstocks show a significant variation in macronutrients in leaf tissues. Grafting increases the yield

(88%–121%) and concentration of P and N in the leaves by up to 6–58% and 6–81%, respectively, compared with self-rooted melon plants (Ruiz et al., 1997). Zhang et al. (2012) found that P uptake and utilization in grafted watermelons are better than those in self-rooted watermelons under low P supply. Various rootstocks perform differently; watermelon grafted onto pumpkin (*Cucurbita moschata* Duch.) performs better than watermelon grafted onto bottle gourd (*Lagenaria siceraria* Standl.). Huang et al. (2013b) found that grafting of watermelon onto Hongdun (*Citrullus lanatus* sp.) and Jingxinzhen No.4 (*C. moschata* Duch.) increases K uptake and whole plant dry mass (1.82 fold) and induces low K tolerance in the watermelon scion. Uygur and Yetisir (2009) worked on watermelons and concluded that the watermelon [*C. lanatus* (Thunb.) Matsum and Nakai] cultivar Crimson Tide grafted onto gourd rootstock (*L. siceraria* Standl.) landraces significantly increases N and K uptake from the soil, especially under salt stress conditions. The concentration of P in the shoots of grafted plants is almost twice that in non-grafted watermelon plants. Therefore, bottle gourds, especially the *Lagenaria* type, can be utilized as a rootstock for watermelon under saline conditions.

Comprehensive mineral nutrient analysis has shown that the concentration of macro and micronutrients in the leaves, fruit rind, fruit flesh, and seeds of grafted watermelon is altered by gourd rootstocks [Ferro and RS841 (*C. maxima* × *C. moschata*) and Argentario and Macis (*Lagenaria* hybrid)]. In leaves, rootstocks increase the N, K, Ca, and Mg concentrations by up to 12–28, 8–36, 13–81, and 12–300%, respectively, and reduce the concentrations of P, Fe, Zn, Mn, and Cu. In fruit rind, flesh, and seeds, rootstocks increase the concentration of all nutrients, thereby proving the superiority of specific graft combinations over self-rooted plants (Yetisir et al., 2013). Watermelon cultivar Zaojia 8424 [*C. lanatus* (Thunb.) Matsum and Nakai] grafted onto bottle gourd cv. Jingxinzhen No.1 (*L. siceraria* Standl.) and pumpkin cv. Qingyanzhen No.1 (*C. maxima* × *C. moschata*) increases the total uptake (mg/plant) and concentration [mg g^{-1} dry weight (DW)] of N, K, Ca, Fe, Mg, and Mn in the roots, stems, leaves, fruit rind, and flesh of grafted plants. The total nutrient uptake of plants grafted onto bottle gourd and pumpkin increases by 30.41 and 49.14%, respectively, at the fruit development stage and by 21.33 and 47.46%, respectively, at the fruit maturation stage compared with non-grafted watermelon plants (Huang et al., 2016a). Another experiment showed that pumpkin rootstock (*C. moschata* Duch.) increases the Mg^{2+} uptake (39%) and whole plant dry mass (1.71 fold) of watermelon plants compared with self-grafted plants under low Mg conditions (Huang et al., 2016b). The *C. maxima* variety Dulce Maravilla clearly increases Fe uptake and translocation to watermelon scions (Rivero et al., 2004).

Grafting is useful in manipulating plant growth and is used in multiple ways. Zhang et al. (2010) reported that when cucumber plants (*Cucumis sativus* L. cv. Xintaimici) are grafted onto *Cucurbita ficifolia*, the uptake of Cu from the soil under Cu stress conditions is significantly reduced. The concentration of Cu in the stem and leaves of the scion is lower in grafted plants than in self-rooted plants; moreover, the concentration of Cu in the roots of grafted plants is higher. This result suggests that the *C. ficifolia* rootstock acts as a Cu accumulator and reduces Cu transport to the scion. However, its sensing, signaling, regulation, and withholding mechanisms still require further explanation. Grafting increases the uptake of K and limits the transport of Na and Cl ions to the scion compared with self-rooted plants under salt stress conditions in cucumber. Grafting also enhances nutrient utilization efficiency as manifested by improved shoot biomass production, yield, and fruit quality (Rouphael et al., 2008; Zhu et al., 2008; Albacete et al., 2009, 2015a,b; Huang et al., 2009; Colla et al., 2012, 2013; Farhadi and Malek, 2015; Gao et al., 2015).

Grafting of tomato (*Solanum lycopersicum* L.) onto Maxifort rootstock (*S. lycopersicum* L. × *Solanum habrochaites*) improves scion growth (11%) and concentration of macro and micronutrients (**Table 1**). However, different forms of nitrogen (NO_3^-, NH_4^+) exert a significant effect on the uptake of other elements; for example, increased availability of NH_4^+ reduces the uptake of Ca and Mg in plant tissues (Borgognone et al., 2013). Savvas et al. (2009) reported that grafting tomato onto He-Man rootstock (*S. lycopersicum* × *S. habrochaites*; Syngenta Seeds, Basel, Switzerland) improves fruit yield (11.5%) and increases the concentrations of Ca, K, and Zn by 18, 8, and 11%, respectively, in tomato leaves and reduces the uptake of Mg (27%) and Fe (27%), especially under low levels of Mn. In pepper and eggplant, rootstocks also show a positive response by modifying ion uptake and acquisition of macro and micronutrients and by providing protection from heavy metals (Leonardi and Giuffrida, 2006; Arao et al., 2008; Penella et al., 2015).

Rootstocks play a pivotal role in fertilizer management because they can ensure the justified utilization of available or applied fertilizers in the soil. Harvestable yield is an important criterion of nutrient utilization efficiency. An overview of reported percentage growth and yield increments obtained through grafting among various vegetables is presented in **Table 1**.

ORNAMENTAL CROPS

Previous studies on ornamental crops have elucidated the effects of rootstock on the nutrient uptake of such crops. Gammon and McFadden (1979) grafted rose onto seven different rootstocks and determined that rootstock combinations significantly increase nutrient uptake and accumulation. *Rosa fortuniana* Lindl. triggered Mn accumulation five times more than *Rosa odorata;* however, *R. odorata* was superior to *R. fortuniana* in terms of K accumulation. Niu and Rodriguez (2008) evaluated the performance of four rose rootstocks [Dr. Huey (*Rosa hybrida* L.), *R. fortuniana* Lindl., *Rosa multiflora* Thunb., and *R. odorata* (Andr.) Sweet] under chloride-or sulfate-dominated salinity and observed that rootstocks behave differentially in terms of Ca, Mg, K, Na, and Cl uptake. *R. multiflora* accumulates more Na than *R. odorata*, and *R. fortuniana* accumulates the least amount. However, *R. multiflora* retains most of Na in the roots, whereas *R. odorata* transports 57% of the absorbed Na to the shoots. According to another study, commercial rose varieties grafted onto different rootstocks significantly differ in macro (P, K, and Mg) and micro (Cl, Mn, Fe, B, Zn, and Na) nutrient concentrations (Cabrera, 2002). The N use efficiency (NUE) in tobacco can be improved by grafting it onto *Nicotiana tabacum*

TABLE 1 | Effects of rootstocks on the nutrient concentration and growth/yield of grafted plants.

Name of crop	Name of rootstock	Plant part used for determination	Increase in nutrients concentration (%)*	Reduction in nutrients concentration (%)*	Yield improvement (%)*	References
Kinnow *(Citrus reticulata* Blanco.)	Nine different citrus rootstocks were used	Leaves	N (4–18), P (11–77), K (3–43)	–	12.5–563[a]	Ahmed et al., 2007
Newhall navel orange (*Citrus sinensis* Osb.)	Citrange [*C. sinensis* (L.) Osb. × *P. trifoliata* (L.) Raf.] and trifoliate orange [*Poncirus trifoliata* (L.) Raf.]	Mature leaves	B (55)	–	3[b]	Liu et al., 2011
		New leaves	B (51)			
		Roots	B (63)			
Apple (*Pyrus Malus*)	Six different *Malus* rootstocks	Leaves	K (25)	–	60[c]	Cong et al., 2014
	M9, MM106, MM111 Apple, and *Malus domestica* cv. Local	Leaves	N (5–34), Mg (5–68), Zn (10–39), Fe (4–34) Mn (11–70)	K (6–19), Ca (10–28)	44[d]	Amiri et al., 2014
Grapes (*Vitis vinifera* L.)	Different grape rootstocks	Petioles	N (8.5–77), P (5–186), K (5–155)	–	–	Ibacache and Sierra, 2009
	41 B (*V. vinifera* × *V. berlandieri*) and 3309 C (*V. riparia* × *V. rupestris*)	Whole plant	N (38), P (21.5), K (18), Ca (35), Mg (12), Zn (16), Mn (94), B (18)	Cu (1)	24[b]	Bavaresco et al., 2003
	Different grape rootstocks	Leaves	N (10–31), P (5–41), K (19–23), Ca (3–20), Mg (26–34), Fe (1–20), B (6–70)	–	30[e]	Zamboni et al., 2016
	Riparia Gloire de Montpellier (RGM) and 110 Richter (*V. vinifera* L.)	Leaves	N (1–14)	–	14–16[e]	Habran et al., 2016
		Petioles	N (9–30)			
	Riparia Gloire de Montpellier (RGM) and 1103 Paulsen (*V. vinifera* L.)	Leaves	N (3), K (44), S (70), Ca (27), Mg (58), Fe (65), Al (46), Mn (83), Cu (43), Zn (57), B (93)	P (33)	152–205[e]	Lecourt et al., 2015
Avocado (*Persea americana*)	Duke and Topa Topa Avocado (*Persea americana*)	Whole plant	N (10), P (5.72), K (2.44), Fe (19), Cu (12.5), Mn (15)	–	5[d]	Slowik et al., 1979
Pistachio (*Pistacia vera* L.)	Badami Pistachio (*Pistacia vera* L.)	Leaves	K (95), Zn (51)	–	–	Sherafati et al., 2011
Melon (*Cucumis melo*)	*C. maxima* × *C. moschata* (Shintoza, RS-841, and Kamel)	Leaves	N (6–81), P (6–58), S (1–4), Mg (1–3), Ca (0–5)	K (4–38)	88–121[d]	Ruiz et al., 1997
	Shintoza (*C. maxima* × *C. moschata*) and Sienne[**] (Cantaloupe type melon)	Leaves	N (27), P (36), K (28), Ca (39), Mg (16), Mn (35), Zn (31), S (5)	Na (232), Cu (566), B (240), Fe (320)	1–26[a], 11–24[d]	Bautista et al., 2011
	Cucurbita maxima Duchesne × *Cucurbita moschata* (pumpkin, squash)	Leaves	Ca (6), Mg (5)	Na (255), K (9)	11.5[d]	Edelstein et al., 2005
	Shintoza (*C. maxima* × *C. moschata*)	Leaves	N (21), P (17), K (19)	–	255[d]	Salehi et al., 2014
Watermelon (*Citrullus lanatus*)	Hongdun (*C. lanatus* sp.)	Xylem sap	K (246)	–	182[b]	Huang et al., 2013b
	Jingxinzhen No.4 (*Cucurbita moschata* Duch.)	Leaves	Mg (39)	–	171[b]	Huang et al., 2016b
	Ferro, RS841 (*Cucurbita maxima* × *C. moschata*), and Argentario and Macis (*Lagenaria* hybrid)	Leaves	N (12–28), K (8–36), Ca (13–81), Mg (12–300)	–	–	Yetisir et al., 2013

(Continued)

TABLE 1 | Continued

Name of crop	Name of rootstock	Plant part used for determination	Increase in nutrients concentration (%)*	Reduction in nutrients concentration (%)*	Yield improvement (%)*	References
	Cucubirta maxima var. Dulce maravilla	Leaves	Fe (193)	–	–	Rivero et al., 2004
		Roots	Fe (143)			
Tomato (*Solanum lycopersicum)*	AR-9704 Tomato (*Solanum lycopersicum* L.)	Leaves	P (68), S (15)	Na (62), Cl (28)	–	Fernández-García et al., 2002
	Maxifort (*S. lycopersicum* L. × *S. habrochaites* S. Knapp and D. M. Spooner)	Leaves	N (0.5), P (13), Ca (10), Fe (9), Mn (3), Cu (18), Zn (17), B (3)	Mg (10)	2[d], 11[b]	Borgognone et al., 2013
	He-Man (*Solanum lycopersicum* × *Solanum habrochaites*)	Leaves	Ca (18), K (8), Ca (11)	Mg (27), Fe (27)	11.5[d]	Savvas et al., 2009
	Solanum lycopersicum cv. Tmknvf2	Leaves	Fe (11.18)	–	–	Rivero et al., 2004
		Roots	Fe (185)			
	Solanum lycopersicum Mill. cv. Radja	Leaves	K (13)	–	20–30[d]	Estañ et al., 2005
	Root localized *IPT*-expressing tomato rootstock (35S::IPT) (*Solanum lycopersicum* Mill.)	Leaves	K (20)	Na (30)	30[d]	Ghanem et al., 2011
Rose (*Rosa centifolia*)	Seven *Rosa* rootstocks	Leaves	N (3–12), P (3–23), K (13–31), Ca (7–25), Mg (8–30), Zn (2–18), Mn (141–410), Fe (3–15), Cu (5–36)	–	223[f]	Gammon and McFadden, 1979

*Compared with self-rooted, self-grafted, or poorly performing rootstock.
**Intermediate scion in the process of double grafting.
[a]Total number of fruits per plant.
[b]Whole plant dry mass.
[c]Shoot dry mass.
[d]Fruit yield per plant on weight basis.
[e]Pruning weights of grapevines.
[f]Flower value index.

H-20 rootstock (Ruiz et al., 2006). Several details on increased nutrient uptake through grafting are summarized in **Table 1**. These pieces of evidence demand the careful selection of the rootstock to enhance nutrient use efficiency in ornamental crops. Grafting is also utilized to produce bonsai plants (an important category of ornamentals); in bougainvillea and several other ornamentals, it is also used to produce plants bearing flowers of different colors or multicolored flowers on the same plant to enhance anesthetics (Relf, 2015). In a recent report, Zhang et al. (2013) observed increased productivity and rooting ability of cuttings obtained from grafted chrysanthemum. In the near future, an increase in the use of grafting is expected in ornamental crops. However, serious efforts are required for the selection of compatible rootstocks in ornamental plants.

MECHANISM

Rootstocks modify the ion uptake in grafted plants. The final concentration of nutrients is a result of uptake, transport, recirculation, and growth. The absorption of nutrients from the soil is affected by numerous factors, including soil properties (pH, cation exchange capacity, and concentration of the nutrients) and root characteristics (root architecture, organic acids and metabolites exudation capacity, and transport ability). This article focuses on root-related mechanisms.

Root System Architecture and Ion Uptake

In cereal crops, modification of the root architecture is a popular means to enhance ion uptake, accumulation, and utilization efficiency, and this means has been discussed in several reviews (Meister et al., 2014; Rogers and Benfey, 2015; Wissuwa et al., 2016). Nutrient uptake and utilization in horticultural crops are enhanced by selecting appropriate rootstocks. Rootstocks play a vital role in manipulating the nutrient status of the scions by directly affecting ion uptake and transport (Amiri et al., 2014). The ion concentration in the roots and shoots of grafted grapevines depends on rootstock genotype (Lecourt et al., 2015). The selected rootstocks have a vigorous root system, i.e., large main roots, many lateral roots and root hair, large total root length, and root surface area. These roots absorb a large amount

of water and nutrients by exploring wide and deep soil volumes (Pérez-Alfocea, 2015). According to a report, the root dry weight of watermelon grafted onto Jingxinzhen No. 4 pumpkin (*C. moschata* Duch.) is 2.24 times that of self-rooted plants (Huang et al., 2013b), and the K uptake efficiency of grafted plants is 2.02 times that of self-rooted plants. Similarly, the root dry weight of a rose cultivar (*Rosa* "BAIore") is thrice that of a poorly performing cultivar *Rosa* "Frontenac" under stress conditions (Harp et al., 2015). Therefore, this vigorous root system of rootstock can capture and transport a large amount of nutrients to the above ground scion. Vigorous rootstocks have high levels of sugars, amino acids, and enzymes and secrete organic acids in the soil, which are important in nutrient mobilization and affect nutrient availability and uptake (Jaitz et al., 2011; Khorassani et al., 2011; Dam and Bouwmeester, 2016). Jiménez et al. (2011) reported that high concentrations of root sucrose, total organic and amino acids, and phosphoenolpyruvate carboxylase activity in the roots of *Prunus* rootstocks subjected to iron deficiency promote root growth and trigger iron uptake. Similarly, under iron-deficient conditions, the roots of *Malus* species secrete acids, reduce the pH of rhizosphere, and significantly increase the activities of root ferric chelate reductase (FCR), thereby leading to increased ferrous uptake (Zha et al., 2014).

Transporters and Ion Uptake

Rootstocks modify ion uptake and transport to the scion by affecting the activities of ion transporters. Transporters are involved in ion uptake, root compartmentation, and translocation of these absorbed ions to aboveground plant parts. Transporters are highly specific under different environmental conditions and in the concentrations of specific nutrients present in the soil. For example, in two citrus rootstocks [Carrizo citrange (*C. sinensis* [L.] Osb. × *P. trifoliata* [L.] Raf.) and Cleopatra mandarin (*C. reshni* Hort. ex Tanaka)], eight different K transporters have been identified (Caballero et al., 2013). Grafting affects the activity of ion transporters. The expression levels of Mg transporter genes *MGT1*, *MGT3*, *MGT4*, *MGT5*, and *MGT7* are much higher in the roots of Jingxinzhen No.4 pumpkin (*C. moschata* Duch.) used as rootstock compared with the roots of self-rooted watermelon cultivar Zaojia 8424 [*C. lanatus* (Thunb.) Matsum and Nakai], especially under low Mg conditions. These higher expression levels enhance the Mg^{2+} uptake of watermelon grafted onto Jingxinzhen No.4 pumpkin rootstock (Huang et al., 2016b). However, the signaling mechanism in the activation of these genes still requires further investigation. Similarly, the activities of ferric-related uptake and transport genes (*NAS1*, *FRD3*, and *NRMAP3*) are significantly increased under iron-deficient conditions in apple rootstock *Malus xiaojinensis*, thereby increasing the ferrous uptake (Zha et al., 2014). Han et al. (2009) reported that a genetically engineered bottle gourd (*L. siceraria* Standl.) rootstock having a modified Arabidopsis Ca^{2+}/H^{+} exchanger *sCAX2B* improves the biomass and quality of watermelon fruits by enhancing nutrient transport to the scion. This transporter provides enhanced Ca^{2+} transporter substrate specificity and decreases Mn transport capability. Gonzalo et al. (2011) studied the response mechanism of two *Prunus* rootstocks [Myrobalan plum (P 2175) and peach–almond hybrid (Felinem)]. Felinem showed an activated expression of FCR and the iron transporter gene. The local signal induced a quick response of the transporter, whereas the FCR gene was expressed later. By contrast, in P 2175, the response appeared later, and long-distance signals appeared to be involved. However, in both situations, signaling molecules were not identified; this mechanism thus requires further investigation.

Grape rootstocks [SO4 and K5BB (VITIS Rauscedo, Società Cooperativa Agricola, Rauscedo, Italy) favor nitrate uptake by affecting the activities of low-affinity nitrate transporter (*VvNRT1.3like*) and high-affinity nitrate transporter (*VvNRT2.4like*) genes in grapevines (Tomasi et al., 2015). In pear rootstock (*Pyrus betulaefolia*), six NH_4^+ transporter genes (*LjAMT;1, LjAMT;2, LjAMT;3, LeAMT;3*, *PbAMT1;3*, and *PbAMT1;5*) have been reported (Mota et al., 2008; Li et al., 2016d); however, the roles of these and other transporters in grafted plants remain unclear. In two citrus rootstocks [Cleopatra mandarin (*C. reshni* hort. ex Tanaka) and Troyer citrange (*C sinensis* × *P trifoliata*)], low-and high-affinity transport systems work depending on the availability of nitrate ions in the external medium (Cerezo et al., 2007). However, the sensing and signaling mechanisms (how plants sense the internal and external concentrations of nitrate and respond accordingly) have not been explained in grafted plants. Non-grafted plants utilize a dual-affinity nitrate transporter (CHL1) and protein kinases (CIPK28 and CIPK8) to sense a wide range of nitrate concentration changes in the soil and to alter their own transport properties (Ho et al., 2009). Another recent study revealed that small peptides are produced in nitrogen-starved roots and then transported to the shoot; this root-to-shoot signaling helps plants adopt under prevailing conditions (Tabata et al., 2014). These pieces of evidence are missing in grafted plants and need further study.

Hormones, miRNAs, and Ion Uptake

Hormones and miRNAs are the key players that affect nutrient absorption and transport by affecting the root growth and activity of ion transporters. Grafting onto rootstocks changes hormonal levels (cytokinin and auxin) in roots and shoots, triggers growth, delays leaf senescence, and helps tolerate environmental stress (Albacete et al., 2009; Van-Hooijdonk et al., 2010; Ghanem et al., 2011). In a previous study, grafting a transient root IPT induction (HSP70::IPT) and wild type (WT) tomato (*S. lycopersicum* L. cv. UC82-B) scions onto root localized *IPT*-expressing tomato rootstock (*35S::IPT*) grown under salt stress conditions (75, 100 mM NaCl) increased root, xylem sap, and leaf bioactive cytokinin by 2–3 times, increased leaf K concentration (20%), and reduced Na concentration (30%) in the transient root IPT induction scion compared with plants grafted onto non-transformed plants. Similarly, *IPT*-expressing tomato rootstock (*35S::IPT*) increased fruit *trans*-zeatin concentrations 1.5–2 fold and fruit yield (30%) in WT tomato scion compared with WT tomato plants grafted onto non-transformed rootstock (Ghanem et al., 2011). Roots of rootstock-grafted apple with more branching (MB) mutant scion show elevated cytokinin and auxin contents and reduced expressions of *MrPIN1, MrARF, MrAHP,* most *MrCRE1* genes, and cell growth-related genes

MrGH3, MrSAUR, and *MrTCH4*. Auxin accumulation and transcription of *MrPIN3, MrALF1*, and *MrALF4* induce lateral root formation in MB-grafted rootstock, and these new roots contribute to nutrient absorption (Li et al., 2016a). miRNAs regulate the expression of transporters involved in nutrient uptake and mobilization (Fujii et al., 2005; Chiou et al., 2006; Sunkar et al., 2007; Valdés-Lopez et al., 2010; Paul et al., 2015). A recent report (Li et al., 2016c) showed that under N or P deficiency, the expression levels of 19 miRNA target genes in the roots of pumpkin (*C. moschata* Duch.)-grafted cucumber (*C. sativus* L.) are higher than those in self-grafted cucumber. Many studies have revealed the role of miRNA 399 in P absorption, transport, metabolism, and homeostasis in plants. P deprivation is rapidly transmitted to the shoots where miRNA 399 is produced, conjugates, changes the activity of PHO2 (an essential transporter of phosphate mobilization), and regulates phosphate homeostasis (Pant et al., 2008). The expressions of miRNA 399 and csa-miR-n08 are higher in pumpkin (*Cucurbita moschata* Duch.)-grafted plants. These affect the expressions of *PHR1* and *E3* (ubiquitin–protein ligase), which are essential for P absorption and metabolism. The PHR1 transcription factor binds to the promoter region of many phosphorous-deficient responsive genes, including those encoding phosphate transporters and protein kinases (Rubio et al., 2001; Todd et al., 2004). Under phosphorous starvation, the activity of miR2111 doubles within 3 h, whereas under N deficiency, the opposite occurs (Pant et al., 2008; Xu et al., 2013). Therefore, the relationship among the expression levels of different miRNAs still requires explanation. Several recently published articles have summarized the role of miRNAs (Liu and Vance, 2010; Zeng et al., 2014; Kulcheski et al., 2015; Paul et al., 2015) and ion transporters (Conte and Walker, 2011; Finazzi et al., 2015; Pinto and Ferreira, 2015; Gu et al., 2016) in nutrient acquisition, transport, and homeostasis. However, information on grafted plants is limited and requires the attention of plant biologists because grafted plants are complex in nature, and their responses are influenced by the genetic makeup of the scion and the rootstock and their interaction.

In conclusion, rootstocks modify nutrient availability to the scion. A vigorous root system, increased secretion of root exudates (organic acids and primary and secondary metabolites), enhanced expression of transport-related genes, increased absorption and transport, improved ion homeostasis, and remobilization capacity of the rootstocks ensure improved nutrient supply to the scion. These nutrients enable scions to increase light energy transformation, CO_2 conductivity, dark reaction activity, and rate of photosynthesis, thereby improving nutrient utilization (Weng, 2000; Sun et al., 2002; Qi et al., 2006; Wei et al., 2006; Huang et al., 2011).

ROOTSTOCK LIMITS THE UPTAKE AND TRANSPORT OF SALTS AND HEAVY METALS

Rootstocks improve the acquisition of essential elements and reduce the uptake and transport of salts (e.g., Na and Cl) and heavy metals (e.g., Cr, Ni, Cd, Sr, and Ti) through ion exclusion or retention. Reciprocal grafting experiments on cucumber (*C. sativus* L.), pumpkin (*C. moschata* Duch.), and melon (*C. melo* L.) rootstocks revealed that pumpkin is salt tolerant. Pumpkin excludes 74% of the available Na, whereas no Na is excluded by melon. Similarly, Na retention in pumpkin rootstock reduces the level of Na in leaves by 46.9%, whereas no decrease is observed in melon rootstock (Edelstein et al., 2011). Estañ et al. (2005) found that grafting a commercial tomato cultivar Jaguar (*S. lycopersicum* L.) onto tomato rootstocks (Radja, Pera, and the hybrid Volgogradskij × Pera) increases fruit yield by up to 80% by regulating saline ions (Na and Cl). Pumpkin-grafted cucumber shows an increased expression of plasma membrane H^+-ATPases (*PMA*) and plasma membrane Na^+/H^+ antiporter (*SOS1*) under NaCl stress conditions compared with self-grafted cucumber. The increased activities of *PMA* and *SOS1* enable the root to pump Na^+ from the cytosol of root cells to the external medium (Lei et al., 2014). Citrus rootstock responds differently to Cl stress, and a number of uncharacterized membrane transporter genes, such as *NRT1-2*, are differentially expressed in poor Cl excluder Carrizo citrange (*C. sinensis* × *P. trifoliata*) and efficient Cl excluder Cleopatra mandarin (*C. reshni* hort. ex Tanaka) rootstocks (Brumós et al., 2009). The strong repression of the *ICln*gene in Cleopatra mandarin regulates Cl uptake and transport to the shoot. It reduces the net Cl loading to the root xylem and thus enhances the Cl tolerance of Cleopatra mandarin (*C. reshni* hort. ex Tanaka) (Brumós et al., 2010). Transporters also help enhance salt stress tolerance. Overexpression of a *Malus* Na^+/H^+ anti-porter gene improves the salt tolerance of M26 dwarfed apple rootstock (Li et al., 2013). Rootstocks reduce Na and Cl loading and transport to the scion while increasing the uptake of K, Ca, and Mg ions and allow small osmotic potentials with a low energy cost. Therefore, rootstocks increase the tolerance of scion species to salt and toxic elements.

Grafting cucumber (*C. sativus* L.) onto *C. maxima* × *C. moschata* rootstocks reduces the absorption and transport of Cd and Ni to the scion. The absorption of Cd depends on rootstock genotype (Savvas et al., 2013). Heavy metals also affect the availability of essential nutrients; however, the negative effect can be minimized by grafting onto appropriate rootstocks. Root structure (genotype) and transporter activities appear to be involved in the reduction of hazardous ion absorption and transport. In a reciprocal grafting experiment, Xin et al. (2013) found that spinach shoot Cd concentration is unrelated to root Cd absorption; it depends on Cd transport from the root to the shoot. The thick phellem (outer zone of periderm) and outer cortex cell walls of the water spinach (*Ipomoea aquatic* Forsk.) rootstock QLQ retain more Cd in the root compared with water spinach rootstock T308. Apple rootstock (*Malus Baccata* Borkh.) reduces the influx of Cd and shows the least amount of Cd in leaf petioles compared with other apple rootstocks (*Malus hupehensis* Rehd., *M. micromalus* "qingzhoulinqin," and *M. robusta* Rehd.). *M. Baccata* has a low transcript level for Cd uptake and transport genes (*HA7, FRO2-like, NRAMP1,* and *NRAMP3*) and a strong transcript level for detoxification genes (*NAS1 and MT2*). The reduced

expression of Cd transport genes results in reduced uptake and transport of Cd (Zhou et al., 2016). Repression of Cd uptake and transport genes occurs through a local signal or as a result of long-distance signaling, although this issue remains unclear. Thus, investigations about the sensing and signaling mechanisms of heavy metals in grafted plants are required.

FUTURE PERSPECTIVES

Although grafting is a centuries-old phenomenon currently practiced at the commercial scale, the physiological and molecular bases of grafting remain unclear. With *Arabidopsis* as a model plant, the basic scientific mechanism of grafting is being investigated. Rootstocks and scions affect each other; their interaction mechanism also requires further attention. Grafting compatibility between the rootstock and scion is important for uninterrupted flow of water, nutrients, and carbohydrates. Grafting incompatibility occurs when either of the plant parts (rootstock or scion) completely or partially fails to grow after successful grafting and in several latter stages of plant growth. Overgrowth of the scion over the rootstock, overgrowth of the rootstock over the scion, and bud union crease are common symptoms of incompatibility. Double grafting can resolve compatibility issues, but it complicates the process of grafted seedling production and increases the production cost. Grafting incompatibility may be related to defense responses. Cookson et al. (2014) observed a coordinated upregulation of stress response-related genes in hetero-grafts compared with self-grafted grapevines (*Vitis* spp.). In a recent study, Melnyk et al. (2015) revealed that auxin response genes *IAA18, IAA28*, and *ALF4* are responsible for vascular reconnection at the graft junction. Although authors have not linked these genes with incompatibility, the roles of these genes in incompatibility cannot be overlooked and require further investigation. Crease formation affects water and nutrient transport; however, to what extent this effect impairs the availability of nutrients to the scion remains unclear. Similarly, different methods of grafting are utilized for fruits and vegetables, but their effects on the quality of the vascular connection, crease development, and nutrient supply have not been considered to date. Detailed histochemical investigations are required to study the cell and vascular tissue structures at graft junctions and their relationship with water and nutrient transport. The rootstock and scion are important, but the rootstock is considered critical. No failure caused by scion variety has been reported in the fruit industry in any country, but a number of examples show failure caused by inappropriate rootstock (Castle, 2010). Therefore, in perennial fruit plants, the choice of proper/compatible rootstock is highly significant because once an orchard is established; it remains productive for a long time. Similarly, selecting compatible and appropriate rootstocks for important vegetables and ornamental crops need consideration. Although large numbers of rootstocks are available and used for different crops, improved rootstocks with improved characteristics, such as multi-disease resistance and enhanced nutrient absorption and utilization efficiencies, are still lacking.

Rootstocks enable increased water and nutrient absorption through efficient uptake systems and/or their capacity to explore wide and deep soil volumes. However, these properties should be transferred to increase yield or improve efficiency. This transfer requires well-designed studies on yield responses vs. a gradient of nutrient/water application to the plant. The accumulation of a given nutrient in the leaves during vegetative growth is not an indicator of nutrient use efficiency and should be considered in relation to the total nutrients absorbed by the plant and the harvestable yield produced (Pérez-Alfocea, 2015). Moreover, the response of rootstocks under different growing conditions changes considerably (Cong et al., 2014). Rootstocks are also inherently selective in the absorption of different nutrients. Fernández-García et al. (2002) observed an increase in the uptake of P and Ca and a decrease in the uptake of N, K, S, and Mg by grafting Fanny and Goldmar (*S. lycopersicum* L.) onto AR-9704 (*S. lycopersicum* L.). Nutrient-specific rootstock breeding is currently eliciting the attention of scientists (Venema et al., 2011). Macronutrients, such as P and K, are finite in nature and costly, so they are of particular interest. With the passage of time, linkage map locations for quantitative trait loci (QTLs) have become available for nutrient uptake and transport. For example, several QTLs controlling the concentration of nutrients in the leaves of tomato and apple rootstocks have been found (Fazio et al., 2013; Asins et al., 2015). These QTLs allow scientists to alter the root architecture of plants as needed. Several transgenic rootstocks have been reported to control fan leaf virus in grapes (Gambino et al., 2010), fungal diseases in citrus (Mitani et al., 2006), pathogen damage in tomato (Haroldsen et al., 2012), and nutrient absorption in tomato and watermelon (Han et al., 2009; Ghanem et al., 2011). Thus, nutrient-efficient transgenic rootstocks are expected to become commercially available for different horticultural crops in the near future. The use of genetically engineered nutrient-efficient rootstocks (transgrafting) and scions will extend the utility of grafting by combining an ancient technique with molecular strategies of the modern era (Goldschmidt, 2014), leading to improved nutrient use efficiency. However, the acceptability of genetically modified crops by the public is a question that needs to be addressed.

Remarkable achievements have been made in the field of ion transporter in *Arabidopsis*, rice, wheat, and other crops. However, a limited number of studies related to the uptake and transport of essential nutrients have been performed on grafted plants. Thus, further study is needed to thoroughly understand the sensing, signaling, uptake, and transport mechanisms in grafted plants. This information will be helpful for breeding programs to develop nutrient-efficient rootstocks. Grafting in horticultural crops can also help understand the basic biology of the grafting mechanism, the reasons for incompatibility, sensing and signaling of nutrients, ion uptake and transport, the mechanism involved in the accumulation of heavy metals in the rootstock, and the restriction of heavy metal transport to the scions. Moreover, vegetable grafting studies can be performed

quickly, and the results can be compared with those on self-rooted or self-grafted plants. Imperative conclusions can be obtained for commercial adoption.

Several approaches, such as the use of plant-growth-promoting rhizobacteria (PGPR), can be combined with grafting to further enhance nutrient uptake and utilization efficiency. These PGPR act in diverse ways, including the production or degradation of important plant growth hormones, which in turn controls root growth and affects nutrient absorption (Dodd et al., 2010; Wang et al., 2016b). The use of arbuscular mycorrhizal fungi enhances the acquisition of P, N, Mg, and Ca, maintains the K:Na ratio, affects nodulation and nitrogen fixation, and alters gene expression (*PIP*, Na/H antiporters, *Lsnced, Lslea,* and *LsP5CS*), thereby improving plant growth (Parniske, 2008; Evelin et al., 2009; Kumar et al., 2015; Miceli et al., 2016; Wang et al., 2016b). Single- and double-root grafting of cucumber increase the population of soil actinomycetes (bacteria) and reduce the population of fungi (*Fusarium oxysporum*) (Xie et al., 2012). However, for other crops, whether the rootstock and scion affect each other's soil microbiota and their effect on the nutrient absorption of rootstocks remain largely unknown and thus need further study. The use of natural (humic acid, root exudates, phytosiderophores) and synthetic chelators [ethylenediaminetetraacetic acid (EDTA), [(ethylenediamine-N, N'-bis (2-hydroxyphenylacetic acid) (EDDHA)], diethylenetriamine pentaacetic acid (DTPA)] is reported to enhance nutrient (Fe, Zn, Cu, Mn, etc.) mobilization and phyto-availability; however, the suitability and efficacy of these chelators in grafted plants need investigation (Treeby et al., 1989; Bocanegra et al., 2006). Exogenous application of plant growth regulators (e.g., auxin) and several other novel substances (e.g., melatonin) is currently being considered by scientists to alter root architecture and enhance nutrient uptake (Nawaz et al., 2016). However, further studies are required to standardize the concentration and method of application of these substances for grafted plants.

AUTHOR CONTRIBUTIONS

MN, MI, QK, and FC wrote the manuscript, YH, WA, and ZB revised, and finally approved the manuscript for submission. All authors declare no competing financial interests.

ACKNOWLEDGMENTS

We are thankful to Prof. Sergey Shabala from University of Tasmania, Australia for providing comments and helping in revision of this manuscript. This work was supported by National Natural Science Foundation of China (31201660, 31471919, and 31410303012), The International Science and Technology Cooperation Program of China (2015DFG32310), China Agriculture Research System (CARS-26-16), and The Fundamental Research Funds for the Central Universities (2013PY086).

REFERENCES

Ahmed, W., Nawaz, M. A., Iqbal, M. A., and Khan, M. M. (2007). Effect of different rootstocks on plant nutrient Status and yield in Kinnow mandarin (C*itrus reticulata* Blanco). *Pak. J. Bot.* 39, 1779–1786. Available online at: http://www.pakbs.org/pjbot/PDFs/39(5)/PJB39(5)1779.pdf

Ahmed, W., Pervez, M. A., Amjad, M., Khalid, M., Ayyub, C. M., and Nawaz, M. A. (2006). Effect of stionic combination on the growth and yield of Kinnow mandarin (C*itrus reticulata* Blanco.). *Pak. J. Bot.* 38, 603–612. Available online at: http://www.pakbs.org/pjbot/PDFs/38(3)/PJB38(3)603.pdf

Albacete, A., Martínez-Andújar, C., Ghanem, M. E., Acosta, M., Sánchez-Bravo, J., Asins, M. J., et al. (2009). Rootstock-mediated changes in xylem ionic and hormonal status are correlated with delayed leaf senescence and increased leaf area and crop productivity in salinized tomato. *Plant Cell Environ.* 32, 928–938. doi: 10.1111/j.1365-3040.2009.01973.x

Albacete, A., Martínez-Andújar, C., Pérez-Alfocea, F., Ruiz-Lozano, J. M., and Asins, M. J. (2015b). "Rootstock-mediated variation in tomato vegetative growth under low potassium or phosphorous supplies," in *Proceeding of the First International Symposium on Vegetable Grafting. Acta Horticulturae,* Vol. 1086, eds Z. Bie Y. Huang, and M. A. Nawaz (Wuhan), 147–152.

Albacete, A., Martinez-Anujar, C., Marinez-Pérez, A., Thompson, A. J., Dodd, I. C., and Pérez-Alfocea, F. (2015a). Unravelling rootstock×scion interactions to improve food Security. *J. Exp. Bot.* 66, 2211–2226. doi: 10.1093/jxb/erv027

Albrigo, L. G. (1977). Rootstocks affect 'Valencia' orange fruit quality and water balance. *Proc. Int. Soc. Citriculture* 1, 62–65.

Aloni, B., Cohen, R., Karni, L., Aktas, H., and Edelstein, M. (2010). Hormonal signaling in rootstock–scion interactions. *Sci. Hortic.* 127, 119–126. doi: 10.1016/j.scienta.2010.09.003

Amiri, M. E., Fallahi, E., and Safi-Songhorabad, M. (2014). Influence of rootstock on mineral uptake and scion growth of 'golden delicious' and 'Royal Gala' apples. *J. Plant Nutr.* 37, 16–29. doi: 10.1080/01904167.2013.792838

Arao, T., Takeda, H., and Nishihara, E. (2008). Reduction of cadmium translocation from roots to shoots in eggplant (*Solanum melongena*) by grafting onto *Solanum torvum* rootstock. *Soil Sci. Plant Nutr.* 54, 555–559. doi: 10.1111/j.1747-0765.2008.00269.x

Arwiyanto, T., Lwin, K., Maryudani, Y., and Purwantoro, A. (2015). "Evaluation of local *Solanum torvum* as a rootstock to control of *Ralstonia solanacearum* in Indonesia," in *Proceeding of the First International Symposium on Vegetable Grafting. Acta Horticulturae,* Vol. 1086, eds Z. Bie Y. Huang, and M. A. Nawaz (Wuhan), 101–106.

Asins, M. J., Raga, V., Roca, D., Belver, A., and Carbonell, E. A. (2015). Genetic dissection of tomato rootstock effects on scion traits under moderate salinity. *Theor. Appl. Genet.* 128, 667–679. doi: 10.1007/s00122-015-2462-8

Bautista, A. S., Calatayud, A., Nebauer, S. G., Pascual, B., Maroto, J. V., and Lopez-Galarza, S. (2011). Effects of simple and double grafting melon plants on mineral absorption, photosynthesis, biomass and yield. *Sci. Hortic.* 130, 575–580. doi: 10.1016/j.scienta.2011.08.009

Bavaresco, L., Giachino, E., and Pezzutto, S. (2003). Grapevine rootstock effects on lime-induced chlorosis, nutrient uptake, and source–sink relationships. *J. Plant Nutr.* 26, 1451–1465. doi: 10.1081/PLN-120021054

Bhatt, R. M., Upreti, K. K., Divya, M. H., Bhat, S., Pavithra, C. B., and Sadashiva, A. T. (2015). Interspecific grafting to enhance physiological resilience to flooding stress in tomato (*Solanum lycopersicum* L.). *Sci. Hortic.* 182, 8–17. doi: 10.1016/j.scienta.2014.10.043

Bocanegra, M. P., Lobartini, J. C., and Orioli, G. A. (2006). Plant uptake of iron chelated by humic acids of different molecular weights. *Commun. Soil Sci. Plant Anal.* 37, 239–248. doi: 10.1080/00103620500408779

Borgognone, D., Colla, G., Rouphael, Y., Cardarelli, M., Reac, E., and Schwarzd, D. (2013). Effect of nitrogen form and nutrient solution pH on growth and mineral composition of self-grafted and grafted tomatoes. *Sci. Hortic.* 149, 61–69. doi: 10.1016/j.scienta.2012.02.012

Brumós, J., Colmenero-Flores, J. M., Conesa, A., Izquierdo, P., Sánchez, G., Iglesias, D. J., et al. (2009). Membrane transporters and carbon metabolism implicated in chloride homeostasis differentiate salt stress responses in tolerant and sensitive Citrus rootstocks. *Funct. Integr. Genomics* 9, 293–309. doi: 10.1007/s10142-008-0107-6

Brumós, J., Talón, M., Bouhlal, R., and Colmenero-Flores, J. M. (2010). Cl- homeostasis in includer and excluder citrus rootstocks: san transport mechanisms and identification of candidate genes. *Plant Cell Environ.* 33, 2012–2027. doi: 10.1111/j.1365-3040.2010.02202.x

Caballero, F., García-Sánchez, F., Gimeno, V., Syvertsen, J. P., Martínez, V., and Rubio, F. (2013). High-affinity potassium uptake in seedlings of two citrus rootstocks Carrizo citrange (*Citrus sinensis* [L.] Osb. × *Poncirus trifoliata* [L.] *Raf.) and Cleopatra mandarin (Citrus reshni Hort. ex Tanaka). Aust. J. Crop Sci.* 7, 538–542. Available online at: http://www.crec.ifas.ufl.edu/academics/faculty/syvertsen/PDF/2013_Caballero_et_al.pdf

Cabrera, R. I. (2002). Rose yield, dry matter partitioning and nutrient status responses to rootstock selection. *Sci. Hortic.* 95, 75–83. doi: 10.1016/S0304-4238(02)00020-1

Cantero-Navarro, E., Romero-Aranda, R., Fernández-Muñoz, R., Martínez-Andújar, C., Pérez Alfocea, F., and Albacete, A. (2016). Improving agronomic water use efficiency in tomato byrootstock-mediated hormonal regulation of leaf biomass. *Plant Sci.* 251, 90–100. doi: 10.1016/j.plantsci.2016.03.001

Castle, W. S. (2010). A career perspective on citrus rootstocks, their development, and commercialization. *HortScience* 45, 11–15. Available online at: http://hortsci.ashspublications.org/content/45/1/11.full.pdf+html

Cerezo, M., Camañes, G., Flors, V., Primo-Millo, E., and García-Agustín, P. (2007). Regulation of nitrate transport in citrus rootstocks depending of nitrogen availability. *Plant Signal. Behav.* 2, 337–342. doi: 10.4161/psb.2.5.4578

Chiou, T. J., Aung, K., Lin, S. I., Wu, C. C., Chiang, S. F., and Su, C. L. (2006). Regulation of phosphate homeostasis by microRNA in Arabidopsis. *Plant Cell* 18, 412–21. doi: 10.1105/tpc.105.038943

Colla, G., Rouphael, Y., Jawad, R., Kumar, P., Rea, E., and Cardarelli, M. (2013). The effectiveness of grafting to improve NaCl and $CaCl_2$ tolerance in cucumber. *Sci. Hortic.* 164, 380–391. doi: 10.1016/j.scienta.2013.09.023

Colla, G., Rouphael, Y., Rea, E., and Cardarelli, M. (2012). Grafting cucumber plants enhance tolerance to sodium chloride and sulfate salinization. *Sci. Hortic.* 135, 177–185. doi: 10.1016/j.scienta.2011.11.023

Cong, C., Chao, L., Cui-ying, L., Xiao-yu, K., Yang-jun, Z., and Feng-wang, M. (2014). Differences in the efficiency of potassium (K) uptake and use in five apple rootstock genotypes. *J. Integr. Agric.* 13, 1934–1942. doi: 10.1016/S2095-3119(14)60839-X

Conte, S. S., and Walker, E. L. (2011). Transporters contributing to iron trafficking in plants. *Mol. Plant.* 4, 464–476. doi: 10.1093/mp/ssr015

Cookson, S. J., Moreno, M. J. C., Hevin, C., Mendome, L. Z. N., Delrot, S., Magnin, N., et al. (2014). Heterografting with nonself rootstocks induces genes involved in stress responses at the graft interface when compared with autografted controls. *J. Exp. Bot.* 65, 2473–2481. doi: 10.1093/jxb/eru145

Covarrubias, J. I., Retamales, C., Donnini, S., Rombolà, A. D., and Pastenes, C. (2016). Contrasting physiological responses to iron deficiency in Cabernet Sauvignon grapevines grafted on two rootstocks. *Sci. Hortic.* 199, 1–8. doi: 10.1016/j.scienta.2015.12.013

Dam, N. M. V., and Bouwmeester, H. J. (2016). Metabolomics in the rhizosphere: tapping into belowground chemical communication. *Trends Plant Sci.* 21, 256–265. doi: 10.1016/j.tplants.2016.01.008

Davis, A. R., Perkins-Veazie, P., Sakata, Y., López-Galarza, S., Maroto, J. V., Lee, S. G., et al. (2008). Cucurbit grafting. *Crit. Rev. Plant Sci.* 27, 50–74. doi: 10.1080/07352680802053940

Dodd,. I. C., Zinovkina, N. Y., Safronova, V. I., and Belimov, A. A. (2010). Rhizobacterial mediation of plant hormone status. *Ann. Appl. Biol.* 157, 361–379. doi: 10.1111/j.1744-7348.2010.00439.x

Dor, E., Alperin, B., Wininger, S., Ben-Dor, B., Somvanshi, V. S., Koltai, H., et al. (2010). Characterization of a novel tomato mutant resistant to the weedy parasites *Orobanche* and *Phelipanche* spp. *Euphytica* 171, 371–380. doi: 10.1007/s10681-009-0041-2

Edelstein, M., Ben-Hur, M., Cohen, R., Burger, Y., and Ravina, I. (2005). Boron and salinity effects on grafted and non-grafted melon plants. *Plant Soil* 269, 273–284. doi: 10.1007/s11104-004-0598-4

Edelstein, M., Cohen, R., Baumkoler, F., and Ben-Hur, M. (2016). Using grafted vegetables to increase tolerance to salt and toxic elements. *Israel J. Plant Sci.* 2016, 1–18. doi: 10.1080/07929978.2016.1151285

Edelstein, M., Plaut, Z., and Ben-Hur, M. (2011). Sodium and chloride exclusion and retention by non-grafted and grafted melon and Cucurbita plants. *J. Exp. Bot.* 62, 177–184. doi: 10.1093/jxb/erq255

Esmaeili, M., Salehi, R., Taheri, M. R., Babalar, M., and Mohammadi, H. (2015). "Effect of different nitrogen rates on fruit yield and quality of grafted and non-grafted muskmelon," in *Proceeding of the First International Symposium on Vegetable Grafting. Acta Horticulturae,* Vol. 1086, eds Z. Bie Y. Huang, and M. A. Nawaz (Wuhan), 255–260.

Estañ, M. T., Martinez-Rodriguez, M. M., Pérez-Alfocea, F., Flowers, T. J., and Bolarin, M. C. (2005). Grafting raises the salt tolerance of tomato through limiting the concentration of sodium and chloride to the shoot. *J. Exp. Bot.* 56, 703–712. doi: 10.1093/jxb/eri027

Evelin, H., Kapoor, R., and Giri, B. (2009). Arbuscularmycorrhizal fungi in alleviation of salt stress: a review. *Ann. Bot.* 104, 1263–1280. doi: 10.1093/aob/mcp251

Farhadi, A., and Malek, S. (2015). "Evaluation of graft compatibility and organoleptic traits of greenhouse cucumber seedlings grafted on different rootstocks," in *Proceeding of the First International Symposium on Vegetable Grafting. Acta Horticulturae,* Vol. 1086, eds Z. Bie Y. Huang, and M. A. Nawaz (Wuhan), 219–224. Available online at: https://www.cabdirect.org/cabdirect/abstract/20143073666

Fazio, G., Kviklys, D., Grusak, M. A., and Robinson, T. L. (2013). Phenotypic diversity and QTL mapping of absorption and translocation of nutrients by apple rootstocks. *Aspects Appl. Biol.* 119, 37–50.

Fernández-García, N., Martínez, V., Cerdá, A., and Carvajal, M. (2002). Water and nutrient uptake of grafted tomato plants grown under saline Conditions. *J. Plant Physiol.* 159, 899–905. doi: 10.1078/0176-1617-00652

Finazzi, G., Petroutsos, D., Tomizioli, M., Flori, S., Sautron, E., Villanova, V., et al. (2015). Ions channels/transporters and chloroplast regulation. *Cell Calcium* 58, 86–97. doi: 10.1016/j.ceca.2014.10.002

Fuentes, I., Stegemann, S., Golczyk, H., Karcher, D., and Bock, R. (2014). Horizontal genome transfer as an asexual path to the formation of new species. *Nature* 511, 232–235. doi: 10.1038/nature13291

Fujii, H., Chiou, T. J., Lin, S. I., Aung, K., and Zhu, J. K. (2005). A miRNA involved in phosphate starvation responses in *Arabidopsis*. *Curr. Biol.* 15, 2038–2043. doi: 10.1016/j.cub.2005.10.016

Gambino, G., Perrone, I., Carra, A., Chitarra, W., Boccacci, P., Marinoni, D. T., et al. (2010). Transgene silencing in grapevines transformed with GFLV resistance genes: analysis of variable expression of transgene, siRNAs production and cytosine methylation. *Transgenic Res.* 19, 17–27. doi: 10.1007/s11248-009-9289-5

Gammon, N. Jr., and McFadden, S. E. Jr. (1979). Effect of rootstocks on greenhouse rose flower yield and leaf nutrient levels. *Comm. Soil Sci. Plant Anal.* 10, 1171–1184. doi: 10.1080/00103627909366970

Gao, Y., Tian, Y., Liang, X., and Gao, L. (2015). Effects of single-root-grafting, double-root grafting and compost application on microbial properties of rhizosphere soils in Chinese protected cucumber (*Cucumis sativus* L.) production systems. *Sci. Hortic.* 186, 190–200. doi: 10.1016/j.scienta.2015.02.026

Gerendás,. J., Abbadi, J., and Sattelmacher, B. (2008). Potassium efficiency of safflower (*Carthamus tinctorius* L.) and sunflower (*Helianthus annuus* L.). *J. Plant Nutr. Soil Sci.* 171, 431–439. doi: 10.1002/jpln.200720218

Ghanem, M. E., Albacete, A., Smigocki, A. C., Frebort, I., Pospisilova, H., Martinez-Andujar, C., et al. (2011). Root-synthesised cytokinins improve shoot growth and fruit yield in salinised tomato (*Solanum lycopersicum* L.). *J. Exp. Bot.* 62, 125–140. doi: 10.1093/jxb/erq266

Goldschmidt, E. E. (2014). Plant grafting: new mechanisms, evolutionary implications. *Front. Plant Sci.* 5:727. doi: 10.3389/fpls.2014.00727

Gonzalo, M. J., Moreno, M. A., and Gogorcena, Y. (2011). Physiological responses and differential gene expression in Prunus rootstocks under iron deficiency conditions. *J. Plant Physiol.* 168, 887–893. doi: 10.1016/j.jplph.2010.11.017

Gregory, P. J., Atkinson, C. J., Bengough, A. G., Else, M. A., Fernandez-Fernandez,. F., Harrison, R. J., et al. (2013). Contributions of roots and rootstocks to sustainable, intensified crop production. *J. Exp. Bot.* 64, 1209–1222. doi: 10.1093/jxb/ers385

Gu, M., Chen, A., Sun, S., and Xu, G. (2016). Complex regulation of plant phosphate transporters and the gap between molecular mechanisms and practical application: what is missing? *Mol. Plant.* 9, 396–416. doi: 10.1016/j.molp.2015.12.012

Habran, A., Commisso, M., Helwi, P., Hilbert, G., Negri, S., Ollat, N., et al. (2016). Roostocks/scion/nitrogen Interactions affect secondary metabolism in the grape berry. *Front. Plant Sci.* 7:1134. doi: 10.3389/fpls.2016.01134

Han, J. S., Park, S., Shigaki, T., Hirschi, K. D., and Kim, C. K. (2009). Improved watermelon quality using bottle gourd rootstock expressing a Ca2+/H+ antiporter. *Mol. Breeding* 24, 201–211. doi: 10.1007/s11032-009-9284-9

Haroldsen, V. M., Chi-Ham, C. L., and Bennett, A. B. (2012). Transgene mobilization and regulatory uncertainty for non-GE fruit products of transgenic rootstocks. *J. Biotechnol.* 161, 349–353. doi: 10.1016/j.jbiotec.2012.06.017

Harp, D. A., Kay, K., Zlesak, C. D., and George, S. (2015). The effect of rose root size on drought stress tolerance and landscape plant performance. *Texas J. Agric. Nat. Resour.* 28, 82–88. Available online at: http://txjanr.agintexas.org/index.php/txjanr/article/view/13/8

Ho, C. H., Lin, S. H., Hu, H. C., and Tsay, Y. F. (2009). CHL1 functions as a nitrate sensor in plants. *Cell* 138, 1184–1194. doi: 10.1016/j.cell.2009.07.004

Hrotko, K., Magyar, L., Borsos, G., and Gyeviki, M. (2014). Rootstock effect on nutrient concentration of sweet cherry leaves. *J. Plant Nutr.* 37, 395–1409. doi: 10.1080/01904167.2014.911317

Huang, Y., Bie, Z. L., Liu, Z. X., Zhen, A., and Jiao, X. R. (2011). Improving cucumber photosynthetic capacity under NaCl stress by grafting onto two salt-tolerant pumpkin rootstocks. *Biol. Plant.* 55, 285–290. doi: 10.1007/s10535-011-0040-8

Huang, Y., Bie, Z., Liu, P., Niu, M., Zhen, A., Liu, Z., et al. (2013a). Reciprocal grafting between cucumber and pumpkin demonstrates the roles of the rootstock in the determination of cucumber salt tolerance and sodium accumulation. *Sci. Hortic.* 149, 47–54. doi: 10.1016/j.scienta.2012.04.018

Huang, Y., Jiao, Y., Nawaz, M. A., Chen, C., Liu, L., Lu, Z., et al. (2016b). Improving magnesium uptake, photosynthesis and antioxidant enzyme activities of watermelon by grafting onto pumpkin rootstock under low magnesium. *Plant Soil* 1–18. doi: 10.1007/s11104-016-2965-3. Available online at: http://link.springer.com/article/10.1007/s11104-016-2965-3/fulltext.html

Huang, Y., Li, J., Hua, B., Liu, Z., Fan, M., and Bie, Z. (2013b). Grafting onto different rootstocks as a means to improve watermelon tolerance to low potassium stress. *Sci. Hortic.* 149, 80–85. doi: 10.1016/j.scienta.2012.02.009

Huang, Y., Tang, R., Cao, Q., and Bie, Z. (2009). Improving the fruit yield and quality of cucumber by grafting onto the salt tolerant rootstock under NaCl stress. *Sci. Hortic.* 122, 26–31. doi: 10.1016/j.scienta.2009.04.004

Huang, Y., Zhao, L. Q., Kong, Q. S., Cheng, F., Niu, M. L., Xie, J. J., et al. (2016a). Comprehensive mineral nutrition analysis of watermelon grafted onto two different rootstocks. *Hortic. Plant J.* 2, 105–113. doi: 10.1016/j.hpj.2016.06.003

Ibacache, G. A., and Sierra, B. C. (2009). Influence of rootstocks on nitrogen, phosphorus and potassium content in petioles of four table grape varieties. *Chilean J. Agric. Res.* 69, 503–508. doi: 10.4067/S0718-58392009000400004

Jaitz, L., Mueller, B., Koellensperger, G., Huber, D., Oburger, E., Puschenreiter, M., et al. (2011). LC-MS analysis of low molecular weight organic acids derived from root exudation. *Anal. Bioanal. Chem.* 400, 2587–2596. doi: 10.1007/s00216-010-4090-0

Jiménez, S., Ollat, N., Deborde, C., Maucourt, M., Rellan-Alvarez, R., Moreno, M. A., et al. (2011). Metabolic response in roots of *Prunus* rootstocks submitted to iron chlorosis. *J. Plant Physiol.* 168, 415–423. doi: 10.1016/j.jplph.2010.08.010

Khorassani, R., Hettwer, U., Ratzinger, A., Steingrobe, B., Karlovsky, P., and Claassen, N. (2011). Citramalic acid and salicylic acid in sugar beet root exudates solubilize soil phosphorus. *BMC Plant Biol.* 11, 121. doi: 10.1186/1471-2229-11-121

Kubota, C., and McClure, M. A. (2008). Vegetable grafting: history, use, and current technology status in North America. *HortScience* 43, 1664–1669. Available online at: http://hortsci.ashspublications.org/content/43/6/1664.full.pdf+html

Kulcheski, F. R., Côrrea, R., Gomes, I. G., Lima, J. C., and Margis, R. (2015). NPK macronutrients and microRNA homeostasis. *Front. Plant Sci.* 6:451. doi: 10.3389/fpls.2015.00451

Kumar, P., Lucini, L., Rouphael, Y., Cardarelli, M., Kalunke, R. M., and Colla,. G. (2015). Insight into the role of grafting and arbuscular mycorrhiza on cadmium stress tolerance in tomato. *Front. Plant Sci.* 6:477. doi: 10.3389/fpls.2015.00477

Lecourt, J., Lauvergeat, V., Ollat, N., Vivin, P., and Cookson, S. J. (2015). Shoot and root ionome responses to nitrate supply in grafted grapevines are rootstock genotype dependent. *Aust. J. Grape Wine Res.* 21, 311–318. doi: 10.1111/ajgw.12136

Lee, J. M. (1994). Cultivation of grafted vegetables I. Current status, grafting methods, and benefits. *HortScience* 29, 235–239.

Lee, J. M., and Oda, M. (2003). "Grafting of herbaceous vegetable and ornamental crops," in: *Horticultural Reviews,* Vol. 28, ed J. Janick (New York, NY: John Wiley and Sons), 61–124.

Lee, J. M., Kubota, C., Tsao, S. J., Bie, Z., Echevarria, P. H., Morra, L., et al. (2010). Current status of vegetable grafting: diffusion, grafting techniques, automation. *Sci. Hortic.* 127, 93–105. doi: 10.1016/j.scienta.2010.08.003

Lei, B., Huang, Y., Xie, J. J., Liu, Z. X., Zhen, A., Fan, M. L., et al. (2014). Increased cucumber salt tolerance by grafting on pumpkin rootstockand after application of calcium. *Biol. Plant.* 58, 179–184. doi: 10.1007/s10535-013-0349-6

Leonardi, C., and Giuffrida, F. (2006). Variation of plant growth and macronutrient uptake in grafted tomatoes and eggplants on three different rootstocks. *Eur. J. Hortic. Sci.* 71, 97–101. Available online at: https://www.researchgate.net/publication/235799269_Variation_of_plant_growth_and_macronutrient_uptake_in_grafted_tomatoes_and_eggplants_on_three_different_rootstocks

Li, C., Wei, Z., Liang, D., Zhou, S., Li, Y., Liu, C., et al. (2013). Enhanced salt resistance in apple plants overexpressing a Malus vacuolar Na/H antiporter gene is associated with differences in stomatal behavior and photosynthesis. *Plant Physiol. Biochem.* 70, 164–173. doi: 10.1016/j.plaphy.2013.05.005

Li, C., Yu, X., Bai, L., He, C., and Yansu, L. (2016c). Responses of miRNAs and their target genes to nitrogen- or phosphorus-deficiency in grafted cucumber seedlings. *Hortic. Environ. Biotechnol.* 57, 97–112. doi: 10.1007/s13580-016-0092-y

Li, G., Ma, J., Tan, M., Mao, J., An, N., Sha, G., et al. (2016a). Transcriptome analysis reveals the effects of sugar metabolism and auxin and cytokinin signaling pathways on root growth and development of grafted apple. *BMC Genomics* 17:150. doi: 10.1186/s12864-016-2484-x

Li, H., Han, J. L., Chang, Y. H., Lin, J., and Yang, Q. S. (2016d). Gene characterization and transcription analysis of two new ammonium transporters in pear rootstock (*Pyrus betulaefolia*). *J. Plant Res.* 129, 737–748. doi: 10.1007/s10265-016-0799-y

Li, H., Wang, Y., Wang, Z., Guo, X., Wang, F., Xia, X. J., et al. (2016b). Microarray and genetic analysis reveals that csa-miR159b plays a critical role in abscisic acid-mediated heat tolerance in grafted cucumber plants. *Plant Cell Environ.* 39, 1790–1804. doi: 10.1111/pce.12745

Liu, G. D., Jiang, C. C., and Wang, Y. H. (2011). Distribution of boron and its forms in young "Newhall" navel orange (*Citrus sinensis* Osb.) plants grafted on two rootstocks in response to deficient and excessive boron. *Soil Sci. Plant Nutr.* 57, 93–104. doi: 10.1080/00380768.2010.551299

Liu, G. D., Wang, R. D., Liu, L. C., Wu, L. S., and Jiang, C. C. (2013). Cellular boron allocation and pectin composition in two citrus rootstock seedlings differing in boron-deficiency response. *Plant Soil* 370, 555–565. doi: 10.1007/s11104-013-1659-3

Liu, J., and Vance, C. P. (2010). Crucial roles of sucrose and microRNA399 in systemic signaling of P deficiency. A tale of two team players? *Plant Signal. Behav.* 5, 1–5. doi: 10.4161/psb.5.12.13293

López-Marín, J., González, A., Pérez-Alfocea, F., Egea-Gilabert, C., and Fernández, J. A. (2013). Grafting is an efficient alternative to shading screens to alleviate thermal stress in greenhouse grown sweet pepper. *Sci. Hortic.* 149, 39–46. doi: 10.1016/j.scienta.2012.02.034

Louws, F. J., Rivard, C. L., and Kubota, C. (2010). Grafting fruiting vegetables to manage soil borne pathogens, foliar pathogens, arthropods and weeds. *Sci. Hortic.* 127, 127–146. doi: 10.1016/j.scienta.2010.09.023

Mei, L., Sheng, O., Peng, S., Zhou, G., Wei, Q., and Li, Q. (2011). Growth, root morphology and boron uptake by citrus rootstock seedlings

differing in boron-deficiency responses. *Sci. Hortic.* 129, 426–432. doi: 10.1016/j.scienta.2011.04.012

Meister, R., Rajani, M. S., Ruzicka, D., and Schachtman, D. P. (2014). Challenges of modifying root traits in crops for agriculture. *Trends Plant Sci.* 19, 779–788. doi: 10.1016/j.tplants.2014.08.005

Melnyk, C. W., and Meyerowitz, E. M. (2015). Plant grafting. *Curr. Biol.* 25, R183–R188. doi: 10.1016/j.cub.2015.01.029

Melnyk, C. W., Schuster, C., Leyser, O., and Meyerowitz, E. M. (2015). A developmental framework for graft formation and vascular reconnection in *Arabidopsis thaliana*. *Current Biol.* 25, 1306–1318. doi: 10.1016/j.cub.2015.03.032

Mestre, L., Reig, G., Betrán, J. A., Pinochet, J., and Moreno, M. A. (2015). Influence of peach-almond hybrids and plum-based rootstocks on mineral nutrition and yield characteristics of 'Big Top' nectarine in replant and heavy-calcareous soil conditions. *Sci. Hortic.* 192, 475–481. doi: 10.1016/j.scienta.2015.05.020

Miceli, A. C., Moncada, R. A., Piazza, G., Torta, L., D'Anna, F., and Vetrano, F. (2016). Yield and quality of mini-watermelon as affected by grafting and mycorrhizal inoculum. *J. Agric. Sci. Technol.* 18, 505–516. Available online at: http://jast.modares.ac.ir/article_14314_8201b9c9312c76336d62b1329c4c91f1.pdf

Miles, C., Wimer, J., and Inglis, D. (2015). "Grafting eggplant and tomato for Verticillium wilt resistance," in *Proceeding of the First International Symposium on Vegetable Grafting. Acta Horticulturae,* Vol. 1086, eds Z. Bie Y. Huang, and M. A. Nawaz (Wuhan), 113–118.

Mitani, N., Kobayashi, S., Nishizawa, Y., Kuniga, T., and Matsumoto, R. (2006). Transformation of trifoliate orange with rice chitinase gene and the use of the transformed plant as a rootstock. *Sci. Hortic.* 108, 439–441. doi: 10.1016/j.scienta.2006.02.006

Mota, M., Neto, C., and Oliveira, C. M. (2008). Identification of gene coding for Nh_4^+ transporters in 'Rocha' Pear/BA29. *Acta Hort.* (ISHS) 800, 365–372. doi: 10.17660/ActaHortic.2008.800.46

Mudge, K., Janick, J., Scofield, S., and Goldschmidt, E. E. (2009). "A history of grafting," in *Horticultural Reviews,* Vol. 35, ed J. Janick (New Jersey: John Wiley and Sons Inc), 437–493.

Nawaz, M. A., Huang, Y., Bie, Z., Ahmed, W., Reiter, R. J., Niu, M., et al. (2016). Melatonin: current status and future perspectives in plant science. *Front. Plant Sci.* 6:1230. doi: 10.3389/fpls.2015.01230

Niu, G., and Rodriguez, D. S. (2008). Responses of growth and ion uptake of four rose rootstocks to chloride- or sulfate-dominated salinity. *J. Am. Soc. Hortic. Sci.* 133, 663–669. Available online at: http://journal.ashspublications.org/content/133/5/663.full.pdf

Pant, B. D., Buhtz, A., Kehr, J., and Scheible, W. R. (2008). MicroRNA399 is a long-distance signal for the regulation of plant phosphate homeostasis. *Plant J.* 53, 731–738. doi: 10.1111/j.1365-313X.2007.03363.x

Parniske, M. (2008). Arbuscular mycorrhiza: the mother of plant root endosymbioses. *Nat. Rev. Microbiol.* 6, 763–775. doi: 10.1038/nrmicro1987

Paul, S., Datta, S. K., and Datta, K. (2015). miRNA regulation of nutrient homeostasis in plants. *Front. Plant Sci.* 6:232. doi: 10.3389/fpls.2015.00232

Penella, C., Landi, M., Guidi, L., Nebauer, S. G., Pellegrini, E., Bautista, A. S., et al. (2016). Salt-tolerant rootstock increases yield of pepper under salinity through maintenance of photosynthetic performance and sinks strength. *J. Plant Physiol.* 193, 1–11. doi: 10.1016/j.jplph.2016.02.007

Penella, C., Nebauer, S. G., Quinones, A., Bautista, A. S., López-Galarza, S., and Calatayud, A. (2015). Some rootstocks improve pepper tolerance to mild salinity through ionic regulation. *Plant Sci.* 230, 12–22. doi: 10.1016/j.plantsci.2014.10.007

Pérez-Alfocea, F. (2015). "Why should we investigate vegetable grafting?," in *Proceeding of the First International Symposium on Vegetable Grafting. Acta Horticulturae,* Vol. 1086, eds Z. Bie Y. Huang, and M. A. Nawaz (Wuhan), 21–30.

Pérez-Alfocea, F., Albacete, A., Ghanem, M. E., and Dodd, I. C. (2010). Hormonal regulation of source-sink relations to maintain crop productivity under salinity: a case study of root-to-shoot signalling in tomato. *Funct. Plant Biol.* 37, 592–603. doi: 10.1071/FP10012

Pinto, E., and Ferreira, I. M. P. L. V. O. (2015). Cation transporters/channels in plants: tools for nutrient biofortification. *J. Plant Physiol.* 179, 64–82. doi: 10.1016/j.jplph.2015.02.010

Pulgar, G., Villora, G., Moreno, D. A., and Romero, L. (2000). Improving the mineral nutrition in grafted watermelon plants: nitrogen metabolism. *Biol. Plant.* 43, 607–609. doi: 10.1023/A:1002856117053

Qi, H. Y., Li, T. L., Liu, Y. F., and Li, D. (2006). Effects of grafting on photosynthesis characteristics, yield, and sugar content in melon. *J. Shenyang Agric. Univ.* 37, 155–158. Available online at: http://en.cnki.com.cn/Article_en/CJFDTOTAL-SYNY200602006.htm

Relf, D. (2015). *The Art of Bonsai.* Blacksburg, VA: Communications and marketing, College of Agriculture and Life Sciences, Virginia Polytechnic Institute and State University. Publication No. 426 601, 1–6.

Rengel, Z., and Damon, P. M. (2008). Crops and genotypes differ in efficiency of potassium uptake and use. *Physiol. Plant.* 133, 624–636. doi: 10.1111/j.1399-3054.2008.01079.x

Rivero, R. M., Ruiz, J. M., and Romero, L. (2004). Iron metabolism in tomato and watermelon plants: influence of grafting. *J. Plant Nutr.* 27, 2221–2234. doi: 10.1081/PLN-200034708

Rogers, E. D., and Benfey, P. N. (2015). Regulation of plant root system architecture: implications for crop advancement. *Curr. Opin. Biotechnol.* 32, 93–98. doi: 10.1016/j.copbio.2014.11.015

Rouphael, Y., Cardarelli, M., Rea, E., and Colla, G. (2008). Grafting of cucumber as a means to minimize copper toxicity. *Environ. Exp. Bot.* 63, 49–58. doi: 10.1016/j.envexpbot.2007.10.015

Rouphael, Y., Schwarz, D., Krumbein, A., and Colla, G. (2010). Impact of grafting on product quality of fruit vegetables. *Sci. Hortic.* 127, 172–179. doi: 10.1016/j.scienta.2010.09.001

Rubio, V., Linhares, F., Solano, R., Martin, A. C., Iglesias, J., Leyva, A., et al. (2001). A conserved MYB transcription factor involved in phosphate starvation signaling both in vascular plants and in unicellular algae. *Genes Dev.* 15, 2122–2133. doi: 10.1101/gad.204401

Ruiz, J. M., Belakbir, A., Lhpez-Cantarero, I., and Romero, L. (1997). Leaf-macronutrient content and yield in grafted melon plants. A model to evaluate the influence of rootstock genotype. *Sci. Hortic.* 71, 227–234. doi: 10.1016/S0304-4238(97)00106-4

Ruiz, J. M., Rivero, R. M., Cervilla, L. M., Castellano, R., and Romero, L. (2006). Grafting to improve nitrogen-use efficiency traits in tobacco plants. *J. Sci. Food Agric.* 86, 1014–1021. doi: 10.1002/jsfa.2450

Salehi, R., Kashi, A., Lee, J. M., and Javanpour, R. (2014). Mineral concentration, sugar content and yield of Iranian 'Khatooni' melon affected by grafting, pruning and thinning. *J. Plant Nutr.* 37, 1255–1268. doi: 10.1080/01904167.2014.888740

Santa-Cruz, A., Martinez-Rodriguez, M. M., Perez-Alfocea, F., Romero-Aranda, R., and Bolarin, M. C. (2002). The rootstock effect on the tomato salinity response depends on the shoot genotype. *Plant Sci.* 162, 825–831. doi: 10.1016/S0168-9452(02)00030-4

Santa-Maria, G. E., Moriconi, J. I., and Oliferuk, S. (2015). Internal efficiency of nutrient utilization: what is it and how to measure it during vegetative plant growth? *J. Exp. Bot.* 66, 3011–3018. doi: 10.1093/jxb/erv162

Savvas, D., Colla, G., Rouphael, Y., and Schwarz, D. (2010). Amelioration of heavy metal and nutrient stress in fruit vegetables by grafting. *Sci. Hortic.* 127, 156–161. doi: 10.1016/j.scienta.2010.09.011

Savvas, D., Ntatsi, G., and Barouchas, P. (2013). Impact of grafting and rootstock genotype on cation uptake by cucumber (*Cucumis sativus* L.) exposed to Cd or Ni stress. *Sci. Hortic.* 149, 86–96. doi: 10.1016/j.scienta.2012.06.030

Savvas, D., Papastavrou, D., Ntatsi, G., Ropokis, A., and Olympios, C., Hartmann, H., et al. (2009). Interactive effects of grafting and manganese supply on growth, yield, and nutrient uptake by tomato. *HortScience* 44, 1978–1982. Available online at: http://hortsci.ashspublications.org/content/44/7/1978.full.pdf

Schwarz, D., Öztekin, G. B., Tüzel, Y., Brückner, B., and Krumbein, A. (2013). Rootstocks can enhance tomato growth and quality characteristics at low potassium supply. *Sci. Hortic.* 149, 70–79. doi: 10.1016/j.scienta.2012.06.013

Schwarz, D., Rouphael, Y., Colla, G., and Venema, J. H. (2010). Grafting as a tool to improve tolerance of vegetables to abiotic stresses: thermal stress, water stress and organic pollutants. *Sci. Hortic.* 127, 162–171. doi: 10.1016/j.scienta.2010.09.016

Sherafati, A., Hokmabadi, H., and Taheri, M. (2011). Effects of some rootstocks on mineral nutrient uptake in two pistachio cultivars (*Pistacia vera* L.). *Acta Hortic.* 912, 97–201. doi: 10.17660/actahortic.2011.912.28

Slowik, K., Labanauskas, C. K., Stolzy, L. H., and Zentmyer, G. A. (1979). Influence of rootstocks, soil oxygen, and soil moisture on the uptake and translocation of nutrients in young avocado.*J. Am. Soc. Hortic. Sci.* 104, 172–175.

Sorgona, A., Abenavoli, M. A., Gringeri, P. G., and Cacco, G. (2006). A comparison of nitrogen use efficiency definitions in citrus rootstocks. *Sci. Hortic.* 109, 389–393. doi: 10.1016/j.scienta.2006.06.001

Suchoff, D., Gunter, C., Schulthesis, J., and Louws, F. J. (2015). "On farm grafted tomato trial to manage bacterial wilt," in *Proceeding of the First International Symposium on Vegetable Grafting. Acta Horticulturae,* Vol. 1086, eds Z. Bie Y. Huang, and M. A. Nawaz (Wuhan),119–127.

Sun, Y., Huang, W., Tian, X. H., Wu, Y., Zhou, C. T., and Ding, Q. (2002). Study on growth situation, photosynthetic characteristics and nutrient absorption of grafted cucumber seedlings. *J. Plant Nutr. Fert. Sci.* 8, 81–185, 209. Available online at: http://www.plantnutrifert.org/EN/abstract/abstract2236.shtml

Sunkar, R., Chinnusamy, V., and Zhu, J. K. (2007). Small RNAs as big players in plant abiotic stress responses and nutrient deprivation. *Trends Plant Sci.* 12, 301–309. doi: 10.1016/j.tplants.2007.05.001

Tabata, R., Sumida, K., Yoshii, T., Ohyama, K., Shinohara, H., and Matsubayashi, Y. (2014). Perception of root-derived peptides by shoot LRR-RKs mediates systemic N-demand signaling. *Science* 346, 343–346. doi: 10.1126/science.1257800

Todd, C. D., Zeng, P., Huete, A. M. R., Hoyos, M. E., and Polacco, J. C. (2004). Transcripts of MYB-like genes respond to phosphorous and nitrogen deprivation in Arabidopsis. *Planta* 219, 1003–1009. doi: 10.1007/s00425-004-1305-7

Tomasi, N., Monte, R., Varanini, Z., Cesco, S., and Pinton, R. (2015). Induction of nitrate uptake in Sauvignon Blanc and Chardonnay grapevines depends on the scion and is affected by the rootstock. *Aust. J. Grape Wine Res.* 21, 331–338. doi: 10.1111/ajgw.12137

Treeby, M., Marschner, H., and Romheld, V. (1989). Mobilization of iron and other micronutrients cations from a calcerous soil by plant-borne, microbial, and synthetic metal chelators. *Plant Soil* 114, 217–226. doi: 10.1007/BF02220801

Tsaballa, A., Athanasiadis, C., Pasentsis, K., Ganopoulos, I., Nianiou-Obeidat, I., and Tsaftaris, A. (2013). Molecular studies of inheritable grafting induced changes in pepper (*Capsicum annuum*) fruit shape. *Sci. Hortic.* 149, 2–8. doi: 10.1016/j.scienta.2012.06.018

Uygur, V., and Yetisir, H. (2009). Effects of rootstocks on some growth parameters, phosphorous and nitrogen uptake by watermelon under salt stress. *J. Plant Nutr.* 32, 629–643. doi: 10.1080/01904160802715448

Valdés-Lopez, O., Yang, S. S., Aparicio-Fabre, R., Graham, P., Reyes, J. L., Vance, C. P., et al. (2010). MicroRNA expression profile in common bean (*Phaseolus vulgaris*) under nutrient deficiency stresses and manganese toxicity. *New Phytol.* 187, 805–818. doi: 10.1111/j.1469-8137.2010.03320.x

Van-Hooijdonk, B. M., Woolley, D. J., Warrington, I. J., and Tustin, D. S. (2010). Initial alteration of scion architecture by dwarfing apple rootstocks may involve shoot–root–shoot signalling by auxin, gibberellin, and cytokinin. *J. Hortic. Sci. Biotechnol.* 85, 59–65. doi: 10.1080/14620316.2010.11512631

Venema, J. H., Elzenga, J. T. M., and Bouwmeester, H. J. (2011). "Selection and breeding of robust rootstocks as a tool to improve nutrient-use efficiency and abiotic stress tolerance in tomato," in *Proceeding First International Conference on Organic Greenhouse Horticulture. Acta Horticulture,* Vol. 915, eds M. Dorais, and S. D. Bishop (Bleiswijk), 109–116.

Wahb-Allah, M. A. (2014). Effectiveness of grafting for the improvement of salinity and drought tolerance in tomato (*Solanum lycopersicon* L.). *Asian J. Crop Sci.* 6, 112–122. doi: 10.3923/ajcs.2014.112.122

Wang, N., Wei, Q., Yan, T., Pan, Z., Liu, Y., and Peng, S. (2016a). Improving the boron uptake of boron-deficient navel orange plants under low boron conditions by inarching boron-efficient rootstock. *Sci. Hortic.* 199, 49–55. doi: 10.1016/j.scienta.2015.12.014

Wang, P., Wu, S. H., Wen, M. X., Wang, Y., and Wu, Q. S. (2016b). Effects of combined inoculation with *Rhizophagus intraradices* and *Paenibacillus mucilaginosus* on plant growth, root morphology, and physiological status of trifoliate orange (*Poncirus trifoliata* L. *Raf.)* seedlings under different levels of phosphorus. *Sci. Hortic.* 205, 97–105. doi: 10.1016/j.scienta.2016.04.023

Warschefsky, E. J., Klein, L. L., Frank, M. H., Chitwood, D. H., Londo, J. P., Eric, J. B., et al. (2016). Rootstocks: diversity, domestication, and impacts on shoot phenotypes. *Trends Plant Sci.* 21, 418–437. doi: 10.1016/j.tplants.2015.11.008

Wei, S., Wu, Y. Z., and Huang, J. (2006). Effects of rootstocks on growth and photosynthetic properties of grafted plants of netted melon. *Acta Agric. Shanghai* 22, 114–117.

Weng, J. H. (2000). The role of active and passive water uptake in maintaining leaf water status and photosynthesis in tomato under water deficit. *Plant Prod. Sci.* 3, 296–298. doi: 10.1626/pps.3.296

Wissuwa, M., Kretzschmar, T., and Rose, T. J. (2016). From promise to application: root traits for enhanced nutrient capture in rice breeding. *J. Exp. Bot.* doi: 10.1093/jxb/erw061. Available online at: http://jxb.oxfordjournals.org/content/early/2016/03/23/jxb.erw061.full.pdf+html

Xie, Y. F., Tian, Y. Q., Li, S., Yao, K. Q., Ma, Z. M., Yang, Y. T., et al. (2012). Effects of single-root-grafting and double-root-grafting on cucumber rhizosphere soil microorganism and enzyme activity. *China Vegetables* 24, 62–68. Available online at: http://xueshu.baidu.com/s?wd=paperuri%3A%28455933d794c8eadae778d00930553aa3%29&filter=sc_long_sign&tn=SE_xueshusource_2kduw22v&sc_vurl=http%3A%2F%2Fen.cnki.com.cn%2FArticle_en%2FCJFDTotal-ZGSC201224016.htm&ie=utf-8&sc_us=4674814618225490452

Xin, J., Huang, B., Yang, J., Yang, Z., Yuan, J., and Mu, Y. (2013). Role of roots in cadmium accumulation of two water spinach cultivars: reciprocal grafting and histochemical experiments. *Plant. Soil* 366, 425–432. doi: 10.1007/s11104-012-1439-5

Xu, F., Liu, Q., Chen, L., Kuang, J., Walk, T., Wang, J., et al. (2013). Genome-wide identification of soybean microRNAs and their targets reveals their organ-specificity and responses to phosphate starvation. *BMC Genomics* 14:66. doi: 10.1186/1471-2164-14-66

Yetisir, H., Özdemir, A. E., Aras, V., Candır, E., and Aslan, O. (2013). Rootstocks effect on plant nutrition concentration in different organ of grafted watermelon. *Agric. Sci.* 4, 230–237. doi: 10.4236/as.2013.45033

Zamboni, M., Garavani, A., Gatti, M., Vercesi, A., Parisi, M. G., Bavaresco, L., et al. (2016). Vegetative, physiological and nutritional behavior of new grapevine rootstocks in response to different nitrogen supply. *Sci. Hortic.* 202, 99–106. doi: 10.1016/j.scienta.2016.02.032

Zarrouk, O., Gogorcena, Y., Gomez-Aparisi, J., Betran, J. A., and Moreno, M. A. (2005). Influence of almond peach hybrids rootstocks on flower and leaf mineral concentration, yield and vigour of two peach cultivars. *Sci. Hortic.* 106, 502–514. doi: 10.1016/j.scienta.2005.04.011

Zen, Y. A., Zhu, Y. L., Huang, B. J., and Yang, L. F. (2004). Effects of *Cucurbita ficifolia* as rootstock on growth, fruit setting, disease resistance and leaf nutrient element contents in *Cucumis sativus*, *J. Plant Resour. Environ.* 13, 15–19. Available online at: http://en.cnki.com.cn/Article_en/CJFDTOTAL-ZWZY200404004.htm

Zeng, H., Wang, G., Hu, X., Wang, H., Du, L., and Zhu, Y. (2014). Role of microRNAs in plant responses to nutrient stress. *Plant Soil* 374, 1005–1021. doi: 10.1007/s11104-013-1907-6

Zha, Q., Wang, Y., Zhang, X. Z., and Han, Z. H. (2014). Both immanently high active iron contents and increased root ferrous uptake in response to low iron stress contribute to the iron deficiency tolerance in *Malus xiaojinensis*. *Plant Sci.* 214, 47–56. doi: 10.1016/j.plantsci.2013.10.002

Zhang, J., Chen, S., Liu, R., Jiang, J., Chen, F., and Fang, W. (2013). Chrysanthemum cutting productivity and rooting ability are improved by grafting. *Sci. World J.* 2013:286328. doi: 10.1155/2013/286328

Zhang, L., Meng, X. X., Liu, N., Yang, J. H., and Zhang, M. F. (2012). Effects of grafting on phosphorus uptake and utilization of watermelon at early stage under low phosphorus stress. *J. Fruit Sci.* 29, 120–124. doi: 10.13925/j.cnki.gsxb.2012.01.024

Zhang, Z. K., Li, H., Zhang, Y., Huang, Z. J., Chen, K., and Liu, S. Q. (2010). Grafting enhances copper tolerance of cucumber through regulating nutrient uptake and antioxidative system. *Agric. Sci. China.* 9, 1758–1770. doi: 10.1016/S1671-2927(09)60274-1

Zhao, X., Guo, Y., Huber, D. J., and Lee, J. (2011). Grafting effects on postharvest ripening and quality of 1-methylcyclopropene-treated muskmelon fruit. *Sci. Hortic.* 130, 581–587. doi: 10.1016/j.scienta.2011.08.010

Zhou, J., Wan, H., Qin, S., He, J., Lyu, D., and Li, H. (2016). Net cadmium flux and gene expression in relation to differences in cadmium accumulation and translocation in four apple rootstocks. *Environ. Exp. Bot.* 130, 95–105. doi: 10.1016/j.envexpbot.2016.05.012

Zhu, J., Bie, Z., Huang, Y., and Han, X. (2008). Effect of grafting on the growth and ion concentrations of cucumber seedlings under NaCl stress. *Soil Sci. Plant Nutr.* 54, 895–902. doi: 10.1111/j.1747-0765.2008.00306.x

Conflict of Interest Statement: The authors declare that the research was conducted in the absence of any commercial or financial relationships that could be construed as a potential conflict of interest.

frontiers in Plant Science

ORIGINAL RESEARCH
published: 25 August 2016
doi: 10.3389/fpls.2016.01255

Photosynthate Regulation of the Root System Architecture Mediated by the Heterotrimeric G Protein Complex in *Arabidopsis*

Yashwanti Mudgil[1,2], Abhijit Karve[3†], Paulo J. P. L. Teixeira[2], Kun Jiang[2†], Meral Tunc-Ozdemir[2] and Alan M. Jones[2,4]*

[1] Department of Botany, University of Delhi, Delhi, India, [2] Department of Biology, University of North Carolina at Chapel Hill, Chapel Hill, NC, USA, [3] Brookhaven National Lab, Upton, NY, USA, [4] Department of Pharmacology, University of North Carolina at Chapel Hill, Chapel Hill, NC, USA

OPEN ACCESS

Edited by:
Janin Riedelsberger, University of Talca, Chile

Reviewed by:
Yong-Ling Ruan, University of Newcastle, Australia
Christina Kuehn, Humboldt University of Berlin, Germany

***Correspondence:**
Yashwanti Mudgil
ymudgil@gmail.com
ymudgil@botany.du.ac.in

†Present address:
Kun Jiang, College of Life Sciences, Zhejiang University, Hangzhou, China;
Abhijit Karve, Purdue Research Foundation, West Lafayette, IN, USA

Specialty section:
This article was submitted to Plant Physiology, a section of the journal Frontiers in Plant Science

Received: *16 May 2016*
Accepted: *08 August 2016*
Published: *25 August 2016*

Citation:
Mudgil Y, Karve A, Teixeira PJPL, Jiang K, Tunc-Ozdemir M and Jones AM (2016) Photosynthate Regulation of the Root System Architecture Mediated by the Heterotrimeric G Protein Complex in Arabidopsis. Front. Plant Sci. 7:1255. doi: 10.3389/fpls.2016.01255

Assimilate partitioning to the root system is a desirable developmental trait to control but little is known of the signaling pathway underlying partitioning. A null mutation in the gene encoding the Gβ subunit of the heterotrimeric G protein complex, a nexus for a variety of signaling pathways, confers altered sugar partitioning in roots. While fixed carbon rapidly reached the roots of wild type and *agb1-2* mutant seedlings, *agb1* roots had more of this fixed carbon in the form of glucose, fructose, and sucrose which manifested as a higher lateral root density. Upon glucose treatment, the *agb1-2* mutant had abnormal gene expression in the root tip validated by transcriptome analysis. In addition, PIN2 membrane localization was altered in the *agb1-2* mutant. The heterotrimeric G protein complex integrates photosynthesis-derived sugar signaling incorporating both membrane-and transcriptional-based mechanisms. The time constants for these signaling mechanisms are in the same range as photosynthate delivery to the root, raising the possibility that root cells are able to use changes in carbon fixation in real time to adjust growth behavior.

Keywords: photosynthetic partitioning, positron electron tomography imaging, AGB1, lateral root density, glucose, gene expression, PIN2-GFP

INTRODUCTION

An intrinsic characteristic of any plant species is its root system architecture (RSA). Although RSA is plastic in development, the features that constitute the RSA, such as lateral root density and lateral root primordial position, remain constant over different root mass volumes (**Figures 1A,B**) (Dubrovsky et al., 2006; Moreno-Risueno et al., 2010; Dubrovsky et al., 2011; Szymanowska-Pulka, 2013). Environmental variables for RSA are light, water, and nutrients. Given that roots are subterranean, the light effect is most likely due to the amount of sugar in the form of fixed carbon (photosynthate) that roots receive (Kircher and Schopfer, 2012; Colaneri and Jones, 2014; Gupta et al., 2015). Sucrose is produced in the cytosol of photosynthesizing cells and is the predominant sugar to be transported through phloem to the carbon sink tissues where this disaccharide sucrose is converted back to the monosaccharides, glucose and fructose, by cell wall invertases (Ruan, 2014).

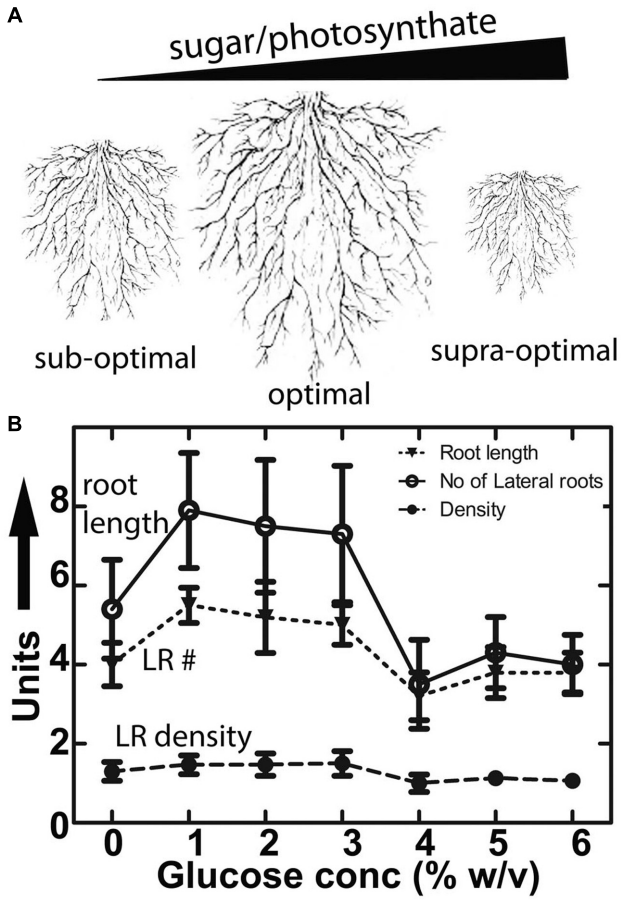

FIGURE 1 | Conserved architecture of plant root growth in nature and the lab. (A) Diagrammatic representation of roots of different size showing constant lateral root density and lateral root primordial position grown under sub-optimal, optimal and supra-optimal nutrient conditions. **(B)** Primary root length (mm), number of lateral roots (per root) and lateral root density (roots per mm) in Col-0 in the presence of different concentrations of glucose. Values represent the mean of 3 independent experiments ($n = 10$ each); bars represent the standard error.

Recently, an accumulating body of evidence suggests that sugars also function as signaling molecules on RSA (Hanson and Smeekens, 2009; Smeekens et al., 2010; Kircher and Schopfer, 2012; Moghaddam and den Ende, 2013). Under laboratory conditions, exogenous application of sugars (D-glucose and sucrose) at a low concentration stimulates primary root elongation and lateral root development (Freixes et al., 2002; Lee-Ho et al., 2007; Booker et al., 2010; Roycewicz and Malamy, 2012; Gupta et al., 2015).

An increase in the available photosynthate stimulates root development (Rogers et al., 2006; Hachiya et al., 2014). Specifically, elevated CO_2 levels increase lateral root formation (Crookshanks et al., 1998; Smith et al., 2013). Reciprocally, nutrient deficiencies that increase the root-to-shoot ratio and alter RSA are associated with an accumulation of sugars (Liu et al., 2009; Giehl et al., 2014). While it is clear that photosynthetic rates in above-ground tissues are associated with the extent and pattern of growth in roots (Kircher and Schopfer, 2012), how at the cellular level this growth is coordinated remains unknown.

It was suggested that putative crosstalk between sugar and hormones, mainly auxin homeostasis/signaling triggers changes in RSA (Gupta et al., 2009, 2015; Mishra et al., 2009; Booker et al., 2010; Lilley et al., 2012; Sairanen et al., 2012). Auxin and sugar act in concert and the availability of free sugars regulate the biosynthesis and degradation of auxin (Lilley et al., 2012; Sairanen et al., 2012). The physiological role of this concerted auxin-sugar action is control of cell division and elongation (Wang and Ruan, 2013).

Plants have at least two glucose sensing pathways; one is metabolism based, mediated by HEXOKINASE1 (HXK1); (Cho et al., 2006, 2007) and the other is based on extracellular sugar mediated by the receptor-like protein called AtRGS1. In *Arabidopsis*, AtRGS1-mediated sugar sensing is coupled by the heterotrimeric G protein complex comprised of a Gα subunit (GPA1) and a Gβγ dimer (AGB1 and AGG, respectively) (Chen and Jones, 2004; Grigston et al., 2008; Phan et al., 2012; Urano et al., 2012a,b; Bradford et al., 2013). We previously established that loss-of-function alleles for AGB1 alter RSA by increased root mass and altered auxin signaling (Ullah et al., 2003). Synergism between auxin and glucose on root growth and lateral root formation is altered in *agb1* mutants indicating G protein action in RSA maintenance (Booker et al., 2010).

The present work provides data suggesting a G protein mediated signaling mechanism for photosynthate partitioning to roots. The heterotrimeric G protein mediates sensing of nutritional state/sugar levels that integrate sink carbohydrate levels to maintain root architecture. The G protein complex lies apically in the sugar pathway controlling photosynthate partitioning in lateral roots. More importantly, this study provides substantial support for G protein functioning as a sensor that integrates sink carbohydrate levels to maintain root growth, in which sugar acts as a signal to regulate transcriptional changes.

MATERIALS AND METHODS

Accession Number Details of the Genes Used in the Study

HXK1, At4G29130; RGS1, At3G26090; AGB1, At4G34460. All RNA-seq libraries produced in this study can be accessed at the NCBI Sequence Read Archive under accession number SRP059460 or at the link http://www.ncbi.nlm.nih.gov/sra/?term=SRP059460.

Plant Material and Growth Conditions

Arabidopsis thaliana ecotype Columbia (Col-0) was used in this study unless otherwise indicated. The G protein mutants and transgenic lines were previously described (Ullah et al., 2003; Chen et al., 2006; Trusov et al., 2007). The *hxk1*-3 is a Columbia null allele (Huang et al., 2015). Seeds were germinated after stratification at 22°C under short-day conditions (8-h light/16-h dark, light intensity 200 μmol $m^{-2}s^{-1}$) or in the dark. The PIN2 reporter lines were described by Wisniewska et al. (2006). The *agb1*-2 null allele was introgressed by genetic crossing.

$^{11}CO_2$ Pulse Chase Experiment and Measurements of Sugars

The $^{11}CO_2$ fixation experiment used 14 days-old Col-0 and *agb2-1* seedlings grown on MS plates under constant light. ^{11}C, a short-lived radioisotope ($t_{1/2} = 20.4$ min) was used to study the allocation and partitioning of [^{11}C]-photosynthate. The high specific activity of ^{11}C, allows a short 5–10 s pulse rather than a continuous stream of 1–2 h needed when using ^{14}C. Given the high rate of transport of photosynthate observed for *Arabidopsis*, ^{11}C provides greater temporal (for analyte) and spatial (for PET imaging) than ^{14}C. ^{11}C was made by irradiating a nitrogen gas (N_2) target with 17-MeV protons from the TR-19 cyclotron (Ebco Industries) at Brookhaven National Laboratory to induce the $^{14}N(p,\alpha)^{11}C$ nuclear transformation (Ferrieri and Wolf, 1983). Carbon dioxide labeled with ^{11}C was captured on a molecular sieve (4 Å), desorbed, and quickly released into an air stream at 200 ml min^{-1} as a discrete pulse to the targeted seedling fixed inside a 5 × 10-cm airtight cell maintained at 21°C and fitted with red/blue light-emitting diodes (120 μmol $m^{-2}s^{-1}$) to ensure a steady level of fixation. In general, plants were pulsed with 20–30 mCi (740-1110 GBq) of $^{11}CO_2$ as a 30-s pulse in a continuous stream of air. After pulsing, the seedlings were chased with normal air for 60 min. Roots and shoots were harvested at 20 and 60 min and placed into separate scintillation vials and radiation quantitated using a γ counter (Picker). For positron emission tomography imaging (PET), 3-week-old plants were transferred to the PET camera 10 min after pulsing. All radioactivity measurements were decay corrected to a standard zero time of each study to quantify allocation of ^{11}C-photosynthate to the roots. After radioactivity measurements, ^{11}C-labeled sugars and total sugars (^{12}C) were analyzed by high performance thin layer chromatography followed by autoradiography as described by Babst et al. (2013). The sugar and the radioactivity data was normalized by the fresh weight of the tissue.

Positron Electron Tomography (PET) Imaging

For PET imaging, a 30-s pulse of $^{11}CO_2$ was administered to the youngest fully expanded leaf of a sorghum plant at grain filling stage. After 90 min incubation, the sorghum plant was scanned in a PET camera (HR+, SEMENS). The data was acquired over 30 min. The image was reconstructed and analyzed using an AMIDE medical image data examiner[1]. Validation of this method is described by Karve et al. (2015).

Glucose Assays

To observe the effect of sugar on plant development, 4-day-old seedlings germinated on ½X MS media without sugar were transferred to plates containing various amount of sugars and grown vertically for 7 days. Primary root length and number of lateral roots were quantified using 10 seedlings per replicate and each experiment was repeated three times.

[1]http://amide.sourceforge.net/

Microscopy Imaging and Analysis

Arabidopsis PIN2-GFP in the Col-0 and *agb1*-2 backgrounds were imaged using a Zeiss LSM710 confocal laser scanning microscope equipped with an Apochromat40 (NA 1.2) water-immersion objective excited by a Multiline Argon laser (458/488/514 nm) excitation 488 nm and emission 520–560 nm. Fluorescence intensity measurements were performed with ImageJ (Albrechtova et al., 2014) and data was graphed with GraphPad Prizm (La Jolla, CA, USA).

Auxin Analysis

Root tissue from the 7-day old seedlings was harvested below the root shoot junction, flash frozen in liquid nitrogen stored in 0.5 ml tubes in −80°C. Lyophilized samples were overnight shipped to the Department of Horticulture at the University of Minnesota where analysis for total and free auxin was performed exactly as described by Liu et al. (2012). The experiment was performed in triplicate. Each sample (treatment by genotype) had approximately 70–80 roots, roughly 25 mg of fresh weight.

RNA Sample Preparation and Next-Generation Sequencing

Wild type and *agb1*-2 seedlings were grown vertically on ½ X MS, and 0.75% Phyto agar, 22° C, in the dark for 5 days followed by treatment with 2% glucose (gluc) in ½ X liquid MS for 4h in dark. The latter was achieved by pouring the liquid solution onto the plates which were then kept still for the 4 h duration. Control seedlings were treated with ½ X liquid MS. After treatment, the apical 1 mm region of roots, primarily the RAM, was harvested under a microscope using ultra sharp razor blades and snap-frozen in liquid nitrogen followed by RNA isolation using the RNeasy Plant Mini Kit (Qiagen) following the manufacturer's protocol. Approximately 150 root tips were harvested per treatment by genotype.

mRNA-seq libraries were prepared with the Illumina TruSeq Stranded RNA library prep kit (RS-122-2201) as per the manufacturer's protocol. One hundred nano-grams of total mRNA per sample were used in each preparation. Size selection (250–450 bp) was performed in each cDNA libraries using a 0.6X-0.8Xfd dual- Solid Phase Reversible Immobilization (SPRI) procedure provided by the manufacturer (SPRIselect reagent kit, item B23317, Beckman Coulter). A total of 12 libraries were prepared (two conditions, two genotypes, three replicates per genotype/condition) using different barcoded adaptors to allow the pooling of the libraries prior to sequencing. Quality control indicated that all libraries except one had >98% mapped sequence. The one library (*agb1*-2, control) that did not meet this condition was excluded, thus only two replicates were used for this condition.

Gene Expression Analysis

The Illumina HiSeq2000 sequencer was used to generate an average of 55 million single-end reads (50 bp) for each of the libraries. The resulting RNA-seq reads were then aligned against the *Arabidopsis* genome (TAIR10) using TopHat (Trapnell et al., 2009). A maximum of two mismatches were allowed in the

alignment and reads mapping to multiple positions in the reference were discarded. Reads mapping to each *Arabidopsis* gene were then counted by the HTSeq software (Anders et al., 2014) using default parameters. Differentially expressed genes between conditions were identified using the edgeR package (Robinson et al., 2010) with a false discovery rate (FDR) threshold of 0.05. A subset of 978 genes differentially expressed by the glucose treatment in at least one of the genotypes was submitted to hierarchical clustering based on the Euclidean distance of their *z*-score normalized expression values. Sets of genes belonging to sub-clusters in this analysis were submitted to Gene Ontology (GO – biological process) enrichment analyses using the PlantGSEA database (Yi et al., 2013) and the Bingo plugin for Cytoscape (Maere et al., 2005).

RESULTS AND DISCUSSION

Sugar Control of Lateral Root Density Mediated by AGB1

Adding glucose or sucrose to media for optimal *Arabidopsis* seedling growth is standard lab practice but paradoxically it is not clear why 1–2% sugar in the agar medium is optimal since this amount does not occur in soils. The fact that there is an optimum concentration for root growth (**Figure 1A**) suggests that sugar is acting on RSA as a signal and not as a growth-limiting metabolite. **Figure 1B** shows that glucose both promoted and inhibited primary root growth and lateral root formation depending on the glucose concentration, but the overall architecture was not affected in wild type seedlings. That is primarily because while root length and lateral root number co-vary depending on glucose concentration, lateral root density remains constant for wild type (**Figure 1B**). We tested Gα (*gpa1-4*), Gβ (*agb1*-2) and Gαβ subunit double mutants (*agb1-2gpa1-4*) of the heterotrimeric G protein complex to discern any involvement of G protein subunits (**Figure 2**). We found that the developmental property of "fixed root density," while developmentally plastic, is genetically encoded because loss of the Gβ caused lateral root density to increase with increased glucose amount (**Figure 2**, $P = <0.005$). To determine if this behavior is due to osmotic pressure, we tested root growth in the presence of various concentrations of the osmoticant mannitol and found that *agb1*-2 behaved like wild type (**Supplementary Figure S1**, $P \geq 0.1$).

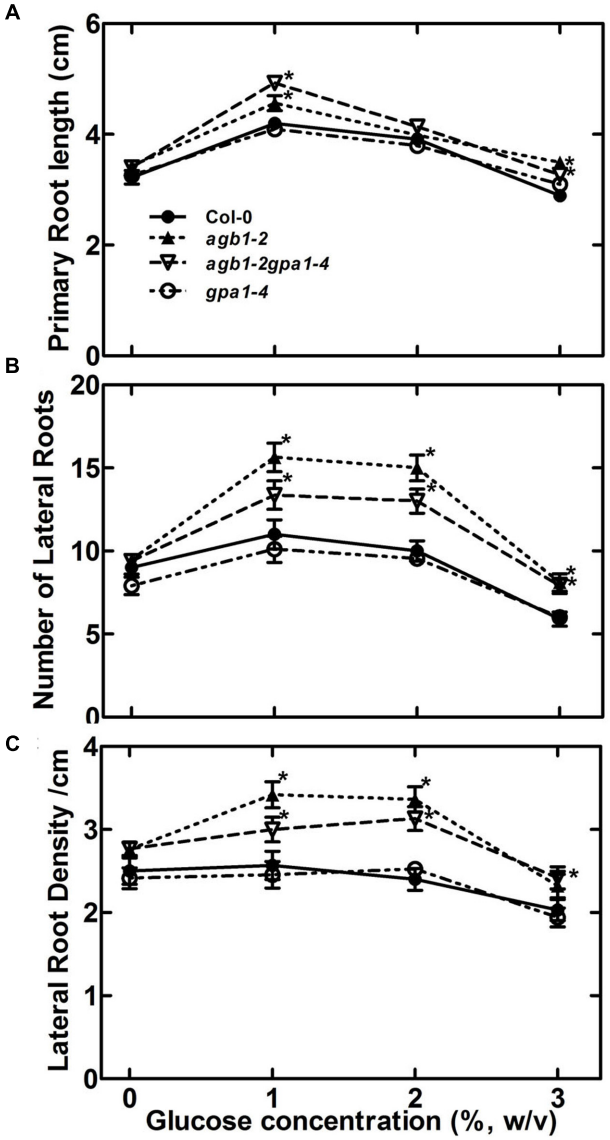

FIGURE 2 | Role of G protein subunits in sensing sugar in RSA maintenance. (A) Primary root length of 11-day-old seedlings of Gα, Gβ and Gαβ double subunit mutants (indicated genotypes) were grown on ½ X MS, and 0.75% agar, 22°C, 8:16 light: dark cycle for 4 days followed by 7 days of vertical growth on different concentrations of glucose. **(B)** Lateral root number **(C)** Lateral root density. All experiments were repeated 3 times with 10–15 seedlings of each genotype per trial. Error bars represent standard error Student's *t*-test results are based on difference between the wild type and indicated genotype shown as asterisks:*$P < 0.05$.

Effects of Glucose on RSA of Sugar-Sensing Mutants

Glucose modulation of the RSA (**Figure 1**) suggests the existence of a glucose-sensing mechanism that refines root development according to the amount of the translocated sucrose as the major form of assimilated carbon from source (leaves) to the sink tissue (roots). Phloem translocated sucrose is metabolized to glucose and fructose in the roots by invertases which determine sink strength. Both HXK1-dependent and -independent mechanisms contribute to glucose sensing in plants (Rolland et al., 2006; Hanson and Smeekens, 2009). Therefore, we performed phenotypic analysis on an *HXK1* null mutant (*hxk1*-3*)* and *AtRGS1* (*rgs1*-2*)*. Compared to its wild type Col-0, the *hxk1*-3 mutant displayed attenuated glucose effects, reduced primary root length and lateral root number ($P \leq 0.005$) and showed insensitivity to glucose compared to the control (**Figure 3**). Root density of *hxk1*-3 was at the wild type level for all the tested glucose concentrations, however, this was because *hxk1* roots were not responsive to glucose with regard to both lateral root

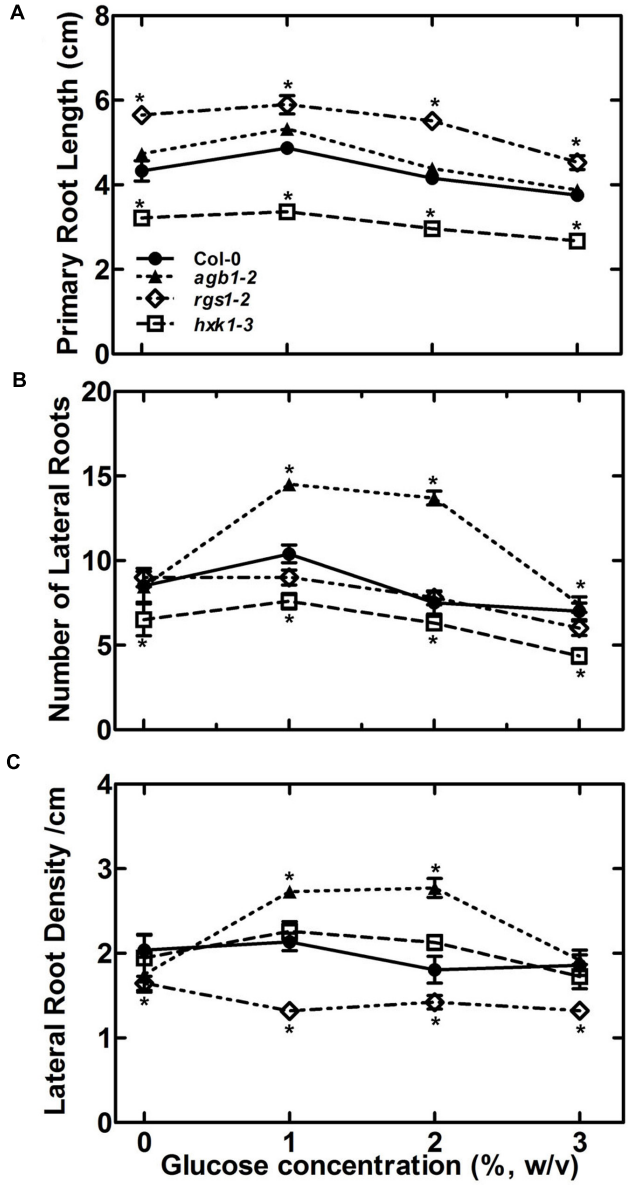

FIGURE 3 | The sugar sensing mechanism in RSA maintenance may involve both HEXOKINASE 1(*HXK1)* and REGULATOR of G SIGNALING 1 (*RGS1).* Effect of glucose on RSA in terms of primary root length **(A)**, number of lateral roots **(B)** and lateral root density **(C)** was compared for wild type, *agb1-2*, *hxk1-3* and *rgs1-2* mutant. All experiments were repeated three times with 10–15 seedlings used for each genotype in each trial. Error bars represent standard error Student's *t*-test results are based on difference between the wild type and indicated genotype shown as asterisks: $*P < 0.05$.

number and root length. Overall, the root system is poorly developed therefore it is difficult to conclude whether HXK1 plays a glucose signaling role or solely a metabolic role in roots (**Figures 3A–C**). Loss of *AtRGS1* conferred an increase in primary root length ($P \leq 0.005$), insensitivity to exogenous glucose at the lower range (**Figure 3A**), and sugar-induced lateral root number compared to wild type (**Figure 3B**). Lateral root density of the *rgs1*-2 mutant was slightly lower over the entire tested range compared to *hxk1*-3 and Col-0 ($P \leq 0.005$, **Figure 3C**). Therefore, we speculate that both HXK1 and RGS1 are involved in this glucose response but function differently.

Dynamics of the Allocation of Leaf-Fixed Carbon to Roots

As discussed above, the evidence supports the conclusion that the source of sugars affecting RSA is from fixed carbon but it is unclear if the rate at which these sugars are produced is distributed to roots within a time scale over which G signaling operates (Fu et al., 2014). As discussed above, sugar strongly affected primary root growth and lateral root formation, but the overall RSA was not affected in wild type seedlings; i.e., the lateral root density was constant over a range of sugar concentration. Possible explanations are that AGB1 negatively regulates the amount of sugars fixed or affects the amount and/or gradients of auxin or both.

To test the first possibility, we quantitated the photosynthesis-derived sugar flux to the roots in *agb1-2* and wild type Col-0 seedlings by γ counting (**Figure 4**). Roots may sense photosynthetic activity by the amount, duration and frequency of the sugar present. For this to operate, sugars from fixed CO_2 must reach roots quickly enough (minutes) for root cells to be able to sense the dynamics of carbon fixation. Photosynthesis-derived sugar flux to the roots in *agb1-2* and wild type Col-0 seedlings was determined using 14-d-old seedlings treated with a pulse of the short-lived radiotracer $^{11}CO_2$ and chased with $^{12}CO_2$ (**Figure 4A**). Quantitation in harvested tissue was made by counting radioactive γ that are formed as a product of positron annihilation. After 20 min, approximately 2% of the radiolabeled photosynthate had already reached the roots in both Col-0 and *agb2-1* seedlings (**Figure 4A**, photoassimilate allocation). The rate of movement was estimated to be 0.5–0.8 cm min^{-1}. By 60 min, the absolute amount increased approximately 5–6 fold, suggesting the time scale for a linear response is minutes.

The allocation of the newly fixed carbon to roots partitioned into at least three soluble sugars (glucose, fructose and sucrose). The total amount of [^{11}C] photosynthate partitioned to the roots did not differ between the two genotypes at the tested time points, indicating comparable photoassimilate allocation in the absence of AGB1 (**Figure 4A**). However, after 60 min, almost twice as much [^{11}C] glucose, [^{11}C] fructose, and [^{11}C] sucrose in the *agb1-2* roots was found compared to Col-0 (**Figure 4A**, photosynthate to sugars = 3 hexoses combined, $P < 0.001$). However, total sugars (i.e., not immediately fixed ^{11}C) were not statistically different between genotypes (**Figure 4A**, photosynthate to sugars inset) indicating that over time the difference in the fixed sugars reached a new equilibrium. Most of the difference in the fixed [^{11}C] sugars was due to an increased amount of [^{11}C] glucose (**Figure 4A**, photosynthate to glucose, $P < 0.001$).

Attempts to visualize allocated carbon in *Arabidopsis* by positron emission tomography (PET) did not yield sufficient resolution due to the small plant size. Irrespective of the size of the plant, phloem sap flow velocity varies only slightly between diverse plant species (Windt et al., 2006). Therefore, to visualize

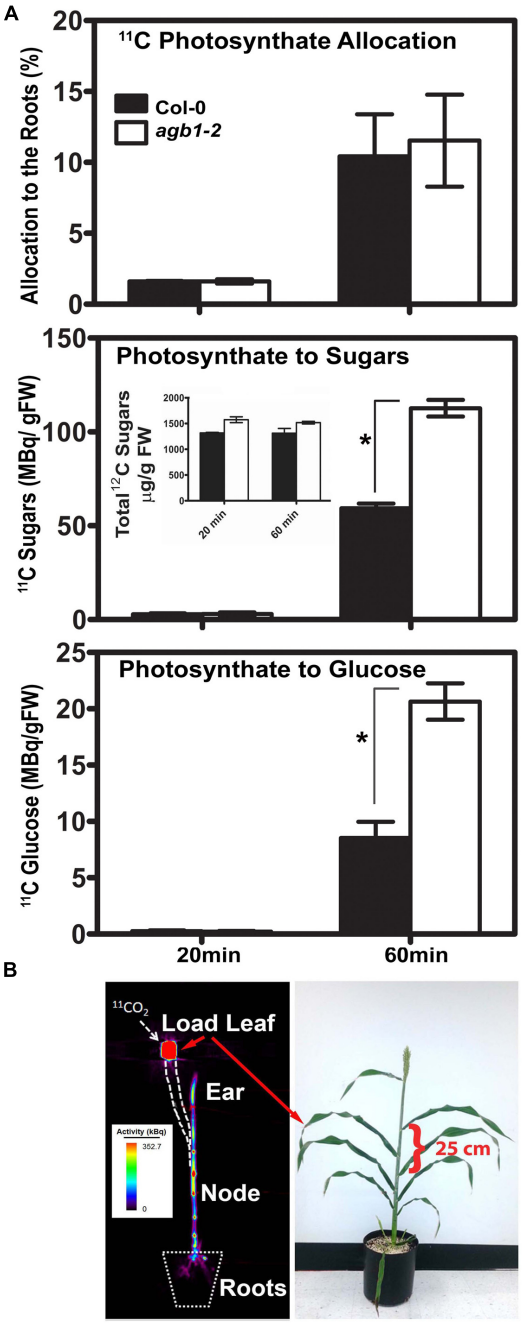

FIGURE 4 | Positron electron tomography imaging of allocation and partitioning of photoassimilate. (A) Top panel. Total allocation of [^{11}C] CO_2 in the roots of Col (solid bars) and *agb1*-2 (open bars) at the indicated times. Middle panel. Partitioning of newly fixed $^{11}CO_2$ to soluble sugars (glucose, fructose and sucrose) in the roots of Col (solid bars) and *agb1*-2 (open bars) at the indicated times. (Inset) Total non-radioactive [^{12}C] sugars (glucose, fructose and sucrose) in the roots of Col (solid bars) and *agb1*-2 (open bars) at the indicated times. Non-radioactive [^{12}C] sugars were extracted and analyzed by thin layer chromatography as described previously (Babst et al., 2013). Numbers represent the average of 3 independent experiments ($n = 10$ each) and error bars represent SE. Lower panel. Partitioning of newly fixed $^{11}CO_2$ to glucose in the roots. Percentage values were calculated as

(Continued)

FIGURE 4 | (Continued)

radioactivity in the roots relative to the total seedling activity. Radioactivity (MBq/g FW) represent the mean of 3 independent experiments ($n = 10$ each) and error bars represent the standard error. **(B)** Fixed carbon is rapidly distributed to tissue sinks. (Left panel) The image shows the distribution of ^{11}C-labeled photoassimilate in different parts of in an intact sorghum plant shown in the right panel imaged 2 h after $^{11}CO_2$ administration to the load leaf at the position indicated. Heat scale represents activity/pixel. Load leaf = site of $^{11}CO_2$ administration. Velocity was 1.25 cm min^{-1}. A distance of 25 cm is indicated by the bracket. Student's *t*-test results are based on difference between the means. Asterisks indicate $P < 0.001$.

and quantitate this rapid carbon allocation, we used sorghum because of its larger size, in particular the greater distance between the leaf and sink tissues. The first fully expanded mature leaf of sorghum during a grain filling stage was pulsed with $^{11}CO_2$ for 30 sec. PET images were taken 90 min after $^{11}CO_2$ exposure. High levels of radiation were detected in the stem, particularly high at nodes, and in the grain head. Remarkably $^{11}CO_2$ was observed ~100 cm away from the loading site traveling at a rate of at least 1.25 cm min^{-1}. Photoassimilate was observed in the roots within minutes (**Figure 4B**).

Feedback Loop Controlling Glucose Economy

There are three possible explanations why the *agb1* mutant root had higher levels of sugar: (**1**) less sugar is secreted from the *agb1*-2 root compared to the wild type. Root exudation plays a major role in maintaining root-soil contact by modifying biochemical and physical properties of the rhizosphere. Compounds such as amino acids and, to a much lesser degree, sugars are secreted by plants roots in order to promote microbial and fungal growth (Chaparro et al., 2014). (**2**) It is possible that the flux of glucose, fructose and sucrose to the roots is higher in the *agb1*-2 mutant. If this were true, we would expect to see a higher total of fixed $^{11}CO_2$ in the root yet this did not occur (**Figure 4A**). (**3**) It is possible that sugar metabolism is altered in the *agb1*-2 mutant. We favor this last which is consistent with our observation that 22% of the interacting partners to the G protein core described in the G protein interactome are annotated as "metabolic processes" (Klopffleisch et al., 2011). This includes half of the enzymes in glycolysis, two enzymes in the Krebs cycle, and one cytosolic enzyme in the glucose shunt (Colaneri and Jones, 2014). Our previous study using *promoter-AGB1*::GUS lines showed that AGB1 transcript levels are sugar inducible in the root tip indicating involvement of feedback loops (Mudgil et al., 2009).

Sugar Effect on Auxin Levels in AGB1 Mutant Roots

There exists a complex interplay between glucose and auxin in the regulation of root (Mishra et al., 2009; Booker et al., 2010) and shoot development (Mishra et al., 2009; Booker et al., 2010; Barbier et al., 2015). In addition, both sugar and auxin increase lateral root number (Boerjan et al., 1995; Mishra et al., 2009; Kircher and Schopfer, 2012; Roycewicz and Malamy, 2012). Glucose induces the expression of a subset of genes

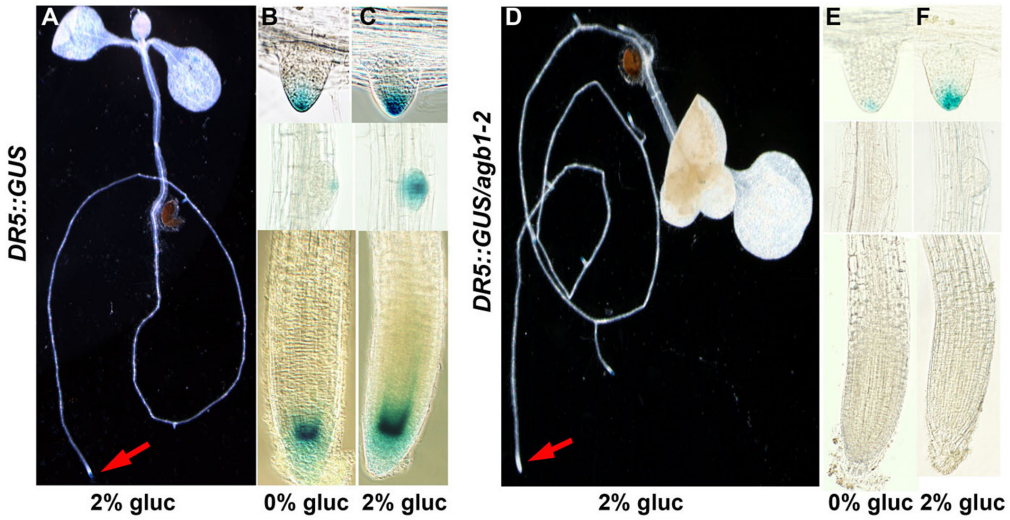

FIGURE 5 | Glucose-induced auxin maxima in *agb1*-2 mutant roots. *DR5::GUS* is a synthetic, auxin-inducible gene promoter reporter used to detect auxin maxima or auxin signaling. **(A–C)** Wild type and *agb1*-2 **(D–F)** seedlings were treated with 2% glucose (gluc) for 4 h **(A,C,D,F)** and compared to the untreated controls **(B,E)**. Arrows point to the root tip. Compared to wild type, glucose did not increase DR5-driven expression of GUS in the *agb1*-2 root tips (*cf.* **B,C**; lower panels to **E,F**; lower panels) and lateral root primordial (*cf.* **B,C**; middle panels to **E,F**; middle panels), although *DR5::GUS* expression occurred in emergent lateral roots (*cf.* **B,C;** upper panels to **E,F**; upper panels).

involved in auxin biosynthesis pathways, and auxin biosynthesis and metabolism rates corresponds to endogenous hexose levels (Sairanen et al., 2012).

The G protein complex may mediate a sugar-induced increase in auxin level by increased auxin synthesis overall and/or increased auxin maxima patterning by altering auxin transport. Genetic ablation of *AGB1* confers enhanced basipetal auxin transport (Mudgil et al., 2009) and sugar increases basipetal auxin transport associated with increased auxin levels (Mishra et al., 2009; Sairanen et al., 2012). Moreover, local auxin gradients generated by directional transport of auxin coincide with the site of organogenesis (Benková et al., 2003; Dubrovsky et al., 2008). Based on these findings, we hypothesized that AGB1 plays an important role in setting up local auxin gradients in response to glucose and therefore modulate expression of auxin-responsive genes. To test this hypothesis, we used the auxin reporter *DR5::GUS* that measures overall transcriptional output of auxin signaling (Friml et al., 2003; Sauer and Friml, 2011). To examine the effect of sugar on local auxin gradients/signaling, 5-day-old wild type and *agb1*-2 seedlings were treated with D-glucose (2%) for 4 h in the dark. In wild type roots, glucose stimulates *DR5::GUS* staining in different regions of the root (RAM, initiating primordia and emerged roots) (**Figures 5A–C**), whereas in the absence of AGB1, *DR5::GUS* expression was undetectable in the RAM (cf. **Figures 5A,D**, red arrows), and absent in the early stages of lateral root primordia development whether or not treated with sugar (cf. **Figures 5B,C** with **Figures 5E,F** center panels), whereas the RAM of the emergent lateral roots showed glucose-induced *DR5::GUS* expression (**Figures 5E,F**, top panels). These results indicate that AGB1 is necessary to attain sugar-induced, local auxin maxima/signaling at the site of cell division in the primary RAM and in the early stages of lateral root initiation. The absence of DR5::GUS staining in seedlings lacking AGB1 indicates either reduced auxin at the meristem or attenuated auxin signaling.

To distinguish between these two possibilities, we measured total endogenous auxin level in 5-day-old roots (**Supplementary Figure S2**). No significant difference in auxin level was found between *agb1*-2 and wild type roots or between control and glucose-treated roots ($P > 0.05$). This indicates that total auxin *per se* is not important for altering RSA and that auxin distribution and/or auxin signaling is glucose and AGB1 dependent.

AGB1 Mediated Glucose Sensing Converge on PIN2 Protein Localization

The polarity of the auxin transport facilitator PIN2 is regulated by auxin, ethylene, cytokinin, strigolactone, and light (Habets and Offringa, 2014; Koltai, 2014; Luschnig and Vert, 2014). These signals regulates PIN action in the root (Wisniewska et al., 2006; Ruzicka et al., 2007; Laxmi et al., 2008; Ruzicka et al., 2009; Ding et al., 2011; Shinohara et al., 2013). We previously reported that sugar signaling shows dose and duration reciprocity (Fu et al., 2014). We tested if changes in sugar levels affect polar auxin transport via G proteins by controlling PIN2-GFP protein level/localization expressed under the control of the native PIN2 promoter (**Figure 6**). Glucose (3%) caused little or no detectable change in PIN2-GFP localization ($P > 0.05$) in the wild type root (*cf.* **Figures 6B,D**, quantitation in **Figure 6A**). In the *agb1*-2 roots, the internal PIN2-GFP level was higher compared to Col-0 (*cf.* **Figures 6B,C**), consistent with our previously reported increase in basipetal auxin transport in *agb1*-2 (Mudgil et al., 2009). In contrast to the lack of an effect in wild type, the 3% glucose

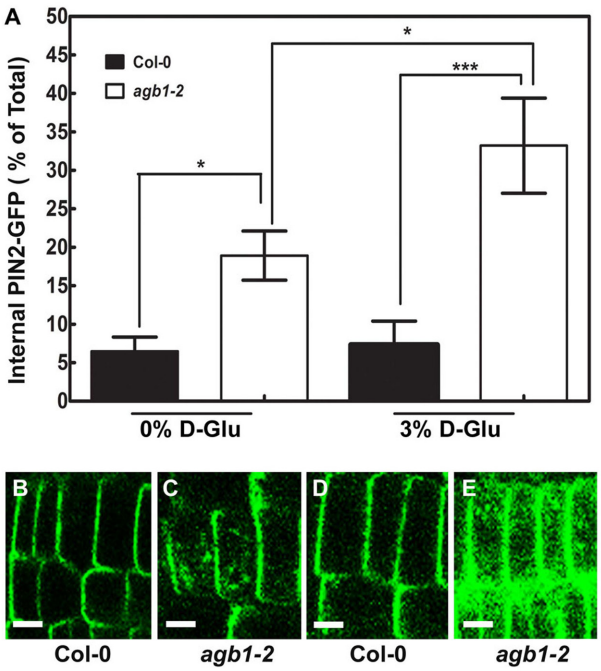

FIGURE 6 | Altered subcellular localization of PIN2-GFP in the *agb1*-2 mutant. (A) Quantitation of PIN2-GFP subcellular localization in Col-0 and *agb1*-2 root tip cells grown with or without supplemental 3% glucose. Fluorescence intensities in multiple seedlings were measured using ImageJ software and compared using Student's *t*-test, shown as asterisks:*$P < 0.05$; ***$P < 0.0005$. PIN2-GFP localization in Col-0 root tip cells **(B,D)** grown without (–) or with (+) supplemental 3% glucose, respectively. **(C,E)** Amount of PIN2-GFP internalized in *agb1*-2 root tip cells grown without (–) or with (+) supplemental 3% glucose, respectively. Scale bars represent 5 μm. In order to compare directly these genotypes, *PIN2-GFP/agb1*-2 lines were obtained by crossing *agb1-2* plants into the *PIN2-GFP* line shown in panels B and D. This experiment was repeated three times and reproducible *PIN2-GFP* localization pattern was observed upon glucose treatment.

treatment in the *agb1*-2 mutant further increased the amount of internalized PIN2-GFP which appeared as a punctate pattern in these cells ($P < 0.05$) (*cf.* **Figures 6C,E**) indicating AGB1 attenuates sugar-mediated PIN2-GFP localization/ recycling.

Sugar-Mediated Auxin Signaling in the AGB1 Mutant

We previously showed that a set of auxin-regulated genes are misregulated in the *agb1*-2 mutant, including genes known to be important for lateral root development (Ullah et al., 2003). Therefore, RNA-Seq was used to test the hypothesis that AGB1 mediates glucose regulation of gene expression in the 1-mm apical root tip. Triplicate libraries of each control and glucose treated roots were prepared, bar-coded and subjected to sequencing resulting in at least 40 million and as high as 65 million reads for each library. Such high coverage enabled us to have confidence in low expressed genes while maintaining a stringent FDR setting of 5% (FDR = 0.05). There were 978 unique elements (**Figure 7A**). Glucose-repressed genes were similar in the two genotypes. There were 264 genes repressed by glucose

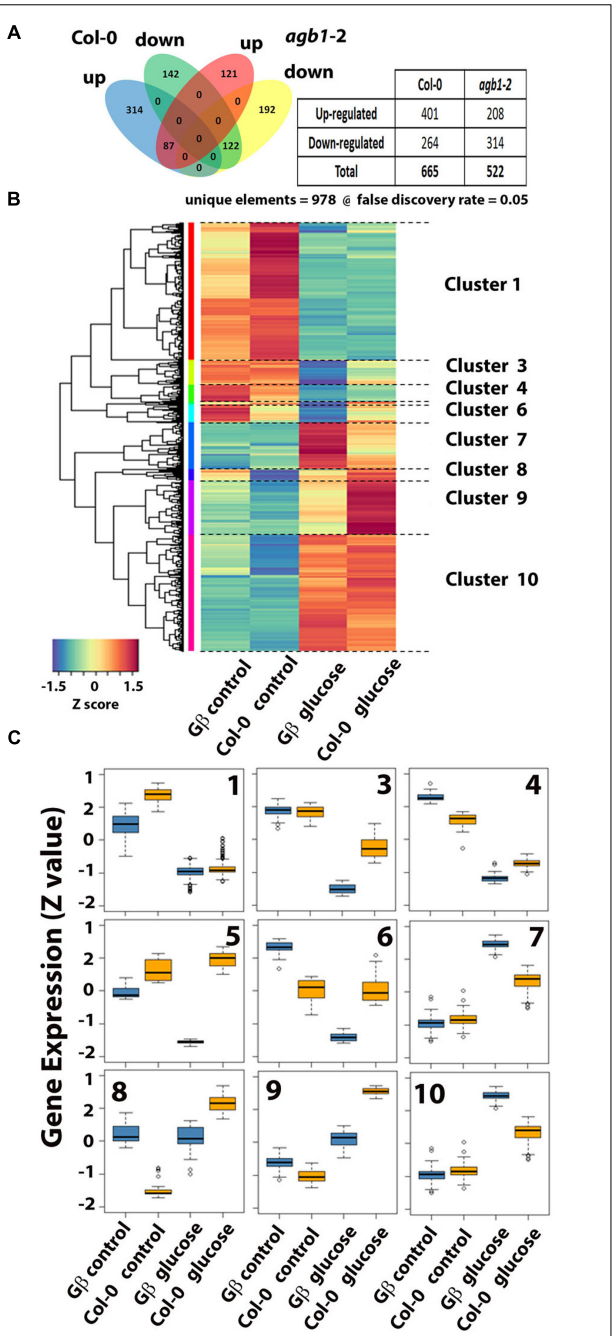

FIGURE 7 | Glucose-induced gene expression in the 1-mm root tips of wild type and *agb1*-2 mutant. Five-day old, etiolated seedlings were treated with glucose for 4 h and the apical 1-mm of roots was harvested for RNA profiling as described in Materials and Methods. **(A)** Venn diagram quantitating genes that were differentially expressed in the two genotypes. The table inset summarizes the number of genes scored as up or down regulated in each genotype. **(B)** Cluster analysis of the genes that have altered expression displayed as a heat map. Ten distinct clusters were formed. Clusters 2 and 5 had too few genes to label. **(C)** The expression profile of each cluster is shown as a box plot. The top of the rectangle indicates the third quartile, the horizontal line indicates the median, and the bottom of the rectangle indicates the first quartile. The vertical line from the top indicates the maximum value, and the other vertical line extending from the bottom indicates the minimum value.

in Col-0 and 314 in *agb1*-2. The genotypes shared 122 of these genes and the remaining are exclusive of each genotype (i.e., 142 in Col-0 and 192 in *agb1*-2). A greater difference between genotypes was observed for glucose-induced genes. There were 401 genes that increased expression upon glucose treatment in wild type. There were 208 up-regulated by glucose in *agb1*-2 with only 87 of them shared by Col-0 and the remaining 121 were statistically significant in *agb1*-2 only. This analysis indicated that AGB1 plays a direct or indirect role in glucose-regulated gene expression.

Gene Ontology analysis revealed that genes repressed by glucose independently of G signaling are related to metabolism of several types, including sucrose, organic acids, and amino acids (**Supplementary Table S1**). Genes with increased expression by glucose independently of G signaling are primarily related to cell wall processes. Genes for which AGB1 is required for proper expression are related to responses to stress. Genes with expression that was repressed compared to wild type were predominantly related to stress responsiveness. The GO analysis indicated that AGB1 is positively regulating genes that are involved in biotic stress, both innate immunity and effector-induced defense (**Supplementary Table S1**, underlined annotations, 23 of 37 genes with $P < 0.003$). This is consistent with the hyper susceptibility of the *agb1* mutants to *Pseudomonas*, necrotrophic and hemibiotrophic fungi, and oomycetes (Urano et al., 2013). AGB1 negatively regulates genes involved in photon capture (**Supplementary Table S1**, underlined annotations, 8 of 24 genes with $P < 0.002$) and genes related to biotic stress (10 of the remaining 16, $P < 0.002$). While it is known that *agb1* mutants have altered sensitivity to several abiotic stresses (Urano et al., 2013), a role for AGB1 in photosynthesis has not previously been reported. AGB1 control of photosynthesis genes seems relevant but it is surprising for these genes to be altered in the root tip.

Annotations provide a generalized view of pathway function; therefore we used "genotype by treatment" cluster analysis of individual gene responses and presented it as a heat map (**Figure 7B**). We organized the 978 differentially expressed genes in our experiment into 10 clusters, with one cluster having only 2 genes (Cluster #2). The distribution of expression level for the individual cluster is compared across treatment and genotype. The PlantGSEA (Yi et al., 2013) server returned informative function information for the gene cluster confirming the analysis performed on the 978 unique elements (**Figure 7A**). Clusters 4 and 6 share overlap with gene sets involved in plant defense, cluster #1 overlaps with genes involved in sugar signaling and metabolism, cluster #3 with plant hormone pathways, cluster #7 with protein folding, and cluster #10 with light and ROS responses.

The hypothesis is that glucose acts on auxin signaling output through apical auxin signaling, therefore the Aux/IAA gene family was inspected closely for differences in glucose regulation between Col-0 and the *agb1*-2 mutant (**Supplementary Figure S3**). Among the *IAA* genes, some were regulated by glucose and all of these in the *agb1* mutant were comparable in expression to wild type. While *IAA4, IAA5, IAA6* appear to be different from wild type, the differences were not supported statistically. Although one possible difference between genotypes may be with *IAA34*. In the control condition, *IAA34* was ∼3 fold repressed in *agb1*-2 relative to Col-0. While the FDR is not significant (FDR = 1), the p-value is 0.054991, supporting a possible trend, albeit weak. *IAA34* is one of two *IAA* genes encoding IAA proteins lacking the destruction box, DII. No functional information on IAA34 is available at this time to enable speculation on whether or not it could be a component of glucose-induced, AGB1-affected lateral root formation. On the other hand, *IAA19*, which is known to play a role in lateral root development and shown here to be glucose induced does not require AGB1. Therefore, we conclude that glucose induction of the IAA gene family members is not a prominent part of the AGB1 mechanism.

Because members of the recently described central regulator PHYTOCHROME-INTERACTING FACTOR (PIF) sense changes in sugar levels and regulate the RSA (Salisbury et al., 2007; Kircher and Schopfer, 2012; Lilley et al., 2012), we examined the expression of the 7 PIF genes but found these all to be poorly expressed in root tips (RPKM < 1.0) and there were no differences between wild type and *agb1*-2.

At least 12 well-expressed genes with profound difference in glucose responsiveness in the *agb1*-2 mutant relative to wild type were identified (**Figure 8**). Many other genes were noted but did not meet the threshold of expression (RPKM > 1.0). Two genes that were completely repressed in the *agb1*-2 mutant are at loci At1g53480 and At3g01345 (**Figure 8**). At3g01345 encodes a putative *O*-glycosyl hydrolase. This is interesting because AGB1 is required for the expression of the *0*-glycosyl transferase, *TBL26* (Grigston et al., 2008), although the significance of glycosyl modification in AGB1-modulated lateral root formation is not presently obvious. At1g53480 encodes MRD1 (*MTO*1 responding down). This gene is down-regulated in the *mto1*-1 mutant that over-accumulates soluble methionine. AGB1 interacts with ARD1 in the methionine salvage pathway in *Arabidopsis* (Friedman et al., 2011), but again, the significance of this connection is not obvious. Among the other profoundly misregulated genes (**Figure 8**), At1g66160 physically interacts with AGB1 (Kobayashi et al., 2012). This gene encodes a U-box ligase. Both AGB1 and this E3 ligase play roles in innate immunity (González-Lamothe et al., 2006; Gilroy et al., 2011; Yaeno et al., 2011; Liu et al., 2013; Lorek et al., 2013; Torres et al., 2013), suggesting convergence between root development and defense.

Summary

While it is accepted that the root system is a sink for photosynthesis-fixed sugars (Freixes et al., 2002; Macgregor et al., 2008), it was not known if these sugars act as signaling elements to control the architecture of the root. We showed that RSA is genetically encoded and that one of these genes points to signaling mediated by the heterotrimeric G protein pathway. We established that G proteins sense the dose of the sugar signal/carbon nutrient status in roots (which operates under dose and duration constraints) and positively affect RSA (**Figures 1** and **2**).

We found higher levels of glucose, fructose, and sucrose in the absence of the G protein beta subunit, the *agb1* mutant

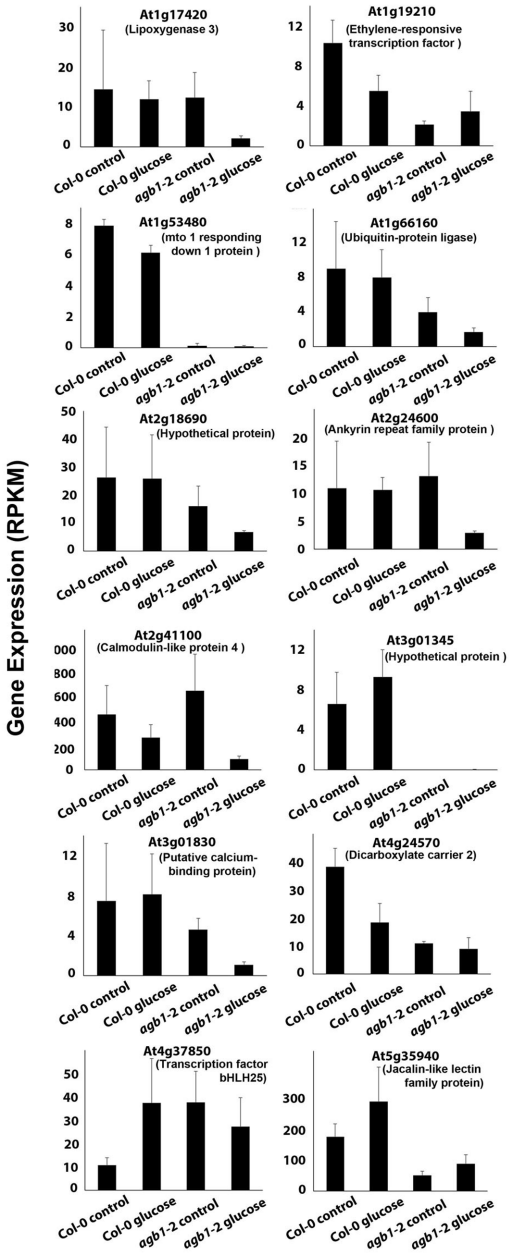

FIGURE 8 | Glucose regulation of genes that differ between wild type and *agb1*-2 root tips. Genes that are differentially expressed (FDR $\leq$ 0.05) between the two genotypes in at least one of the conditions (control and glucose treatment) are shown. Normalized gene expression is shown as reads per kb per million reads (RPKM).

root. It is possible that sugar metabolism is altered in the *agb1*-2 mutant. Considering the velocity at which sugars arrive from the mesophyll to the root system (**Figure 4**), it is plausible that roots monitor photosynthesis with a resolution of minutes to hours. This is certainly the case for the shoot although monitoring occurs with a much longer time scale (Mason et al., 2014). Mason and coworkers showed that sugars are directly responsible for release of axillary bud dormancy. Because AGB1 acts like a negative regulator of lateral root density, G proteins may dampen the fluctuation of sugars and in that sense is part of a fluctuation sensor.

We established that G proteins mediate the glucose effect on RSA (**Figure 2**), through auxin patterning and transcriptional control (**Figure 6**, **7**, and **8**). Both HXK1 and RGS1 are involved in this glucose response but function differently (**Figure 3**). AGB1 plays an important role as a sensor component of glucose or carbon nutrient status in roots and modulates root growth. The steady-state levels of soluble sugar are higher in the absence of AGB1, indicating positive regulation within this pathway. Because glucose affects the posttranslational stability of N-MYC DOWN REGULATED LIKE 1 (NDL1) protein (Mudgil et al., 2009, 2013) in an AGB1-dependent manner, NDL1 stability may be part of this proposed feedback mechanism.

This work raises the possibility that fixed sugars derived through photosynthesis act as signals that regulate the RSA and we speculate that the roots may also signal back. This feedback from roots to shoots already has been proposed in a different signaling pathway in which AGB1 is also involved. Applied methyl jasmonate (MeJA) increased the allocation of ^{11}C-labeled photosynthate to sink leaves and roots (Ferrieri et al., 2013). Because chilling the roots to 5°C inhibited the MeJA-induced increase allocation to sink leaves, feedback signaling from the roots was proposed. While AGB1 was not shown to be directly involved in this particular MeJA pathway, it was shown that AGB1 is essential for MeJA signaling in fungal resistance (Llorente et al., 2005; Trusov et al., 2007, 2009).

AUTHOR CONTRIBUTIONS

YM designed and conducted experiments, analyzed data, wrote and edited the manuscript (final root assays, prepared root tips for cDNA libraries and auxin quantification, PIN, DR-5-GUS localization); AK edited the manuscript and conducted experiments (PET assay, γ quantitation, sugar analyses); PT edited the manuscript and performed all the bioinformatics analyses; KJ performed experiments (preliminary root growth assay); MT-O analyzed data (PIN2 DATA analysis); AJ designed and performed experiments, analyzed data, wrote the manuscript, and managed the project.

FUNDING

Work in the Jones Lab is supported by grants from the NIGMS (R01GM065989), DOE (DE-FG02-05er15671), and NSF (MCB-0723515, MCB-1158054, and MCB-0718202). The Division of Chemical Sciences, Geosciences, and Biosciences, Office of Basic Energy Sciences of the US Department of Energy funded the majority of the work in this study. YM was supported by DBT CREST award (2011–2012) from the Government of INDIA and Delhi University R&D and DU-DST PURSE grant. PT is supported by The Pew Latin American Fellows Program in the Biomedical Sciences.

ACKNOWLEDGMENTS

We thank Jerry Cohen, Department of Horticultural Science and Microbial and Plant Genomics Institute at the University of Minnesota, for facilitating the microanalyses of auxin. The auxin measurements were conducted by Molly Kreiser and Jayanti Suresh. We thank Nguyen Phan and Alejandro Colaneri for technical assistance.

SUPPLEMENTARY MATERIAL

The Supplementary Material for this article can be found online at: http://journal.frontiersin.org/article/10.3389/fpls.2016.01255

FIGURE S1 | G protein sensing glucose levels is specific and not shown by osmotic control mannitol (A) Primary root length (B) Lateral root number (C) Lateral root density of the various G protein mutants genotypes used in Figure 2. Glucose was replaced with the corresponding concentrations of mannitol. Experiments were performed three times with10–15 seedlings used for each genotype. MIXED ANOVA analysis followed by box cox test (Box and Cox, 1964) indicated that there was no significant difference between genotypes on different concentrations of mannitol ($P > 0.1$).

FIGURE S2 | Auxin measurements in the whole root of *agb1-2* and Col-0 in the presence and absence of 2% D-glucose. Physical quantitation was performed by mass spectrometry as described in the Materials and Methods. Total free IAA is displayed as ng per g fresh weight of root tissue in whisker plots. Horizontal lines = means, bars represent STD. Symbols are the individual measurements. ANOVA analysis indicated that all values are not statistically different ($P < 0.05$).

FIGURE S3 | *IAA* genes expression in wild type and *agb1-2* mutant without (control) or with glucose treatment in 1/2 MS liquid without sugar. Expression profile of 28 out of 29 analyzed *IAA* genes showed no difference in expression upon glucose treatment in *agb1* mutant background compared to wild type. Minor visible differences were not supported statistically. Only one *IAA, IAA34* showed ∼3 fold repression in *agb1*-2 compared to Col-0 upon glucose treatment. While the FDR is not significant (FDR = 1), the *P*-value is 0.054991.

TABLE S1 | Gene Ontology (GO) Analysis Genotype by treatment

REFERENCES

Albrechtova, J., Kubinova, Z., Soukup, A., and Janacek, J. (2014). Image analysis: basic procedures for description of plant structures. *Methods Mol. Biol.* 1080, 67–76. doi: 10.1007/978-1-62703-643-6_5

Anders, S., Pyl, P., and Huber, W. (2014). HTSeq-A Python framework to work with high-throughput sequencing data. *Bioinformatics* 31, 166–169. doi: 10.1093/bioinformatics/btu638

Babst, B. A., Karve, A. A., and Judt, T. (2013). Radio-metabolite analysis of carbon-11 biochemical partitioning to non-structural carbohydrates for integrated metabolism and transport studies. *Plant Cell Physiol.* 54, 1016–1025. doi: 10.1093/pcp/pct045

Barbier, F. F., Lunn, J. E., and Beveridge, C. A. (2015). Ready, steady, go! A sugar hit starts the race to shoot branching. *Curr. Opin. Plant Biol.* 25, 39–45. doi: 10.1016/j.pbi.2015.04.004

Benková, E., Michniewicz, M., Sauer, M., Teichmann, T., Seifertová, D., Jürgens, G., et al. (2003). Local, efflux-dependent auxin gradients as a common module for plant organ formation. *Cell* 115, 591–602. doi: 10.1016/S0092-8674(03)00924-3

Boerjan, W., Cervera, M. T., Delarue, M., Beeckman, T., Dewitte, W., Bellini, C., et al. (1995). Superroot, a recessive mutation in *Arabidopsis*, confers auxin overproduction. *Plant Cell* 7, 1405–1419. doi: 10.2307/3870131

Booker, K. S., Schwarz, J., Garrett, M. B., and Jones, A. M. (2010). Glucose attenuation of auxin-mediated bimodality in lateral root formation is partly coupled by the heterotrimeric G protein complex. *PLoS ONE* 5:e12833. doi: 10.1371/journal.pone.0012833

Box, G., and Cox, D. (1964). An analysis of transformations. *J. R. Stat. Soc. Series B* 26, 211–252.

Bradford, W., Buckholz, A., Morton, J., Price, C., Jones, A. M., and Urano, D. (2013). Eukaryotic G protein signaling evolved to require G protein-coupled receptors for activation. *Sci. Signal.* 6:ra37. doi: 10.1126/scisignal.2003768

Chaparro, J. M., Badri, D. V., and Vivanco, J. M. (2014). Rhizosphere microbiome assemblage is affected by plant development. *ISME J.* 8, 790–803. doi: 10.1038/ismej.2013.196

Chen, J. G., Gao, Y., and Jones, A. M. (2006). Differential roles of *Arabidopsis* heterotrimeric G-protein subunits in modulating cell division in roots. *Plant Physiol.* 141, 887–897. doi: 10.1104/pp.106.079202

Chen, J. G., and Jones, A. M. (2004). AtRGS1 function in *Arabidopsis thaliana*. *Methods Enzymol.* 389, 338–350. doi: 10.1016/S0076-6879(04)89020-7

Cho, Y. H., Yoo, S. D., and Sheen, J. (2006). Regulatory functions of nuclear hexokinase1 complex in glucose signaling. *Cell* 127, 579–589. doi: 10.1016/j.cell.2006.09.028

Cho, Y. H., Yoo, S. D., and Sheen, J. (2007). Glucose signaling through nuclear hexokinase1 complex in *Arabidopsis*. *Plant Signal. Behav.* 2, 123–124. doi: 10.4161/psb.2.2.3894

Colaneri, A. C., and Jones, A. M. (2014). The wiring diagram for plant G signaling. *Curr. Opin. Plant Biol.* 22, 56–64. doi: 10.1016/j.pbi.2014.09.004

Crookshanks, M., Taylor, G., and Dolan, L. (1998). A model system to study the effects of elevated CO_2 on the developmental physiology of roots: the use of *Arabidopsis thaliana*. *J. Exp. Bot.* 49, 593–597. doi: 10.1093/jxb/49.320.593

Ding, Z., Galvan-Ampudia, C. S., Demarsy, E., Langowski, L., Kleine-Vehn, J., Fan, Y., et al. (2011). Light-mediated polarization of the PIN3 auxin transporter for the phototropic response in *Arabidopsis*. *Nat. Cell Biol.* 13, 447–452. doi: 10.1038/ncb2208

Dubrovsky, J. G., Gambetta, G. A., Hernandez-Barrera, A., Shishkova, S., and Gonzalez, I. (2006). Lateral root initiation in *Arabidopsis*: developmental window, spatial patterning, density and predictability. *Ann. Bot.* 97, 903–915. doi: 10.1093/aob/mcj604

Dubrovsky, J. G., Napsucialy-Mendivil, S., Duclercq, J., Cheng, Y., Shishkova, S., Ivanchenko, M. G., et al. (2011). Auxin minimum defines a developmental window for lateral root initiation. *New Phytol.* 191, 970–983. doi: 10.1111/j.1469-8137.2011.03757.x

Dubrovsky, J. G., Sauer, M., Napsucialy-Mendivil, S., Ivanchenko, M. G., Friml, J., Shishkova, S., et al. (2008). Auxin acts as a local morphogenetic trigger to specify lateral root founder cells. *Proc. Natl. Acad. Sci. U.S.A.* 105, 8790–8794. doi: 10.1073/pnas.0712307105

Ferrieri, A. P., Agtuca, B., Appel, H. M., Ferrieri, R. A., and Schultz, J. C. (2013). Temporal changes in allocation and partitioning of new carbon as 11C elicited by simulated herbivory suggest that roots shape aboveground responses in *Arabidopsis*. *Plant Physiol.* 161, 692–704. doi: 10.1104/pp.112.208868

Ferrieri, R. A., and Wolf, A. P. (1983). The chemistry of positron emitting nucleogenic atoms with regard to preparation of labeled compounds of practical utility. *Radiochim. Acta* 344, 69–83.

Freixes, S., Thibaud, M. C., Tardieu, F., and Muller, B. (2002). Root elongation and branching is related to local hexose concentration in *Arabidopsis thaliana* seedlings. *Plant Cell Environ.* 25, 1357–1366. doi: 10.1046/j.1365-3040.2002.00912.x

Friedman, E. J., Wang, H. X., Perovic, I., Deshpande, A., Pochapsky, T. C., Temple, B. R. S., et al. (2011). ACI-REDUCTONE DIOXYGENASE 1 (ARD1) is an effector of the heterotrimeric G protein beta subunit in *Arabidopsis*. *J. Biol. Chem.* 286, 30107–30118. doi: 10.1074/jbc.M111.227256

Friml, J., Vieten, A., Sauer, M., Weijers, D., Schwarz, H., Hamann, T., et al. (2003). Efflux-dependent auxin gradients establish the apical-basal axis of *Arabidopsis*. *Nature* 426, 147–153. doi: 10.1038/nature02085

Fu, Y., Lim, S., Urano, D., Tunc-Ozdemir, M., Phan, N., Elston, T., et al. (2014). Reciprocal encoding of signal intensity and duration in a glucose-sensing circuit. *Cell* 156, 1084–1096. doi: 10.1016/j.cell.2014.01.013

Giehl, R. F. H., Gruber, B. D., and von Wirén, N. (2014). It's time to make changes: modulation of root system architecture by nutrient signals. *J. Exp. Bot.* 65, 769–778. doi: 10.1093/jxb/ert421

Gilroy, E. M., Taylor, R. M., Hein, I., Boevink, P., Sadanandom, A., and Birch, P. R. J. (2011). CMPG1-dependent cell death follows perception of diverse pathogen elicitors at the host plasma membrane and is suppressed by *Phytophthora infestans* RXLR effector AVR3a. *New Phytol.* 190, 653–666. doi: 10.1111/j.1469-8137.2011.03643.x

González-Lamothe, R., Tsitsigiannis, D. I., Ludwig, A. A., Panicot, M., Shirasu, K., and Jones, J. D. G. (2006). The U-Box protein CMPG1 is required for efficient activation of defense mechanisms triggered by multiple resistance genes in tobacco and tomato. *Plant Cell* 18, 1067–1083. doi: 10.1105/tpc.106.040998

Grigston, J. C., Osuna, D., Scheible, W. R., Liu, C., Stitt, M., and Jones, A. M. (2008). D-Glucose sensing by a plasma membrane regulator of G signaling protein, AtRGS1. *FEBS Lett.* 582, 3577–3584. doi: 10.1016/j.febslet.2008.08.038

Gupta, A., Singh, M., and Laxmi, A. (2015). Interaction between Glucose and Brassinosteroid during regulation of lateral root development in *Arabidopsis*. *Plant Physiol.* 168, 307–320. doi: 10.1104/pp.114.256313

Gupta, A., Singh, M., Mishra, B. S., Kushwah, S., and Laxmi, A. (2009). Role of glucose in spatial distribution of auxin regulated genes. *Plant Signal. Behav.* 4, 862–863. doi: 10.4161/psb.4.9.9421

Habets, M. E. J., and Offringa, R. (2014). PIN-driven polar auxin transport in plant developmental plasticity: a key target for environmental and endogenous signals. *New Phytol.* 203, 362–377. doi: 10.1111/nph.12831

Hachiya, T., Sugiura, D., Kojima, M., Sato, S., Yanagisawa, S., Sakakibara, H., et al. (2014). High CO_2 triggers preferential root growth of *Arabidopsis thaliana* via two distinct systems under low pH and low N stresses. *Plant Cell Physiol.* 55, 269–280. doi: 10.1093/pcp/pcu001

Hanson, J., and Smeekens, S. (2009). Sugar perception and signaling–an update. *Curr. Opin. Plant Biol.* 12, 562–567. doi: 10.1016/j.pbi.2009.07.014

Huang, J. P., Tunc-Ozdemir, M., Chang, Y., and Jones, A. M. (2015). Cooperative control between AtRGS1 and AtHXK1 in a WD40-repeat protein pathway in *Arabidopsis thaliana*. *Front. Plant Sci.* 6:851. doi: 10.3389/fpls.2015.00851

Karve, A. A., Alexoff, D. A., Kim, D., Schuller, M. J., Ferrieri, R. A., and Babst, B. A. (2015). In vivo quantitative imaging of photoassimilate transport dynamics and allocation in large plants using a commercial positron emission tomography (PET) scanner. *BMC Plant Biol.* 15:273. doi: 10.1186/s12870-015-0658-3

Kircher, S., and Schopfer, P. (2012). Photosynthetic sucrose acts as cotyledon-derived long-distance signal to control root growth during early seedling development in *Arabidopsis*. *Proc. Natl. Acad. Sci. U.S.A.* 109, 11217–11221. doi: 10.1073/pnas.1203746109

Klopffleisch, K., Phan, N., Augustin, K., Bayne, R. S., Booker, K. S., Botella, J. R., et al. (2011). *Arabidopsis* G-protein interactome reveals connections to cell wall carbohydrates and morphogenesis. *Mol. Syst. Biol.* 7:532. doi: 10.1038/msb.2011.66

Kobayashi, S., Tsugama, D., Liu, S., and Takano, T. (2012). A U-Box E3 ubiquitin ligase, PUB20, interacts with the *Arabidopsis* G-Protein β subunit, AGB1. *PLoS ONE* 7:e49207. doi: 10.1371/journal.pone.0049207

Koltai, H. (2014). Receptors, repressors, PINs: a playground for strigolactone signaling. *Trends Plant Sci.* 19, 727–733. doi: 10.1016/j.tplants.2014.06.008

Laxmi, A., Pan, J., Morsy, M., and Chen, R. (2008). Light plays an essential role in intracellular distribution of auxin efflux carrier PIN2 in *Arabidopsis thaliana*. *PLoS ONE* 3:e1510. doi: 10.1371/journal.pone.0001510

Lee-Ho, E., Walton, L. J., Reid, D. M., Yeung, E. C., and Kurepin, L. V. (2007). Effects of elevated carbon dioxide and sucrose concentrations on *Arabidopsis thaliana* root architecture and anatomy. *Can. J. Bot.* 85, 324–330. doi: 10.1139/b07-009

Lilley, J. L., Gee, C. W., Sairanen, I., Ljung, K., and Nemhauser, J. L. (2012). An endogenous carbon-sensing pathway triggers increased auxin flux and hypocotyl elongation. *Plant Physiol.* 160, 2261–2270. doi: 10.1104/pp.112.205575

Liu, J., Ding, P., Sun, T., Nitta, Y., Dong, O., Huang, X., et al. (2013). Heterotrimeric G proteins serve as a converging point in plant defense signaling activated by multiple receptor-like kinases. *Plant Physiol.* 161, 2146–2158. doi: 10.1104/pp.112.212431

Liu, T. Y., Chang, C. Y., and Chiou, T. J. (2009). The long-distance signaling of mineral macronutrients. *Curr. Opin. Plant Biol.* 12, 312–319. doi: 10.1016/j.pbi.2009.04.004

Liu, X., Hegeman, A., Gardner, G., and Cohen, J. (2012). Protocol: high-throughput and quantitative assays of auxin and auxin precursors from minute tissue samples. *Plant Methods* 8:31. doi: 10.1186/1746-4811-8-31

Llorente, F., Alonso-Blanco, C., Sanchez-Rodriguez, C., Jorda, L., and Molina, A. (2005). ERECTA receptor-like kinase and heterotrimeric G protein from *Arabidopsis* are required for resistance to the necrotrophic fungus *Plectosphaerella cucumerina*. *Plant J.* 43, 165–180. doi: 10.1111/j.1365-313X.2005.02440.x

Lorek, J., Griebel, T., Jones, A., Kuhn, H., and Panstruga, R. (2013). The role of *Arabidopsis* heterotrimeric G-protein subunits in MLO2 function and MAMP-triggered immunity. *Mol. Plant Microbe Interact.* 26, 991–1003. doi: 10.1094/MPMI-03-13-0077-R

Luschnig, C., and Vert, G. (2014). The dynamics of plant plasma membrane proteins: PINs and beyond. *Development* 141, 2924–2938. doi: 10.1242/dev.103424

Macgregor, D. R., Deak, K. I., Ingram, P. A., and Malamy, J. E. (2008). Root system architecture in *Arabidopsis* grown in culture is regulated by sucrose uptake in the aerial tissues. *Plant Cell* 20, 2643–2660. doi: 10.1105/tpc.107.055475

Maere, S., Heymans, K., and Kuiper, M. (2005). BiNGO: a Cytoscape plugin to assess overrepresentation of gene ontology categories in biological networks. *Bioinformatics* 21, 3448–3449. doi: 10.1093/bioinformatics/bti551

Mason, M. G., Ross, J. J., Babst, B. A., Wienclaw, B. N., and Beveridge, C. A. (2014). Sugar demand, not auxin, is the initial regulator of apical dominance. *Proc. Natl. Acad. Sci. U.S.A.* 111, 6092–6097. doi: 10.1073/pnas.1322045111

Mishra, B. S., Singh, M., Aggrawal, P., and Laxmi, A. (2009). Glucose and auxin signaling interaction in controlling *Arabidopsis thaliana* seedlings root growth and development. *PLoS ONE* 4:e4502. doi: 10.1371/journal.pone.0004502

Moghaddam, M. R., and den Ende, W. V. (2013). Sugars, the clock and transition to flowering. *Front. Plant Sci.* 4:22. doi: 10.3389/fpls.2013.00022

Moreno-Risueno, M. A., Van Norman, J. M., Moreno, A., Zhang, J., Ahnert, S. E., and Benfey, P. N. (2010). Oscillating gene expression determines competence for periodic *Arabidopsis* root branching. *Science* 329, 1306–1311. doi: 10.1126/science.1191937

Mudgil, Y., Ghawana, S., and Jones, A. M. (2013). N-MYC down-regulated-like proteins regulate meristem initiation by modulating auxin transport and MAX2 expression. *PLoS ONE* 8:e77863. doi: 10.1371/journal.pone.0077863

Mudgil, Y., Uhrig, J. F., Zhou, J., Temple, B., Jiang, K., and Jones, A. M. (2009). *Arabidopsis* N-MYC DOWNREGULATED-LIKE1, a positive regulator of auxin transport in a G protein-mediated pathway. *Plant Cell* 21, 3591–3609. doi: 10.1105/tpc.109.065557

Phan, N., Urano, D., Srba, M., Fischer, L., and Jones, A. (2012). Sugar-induced endocytosis of plant 7TM-RGS proteins. *Plant Signal. Behav.* 8, e22814. doi: 10.4161/psb.22814

Robinson, M. D., McCarthy, D. J., and Smyth, G. K. (2010). edgeR: a Bioconductor package for differential expression analysis of digital gene expression data. *Bioinformatics* 26, 139–140. doi: 10.1093/bioinformatics/btp616

Rogers, H. H., Peterson, C. M., McCrimmon, J. N., and Cure, J. D. (2006). Response of plant roots to elevated atmospheric carbon dioxide. *Plant Cell Environ.* 15, 749–752. doi: 10.1111/j.1365-3040.1992.tb01018.x

Rolland, F., Baena-Gonzalez, E., and Sheen, J. (2006). Sugar sensing and signaling in plants: conserved and novel mechanisms. *Annu. Rev. Plant Biol.* 57, 675–709. doi: 10.1146/annurev.arplant.57.032905.105441

Roycewicz, P., and Malamy, J. E. (2012). Dissecting the effects of nitrate, sucrose and osmotic potential on *Arabidopsis* root and shoot system growth in laboratory assays. *Philos. Trans. R. Soc. Lond. B Biol. Sci.* 367, 1489–1500. doi: 10.1098/rstb.2011.0230

Ruan, Y. L. (2014). Sucrose metabolism: gateway to diverse carbon use and sugar signaling. *Annu. Rev. Plant Biol.* 65, 33–67. doi: 10.1146/annurev-arplant-050213-040251

Ruzicka, K., Ljung, K., Vanneste, S., Podhorska, R., Beeckman, T., Friml, J., et al. (2007). Ethylene regulates root growth through effects on auxin biosynthesis and transport-dependent auxin distribution. *Plant Cell* 19, 2197–2212. doi: 10.1105/tpc.107.052126

Ruzicka, K., Simaskova, M., Duclercq, J., Petrasek, J., Zazimalova, E., Simon, S., et al. (2009). Cytokinin regulates root meristem activity via modulation of the polar auxin transport. *Proc. Natl. Acad. Sci. U.S.A.* 106, 4284–4289. doi: 10.1073/pnas.0900060106

Sairanen, I., Novak, O., Pencik, A., Ikeda, Y., Jones, B., Sandberg, G., et al. (2012). Soluble carbohydrates regulate auxin biosynthesis via PIF proteins in *Arabidopsis*. *Plant Cell* 24, 4907–4916. doi: 10.1105/tpc.112.104794

Salisbury, F. J., Hall, A., Grierson, C. S., and Halliday, K. J. (2007). Phytochrome coordinates *Arabidopsis* shoot and root development. *Plant J.* 50, 429–438. doi: 10.1111/j.1365-313X.2007.03059.x

Sauer, M., and Friml, J. (2011). Fleeting hormone cues get stabilized for plant organogenesis. *Mol. Syst. Biol.* 7, 507–507. doi: 10.1038/msb.2011.45

Shinohara, N., Taylor, C., and Leyser, O. (2013). Strigolactone can promote or inhibit shoot branching by triggering rapid depletion of the auxin efflux protein PIN1 from the plasma membrane. *PLoS Biol.* 11:e1001474. doi: 10.1371/journal.pbio.1001474

Smeekens, S., Ma, J., Hanson, J., and Rolland, F. (2010). Sugar signals and molecular networks controlling plant growth. *Curr. Opin. Plant Biol.* 13, 274–279. doi: 10.1016/j.pbi.2009.12.002

Smith, A. R., Lukac, M., Bambrick, M., Miglietta, F., and Godbold, D. L. (2013). Tree species diversity interacts with elevated CO_2 to induce a greater root system response. *Glob. Chang. Biol.* 19, 217–228. doi: 10.1111/gcb.12039

Szymanowska-Pulka, J. (2013). Form matters: morphological aspects of lateral root development. *Ann. Bot.* 112, 1643–1654. doi: 10.1093/aob/mct231

Torres, M. A., Morales, J., Sánchez-Rodríguez, C., Molina, A., and Dangl, J. L. (2013). Functional interplay between *Arabidopsis* NADPH oxidases and heterotrimeric G protein. *Mol. Plant Microbe Interact.* 26, 686–694. doi: 10.1094/mpmi-10-12-0236-r

Trapnell, C., Pachter, L., and Salzberg, S. (2009). TopHat: discovering splice junctions with RNA-Seq. *Bioinformatics* 25, 1105–1111. doi: 10.1093/bioinformatics/btp120

Trusov, Y., Rookes, J. E., Tilbrook, K., Chakravorty, D., Mason, M. G., Anderson, D., et al. (2007). Heterotrimeric G protein gamma subunits provide functional selectivity in Gbetagamma dimer signaling in *Arabidopsis*. *Plant Cell* 19, 1235–1250. doi: 10.1105/tpc.107.050096

Trusov, Y., Sewelam, N., Rookes, J. E., Kunkel, M., Nowak, E., Schenk, P. M., et al. (2009). Heterotrimeric G proteins-mediated resistance to necrotrophic pathogens includes mechanisms independent of salicylic acid-, jasmonic acid/ethylene- and abscisic acid-mediated defense signaling. *Plant J.* 58, 69–81. doi: 10.1111/j.1365-313X.2008.03755.x

Ullah, H., Chen, J. G., Temple, B., Boyes, D. C., Alonso, J. M., Davis, K. R., et al. (2003). The beta-subunit of the *Arabidopsis* G protein negatively regulates auxin-induced cell division and affects multiple developmental processes. *Plant Cell* 15, 393–409. doi: 10.1105/tpc.006148

Urano, D., Chen, J.-G., Botella, J. R., and Jones, A. M. (2013). Heterotrimeric G protein signalling in the plant kingdom. *Open Biol.* 3:120186. doi: 10.1098/rsob.120186

Urano, D., Jones, J. C., Wang, H., Matthews, M., Bradford, W., Bennetzen, J. L., et al. (2012a). G protein activation without a GEF in the plant kingdom. *PLoS Genetics* 8:e1002756. doi: 10.1371/journal.pgen.1002756

Urano, D., Phan, N., Jones, J. C., Yang, J., Huang, J., Grigston, J., et al. (2012b). Endocytosis of the seven-transmembrane RGS1 protein activates G-protein-coupled signalling in *Arabidopsis*. *Nat. Cell Biol.* 14, 1079–1088. doi: 10.1038/ncb2568

Wang, L., and Ruan, Y.-L. (2013). Regulation of cell division and expansion by sugar and auxin signaling. *Front. Plant Sci.* 4:163. doi: 10.3389/fpls.2013.00163

Windt, C. W., Vergeldt, F. J., de Jager, P. A., and van As, H. (2006). MRI of long-distance water transport: a comparison of the phloem and xylem flow characteristics and dynamics in poplar, castor bean, tomato and tobacco. *Plant Cell Environ.* 29, 1715–1729. doi: 10.1111/j.1365-3040.2006.01544.x

Wisniewska, J., Xu, J., Seifertova, D., Brewer, P. B., Ruzicka, K., Blilou, I., et al. (2006). Polar PIN localization directs auxin flow in plants. *Science* 312:883. doi: 10.1126/science.1121356

Yaeno, T., Li, H., Chaparro-Garcia, A., Schornack, S., Koshiba, S., Watanabe, S., et al. (2011). Phosphatidylinositol monophosphate-binding interface in the oomycete RXLR effector AVR3a is required for its stability in host cells to modulate plant immunity. *Proc. Natl. Acad. Sci. U.S.A.* 108, 14682–14687. doi: 10.1073/pnas.1106002108

Yi, X., Du, Z., and Su, Z. (2013). PlantGSEA: a gene set enrichment analysis toolkit for plant community. *Nucleic Acids Res.* 41, W98–W103. doi: 10.1093/nar/gkt281

Conflict of Interest Statement: The authors declare that the research was conducted in the absence of any commercial or financial relationships that could be construed as a potential conflict of interest.

frontiers in Plant Science

ORIGINAL RESEARCH
published: 23 June 2016
doi: 10.3389/fpls.2016.00904

Contributions of Root WSC during Grain Filling in Wheat under Drought

Jingjuan Zhang[1], Bernard Dell[1], Wujun Ma[1], Rudy Vergauwen[2], Xinmin Zhang[1], Tina Oteri[3], Andrew Foreman[3], Damian Laird[3] and Wim Van den Ende[2]*

[1] School of Veterinary and Life Sciences, Murdoch University, Murdoch, WA, Australia, [2] Laboratory of Molecular Plant Biology, KU Leuven, Leuven, Belgium, [3] School of Engineering and Information Technology, Murdoch University, Murdoch, WA, Australia

As the first organ in plants to sense water-deficit in the soil, roots have important roles for improving crop adaption to water limited environments. Stem water soluble carbohydrates (WSC) are a major carbon source for grain filling under drought conditions. The contributions of root WSC during grain filling under drought has not been revealed. Wheat parental lines of Westonia, Kauz and their derived four double haploid (DH) lines, namely, DH 125, DH 139, DH 307, and DH 338 were used in a field drought experiment with four replications. Through measurements of the root and stem WSC components, and the associated enzyme activities during grain filling, we identified that the levels of root WSC and fructan were one third of the levels in stems. In particular, root glucose and 6-kestose levels were one third of the stem, while the root fructose and bifurcose level were almost half of the stem and sucrose level was two third of the stem. The accumulation and the degradation patterns of root fructan levels were similar to that in the stem, especially under drought. Correlations between root fructan levels and grain assimilation were highly significant, indicating that under terminal drought, root WSC represents a redistributed carbon source for grain filling rather than deep rooting. The significantly higher root sucrose levels under drought suggest that sucrose may act as a signal under drought stress. As compared with stem fructose levels, the earlier increased root fructose levels in DH 307, DH 139, and DH 338 provided agile response to drought stress. Our root results further confirmed that β-(2–6) linkages predominate in wheat with patterns of 6-kestose being closely correlated with overall fructan patterns. Further research will focus on the roles of 6-FEH during fructan remobilization in stems.

Keywords: 6-kestose, deep rooting, fructan remobilization, grain assimilation, osmotic adjustment, root water soluble carbohydrates (WSC), terminal drought stress

OPEN ACCESS

Edited by:
Janin Riedelsberger, University of Talca, Chile

Reviewed by:
Mingxiang Liang, Nanjing Agricultural University, China
Xiping Deng, Northwest A&F University, China

****Correspondence:***
Jingjuan Zhang
j.zhang@murdoch.edu.au

Specialty section:
This article was submitted to Plant Physiology, a section of the journal Frontiers in Plant Science

Received: *09 May 2016*
Accepted: *08 June 2016*
Published: *23 June 2016*

Citation:
Zhang J, Dell B, Ma W, Vergauwen R, Zhang X, Oteri T, Foreman A, Laird D and Van den Ende W (2016) Contributions of Root WSC during Grain Filling in Wheat under Drought. Front. Plant Sci. 7:904. doi: 10.3389/fpls.2016.00904

INTRODUCTION

Along with global warming, drought is considered to be one of the prime abiotic stresses in the world. For producing sustainable crop yield, drought tolerance is the most desirable trait for breeders. Drought tolerance can be defined in different ways, including drought avoidance, high water use efficiency and growth recovery following rewatering (Passioura, 2012).

In wheat, before flowering, stem, and roots are the major sinks (Xue et al., 2008; Paul and Lawlor, 2014). Plant survival during the drought conditions can be supported by osmotic adjustment. Most of the adjustment can usually be resulted by increases in concentration of common solutes,

including sugars, organic acids, amino acids, and inorganic ions (especially K^+). Some results show that dehydration tolerance can be promoted by osmotic adjustment, but this does not always lead to higher productivity (McCree and Richardson, 1987). Plant turgor and root growth can be maintained at lower water potentials. Drought stress enhances root extension into deeper, moist soil (Fukai and Cooper, 1995). Thus, varieties with deep roots become an important practical way to select for drought tolerance (Fukai and Cooper, 1995; Price et al., 1997; Wasson et al., 2012). However, root elongation is limited by soil impedance. Deep rooting is significantly limited while penetrometer resistances are more than 2 MPa, air-filled volume is less than 10%, and a matric potential is higher than -1.5 MPa (Bengough et al., 2011; Lynch and Wojciechowski, 2015). Root growth is reduced and stressed roots develop a pronounced suberisation of the apoplast to minimize water losses for plant survival (Steudle, 2000).

When drought occurs during the reproductive and grain filling stages of wheat, general responses including stomatal closure, photosynthesis limitation, osmotic adjustment, abscisic acid (ABA) accumulation, and root elongation would occur. Male sterility is a particular phenotype during such process (Blum, 2007). When drought stress becomes severe, the phloem translocation mechanisms may be affected directly, since phloem transport relies on water transport processes in the xylem. However, it was demonstrated that phloem translocation remained unaffected until late in the stress period, when other processes, such as photosynthesis, had already been strongly inhibited (Taiz and Zeiger, 2002). Because of this relative insensitivity of translocation to stress, plant reserves can be mobilized, for example, to grain. The continuing translocation of assimilates could be a key ability for drought tolerance.

Under drought stress, stem water soluble carbohydrate (WSC), mainly fructans, represents a long-term carbon storage form functioning as a major carbon source for grain filling (Pollock, 1986; Pollock and Cairns, 1991). The high remobilization efficiency of stem WSC could contribute to high water use efficiency (Passioura, 2012; Zhang et al., 2015a). Fructans may also be involved in osmoregulation under drought (Schnyder, 1993; Turner et al., 2008). Stem fructans may also contribute to recovery mechanisms under biotic and abiotic stresses (Schnyder, 1993; Yang and Zhang, 2006; Valluru and Van den Ende, 2008; Livingston et al., 2009). Furthermore, sucrose, hexoses (Hex) and small fructans may act as phloem-mobile signaling molecules under stress, contributing to stress tolerance and disease prevention (Van den Ende, 2013; Ruan, 2014).

There are different fructan types in wheat, predominantly graminan- and levan-type fructans in which β-(2–6) linkages predominate, besides some small inulin-type fructans (Pollock and Cairns, 1991). 1-SST (sucrose: sucrose 1-fructosyl-transferase), 1-FFT (fructan: fructan 1-fructosyltransferase), and 6-SFT (sucrose: fructan 6-fructosyltransferase) are the main fructosyltransferases involved. Fructans are degraded into sucrose and fructose by linkage-specific fructan exohydrolases, for example, 1-FEH, 6-FEH, and 6&1-FEH (Van den Ende et al., 2003; Kawakami et al., 2005; Van Riet et al., 2006, 2008; Xue et al., 2008). Sucrose is hydrolyzed to Hex through different types of invertases (INVs), among which soluble acid-type vacuolar invertase is the most prominent form in wheat roots (Königshofer and Löppert, 2015).

Carbohydrate metabolism has previously been studied in wheat roots under cold and salinity stresses (Santoiani et al., 1993; Kafi et al., 2003). Chilling stimulated high degree of polymerization (DP) fructan synthesis associated with higher sucrose levels and higher 1-SST and sucrose phosphate synthase (SPS) activities whereas INV and FEH activities remained unaffected. Cold temperature decreased shoot and root growth and increased carbohydrate levels in different wheat cultivars (Equiza et al., 1997), as it does in many other species (Tarkowski and Van den Ende, 2015). In ryegrass, lines adapted to cold climates produced more high DP fructans as compared to lines adapted to warmer environments when subjected to cold stress (Abeynayake et al., 2015). Under salt stress, contents of proline, soluble and insoluble carbohydrates increased in leaves, apices and roots but were lower in the maturing seeds of a salt-sensitive wheat cultivar (cv. Ghods) as compared to salt tolerant cultivars (Kafi et al., 2003).

So far, wheat stem WSC dynamics have been well studied under an array of stresses. However, carbohydrate dynamics in drought-stressed wheat roots remains unknown. At grain filling stage, the three hypotheses for contributions of root WSC would be: (i) as an energy source for root growing deeper to utilize the moisture in deep soil; (ii) as an osmoregulation factor for maintaining plant vigor and keep plant survive; and (iii) as a redistributed carbon source for grain filling. To better understand the root responses to drought at the grain filling stage, glucose, fructose, sucrose and different types of fructans were examined in wheat roots alongside stems under different water regimes. Enzyme activities involved in fructan biosynthesis and degradation along with vacuolar invertase activity were analyzed in parallel, with the objective to: (i) understand the potential function of root WSC and (ii) identify key enzymes during the process.

MATERIALS AND METHODS

Plant Materials

Wheat varieties, Westonia, Kauz and their double haploid (DH) lines DH 125, DH 139, DH 307, and DH 338 were selected from a population of 225 lines and used in a field drought experiment. Westonia and Kauz were developed in Western Australia (WA) and the International Maize and Wheat Improvement Center (CIMMYT, Mexico), respectively. Westonia produces consistent high yield in medium and low rainfall regions as Kauz is considered as drought tolerant variety (Butler et al., 2005). Both varieties contain high stem WSC levels (∼40%) after anthesis but they show different responses to the drought stress as explained previously (Zhang et al., 2009, 2015b). DH 125, DH 139, DH 307, and DH 338 were selected based on genetic diversity and flowering time (Zhang et al., 2015b). Previous results showed that DH 139 and DH 307 are genetically close to Westonia while DH 125 and DH 338 are close to Kauz.

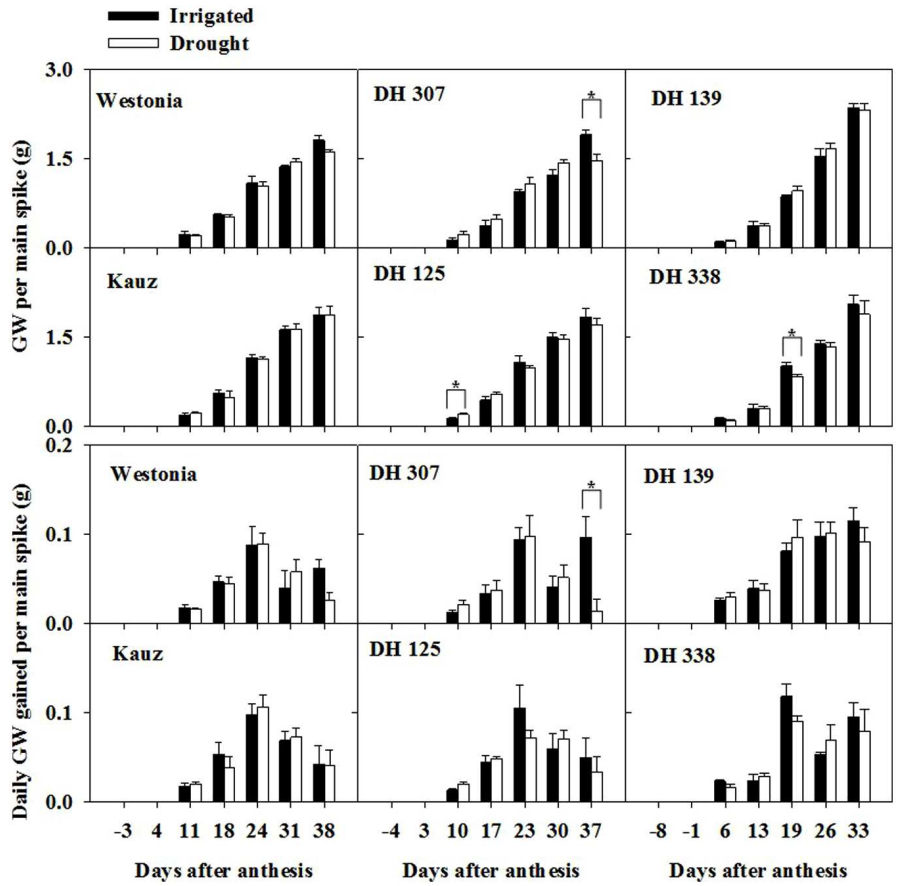

FIGURE 1 | Time-dependent grain weight per main spike and daily grain weight gains for DH 307, DH 125, DH 139, DH 338, and the parental lines of Westonia and Kauz under irrigated and drought conditions. The vertical bars represent SE. An asterisk (*) identifies significantly different values at $P < 0.05$ in *t*-test

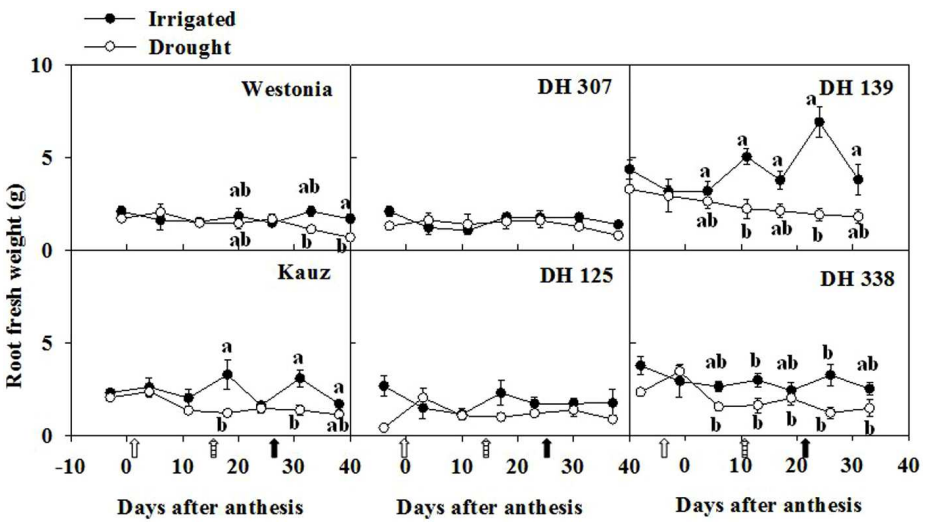

FIGURE 2 | Time-dependent root fresh weight of six plants for DH 307, DH 125, DH 139, DH 338, and the parental lines of Westonia and Kauz under irrigated and drought conditions. The vertical bars represent SE. Values with the same letter are statistically not different at $P = 0.05$. Open, dashed and closed arrows indicate start of drought treatment, 6 and 10 mm of rainfall, respectively.

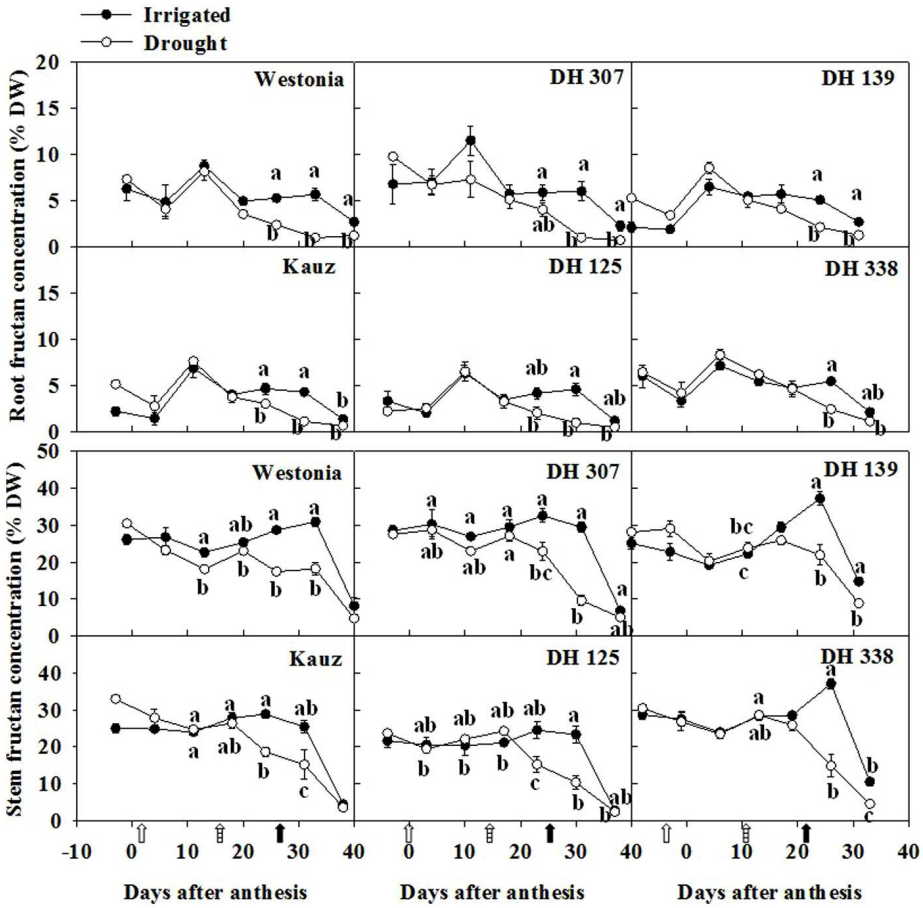

FIGURE 3 | Fructan levels in roots and stems of DH 307, DH 125, DH 139, DH 338, and the parental lines of Westonia and Kauz under drought and irrigated conditions in the field, respectively. The vertical bars represent SE. Values with the same letter are statistically not different at $P = 0.05$. Open, dashed and closed arrows indicate start of drought treatment, 6 and 10 mm of rainfall, respectively.

DH 139 contains the 1-FEH w3 Westonia type of allele while the three other DH lines contain the Kauz type of 1-FEH w3 alleles (Zhang et al., 2015b). DH 307 and DH 125 flower at a similar time, while DH 139 and DH 338 flower relatively later. Under drought, the losses in the grain weight per spike in DH 307, DH 125, and DH 338 were less than in DH 139 (data not shown).

Field Experiment

The field drought trial was carried out in 2013 at Merredin field station, Western Australia (31.5° S, 118.3° E). Parental lines of Westonia and Kauz and DH 125, DH 139, DH 307, and DH 338 were planted in 10 m^2 plots, in a randomized trial with four replicates sown on the 20th of June for both drought and irrigated treatments. Drought treatment was initiated at average anthesis time (the 24th of September, 2013) of these lines. Besides 16 mm of rainfall (6 and 10 mm rainfall on the 9–10th and 20–21st of October, 2013), irrigated plots received 15 mm water on a weekly basis for four weeks after the average anthesis time. Twelve neutron probes (down to 1.5 m depth) were distributed evenly in each treatment block to monitor soil moisture. During the drought treatment, soil water content was significantly reduced by 40% at 10 cm depth and reduced by 15 and 8% at 30 and 50 cm depth, respectively, in the late sowing trial between 20 and 30 days after anthesis (DAA) (Supplementary Figure S1).

Plant Harvest

Six plants of each plot were sampled weekly between 11:00 and 17:00 (Zhang et al., 2008) from 1-week pre-anthesis to 6-weeks post-anthesis. A shovel was used to dig out the plants, including almost their entire root system above 20–30 cm depth. Plants were separated from each other after the soil was gently removed. The six main stems of the six plants were immediately placed on dry ice and subsequently stored in a −20°C freezer. The stem samples for the WSC extraction were processed as described previously (Zhang et al., 2008). Roots from the six plants in each plot were combined to provide one root sample per plot. Roots were rinsed free of soil on a sieve with 2 mm apertures, immediately surface dried using tissue paper then the root fresh weight was recorded. The roots were stored (−20°C) afterwards. Once frozen, each

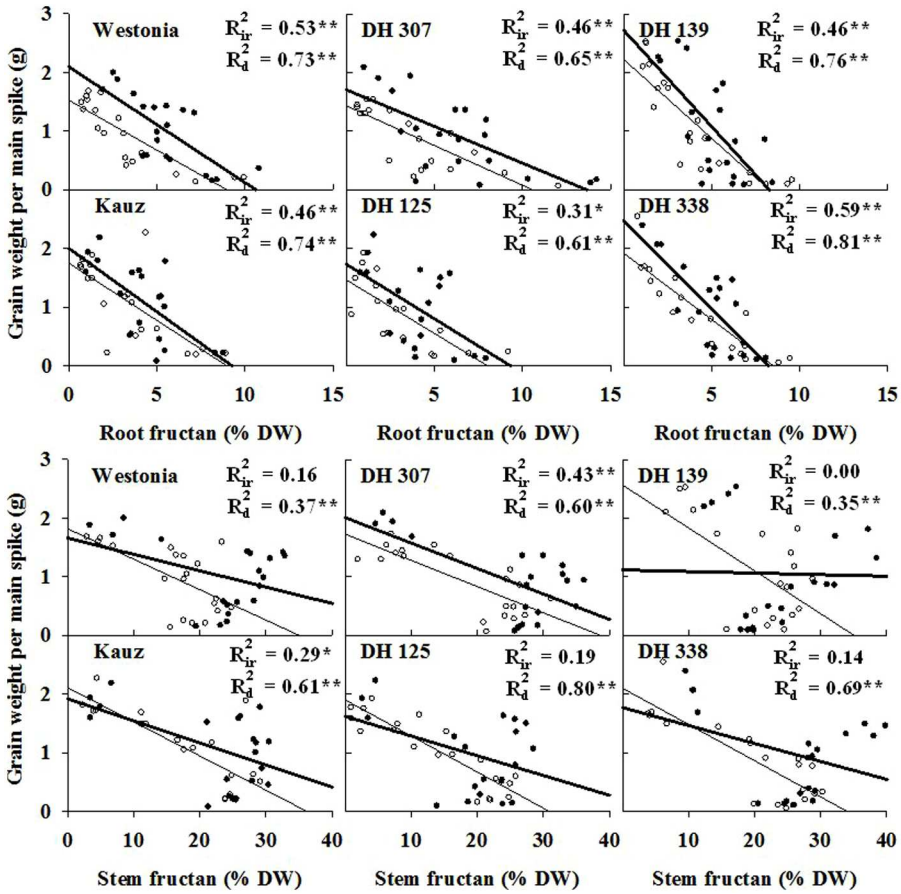

FIGURE 4 | The correlations of grain weight per main spike and fructan concentration in roots and stems (sheath included) starting from six days after anthesis (DAA) in DH 307, DH 125, DH 139, DH 338, and the parental lines of Westonia and Kauz under irrigated (closed circles and thick lines) and drought conditions (open circles and thin lines), respectively. R^2_{ir} and R^2_d represent the correlations under irrigated and drought conditions, respectively. Asterisks (*) and (**) represent the significant levels at $P < 0.05$ and $P < 0.01$, respectively.

root sample was ground to fine powder using a TissueLyser II (Qiagen) in a 4°C temperature controlled room. Samples were then subdivided for enzyme analysis, and WSC and WSC components analysis, as described previously (Zhang et al., 2015a). The six heads were combined and stored (−20°C). Four out of six heads were randomly selected, freeze dried and oven dried. Seeds were taken by hand threshing for grain weight (GW) assimilation measurements. Data were generated weekly, including thousand grain weight (TGW), kernel number per spike (KN), and grain weight (GW) per spike from main stems. At harvest time, 1 m^2 of each plot was harvested and grain weight (GW) per m^2, GW per tiller, KN per tiller, and TGW were recorded.

Carbohydrate Analysis

Total WSC were extracted from stem and root powder using the deionized water and anthrone reagent (Fales, 1951; Yemm and Willis, 1954). The WSC content was analyzed as previously described (Zhang et al., 2015b). Briefly, WSC components were separated by high-performance anion exchange chromatography with integrated pulsed amperometric detection (HPAEC–IPAD) and quantified using peak area comparison. The glucose, fructose, sucrose, 1-kestose, 6-kestose, neokestose, nystose, and bifurcose were used as external standards. Total fructan concentration was calculated as described previously (Zhang et al., 2015a).

Enzyme Activity Measurements

For reducing the high overall work load, the root samples of Westonia, Kauz, DH 125 and DH 307 were selected for sugar related enzyme activity measurements. Protein extraction and enzyme activity measurements were undertaken as described previously (Zhang et al., 2015b).

Statistical Analysis

Analysis of variance (ANOVA) in IBM SPSS statistics v 21 was used for phenotype data analysis. Significant groupings were identified by *post hoc* Tukey's Multiple Range tests. The data pair significant analysis was detected by the Student's *t*-test. The correlation significance level was determined by Pearson bivariate analysis.

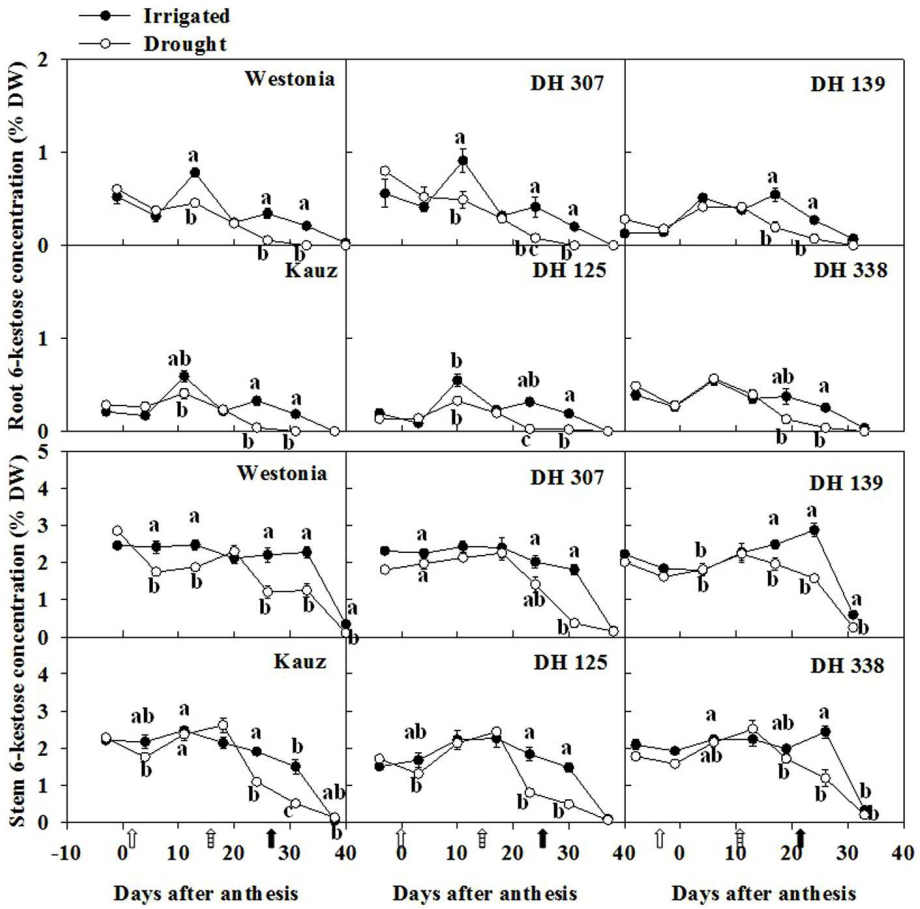

FIGURE 5 | The levels of 6-kestose in roots and stems of DH 307, DH 125, DH 139, DH 338, and the parental lines of Westonia and Kauz under drought and irrigated conditions in the field, respectively. The vertical bars represent SE. Values with the same letter are statistically not different at $P = 0.05$. Open, dashed and closed arrows indicate start of drought treatment, 6 and 10 mm of rainfall, respectively.

RESULTS

Root Fructan and Grain Assimilation

Under drought, grain yield losses per square meter were only significant for the late flowering lines DH 139 and DH 338 (Supplementary Table S1). The reduction in grain weight per tiller under drought was significant in DH 307 and DH 139. The KN per tiller was only significantly affected in DH 139 under drought. A significant TGW loss appeared in most lines, with the exception of Kauz and DH 139.

The grain assimilation patterns from the main stem were different among lines and treatments. Under drought, the daily grain weight (GW) peaked around 23–24 DAA before decreasing, except for DH 139 and DH 338 (**Figure 1**). In irrigated plants, the daily assimilation rate patterns were similar between Kauz and DH 125 and similar under drought, while the other lines still showed enhanced rates towards the end of the sampling period under irrigated conditions. The daily GW assimilation was significantly higher in DH 307 irrigated plants at the last sampling time as compared to that under drought (**Figure 1**), which may account for the significantly higher GW per main spike and final GW per tiller under irrigated conditions (**Figure 1**; Supplementary Table S1).

As root growth relies on the sucrose supplies from photosynthesis, root WSC levels may reflect root development under different water regimes. Root fresh weight significantly increased in Kauz and DH 139 under irrigated conditions (**Figure 2**). The root fresh weight differences between irrigated and drought conditions were less prominent in the other lines. The highest WSC level in roots was around 10–15% of dry weight (DW), which was approximately one third of the level recorded in stems (30–45% of DW) (Supplementary Figure S2). Between 25 and 30 DAA, WSC concentration in roots decreased significantly in all lines under drought. These significant differences were maintained up to the last sampling date in some lines (DH 307, DH 139, and Westonia; Supplementary Figure S2).

As fructans are the major storage form of stem WSC (Pollock and Cairns, 1991; Zhang et al., 2015a), the root fructan level was examined. The maximal root fructan concentration was around 7–10% of DW (**Figure 3**). Similar to root WSC, the root fructan level was about one third of the stem fructan level (25–30% of DW) and it decreased significantly after 20 DAA in all lines.

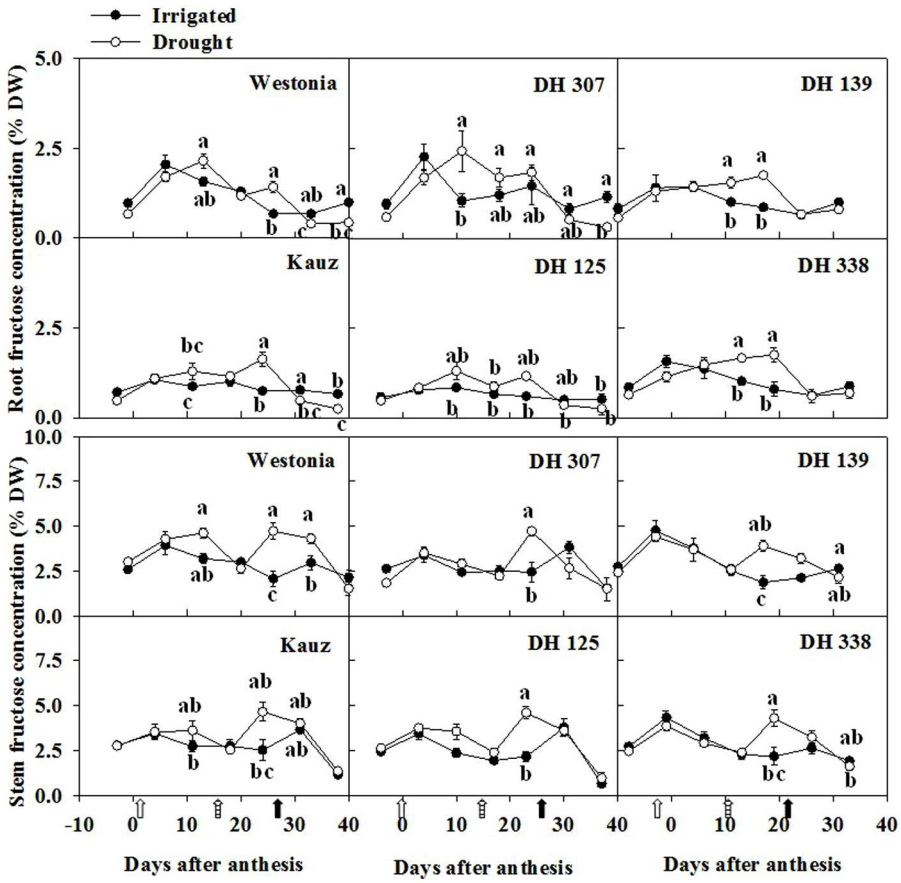

FIGURE 6 | The levels of fructose in roots and stems of DH 307, DH 125, DH 139, DH 338, and the parental lines of Westonia and Kauz under drought and irrigated conditions in the field, respectively. The vertical bars represent SE. Values with the same letter are statistically not different at $P = 0.05$. Open, dashed and closed arrows indicate start of drought treatment, 6 and 10 mm of rainfall, respectively.

This implies that the concentrations of WSC in roots and stems are inter-related and statistical analysis showed a high significant correlation ($P < 0.01$) in Kauz, DH 125, and DH 338 under both water regimes (Supplementary Figure S3). It was well correlated in DH 307 drought plants ($R^2 = 0.53^{**}$, $P < 0.01$) while the correlation was lower ($R^2 = 0.26^{*}$, $P < 0.05$) under irrigated conditions.

Since fructans are recognized sources for grain filling, the association between root fructan degradation and grain assimilation was examined. Significant correlations ($P < 0.01$) between grain weight and fructan level were detected under both water regimes in all lines (**Figure 4**). Overall, correlations were superior under drought as compared to irrigated conditions (**Figure 4**). Moreover, with the exception of DH 125 under drought, correlative parameters were even better for root fructans as compared to stem fructans (**Figure 4**).

Similar to total fructan levels, the 6-kestose level in roots was almost one third of that in stems. After anthesis, 6-kestose increased in irrigated plants up to about 10 DAA and decreased gradually afterwards (**Figure 5**). Under drought, only a slight increase occurred, followed by a significant decrease between 20 and 30 DAA in Westonia, Kauz, DH 307, and DH 125 (**Figure 5**). In the stem, 6-kestose levels became significantly lower under drought in all DH lines between 20 and 30 DAA (**Figure 5**). Overall, root and stem 6-kestose correlated well with root and stem total fructans (Supplementary Figure S4). The bifurcose level in roots was almost half of the level in stems (Supplementary Figure S5). The bifurcose patterns resembled those of 6-kestose, with some line-specific variations (**Figure 5**; Supplementary Figure S5). Levels of 1-kestose and 1,1-nystose in roots were hardly detectable. In stems, 1-kestose levels were below 1% in all lines and much lower than 6-kestose and bifurcose, decreasing slightly in all lines and under both treatments (data not shown).

Fructose, Glucose, and Sucrose Dynamics

Along with the root fructan degradation, the fructose, glucose and sucrose were examined. In general, fructose levels in roots were half of the levels in stems. For all lines, except for DH 125, there were one or two dates at which the root fructose levels became significantly higher under drought than under comparable irrigated conditions (**Figure 6**). With the exception

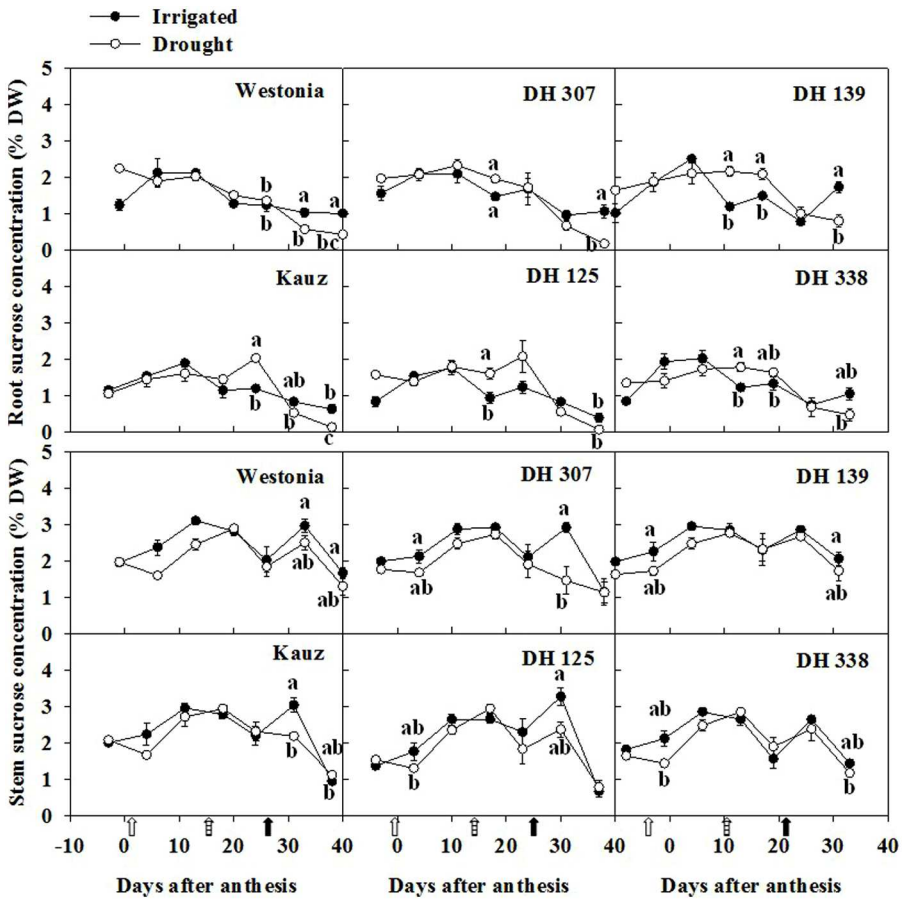

FIGURE 7 | The levels of sucrose in roots and stems of DH 307, DH 125, DH 139, DH 338, and the parental lines of Westonia and Kauz under drought and irrigated conditions in the field, respectively. The vertical bars represent SE. Values with the same letter are statistically not different at $P = 0.05$. Open, dashed and closed arrows indicate start of drought treatment, 6 and 10 mm of rainfall, respectively.

of Kauz, differences in stem fructose levels between drought and irrigated plants were more extended. The early increase of fructose in DH 307 roots did not appear in stems. The glucose levels in roots were approximately one third of the levels in stems. For all lines, except for DH 125, DH 307, and Westonia, there were one or two dates at which the root glucose levels became significantly higher under drought (Supplementary Figure S6). In drought treated plants, the root glucose level in DH 307 was significantly higher than that in DH 125. In stems, glucose levels were significantly higher under drought, at least at one point in time, for all lines (Supplementary Figure S6). After 10 DAA, patterns of glucose and fructose were very similar (**Figure 6**; Supplementary Figure S6). In general, root sucrose levels were only slightly lower than those in stems (**Figure 7**). Interestingly, root sucrose levels under drought became significantly higher over the 15–20 DAA intervals in all lines, except for DH 307 and Westonia (**Figure 7**).

Fructan and Sucrose Metabolic Enzymes

Since fructan biosynthetic and breakdown enzymes influence fructan levels and other WSC components, the activities of the enzymes involved in fructan and sucrose metabolism were investigated. In roots, the enzyme activities of 1-SST, 6-SST, and 1-FFT were extremely low (data not shown), and did not correlate with increasing fructan levels around 10 DAA in most lines. Hydrolytic activities (1-FEH, 6-FEH, and vacuolar invertase) increased in some lines over the sampling period but no significantly higher activities could be detected between drought and irrigated conditions (**Figure 8**). At 10 DAA in irrigated plants, 1-FEH and 6-FEH activities were significantly higher in Westonia than in Kauz. At 30 DAA in irrigated plants, 1-FEH and 6-FEH activities were significantly higher in DH 307 as compared to DH 125 (**Figure 8**).

DISCUSSION

Wheat stem WSC is recognized as a storage carbon source for grain filling and fructans are the main component (Schnyder, 1993; Yang et al., 2000; Zhang et al., 2015a, b). Equivalent to one third of the stem WSC level, the root WSC may be as a redistributed carbon source pool for grain filling. Thus, the decrease of root WSC may be associated with the grain

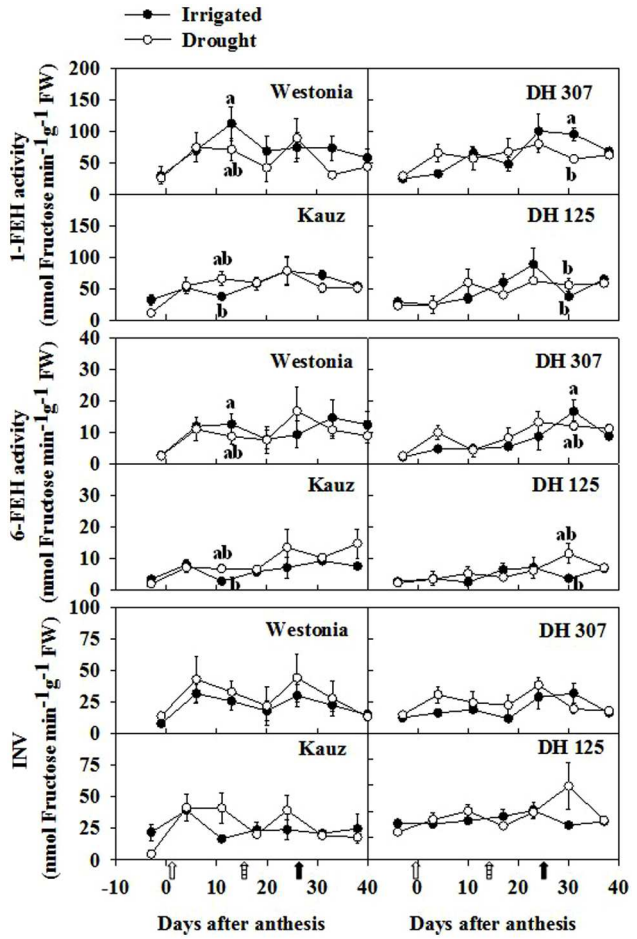

FIGURE 8 | Enzyme activities of 1-FEH, 6-FEH, and INV at fresh level in roots of DH 307, DH 125, DH 139, DH 338, and the parental lines of Westonia and Kauz under drought (open circles) and irrigated conditions (closed circles) in the field. Open, dashed and closed arrows indicate start of drought treatment, 6 and 10 mm of rainfall, respectively.

assimilation rate as indicated by Lopes and Reynolds (2010). Root fructan and 6-kestose levels peaked around 10 DAA under both water regimes. Afterwards, they decreased significantly under drought. During wheat grain development, the basic structure of the endosperm is established after 10 DAA and thereafter, the deposition of storage components (starch and proteins) is initiated (Shewry et al., 2012). The rapid grain filling period is between 14 and 28 DAA (Shewry et al., 2012). According to our data, the most active grain filling period was between 18 and 24 DAA (**Figure 1**). For late flowering lines, this period extended to 33 DAA (**Figure 1**). The period of rapid grain filling correlated well with the decrease in the root WSC level. The likely remobilization of the root WSC to grain was also strongly supported by the significant correlation between root fructan level and GW assimilation. The degradation of root fructan was more distinct under drought, indicating that root fructan remobilization was more efficient than under irrigated conditions.

Fructans in wheat include β-(2–1) and β-(2–6) linkages and the latter is the predominant form (Bancal et al., 1993; Bonnett and Simpson, 1995; Van den Ende et al., 2003). From our results, the patterns of 6-kestose and total fructan were very similar in the stems and roots. The correlations between 6-kestose and total fructan were highly significant in both stems and roots under two water regimes. Our results further support that β-(2–6) linkages are the predominant form of fructan in wheat.

Studies under controlled environments in wheat (Santoiani et al., 1993; Equiza et al., 1997; Kafi et al., 2003) have demonstrated that levels of fructan and monosaccharides accumulate in roots under cold and salinity stresses. By contrast, our study was conducted under field conditions, with wheat plants going through natural drought. In contrast to the above-mentioned results, root fructan levels decreased significantly under drought in all lines. The differences are probably due to the growth stages at sampling and the related different function of the root WSC. In the previous studies (Santoiani et al., 1993; Equiza et al., 1997; Kafi et al., 2003), the root samples were taken before flowering. Our drought stress commenced at flowering and the root samples were taken during grain filling. It seems that plants tend to accumulate more WSC in root under abiotic stress before anthesis and use mechanisms of the osmotic adjustment for surviving. At the grain filling stage, although in the process of the root fructan degradation, the significant high levels of sucrose, fructose and glucose in drought plants would act as osmoregulators, the main function of root WSC may be as partial fructan pools for translocation to grain, as growing seeds is a priority for plants during terminal drought.

A wheat growth study on four soil types in WA revealed that wheat roots grew more rapidly during seedling and anthesis stages, while growth rates reduced during tillering and grain filling stages (Tennant, 1976; Watt et al., 2013), suggesting that tillering and grain filling are more costly (in terms of energy/carbon sources) as compared with root growth. Ideally, the ability of deep rooting allows plants to reach moisture from deeper soil layers to produce relatively high grain yields in dry environments. Indeed, root depths (sampled between 7 and 12 DAA) were positively correlated with wheat yield under terminal or intermittent drought (Lopes and Reynolds, 2010). However, root elongation is affected by soil type, the level of water deficiency and soil compaction (Bengough et al., 2011; Lynch and Wojciechowski, 2015). Moreover, under severe and persistent drought stress, root growth is reduced. For minimizing water losses, stressed roots develop a suberized interface between living tissue and the rhizosphere (Steudle, 2000). Consequently, under severe drought, apart from as an energy source to develop suberisation, the major contributions of root WSC reserves is most likely to serve as a carbon source for grain filling rather than for deep rooting. In this study, weather was not perfect for the drought experiment. There were two rain falls (6 mm on the 9–10th of October and 10 mm on the 20–21st of October) and the evaporations on those days were 4.2 and 5.8 mm, respectively. Apart from the evaporation, the little moisture from the 6 mm rainfall mainly stayed on the soil surface and was probably not enough to help plants develop deep roots. The 10 mm rainfall happened at the late grain fill stage. Apart from the high

evaporation (5.8 mm), the rest moisture mainly remained on the top layer of the soil and might favor the grain assimilation in the late flowering lines (DH 139 and 338). It seems very unlikely that this moisture would have helped root elongation instead of grain filling. Since grain filling is clearly the dominant physiological process during these late developmental stages (Tennant, 1976; Lopes and Reynolds, 2010).

Levels of sucrose are proportionally higher in roots, its concentration being two thirds of that in the stem, while the concentrations of other sugars are much lower than those in the stem. Continuous import of leaf-derived photosynthetic sucrose is required to sustain root growth (Nagel et al., 2006), since root carbohydrate reserves cannot sustain root growth for a long time (Eliasson, 1968). During drought stress, photosynthesis can be affected (Zhang et al., 2009), and general growth is affected more than photosynthesis (Vandoorne et al., 2012), explaining why significantly higher levels of sucrose remained in four out of six lines under drought as compared to irrigated plants. In irrigated plants, the lower levels of sucrose in Kauz and DH 139 correlated with higher root fresh weights ($P < 0.05$), in agreement with high sucrose influxes from the leaves and continuous sucrose hydrolysis to sustain root growth. Genotypic differences in root sucrose levels were observed between Westonia and the other lines, and this requires further investigation.

In summary, the levels of root WSC, fructans, glucose and 6-kestose account for one third of that in stems. Root fructose and bifurcose levels were almost half of the stem and the sucrose level was two thirds of the stem. Different from abiotic stresses studied before anthesis, during the grain filling stage, the degradation patterns of root fructan levels and the significantly high correlations with grain assimilation under drought indicate that the root WSC as a partial carbon source for grain filling rather than deep rooting as growing seeds is the priority under terminal drought. Overall, root WSC may represent a redistributed carbon source for grain filling next to stem WSC. Our results further reflect that fructans with β-(2–6) linkages predominate in wheat and the patterns of 6-kestose resembled those of total fructans. Further research is required into the specific roles of root and stem 6-FEHs under terminal drought.

AUTHOR CONTRIBUTIONS

JZ and WV designed the experiments. JZ and XZ sampled the materials. JZ, RV, XZ, AF, and TO analyzed the carbohydrates. JZ and RV analyzed the enzyme activities. JZ, WV, BD, WM, and DL wrote the manuscript with inputs from the other authors.

FUNDING

This work was supported by Grains Research & Development Corporation 'grant number UMU00039', and the Sir Walter Distinguished Collaborator Scheme at Murdoch University.

ACKNOWLEDGMENTS

The authors are very grateful for the support from the research group of Dr. Ben Biddulph and staff at the Department of Agricultural and Food of Western Australia for helping in operating the field drought experiment. Authors appreciate the assistance of Miss. Yunji Xu, Dr. Hao Luo, and Mrs. Nusrat Khan for sampling and Mr. Timmy Reijnders for preparing 6-kestose and bifurcose sugar references. Westonia and Kauz DH populations were kindly provided by InterGrain, Western Australia.

SUPPLEMENTARY MATERIAL

The Supplementary Material for this article can be found online at: http://journal.frontiersin.org/article/10.3389/fpls.2016.00904

REFERENCES

Abeynayake, S. W., Etzerodt, T. P., Jonaviciene, K., Byrne, S., Asp, T., and Boelt, B. (2015). Fructan metabolism and changes in fructan composition during cold acclimation in perennial ryegrass. *Front. Plant Sci.* 6:329. doi: 10.3389/fpls.2015.00329

Bancal, P., Gibeaut, D. M., and Carpita, N. C. (1993). "Analytical methods for the determination of fructan structure and biosynthesis," in *Science and Technology of Fructans*, eds N. J. Chatterton and M. Suzuki (Boca Raton, FL: CRC Press), 83–118.

Bengough, A. G., Mckenzie, B. M., Hallett, P. D., and Valentine, T. A. (2011). Root elongation, water stress, and mechanical impedance: a review of limiting stresses and beneficial root tip traits. *J. Exp. Bot.* 62, 59–68. doi: 10.1093/jxb/erq350

Blum, A. (2007). *Drought Stress and Its Impact*. Available at: http://www.plantstress.com/

Bonnett, G. D., and Simpson, R. J. (1995). Fructan exohydrolase activities from *Lolium rigidum* that Hydrolyze β-2,1- and β-2,6-Glycosidic linkages at different rates. *New Phytol.* 131, 199–209. doi: 10.2307/2558474

Butler, J. D., Byrne, P. F., Mohammadi, V., Chapman, P. L., and Haley, S. D. (2005). Agronomic performance of Rht alleles in a spring wheat population across a range of moisture levels. *Crop Sci.* 45, 939–947. doi: 10.2135/cropsci2004.0323

Eliasson, L. (1968). Dependence of root growth on photosynthesis in *Populus tremula*. *Physiol. Plant.* 21, 806–810. doi: 10.1111/j.1399-3054.1968.tb07304.x

Equiza, M. A., Miravé, J. P., and Tognetti, J. A. (1997). Differential inhibition of shoot vs. root growth at low temperature and its relationship with carbohydrate accumulation in different wheat cultivars. *Ann. Bot.* 80, 657–663. doi: 10.1006/anbo.1997.0503

Fales, F. W. (1951). The assimilation and degradation of carbohydrates by yeast cells. *J. Biol. Chem.* 193, 113–124.

Fukai, S., and Cooper, M. (1995). Development of drought-resistant cultivars using physiomorphological traits in rice. *Field Crops Res.* 40, 67–86. doi: 10.1016/0378-4290(94)00096-U

Kafi, M., Stewart, W. S., and Borland, A. M. (2003). Carbohydrate and proline contents in leaves, roots, and apices of salt-tolerant and salt-sensitive wheat cultivars1 Russ. *J. Plant Physiol.* 50, 155–162. doi: 10.1023/A:1022956727141

Kawakami, A., Yoshida, M., and Van den Ende, W. (2005). Molecular cloning and functional analysis of a novel 6&1-FEH from wheat (*Triticum aestivum* L.) preferentially degrading small graminans like bifurcose. *Gene* 358, 93–101. doi: 10.1016/j.gene.2005.05.029

Königshofer, H., and Löppert, H.-G. (2015). Regulation of invertase activity in different root zones of wheat (*Triticum aestivum* L.) seedlings in the course

of osmotic adjustment under water deficit conditions. *J. Plant Physiol.* 183, 130–137. doi: 10.1016/j.jplph.2015.06.005

Livingston, D. P. III, Hincha, D., and Heyer, A. (2009). Fructan and its relationship to abiotic stress tolerance in plants. *Cell. Mol. Life Sci.* 66, 2007–2023. doi: 10.1007/s00018-009-0002-x

Lopes, M. S., and Reynolds, M. P. (2010). Partitioning of assimilates to deeper roots is associated with cooler canopies and increased yield under drought in wheat. *Funct. Plant Biol.* 37, 147–156. doi: 10.1071/FP09121

Lynch, J. P., and Wojciechowski, T. (2015). Opportunities and challenges in the subsoil: pathways to deeper rooted crops. *J. Exp. Bot.* 66, 2199–2210. doi: 10.1093/jxb/eru508

McCree, K. J., and Richardson, S. G. (1987). Stomatal closure vs. osmotic adjustment: a comparison of stress response. *Crop Sci.* 27, 539–543. doi: 10.2135/cropsci1987.0011183X002700030024x

Nagel, K. A., Schurr, U., and Walter, A. (2006). Dynamics of root growth stimulation in *Nicotiana tabacum* in increasing light intensity. *Plant Cell Environ.* 29, 1936–1945. doi: 10.1111/j.1365-3040.2006.01569.x

Passioura, J. B. (2012). Phenotyping for drought tolerance in grain crops: when is it useful to breeders? *Funct. Plant Biol.* 39, 851–859. doi: 10.1071/FP12079

Paul, M., and Lawlor, D. (2014). Source/sink interactions underpin crop yield: the case for trehalose 6-phosphate/SnRK1 in improvement of wheat. *Front. Plant Sci.* 5:418. doi: 10.3389/fpls.2014.00418

Pollock, C. J. (1986). Tansley review no. 5 fructans and the metabolism of sucrose in vascular plants. *New Phytol.* 104, 1–24. doi: 10.1111/j.1469-8137.1986.tb00629.x

Pollock, C. J., and Cairns, A. J. (1991). Fructan metabolism in grasses and cereals. *Annu. Rev. Plant Phys.* 42, 77–101. doi: 10.1146/annurev.pp.42.060191.000453

Price, A. H., Tomos, A. D., and Virk, D. S. (1997). Genetic dissection of root growth in rice (*Oryza sativa* L.) I: a hydrophonic screen. *Theor. Appl. Genet.* 95, 132–142. doi: 10.1007/s001220050541

Ruan, Y.-L. (2014). Sucrose metabolism: gateway to diverse carbon use and sugar signaling. *Annu. Rev. Plant Biol.* 65, 33–67. doi: 10.1146/annurev-arplant-050213-040251

Santoiani, C. S., Tognetti, J. A., Pontis, H. G., and Salerno, G. L. (1993). Sucrose and fructan metabolism in wheat roots at chilling temperatures. *Physiol. Plant.* 87, 84–88. doi: 10.1111/j.1399-3054.1993.tb08794.x

Schnyder, H. (1993). The role of carbohydrate storage and redistribution in the source-sink relations of wheat and barley during grain filling- a review. *New Phytol.* 123, 233–245. doi: 10.1111/j.1469-8137.1993.tb03731.x

Shewry, P. R., Mitchell, R. A. C., Tosi, P., Wan, Y., Underwood, C., Lovegrove, A., et al. (2012). An integrated study of grain development of wheat (cv. Hereward). *J. Cereal Sci.* 56, 21–30. doi: 10.1016/j.jcs.2011.11.007

Steudle, E. (2000). Water uptake by roots: effects of water deficit. *J. Exp. Bot.* 51, 1531–1542. doi: 10.1093/jexbot/51.350.1531

Taiz, L., and Zeiger, E. (2002). *Plant Physiology*. Sunderland, MA: Sinauer Associates, Inc.

Tarkowski, Ł. P., and Van den Ende, W. (2015). Cold tolerance triggered by soluble sugars: a multifaceted countermeasure. *Front. Plant Sci.* 6:203. doi: 10.3389/fpls.2015.00203

Tennant, D. (1976). Wheat root penetration and total available water on a range of soil types. *Aust. J. Exp. Agric.* 16, 570–577. doi: 10.1071/EA9760570

Turner, L. B., Cairns, A. J., Armstead, I. P., Thomas, H., Humphreys, M. W., and Humphreys, M. O. (2008). Does fructan have a functional role in physiological traits? Investigation by quantitative trait locus mapping. *New Phytol.* 179, 765–775. doi: 10.1111/j.1469-8137.2008.02495.x

Valluru, R., and Van den Ende, W. (2008). Plant fructans in stress environments: emerging concepts and future prospects. *J. Exp. Bot.* 59, 2905–2916. doi: 10.1093/jxb/ern164

Van den Ende, W. (2013). Multifunctional fructans and raffinose family oligosaccharides. *Front. Plant Sci.* 4:247. doi: 10.3389/fpls.2013.00247

Van den Ende, W., Clerens, S., Vergauwen, R., Van Riet, L., Van Laere, A., Yoshida, M., et al. (2003). Fructan 1-exohydrolases. β-(2,1)-trimmers during graminan biosynthesis in stems of wheat? purification, characterization, mass mapping, and cloning of two fructan 1-exohydrolase isoforms. *Plant Physiol.* 131, 621–631. doi: 10.1104/pp.015305

Van Riet, L., Altenbach, D., Vergauwen, R., Clerens, S., Kawakami, A., Yoshida, M., et al. (2008). Purification, cloning and functional differences of a third fructan 1-exohydrolase (1-FEHw3) from wheat (*Triticum aestivum* L.). *Physiol. Plant.* 133, 242–253. doi: 10.1111/j.1399-3054.2008.01070.x

Van Riet, L., Nagaraj, V., Van den Ende, W., Clerens, S., Wiemken, A., and Van Laere, A. (2006). Purification, cloning and functional characterization of a fructan 6-exohydrolase from wheat (*Triticum aestivum* L.). *J. Exp. Bot.* 57, 213–223. doi: 10.1093/jxb/erj031

Vandoorne, B., Mathieu, A.-S., Van den Ende, W., Vergauwen, R., Périlleux, C., Javaux, M., et al. (2012). Water stress drastically reduces root growth and inulin yield in *Cichorium intybus* (var. sativum) independently of photosynthesis. *J. Exp. Bot.* 63, 4359–4373. doi: 10.1093/jxb/ers095

Wasson, A. P., Richards, R. A., Chatrath, R., Misra, S. C., Prasad, S. V. S., Rebetzke, G. J., et al. (2012). Traits and selection strategies to improve root systems and water uptake in water-limited wheat crops. *J. Exp. Bot.* 63, 3485–3498. doi: 10.1093/jxb/ers111

Watt, M., Moosavi, S., Cunningham, S. C., Kirkegaard, J. A., Rebetzke, G. J., and Richards, R. A. (2013). A rapid, controlled-environment seedling root screen for wheat correlates well with rooting depths at vegetative, but not reproductive, stages at two field sites. *Ann. Bot.* 112, 447–455. doi: 10.1093/aob/mct122

Xue, G.-P., Mcintyre, C. L., Glassop, D., and Shorter, R. (2008). Use of expression analysis to dissect alterations in carbohydrate metabolism in wheat leaves during drought stress. *Plant Mol. Biol.* 67, 197–214. doi: 10.1007/s11103-008-9311-y

Yang, J., and Zhang, J. (2006). Grain filling of cereals under soil drying. *New Phytol.* 169, 223–236. doi: 10.1111/j.1469-8137.2005.01597.x

Yang, J., Zhang, J., Huang, Z., Zhu, Q., and Wang, L. (2000). Remobilization of carbon reserves is improved by controlled soil-drying during grain filling of wheat. *Crop Sci.* 40, 1645–1655. doi: 10.2135/cropsci2000.4061645x

Yemm, E., and Willis, A. (1954). The estimation of carbohydrates in plant extracts by anthrone. *Biochem. J.* 57, 508–514. doi: 10.1042/bj0570508

Zhang, J., Chen, W., Dell, B., Vergauwen, R., Zhang, X., Mayer, J., et al. (2015a). Wheat genotypic variation in dynamic fluxes of WSC components in different stem segments under drought during grain filling. *Front. Plant Sci.* 6:624. doi: 10.3389/fpls.2015.00624

Zhang, J., Dell, B., Conocono, E., Waters, I., Setter, T., and Appels, R. (2009). Water deficits in wheat: fructosyl exohydrolase (1-FEH) mRNA expression and relationship to soluble carbohydrate concentrations in two varieties. *New Phytol.* 181, 843–850. doi: 10.1111/j.1469-8137.2008.02713.x

Zhang, J., Huang, S., Fosu-Nyarko, J., Dell, B., Mcneil, M., Waters, I., et al. (2008). The genome structure of the 1-FEH genes in wheat (*Triticum aestivum* L.): new markers to track stem carbohydrates and grain filling QTLs in breeding. *Mol. Breed.* 22, 339–351. doi: 10.1007/s11032-008-9179-1

Zhang, J., Xu, Y., Chen, W., Dell, B., Vergauwen, R., Biddulph, B., et al. (2015b). A wheat 1-FEH w3 variant underlies enzyme activity for stem WSC remobilization to grain under drought. *New Phytol.* 205, 293–305. doi: 10.1111/nph.13030

Conflict of Interest Statement: The authors declare that the research was conducted in the absence of any commercial or financial relationships that could be construed as a potential conflict of interest.

frontiers in Physiology

REVIEW
published: 27 June 2016
doi: 10.3389/fphys.2016.00243

The Thermodynamic Flow-Force Interpretation of Root Nutrient Uptake Kinetics: A Powerful Formalism for Agronomic and Phytoplanktonic Models

Erwan Le Deunff[1,2]*, *Pierre-Henri Tournier*[3] and *Philippe Malagoli*[4,5]

[1] Université de Caen Basse-Normandie, UFR des Sciences, UMR EVA, Caen, France, [2] Institut National de la Recherche Agronomique, UMR 950, Écophysiologie Végétale and Agronomie Nutritions NCS, Caen, France, [3] Laboratoire Jacques-Louis Lions, INRIA Paris, EPC Alpines and Université Pierre et Marie Curie Paris 06, UMR 7598, Paris, France, [4] Université Clermont Auvergne, Université Blaise Pascal, UMR 547, PIAF, Clermont-Ferrand, France, [5] Institut National de la Recherche Agronomique, UMR 547 PIAF, Clermont-Ferrand, France

The ion influx isotherms obtained by measuring unidirectional influx across root membranes with radioactive or stable tracers are mostly interpreted by *enzyme-substrate-like* modeling. However, recent analyses from ion transporter mutants clearly demonstrate the inadequacy of the conventional interpretation of ion isotherms. Many genetically distinct carriers are involved in the root catalytic function. Parameters *Vmax* and *Km* deduced from this interpretation cannot therefore be regarded as microscopic parameters of a single transporter, but are instead macroscopic parameters (V_m^{app} and K_m^{app}, apparent maximum velocity and affinity constant) that depend on weighted activities of multiple transporters along the root. The *flow-force* interpretation based on the thermodynamic principle of irreversible processes is an alternative macroscopic modeling approach for ion influx isotherms in which macroscopic parameters L_j (overall conductance of the root system for the substrate j) and π_j (thermodynamic parameter when $J_j = 0$) have a straightforward meaning with respect to the biological sample studied. They characterize the efficiency of the entire root catalytic structure without deducing molecular characteristics. Here we present the basic principles of this theory and how its use can be tested and improved by changing root pre- and post-wash procedures before influx measurements in order to come as close as possible to equilibrium conditions. In addition, the constant values of *Vm* and *Km* in the Michaelis-Menten (MM) formalism of *enzyme-substrate* interpretation do not reflect variations in response to temperature, nutrient status or nutrient regimes. The linear formalism of the *flow-force* approach, which integrates temperature effect on nutrient uptake, could usefully replace MM formalism in the 1-3-dimension models of plants and phytoplankton. This formalism offers a simplification of parametrization to help find more realistic analytical expressions and numerical solution for root nutrient uptake.

Keywords: ion transport modeling, influx, efflux, enzyme-substrate modeling, flow-force modeling, nitrate, potassium, phytoplankton

OPEN ACCESS

Edited by:
Janin Riedelsberger, University of Talca, Chile

Reviewed by:
Ingo Dreyer, Universidad de Talca, Chile
Igor Pottosin, Universidad de Colima, Mexico

***Correspondence:**
Erwan Le Deunff
erwan.ledeunff@unicaen.fr

Specialty section:
This article was submitted to Plant Physiology, a section of the journal Frontiers in Physiology

Received: *29 February 2016*
Accepted: *03 June 2016*
Published: *27 June 2016*

Citation:
Le Deunff E, Tournier P-H and Malagoli P (2016) The Thermodynamic Flow-Force Interpretation of Root Nutrient Uptake Kinetics: A Powerful Formalism for Agronomic and Phytoplanktonic Models. Front. Physiol. 7:243. doi: 10.3389/fphys.2016.00243

INTRODUCTION

The kinetic patterns of ion uptake rates across roots, called ion influx isotherms, were first established in the 1960s by the pioneer work of Emanuel Epstein with ^{86}Rb or ^{42}K radioactive tracers for potassium uptake in barley (Epstein et al., 1963). These ion influx isotherms were later extended to other ions with radioactive or stable isotope tracers such as ^{13}N and ^{15}N for nitrate, $^{32}PO_4^{2-}$ and $^{33}PO_4^{2-}$ for phosphate, and $^{35}SO_4^{2-}$ and $^{34}SO_4^{2-}$ for sulfate (Bieleski, 1973; Kochian et al., 1985; Lee and Drew, 1986; Siddiqi et al., 1989, 1990; Faure-Rabasse et al., 2002). The conventional *enzyme-substrate* interpretation of influx isotherms by Epstein's group refers to a dual mechanism of ion transport and defines two distinct transport systems: a high-affinity transport system (HATS) and a low-affinity transport system (LATS). HATS is characterized by a saturable kinetic pattern in the low ion concentration range (<1 mM; Lee and Drew, 1986; Hole et al., 1990; Siddiqi et al., 1990; Aslam et al., 1992), whereas LATS exhibits saturable or linear behavior in the high ion concentration range (>1 mM; Pace and McClure, 1986; Siddiqi et al., 1990; Aslam et al., 1992; Kronzucker et al., 1995a).

The concept of transport systems (kinetic components of ion fluxes across the roots) deduced from the *enzyme-substrate* interpretation of influx isotherms is strengthened by the mathematical deduction of microscopic parameters such as *Vmax* and *Km* for the HATS and sometimes LATS, but shows its weakness in the case of the LATS mechanism when no enzymatic parameter can be set when its behavior is linear (Peuke and Kaiser, 1996). Although ion influx isotherms have been intensively used to validate molecular characterization of ion transporters in mutant analyses, recent analyses of ion transporter mutants for nitrate and potassium clearly demonstrate that the conventional *enzyme-substrate* interpretation is inadequate (Cerezo et al., 2001; Filleur et al., 2001; Li et al., 2007; Britto and Kronzucker, 2008; Alemán et al., 2011). Many carriers provided by genetically distinct gene families are involved in the root catalytic function (Touraine et al., 2001; Britto and Kronzucker, 2008; Alemán et al., 2011), and some transporters show double affinity depending on their phosphorylation status, as observed for the NRT1.1 (renamed NPF6.3) nitrate transporter (Liu and Tsay, 2003; Ho et al., 2009). *Vmax* and *Km* parameters deduced from an *enzyme-substrate* interpretation cannot therefore be regarded as microscopic parameters of a single transporter, but are instead macroscopic parameters (*Vmapp* and *Kmapp*) that reflect the sum of single activities of multiple transporters along the root (Neame and Richards, 1972).

Histochemical GUS (β-glucuronidase) or GFP (Green Fluorescent Protein) activities of *pNRT::GUS* or *pNRT::GFP* in transgenic Arabidopsis plants has revealed that these carriers are located on the different membrane cell layers within the mature root, and can be arranged in series or parallel to form a complex catalytic structure (Guo et al., 2001, 2002; Girin et al., 2007). The concept of transport systems deduced from the interpretation of influx isotherms cannot therefore be merged or confounded with ion transporters because influx components correspond to subsumed activities of multiple transporters along the root (Le Deunff and Malagoli, 2014a,b). Likewise, the copy number of the genes is also increased by endoreduplication in root cells during their elongation (Hayashi et al., 2013) and by a genome redundancy in polyploid crop species such as oilseed rape and wheat. Both situations probably lead to an underestimation of the number of nitrate transporters, hampering the *enzyme-substrate* interpretation of nitrate uptake isotherms. It is also well demonstrated that ion influx is uneven along the roots (Lazof et al., 1992; Reidenbach and Horst, 1997; Colmer and Bloom, 1998; Sorgona et al., 2011).

Conventional measurements of influx rate across the root in kinetic patterns are most often made in transient conditions far removed from equilibrium, because emphasis is laid on unidirectional influx rate across the plasma membrane instead of net flux (Britto and Kronzucker, 2001a,b; Britto and Kronzucker, 2003a; Glass et al., 2002). The pre- and post-wash conditions used for measurements therefore induced thermodynamic perturbations of the root membranes (Britto and Kronzucker, 2001a,b; Szczerba et al., 2006). Thus as shown by Kronzucker and co-workers, the pre- and post-wash conditions used in unidirectional influx measurements exhibit minor discrepancies in the HATS range, but large discrepancies in the LATS range of nutrient ion concentrations (Britto et al., 2006; Szczerba et al., 2006). In alternative approaches such as *flow-force* or compartmental analysis by the tracer efflux method (CATE), the measurements of net influx or efflux rates are more accurate and less chaotic because they are performed in steady-state conditions and are close to equilibrium (Britto et al., 2006). These experimental approaches offer major opportunities to find new solutions to improve formalisms of ion uptake in agronomic models for agricultural purposes.

In this review, we discuss experimental procedures to measure ion influx across the root, and present the basic principles of *flow-force* theory established in the 1970s (Thellier, 1969, 1970a,b; Thellier et al., 1971a,b), how this theory has evolved (Thellier, 1973, 2012; Thellier et al., 2009) and how and why its formalism could be used in agronomic and phytoplankton models of nutrient ion uptake.

EXPERIMENTAL PROTOCOLS FOR ENZYME-LIKE VS. FLOW-FORCE MODELING

Although the effects of local ion status and/or uptake-wash regime on uptake isotherm kinetics have long been recognized as very important factors influencing kinetic responses (Cram and Laties, 1971; Leigh et al., 1973; Ayadi et al., 1974; Tinker and Nye, 2000), they have been discussed only in the recent literature (Britto and Kronzucker, 2001a, 2006; Szczerba et al., 2006). Here we show that experimental procedures used to measure unidirectional ion influx across root membranes to establish ion influx isotherms will be different according to the modeling type chosen: *enzyme-like* or *flow-force*.

Influx Rate Measurements According to Enzyme-Like Interpretation of Root Ion Uptake

In the conventional *enzyme-like* procedure, ion flux measurements across the root membranes at a given temperature (isotherm condition) are made on roots of intact plants (Polley and Hopkins, 1979; Siddiqi et al., 1989, 1990; Delhon et al., 1995; Faure-Rabasse et al., 2002) or excised roots (Epstein et al., 1963; Leigh et al., 1973; Kochian and Lucas, 1982; Kochian et al., 1985). The flux measurements with radioactive or stable tracers of the major nutrient ions present in soil (NO_3^-, NH_4^+, K^+, PO_4^{2-}) are performed over a short period of time: 5–10 min (**Figure 1**), because the half-life of the ion cytoplasmic pool is only 2–7 min (Presland and MacNaughton, 1984; Lee and Clarkson, 1986; Devienne et al., 1994; Muller et al., 1995). It is assumed that this short measurement time allows the assessment of influx from carriers located in the plasma membrane of epidermis root cell layer instead of net flux resulting from the difference between influx and efflux (Walker and Pitman, 1976). It is then critical to accurately determine the time needed to measure unidirectional ion influx, together with the durations of pre- and post-wash to equilibrate the apparent free spaces of the cell wall. As a rule, these durations are deduced from the half-life of tracer exchange between the apoplast and cytosol compartments, obtained by desorption experiments (Presland and MacNaughton, 1984; Lee and Clarkson, 1986; Devienne et al., 1994; Muller et al., 1995; Kronzucker et al., 1995b,c,d).

Pre- and Post-Wash Steps During Unidirectional Measurement of Influx Rate with Ion Tracers in Non-Steady-State or Non-Equilibrium Conditions

The determination of ion influx rate from plants never exposed to the ion of interest except for a 5 min pre-wash solution prior to influx measurement, or directly in labeling solution does not correspond to stationary or equilibrium conditions (**Figure 1**). Unidirectional influx rate values are obtained in a transient state although plants have the same nutrient status because they have been uniformly pre-treated (**Figure 1**). By contrast, the steady-state conditions can be defined as a situation in which ion fluxes in and out of the root cells of a substrate S_j do not fluctuate under given environmental conditions. In this stationary condition, the root system is crossed by a flow of matter or energy but the system properties do not change over time. In addition, the steady-state conditions do not rule out an active transport across the membrane that prevents many diffusive fluxes from ever reaching equilibrium. Such a situation is encountered in short-term isotopic labeling experiments in which the plant growth rate and nutrient solution are held constant (Britto and Kronzucker, 2001b, 2003a; Malagoli et al., 2008). The equilibrium is defined as no further net movement of solute in the lack of driving forces such as difference in concentration or electric field. In conventional pre-wash procedures presented in **Figure 1A**, the conditions for the ion of interest are far removed from the equilibrium or steady state conditions because plants are never exposed to this ion before influx measurements (Siddiqi et al., 1989, 1990; Tinker and Nye, 2000). These situations can be qualified as transient conditions because the system properties change over time. Likewise, during the post-wash step a low temperature is sometime applied to block the activity of influx and efflux carriers (**Figure 1B**). However, this condition may induce strong disturbances in measurements of ion influx from a thermodynamic point of view by modifying influx and efflux velocity characteristics of ion transporters (Britto and Kronzucker, 2001a).

Duration of Pre- and Post-Wash Steps is Determined by Compartmental Analysis by Tracer Efflux

Turnover in the tracer cytosolic pool is calculated from compartmental analysis by tracer efflux (CATE) from plants growing under steady-state conditions (Rauser, 1987; Cram, 1988; Siddiqi et al., 1991; Kronzucker et al., 1995b,c,d). Depending on the ion studied, the plant roots were exposed to a radioactive or stable tracer for 30 min to 1 h allowing both substantial labeling of the cytosolic pool and limited labeling of the vacuolar compartment under steady-state conditions. The plants were then transferred to a non-labeling solution of the same concentration, and a kinetic study of tracer elution due to its efflux was performed to monitor desorption from extra-cellular compartments, and then ion efflux from cytosol to external medium (**Figure 2A**). It is well-established that compartmental analysis from a semi-logarithmic plot of the time-course of ^{13}N radiotracer efflux shows three different phases (**Figure 2B**). The successive phases are linked to the surface liquid film (phase I), cell wall composed of the water free space (WFS) and Donan free space (DFS; phase II) and cytosolic pool (phase III; Rauser, 1987; Kronzucker et al., 1995b,c,d; Britto and Kronzucker, 2003b). From these experiments, duration of ion tracer desorption (i.e., ion exchange between labeled and unlabeled ion in the apoplast) by washing with unlabeled nutrient solution is easily determined by the duration of phases I and II for different ion species (Siddiqi et al., 1989, 1990; Kronzucker et al., 1995b,c,d; Malagoli et al., 2008). The idea is to maximize ion removal from WFS and DFS while minimizing ion loss from the cytosolic pool. However, even in the steady-state conditions used, Kronzucker and co-workers have shown that elution of ^{42}K tracer by washing of barley roots causes disturbance of ion efflux and leads to less accurate measurements of kinetic parameters. Accordingly, a new procedure involving continuous monitoring of bathing solution by removal and replacement of external solution aliquots was defined to improve the estimation of the kinetic constant, called sub-sample CATE (SCATE; Britto et al., 2006).

Alternative Flow-Force Procedure

In the *flow-force* procedure, the main difference is that flux measurements are performed on the roots at or close to equilibrium with the external nutrient solution (Ayadi et al., 1974; Tinker and Nye, 2000). The equilibrium is defined as no further net movement of solute in the absence of driving forces such as difference in concentration, or electric field. Accordingly, the plant roots placed in a non-labeled solution at a given external concentration were not washed before the tracer flux measurements to avoid destroying the initial state of

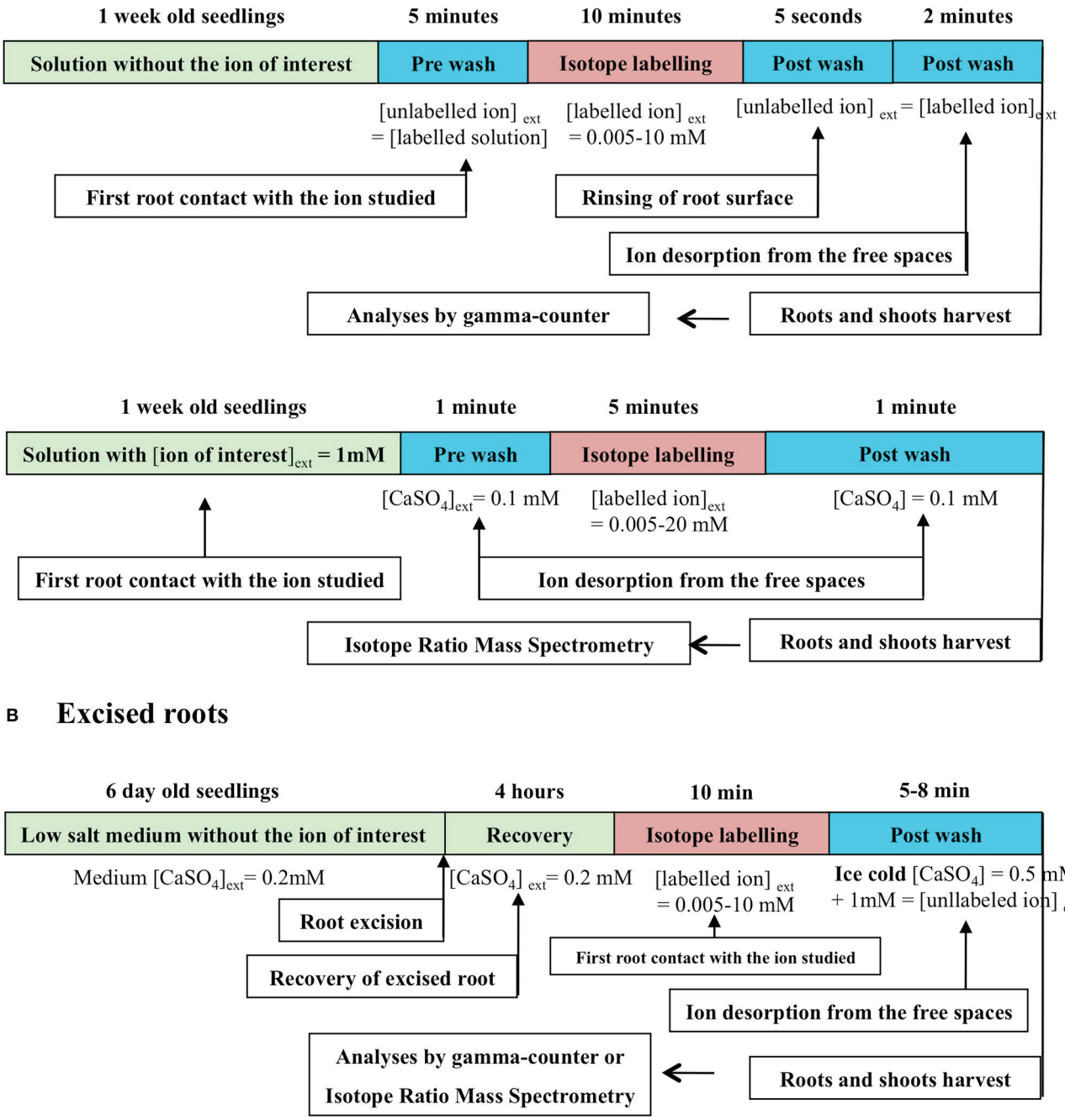

FIGURE 1 | Conventional procedure of ion influx measurements with radioactive or stable ion isotopes by stepwise increase of ion concentrations. (A) Stepwise protocol for nitrate influx isotherms determination in intact plant roots of barley (from Siddiqi et al., 1989, 1990), spruce (Kronzucker et al., 1995a), and Arabidopsis (Filleur et al., 2001). **(B)** Stepwise protocol for K^+ influx isotherms determination of excised roots of 6-day-old dark-grown maize seedlings (from Kochian and Lucas, 1982; Kochian et al., 1985).

equilibrium (**Figure 3**). The external concentration was smoothly increased by adding aliquots with labeled nutrient ion at a higher concentration, and the net flux was measured. The plants were then transferred to non-labeling solution at the same concentration to remove tracer from the cell wall. To some extent, the steady-state conditions used in SCATE procedure are

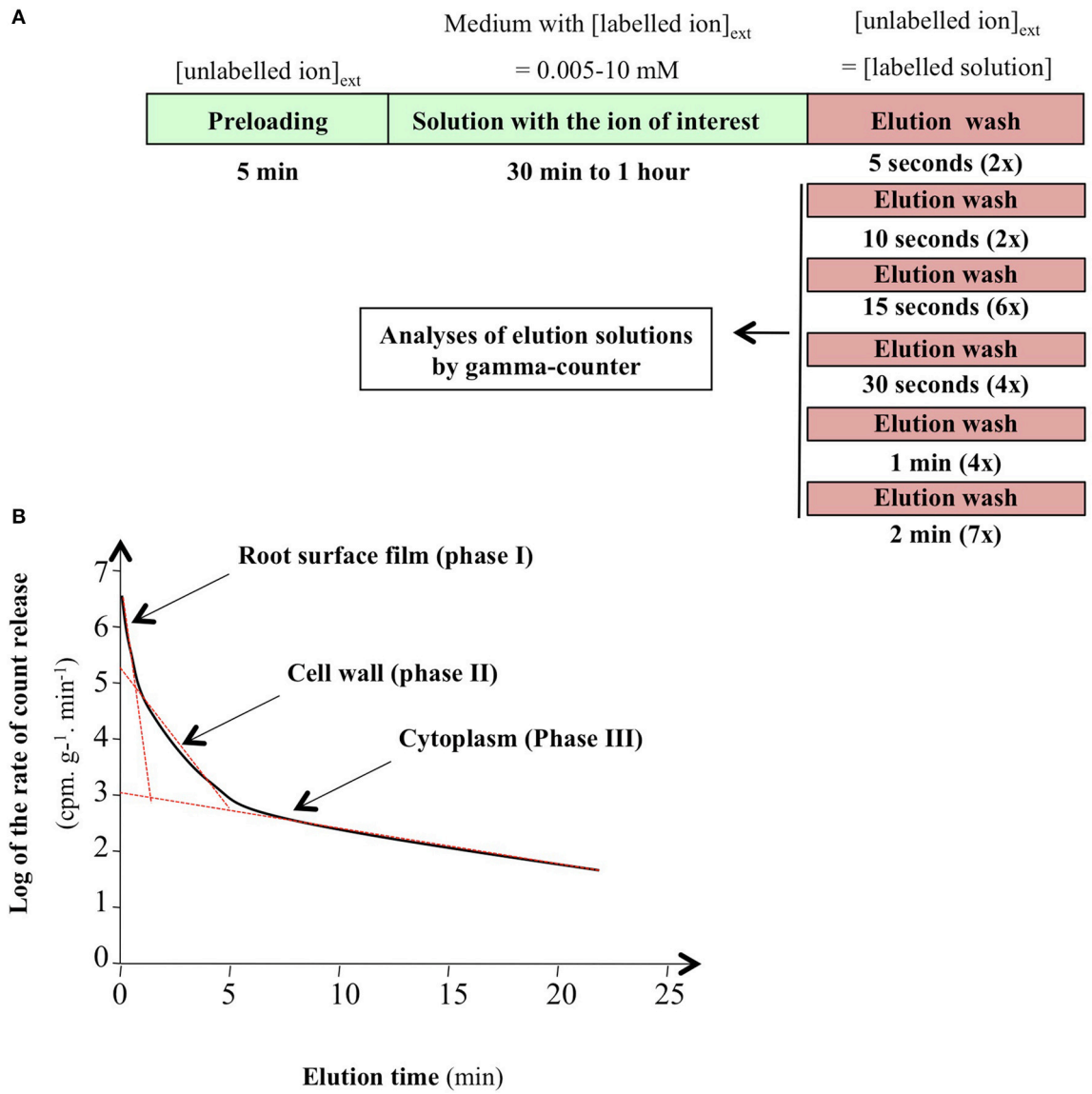

FIGURE 2 | Conventional procedure of root efflux analysis. (A) Stepwise protocol for efflux in intact plant roots of spruce, barley, and rice. **(B)** Representative plot of ion efflux from roots of intact plants. Linear regression on semi-logarithmic plots was used to resolve phase I, II, and III corresponding to ion root surface film, cell wall, and cytosolic pools (from Clarkson, 1974; Kronzucker et al., 1995b; Britto and Kronzucker, 2003b).

close to that which should be followed in the flow-force analysis (Britto et al., 2006).

Does the Broad Range of Applied External Concentrations Have Any Biological Significance in Building Isotherms?

For a long time in the *enzyme-like* conventional procedure, the maximal external ion concentrations used to build the isotherms exceeded those measured in non-anthropized or agricultural soil solutions by one or two orders of magnitude. For example, nutrient solution concentrations used in laboratory studies lay in the range 1 μM to 250 mM for nitrate (Siddiqi et al., 1989, 1990; Kronzucker et al., 1995a,b; Hu et al., 2009), nitrate concentrations being lower than 1 mM in non-anthropized soils and lower or equivalent to 10–20 mM after fertilization in agricultural soils (Reisenauer, 1966; NaNagara et al., 1976; Wolt, 1994; Britto and Kronzucker, 2005; Miller et al., 2007). Likewise, for potassium, the concentrations explored ranged from 1 μM to 10 or 100 mM (Epstein et al., 1963; Polley and Hopkins, 1979; Kochian and Lucas, 1982), typical K^+ concentration in the soil solution ranging only from 1 μM to 6 mM (Maathuis, 2009). Furthermore, in the conventional *enzyme-substrate* wash procedure, measurement errors in unidirectional influx rate are less significant (10%) in a low range of ion concentration. However, the wash procedure induces errors of at least 30%

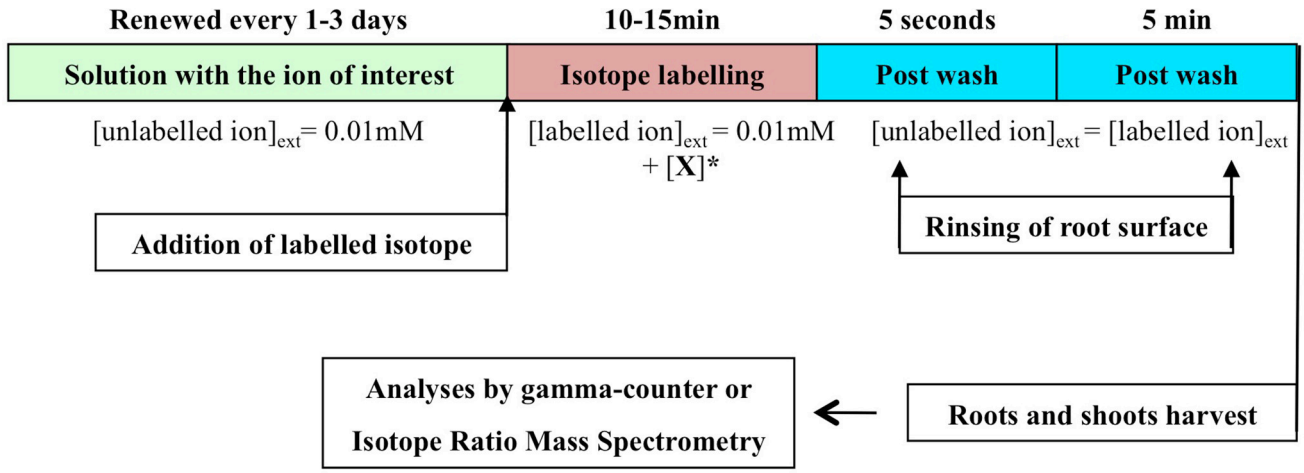

FIGURE 3 | Optimal experimental design for the *Flow-Force* modeling. Stepwise protocol for influx in intact plant roots placed in conditions of steady-state growth. The stepwise increase of labeled ion concentration. = +[X] represents the concentrations of labeled ion needed to reach a desired final concentration for stepwise influx measurements.

in the high range of ion concentrations (Britto et al., 2006). Likewise, in the high range of concentrations for six major nutrient ions (Cl^-, NO_3^-, SO_4^{2-}, K^+, NH_4^+, Na^+), the efflux component increases, and efflux:influx ratios tend toward a value close to 1. Because the anion (A^-) influx is mediated by an electrogenic symport mechanism with a general $A^-/2H^+$ stoichiometry, this result suggests that H^+-ATPase pumps must run twice to counterbalance the anion efflux. Under a broad range of concentrations, this futile ion cycling probably has a large energy cost (Britto and Kronzucker, 2006). Taken all together, these results show that over a high range of ion nutrient concentrations, besides the lack of biological meaning of ion concentrations used, the kinetic patterns of the isotherms cannot be regarded as being accurate measurements of the unidirectional influx owing to the magnitude of the efflux component (Britto and Kronzucker, 2006).

ENZYME-LIKE MODELING

When influx of substrate j (J_j) has been plotted against S_j concentrations in external solution (noted c_j^e), a wide variety of curves can frequently be fitted to experimental data points: (i) curve with one arch, (ii) curve with two arches, or (iii) curve with one arch followed by a quasi-linear response, (iv) curves with more than two arches, and (v) sigmoid curves (**Figure 4**). For example in erythrocytes, sodium uptake between 0 and 150 mM shows a sigmoid rather than a curvilinear relationship (Garrahan and Glynn, 1967). Similarly, depending on the internal concentration of K^+, root influx of K^+ showed an allosteric regulation (Glass, 1976).

Carrier Viewpoint of Enzyme-Like Modeling

The idea of modeling arches given by the experimental points obtained with unidirectional flux of tracer originated from the pioneering work of Emmanuel Epstein and his group (Epstein and Hagen, 1952; Epstein, 1953, 1966). The interpretation of ion influx isotherms is based on applying analogical reasoning to enzyme functioning (Briskin, 1995; Jacoby, 1995). In brief, this reasoning states that the absorption mechanism of a substrate S_j from external to internal is catalyzed by a carrier C. In this case,

$$S_j^e + C \longleftrightarrow CS_j \rightarrow S_j^i + C, \quad (1)$$

where S_j^e and S_j^i represent substrate S_j present in external and internal solution, respectively. CS_j represents the complex formed between S_j and the carrier. This formalism is equivalent to Michaelis–Menten kinetics formalizing an enzymatic transformation of S into P through E activation:

$$S + E \longleftrightarrow ES \rightarrow P + E, \quad (2)$$

where ES represents the enzyme-substrate complex.

The graphs $\{c_j^e, J_j^{ei}(c_j^e)\}$ obtained are curves with one arch (**Figure 2A**), and are modeled by a hyperbola of the Michaelis–Menten type stated to represent the involvement of a single carrier (Cornish-Bowden et al., 2004).

$$v = V\max \cdot [c_s]/(Km + [c_s]), \quad (3)$$

where v is the velocity or "*flow,*" c_s is the external substrate concentration, *Vmax* (maximum velocity) represents the velocity of enzyme saturated by the substrate, and $1/K_m$ is an approximation of the enzyme affinity for the substrate. This equation can also be written:

$$J_j^{ei}(c_j^e) = V\max \cdot [c_j^e]/(Km + [c_j^e]), \quad (4)$$

where *Vmax* is the saturation velocity of carrier C by substrate S_j, and $1/Km$ is an approximation of the affinity of carrier C for substrate S_j.

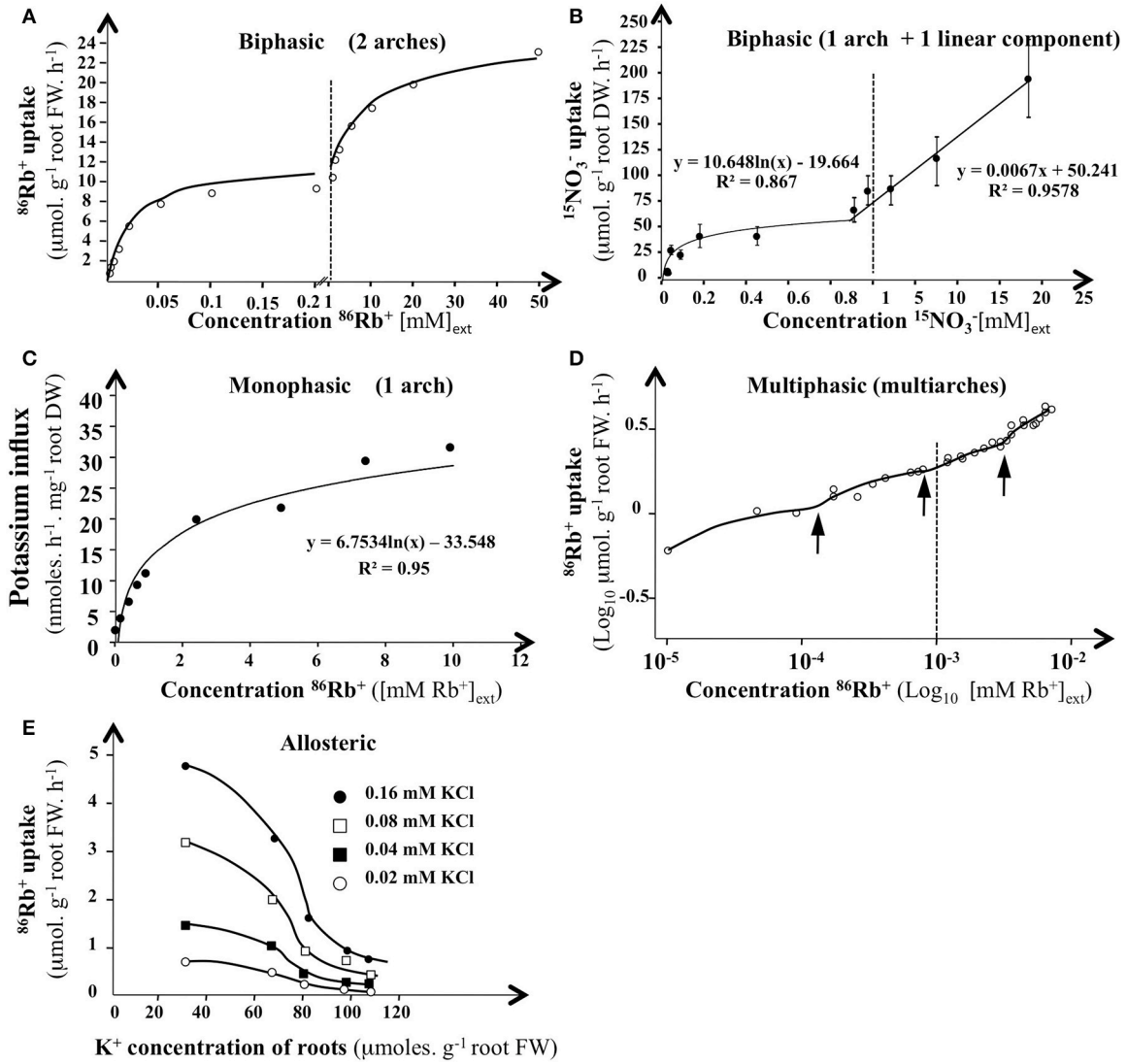

FIGURE 4 | Influx isotherms for K^+ and NO_3^- absorption by plant roots in *H. vulgare* and *Arabidopsis*. (A) Isotherms for $^{42}K^+$ uptake of excised roots from 5-day-old dark-grown barley seedlings. K^+influx rate was measured after 10 min of labeling at 30°C with a nutrient solution of 0.5 mM $CaCl_2$ containing between 0.002 and 50 mM $^{15}NO_3^-$ (adapted from Epstein et al., 1963). **(B)** Isotherms for $^{15}NO_3^-$ of intact roots from 6-weeks-old *Arabidopsis* plants. No_3^-influx rate was measured after 5 min of labeling at 25°C with a complete nutrient solution containing between 0.005 and 20 mM $^{15}NO_3^-$. Bars indicates SE for $n = 6$ (adapted from Filleur et al., 2001). **(C)** Monophasic isotherm interpretation for $^{86}Rb^+$ uptake of roots from 4-5-d-old *Arabidopsis* intact seedlings (adapted from Polley and Hopkins, 1979). **(D)** Multiphasis or discontinuous isotherms interpretation for $^{86}Rb^4$ uptake of excised roots from 6-d-old dark grown maize roots ($log_{10}v$ vs. log_{10} $[Rb^+]_{ext}$) (from Nissen, 1989). K^+ influx rate was measured after 10 or 30 min of labeling at 23°C with a nutrient solution of 0.2 mM $CaSO_4$ and 1 mM MES Buffer pH 6.5 containing between 0.005 and 50mM $^{86}Rb^4$ (Kochian and Lucas, 1982). Arrows indicates transition for potassium uptake. **(E)** Allosteric regulation of $^{86}Rb^+$ influx rate by internal K^+ concentrating 6-d-old intact barley roots. K^+ influx rate was measured after 10 min of labeling at 30° C with a nutrient solution of 0.5 mM $CaSO_4$ containing between 0.02 and 0.16 mM $^{86}Rb^+$(from Glass, 1976).

For the graphs with two arches, we consider that each of the arches reflects the activity of a particular type of carrier considered to play the dominant role in the range of concentrations over which the arch is observed (**Figure 4A**). Each of the arches is then modeled by a Michaelis–Menten hyperbola and characterized by the values of the microscopic parameters *Vmax* and *Km* (*Vm1*, *Km1* for the first hyperbola and *Vm2*, *Km2* for the second, and so on). Because graphs with two arches are those most frequently obtained, it was widely assumed that two types of carriers or mechanisms were most often involved in the absorption process: a low maximum velocity (and so capacity) and HATS (mechanism I, called HATS for High Affinity Transport System) and a high maximum velocity, LATS (mechanism II, called LATS for Low Affinity Transport System).

When the second mechanism shows a linear part (**Figure 4B**), it is considered that the diffusion becomes dominant in the

corresponding concentration range (Kochian and Lucas, 1982; Briskin, 1995; Jacoby, 1995; Britto and Kronzucker, 2008). When the graphs $\{c_j^e, J_j^{ei}(c_j^e)\}$ are sigmoid (**Figure 4E**), it is inferred that the corresponding carriers could be allosteric proteins (Glass, 1976).

In summary, *enzyme-like* modeling seems powerful since it determines the molecular characteristics of the carrier from the macroscopic unidirectional influx measurements of root biological samples (e.g., number of different types of carriers involved, estimated values of *Km* and *Vmax* of these carriers, possible allosteric nature of carriers). However, at the same time, a broad diversity of equations fitting experimental data points is controversial because no unity in the identification of root transporter and associated parameters is allowed.

Discussion of Enzyme-Like Modeling

Theoretical studies based on the modeling of realistic mechanisms for carrier functioning showed, with the help of some simplifying assumptions, that such systems could actually generate pulses obeying the Michaelis–Menten equation (King and Altman, 1956; Schachter, 1972; Wong and Hanes, 1973). However, although the arches of the experimental graphs can be reasonably modeled by a Michaelian hyperbola, this does not mean that hyperbolic Michaelis–Menten fitting is the best of all possible models for these arches made from experimental data points: in other words *enzyme-like* modeling may possibly be satisfactory, but is not necessarily so. Indeed, there is no particular reason plant roots should behave like an enzyme.

Molecular Analyses of Ion Carrier Mutants Are Inconsistent with the Predictions of Enzyme-Like Modeling

In the last two decades the cloning and molecular characterization of new macronutrient carriers such as potassium and nitrate, operating over a wide range of external concentrations, has thrived (Touraine et al., 2001; Britto and Kronzucker, 2008; Wang et al., 2012). The mutant analyses validated the existence of complex carrier systems for root absorption rather than a simple carrier system over low and high ranges of potassium and nitrate concentrations (Alemán et al., 2011; Le Deunff and Malagoli, 2014b; Krapp, 2015). For example, the dual affinities of some K^+ and NO_3^- transporters as a result of protein modifications such as phosphorylation and dephosphorylation invalidate the notion of distinct high and low affinity transport systems established by the *enzyme-like* approach (Liu and Tsay, 2003; Cheong et al., 2007; Ho et al., 2009; Ragel et al., 2015). It also denies the oversimplification of carrier insertion in one single membrane (Crawford and Glass, 1998; Le Deunff and Malagoli, 2014b). In addition, the redundancy of the genes encoding nitrate transporters in *Arabidopsis* operating in a low range of external concentrations (<1 mM) such as NRT2.1, NRT2.2, NRT2.4, NRT2.5, and NRT1.1 (NPF6.3) also invalidates *enzyme-substrate* analogical reasoning (Li et al., 2007; Kiba et al., 2012; Glass and Kotur, 2013; Kotur and Glass, 2014; Lezhneva et al., 2014). Furthermore, the recent discovery of new gene families of nitrate transporters: *CLC* (ChLoride Channel) and *NAXT* (NitrAte eXcretion Transporter) has increased the complexity of the root catalytic device for nitrate (De Angeli et al., 2006; Segonzac et al., 2007). The ClCa transporter is involved in nitrate influx into the vacuole and participates in the short-distance transport of nitrate and the homeostasis for cellular nitrate (Monachello et al., 2009; Krebs et al., 2010). Likewise, impairment of nitrate vacuolar sequestration in a mutant defective in tonoplast proton pump, or inhibition of the proton pump using pharmacological inhibitors, up-regulated the *AtNRT1.5* gene expression and down-regulated *AtNRT1.8* expression (Han et al., 2016). The NRT1.5 nitrate transporter is involved in nitrate xylem loading, while the NRT1.8 gene is responsible for xylem unloading (Lin et al., 2008; Li et al., 2010; Chen et al., 2012; Zhang et al., 2014). These results demonstrate that the regulation of the cytosolic nitrate concentration in roots regulates the long-distance transport of nitrate from roots to shoots and the nitrate influx at the root plasma membrane (Geelen et al., 2000; Monachello et al., 2009). They corroborate the previous conclusion of compartmental analysis by the tracer efflux method showing that influx of nitrate to roots is highly regulated by nitrate import into the vacuole, efflux from the cell and loading into the xylem (Pitman, 1977; Britto and Kronzucker, 2001b, 2003a,b). This molecular complexity will certainly go on increasing with the identification of other genes encoding nitrate carriers involved in nitrate influx and efflux from the vacuole (Migocka et al., 2013) or nitrate xylem loading and unloading (Köhler et al., 2002; Han et al., 2016).

Hence the overall root organ should be considered as a catalytic device across the root radius, formed by a complex of nitrate transporters (CNT) operating at low and high ranges of external concentrations (Tinker and Nye, 2000; Britto and Kronzucker, 2003a). The compartment location and inducibility of nitrate transporters conflicts with the implicit interpretation of *enzyme-substrate* modeling where *Vmax* and *Km* are constant parameters and where nitrate transporters are located in a "single root membrane." This probably explains the varied shapes of isotherms encountered in the literature under the different experimental conditions used (**Figure 4**).

Macroscopic vs. Microscopic Parameters

The above arguments do not completely invalidate the *enzyme-like* modeling approach. It is easier to manipulate the macroscopic values taken by a few parameters (V_m^{app} and K_m^{app}, apparent maximum velocity and affinity constant) than to manipulate the experimental values or even the plot that can be drawn from these values. However, we must face the fact that V_m^{app} and K_m^{app} do not have the molecular meanings we might expect (*Vm* and *Km* from an enzymatic reaction). It is clear that parameters *Vmax* and *Km* are only "apparent" parameters, i.e., they reflect activity of ion uptake at the root level and the subsumed activity of several elemental transporters (Neame and Richards, 1972; Polley and Hopkins, 1979; Briskin, 1995; Tinker and Nye, 2000; Franks, 2009). Unfortunately, V_m^{app} and K_m^{app} are too often regarded as actual values of microscopic parameters at the elemental transporter level (Siddiqi et al., 1989, 1990; Forde and Clarkson, 1999; Tinker and Nye, 2000). For the absorption process, V_m^{app} and K_m^{app} are only macroscopic parameters describing the overall behavior of the root sample

studied for the absorption process considered in the experimental conditions used. The major difficulty in using these macroscopic parameters arises from the fact that we are unable (i) to find a simple meaning for them in relation to the integrated constitution and functioning of the root sample at a molecular level and (ii) to fill the gap between the transporters and the unidirectional or net flux measured at root level. Some of the most serious shortcomings of the *enzyme-substrate* interpretation to describe nutrient ion uptake have been corrected in the ecological models of phytoplankton in the last three decades (see Section: Changes in the Number and Nature of Transporters Involved in Nutrient Uptake Modify *Vmax* and *Km* values and Section: Inducibility of Nutrient Transporters in Relation with Plant Nutrient Status also Modifies Apparent Values of *Vmax* and *Km* below).

FLOW-FORCE MODELING

Stating the Problem

Non-equilibrium thermodynamics may be a useful frame for a macroscopic description of the substrate-absorption in which the parameters have a straightforward meaning with respect to the biological sample studied (Katchalsky and Curran, 1965; Thellier et al., 2009; Thellier, 2012).

Briefly, let us consider a system, the "internal" and "external" compartments of which are termed "i" and "e," respectively. The system may be defined by state variables that are either intensive (temperature [in K], pressure, electric potential, chemical potential of a substance, etc.) or extensive (entropy, volume, quantity of electricity, quantity of a substance, etc.). Intensive and extensive variables can be coupled or "conjugated": temperature/entropy, pressure/volume, electric potential/quantity of electricity, chemical potential of a substance/quantity of that substance. Generally speaking, the properties of extensive variables are such that they cannot be defined at a point but only in macroscopic systems or subsystems (e.g., the volume of a point is meaningless) and they are additive (e.g., with a system made up of subsystems, the content of a substance in the system is the sum of the contents of that substance in the subsystems). By contrast, the properties of intensive variables are defined at a mathematical point and are not additive. For instance, when we speak about "the temperature of a system," we imply that all the points in the system are at that temperature. If one or several state variables of a system do not keep the same value in time, this system is said to undergo a "transformation" (or "process"). Two different types of transformation may occur: (i) an exchange of an extensive variable between the internal, i, and the external, e, compartments of the system and/or (ii) a chemical reaction within the system. Let us consider the case of an exchange. The exchange is driven by forces resulting from potential gradients. In the simple case (that considered here) of an exchange of an extensive variable such as a chemical potential of a substance (S_j) between i and e through an infinitely thin frontier, the driving force is merely the difference in the value of the conjugate intensive variable in e and i. In the case presented, this is the difference in the concentration of substance J (namely, c_j^i and c_j^e). The "*flow*," J_j, of S_j between e and i is the quantity of S_j exchanged per unit of time. Using isotopic tracers, it is easy to measure the influx, J_j^{ei}, and the efflux, J_j^{ie}, of S_j separately with:

$$J_j = J_j^{ei} - J_j^{ie} \tag{5}$$

When close enough to equilibrium (i.e., when c_j^i and c_j^e no longer fluctuate in the case of a substance), the *flow*, J_j, is a linear function of the *force*, X_j (i.e., C_j in the case of a substance):

$$J_j = L_j \cdot X_j, \tag{6}$$

in which the coefficient L_j is termed the "conductance" of the process. Farther away from equilibrium, the relation between *flow* and *force* becomes non-linear (Thellier, 1973).

Application of Flow-Force Relationships to the Transport Process

Transposing Equation (1) for a transport process in cell systems in which i is the cytosol of the root cells and e is the apoplastic spaces results in the net *flow* of a substance S_j:

$$J_j(c_j^e) = J_j^{ei}(c_j^e) - J_j^{ie}(c_j^e), \tag{7}$$

where $J_j(c_j^e)$ is the positive *flow* (influx) from e to i and $J_j^{ie}(c_j^e)$ is the positive *flow* (efflux) from i to e. Based on the general *flow-force* theory as set out above, we may consider that in a biological system (here a root cell) in the presence of two substances S_j and S_k, the *flow* of S_j depends not only on "combined" terms (i.e., difference in concentrations across the cell membrane), but also on "crossed" terms (i.e., the effect of S_k on flow of S_j, for instance). It is said that there is a "coupling" between these two processes. Two well-known examples of couplings are: (i) the coupling between the transport process of a substance, S_j, and a reaction process, R (active transport of first order) and (ii) the coupling of the transport process of a substance, S_j, to the transport process of another substance, S_k (active transport of the second order, Mitchell, 1967; Hanson, 1978). *Flow-force* modeling may be proposed to simulate ion *flows* across the root membrane based on driving forces, and not only the putative enzymatic deduced functioning of carriers (Thellier et al., 2009; Thellier, 2012). To deal with linear equations, the transport process, as governed by differences in substrate concentrations, has to be close enough to equilibrium. If $^{\circ}c_j^e$ is the concentration of the growth medium with which plants have pre-equilibrated, the experiments will have to be carried out using a series of external concentrations of S_j, c_j^e, close enough to $^{\circ}c_j^e$. Accordingly, washing the roots before the absorption experiments (as is commonly reported in numerous influx measurement experiments) would strongly disturb the pre-equilibration value, and so ultimately the thermodynamic conditions and *forces* driving *flow*. Washing (with calcium salt, for instance) before influx measurement should therefore be avoided.

The Optimal Experimental Protocol for Flow-Force Modeling

The experimental protocol (Thellier et al., 2009) best suited to application of the *flow-force* approach is as follows. We prepare a series of growth vessels containing a nutrient solution with the initial concentration ($^{\circ}c_j^e$) of S_j. We dip plant samples in these growth vessels long enough for them to equilibrate with this medium with regard to S_j. Without removing the plant samples from the vessels, we impose various concentrations, c_j^e, of S_j in the growth vessels by adding either small amounts of S_j ($c_j^e > {}^{\circ}c_j^e$) or small volumes of a solution identical to the initial medium except that it contains no S_j ($c_j^e < {}^{\circ}c_j^e$). This enables us to smoothly increase or decrease test concentration of substance J. For each value of c_j^e thereby obtained, influx, J_j^{ie} (c_j^e), and efflux, J_j^{ei} (c_j^i) of S_j can be measured using labeled medium marked with a suitable isotope with unlabeled plant samples (direct influx measurements) or unlabeled medium with pre-labeled plant samples (efflux measurements). Accordingly, the net flux for each value of c_j^e, $J_j(c_j^e)$ can be obtained easily using Equation (3).

The Flow-Force Model

Using reasonable simplifying assumptions such as (i) similar values for the activity coefficient of the substrate in the internal and external media, (ii) quasi-constant transmembrane electrical potential over the range of values of c_j^e, and (iii) constant export of the substrate S_j to the aerial parts over the duration of the experiments, the following equation expressing *flow* of substance J across a membrane can be written:

$$J_j(c_j^e) = RT\lambda_j \ln((c_j^e)/({}^{\circ}c_j^e)) = L_j \ln((c_j^e)/({}^{\circ}c_j^e)), \quad (8)$$

with

$$L_j = RT\lambda_j, \quad (9)$$

where R is the gas constant, T the absolute temperature and λ_j, the overall conductance of the sample for the net uptake of S_j. **Table 1** presents the parameters of models, their symbols and their units. When a change in the experimental conditions causes a change λ_j, an Arrhenius diagram lets us determine whether the change is quantitative or qualitative (see Thellier et al., 2009 for further explanations).

A more general expression of net *flows* that can be used when the simplifying assumptions are not properly fulfilled would be:

$$J_j(c_j^e) = L_j \ln(\pi_j \cdot (c_j^e)), \quad (10)$$

where π_j characterizes the resulting effect of all terms (i.e., activity coefficients, electric potential difference, potential couplings, etc.) other than c_j^e involved in the driving force for the net absorption of S_j by the plant sample under study. This means that when a system of semi-log coordinates is used {ln (c_j^e), $J_j(c_j^e)$}, the plot representing the experimental points is expected to be quasi-linear for the values of c_j^e sufficiently close to the equilibrium concentration $^{\circ}c_j^e$ (Thellier et al., 2009). Hence it is expected that if the experiment is undertaken under optimal conditions (similar values of activities coefficients, no change in electrical potentials across the membrane and constant value of net flux across tonoplast and up to aerial parts), the intersection of plots on the abscissa (i.e., *flow* = 0) estimates π_j as:

$$\ln(1/{}^{\circ}c_j^e) = \ln\pi_j. \quad (11)$$

Conversely, if the experimental protocol is not optimal, then the plot intersects the abscissa again at a point $-\ln \pi_j$, but where π_j is no longer equal to $1/{}^{\circ}c_j^e$, although it remains the result of the contribution of all terms other than c_j^e involved in the driving forces energizing the absorption of S_j. In such a case, difference in activity coefficient, transmembrane potentials and fluxes into cells may all be single or combined candidates contributing in a significant way to *forces* driving *flow*. This underlines the importance of conducting experiments close to equilibrium in order to avoid confounding effects when investigating and ultimately modeling *flows*. In other words, $-\ln \pi_j$, represents a thermodynamic constant that accounts for energy coupling necessary for Sj transport. The plot in **Figure 5** illustrates some examples of representations in semi-log coordinates {ln (c_j^e), $J_j(c_j^e)$} for potassium and nitrate uptake from data points obtained in intact plants and unicellular algae in the literature (Kannan, 1971; Polley and Hopkins, 1979; Faure-Rabasse et al., 2002).

TABLE 1 | Key to symbols used in the text.

Symbol	Description	Unit
e	Apoplastic space of the root cells	
i	Internal space of the root cells	
$^{\circ}c_j^e$	Initial concentration in the bulk solution	mol. m^{-3}
c_j^i	Concentration of S_j component in the cytosol	mol. m^{-3}
c_j^e	Concentration of S_j component in the apoplast	mol. m^{-3}
j	Solute under study	
J_j	Solute influx (based on membrane area)	mol. m^2. s^{-1}
K_m^{app}	Apparent half saturation constant	mol. m^{-3}
Km	Half saturation Michaelis-Menten constant	mol. m^{-3}
L_j	Conductance of the overall root system	mol. $h^{-1}.g^{-1}$ root DW
Ln	Logarithm to base e	
π_j	Effect of all the processes energizing the transport of S_j	$mol^{-1}.m^3$
R	Gas constant	8.314 J mol^{-1} K^{-1}
S_j	Solute concentration of solute J in the bulk solution	mol. m^{-3}
T	Absolute temperature	K or °C
V_m^{app}	Apparent maximal uptake rate	mol. s^{-1}
Vmax	Maximum reaction velocity of Michaelis-Menten	mol. s^{-1}

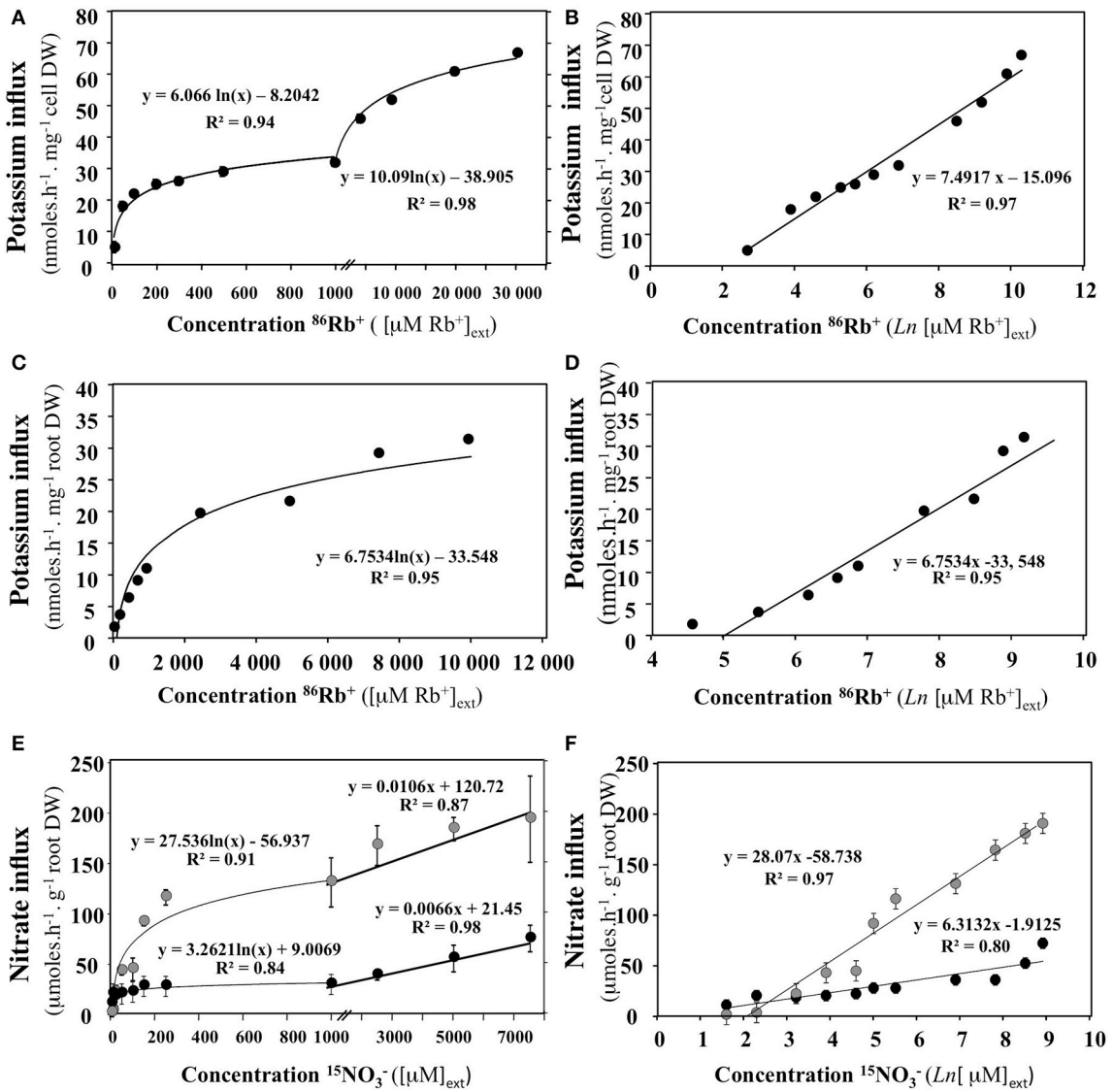

FIGURE 5 | Transformation of nitrate or potassium uptake rate isotherms in semi-log coordinates {ln (c_j^e), $J_j(c_j^e)$}. (A,B) Rate of potassium ($^{86}Rb^+$) uptake by cells of *chlorella pyrenoidosa* as a function of and transformation of the data in semi-log coordinates (From Kannan, 1971). Verticla bars represent ±SD of the means. **(C,D)** Rate of Potassium ($^{86}Rb^+$) uptake by roots of *Arabidpopsis* intact seedlings as a function of KCl concentration in the medium and transformation of the data in semi-log coordinates (from Polley and Hopkins, 1979). **(E,F)** Rate of nitrate uptake by roots of *Brassica napus* intact seedlings as a function of KNO3 concentration in the medium and transformation of the data in semi-log coordinates (from Faure-Rabasse et al., 2002). Plants were either non-induced (grown without NO3 supply, black circles) or induced during 24 h by 1 mM KNO3 prior to measurements (gray circles). Vertical bars indicated ±SD for $N = 3$ when larger than the symbol.

Quantitative/Qualitative Modifications of the Global Conductance, λ_j, in Response to a Change in the Experimental Conditions

When a change in experimental conditions (e.g., use of younger or older plants) causes a change of λ_j, this change can come from quantitative modification of the root catalytic device (which gathers all transporters) involved in the absorption of S_j (change in the number of molecules of carriers) and/or qualitative changes (change in the nature or activity of the carriers). In the range of the biological temperatures [i.e., between 275 (1.85°C) and 305 K (31.85°C)], different values of λ_j are obtained for different temperature values (all the other variables unchanged). Using an Arrhenius plot {1/T, log J_j} or {1/T, λ_j}, the experimental points are expected to lie on a straight line, the slope of which plays a role comparable to that of an activation energy for the overall process of absorption under consideration (Thellier, 1971). When the experiments are carried out with two different conditions (for instance using young or adult plants or at two different external concentrations S_j), if the two plots thus obtained are parallel to each other (similar slope), then the overall

absorption processes differ quantitatively (e.g., the density of carriers at the root epidermis is not the same). By contrast, if the plot slopes are significantly different, then a qualitative change has occurred (e.g., in the specific activity of the carriers). **Figure 6** illustrates the Arrhenius diagram obtained by plotting the logarithm of nitrate influx J_j vs. 1/root temperature at 100 μM and 5 mM external nitrate concentration (Le Deunff and Malagoli, 2014a). Although the experiment was not carried out in the best conditions, the parallel behavior of the two linear curves (**Figure 6B**) highlights that the temperature does not change the root conductance for nitrate at 100 μM and 5 mM. Hence the increase in nitrate influx with temperature is not associated with changes in the catalytic efficacy of the root catalytic device for nitrate (specific activity of carriers), but is instead associated with quantitative changes such as the numbers of nitrate carriers.

Application of Flow-Force Modeling under Suboptimal Experimental Conditions

To our knowledge, no experiment has ever been carried out under the optimal conditions indicated in Section: Application of Flow-Force Relationships to the Transport Process and Section: The Optimal Experimental Protocol for Flow-Force Modeling. However, making a few simplifying hypotheses (in particular the assumption that the efflux remains small compared with the influx over the range of concentrations used, which means that the net *flow* is not too different from the influx), it is possible to apply *flow-force* modeling to the numerous experiments carried out since isotopic tracers became available (Thellier et al., 2009; Le Deunff and Malagoli, 2014a).

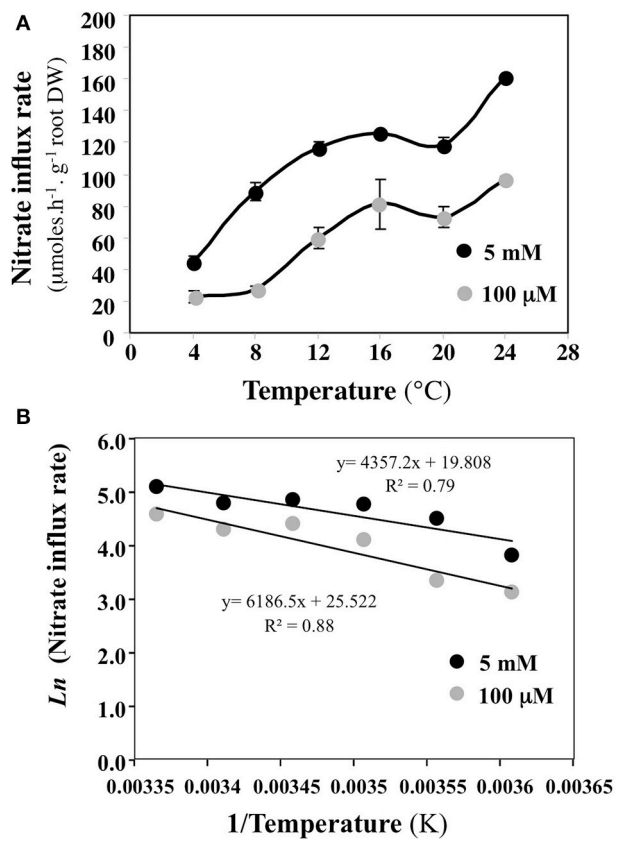

FIGURE 6 | Building an Arrhenius plot from experimental data points to check qualitative or quantitative modifications or the root catalytic device for nitrate uptake. (A) Variations of nitrate uptake rate at 100 μM and 5 mM external nitrate concentration induced by different root temperature treatments. **(B)** Arrhenius diagrams {1/T, log J_j) deduced from nitrate influx rate variations in response to root temperature changes. Vertical bars indicated ±SD for $N = 3$ when larger than the symbol.

Initial Approach to the Problem: The Electrokinetic Formalism

Flow-force modeling of cell transports was initially introduced using the "electrokinetic formulation," based on a formal analogy with classical electrokinetics (Thellier, 1969, 1970a,b, 1973). This does not change the main equations given above. The reason is that classical electrokinetics amounts to *flow-force* modeling in the linear domain.

ATTEMPTS TO CORRECT THE SHORTCOMINGS OF ENZYME-SUBSTRATE INTERPRETATION IN THE NUTRIENT UPTAKE MODELS

For over 50 years, the *enzyme-substrate* interpretation of isotherm kinetics has prevailed, and has been extended to models of nutrient ion uptake in plants (Barber, 1995; Le Bot et al., 1998; Tinker and Nye, 2000; Ma et al., 2008) and phytoplankton (Dugdale, 1967; MacIsaac and Dugdale, 1969; Morel, 1987; Smith et al., 2009, 2014; Aksnes and Cao, 2011; Fiksen et al., 2013). Among all the models, the phytoplankton ecological models of nutrient uptake based on the Michaelis–Menten (MM) formalism show the most noteworthy developments for coping with deviations between simulated and measured outputs. The development of these phytoplankton ecological models encapsulates all the problems encountered by the rigid values of *Vmax* and *Km* provided by the MM models developed in plants (Aksnes and Egge, 1991; Franks, 2009).

Changes in the Number and Nature of Transporters Involved in Nutrient Uptake Modify *Vmax* and *Km* Values

Phytoplankton physiologists have found that one of the main problems of MM models is the rigid values of the *Vmax* and *Km* obtained in short-term experiments in oligotrophic and eutrophic regimes (Aksnes and Egge, 1991; Franks, 2009; Bonachela et al., 2011; Fiksen et al., 2013; Smith et al., 2014). Plant physiologists reached the same conclusion in the 1970s (Nye and Tinker, 1969; Jungk et al., 1990; Barber, 1995; Tinker and Nye, 2000). Several experiments have demonstrated the shortcomings of MM kinetics to describe nutrient ion uptake of phytoplankton (Droop, 1970, 1973; Aksnes and Egge, 1991; Franks, 2009). The observed co-variation of *Vmax* and *Km* values has invalidated the definition of *Km* as an affinity constant, and demonstrated that the *Vmax* and *Km* are only apparent parameters (V_m^{app} and K_m^{app}) and cannot be regarded as constant values depending

for instance on time or internal nutrient status (Neame and Richards, 1972; Aksnes and Egge, 1991; Franks, 2009; Aksnes and Cao, 2011). Hence recent trait-based phytoplankton models provide novel mechanistic expressions to tackle and correct the static expression of the *enzyme-substrate* formalism (Aksnes and Egge, 1991; Aksnes and Cao, 2011; Bonachela et al., 2011; Fiksen et al., 2013; Smith et al., 2014). By deriving equation of nutrient transport at cellular level rather than at enzymatic individual level, Aksnes and Egge (1991) demonstrate that MM modeling is a special case of their mechanistic model. In these models, the uptake of nutrient ions depends on the number and density of uptake sites on the plasmalemma of phytoplankton cells, which determines the plasticity of the uptake apparatus in response to temperature and nutrient diffusion in relation with nutrient regimes (Aksnes and Egge, 1991; Fiksen et al., 2013; Lindemann et al., 2016). In addition, the affinity constant α, defined as the Vmax/Km ratio, is preferred to Km because it represents the area of the cell membrane able to catch nutrient ions and it is proportional to the cell size. The introduction of mechanistic parameters in these extended MM models avoids bias up to 50% in some configurations compared with usual MM models (Fiksen et al., 2013), showing the pertinence of the approach.

Inducibility of Nutrient Transporters in Relation with Plant Nutrient Status Also Modifies Apparent Values of *Vmax* and *Km*

In plants, activities of nutrient transporters such as NO_3^-, PO_4^{2-}, K^+, and SO_4^{2-} are modified by external nutrient availability and pre-treatment with the nutrient under study, which alter nutrient status in plants (Glass, 1976; Siddiqi et al., 1989, 1990; Jungk et al., 1990). Thus in *Arabidopsis*, it has been clearly demonstrated that *AtNRT2.1*, *AtNRT2.2,* and *AtNRT1.1* nitrate transporter genes are induced by external nitrate (Tsay et al., 1993; Amarasinghe et al., 1998; Krapp et al., 1998). Transcriptional induction depends on plant N status, the level induction decreasing with increasing nitrate concentration during the pre-treatment (Siddiqi et al., 1989, 1990). After the induction, a steady de-induction process is observed, with a reversion after 48–72 h to the initial value of nitrate influx rate before induction (Faure-Rabasse et al., 2002; Okamoto et al., 2003). These results demonstrate that depending on plant N status and nitrate pre-treatment, values for the parameters *Vmax* and *Km* can be determined, but are not constant. Although in phytoplankton, inducible behavior of some nutrient carriers such as nitrate transporters has been recently discovered (Rogato et al., 2015), nutrient uptake regulation by N status was already taken into account in trait-based models through a modulating term dependent on the internal nutrient concentration or N/C ratio (Droop, 1970, 1973; Geider et al., 1998; Litchman et al., 2007; Litchman and Klausmeier, 2009; Bonachela et al., 2011).

Despite the quantitative use of the *enzyme-substrate* approach in nutrient uptake models (N, P, K, S) in plants and phytoplankton, the thermodynamic processes involved in nutrient ion uptake and the realistic solutions offered by the *flow-force* modeling approach can no longer be ignored. One of the most severe limitations of MM models in plants and phytoplankton is that temperature, which partly drives biochemical reaction rates and ion diffusion processes, and which in turn modify parameters *Vmax* and *Km*, is not taken into account (Aksnes and Egge, 1991; Tinker and Nye, 2000; Fiksen et al., 2013). Nutrient ion kinetics are established under isothermal conditions. Response of the uptake process to temperature is thus left out of the MM model, even though temperature is a key variable acting either directly (on carrier functioning) or on nutrient availability in the diffusion boundary layer around phytoplankton cells or roots (Aksnes and Egge, 1991; Smith, 2011; Fiksen et al., 2013). The temperature dependence of nutrient influx rate in plants is well illustrated in **Figure 6** for nitrate. Use of *flow-force* formalism for nutrient uptake, which includes the temperature dependence of the uptake, might greatly improve plant and phytoplankton models in response to changes in environmental variables (e.g., temperature, nutritional regimes). Likewise, the nitrate pretreatment with 1 mM KNO_3 for 24 h on previously starved *B. napus* plants induced contrasting root conductance for nitrate and so different catalytic efficiencies (**Figures 5E,F**). Therefore, the embedding in *flow-force* models of the mechanistic approach used in the trait-based approach developed in phytoplankton models (cell size, number of uptake sites per cell, uptake site handling time, affinity of a single uptake site, etc.) should further improve their formalisms and enhance their performance (Lindemann et al., 2016). Attempts at flexible approaches to the uptake parameters in nutrient uptake models such as the introduction of mechanistic support for the uptake sites or cross-combination of the *flow-force* formalism with *in planta* and environmental factor effects, predicts higher and more realistic nutrient uptake rates than the usual MM counterparts (Bonachela et al., 2011; Fiksen et al., 2013; Le Deunff and Malagoli, 2014a; Malagoli and Le Deunff, 2014). Outputs of these new conceptual models demonstrate that usual nutrient uptake models based on the *enzyme-substrate* formalism are inevitably forced by some parameters to match measured nutrient taken up (Ma et al., 2008; Franks, 2009). Unlike phytoplankton nutrient uptake models, the nutrient uptake models in plants also have to allow for the effects of the growth, geometry, and aging of the root system that affect the nutrient uptake. The next sections explain how these effects are taken into account in recent modeling approaches.

Flow-Force Agronomic Models for Nutrient Uptake with One Spatial Dimension

Agronomic models of nutrient ion uptake in one spatial dimension (1-D models) depend on measurements of root distribution profile in the different soil layers from the soil surface to rooting depth along the growth cycle. The relationship between root development and rooting depth is generally described by an experimentally measured heuristic law that gives root distribution for different times throughout the plant growth cycle. This law accounts for the root length density distribution in one spatial dimension (Gerwitz and Page, 1974).

From this framework, a new mechanistic structural-functional model for nitrate uptake was developed for a crop of winter oilseed rape (*Brassica napus* L.). The functional component of the model derives from a revisited conceptual framework that combines the thermodynamic *flow-force* interpretation of nitrate uptake isotherms and environmental and *in planta* effects on nitrate influx (Le Deunff and Malagoli, 2014a). The structural component of the model is based on estimation of root biomass contributing actively to N uptake using the determination of a synthetic parameter IRSA (Integrated Root System Age) that allows assignment of a root absorption capacity at a specific age of the root (Gao et al., 1998; Malagoli and Le Deunff, 2014). This model of one spatial dimension (1-D model) is able to respond more realistically to external nitrate fluctuations throughout the plant growth cycle under field conditions for three levels of N fertilization at both functional and structural levels (Malagoli and Le Deunff, 2014). In this model, it is assumed that convection and diffusion of nitrate ions to the root surface are optimal because the soil water content is close to field capacity. Likewise, no root competition for nitrate uptake or effects of root exudates, microbial activity and mycorrhizae are taken into account. Nitrate influx depends on fluctuation of soil nitrate concentrations, changes in climatic (temperature and PAR) and *in planta* factors (day-night and ontogenetic cycles), and changes in root uptake capacities with aging throughout the plant growth cycle (Le Deunff and Malagoli, 2014b).

Toward Flow-Force Agronomic Models with Two and Three Spatial Dimensions

Two- and three-dimensional models for nutrient ion uptake have been developed to take into account the spatial geometry of root systems and the dynamics of water and nutrient availability and their spatial distribution in soil during the growth cycle (Somma et al., 1998; Roose, 2000; Biondini, 2008; Tournier, 2015). In general, these models were built to find analytical solutions to differential equations provided by equations of soil ion convection-diffusion and root ion influx isotherms (Roose et al., 2001; Roose and Kirk, 2009). Analytical solutions are obtained for one single cylindrical root for isothermal conditions, and then extended to the whole root system (Roose, 2000; Roose et al., 2001). Because analytical solutions can now be derived from almost any form of nutrient uptake function (Roose and Kirk, 2009), we propose to use the thermodynamic *flow-force* linear formalism of nutrient ion isotherms (Equation 10) instead of the non-linear formalism of Michaelis–Menten (Equation 4). This will make parametrization simpler to obtain a more realistic analytical expression for nutrient uptake by a single cylindrical root.

Although parameter L_j in Equation (9; root conductance for substrate S_j) is taken as constant to solve the equations, it may not be truly constant. For example, the effects of fluctuating temperature throughout the growth cycle, spatial heterogeneity of nitrate in the soil, root aging, the day-night cycle and ontogenesis, which modify $J_j(c_j^e)$ through changes in L_j, are not taken into account in this approach (Le Deunff and Malagoli, 2014a,b). Accordingly, obtaining analytical solutions to these equations will not completely solve the problems associated with extension of the uptake behavior of one root segment to the entire root system throughout the plant growth cycle. In particular, the building of a realistic root network is confronted with the patterning process of root systems caused by the spatial heterogeneity of available water and nutrient ions in soil throughout the growth cycle (Drew, 1975; Bao et al., 2014).

Instead of finding analytical solutions and scaling up the uptake behavior of one root segment to the entire root system, mechanistic 3-D models have been developed that numerically solve nonlinear partial differential equations coupling soil water and nutrient transport with root uptake at the single root scale (Somma et al., 1998; Doussan et al., 2006; Javaux et al., 2008; Tournier et al., 2015). Thanks to recent advances in scientific computing, such models are now able to simulate water and nutrient transport with root uptake for realistic root systems, taking advantage of unstructured grids adapted to the complex geometry of the root system and solving the computationally intensive discrete problems on parallel architectures (Tournier, 2015). Like for 2-D models, the *flow-force* formalism can be easily introduced in this type of 3-D model.

CONCLUDING REMARKS

Major benefits of the *flow-force* formulation are that it makes experimentally testable predictions and it expresses the results of macroscopic measurements (i.e., made on an entire biological sample) by macroscopic parameters (L_j and π_j) associated with a biological meaning, without considering molecular characteristics of carriers. It also provides a coordinate graph $\{\ln(c_j^e), J_j(c_j^e)\}$ that is linear if c_j^e values are sufficiently close to the equilibrium concentration of S_j ($^\circ c_j^e$). The kinetic patterns can be improved by changing the pre- and post-wash procedures for roots before net influx rate measurements in order to come as close as possible to equilibrium conditions. In addition, linear formalism of the *flow-force* approach could usefully replace the Michaelis–Menten formalism of the *enzyme-substrate* approach currently used in the phytoplankton and agronomic nutrient ion uptake models (Barber, 1995; Tinker and Nye, 2000; Roose and Kirk, 2009; Tournier, 2015). This would offer a simplification of parametrization to help find more realistic analytical expressions and numerical solutions for ion uptake in 2-D and 3-D models of nutrient uptake in plants.

AUTHOR CONTRIBUTIONS

Substantial contributions to the conception or design of the work: EL, PT, PM. Drafting the work or revising it critically for important intellectual content: EL, PT, PM. Final approval of the version to be published: EL, PT, PM. Agreement to be accountable for all aspects of the work in ensuring that questions related to the accuracy or integrity of any part of the work are appropriately investigated and resolved: EL, PT, PM.

ACKNOWLEDGMENTS

The authors warmly thank Prof. Michel Thellier for early comments, helpful guidelines and constructive discussion on development of the *flow-force* theory and its applicability to nutrient uptake models during the writing of this paper. We also thank the two reviewers for valuable suggestions and comments on drafts of the manuscript.

REFERENCES

Aksnes, D. L., and Cao, F. J. (2011). Inherent and apparent traits in microbial nutrient uptake. *Mar. Ecol. Prog. Ser.* 440, 41–51. doi: 10.3354/meps09355

Aksnes, D. L., and Egge, J. K. (1991). A theoretical model for nutrient uptake in phytoplankton. *Mar. Ecol. Prog. Ser.* 70, 65–72. doi: 10.3354/meps070065

Alemán, F., Nieves-Cordones, M., Martinez, V., and Rubio, F. (2011). Root K^+ acquisition in plants: the *Arabidopsis thaliana* model. *Plant Cell Physiol.* 52, 1603–1612. doi: 10.1093/pcp/pcr096

Amarasinghe, B. H., de Bruxelles, G. L., Braddon, M., Onyeocha, I., Forde, B. G., and Udvardi, M. K. (1998). Regulation of *GmNRT2* expression and nitrate transport activity in roots of soybean (*Glycine max). Planta* 206, 44–52. doi: 10.1007/s004250050372

Aslam, M., Travis, R. L., and Huffaker, R. C. (1992). Comparative kinetics and reciprocal inhibition of nitrate and nitrite uptake in roots of uninduced and induced barley (*Hordeum vulgare* L.) seedlings. *Plant Physiol.* 99, 1124–1133. doi: 10.1104/pp.99.3.1124

Ayadi, A., Stelz, T., Monnier, A., Lassalles, J. P., and Thellier, M. (1974). Application of an electrokinetic formulation to the study of the effect of alkaline-earth cations on the absorption of K^+-ions by *Lemna minor*. *Ann. Bot.* 38, 677–696.

Bao, Y., Aggarwal, P., Robbins, N. E., Sturrock, C. J., Thompson, M. C., Tan, H. Q., et al. (2014). Plant roots use a patterning mechanism to position lateral root branches toward available water. *Proc. Natl. Acad. Sci. U.S.A.* 111, 9319–9324. doi: 10.1073/pnas.1400966111

Barber, S. A. (1995). "Nutrient absorption by plant roots," in *Soil Nutrient Bioavailability: A Mechanistic Approach*, ed S. A. Barber (New York, NY: John Wiley and Sons), 49–84.

Bieleski, R. L. (1973). Phosphate pools, phosphate transport, and phosphate availability. *Annu. Rev. Plant Physiol.* 24, 225–252. doi: 10.1146/annurev.pp.24.060173.001301

Biondini, M. (2008). Allometric scaling laws for water uptake by plant roots. *J. Theor. Biol.* 251, 35–59. doi: 10.1016/j.jtbi.2007.11.018

Bonachela, J. A., Raghib, M., and Levin, S. A. (2011). Dynamic model of flexible phytoplankton nutrient uptake. *Proc. Natl. Acad. Sci. U.S.A.* 108, 20633–20638. doi: 10.1073/pnas.1118012108

Briskin, D. P. (1995). "Solute transport across plant cell membranes: biochemical and biophysical aspects," in *Handbook of Plant and Crop Physiology*, ed M. Pessarakli (New York, NY; Basel; Hong Kong: Marcel Dekker Inc), 387–418.

Britto, D. T., Czczerba, M. W., and Kronzucker, H. J. (2006). A new, non-perturbing, sampling procedure in tracer efflux measurements. *J. Exp. Bot.* 57, 1309–1314. doi: 10.1093/jxb/erj105

Britto, D. T., and Kronzucker, H. J. (2001a). Can unidirectional influx be measured in higher plants? A mathematical approach using parameters from efflux analysis. *New Phytol.* 150, 37–47. doi: 10.1046/j.1469-8137.2001.00080.x

Britto, D. T., and Kronzucker, H. J. (2001b). Constancy of nitrogen turnover kinetics in the plant cell: insights into the integration of subcellular N fluxes. *Planta* 213, 175–181. doi: 10.1007/s004250000497

Britto, D. T., and Kronzucker, H. J. (2003a). Ions fluxes and cytosolic pool size: examining fundamental relationships in transmembrane flux regulation. *Planta* 217, 490–497. doi: 10.1007/s00425-003-1013-8

Britto, D. T., and Kronzucker, H. J. (2003b). The case for cytosolic NO_3^- heterostasis: a critique of a recently proposed model. *Plant Cell Environ.* 26, 183–188. doi: 10.1046/j.1365-3040.2003.00992.x

Britto, D. T., and Kronzucker, H. J. (2005). Plant nitrogen transport and its regulation in changing soil environments. *J. Crop Improv.* 15, 1–42. doi: 10.1300/J411v15n02_01

Britto, D. T., and Kronzucker, H. J. (2006). Futile cycling at the plasma membrane: a Hallmark of low-affinity nutrient transport. *Trends Plant Sci.* 11, 529–534. doi: 10.1016/j.tplants.2006.09.011

Britto, D. T., and Kronzucker, H. J. (2008). Cellular mechanisms of potassium transport in plants. *Physiol. Plant.* 133, 637–650. doi: 10.1111/j.1399-3054.2008.01067.x

Cerezo, M., Tillard, P., Filleur, S., Munos, S., Daniele-Vedele, F., and Gojon, A. (2001). Major alterations of the regulation of root NO_3^- are associated with the mutation of NRT2.1 and NRT2.2 genes in Arabidopsis. *Plant Physiol.* 127, 262–271. doi: 10.1104/pp.127.1.262

Chen, C.-Z., Lv, X.-F., Li, J.-Y., Yi, H.-Y., and Gong, J.-M. (2012). Arabidopsis NRT1.5 is another essential component in the regulation of nitrate reallocation and stress tolérance. *Plant Physiol.* 159, 1582–1590. doi: 10.1104/pp.112.199257

Cheong, Y. H., Pandey, G. K., Grant, J. J., Batistic, O., Li, L., Kim, B.-G., et al. (2007). Two calcineurin B-like calcium sensors, interacting with protein kinase CIPK23, regulate leaf transpiration and root potassium uptake in Arabidopsis. *Plant J.* 52, 223–239. doi: 10.1111/j.1365-313X.2007.03236.x

Clarkson, D. T. (ed.). (1974). *Ion Transport and Cell Structure in Plants.* London: MacGraw-Hill.

Colmer, T. D., and Bloom, A. J. (1998). A comparison of NH_4^+ and NO_3^- net fluxes along roots of rice and maize. *Plant Cell Environ.* 21, 240–246. doi: 10.1046/j.1365-3040.1998.00261.x

Cornish-Bowden, A., Jamin, M., and Saks, V. (2004). "La thermodynamique et la théorie des vitesses absolues," in *Cinétique Enzymatique*, ed J. Bornarel (London: Portland Press Ltd), 25–54.

Cram, W. J. (1988). "Transport of nutrient ions across cell membranes *in vivo*," in *Advances in Plant Nutrition*, eds E. D. Tinker and A. Laüchli (New York, NY: Praeger), 1–53.

Cram, W. J., and Laties, G. G. (1971). The use of short-term and quasi-steady influx in estimating plasmalemma and tonoplast influx in barley root cells at various external and internal chloride. *Aust. J. Biol. Sci.* 24, 633–646.

Crawford, N. M., and Glass, A. D. M. (1998). Molecular and physiological aspects of nitrate uptake in plants. *Trends Plant Sci.* 3, 389–395. doi: 10.1016/S1360-1385(98)01311-9

De Angeli, A., Monachello, D., Ephritikhine, G., Frachisse, J. M., Thomine, S., Gambale, F., et al. (2006). The nitrate/proton antiporter AtCLCa médiates nitrate accumulation in plant vacuoles. *Nature* 442, 939–942. doi: 10.1038/nature05013

Delhon, P., Gojon, A., Tillard, P., and Passama, L. (1995). Diurnal regulation of NO_3^- uptake in soybean plants I. changes in NO_3^- influx, efflux, and N utilization in the plant during the day/night cycle. *J. Exp. Bot.* 46, 1585–1594. doi: 10.1093/jxb/46.10.1585

Devienne, F., Mary, B., and Lamaze, T. (1994). Nitrate transport in intact wheat roots. I. Estimation of cellular fluxes and NO_3^- distribution using compartmental analysis from data of $^{15}NO_3^-$ efflux. *J. Exp. Bot.* 45, 667–676. doi: 10.1093/jxb/45.5.667

Doussan, C., Pierret, A., Garrigues, E., and Pagès, L. (2006). Water uptake by plant roots: II - modelling of water transfer in the soil root-system with explicit account of *flow* within the root system - comparison with experiments. *Plant Soil* 283, 99–117. doi: 10.1007/s11104-004-7904-z

Drew, M. C. (1975). Comparison of the effects of a localized supply of phosphate, nitrate, ammonium and potassium on the growth of the seminal root system, and the shoot in Barley. *New Phytol.* 75, 479–490. doi: 10.1111/j.1469-8137.1975.tb01409.x

Droop, M. R. (1970). Vitamin B, and marine ecology. V. Continuous culture as an approach to nutritional kinetics. *Helgol. Wiss. Meeresunters.* 205, 29–36.

Droop, M. R. (1973). Some thoughts on nutrient limitation in algae. *J. Phycol.* 9, 264–272. doi: 10.1111/j.1529-8817.1973.tb04092.x

Dugdale, R. (1967). Nutrient limitation in the sea: dynamics, identification, and significance. *Limnol. Oceanogr.* 12, 685–695. doi: 10.4319/lo.1967.12.4.0685

Epstein, E. (1953). Mechanism of ion absorption by roots. *Nature* 171, 83–84. doi: 10.1038/171083a0

Epstein, E. (1966). Dual pattern of ion absorption by plant cells and by plants. *Nature* 212, 1324–1327. doi: 10.1038/2121324a0

Epstein, E., and Hagen, C. E. (1952). A kinetic study of the absorption of alkali cations by barley roots. *Plant. Physiol.* 27, 457–474. doi: 10.1104/pp.27.3.457

Epstein, E., Rains, D. W., and Elzam, O. E. (1963). Resolution of dual mechanisms of potassium absorption by barley roots. *Proc. Natl. Acad. Sci. U.S.A.* 49, 684–692. doi: 10.1073/pnas.49.5.684

Faure-Rabasse, S., Le Deunff, E., Laine, P., Macduff, J. H., and Ourry, A. (2002). Effects of nitrate pulses on *BnNRT1* and *BnNRT2* genes mRNA levels and nitrate influx rates in relation to the duration of N deprivation in *Brassica napus* L. *J. Exp. Bot.* 53, 1711–1721. doi: 10.1093/jxb/erf023

Fiksen, ϕ., Follows, M. J., and Aksnes, D. L. (2013). Trait-based models of nutrient uptake in microbes extend the Michaelis-Menten framework. *Limnol. Oceanogr. 58*, 193–202. doi: 10.4319/lo.2013.58.1.0193

Filleur, S., Dorbe, M. F., Cerezo, M., Orsel, M., Granier, F., Gojon, A., et al. (2001). An Arabidopsis T-DNA mutant affected in Nrt2 genes is impaired in nitrate uptake. *FEBS Lett.* 89, 220–224. doi: 10.1016/S0014-5793(01)02096-8

Forde, B. G., and Clarkson, D. T. (1999). Nitrate and ammonium nutrition of plants: physiological and molecular perspectives. *Adv. Bot. Res.* 30, 1–90. doi: 10.1016/S0065-2296(08)60226-8

Franks, P. J. S. (2009). Planktonic ecosystem models: perplexing parametrizations and a failure to fail. *J. Plankton Res.* 31, 1299–1306. doi: 10.1093/plankt/fbp069

Gao, S., Pan, W. L., and Koening, R. (1998). Integrated root system age in relation to plant nutrient uptake activity. *Agron. J.* 90, 505–510. doi: 10.2134/agronj1998.00021962009000040011x

Garrahan, P. J., and Glynn, I. M. (1967). The behaviour of the sodium pump in red cells in the absence of external potassium. *J. Physiol.* 192, 159–174.

Geelen, D., Lurin, C., Bouchez, D., Frachisse, J.-M., Lelièvre, F., Courtiel, B., et al. (2000). Disruption of putative anion channel gene AtCLC-a in *Arabidopsis* suggests a role in the regulation of nitrate content. *Plant J.* 21, 259–267. doi: 10.1046/j.1365-313x.2000.00680.x

Geider, R. J., MacIntyre, H. L., and Kana, T. M. (1998). A dynamic regulatory model of phytoplanktonic acclimation to light, nutrients, and temperature. *Limnol. Oceanogr.* 43, 679–694. doi: 10.4319/lo.1998.43.4.0679

Gerwitz, S., and Page, E. (1974). An empirical mathematical model to describe plant root systems. *J. Appl. Ecol.* 11, 773–781. doi: 10.2307/2402227

Girin, T., Lejay, L., Wirth, J., Widiez, T., Palenchar, P. M., Nazoa, P., et al. (2007). Identification of a 150 bp cis-acting element of the AtNRT2.1 promoter involved in the regulation of gene expression by the N and C status of the plant. *Plant Cell Environ.* 30, 1366–1380. doi: 10.1111/j.1365-3040.2007.01712.x

Glass, A. D. M. (1976). Regulation of potassium absorption in barley roots: an allosteric model. *Plant Physiol.* 58, 33–37. doi: 10.1104/pp.58.1.33

Glass, A. D. M., Britto, D. J., Kaiser, B. N., Kronzucker, H. J., Kumar, A., Okamoto, M., et al. (2002). The regulation of nitrate and ammonium transport systems in plants. *J. Exp. Bot.* 53, 855–864. doi: 10.1093/jexbot/53.370.855

Glass, A. D. M., and Kotur, Z. (2013). A re-evaluation of the role of NRT1.1 in high-affinity nitrate transport? *Plant Physiol.* 163, 1103–1110. doi: 10.1104/pp.113.229161

Guo, F. Q., Wang, R., Chen, M., and Crawford, N. M. (2001). The *Arabidopsis* dual-affinity nitrate transporter gene *AtNRT1.1* (CHL1) is activated and functions in nascent organ development during vegetative and reproductive growth. *Plant Cell* 13, 1761–1777. doi: 10.1105/tpc.13.8.1761

Guo, F. Q., Wang, R., and Crawford, N. M. (2002). The *Arabidopsis* dual-affinity nitrate transporter gene *AtNRT1.1* (CHL1) is regulated by auxin in both shoots and roots. *J. Exp. Bot.* 53, 835–844. doi: 10.1093/jexbot/53.370.835

Han, Y.-L., Song, H.-X., Liao, Q., Yu, Y., Jian, S.-F., Lepo, J. E., et al. (2016). Nitrogen use efficiency is mediated by vacuolar nitrate sequestration capacity in roots of *Brassica napus*. *Plant Physiol.* 170, 1684–1698. doi: 10.1104/pp.15.01377

Hanson, J. B. (1978). Application of the chemiosmotic hypothesis to ion transport across the root. *Plant Physiol.* 62, 129–135. doi: 10.1104/pp.62.3.402

Hayashi, K., Hasegawa, J., and Matsunaga, S. (2013). The boundary of the meristematic and elongation zones in roots: endoreplication precedes rapid cell expansion. *Sci. Rep.* 14:2723. doi: 10.1038/srep02723

Ho, C.-H., Lin, S.-H., Hu, H.-C., and Tsay, Y.-F. (2009). CHL1 Functions as a nitrate sensor in plants. *Cell* 138, 1184–1194. doi: 10.1016/j.cell.2009.07.004

Hole, D. J., Emran, A. M., Fares, Y., and Drew, M. (1990). Induction of nitrate transport in maize roots, and kinetics of influx, measured with nitrogen-13. *Plant Physiol.* 93, 642–647. doi: 10.1104/pp.93.2.642

Hu, H. C., Wang, Y.-Y., and Tsay, Y.-F. (2009). AtCIPK8, a CBL-interacting protein kinase, regulates the low-affinity phase of the primary nitrate response. *Plant J.* 57, 264–278. doi: 10.1111/j.1365-313X.2008.03685.x

Jacoby, B. (1995). "Nutrient uptake by plants," in *Handbook of Plant and Crop Physiology*, ed M. Pessarakli (New York, NY; Basel; Hong Kong: Marcel Dekker Inc), 1–22.

Javaux, M., Schröder, T., Vanderborght, J., and Vereecken, H. (2008). Use of a three- dimensional detailed modeling approach for predicting root water uptake. *Vadose Zone J.* 7, 1079–1088. doi: 10.2136/vzj2007.0115

Jungk, A., Asher, C. J., Edwards, D. G., and Meyer, D. (1990). Influence of phosphate status on phosphate uptake kinetics of maize (*Zea mays*) and soybean (*Glycine max*). *Plant Soil* 124, 175–182. doi: 10.1007/BF00009256

Kannan, S. (1971). Plasmalemma: the seat of dual mechanisms of ion absorption in *Chlorella pyrenoidosa*. *Science* 173, 927–929. doi: 10.1126/science.173.4000.927

Katchalsky, A., and Curran, P. F. (1965). *Non Equilibrium Thermodynamics in Biophysics.* Cambridge, MA: Harvard University Press.

Kiba, T., Feria-Bourrellier, A. B., Lafouge, F., Lezhneva, L., Boutet, S., Orsel, M., et al. (2012). The Arabidopsis nitrate transporter NRT2.4 plays a double role in roots and shoots of N-starved plants. *Plant Cell* 24, 245–258. doi: 10.1105/tpc.111.092221

King, E. L., and Altman, C. (1956). A schematic method for deriving the rate laws for enzyme-catalyzed reactions. *J. Phys. Chem.* 60, 1375–1378. doi: 10.1021/j150544a010

Kochian, V., and Lucas, W. J. (1982). Potassium transport in corn roots. I. Resolution of kinetics into a saturable and linear component. *Plant Physiol.* 70, 1723–1731. doi: 10.1104/pp.70.6.1723

Kochian, V., Xin-Zhi, J., and Lucas, W.J. (1985). Potassium transport in corn roots IV. Characterisation of the linear component. *Plant Physiol.* 79, 771–776. doi: 10.1104/pp.79.3.771

Köhler, B., Wegner, L. H., Osipov, V., and Raschke, K. (2002). Loading of nitrate into the xylem: apoplastic nitrate controls the voltage dependence of X-QUAC, the main anion conductance in xylem-parenchyma cells of barley roots. *Plant J.* 30, 133–142. doi: 10.1046/j.1365-313X.2002.01269.x

Kotur, Z., and Glass, A. D. M. (2014). A 150 kDa plasma membrane complex of AtNRT2.5 and AtNAR2.1 is the major contributor to constitutive high-affinity nitrate influx in *Arabidopsis thaliana*. *Plant Cell Environ.* 38, 1490–1502. doi: 10.1111/pce.12496

Krapp, A. (2015). Plant nitrogen assimilation and its regulation: a complex puzzle with missing pieces. *Curr. Opin. Plant Biol.* 25, 115–122. doi: 10.1016/j.pbi.2015.05.010

Krapp, A., Fraisier, V., Scheible, W. R., Quesada, A., Gojon, A., Stitt, M., et al. (1998). Expression studies of Nrt2; 1Np, a putative high-affinity nitrate transporter: evidence for its role in nitrate uptake. *Plant J.* 14, 723–731.

Krebs, M., Beyhl, D., Gorlich, E., Al-Rasheid, K. A., Marten, I., Stierhof, Y. D., et al. (2010). Arabidopsis V-ATPase activity at the tonoplast is required for efficient nutrient storage but not for sodium accumulation. *Proc. Natl. Acad. Sci. U.S.A.* 107, 3251–3256. doi: 10.1073/pnas.0913035107

Kronzucker, H., Siddiqi, M. Y., and Glass, A. D. M. (1995a). Kinetics of nitrate influx in Spruce. *Plant Physiol.* 109, 319–326.

Kronzucker, H., Siddiqi, M. Y., and Glass, A. D. M. (1995b). Nitrate induction in spruce: an approach using compartmental analysis. *Planta* 196, 683–690. doi: 10.1007/BF01106761

Kronzucker, H., Siddiqi, M. Y., and Glass, A. D. M. (1995c). Compartmentation and flux characteristics of nitrate in spruce. *Planta* 196, 674–682. doi: 10.1007/BF01106760

Kronzucker, H., Siddiqi, M. Y., and Glass, A. D. M. (1995d). Compartmentation and flux characteristic of ammonium in spruce. *Planta* 196, 691–698. doi: 10.1007/BF01106762

Lazof, D. B., Rufty, T. W., and Redinbaugh, M. G. (1992). Localization of nitrate absorption and translocation within morphological regions of the corn root. *Plant Physiol.* 100, 1251–1258. doi: 10.1104/pp.100.3.1251

Le Bot, J., Adamowicz, S., and Robin, P. (1998). Modelling plant nutrition of horticultural crops: a review. *Sci. Hortic.* 74, 47–82. doi: 10.1016/S0304-4238(98)00082-X

Le Deunff, E., and Malagoli, P. (2014a). An updated model for nitrate uptake modelling in plants. I. Functional component: cross-combination of flow–force interpretation of nitrate uptake isotherms, and environmental and in planta regulation of nitrate influx. *Ann. Bot.* 113, 931–938. doi: 10.1093/aob/mcu021

Le Deunff, E., and Malagoli, P. M. (2014b). Breaking conceptual locks in modeling roots absorption of nutrients: reopening the thermodynamic viewpoint of ion transport across the root. *Ann. Bot.* 114, 1555–1570. doi: 10.1093/aob/mcu203

Lee, R. B., and Clarkson, D. T. (1986). Nitrogen-13 studies of nitrate fluxes in barley roots. II. Compartmental analysis from measurements of 13N efflux. *J. Exp. Bot.* 3, 1753–1767. doi: 10.1093/jxb/37.12.1753

Lee, R. C., and Drew, M. C. (1986). Nitrogen-13 studies of nitrate fluxes in barley roots. *II.* Effect of plant N-status on the kinetic parameters of nitrate influx. *J. Exp. Bot.* 185, 1768–1779. doi: 10.1093/jxb/37.12.1768

Leigh, R. A., Wyn Jones, R. G., and Williamson, F. A. (1973). "The possible role of vesicules and ATPases in ion uptake," in *Ions Transport in Plants*, ed W. P. Anderson (London; New York, NY: Academic Press), 407–418.

Lezhneva, L., Kiba, T., Feria-Bourrellier, A. B., Lafouge, F., Boutet-Mercey, S., Zoufan, P., et al. (2014). The Arabidopsis nitrate transporter NRT2.5 plays a role in nitrate acquisition and remobilization in nitrogen-starved plants. *Plant. J.* 80, 230–241. doi: 10.1111/tpj.12626

Li, J.-Y., Fu, Y.-L., Pike, S. M., Bao, J., Tian, W., Zhang,. Y., et al. (2010). The *Arabidopsis* nitrate transporter NRT1.8 functions in nitrate removal from the xylem sap and mediates cadmium tolerance. *Plant Cell* 22, 1633–1646. doi: 10.1105/tpc.110.075242

Li, W., Wang, Y., Okamoto, M., Crawford, N. M., Siddiqi, M. Y., and Glass, A. D. M. (2007). Dissection of the *AtNRT2.1*:*AtNRT2.2* inducible high-affinity nitrate transporter gene cluster. *Plant Physiol.* 143, 425–433. doi: 10.1104/pp.106.091223

Lin, S.-H., Kuo, H.-F., Canivenc, G., Lin, C.-S., Lepetit, M., Hsu, P.-K., et al. (2008). Mutation of the Arabidopsis NRT1.5 nitrate transporter causes defective root-to-shoot nitrate transport. *Plant Cell* 20, 2514–2528. doi: 10.1105/tpc.108.060244

Lindemann, C., Fiksen, Ø., Andersen, K. H., and Aksnes, D. L. (2016). Scaling laws in phytoplankton nutrient uptake affinity. *Front. Mar. Sci.* 3:26. doi: 10.3389/fmars.2016.00026

Litchman, E., and Klausmeier, C. A. (2009). Trait-based community ecology of phytoplankton. *Annu. Rev. Ecol. Evol. Syst.* 39, 615–639. doi: 10.1146/annurev.ecolsys.39.110707.173549

Litchman, E., Klausmeier, C. A., Schofield, O. M., and Falkowski, P. G. (2007). The role of functional traits and trade-offs in structuring phytoplankton communities: scaling from cellular to ecosystem level. *Ecol. Lett.* 10, 1170–1181. doi: 10.1111/j.1461-0248.2007.01117.x

Liu, K.-H., and Tsay, Y.-F. (2003). Switching between the two action modes of the dual-affinity nitrate transporter CHL1 by phosphorylation. *EMBO J.* 22, 1005–1013. doi: 10.1093/emboj/cdg118

Ma, L., Ahuja, L. R., and Bruulsema, T. W. (2008). *Quantififying and Understanding Plant Nitrogen Uptake for Systems Modelling.* Boca Raton, FL: CRC Press.

Maathuis, F. J. M. (2009). Physiological functions of mineral macronutrients. *Curr. Opin. Plant Biol.* 12, 250–258. doi: 10.1016/j.pbi.2009.04.003

MacIsaac, J., and Dugdale, R. C. (1969). The kinetics of nitrate and ammonia uptake by natural populations of marine phytoplankton. *Deep Sea Res.* 16, 45–57. doi: 10.1016/0011-7471(69)90049-7

Malagoli, P., Britto, D. T., Schulze, L. M., and Kronzucker, H. J. (2008). Futile Na^+ cycling at the root plasma membrane in rice (*Oryza sativa* L.): kinetics, energetics, and relationship to salinity tolerance. *J. Exp. Bot.* 59, 4109–4117. doi: 10.1093/jxb/ern249

Malagoli, P., and Le Deunff, E. (2014). An updated model for nitrate uptake modelling in plants II. Assessment of active roots involved on nitrate uptake based on integrated root system age: measured vs modelled outputs. *Ann. Bot.* 113, 939–952. doi: 10.1093/aob/mcu022

Migocka, M., Warzybok, A., Papierniak, A., and Kłobus, G. (2013). NO3−/H+ antiport in the tonoplast of cucumber root cells is stimulated by nitrate supply: evidence for a reversible nitrate-induced phosphorylation of vacuolar NO3−/H+ antiport. *PLoS ONE* 8:e73972. doi: 10.1371/journal.pone.0073972

Miller, A. J., Fan, X., Orsel, M., Smith, S. J., and Wells, D. M. V. (2007). Nitrate transport and signalling. *J. Exp. Bot.* 58, 2297–2306. doi: 10.1093/jxb/erm066

Mitchell, P. (1967). " Active transport and ion accumulation," in *Comprehensive Biochemistry, Vol.* 22, eds M. Florkin and E. H. Stotz (Amsterdam: Elsevier), 167–197.

Monachello, D., Allot, M., Oliva, S., Krapp, A., Daniel-Vedele, F., Barbier-Brygoo, H., et al. (2009). Two anion transporters AtClCa and AtClCe fulfil interconnecting but not redundant roles in nitrate assimilation pathways. *New Phytol.* 183, 88–94. doi: 10.1111/j.1469-8137.2009.02837.x

Morel, F. M. M. (1987). Kinetics of nutrient uptake and growth in phytoplankton. *J. Phycol.* 23, 137–150.

Muller, B., Tillard, P., and Touraine, B. (1995). Nitrate fluxes in soybean seedlings roots and their response to amino acids: an approach using ^{15}N. *Plant Cell Environ.* 18, 1267–1279. doi: 10.1111/j.1365-3040.1995.tb00186.x

NaNagara, T., Phillips, R. E., and Leggett, J. E. (1976). Diffusion and mass *flow* of nitrate-nitrogen into corn roots grown under field conditions. *Agron. J.* 68, 67–72. doi: 10.2134/agronj1976.00021962006800010018x

Neame, K. D., and Richards, T. G. (1972). "Multiple carriers," in *Elementary Kinetics of Membrane Carrier Transport*, eds K. D. Neame and T. G. Richards (Oxford, London: Blackwell Scientific Publications), 80–94.

Nissen, P. (1989). Multiphasic uptake of potassium by corn roots: no linear component. *Plant Physiol.* 89, 231–237.

Nye, P. H., and Tinker, P. B. (1969). The concept of a root demand coefficient. *J. Appl. Ecol.* 6, 293–300. doi: 10.2307/2401543

Okamoto,. M., Vidmar, J. J., and Glass, A. D. M. (2003). regulation of NRT1 and NRT2 gene families of *Arabidopsis thaliana*: responses to nitrate provision. *Plant Cell Physiol.* 44, 304–317. doi: 10.1093/pcp/pcg036

Pace, G. M., and McClure, P. R. (1986). Comparison of nitrate uptake kinetic parameters across maize inbred line. *J. Plant. Nutr.* 9, 1095–1111. doi: 10.1080/01904168609363512

Peuke, A. D., and Kaiser, W. M. (1996). Nitrate or ammonium uptake and transport, and rapid regulation of nitrate reduction in higher plants. *Prog. Bot.* 57, 93–113. doi: 10.1007/978-3-642-79844-3_7

Pitman, M. G. (1977). Ion transport in the xylem. *Annu. Rev. Plant Physiol.* 28, 71–89. doi: 10.1146/annurev.pp.28.060177.000443

Polley, D., and Hopkins, J. W. (1979). Rubidium (potassium) uptake by Arabidopsis. A comparison of uptake by cells in suspension culture and by roots of intact seedlings. *Plant Physiol.* 64, 374–378. doi: 10.1104/pp.64.3.374

Presland, M. R., and MacNaughton, G. S. (1984). Whole plant studies using radioactive 13-nitrogen. II. A compartmental model for the uptake and transport of nitrate ions by *Zea mays. J. Exp. Bot.* 35, 1277–1288. doi: 10.1093/jxb/35.9.1277

Ragel, P., Rodenas, R., Garcia-Martin, E., Andrés, Z., Villalta, I., Nieves-Cordones, M., et al. (2015). CIPK23 regulates HAK5-mediated high-affinity K^+ uptake in Arabidopsis roots. *Plant Physiol.* 169, 2863–2873. doi: 10.1104/pp.15.01401

Rauser, W. E. (1987). Compartmental efflux analysis and removal of extracellular cadmium from roots. *Plant Physiol.* 85, 62–65. doi: 10.1104/pp.85.1.62

Reidenbach, G., and Horst, W. J. (1997). Nitrate-uptake capacity of different root zones of *zea mays* (L.) *in vitro* and *in situ*. *Plant Soil* 196, 295–300. doi: 10.1007/978-94-009-0047-9_214

Reisenauer, H. M. (1966). "Mineral nutrients in soil solution," in *Environmental Biology*, eds P. L. Altman and D. S. Dittmer (Bethesda, MD: Federation of American Societies for Experimental Biology), 507–508.

Rogato, A., Amato, A., Ludicone, D., Chiurazzi, M., Immacolata, M., and Ribera d'Alcalà, M. (2015). The diatom molecular toolkit to handle nitrogen uptake. *Mar. Genomics* 24, 95–108. doi: 10.1016/j.margen.2015.05.018

Roose, T. (2000). *Mathematical Model of Plant Nutrient Uptake*. D. Phil. thesis, University of Oxford, Oxford, UK.

Roose, T., Fowler, A. C., and Darrah, P. R. (2001). A mathematical model of plant nutrient uptake. *J. Math. Biol.* 42, 347–360. doi: 10.1007/s002850000075

Roose, T., and Kirk, G. J. D. (2009). The solution of convection-diffusion equations for solute transport to plant roots. *Plant Soil* 316, 257–264. doi: 10.1007/s11104-008-9777-z

Schachter, H. (1972). "The use of steady-state assumption to derive kinetic formulations for the transport of a solute across a membrane," in *Metabolic Transport*, Vol. VI, ed L. E. Hokin (New York, NY; London: Academic Press), 1–15

Segonzac, C., Boyer, J.-C., Ipotesi, E., Szponarski, W., Tillard, P., Touraine, B., et al. (2007). Nitrate efflux at the root plasma membrane: identification of an *Arabidopsis* excretion transporter. *Plant Cell* 19: 3760–3777. doi: 10.1105/tpc.106.048173

Siddiqi, M. Y., Glass, A. D. M., and Ruth, T. J. (1991). Studies of the uptake of nitrate in barley. III. comparmentation of NO_3^-. *J. Exp. Bot.* 42, 1455–1463. doi: 10.1093/jxb/42.11.1455

Siddiqi, M. Y., Glass, A. D. M., Ruth, T. J., and Fernando, M. (1989). Studies of the regulation of nitrate influx by Barley seedlings using $^{13}NO_3^-$. *Plant Physiol.* 90, 806–813. doi: 10.1104/pp.90.3.806

Siddiqi, M. Y., Glass, A. D. M., Ruth, T. J., and Rufty, T. W. (1990). Studies of the uptake of nitrate in Barley: I. Kinetics of $^{13}NO_3^-$ influx. *Plant Physiol.* 93, 1426–1432. doi: 10.1104/pp.93.4.1426

Smith, S. L. (2011). Consistently modeling the combined effects of temperature and concentration on nitrate uptake in the ocean. *J. Geophys. Res.* 116, 1–12. doi: 10.1029/2011jg001681

Smith, S. L., Merico, A., Hohn, S., and Brandt, G. (2014). Sizing-up nutrient uptake kinetics: combining a physiological trade-off with size-scaling of phytoplankton traits *Mar. Ecol. Prog. Ser.* 511, 33–39. doi: 10.3354/meps10903

Smith, S. L., Yamanaka, Y., Pahlow, M., and Oschlies, A. (2009). Optimal uptake kinetics: physiological acclimation explains the pattern of nitrate uptake by phytoplankton in the ocean. *Mar. Ecol. Prog. Ser.* 384, 1–12. doi: 10.3354/meps08022

Somma, F., Hopmans, J., and Clausnitzer, V. (1998). Transient three-dimensional modeling of soil water and solute transport with simultaneous root growth, root water and nutrient uptake. *Plant Soil* 202, 281–293. doi: 10.1023/A:1004378602378

Sorgona, A., Lupini, A., Mercati, F., Di Dio, L., Sunseri, F., and Abenavoli, M. R. (2011). Nitrate uptake along the maize primary root: an integrated physiological and molecular approach. *Plant Cell Environ.* 34, 1127–1140. doi: 10.1111/j.1365-3040.2011.02311.x

Szczerba, M. W., Britto, D. T., and Kronzucker, H. (2006). The face value of ion fluxes: the challenge of determining influx in the low-affinity transport range. *J. Exp. Bot.* 57, 3293–3300. doi: 10.1093/jxb/erl088

Thellier, M. (1969). Interprétation électrocinétique de l'absorption minérale chez les végétaux. *Bull. Soc. Franç. Physiol. Végét.* 15, 127–139.

Thellier, M. (1970a). An electrokinetic interpretation of biological systems and its application to the study of mineral salt absorption. *Ann. Bot.* 34, 983–1009.

Thellier, M. (1970b). Comportement semi-conducteur des structures catalytiques cellulaires et loi d'Arrhenius. *CR Acad. Sci. Paris (série D) 270*, 1032–1034.

Thellier, M. (1971). Non-equilibrium thermodynamics and electrokinetic interpretation of biological systems. *J. Theor. Biol.* 31, 389–393. doi: 10.1016/0022-5193(71)90017-8

Thellier, M. (1973). "Electrokinetic formulation of ionic absorption by plants samples," in *Ions Transport in Plants*, ed W. P. Anderson (London: Academic Press), 47–63.

Thellier, M. (2012). A half-century adventure in the dynamics of living systems. *Prog. Bot.* 73, 3–53. doi: 10.1007/978-3-642-22746-2_1

Thellier, M., Ripoll, C., Norris, V., Nikolic, M., and Römheld, V. (2009). Solute uptake in plants: a *Flow*/Force interpretation. *Prog. Bot.* 70, 53–68. doi: 10.1007/978-3-540-68421-3_3

Thellier, M., Stelz, T., and Ayadi, A. (1971b). Application des relations et de la loi d'Onsager à l'interprétation d'interactions entre processus cellulaires globaux. *CR Acad. Sci. Paris (série D) 273*, 2346–2349.

Thellier, M., Thoiron, B., and Thoiron, A. (1971a). Electrokinetic formulation of overall kinetics of *in vivo* processes. *Physiol. Vég.* 9, 65–82.

Tinker, P. B., and Nye, P. H. (2000). "The uptake properties of the root system," in *Solutes Movement in the Rhizosphere*, eds P. B. Tinker and P. H. Nye (New York, NY; Oxford: University Press), 95–129.

Touraine, B., Daniel-Vedele, F., and Forde, B. G. (2001). "Nitrate uptake and its regulation," in *Plant Nitrogen,* eds P. J. Lea and J. -F. Morot-Gaudry (Berlin; Heidelberg: INRA and Springer-Verlag), 1–36.

Tournier, P.-H. (2015). *Absorption de l'eau et des Nutriments par les Racines des Plantes: Modélisation, Analyse et Simulation*. General Mathematics thesis, Université Pierre et Marie Curie, Paris VI.

Tournier, P. H., Hecht, F., and Comte, M. (2015). Finite element model of soil water and nutrient transport with root uptake: explicit geometry and unstructured adaptive meshing. *Trans. Porous Med.* 106, 487–504. doi: 10.1007/s11242-014-0411-7

Tsay, Y.-F., Schroeder, J. J., Feldmann, K. A., and Crawford, N. M. (1993). The herbiside sensitivity gene *CHL1* of *Arabidopsis* encodes a nitrate-inducible nitrate transporter. *Cell* 72, 705–713. doi: 10.1016/0092-8674(93)90399-B

Walker, N. A., and Pitman, M. G. (1976). "Measurements of fluxes across membranes," in *Encyclopedia of Plant Physiol, Vol. 2*, *Part A,* eds U. Lüttge and M. G. Pitman (Berlin; Heildelberg; New York, NY: Springer-Verlag), 93–126.

Wang, Y.-Y., Hsu, P.-K., and Tsay, Y.-F. (2012). Uptake, allocation and signalling of nitrate. *Trends Plant Sci.* 17, 458–467. doi: 10.1016/j.tplants.2012.04.006

Wolt, J. D. (1994). "Soil solution chemistry: application to environmental science and agriculture," in *Soil Solution Chemistry: Application to Environmental Science and Agriculture*, ed J. D. Wolt (New York, NY: Wiley and Sons, Inc), 345.

Wong, J. T., and Hanes, C. S. (1973). Topological analysis of enzymic mechanisms. *Acta Biol. Med. Ger.* 31, 507–514.

Zhang, G., Yi, H.-Y., and Gong, J.-M. (2014). The *Arabidopsis* ethylene/jasmonic acid-NRT signalling module coordinates nitrate reallocation and the trade-off between growth and environmental adaptation. *Plant Cell* 26, 3984–3998. doi: 10.1105/tpc.114.129296

Conflict of Interest Statement: The authors declare that the research was conducted in the absence of any commercial or financial relationships that could be construed as a potential conflict of interest.

The reviewer, ID, and handling Editor declared their shared affiliation, and the handling Editor states that the process nevertheless met the standards of a fair and objective review

frontiers in Plant Science

ORIGINAL RESEARCH
published: 23 June 2016
doi: 10.3389/fpls.2016.00914

Modeling Root Zone Effects on Preferred Pathways for the Passive Transport of Ions and Water in Plant Roots

Kylie J. Foster and Stanley J. Miklavcic *

Phenomics and Bioinformatics Research Centre, School of Information Technology and Mathematical Sciences, University of South Australia, Mawson Lakes, SA, Australia

We extend a model of ion and water transport through a root to describe transport along and through a root exhibiting a complexity of differentiation zones. Attention is focused on convective and diffusive transport, both radially and longitudinally, through different root tissue types (radial differentiation) and root developmental zones (longitudinal differentiation). Model transport parameters are selected to mimic the relative abilities of the different tissues and developmental zones to transport water and ions. For each transport scenario in this extensive simulations study, we quantify the optimal 3D flow path taken by water and ions, in response to internal barriers such as the Casparian strip and suberin lamellae. We present and discuss both transient and steady state results of ion concentrations as well as ion and water fluxes. We find that the peak in passive uptake of ions and water occurs at the start of the differentiation zone. In addition, our results show that the level of transpiration has a significant impact on the distribution of ions within the root as well as the rate of ion and water uptake in the differentiation zone, while not impacting on transport in the elongation zone. From our model results we infer information about the active transport of ions in the different developmental zones. In particular, our results suggest that any uptake measured in the elongation zone under steady state conditions is likely to be due to active transport.

Keywords: Casparian strip, suberin lamellae, elongation zone, differentiation zone, transpiration, salt uptake

OPEN ACCESS

Edited by:
Janin Riedelsberger, University of Talca, Chile

Reviewed by:
Ingo Dreyer, University of Talca, Chile
Xiaoxian Zhang, Rothamsted Research, UK

***Correspondence:**
Stanley J. Miklavcic
stan.miklavcic@unisa.edu.au

Specialty section:
This article was submitted to Plant Physiology, a section of the journal Frontiers in Plant Science

Received: *03 March 2016*
Accepted: *09 June 2016*
Published: *23 June 2016*

Citation:
Foster KJ and Miklavcic SJ (2016) Modeling Root Zone Effects on Preferred Pathways for the Passive Transport of Ions and Water in Plant Roots. Front. Plant Sci. 7:914. doi: 10.3389/fpls.2016.00914

1. INTRODUCTION

Plant roots are responsible for the uptake of water and nutrients, as well as any potentially toxic ions, from the soil. This uptake varies along the longitudinal axis of roots, particularly across the different developmental zones, as a result of both changes in internal root anatomy (e.g., Zhou et al., 2011) and changes in the functional expression of transporters. There has been extensive investigation into the identification of ion transporters and their role in the uptake and transport of ions in plant roots (Barberon and Geldner, 2014). However, understanding how changes in root anatomy influence the transport of ions and water is also important for improving our understanding of root function. In this paper we utilize mathematical modeling to explore the effects of cell differentiation on the preferred pathways for the passive uptake of ions and water by plant roots. This model is an extension of previous efforts (Foster and Miklavcic, 2013, 2014), which have already highlighted the intrinsic coupling of ions in their transport through the root.

Plant roots can be divided longitudinally into anatomically distinct developmental zones, each of which have different abilities to take up and transport ions and water. For example, *Arabidopsis thaliana* primary roots consist of three distinct zones (Dolan et al., 1993): the meristematic zone, followed by the elongation zone (EZ) and then the differentiation zone (DZ). In the EZ the cells lengthen in preparation for differentiation, while in the DZ the cells become fully differentiated (Dolan et al., 1993). This process of cell differentiation can significantly affect the transport of ions and water. For example, in the primary development stage of the endodermis the Casparian strip (CS) develops in the cell wall of adjacent endodermal cells. The CS is a barrier that consists predominantly of lignin (Naseer et al., 2012) which blocks the passive uptake of ions (and possibly water) via the non-selective, apoplastic pathway (Geldner, 2013; Barberon and Geldner, 2014). In addition, the suberin lamellae (SL) forms in the secondary development stage of the endodermis. The SL forms between the plasma membrane and the primary cell wall of the endodermal cells. This barrier eventually covers the entire cell and inhibits the uptake of water and solutes via transporters across the plasma membrane of the affected endodermal cells (Geldner, 2013; Barberon and Geldner, 2014). On the other hand, the SL does not sever the plasmodesmatal connections between the cells. Hence, this disruption of the selective pathway forces solutes and water to enter the symplastic pathway in the outer regions of the root in order to enter the stele (Geldner, 2013).

Numerous experiments, conducted over many decades, have investigated the uptake of ions and water along the longitudinal axis of roots and how this uptake relates to root anatomy (e.g., Graham et al., 1974; Lüttge, 1983; Zhou et al., 2011). Similarly, experimental measurements of how transport properties (such as hydraulic conductivity) vary across different developmental zones have been carried out (e.g., Melchior and Steudle, 1993; Frensch et al., 1996). In addition, experiments have been conducted to identify the cell-specific distribution of ions across roots in order to gain information about transport mechanisms, including the importance of root structures such as the endodermal barriers as control points in the uptake process (e.g., Lauchli et al., 2008). An improved understanding of this uptake has important implications for better understanding root function, including the transport of nutrients and the response of plants to various stresses. Clearly, the spatial distribution of ion transporters has a significant influence on the uptake of ions along the length of the root as well as on the distribution of ions within the root. However, the focus of this work is on the effects of cell differentiation on uptake. Direct experimental testing of the roles of anatomically distinct root zones has proved difficult (Barberon and Geldner, 2014). Genetic advances, such as the recent identification of *sgn3*, an *Arabidopsis* mutant with a nonfunctional CS (Pfister et al., 2014), are important. To complement these experimental efforts mathematical modeling can provide an opportunity to examine in detail the spatial distribution of ion and water fluxes, as well as ion concentrations, and how these vary over time. Modeling also provides the ability to explore directly the effects of cell differentiation on ion and water transport. For example, the role of endodermal barriers can be examined by comparing model scenarios where the barriers are present to those where the barriers are absent (e.g., Foster and Miklavcic, 2014; Sakurai et al., 2015). Modeling also allows us to determine the relative contributions of different driving forces, such as diffusion and convection, to the overall transport process. Finally, it is relevant to consider how much of the observed ion uptake and concentration distributions can be explained by passive processes. This would be difficult or impossible to explore experimentally, whereas modeling can simulate scenarios in which uptake in a root occurs by passive processes without the interference of active transporters.

Previous simulations of solute uptake by plant roots have typically investigated radial, rather than axial, variations in root transport properties. For example, Claus et al. (2013) and Sakurai et al. (2015) developed models of the uptake of zinc and silicon, respectively, in the DZ. Their efforts focused on the radial distribution of these solutes (including the effects of apoplastic transport barriers) and as a result they did not consider any variations in transport properties along the longitudinal axis of the root. In contrast, Shimotohno et al. (2015) modeled the uptake and spatial distribution of boron in a plant root, including axial variation in the model root transport properties to simulate different root developmental zones. The emphasis of the simulations conducted by Shimotohno et al. (2015), however, was on the root tip and hence the effects of endodermal barriers and functional xylem were not simulated. All of the transport models described above included transport via membrane transporters. However, none of these models simulated transport in a plant root which had a zone of undifferentiated cells as well as a zone in which functional xylem and endodermal barriers were present.

Convection is likely to be an important driving force for ion transport, particularly in the DZ where functional xylem is present. However, convection is often not modeled in root ion transport simulations. An exception is the zinc model developed by Claus et al. (2013) which included convection in the symplast via a constant water flow rate. Claus et al. (2013) identified that this convection was an important factor affecting the radial zinc concentration pattern. However, this model did not incorporate all of the interactions between solutes and water. In particular, the osmotic effects of ion concentrations on water transport were not modeled.

In this study we extend our compartmental model of ion and water transport in a plant root (Foster and Miklavcic, 2013, 2014) to simulate different developmental zones along the longitudinal axis of the root. We include both the EZ and the DZ, incorporating the transition from non-functional to functional xylem and the development of the endodermal barriers. In contrast to the ion transport models discussed above, we focus on passive transport and include interactions between ion and water transport. As assumed previously (Foster and Miklavcic, 2013, 2014), we do not explicitly consider the apoplastic and symplastic pathways separately. Instead, the transport parameters, fluxes and concentrations are a composite representation of both pathways.

Using our model, we identify that the main steady state, passive, uptake of ions and water occurs at the start of the DZ. In contrast, the passive uptake in the EZ at steady state is negligible due to the insignificant level of convection in this region. From

this we conclude that any significant uptake in the EZ under steady state conditions is likely to be driven by active transport. In addition, we show that the level of transpiration has a significant effect on the pattern of ion distribution (both radially and axially) in the DZ and on the rate of ion and water uptake into the aerial parts of the plant. This has important implications for both modeling and experimental efforts.

2. MODEL OF WATER AND ION TRANSPORT

2.1. Model Root Structure

In this compartmental model we simulate the passive uptake and transport of multiple ions and water through a plant root. The model root consists of a single, flat ended, right cylinder (**Figure 1A**). The anatomy of the root is modeled on the structure of *Arabidopsis* primary roots. The model includes radial variation in transport properties to represent the different tissue types, as well as longitudinal variation in transport parameters to represent the different developmental zones (the EZ and DZ). Due to the compartmental nature of the model, the root is discretized radially into consecutive annular cylinders which represent the different tissue types present in *Arabidopsis* roots: the epidermis, cortex, endodermis, pericycle and xylem (see **Figure 1**). In addition, the model root is further discretized along the longitudinal axis with the height of each compartment reflecting the height of an individual cell. Hence, the height of each compartment varies across the EZ (see **Figure 1B**).

For simplicity we assume axial symmetry. Therefore, the features of the model root are independent of the angle around the central axis, instead they depend only on the radial and axial coordinates. As a result, any modeled disruption of the endodermal barriers (e.g., due to the presence of passage cells) is represented as a disruption of the barrier for the full circumference of the endodermis at the relevant location along the length of the root (see **Figure 1A**).

As an extension of our previous work (Foster and Miklavcic, 2013, 2014) both axial and radial flow of water and solutes is modeled in all of the root tissues. This allows us to investigate the effects of changes in root anatomical structure that occur along the length of the root. To capture the interactions between water and ion transport, we model their uptake as a coupled system. Radial and axial flows of water occur due to both osmotic and hydraulic pressure gradients, while both radial and axial flows of ions are driven by local concentration differences, electric field effects and convection. This is a compartmental model in which the root is divided into model compartments (see **Figures 1B,C**), with the hydrostatic pressure and concentration of each ion assumed to be uniform throughout each model compartment. The discretization of the root into compartments is described in further detail in the Supplementary Material. As this is a composite model water and ion fluxes are not explicitly separated into apoplastic and symplastic contributions. Instead, the transport parameters, fluxes and concentrations are composites of both pathways. This model does not explicitly include transport via active transporters. To our advantage, it can be used to examine how much of the observed behavior of ions in plant roots can be explained by passive processes.

The focus of this report is on the transport of solutes up into the plant rather than transport of any solutes (such as sucrose) down into the root. Hence, we assume that the transpiration stream occurring in the xylem is the dominant function of the vascular bundle.

2.2. Forces Driving Ion and Water Transport

In this section we outline the methods used to model ion and water transport. The detailed model equations are provided in the Supplementary Material.

We assume that the root consists of rigid and completely water filled compartments. The radial and axial flow of water in tissue regions where cell membranes are present is driven by both hydraulic and osmotic pressure gradients. Hence, the flow rate of water in these regions is modeled using non-equilibrium thermodynamics (Katchalsky and Curran, 1965). We use the van't Hoff relation to calculate the osmotic pressure in these regions (Katchalsky and Curran, 1965). In contrast, axial transport in the mature xylem is not interrupted by cell membranes and hence, the axial flow of water in the xylem is driven by hydraulic pressure gradients only. This water flow is modeled as linearly proportional to the hydraulic pressure gradient, using Darcy's Law.

The radial and axial transport of ions in the model plant root is governed by a chemical potential contribution (arising from concentration differences), an electric field contribution (due to electric potential differences) and by convection. This is modeled using the extended Nernst-Planck equation (van der Horst et al., 1995). The electric potential is determined by solving Poisson's equation as described previously (Foster and Miklavcic, 2013, 2014). The transport of ions and water are interdependent due to both the contribution of water transport to the convection of the ions as well as the contribution of the ions to the osmotic pressure driving water transport.

2.3. Model Parameters

Table 1 summarizes the parameter values used in the model simulations. The boundary conditions are described in Section 2.4.

The values of several model transport parameters were used to model the anatomical changes that occur across the different root tissues and root developmental zones. For example, the increased resistance to transport due to the CS and subsequently the SL were represented by changing the value of transport parameters at the endodermis-pericycle interface in the DZ, without changing the values adopted for the other tissue layers. In particular, the reduced diffusion due to these barriers was modeled by decreasing the radial diffusive permeability of each ion (k^{rad}) by an order of magnitude for each barrier. Simultaneously, the reduced water transport and convection due to these barriers was modeled by decreasing the radial water permeability (L_p^{rad}) by an order of magnitude and increasing the radial reflection coefficient of each ion (σ^{rad}) by 0.2 units for each barrier.

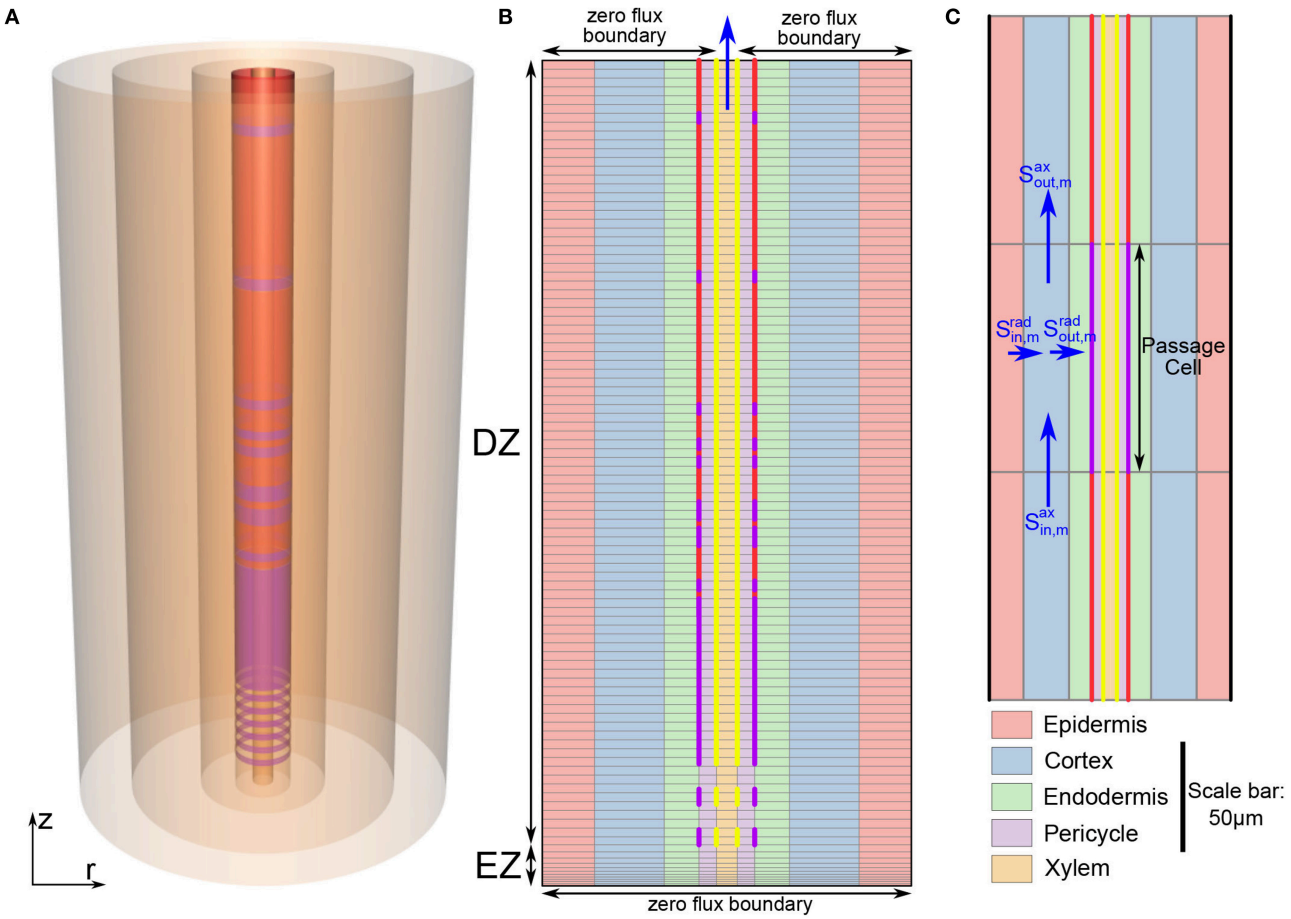

FIGURE 1 | (A) Schematic of the model root showing the radial discretization used to represent the different root tissue types (from outermost region to innermost region: the epidermis, cortex, endodermis, pericycle, and xylem). The purple and red cylinders show the location of the CS and SL, respectively. **(B)** Schematic longitudinal cross-section of the model root. The light gray lines show the radial and axial discretization. The different tissue types are highlighted by different colors, while the extent of different developmental zones (EZ and DZ) are indicated by arrows. Some of the model boundary conditions are also indicated. For visual clarity, the *z* and *r* axes are scaled differently. **(C)** Expanded view of a small section of the root cross-section in **(B)** showing the location of a passage cell. The *z* and *r* axes are here drawn to the same scale (refer to the scale bar) highlighting the actual relative axial to radial proportions. The blue arrows indicate ion fluxes. In **(B,C)**, vertical purple lines indicate the location of the CS, vertical red lines represent SL and yellow lines represent functional xylem. Purple dashed lines indicate incomplete CS while yellow dashed lines represent the transition from non-functional to functional xylem. The root dimensions are given in **Table 1**. The coordinate system (r, z) is as shown in **(A)**. Gravity force is in the direction of decreasing *z*.

The functional CS and xylem were assumed to begin at the 12th cell from the start of the EZ (Naseer et al., 2012). To represent the observed gradual, patchy appearance of the CS in the early stages of endodermal cell differentiation (Roppolo et al., 2011) k^{rad}, L_p^{rad} and σ^{rad} were changed gradually across several axial model compartments from values equal to the surrounding tissues to values representing the fully formed, continuous CS. This region of developing CS is represented by dashed purple lines in **Figure 1B**. Similarly, the development of the xylem from non-functional to functional xylem in the transition from the EZ to the DZ was modeled by changing the axial water permeability (L_p^{ax}) and the axial reflection coefficient of each ion (σ^{ax}) across several axial model compartments (dashed yellow lines in **Figure 1B**).

In the early stages of secondary endodermal cell differentiation, the SL is patchy. As the root matures the SL becomes a more continuous barrier, with the presence of only an occasional passage cell (Geldner, 2013). To model this observed behavior we assumed that the probability of the existence of a passage cell (i.e., a cell unaffected by SL) at a given location decreased along the length of the root. To achieve this, we used a scalar random generator to assign each endodermal cell as either a passage cell (with a probability of $\exp\left(-\frac{j}{30}\right)$) or a cell affected by SL (with a probability of $1-\exp\left(-\frac{j}{30}\right)$). Here j refers to the number of cells from the start of the EZ. The possibility of the SL first appearing was assumed to occur starting from the 38th cell from the start of the EZ (Naseer et al., 2012). This process provided a realistic distribution of passage cells (see **Figure 1B**).

2.4. Computational Details

The discretization of our model root is discussed in detail in the Supplementary Material. However, one major difference between our current model and our previous root model (Foster and

TABLE 1 | Summary of parameters used and their source.

Parameter	Value
Root hydraulic conductivity, L_p	5.5×10^{-8} ms^{-1}MPa^{-1} (Unless otherwise stated)
Solute permeability, k_m	3×10^{-9} ms^{-1} (Unless otherwise stated)
Reflection coefficient, σ_m	0.5 (Unless otherwise stated)
Axial xylem water permeability, k^{ax}	5×10^{-13} m^2
Dynamic viscosity, μ	1.002×10^{-3} Pa s
Water density, ρ	1.0×10^3 kg m^{-3}
Relative permittivity, ϵ_r	80
Thickness of epidermis	15 μm
Thickness of cortex	20 μm
Thickness of endodermis	10 μm
Thickness of pericycle	5 μm
Radius of xylem	3 μm
Concentration of ions in soil	100 mM

Unless otherwise stated the transport parameters in the radial and axial directions are assumed to be equal. Root hydraulic conductivity was obtained from Javot et al. (2003), Ranathunge and Schreiber (2011), and Sutka et al. (2011). Solute permeabilities were obtained from Ranathunge and Schreiber (2011). Reflection coefficients were obtained from Boursiac et al. (2005) and Ranathunge and Schreiber (2011). Axial water permeability in the xylem was calculated using Poiseuille's Equation. The thicknesses of the root sections were obtained from Dolan et al. (1993), Scheres et al. (1995), Mattsson et al. (1999), Casimiro et al. (2003), and Javot et al. (2003).

Miklavcic, 2013, 2014) is that the axial discretization of the root includes a region of varying compartment height to model the EZ (see **Figure 1B**).

The nonlinear, coupled system of ordinary differential equations, resulting from the model setup described in Section 2.2 and the Supplementary Material, was solved numerically in MATLAB using the ode15s package. Poisson's equation was solved numerically using finite difference methods to determine ψ as described in Foster and Miklavcic (2014). The hydraulic pressure in each compartment was determined at each time step by solving a linear system of equations as described in Foster and Miklavcic (2014).

The boundary conditions in the soil consist of a linear hydrostatic hydraulic pressure gradient and a fixed bulk concentration of four monovalent ions (two monovalent cation-anion pairs). The root is assumed to be vertical (see **Figure 1**), with the top of the root aligned with the surface of the external medium. Hence, as a result of the assumption of a hydrostatic pressure gradient outside the root, the pressure in the external medium at the top of the root is atmospheric, with this external pressure increased by $\rho \times g \times L$ at the bottom of the root (here, ρ is the density of water, g is the acceleration due to gravity and L is the length of the root). These ideal boundary conditions assume that the root is surrounded by an infinite reservoir of both mobile ions and water and hence can be thought to be representative of the external conditions in, say, hydroponics experiments. In contrast, under actual field conditions there is usually a limited supply of water and solutes in the soil. Deviation from these ideal conditions may occur in practice for various reasons, such as non-uniform soil conditions, water depletion in the soil due to environmental factors (global effects) and uptake into the root (local effects). These non-uniform boundary effects could be included in future simulations by including the simultaneous modeling of water and ion transport in the soil. However, the focus of our work currently is on the response within the root and hence we have chosen to adopt the simplest of external conditions. Our model establishes a basic understanding of the root transport response under optimal external conditions. There is zero flux of water and ions across the bottom boundary of the root (as shown in **Figure 1B**).

The boundary conditions across the top of the root represent the connectivity of the root to the aerial sections of the plant. It is clear that the axial flow of water and ions up through the xylem into the stem should be significant and hence a zero flux boundary condition across the top of the root would not be appropriate. However, it is less clear how much flow occurs axially out of the other tissue types. Hence, we carried out model simulations for a range of boundary conditions at the top boundary of the model root. These included: axial flux of water and ions out of only the xylem with constant concentrations and hydrostatic pressure at the xylem boundary; axial flux out of only the xylem with a constant hydrostatic pressure and no concentration gradients across the xylem boundary; identical boundary conditions across the top of the root for all tissue types with constant concentrations and pressure at the boundary; and identical boundary conditions across the top of the root for all tissue types with a constant pressure and no concentration gradients across the boundary. We explored a wide range of values for the fixed hydrostatic pressure as well as the ion concentrations at the boundary. The pressure at the top boundary of the root (P_b) significantly affected the simulation results. This is unsurprising since P_b simulates the level of transpiration, which is one of the key driving forces in our model. However, the remaining changes to the boundary conditions that were investigated led to only negligible changes in the simulation results, with only the fluxes and ion concentrations in the top three cell layers of the root affected. For the simulations shown in Section 3 we assume there is zero flux axially out of the outer four tissue regions at the top boundary of the root and there is a constant pressure and no concentration gradients across the top of the xylem (see **Figure 1B**). In Section 3 we explore the effects of different P_b values, which represent the effects of different transpiration conditions.

For the majority of the simulations the root is initially empty of ions. However, as found in our previous work (Foster and Miklavcic, 2013) the steady state model results are independent of the initial conditions. In all instances the root is completely filled with water.

3. RESULTS

The Endodermal Barriers Significantly Inhibit the Passive Influx of Ions and Water into the DZ

Figure 2 shows the steady state ion concentration (colormap) and ion flux (arrows) results for different endodermal barrier scenarios. In **Figure 2A** the root is unprotected by endodermal

barriers. In **Figure 2B**, the CS is present which blocks the apoplastic pathway at the endodermis. In **Figure 2C**, both the CS and a solid, uninterrupted SL barrier are present. Hence, both the apoplastic and selective transport pathways are affected at the endodermis. Finally, **Figure 2D** represents the most realistic scenario in which both the CS and the SL are present with a gradual introduction of the SL and passage cells occurring along the length of the root. At the passage cell locations the SL is absent but the CS is still present (Peterson and Enstone, 1996).

In all of the scenarios, there is no significant uptake (i.e., net radial flux across the root surface) of solutes or water at steady state in the EZ (see arrows in **Figure 2**). As there is no functional xylem in the EZ, there is no convection of ions further up into the root. The influence of the conductive xylem extends only a few cells into the EZ, and hence this region is hydraulically isolated from the rest of the root. Therefore, diffusion is the main mechanism of ion transport in this region. As a result, at steady state the concentration of ions in the EZ for all four scenarios is equal to the bulk concentration in the soil.

In contrast, the introduction of the endodermal barriers has a strong effect on the amount and location of ion and water uptake in the DZ (see arrows in **Figure 2**). When there are no endodermal barriers present, the main uptake of water and ions occurs throughout the region where the xylem is, or is close to, fully functional (**Figure 2A**). However, when the endodermal barriers are present, the main uptake occurs closer to the root tip where the CS is not yet fully developed (giving an average net radial ion flux of 15.19 nmol $s^{-1}m^{-2}$ across the root surface in this region at steady state for the scenario shown in **Figure 2D**), despite the fact that in this region the xylem is *not* fully functional (**Figures 2B–D**). The SL substantially blocks water and solute uptake with an average ion flux of 0.58 nmol $s^{-1}m^{-2}$ across the root surface in the region where the SL is fully developed (excluding passage

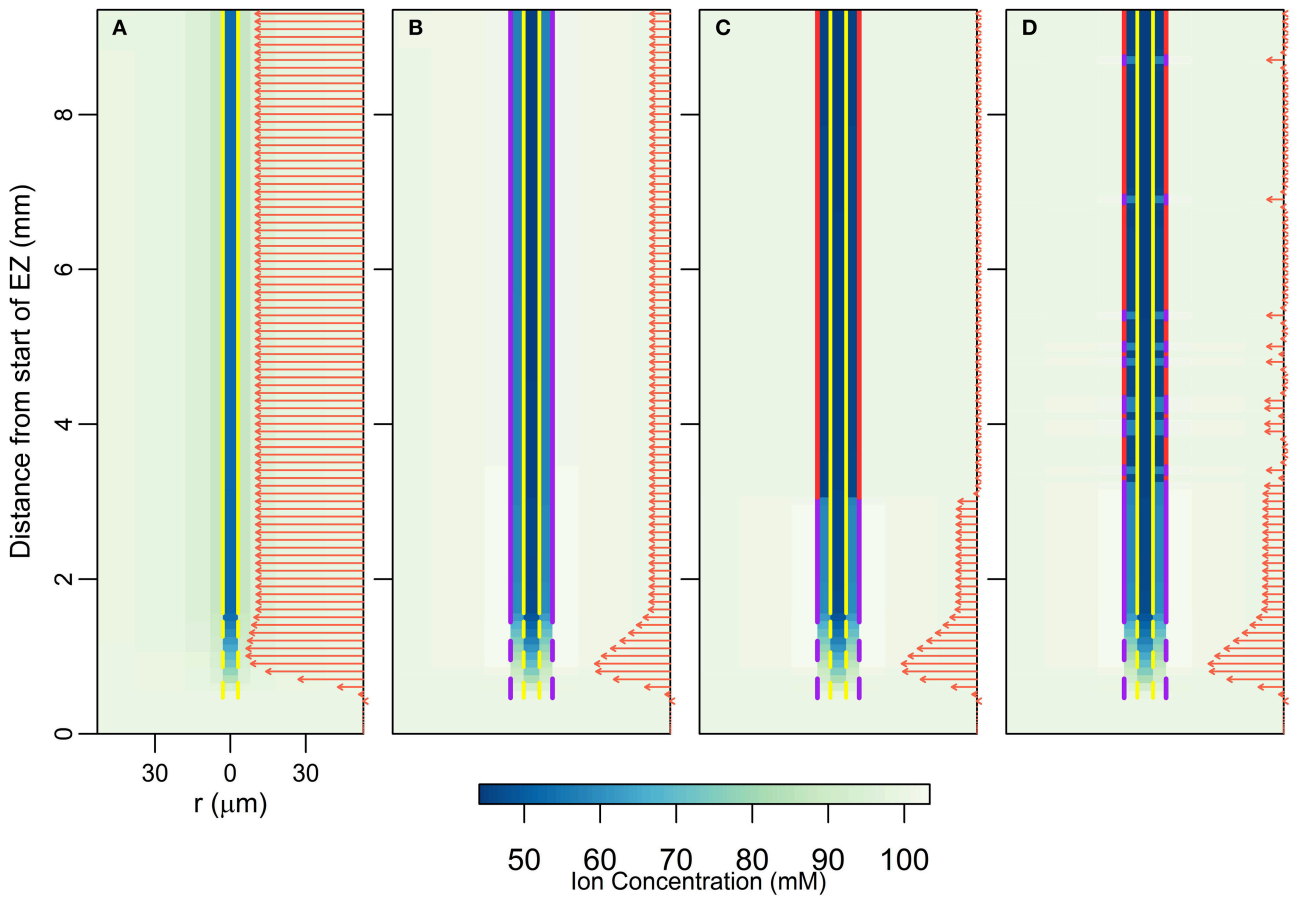

FIGURE 2 | Plots of steady state ion concentrations (colormaps) and ion fluxes (arrows) for four different root structures: (A) no endodermal barriers present, (B) CS present, (C) CS and SL present, (D) CS and SL with passage cells present. Yellow vertical lines show the presence of functional xylem with dashed lines near the root tip indicating the gradual increase in conductivity as the xylem develops. Purple vertical lines represent the presence of the CS; dashed lines near the root tip indicate the gradual appearance of the barrier. Red vertical lines show the location of the SL, with gaps identifying the location of passage cells. The arrows show the magnitude of net radial solute flux across the root surface (in mol s^{-1}), with the same scale used across all four subfigures. These arrows are also indicative of the corresponding water flow rates. All simulations assume 100 mM of 2 monovalent cations and 2 monovalent anions in the soil (e.g., 100 mM NaCl and 100 mM KNO_3). All ions are assumed to have identical transport properties and the transport parameters used are provided in **Table 1**. Refer to Section 2.3 for an explanation of the simulation of the endodermal barriers and xylem development. These simulations were carried out using $P_b = -0.5$ MPa.

cell locations) compared to 6.73 nmol $s^{-1}m^{-2}$ in the region where the CS is fully developed (**Figures 2C,D**). However, at the location of passage cells there is increased uptake, with an average ion flux across the root surface of 5.71 nmol $s^{-1}m^{-2}$ at their location (**Figure 2D**). This enhanced uptake supports the idea that passage cells function as key entry points into the stele (Peterson and Enstone, 1996; Andersen et al., 2015). The role of passage cells is explored further in the following sections.

In terms of ion concentrations, the main effects of the introduction of each barrier include an increase in the concentration gradient across the barrier, as well as a decrease in the concentration gradient across the tissues inside the barrier (i.e., the pericycle-xylem interface). Both of these changes result from relatively large reductions in the concentrations of ions in the pericycle, with smaller changes in concentrations in the xylem and endodermis also occurring. The introduction of the first barrier (the CS) causes the greatest change, with the introduction of a further barrier (the SL) having a less significant impact.

The results shown in **Figure 2** were simulated using a pressure boundary of −0.5 MPa at the top of the root (see Section 2.4 for further details about the boundary conditions). However, the discussion in this section is valid at lower transpiration conditions. The effects of different transpiration conditions are discussed in the following sections.

The Endodermal Barriers Reduce the Rate of Ion and Water Uptake into the Shoot, with Greater Reductions at Higher Transpiration Rates

Considering the relatively small changes in ion concentrations in the xylem, with the introduction of the endodermal barriers (**Figure 2**), it may at first glance appear that these barriers have minimal impact on the transport occurring within the xylem. However, other changes in root function occur in response to the introduction of each barrier. In particular, there are substantial decreases in both axial ion and water flow rates in the xylem (**Figure 3**). Importantly, it is this rate of axial transport out of the top of the root that determines the amount of ions and water entering the stem from the root.

The introduction of each endodermal barrier leads to reduced transport of both ions and water from the root into the aerial parts of the plant (**Figure 3**). The effect of each barrier becomes more significant as the transpiration rate increases (represented by a more negative P_b). These results show the compromise inherent in the function of the endodermal barriers: the entry of harmful ions into the xylem must be minimized while still maintaining the uptake of beneficial ions and water. The model simulations show a small increase in the axial flow rates of ions and water at the top of the root due to the presence of passage cells (see **Figure 3**, purple dot-dashed line vs. green dotted line), with a higher number of passage cells resulting in a larger increase (results not shown). These results support the idea that one function of passage cells is to enhance the uptake of water and at least some ions (Peterson and Enstone, 1996).

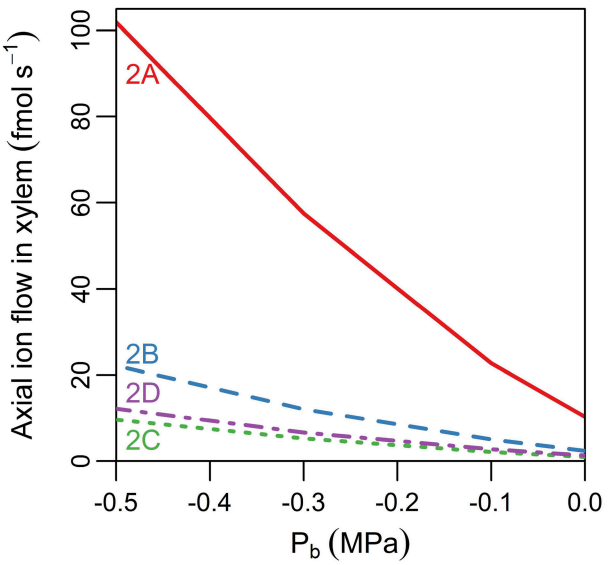

FIGURE 3 | Line plot showing the steady state axial flux of ions out of the top of the root xylem as a function of pressure at the top of the root, P_b (representing different rates of transpiration), and of the barriers present in the endodermis (different line types). The scenarios considered are: no endodermal barriers (solid red line); CS only (dashed blue line); both CS and SL present with no passage cells (green dotted line); and both CS and SL with passage cells present (purple dot-dashed line). The labels indicate the corresponding scenarios in **Figure 2**. The axial fluxes into the xylem compartment three cells down from the top of the root were used to minimize the influence of the flux boundary conditions chosen at the top of the root. The solute fluxes shown are also indicative of the corresponding water flow rates. All simulations assume 100 mM of 2 monovalent cations and 2 monovalent anions in the soil. All ions are assumed to have identical transport properties and the transport parameters used in the simulations are provided in **Table 1**.

Delayed Development of CS Relative to Functional Xylem Significantly Enhances Passive Ion and Water Uptake

In *Arabidopsis* primary roots, the xylem has been observed to appear in conjunction with the CS (Alassimone et al., 2010). We have thus far assumed that the development of the CS and functional xylem is coincident along the length of the root (**Figure 2**). However, exposure to various stresses (e.g., salinity) can influence the development of the endodermal barriers (Enstone et al., 2002) as well as the xylem (Cruz et al., 1992; Reinhardt and Rost, 1995), altering their position relative to the root tip and to each other. In **Figure 4** we explore the physiological effects of shifting the first points of development of the xylem and CS, both together and relative to each other. **Figures 4A–F** show the different locations considered, with vertical lines showing the positions of the CS (purple lines) and functional xylem (yellow lines). The arrows indicate the ion fluxes across the root surface, but are also representative of the water flow rates. Although the results in **Figures 4A–F** assume $P_b = -0.3$ MPa, the qualitative behavior is very similar for other transpiration conditions; the peak in uptake, however, becomes

less pronounced as the transpiration rate decreases. **Figure 4G** shows the rate of ion transport out of the top of the root xylem for the scenarios shown in **Figures 4A–F** for a range of transpiration conditions. The different positions shown in **Figures 4A–F** have only a minimal effect on the concentration of the ions in the root xylem at the top of the model root (results not shown).

A key result is that it is the *relative* location of the first points of development of the xylem and the CS that has the largest effect on the axial transport of water and ions up out of the root (**Figure 4G**). If any length of xylem is unprotected by the endodermal barrier, due to either delayed development of the CS (**Figure 4A**) or early maturation of the xylem (**Figure 4B**), there is increased transport of water and ions radially into the root and hence out of the xylem at the top of the root (green lines in **Figure 4G**). In contrast, if the CS develops before the xylem (**Figures 4E,F**) this transport is reduced (red lines in **Figure 4G**).

These results suggest that experiments examining the development of endodermal barriers could also quantify the development of the xylem and the relative positions of the two. In particular, examining the relative development of the CS and xylem and how this correlates with applied stresses could provide useful insights into the stress response of plants. For example, salt stress has been observed to result in the endodermal barriers developing closer to the root tip due to a reduction in the root growth rate as well as accelerated maturation of the barriers (Enstone et al., 2002). The observed reduced root growth rate would presumably also lead to the xylem developing closer to the root tip. However, the accelerated maturation rate of the barriers could lead to the CS developing closer to the root tip than the xylem (similar to the scenario shown in **Figure 4E**). This could be a favorable adaptation to salt stress as it would result in reduced passive uptake of ions (**Figure 4G**), although it would also lead to reduced water uptake. Similarly, when comparing the development of endodermal barriers across species or varieties in order to explain differences in their transport abilities it would seem important to consider the relative development of the xylem and CS.

Altered development of the SL can be correlated with altered development in the CS (Enstone et al., 2002). Hence, we also explored scenarios representing this correlation. We found similar behavior to that shown in **Figure 4**, with the additional feature that any reduction in the total length of the SL resulted in increased axial flow of ions in the xylem (results not shown).

In all of the scenarios considered, the peak uptake of water and solutes into the root occurs in the region where the xylem is present and either the CS is not present or is still developing. This agrees with the experimentally observed pattern of rapid uptake of water in the young region of the root (Graham et al., 1974; Clarkson and Robards, 1975). In contrast, the experimentally observed uptake of ions is more variable (Lüttge, 1983). This variability is unsurprising due to the variation in the types and locations of ion specific transporters. However, for some ions, peak uptake has been observed in this young region of the root; an example of this is calcium (Robards et al., 1973; White, 2001). It is worth noting that the modeled peak in ion uptake is not significantly affected even if the ions have differing diffusive

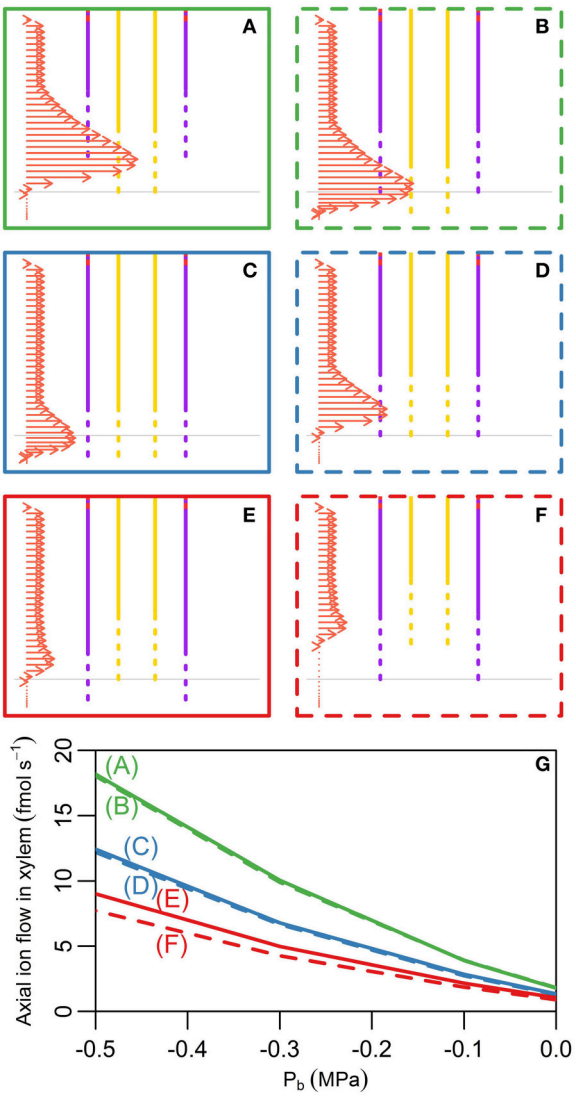

FIGURE 4 | (A–F) Plots showing the lower section of the model root, indicating the different initial positions of development of the CS and functional xylem that were explored. Purple (yellow) vertical lines indicate the presence of the CS (functional xylem). Dotted lines represent the gradual development of the CS and xylem, while solid lines represent fully functioning CS and xylem. Horizontal gray lines show the location of the start of the CS and xylem used in the model simulations shown in all other figures. The arrows show the net radial solute flux across the surface of the root at steady state for each scenario, these flows are indicative of the solute fluxes into the xylem. The same scale is used for the arrows across all six subfigures. Although these arrows show solute fluxes, they are also indicative of the corresponding water flow rates. The arrows shown represent the model results for $P_b = -0.3$ MPa. **(G)** Line plots showing the steady state axial solute fluxes out of the top of the model xylem as a function of the pressure boundary condition (representing the transpiration rate) and the relative positions of the initial development of the CS and xylem. The axial fluxes into the xylem compartment three cells down from the top of the root were used to minimize the influence of the type of flux boundary conditions chosen at the top of the root. The line colors and styles in **(G)** match the colors and styles of the boxes around the corresponding scenario in **(A–F)**. All simulations assume 100 mM of 2 monovalent cations and 2 monovalent anions in the soil. All ions are assumed to have identical transport properties and the transport parameters used in the simulations are provided in **Table 1**.

permeabilities (results not shown). Our results show that the location of the peak in uptake is less obvious if the CS extends beyond the xylem (compare **Figures 4E,F** to **Figures 4C,D**) or if the transpiration level is low (see the next section). Hence, differences in the anatomy of plant roots as well as experimental conditions may affect the extent and prominence of the peak in uptake.

The model results in **Figures 4A–F** show the locations of peak uptake. However, they do not specify which region of the root contributes the most to the total uptake of ions and water. Due to the longer length of the mature region of the root compared to the short length of the high uptake region, the mature region may contribute more to the overall uptake of ions and water. The presence of lateral roots also contributes to the uptake in the more mature regions of the root.

Low vs. High Transpiration Leads to Significantly Different Spatial Distributions of Ions in the DZ, but Not in the EZ

Figures 3, **4G** initiated a study of the effect of transpiration on the rate of ion and water uptake. In this section we explore in greater detail the influence of transpiration on the distribution of ions within the root (**Figure 5**). The effect of varying the transpiration level is particularly felt in the DZ, with the level of transpiration influencing both the axial and radial distribution of ions.

The qualitative behavior of the axial distribution of ions in the DZ varies depending on the level of transpiration. Under high transpiration there is a steady decline in concentration in the xylem along the length of the root in the DZ (**Figure 5B** and red dotted line in **Figure 5C**), whereas under low transpiration conditions the ion concentrations in the xylem increase along the length of the root in the DZ (**Figure 5A** and solid red line in **Figure 5C**). This dichotomy arises from the competing effects of diffusion and convection. High transpiration results in ions being convected away faster than can be replaced by diffusion, while under low transpiration the low level of convection cannot offset the influx of ions by diffusion into the xylem from the surrounding tissues.

In terms of the radial distribution of ions in the DZ, the concentration of ions in the xylem and pericycle is lower at higher levels of transpiration (**Figure 5B** and dotted lines in **Figure 5C** compared to **Figure 5A** and solid lines in **Figure 5C**) due to greater convection up and out of the root. In addition, at higher levels of transpiration there is a build up of ions in the endodermis at locations where only the CS is present (including at passage cell locations), while this build up is not evident at lower transpiration levels (green dotted lines compared to solid lines in **Figure 5C**). **Figures 5D,E** highlight how the interactions between diffusion and convection generate these contrasting results. In particular, where only the CS is present, a high level of convection (red arrows in **Figure 5E**) is required to offset the process of diffusion, which counteracts the formation of any concentration gradients (see yellow arrows in **Figure 5E**). In contrast, at low levels of transpiration, the inward convection of ions is small or even reversed due to osmotic pressure gradients (red arrows in **Figure 5D**) and hence there is no build up of ions outside the endodermal barriers. Overall these results point to the importance of considering the effect of the level of transpiration when experimentally investigating the function of endodermal barriers, particularly when using the presence of a build up of ions outside the CS as an experimental measure of how well it is functioning as a barrier (e.g., Lauchli et al., 2008).

In contrast to the results in the DZ, the steady state concentrations in the EZ are identical and equal to the ion concentrations in the soil for both transpiration scenarios (see **Figures 5A–C**). Since there is only negligible convection in the EZ, transpiration conditions do not influence the uptake of ions in this hydraulically isolated region of the root. Similarly, for both transpiration scenarios the concentration of ions in the xylem and pericycle decreases through the transition zone from the EZ to the DZ due to the development of a functional xylem . However, this decrease is more pronounced under higher transpiration conditions (see **Figures 5A–C**).

The effect of passage cells on the distribution of ions extends across several tissue regions (see **Figure 5C**). There are higher levels of both diffusion and convection across the endodermis in the vicinity of passage cells compared to the surrounding cells which are affected by the SL (**Figures 5D,E**). Where there are passage cells, ions build up in the pericycle as both diffusion and convection draw ions in from the surrounding outer tissues (see the yellow diffusive and red convective arrows in **Figures 5D,E**). Again, these results confirm the function of passage cells as key entry points into the stele (Peterson and Enstone, 1996).

The arrows in **Figures 5A,B** show that the pattern of ion *uptake* is not qualitatively affected by the level of transpiration. However, the magnitude of ion uptake is strongly dependent on the rate of transpiration.

The significant differences in the distribution of ions for the different transpiration conditions are supported by experimental observations. For example, Møller et al. (2009) found that the measured radial distribution of Na^+ and K^+ differed substantially between plants grown in conditions where there was little or no transpiration and those plants grown in transpiring conditions. In addition, our predicted increase in the magnitude of water uptake along the length of the root for higher transpiration conditions (**Figures 5A,B**) has also been observed experimentally (e.g., Sanderson, 1983).

Measurements of Transient vs. Steady State Ion Fluxes Reflect Different Aspects of Root Function

The design of experiments to measure the fluxes of ions and/or water across root surfaces (e.g., Zhou et al., 2011) should incorporate an appropriate time frame to match the purpose of the experiment, i.e., are transient or steady state conditions appropriate? Transient ion fluxes demonstrate which regions along the length of the root fill up most rapidly, while steady state fluxes indicate the regions through which the main uptake occurs over time. This is highlighted in **Figure 6**, which shows how the ion concentrations (colormap) and the radial solute fluxes (arrows) change over time. For clarity only the net radial solute fluxes into the epidermis and pericycle are shown in

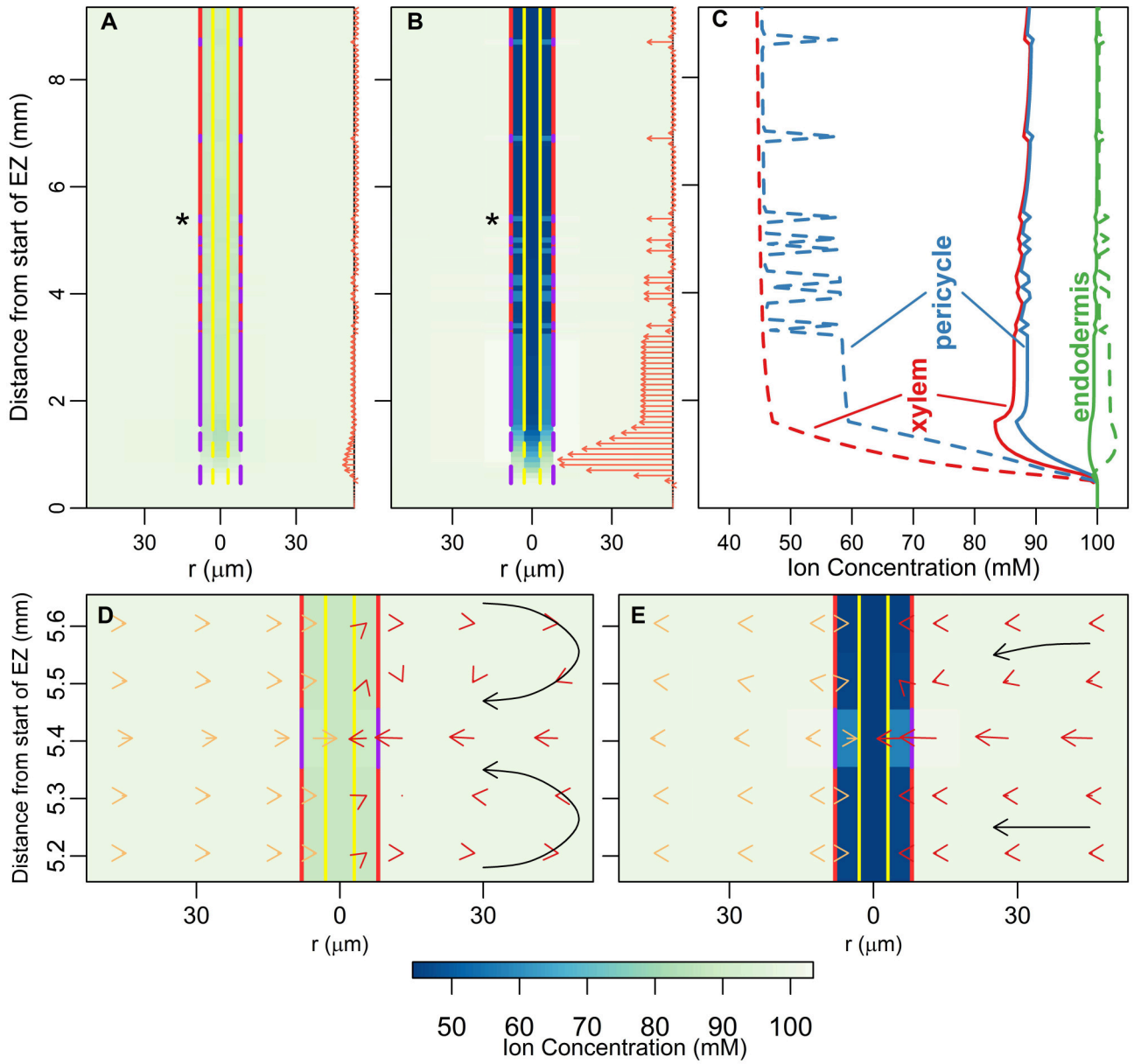

FIGURE 5 | (A,B) Plots of steady state ion concentrations (colormaps) and ion fluxes (arrows) for two different transpiration conditions: $P_b = 0$ MPa and $P_b = -0.5$ MPa respectively. The arrows are also indicative of water flow rates. The same scale is used for the arrows in **(A,B)**. **(C)** Line plots of ion concentrations in **(A)** (solid lines) and **(B)** (dotted lines). The line colors refer to tissue regions: xylem (red lines), pericycle (blue lines) and endodermis (green lines). **(D,E)** show zoomed-in sections of results in **(A,B)**, respectively, at the location of the passage cell indicated by asterisks. Yellow arrows on the left show the diffusive component of the total ion flow, red arrows on the right show the convective component (adding the two together gives the total flow). The arrows are shown in the center of their corresponding model compartment. The arrows in **(D,E)** are drawn to different scales for clarity, an equal length arrow in **(E)** represents a 10 times larger flux than in **(D)**. The black arrows highlight the convective flow path and are not drawn to scale. All simulations assume 100 mM of 2 monovalent cations and 2 monovalent anions in the soil. All ions are assumed to have identical transport properties and the transport parameters used in the simulations are provided in **Table 1**.

Figure 6, rather than the fluxes into all of the root tissues. As in previous figures, the arrows in **Figure 6** also represent the water flow rates, which are in direct proportion to the ion fluxes. The results indicate that the solute fluxes at the surface are not representative of those in the inner regions of the root until the system is at or near steady state (**Figures 6A–C**). However, when the system is at steady state (**Figure 6D**), solute fluxes across the root surface are representative of where the main uptake of ions into the inner regions occurs. This is provided there are no large vertical fluxes in the intervening regions. Further complications in flux measurements would arise if the ions being measured are converted to other forms before reaching the stele (e.g., the reduction of nitrate to nitrite).

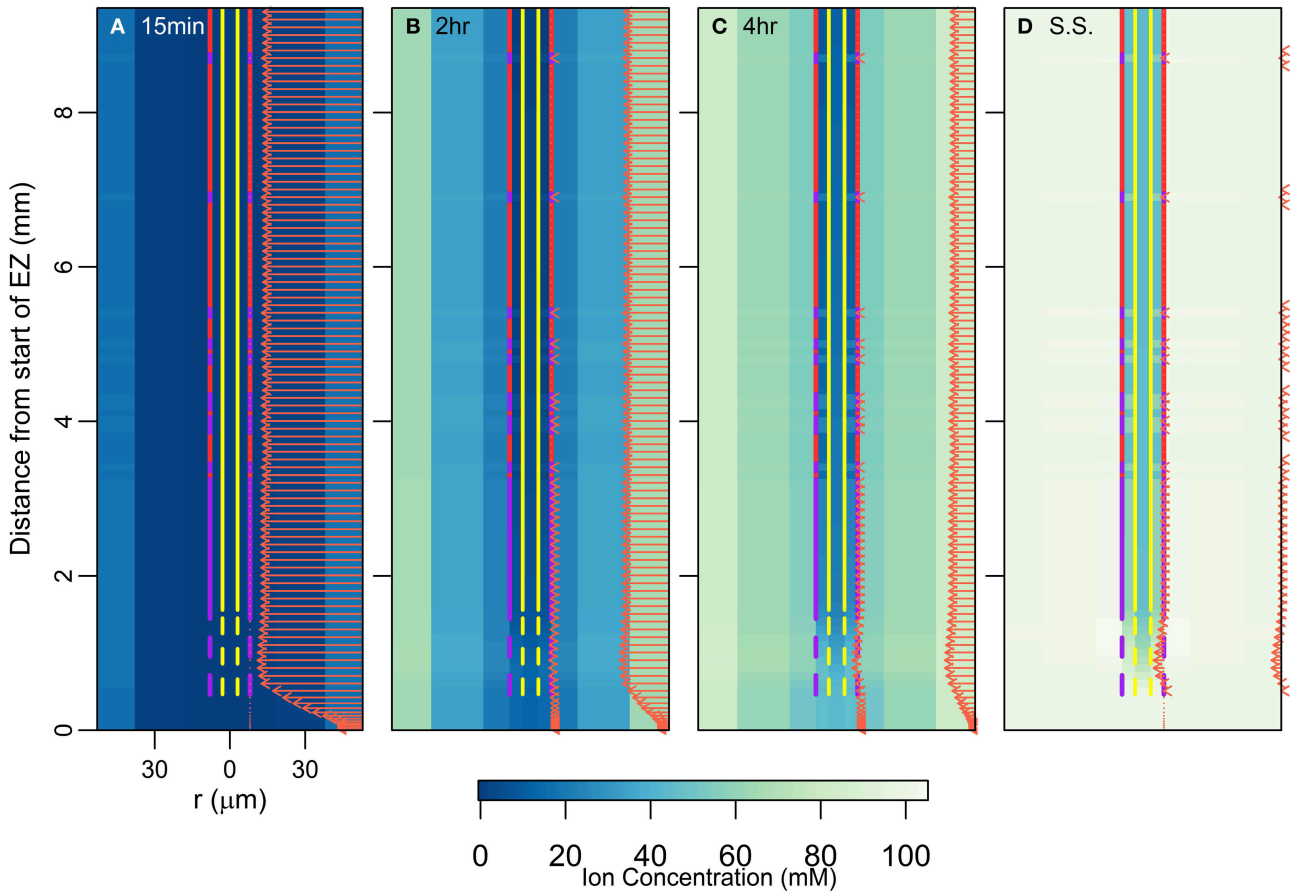

FIGURE 6 | Plots of transient ion concentrations (colormap) and ion fluxes (arrows) for the root structure shown in Figure 2D. For clarity only the net radial solute fluxes across the root surface (into the epidermis) and across the endodermis-pericycle interface are shown. The initial condition for this simulation was the steady state result for a simulation carried out with 100 mM of 1 monovalent cation and 1 monovalent anion in the soil (e.g., KNO_3). The simulation was then carried out assuming 100 mM of 2 monovalent cations and 2 monovalent anions in the soil (e.g., the existing KNO_3 with NaCl added). The results shown are for the added ions. The results show the changes over time after the ions were added: **(A)** 15 min after, **(B)** 2 h after, **(C)** 4 h after, **(D)** at steady state (approximately 1 day after). These simulations were carried out using $P_b = -0.5$ MPa. All ions are assumed to have identical transport properties and the transport parameters used in the simulations are provided in **Table 1**.

4. DISCUSSION

Our work focuses on the passive uptake of ions and water, in particular, exploring the interaction between the processes of diffusion and convection. The results therefore show the ion uptake patterns and concentration distributions that can be explained by passive processes and their interaction with cell differentiation. However, using these results one can also infer information about the active transport of ions. In particular, our results describe the pattern of ion and water uptake that occurs when only passive processes operate (arrows in **Figure 2D**) and highlight that qualitatively this pattern is relatively unaffected by either differences in the level of transpiration (arrows in **Figures 5A,B**) or differences in cell development (**Figures 4A–F**), although the magnitudes can be substantially affected. Hence, an ion uptake pattern that qualitatively differs substantially from **Figure 2D** would indicate the operation of an active transport mechanism. For example, any significant uptake of ions in the EZ at steady state is likely to be driven by active processes as there is only minimal passive uptake in this region (see arrows in **Figures 2D**, **6D**). Similarly, any significant uptake of water in this region is likely to be driven by osmotic pressure gradients developed by the active transport of ions.

It is no surprise that the level of transpiration has a very significant effect on the rate of ion and water uptake (**Figures 3**, **4G** and arrows in **Figure 5**), as well as on the spatial distribution of ions radially and axially inside the DZ of the root (**Figure 5**). Indeed, the level of impact that transpiration has on the spatial distribution of ions is of a similar scale to the level of impact of the presence of the endodermal barriers (compare **Figures 2**, **5**). Our results support the experimental findings of Møller et al. (2009) that different transpiration conditions lead to differences in the radial distribution of ions across plant roots. In addition, our results highlight the fact that some transport behavior becomes more distinct as the level of transpiration increases, e.g., the influence of the endodermal

barriers on ion uptake (**Figure 3**), as well as the positions of peak uptake (**Figures 5A,B**). Hence, our findings suggest that the results of ion and water measurements conducted on non-transpiring plants or excised roots (with no suction applied to cut end) are likely to differ substantially from measurements conducted on intact, transpiring plants. In particular, the effects of convective processes will be more obvious under higher transpiring conditions, whereas under low or non-transpiring conditions the effects of active processes are likely to be more obvious, although under all growth conditions the transport will also be affected by diffusion. These differences need to be considered when attempting to compare the results of experiments conducted under different transpiration conditions (see e.g., Møller and Tester, 2007).

The effects of the transpiration level also have ramifications for other modeling efforts. Firstly, our more detailed simulations of water transport concur with previous modeling findings that the level of convection is a significant factor in determining the radial distribution of ions (Claus et al., 2013). Convection is clearly an essential mechanism to include in models of ion transport in roots in which functional xylem is present. Secondly, the distinctly different patterns of ion distribution resulting from differing transpiration levels (**Figures 5A–C**) suggest the importance of investigating the interactions between convective and membrane transport processes in any study of the effects of membrane transporters on the pattern of solute distribution (e.g., Claus et al., 2013; Sakurai et al., 2015). Thirdly, convection does not seem to be significant in regions of root where the xylem is not conductive, such as in the EZ. In our case, the zone of influence of the xylem extended only a few cells in the direction of the root tip from the initial conductive cells. These findings support earlier assumptions that it is unnecessary to include convection when modeling ion transport in regions where the xylem is not functional (e.g., Shimotohno et al., 2015). Hence, while it is not necessary for convection to be incorporated into models of ion transport in the meristematic zone and the EZ, it may be very important for convection to be considered in the more mature regions of the root.

It has been suggested that passage cells function as low resistance pathways for the uptake of water and at least some ions (Peterson and Enstone, 1996). Our findings (**Figures 2D**, **3**, **5**) give this position some support. This role has been suggested due to the consistent positioning of passage cells adjacent to protoxylem poles (Peterson and Enstone, 1996). However, there is currently very limited direct experimental evidence identifying the function of passage cells (Andersen et al., 2015). To investigate the role of passage cells further it would be necessary to differentiate between the apoplastic and symplastic pathways.

Our efforts to model transport within a single root do not include contributions from lateral roots to the uptake of ions and water. Not only do lateral roots increase the root surface area available for uptake, their formation also interrupts the CS (Vermeer et al., 2014), potentially allowing leakage of ions and water across the endodermis. Hence, the influx of ions and water at the location of lateral root formation would likely be similar to the modeled influx found at the location of passage cells (e.g., **Figure 2D**).

In this paper we have explored passive transport processes. However, to investigate the uptake and transport of specific ions (such as K^+ or Na^+) it is necessary to incorporate models of active transport, such as the model we have developed recently (Foster and Miklavcic, 2015). Such a challenge requires the explicit modeling of symplastic and apoplastic pathways, which would allow us to investigate more specific aspects of cell differentiation that cannot be included in the current model. For example, one of the suspected functions of the CS is to prevent backflow of ions out of the stele under low transpiration conditions (Enstone et al., 2002). An investigation of this process would require active transport mechanisms to be included since it is thought that active transport is responsible for the build up of ions in the xylem under low or non-transpiring conditions (Enstone et al., 2002). In addition, a more complex model would allow a clearer separation of the function of the CS (which blocks the apoplastic pathways) from the function of the SL (which is thought to block uptake into the symplastic pathway), including a further exploration of the role of passage cells.

5. CONCLUSIONS

In this paper we have presented the results of simulations of the transport of ions and water in a plant root via passive transport processes. The model root incorporates both different tissue types and different developmental zones. As in our previous works (Foster and Miklavcic, 2013, 2014), the model includes the self-consistent interaction between the transport of ions and water. We have used the model to simulate a wide range of transport scenarios and found that, in all instances where the endodermal barriers were present, the peak uptake of water and ions occurred at the start of the DZ. In addition, we found that there was no substantial uptake in the EZ at steady state due to the lack of functional xylem in this region. From this we infer that any observed uptake of ions (or water) in this developmental zone under steady state conditions is likely to be due to active transport processes. The results also highlight that the level of transpiration has a significant impact on water and ion transport in the DZ. This should be taken into consideration both when conducting experiments and developing models to examine transport in this developmental zone.

We have used our model of passive transport to infer information about active transport processes. However, more detailed modeling is required to examine the transport of specific ions. For example, combining a single cell model of active and passive transport of ions as well as water, which we have developed previously (Foster and Miklavcic, 2015), with the root model presented here would allow more detailed exploration of ion transport (specifically Na^+, K^+, and Cl^-) across the different developmental zones. For example, it would allow an examination of how each of the endodermal barriers influence the different transport pathways. This is the subject of ongoing efforts. Nevertheless, the passive processes of diffusion and

convection modeled in this paper are fundamental to ion uptake. Hence, the results discussed in this paper establish a baseline of transport phenomenon on which active transport mechanisms are imposed and with which active transport mechanisms interact.

AUTHOR CONTRIBUTIONS

The authors were equal contributors to the design of simulations, analysis of results and drafting of the paper. KF performed the simulations.

FUNDING

This project is supported by an Australian Postgraduate Award and a Grains Industry Research Scholarship from the Grains Research and Development Corporation for KF.

SUPPLEMENTARY MATERIAL

The Supplementary Material for this article can be found online at: http://journal.frontiersin.org/article/10.3389/fpls.2016.00914

REFERENCES

Alassimone, J., Naseer, S., and Geldner, N. (2010). A developmental framework for endodermal differentiation and polarity. *Proc. Natl. Acad. Sci. U.S.A.* 107, 5214–5219. doi: 10.1073/pnas.0910772107

Andersen, T. G., Barberon, M., and Geldner, N. (2015). Suberization - the second life of an endodermal cell. *Curr. Opin. Plant Biol.* 28, 9–15. doi: 10.1016/j.pbi.2015.08.004

Barberon, M., and Geldner, N. (2014). Radial transport of nutrients: the plant root as a polarized epithelium. *Plant Physiol.* 166, 528–537. doi: 10.1104/pp.114.246124

Boursiac, Y., Chen, S., Luu, D.-T., Sorieul, M., van den Dries, N., and Maurel, C. (2005). Early effects of salinity on water transport in *Arabidopsis* roots. Molecular and cellular features of aquaporin expression. *Plant Physiol.* 139, 790–805. doi: 10.1104/pp.105.065029

Casimiro, I., Beeckman, T., Graham, N., Bhalerao, R., Zhang, H., Casero, P., et al. (2003). Dissecting *Arabidopsis* lateral root development. *Trends Plant Sci.* 8, 165–171. doi: 10.1016/S1360-1385(03)00051-7

Clarkson, D. T., and Robards, A. W. (1975). *The Endodermis, Its Structural Development and Physiological Role*. London: Academic Press.

Claus, J., Bohmann, A., and Chavarra-Krauser, A. (2013). Zinc uptake and radial transport in roots of *Arabidopsis thaliana*: a modelling approach to understand accumulation. *Ann. Bot.* 112, 369–380. doi: 10.1093/aob/mcs263

Cruz, R. T., Jordan, W. R., and Drew, M. C. (1992). Structural changes and associated reduction of hydraulic conductance in roots of *Sorghum bicolor L.* following exposure to water deficit. *Plant Physiol.* 99, 203–212. doi: 10.1104/pp.99.1.203

Dolan, L., Janmaat, K., Willemsen, V., Linstead, P., Poethig, S., Roberts, K., et al. (1993). Cellular organisation of the *Arabidopsis thaliana* root. *Development* 119, 71–84.

Enstone, D. E., Peterson, C. A., and Ma, F. (2002). Root endodermis and exodermis: structure, function, and responses to the environment. *J. Plant Growth Regul.* 21, 335–351. doi: 10.1007/s00344-003-0002-2

Foster, K. J., and Miklavcic, S. J. (2013). Mathematical modelling of the uptake and transport of salt in plant roots. *J. Theor. Biol.* 336, 132–143. doi: 10.1016/j.jtbi.2013.07.025

Foster, K. J., and Miklavcic, S. J. (2014). On the competitive uptake and transport of ions through differentiated root tissues. *J. Theor. Biol.* 340, 1–10. doi: 10.1016/j.jtbi.2013.09.004

Foster, K. J., and Miklavcic, S. J. (2015). Toward a biophysical understanding of the salt stress response of individual plant cells. *J. Theor. Biol.* 385, 130–142. doi: 10.1016/j.jtbi.2015.08.024

Frensch, J., Hsiao, T., and Steudle, E. (1996). Water and solute transport along developing maize roots. *Planta* 198, 348–355. doi: 10.1007/BF00620050

Geldner, N. (2013). The endodermis. *Ann. Rev. Plant Biol.* 64, 531–558. doi: 10.1146/annurev-arplant-050312-120050

Graham, J., Clarkson, D. T., and Sanderson, J. (1974). *Water Uptake by the Roots of Marrow and Barley Plants*. Agricultural Resource Council Letcombe Laboratory Annual Report 1973, 9–12.

Javot, H., Lauvergeat, V., Santoni, V., Martin-Laurent, F., Güçlü, J., Vinh, J., et al. (2003). Role of a single aquaporin isoform in root water uptake. *Plant Cell Online* 15, 509–522. doi: 10.1105/tpc.008888

Katchalsky, A., and Curran, P. F. (1965). *Nonequilibrium Thermodynamics in Biophysics*. Cambridge: Harvard University Press. doi: 10.4159/harvard.9780674494121

Lauchli, A., James, R. A., Huang, C. X., McCully, M., and Munns, R. (2008). Cell-specific localization of Na^+ in roots of durum wheat and possible control points for salt exclusion. *Plant Cell Environ.* 31, 1565–1574. doi: 10.1111/j.1365-3040.2008.01864.x

Lüttge, U. (1983). "Import and export of mineral nutrients in plant roots," in *Inorganic Plant Nutrition*, eds A. Läuchli and R. L. Bieleski (New York, NY: Springer-Verlag), 181–211.

Mattsson, J., Sung, Z., and Berleth, T. (1999). Responses of plant vascular systems to auxin transport inhibition. *Development* 126, 2979–2991.

Melchior, W., and Steudle, E. (1993). Water transport in onion (*Allium cepa* L.) roots (changes of axial and radial hydraulic conductivities during root development). *Plant Physiol.* 101, 1305–1315.

Møller, I. S., Gilliham, M., Jha, D., Mayo, G. M., Roy, S. J., Coates, J. C., et al. (2009). Shoot Na^+ exclusion and increased salinity tolerance engineered by cell type-specific alteration of Na^+ transport in *Arabidopsis*. *Plant Cell* 21, 2163–2178. doi: 10.1105/tpc.108.064568

Møller, I. S., and Tester, M. (2007). Salinity tolerance of *Arabidopsis*: a good model for cereals? *Trends Plant Sci.* 12, 534–540. doi: 10.1016/j.tplants.2007.09.009

Naseer, S., Lee, Y., Lapierre, C., Franke, R., Nawrath, C., and Geldner, N. (2012). Casparian strip diffusion barrier in *Arabidopsis* is made of a lignin polymer without suberin. *Proc. Natl. Acad. Sci. U.S.A.* 109, 10101–10106. doi: 10.1073/pnas.1205726109

Peterson, C. A., and Enstone, D. E. (1996). Functions of passage cells in the endodermis and exodermis of roots. *Physiol. Plant.* 97, 592–598. doi: 10.1111/j.1399-3054.1996.tb00520.x

Pfister, A., Barberon, M., Alassimone, J., Kalmbach, L., Lee, Y., Vermeer, J. E. M., et al. (2014). A receptor-like kinase mutant with absent endodermal diffusion barrier displays selective nutrient homeostasis defects. *eLife* 3:e03115. doi: 10.7554/eLife.03115

Ranathunge, K., and Schreiber, L. (2011). Water and solute permeabilities of *Arabidopsis* roots in relation to the amount and composition of aliphatic suberin. *J. Exp. Bot.* 62, 1961–1974. doi: 10.1093/jxb/erq389

Reinhardt, D. H., and Rost, T. L. (1995). On the correlation of primary root growth and tracheary element size and distance from the tip in cotton seedlings grown under salinity. *Environ. Exp. Bot.* 35, 575–588. doi: 10.1016/0098-8472(95)00018-6

Robards, A. W., Jackson, S. M., Clarkson, D. T., and Sanderson, J. (1973). The structure of barley roots in relation to the transport of ions into the stele. *Protoplasma* 77, 291–311. doi: 10.1007/BF01276765

Roppolo, D., De Rybel, B., Tendon, V. D., Pfister, A., Alassimone, J., Vermeer, J. E. M., et al. (2011). A novel protein family mediates Casparian strip formation in the endodermis. *Nature* 473, 380–383. doi: 10.1038/nature10070

Sakurai, G., Satake, A., Yamaji, N., Mitani-Ueno, N., Yokozawa, M., Feugier, F. G., et al. (2015). *In silico* simulation modeling reveals the importance of the Casparian strip for efficient silicon uptake in rice roots. *Plant Cell Physiol.* 56, 631–639. doi: 10.1093/pcp/pcv017

Sanderson, J. (1983). Water uptake by different regions of the barley root. Pathways of radial flow in relation to development of the endodermis. *J. Exp. Bot.* 34, 240–253. doi: 10.1093/jxb/34.3.240

Scheres, B., Di Laurenzio, L., Willemsen, V., Hauser, M. T., Janmaat, K., Weisbeek, P., et al. (1995). Mutations affecting the radial organisation of the *Arabidopsis* root display specific defects throughout the embryonic axis. *Development* 121, 53–62.

Shimotohno, A., Sotta, N., Sato, T., De Ruvo, M., Mare, A. F., Grieneisen, V. A., et al. (2015). Mathematical modeling and experimental validation of the spatial distribution of boron in the root of *Arabidopsis thaliana* identify high boron accumulation in the tip and predict a distinct root tip uptake function. *Plant Cell Physiol.* 56, 620–630. doi: 10.1093/pcp/pcv016

Sutka, M., Li, G., Boudet, J., Boursiac, Y., Doumas, P., and Maurel, C. (2011). Natural variation of root hydraulics in *Arabidopsis* grown in normal and salt-stressed conditions. *Plant Physiol.* 155, 1264–1276. doi: 10.1104/pp.110.163113

van der Horst, H. C., Timmer, J. M. K., Robbertsen, T., and Leenders, J. (1995). Use of nanofiltration for concentration and demineralization in the dairy industry: model for mass transport. *J. Membrane Sci.* 104, 205–218. doi: 10.1016/0376-7388(95)00041-A

Vermeer, J. E. M., von Wangenheim, D., Barberon, M., Lee, Y., Stelzer, E. H. K., Maizel, A., et al. (2014). A spatial accommodation by neighboring cells is required for organ initiation in *Arabidopsis*. *Science* 343, 178–183. doi: 10.1126/science.1245871

White, P. J. (2001). The pathways of calcium movement to the xylem. *J. Exp. Bot.* 52, 891–899. doi: 10.1093/jexbot/52.358.891

Zhou, Q., Wang, L., Cai, X., Wang, D., Hua, X., Qu, L., et al. (2011). Net sodium fluxes change significantly at anatomically distinct root zones of rice *Oryza sativa L.* seedlings. *J. Plant Physiol.* 168, 1249–1255. doi: 10.1016/j.jplph.2011.01.017

Conflict of Interest Statement: The authors declare that the research was conducted in the absence of any commercial or financial relationships that could be construed as a potential conflict of interest.

The reviewer ID and handling Editor declared their shared affiliation, and the handling Editor states that the process nevertheless met the standards of a fair and objective review.

frontiers in Plant Science

HYPOTHESIS AND THEORY
published: 27 June 2016
doi: 10.3389/fpls.2016.00912

Cooperation through Competition—Dynamics and Microeconomics of a Minimal Nutrient Trade System in Arbuscular Mycorrhizal Symbiosis

*Stephan Schott, Braulio Valdebenito, Daniel Bustos, Judith L. Gomez-Porras, Tripti Sharma and Ingo Dreyer**

Facultad de Ingeniería, Centro de Bioinformática y Simulación Molecular, Universidad de Talca, Talca, Chile

In arbuscular mycorrhizal (AM) symbiosis, fungi and plants exchange nutrients (sugars and phosphate, for instance) for reciprocal benefit. Until now it is not clear how this nutrient exchange system works. Here, we used computational cell biology to simulate the dynamics of a network of proton pumps and proton-coupled transporters that are upregulated during AM formation. We show that this minimal network is sufficient to describe accurately and realistically the nutrient trade system. By applying basic principles of microeconomics, we link the biophysics of transmembrane nutrient transport with the ecology of organismic interactions and straightforwardly explain macroscopic scenarios of the relations between plant and AM fungus. This computational cell biology study allows drawing far reaching hypotheses about the mechanism and the regulation of nutrient exchange and proposes that the "cooperation" between plant and fungus can be in fact the result of a competition between both for the same resources in the tiny periarbuscular space. The minimal model presented here may serve as benchmark to evaluate in future the performance of more complex models of AM nutrient exchange. As a first step toward this goal, we included SWEET sugar transporters in the model and show that their co-occurrence with proton-coupled sugar transporters results in a futile carbon cycle at the plant plasma membrane proposing that two different pathways for the same substrate should not be active at the same time.

Keywords: computational cell biology, phosphate, plant biophysics, proton-coupled transport, sugar

OPEN ACCESS

Edited by:
Mike Blatt,
University of Glasgow, UK

Reviewed by:
Xinguang Zhu,
Chinese Academy of Sciences, China
Igor Pottosin,
Universidad de Colima, Mexico

****Correspondence:***
Ingo Dreyer
idreyer@utalca.cl

Specialty section:
This article was submitted to Plant Physiology, a section of the journal Frontiers in Plant Science

Received: *04 May 2016*
Accepted: *09 June 2016*
Published: *27 June 2016*

Citation:
Schott S, Valdebenito B, Bustos D, Gomez-Porras JL, Sharma T and Dreyer I (2016) Cooperation through Competition—Dynamics and Microeconomics of a Minimal Nutrient Trade System in Arbuscular Mycorrhizal Symbiosis. Front. Plant Sci. 7:912. doi: 10.3389/fpls.2016.00912

INTRODUCTION

Land plants established diverse forms of mutualistic and reciprocally beneficial symbiotic relationships with microorganisms (Marschner, 2012). In the most prevalent symbiosis known, arbuscular mycorrhizal fungi (AMF) from the phylum Glomeromycota colonize the root systems and modulate plant growth by enhancing the availability of nutrients (Parniske, 2008; Bonfante and Genre, 2010; Smith and Smith, 2011; Harrison, 2012; van der Heijden et al., 2015). Here, the plant benefits in particular from the phosphorus supply by the fungus and provides the fungus in return with energy-rich photosynthetic carbohydrates (Karandashov and Bucher, 2005; Kiers et al., 2011; Smith et al., 2011). The fungus with its extensive network of extra-radical hyphae extends beyond

root depletion zones and can explore larger soil volumes; it thus secures new regions for nutrient mining.

When a hypha from a germinating soil-borne spore of an AM fungus comes into contact with a host root, it starts to penetrate deep into the parenchyma cortex and then differentiates into highly branched arbuscular structures. As a response, the infected cells undergo major modifications by altering their transcriptional activity, shrinking the vacuoles, reorganizing the cytoskeleton and extending the plant plasma membrane that it surrounds the arbuscule (Gianinazzi-Pearson, 1996; Harrison, 2012). The fractal-like structure of fungal and plant plasma membranes significantly increases the interaction surface between fungus and plant. The symbiotic interface, the periarbuscular space, separates the two plasma membranes by 100 nm or less and is a specialized apoplastic zone for nutrient exchange between the mycorrhizal symbionts (Gianinazzi-Pearson, 1996).

Along with the morphological changes, gene expression is also largely re-programmed in arbuscule containing cells (Harrison, 2012). In particular, the expression of certain types of transmembrane transporters is stimulated. So far it was known that at the plant side, genes coding for H^+-ATPases, proton-coupled sugar transporters, and proton-coupled phosphate transporters are activated in arbuscule containing cells (Gianinazzi-Pearson, 1996; Harrison, 1996, 2012; Rausch et al., 2001; Harrison et al., 2002; Paszkowski et al., 2002; Javot et al., 2007; Krajinski et al., 2014), while at the fungal side, this transporter set is complemented by proton pumps as well as sugar and phosphate transporters that are homologous to the plant transporters (Harrison and van Buuren, 1995; Karandashov and Bucher, 2005; Ramos et al., 2008; Helber et al., 2011; Doidy et al., 2012). Very recently it was shown that in plant cells also carbon transporters of the SWEET type are upregulated during arbuscule formation (Manck-Götzenberger and Requena, 2016).

The exchange of phosphate (P) for carbon (C) is seen as a highly cooperative process. Plants can detect, discriminate, and reward the best fungal partners with more carbohydrates. In turn, their fungal partners enforce cooperation by increasing nutrient transfer only to those roots providing more carbohydrates (Kiers et al., 2011). This exchange of nutrients has been considered as an ideal example to test biological market theory (Noë and Hammerstein, 1995; Schwartz and Hoeksema, 1998; Hoeksema and Schwartz, 2003) and was addressed by Kiers et al. (2011) proposing that AMF symbiosis functions analogous to a market economy, where there are partners on both sides of the interaction and higher quality services are remunerated in both directions. However, the terms of trade between the partners are still under debate (Fitter, 2006; Smith and Smith, 2015). In particular, the molecular components involved in the efflux of P across the fungal plasma membrane and in the export of carbohydrates from the plant have not been clarified yet (Bonfante and Genre, 2010; Smith and Smith, 2011; Johri et al., 2015).

Interestingly both, plant and fungus, are equipped with electrically identical transporters: (i) proton pumps, (ii) H^+/sugar transporters that commonly use the electrochemical proton gradient for the uptake of sugars (Klepek et al., 2005), and (iii) phosphate transporters with a stoichiometry of nH^+:Pi^- ($n > 1$) that normally harvest the electrochemical proton gradient for the uptake of phosphate (Preuss et al., 2011). In principle, these transporter types might be sufficient for nutrient exchange as proton-coupled transporters are not only suited for the uptake of nutrients but also for their release; a transport mode that is often overseen. They work as perfect molecular machines that transport their substrate(s) along the coupled electrochemical gradients without rectification preferences (Carpaneto et al., 2005; Preuss et al., 2011).

To test whether the known proton-coupled transporters are sufficient for the nutrient exchange between plant and fungus we simulated in this study the transporter network in the AM interaction zone *in silico*. We show that a network of these transporters, which have been considered so far to mediate sugar or phosphate uptake only, functions in fact as a nutrient trade system with all properties that are observed in AM symbiosis. The presented computational cell biological data allow insights that are far beyond the reach of any wet-lab experimental technique available at the moment. The data suggest particular market forces of the P-C-exchange between plant and AM fungus, where their "cooperation" is the result of a competition of both for the same resources in the periarbuscular space. On the basis of this minimal model we evaluate the performance of the nutrient trade system if additionally sugar channels of the SWEET type are included.

MATERIALS AND METHODS

Geometry of the Plant Fungus Interface

A small sector of the interaction zone at an arbuscule can be approximated by two parallel plasma membranes separated by ~80–100 nm (**Figure 1A**). In this three compartment model the plant cytoplasm and the fungal cytoplasm are rather huge compared to the volume of the periarbuscular space. Fluxes between the compartments that strongly change the apoplastic concentration do not have a significant impact on the cytoplasmic concentrations; therefore, cytoplasmic concentrations were kept constant in the simulations. In the considered sector of the periarbuscular space, the concentrations could be contemplated without spatial imbalances as these gradients would quickly dissipate by diffusion in this tiny volume. Transport of sugar or phosphate across both membranes was mediated by H^+/sugar (H/C) and H^+/phosphate (H/P) cotransporters. H^+-ATPases were gathered with other potential ionic conductances in a background conductance (**Figure 1B**).

Mathematical Description of Transporter Activities

Voltage dependence of the H^+-ATPase driven background conductance was approximated by the sigmoidal function $I_{background} = I_{BG} = I_{BGmax} \times (1 - \exp[-(V_m - V_0) \times F/(RT)])/(1 + \exp[-(V_m - V_0) \times F/(RT)])$ (**Figure 2A**). Here, V_m is the voltage at the respective plasma membrane. The important feature of the H^+-ATPase driven background current is that it reverts its direction at a certain voltage, V_0, the equilibrium voltage. Positive of V_0, I_{BG} is positive, which means that

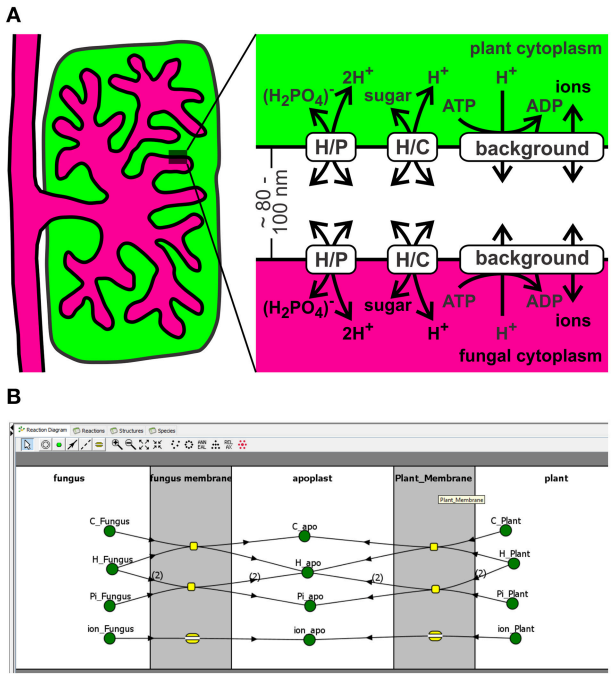

FIGURE 1 | A minimal transporter network for nutrient exchange in arbuscular mycorrhizal symbiosis. (A) The exchange zone was modeled as a three-compartment system with the 100 nm thick interfacial apoplast between plant and fungus and 50-fold larger cytoplasmic volumes. Note that different cytoplasms/apoplasm values do not qualitatively change the obtained results. The pH values were kept constant to pHcyt = 7.0 and pHapo = 6.0 to reflect the proton-buffer capacities (see also Discussion for the flexibility of these values). Transport of sugar or phosphate was mediated by H^+/sugar (H/C) and H^+/phosphate (H/P) cotransporters. The background conductance gathers the H^+-ATPase and other potential ionic conductances. In order to include the exchange of nitrogen sources, the network could be enlarged by NH_4^+-channels and electrogenic H^+/NO_3^-, H^+/amino acid or H^+/peptide co-transporters (Smith and Smith, 2011; Casieri et al., 2013). The qualitative conclusions would be identical to the considered P/C-exchange system. **(B)** Screenshot of the implementation of the three compartment model in VCell.

protons or other positive charges are exported from the cell, while negative of V_0, I_{BG} is negative, which means that cations (e.g., H^+, K^+, NH_4^+) flow into the cell and/or anions (e.g., NO_3^-) flow out of the cell. The value V_0 can be influenced by the activity of the H^+-ATPase. A larger activity increases the efflux of positive charges and drives V_0 to more negative voltages. I_{BGmax} is the maximal background current. RT/F $\sim$ 25 mV is a factor composed of gas constant, temperature and Faraday constant. Also the current voltage characteristics of proton-coupled H^+/X cotransporters $I_{H/X}$ revert their direction at a certain voltage, $E_{H/X}$, $I_{H/X}(E_{H/X}) = 0$. According to the enlarged Nernst-equation $E_{H/X}$ depends on the concentrations of protons and the co-transported molecule X at both sides of the membrane: $E_{H/X} = RT/F \times [n_x \times \ln(H_{apo}/H_{cyt}) + \ln(X_{apo}/X_{cyt})]/(n_x + z_x)$ (Nour-Eldin et al., 2012). Here, z_x is the valence of the ion/metabolite X, $z_C = 0$ in case of sugar and $z_P = -1$ in case of phosphate, $H_2PO_4^-$; n_x is the number of protons transported per one particle X. Positive of $E_{H/X}$, $I_{H/X}$ is positive, which means that H^+/X flow from the cell, while negative of $E_{H/X}$ H^+/X flow into the cell; $I_{H/X}$ is negative. At voltages, which are not too far from this equilibrium voltage, the current voltage dependence of H^+/X cotransporters can be approximated by a linear function according to the first-order Taylor approximation (Gajdanowicz et al., 2011) resulting in $I_{H/X} = G_{H/X} \times (V_m - E_{H/X})$ (**Figures 2B,C**). Here, $G_{H/X}$ is the conductance of the transporter. For $E_{H/C}$ and $E_{H/P}$, we set $n_C = 1$ without loss of generality for the sugar transporters (Carpaneto et al., 2005) and $n_P = 2$ for the phosphate transporters (Preuss et al., 2011). Different values, considering the conditions $n_C > 0$ and $n_P > 1$, respectively, do not change the results qualitatively. The transporter network is determined by the concentrations of H^+, phosphate and carbon in the different compartments (H_{cyt}^{plant}, H_{apo}, H_{cyt}^{fungus}, P_{cyt}^{plant}, P_{apo}, P_{cyt}^{fungus}, C_{cyt}^{plant}, C_{apo}, C_{cyt}^{fungus}) and the 10-not fully independent-parameters V_m^{plant}, V_m^{fungus}, I_{BGmax}^{plant}, I_{BGmax}^{fungus}, $V_0^{plant} = V_p^0$, $V_0^{fungus} = V_f^0$, $G_{H/P}^{plant}$, $G_{H/P}^{fungus}$, $G_{H/C}^{plant}$, $G_{H/C}^{fungus}$. To reflect the pH buffer capacities, the pH-values in the apoplast and the cytosols were set constant to $pH_{apo} = 6.0$; $pH_{cyt}^{plant} = pH_{cyt}^{fungus} = 7.0$. Sugar-flux through SWEET channels was modeled as a diffusion process: $J_{SWEET} = Diff_{SWEET} \times (C_{cyt}^{plant} - C_{apo})$. The diffusion factor $Diff_{SWEET}$ reflects the activity of SWEETs and was screened in the entire range from 0 to ∞.

Computational Cell Biology

The behavior of the transporter network was mathematically simulated using Virtual Cell Modeling and Analysis Software (**Figure 1B**) developed by the National Resource for Cell Analysis and Modeling, University of Connecticut Health Center (Loew and Schaff, 2001). The model source code is provided in the Supplementary Material.

Parameter Screening and Determination of Marginal Costs and Marginal Revenues

For each tested parameter the simulations were repeated with 28 logarithmically distributed values. As shown in the mathematical appendix (Supplementary Material), the dependency of the H/C- and H/P-fluxes on a certain parameter follows one of three possible equation types. The obtained H/P and H/C fluxes in equilibrium were used to determine the parameters in the respective equation. All non-linear fits were characterized by a regression coefficient of $r^2 = 1$, i.e., no variance, indicating the precise description of the simulation results by the independently derived mathematical equations. The parameters were then used to calculate the first derivatives and thus the marginal costs (MC) and marginal revenues (MR). In our study, compared MC and MR are always expressed in different "currencies" (C per time or P per time). To be able to compare MR and MC, the MR-values were converted into the MC-currency by a factor that indicates the internal value of the traded good for the respective organism.

RESULTS

Previous wet-lab studies provided evidence that the fungus and the plant express proton-coupled phosphate and sugar transporters during AM formation (Harrison and van Buuren,

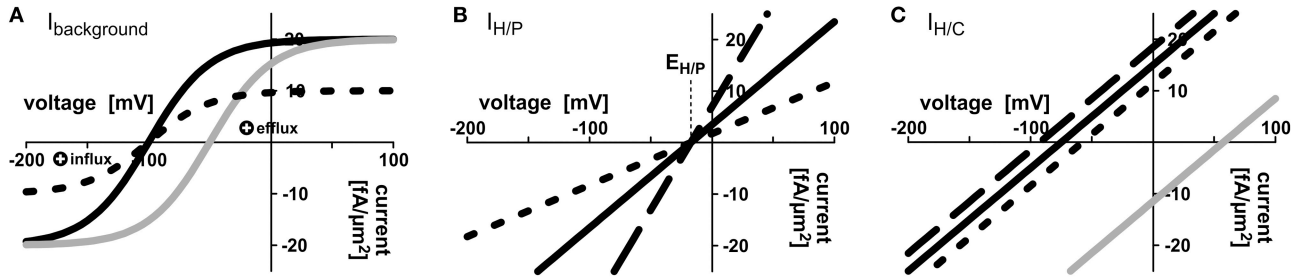

FIGURE 2 | Mathematical description of transporter activities. (A) Voltage dependence of the background conductance $I_{background} = I_{BG} = I_{BGmax} \times (1 - \exp[-(V - V_0) \times F/(RT)])/(1 + \exp[-(V - V_0) \times F/(RT)])$; here $V_0 = -100$ mV (*black curves*) or $V_0 = -50$ mV (*gray curve*); $I_{BGmax} = 20$ fA/µm^2 (*solid lines*), $I_{BGmax} = 10$ fA/µm^2 (*dotted line*). **(B,C)** Voltage dependencies of the **(B)** H/P and **(C)** H/C cotransporters were approximated by first-order Taylor approximation. **(B)** $I_{H/P} = G_{H/P} \times (V - RT/F \times [2 \times \ln(H_{apo}/H_{cyt}) + \ln(P_{apo}/P_{cyt})])$; $G_{H/P} = 200$ fA/(µm$^2 \times$ V) (*solid line*), $G_{H/P} = 400$ fA/(µm$^2 \times$ V) (*dashed line*), $G_{H/P} = 100$ fA/(µm$^2 \times$ V) (*dotted line*). $P_{cyt} = 2$ mM, $P_{apo} = 10$ µM, $pH_{cyt} = 7.0$, $pH_{apo} = 6.0$, i.e. $E_{H/P} = -17.3$ mV. **(C)** $I_{H/C} = 200$ fA/(µm$^2 \times$ V) $\times$ (V − RT/F $\times$ [ln(H_{apo}/H_{cyt}) + ln(C_{apo}/C_{cyt})]); $C_{cyt} = 2$ mM (*solid lines*), $C_{cyt} = 4$ mM (*dashed line*), $C_{cyt} = 1$ mM (*dotted line*), $C_{apo} = 10$ µM (*black lines*) or $C_{apo} = 2$ mM (*gray line*). The basic settings of the transporter network were: $P_{cyt}^{plant} = 1.5$ mM, $P_{cyt}^{fungus} = 3.0$ mM, $C_{cyt}^{plant} = 2$ mM, $C_{cyt}^{fungus} = 1$ mM, $pH_{apo} = 6.0$, $pH_{cyt}^{plant} = 7.0$, $pH_{cyt}^{fungus} = 7.0$, $G_{H/P}^{plant} = 200$ fA/(µm$^2 \times$ V), $G_{H/P}^{fungus} = 200$ fA/(µm$^2 \times$ V), $G_{H/C}^{plant} = 200$ fA/(µm$^2 \times$ V), $G_{H/C}^{fungus} = 200$ fA/(µm$^2 \times$ V), $I_{BGmax}^{plant} = 20$ fA/µm^2, $I_{BGmax}^{fungus} = 20$ fA/µm^2, $V_p^0 = V_0^{plant} = -75$ mV, $V_f^0 = V_0^{fungus} = -75$ mV. The free-running parameters in *in silico* simulations were the apoplastic concentrations P_{apo} and C_{apo}, and the voltages at the plant and fungal plasma membrane V_p, V_f.

1995; Gianinazzi-Pearson, 1996; Harrison, 1996; Rausch et al., 2001; Harrison et al., 2002; Paszkowski et al., 2002; Javot et al., 2007; Helber et al., 2011; Casieri et al., 2013). In an attempt to test if these known transporters are sufficient to explain the nutrient exchange in AM symbiosis between plants and mycorrhizal fungi we took this transporter network as basis and also included H^+-ATPase-driven background conductances in both membranes (**Figure 1**), then described all transporters mathematically (**Figure 2**) and carried out computational cell biology (dry-lab) experiments using VCell software (Loew and Schaff, 2001).

A Few Molecules Change Largely the Concentration in the Tiny Periarbuscular Space

The interfacial apoplast between plant and fungus is a very tiny compartment with thickness of about 80–100 nm (Balestrini and Bonfante, 2005). If we now consider exemplarily a membrane patch of 1 × 1 µm, the volume between the plant and fungal plasma membrane patches is 0.8–1 × 10^{-4} pL. The transport of 500–600 sugar/phosphate molecules across the membrane patch changes the apoplastic sugar/phosphate concentration by 10 µM, a concentration change that can be achieved by the activity of a single transporter per patch within a second as proton-coupled transporters usually transport ∼500 molecules per second (Derrer et al., 2013). These spatial conditions are considered in the cell biological simulations in order to reflect the real dimensions.

The H^+-Coupled Transporter Network Establishes a Defined Nutrient Exchange System

To elucidate whether the stability of the transporter network depends on the starting conditions, we tested a broad range of values. Irrespective of the starting condition the arbuscular transporter network (**Figure 1**) quickly attains a defined equilibrium state, at which the voltage at both membranes and the apoplastic sugar and phosphate concentrations are constant (**Figures 3A,B**). In **Figure 3**, the equilibration processes for two different starting conditions are shown. The apoplastic concentrations at equilibrium are in the micromolar or even sub-micromolar range (**Figure 3B**), which means that only a few phosphate or sugar molecules are left in the periarbuscular space. Interestingly, despite this emptiness, there is still a constant flux of phosphate from the fungus to the plant as indicated by a positive $I_{H/P}$ current across the fungal membrane and a negative $I_{H/P}$ current of the same amplitude across the plant membrane. This phosphate flux is accompanied by a sugar flux in the inverse direction (**Figure 3C**). Thus, the simple transporter network shown in **Figure 1** appears to be not only involved in nutrient uptake but is also well suited to mediate the P/C-exchange observed in arbuscular fungal symbiosis. In this nutrient exchange, the H/C efflux at the plant is accompanied by a positive electric $I_{H/C}$ current, which corresponds to a released electrochemical energy. This energy, in turn, is re-used by the plant for phosphate uptake by the electrogenic H/P-transporter. The positive $I_{H/C}$ current compensates the negative $I_{H/P}$ current. At the fungal membrane it is the other way round. Here, the released electrochemical energy from phosphate efflux energizes sugar uptake. The simple nutrient exchange system is highly energy-efficient.

Demand and Supply Strategy in Nutrient Deal

To get more insights into the dynamics of the transporter system, we systematically analyzed its properties in dry-lab experiments. At first, we repeated the simulations with different phosphate and sugar concentrations in the cytosol of the plant and the fungus (**Figure 4**). If the sugar concentration in the plant cytosol is increased, both H/P- and H/C-fluxes are stimulated (**Figure 4A**).

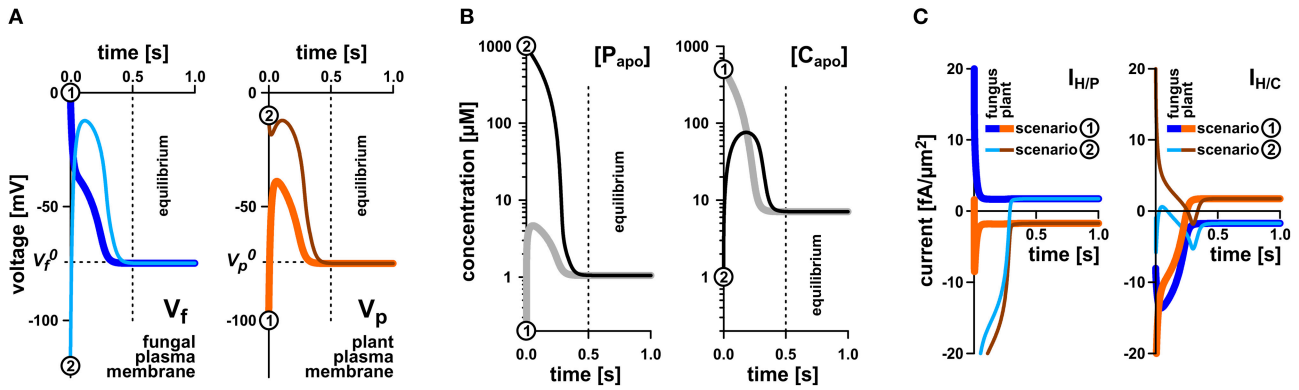

FIGURE 3 | Rapid equilibration of the nutrient uptake system. (A) Time course of equilibration of the membrane voltages at the fungal plasma membrane (left) and the plant plasma membrane (right). (**B**) Time course of equilibration of the apoplastic phosphate (left) or sugar concentrations (right). (**C**) Time course of equilibration of proton-couplesd phosphate ($I_{H/P}$, left) and sugar fluxes ($I_{H/C}$, right) across the plant and fungal plasma membrane. Irrespective of the starting conditions (apoplastic P and C concentrations and voltages at the fungal and plant plasma membranes) the system reaches quickly an equilibrium that depends on the P and C concentrations in the cytosols of plant and fungus and the relative settings of the transporters. The equilibration processes for two different starting conditions [1, *thicker lines, gray* in **(B)**, *dark blue* or *orange* in **(A,C)**, and 2, *thinner lines, black* in **(B)**, *light blue* and *brown* in **(A,C)**] are shown. Please note that the equilibration time depends on the expression level of the transporters. In this study, a rather low expression level was chosen. The overall increase of the expression level would result in faster equilibration. In equilibrium there is still a continuous flux of phosphate from the fungus to the apoplast (**C**, left, positive current) and from the apoplast to the plant (**C**, left, negative current). Similarly, there is a constant flux of sugar from the plant via the apoplast to the fungus (**C**, right).

Although one parameter is changed only, the increased C-gradient not only induces a larger sugar flux from the plant to the fungus but, due to the electrogenic nature of the H/C and H/P transport, also induces a larger phosphate flux in the inverse direction. The same phenomenon manifests if the phosphate concentration in the fungus is increased (**Figure 4D**), if the sugar concentration in the fungus is reduced (**Figure 4B**), or if the phosphate concentration in the plant is decreased (**Figure 4C**). Actually, the fluxes depend on the sugar and phosphate gradients between plant and fungus, which reflect "supply" and "demand" of the partners. More sugar in the plant cytosol (**Figure 4A**) or more phosphate in the fungal cytosol (**Figure 4D**) can be considered as a higher supply, while less sugar in the fungus (**Figure 4B**) or less phosphate in the plant (**Figure 4C**) represent a higher demand. Interestingly, the change of only one parameter is sufficient to enhance both, P and C transport. And in this it is irrelevant whether one partner provides higher supply (reciprocal reward (Kiers et al., 2011), **Figures 4A,D**) or gestures a higher demand (**Figures 4B,C**).

Plant and Fungus Interact on Equal Terms

The two symbionts can control the nutrient fluxes not only via their cytosolic phosphate and sugar concentrations but also by regulating the activity of the transporters. If, for instance, the plant invests more energy to fuel H^+-ATPases, its membrane voltage gets more negative (**Figure 2A**, shift from gray to black solid curve, V_p^0 gets more negative). As a consequence, the C-loss of the plant gets smaller while its P-gain gets larger (**Figure 5A**, 1). In comparison to the situation in **Figure 3**, now the plant energizes the P-uptake not only by the electrochemical energy of H/C-release, but invests energy from a different source (e.g., ATP hydrolysis). Such a situation is considered as standard if the plant is absorbing P from the surrounding soil. However, in AM symbiosis, the improvement of the plant's P/C-balance is at the cost of the fungus' C/P-balance. In return, the fungus can positively influence its C/P-balance by also investing more energy to fuel H^+-ATPases resulting in a negative shift of V_f^0 and a more negative voltage at the fungal membrane (**Figure 5A**, 2). Remarkably, by larger energy investment the fungus could even invert the P-efflux into an influx; similarly, the plant could invert the C-efflux into an influx. Thus, as one organism can absorb both, C and P, each partner could in principle exploit the other. Plant and fungus are therefore in a kind of "arms race" with a "balance of power" at $V_p^0 = V_f^0$ (or $\Delta V_0 = V_f^0 - V_p^0 = 0$, **Figures 5A**, **6**). As a consequence, apoplastic [P] and [C] are very low (**Figures 5B,C**; see also above). These low concentrations have a positive side-effect since it allows each partner to monitor the cooperativity of the other (**Figure 7**). In an example that should illustrate this fact we consider an H/C-transporter, a cytosolic C-concentration of $[C]_{cyt} = 2$ mM and a pH difference between cytosol and apoplast of 1. In case the apoplastic C-concentration is initially $[C]_{apo} = 10\,\mu M$, the H/C-transporter does not transport in either direction if the membrane voltage is $V = E_{H/C} \approx -75$ mV. More positive of $E_{H/C}$ the H/C-flux is out of the cell while more negative of $E_{H/C}$ it is into the cell (**Figure 7**, black curve). The increase of $[C]_{apo}$ by additional $5\,\mu M$ shifts this equilibrium voltage by about 10 mV more positive to $E_{H/C} \approx -65$ mV (**Figure 7**, gray dashed curve). It can be observed that a change of $[C]_{apo}$ by $5\,\mu M$ converts an initial H/C-efflux into an influx, if the membrane voltage is kept at -70 mV. Now, considering the same change in concentration, in an upper range limit (from $[C]_{apo} = 1000\,\mu M$ to $[C]_{apo} = 1005\,\mu M$), the equilibrium voltage is $E_{H/C} \approx +40$ mV (**Figure 7**, blue curve). The increase of $[C]_{apo}$ by additional $5\,\mu M$ has no remarkable effect neither on the equilibrium voltage, nor on the flux direction at a certain voltage (**Figure 7**, yellow dashed curve). Thus, due to the low apoplastic concentrations of the exchanged nutrients

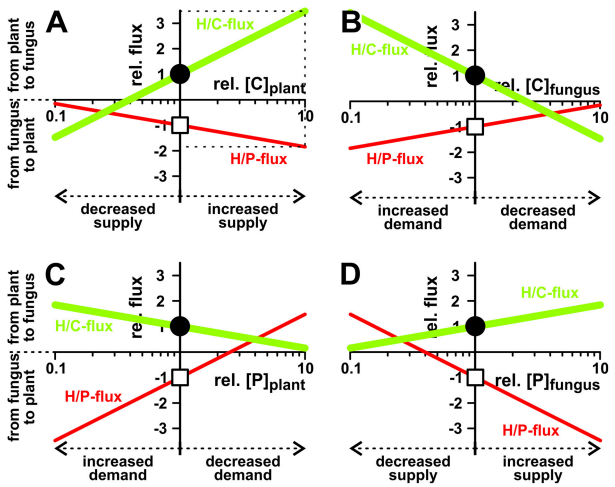

FIGURE 4 | Dependency of nutrient exchange on supply and demand. Proton-coupled sugar (H/C, *green curves, lighter/bigger in gray scale*) and phosphate (H/P, *red curves, darker/smaller in gray scale*) fluxes in equilibrium as a function of varying cytosolic concentrations of **(A,B)** sugar ([C]) and **(C,D)** phosphate ([P]) in the plant **(A,C)** and the fungus **(B,D)**. For better comparison, concentrations, and fluxes were normalized. As reference we chose the H/C-flux across the plant membrane in equilibrium of the condition shown in **Figure 3**. The reference condition ($[C]_{plant}$ = 2 mM, $[C]_{fungus}$ = 1 mM, $[P]_{plant}$ = 1.5 mM, $[P]_{fungus}$ = 3 mM) is indicated by the position of the vertical axes and the circles (H/C) and squares (H/P). Concentration changes in [C] and [P] are displayed as relative changes. For instance, a value of $[C]_{plant}$ = 4 mM correlates with rel.$[C]_{plant}$ = 2, i.e., a doubling of the C-concentration in the plant, while halving the concentration to $[C]_{plant}$ = 1 mM correlates with rel.$[C]_{plant}$ = 0.5. Likewise, fluxes are displayed as relative fluxes: rel.flux = flux/(H/C-$flux_{in\ reference\ condition}$). The dotted lines in **(A)** exemplify the reading of the figure: Compared to the reference condition, a 10-fold increase of $[C]_{plant}$ (rel.$[C]_{plant}$ = 10) would result in a 3.5-fold increase in H/C-flux (rel.flux = 3.5) and a 1.8-fold increase in H/P-flux (rel.flux = −1.8).

in the tiny volume of the periarbuscular space one partner can sense within seconds or even faster the activity and therefore cooperativity of the other symbiont.

In a different scenario plant and fungus can regulate their proton coupled transporters to modify the fluxes for their benefits (**Figure 8**). Increasing the activity of any of the four transporter types increases the fluxes of both, sugar and phosphate. Nevertheless, if one partner may decide to reduce its nutrient loss, it does not need to sacrifice fully its nutrient gain. In principle, the plant could switch off the activity of its sugar transporters (H/C) and would still benefit from significant phosphate supply by the fungus (**Figure 8A**, arrow). In this case the plant acts solely with a proton pump-driven proton-coupled phosphate transporter and uses the energy from ATP hydrolysis for the uptake of phosphate. Similarly, the fungus could shut down its phosphate transporters without losing all sugar supply (H/P; **Figure 8B**, arrow) and would switch into a proton pump-driven uptake mode.

Basic Microeconomic Principles Provide the Driving Forces for a Cooperative Behavior

In their trade of nutrients plant and fungus are participants in a local economy. Therefore, we had to cross disciplines and analyzed the transporter system in scientific terms not only from a biological but also from an economical perspective. In the simplest notion both, plant and fungus, are considered as selfish partners in a bi-polar economy. They neither exhibit altruistic behavior nor any other long-term collaboration strategy. Instead, each is only interested in maximizing the gain for reasonable costs. The gain of the plant is accumulation of phosphate per time and that of the fungus is accumulation of sugar per time. The main cost for the plant is the loss of sugar per time and for the fungus is the loss of phosphate per time.

We started the economic considerations with a game theoretical scenario. When plant and fungus play the "game of nutrient exchange," one partner may suddenly decide to cut off the other from nutrient supply, while still benefiting from an influx, albeit slightly reduced (**Figure 8**). A reasonable reaction of the cheated partner on such an event would be the cessation of supply for its part. Without activities of neither the H/C-transporter in the plant nor the H/P-transporter in the fungus there is no phosphate-sugar exchange anymore. Thus, at first glance, the system presented in **Figure 1** does not appear to be well-suited for nutrient exchange as it would be stable in a Nash-equilibrium that is not favorable for both sides, similar to the well-known prisoners' dilemma. However, in contrast to the prisoners, who could choose between two options only, plant and fungus have a continuum of options and can adjust their transporter activities smoothly. In this case, the optimal condition, i.e., the Nash-equilibrium, can be determined by the relationship between marginal costs and marginal revenues (**Figure 9**). To assess which might be the optimal expression and activity level of a certain transporter, we compare the additional revenue for the respective organism with the additional costs when increasing the activity level a bit more. If the marginal revenue is still larger than the marginal costs it is worth for the organism to increase the activity level further until the marginal revenue equals the marginal costs. Upon a further increase of the transporter activity the marginal costs would be higher than the marginal revenue, which would not be optimal for the organism. Thus, the intersection of marginal revenue and marginal cost curves defines a stable economic equilibrium.

To evaluate the economically optimal activity of H/C-transporters in the plant plasma membrane, the marginal revenue is calculated from the H/P-flux curve in **Figure 8A** and the marginal cost from the H/C-flux curve. On top of these expenses other fixed costs for the expression and functional maintenance of the transporter can be considered. The plant generates a benefit as long as the marginal revenue curve is above the marginal cost curve (**Figures 10A–C**). This condition sets the economical limit for the activity of the H/C-transporters. As shown in **Figure 10**, the higher the plant values the traded phosphate the more H/C-transporters can be active. A low phosphate value can certainly result in the non-cooperative scenario described above, in which the plant does not maintain functional H/C-transporters (**Figure 10A**).

Based on economic principles we thus postulate the regulation of the plant H/C-transporter in response to the plant's phosphate status. Although this signaling cascade remains to be elucidated in wet-lab experiments, several experimental findings are well

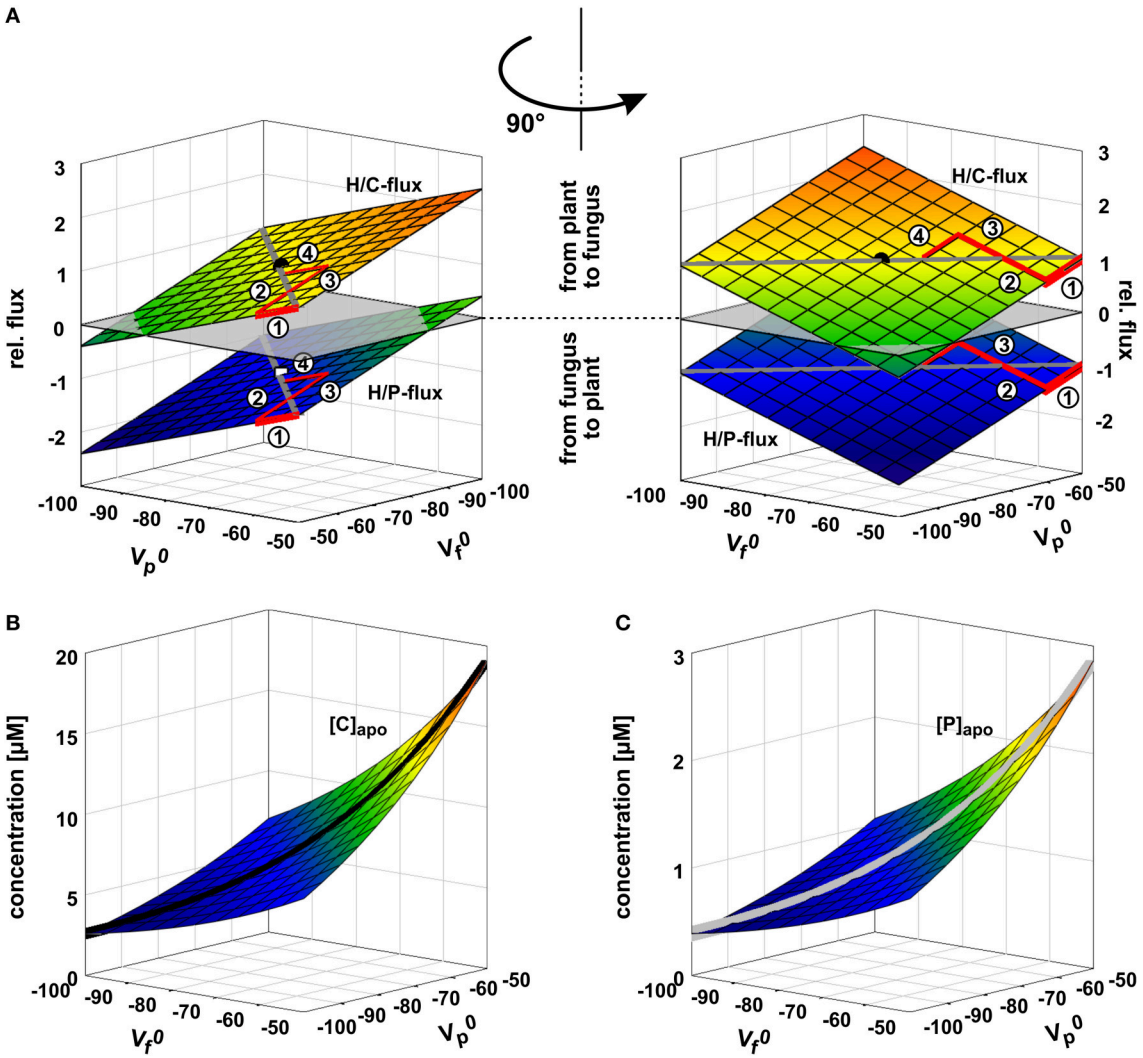

FIGURE 5 | Arms race in adjusting the zero-current voltages of the background conductance. (A) Relative phosphate (H/P) and sugar (H/C) fluxes as a function of the zero-current voltages of the plant's (V_p^0) and fungus' (V_f^0) background conductances. V_p^0 and V_f^0 are strongly influenced by the activity of H^+-ATPases; a higher pump activity drives the values to more negative voltages. If the plant unilaterally invests more pump energy, V_p^0 gets more negative and the plant benefits from a higher P-influx while reducing the C-efflux. In its extreme the plant could even achieve a C-flux from the fungus to the plant (negative values for H/C-flux). The gain of the plant is at the cost of the fungus. In return, the fungus can also invest pump energy and drive V_f^0 more negative with positive consequences for its C/P-balance but at the cost of the plant. The arms race between plant and fungus ($1 \rightarrow 2 \rightarrow 3 \rightarrow 4 \rightarrow \ldots$) as equal partners ends in a draw at which $\Delta V_0 = V_f^0 - V_p^0 = 0$ with negative V_p^0 and V_f^0 values. The dot indicates the condition chosen for the other simulations in this study ($V_p^0 = V_f^0 = -75$ mV). **(B,C)** Apoplastic carbon/sugar (**B**, [C]) and phosphate (**C**, [P]) concentrations at equilibrium of the transporter network as a function of V_p^0 and V_f^0. During the arms race between plant and fungus both concentrations decline (*black* and *gray curves*).

in line with such a mechanism. For instance, if the plant gets significant amounts of phosphate from other sources like mineral fertilizers or other symbiotic organisms, the phosphate provided by the fungus is of lesser value for the plant and the plant declines its cooperativity toward the fungus (Cowden and Peterson, 2009; Verbruggen and Kiers, 2010; Kiers et al., 2011; Wyatt et al., 2016).

At the fungal side of the periarbuscular space we can consider the microeconomic situation for the activity of the fungal H/C-transporter. In this case, sugar is the desired good and phosphate is the currency to pay with. As shown in **Figures 10D–F**, from an economic point of view it makes sense for the fungus to maintain a high H/C-transporter activity even for a lower carbon value.

The economically optimal activity of phosphate transporters can be analyzed in a similar manner with analogous results: In economically optimal conditions the fungal H/P-transporter activity strongly depends on the value that sugar has for the fungus while throttling the plant H/P-transporter is not as price dependent (not shown).

Also the sugar and phosphate supply is subject to market forces (**Figures 4**, **10G,H**). Although one partner could

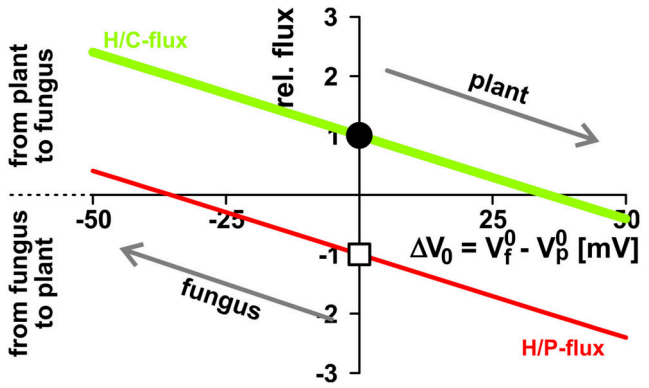

FIGURE 6 | Opposite interests of plant and fungus maintain a balance of power. The activity of H^+-ATPases influences the zero-current potentials (plant: V_p^0; fungus: V_f^0) of the background conductances at the plasma membranes. The proton-coupled sugar (H/C, *green, lighter/bigger in gray scale*) and phosphate (H/P, *red, darker/smaller in gray scale*) fluxes depend on the difference $\Delta V_0 = V_f^0 - V_p^0$. The plant has the interest to drive V_p^0 more negative (and therefore to drive ΔV_0 more positive) to reduce the loss in sugar and to increase the gain in phosphate, while the fungus tends to reduce the loss of phosphate and to increase the gain of sugar by driving V_f^0 (and ΔV_0) more negative. Between equal partners the different forces balance at $\Delta V_0 = 0$. For further details, see also **Figure 5**. For better comparison, fluxes were normalized, as explained in **Figure 4**, to the H/C-flux across the plant membrane in equilibrium of the condition shown in **Figure 3** and displayed as relative changes. Circle (H/C) and square (H/P) indicate this reference condition.

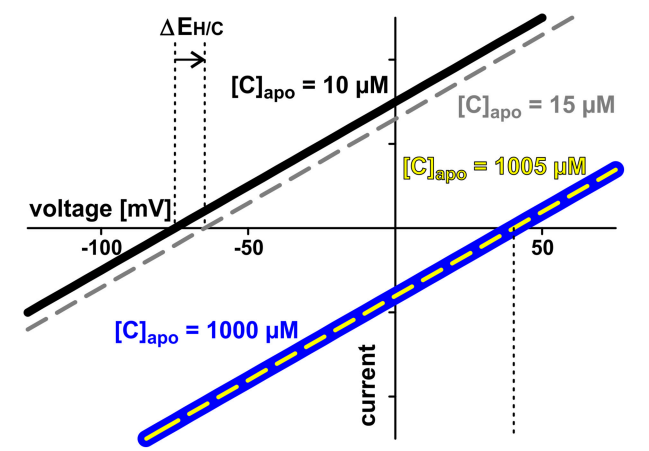

FIGURE 7 | Low apoplastic concentrations facilitate sensing by proton-coupled transporters. Exemplarily the current voltage curves of a proton-coupled H/C-transporter are shown. The cytosolic sugar concentration is $[C]_{cyt} = 2$ mM in all cases. Two cases are considered: In case 1 (*black* and *gray curves*) the apoplastic concentration is initially $[C]_{apo} = 10\,\mu M$ (*black*). The increase by additional 5 µM shifts the current voltage characteristics to less negative voltages ($\Delta E_{H/C}$, *gray, dashed*). The transporter senses the 5 µM difference. The modified properties feedback on the entire transporter network. In case 2 (*blue* and *yellow curves*) the apoplastic concentration is initially $[C]_{apo} = 1000\,\mu M$ (*blue*) and increase of the same magnitude (5 µM) does not change the current voltage characteristics (*yellow*). The transporter cannot sense the difference between $[C]_{apo} = 1000\,\mu M$ and $[C]_{apo} = 1005\,\mu M$. There is no feedback of the concentration change to the transporter network.

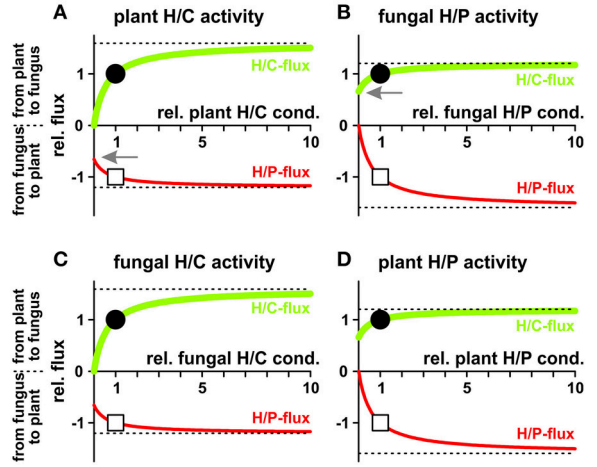

FIGURE 8 | Dependency of proton-coupled sugar (H/C, *green*) and phosphate (H/P, *red*) fluxes on the activity of plant and fungal transporters. (A) Fluxes as a function of the activity of the plant H/C-transporter. **(B)** Fluxes as a function of the activity of the fungal H/P-transporter. **(C)** Fluxes as a function of the activity of the fungal H/C-transporter. **(D)** Fluxes as a function of the activity of the plant H/P-transporter. For better comparison, fluxes were normalized, as explained in **Figure 4**, to the H/C-flux across the plant membrane in equilibrium of the condition shown in **Figure 3** and displayed as relative changes. Circle (H/C) and square (H/P) indicate the reference condition. If, *ceteris paribus*, all plant H/C-transporters are turned off, the sugar flux vanishes while there is still a significant phosphate flux from the fungus to the plant (**A**, arrow). If, *ceteris paribus*, all fungal H/P-transporters are shut down, the phosphate flux vanishes while there is still a significant sugar flux from the plant to the fungus (**B**, arrow). The dotted lines indicate the maximal fluxes that can be achieved at infinitely high expression and activity levels.

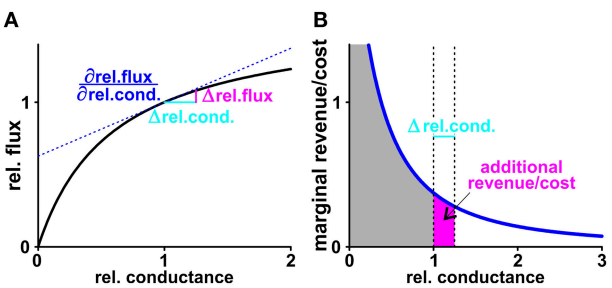

FIGURE 9 | Marginal revenue/marginal cost. (A) The black curve shows exemplarily the dependency of the normalized sugar flux on the normalized conductance of the plant H/C-transporter. The normalization process results in unit-less values: Doubling the conductance from $G_{H/C}^{plant} = 200$ fA/(µm^2 ×V) to 400 fA/(µm^2 ×V) is equivalent to a shift of the relative conductance from 1 to 2. This change increases the H/C-flux from 1.74 to 2.13 fA/µm^2, which is equivalent to an increase in the relative flux from 1 to 1.22. If the rel.conductance changes by the small amount Δrel.cond. (*light blue*) there is an additional H/C-flux (Δrel.flux, *magenta*) from the plant. At the limit $\Delta\,\text{rel.cond.} \to 0$ the additional flux can be calculated as $\Delta\,\text{rel.flux} = \frac{\partial \text{rel.flux}}{\partial \text{rel.cond.}} \cdot \Delta\,\text{rel.cond.}$ with the derivative of the black curve $\frac{\partial \text{rel.flux}}{\partial \text{rel.cond.}}$ at the starting point (*blue*, *dashed line*). **(B)** The derivative of the black curve is the marginal cost curve (*blue*). The surface below the curve down to the axis (*gray*) indicates the total cost. For a small change Δrel.cond. (*light blue*) the additional surface (*magenta*) indicates the additional cost superimposed by this change. Calculations of marginal revenues are equivalent to the considerations for "costs" outlined here in detail.

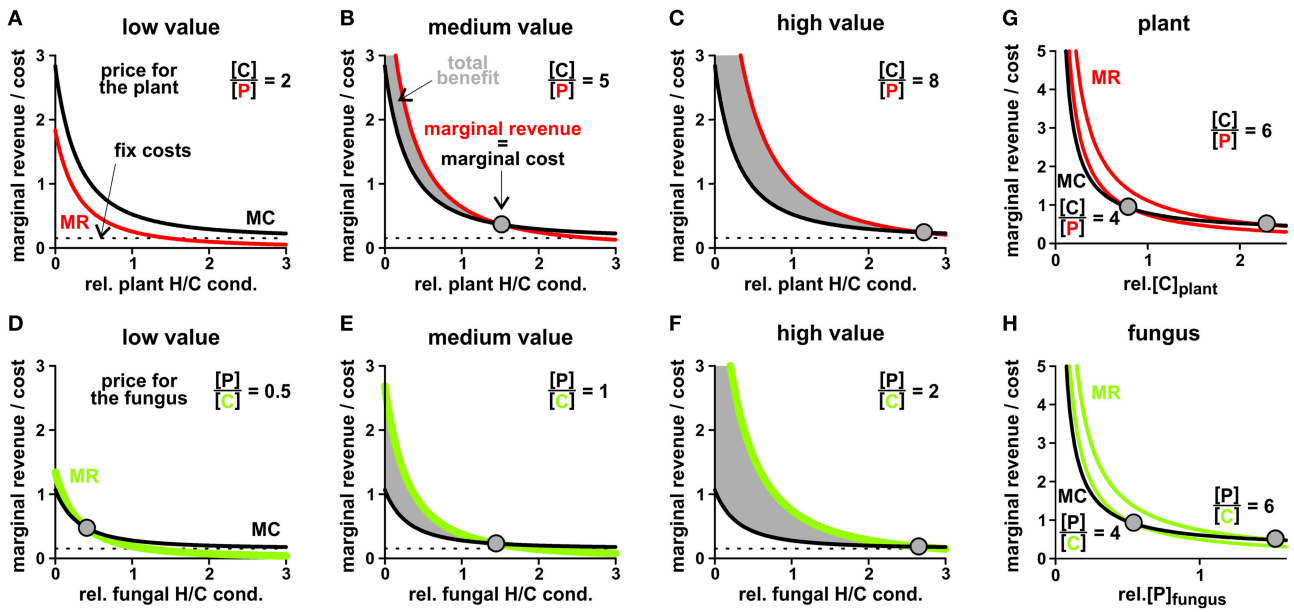

FIGURE 10 | Price-dependent economic optimisation of transporter activity and cytosolic concentrations. (A–C) Adjustment of the plant H/C-transporter activity in three different scenarios: the phosphate provided by the fungus is **(A)** of low value (1 P values 2 C for the plant), **(B)** medium value (C/P = 5) and **(C)** high value for the plant (C/P = 8). In all cases, the revenue of the plant in terms of delivered P increases (**Figure 8**), however, the marginal revenue (*MR*, *red*) decreases with increasing transporter activity (relative plant H/C conductance). The plant "pays" a carbon source and may have additional fix costs for the expression and maintenance of functional transporters (marginal cost curve, *MC*, *black*). The intersection of the MR with the MC curve indicates the point of economic equilibrium, at which the marginal revenue equals the marginal costs (*dots*). At a higher H/C-transporter activity the additional costs of the plant would be higher than its additional revenue, while at a lower activity the plant would not make maximal profit. Please note that in **(A)** the two curves do not intersect; the economical equilibrium is at zero, i.e. no plant H/C-transporter activity. **(D–F)** Adjustment of the fungal H/C-transporter activity in three different scenarios: the carbon source provided by the plant is **(D)** of low value (2 C values 1 P for the fungus), **(E)** medium value (P/C = 1) and **(F)** high value for the fungus (P/C = 2). The marginal revenues for the carbon source (*MR*, *green*) are compared with the marginal cost curve (MC, *black*) for phosphate and potential fix costs. **(G,H)** Price-dependent economic optimisation of nutrient supply. **(G)** Marginal cost = additional carbon/sugar release (*MC*, *black*) and marginal revenue = additional phosphate gain (*MR*, *red*) as a function of the cytosolic sugar ([C]) concentration in the plant for two different plant-specific C/P values. With increasing C/P value the economic equilibrium shifts to higher cytosolic [C] levels. **(H)** Marginal cost = additional phosphate release (*MC*, *black*) and marginal revenue = additional carbon/sugar gain (*MR*, *green*) as a function of the cytosolic phosphate ([P]) concentration in the fungus for two different fungus-specific P/C values. With increasing P/C value the economic equilibrium shifts to higher cytosolic [P] levels. Please note: The MC and MR curves do not have units as they are the first derivatives of the unit-less relative P- and C-fluxes plus the fix costs in case of MC. To be able to compare MR with MC their different "currencies" (C per time or P per time) were converted by the indicated conversion factor, which indicates the individual value for the respective organism.

theoretically achieve nutrient gain for zero or even negative costs by keeping the cytosolic concentrations very low, the total benefit is maximized if significant amounts of P and C, respectively, are provided. Also here, the optimal conditions depend on the organism-specific internal value of the traded good (**Figures 10G,H**). Thus, the simple transporter system is highly flexible and both partners can control nutrient exchange at several set screws.

Increasing Complexity by Expanding the Model

The presented minimal model for a nutrient trade system explains very well observed phenomena. It can thus serve as benchmark to evaluate the performance of alternative and/or enlarged models for nutrient exchange. P and C sources might be transported not only via proton-coupled transporters but by diffusion facilitators. For instance, P could also be transported via phosphate-permeable anion channels (Dreyer et al., 2012) and C could be transported in neutral form as sugar through sugar channels (Chen et al., 2010) or as organic acid through channels of the ALMT type (Dreyer et al., 2012). Models that also contain ion channels are predominantly developed for guard cells (Hills et al., 2012; Blatt et al., 2014; Minguet-Parramona et al., 2016). Here, we increased the complexity of the minimal model by integrating sugar channels of the SWEET type for sugar release (**Figure 11**) from the plant as they have been found to be also upregulated during arbuscule formation (Manck-Götzenberger and Requena, 2016). However, under the dry lab conditions tested in this work, the functional expression of sugar diffusion facilitators (SWEET) in addition to the H/C-transporter impairs the plant's nutrient deal. Without active SWEET channels, there is a constant sugar flux from the plant cytosol to the periarbuscular space and from the periarbuscular space to the fungus (**Figure 11B**, black circle). In return there is a constant flux of phosphate from the fungus via the periarbuscular space to the plant (**Figure 11B**, white square).

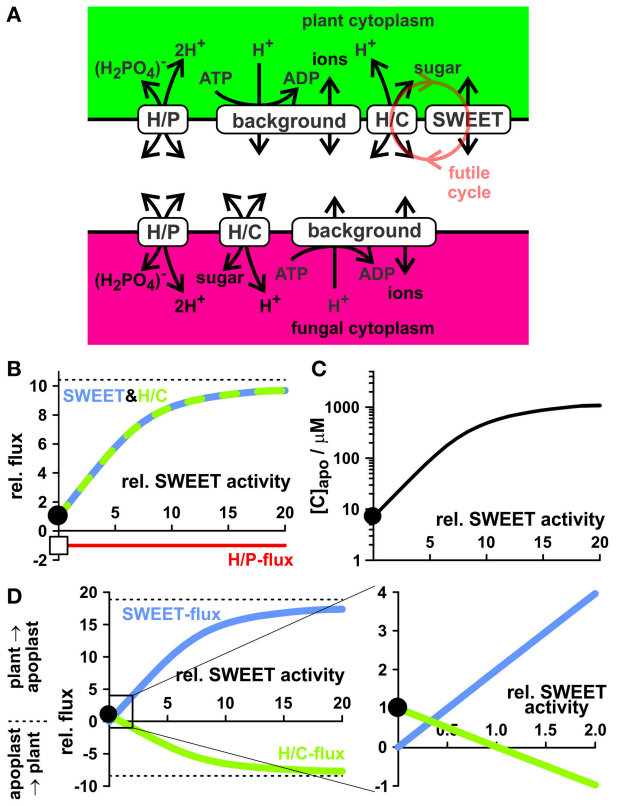

FIGURE 11 | The futile cycling of sugar. (A) Transporter network that allows the efflux of electroneutral sugar molecules from the plant to the periarbuscular space via proton-coupled transporters (H/C) and sugar channels (SWEET). The red circle indicates the futile sugar cycle that results from the co-existence of active H/C and SWEET transporters. **(B)** Dependency of the sugar/phosphate exchange between plant and fungus on the activity of SWEET channels. Without active SWEET channels, there is a constant sugar flux from the plant cytosol to the periarbuscular space and from the periarbuscular space to the fungus. All displayed fluxes are normalized to this H/C-flux (*black circle*). In return there is a constant flux of phosphate from the fungus via the periarbuscular space to the plant (*white square*). Upon increasing the activity of the SWEET channel, this phosphate flux is not affected while the sugar flux from the plant to the fungus rises. The dotted line indicates the maximal flux that can be achieved at infinitely high SWEET activity levels. **(C)** Activation of SWEET channels floods the apoplast with sugar. Equilibrium apoplastic sugar concentration as a function of the activity of SWEET channels. **(D)** Sugar flux through H/C and SWEET from the plant to the apoplast and from the apoplast to the plant as a function of the activity of SWEET channels. The right panel is an enlargement of the black rectangle in the left panel. Without active SWEET channels the transmembrane sugar gradient drives H^+/sugar efflux via H/C-transporters. Here, each sugar molecule transports a proton from the plant cytosol to the apoplast and assists the H^+-ATPase in charging the proton gradient that can be harvested by the H/P transporter for phosphate uptake. With increasing SWEET activity more and more sugar flows without piggybacked proton from the cytosol to the apoplast and is re-taken up by H/C-transporters. Activity of SWEET channels was normalized, so that at a relative activity of 1 the flux through H/C-transporters reverts its direction.

Upon increasing the activity of SWEET channels, this phosphate flux is not affected while the sugar flux from the plant to the fungus rises. Jointly, also the apoplastic sugar concentration rises (**Figure 11C**) and the altered H^+/sugar gradient modifies the transport direction of the H/C-transporters. They turn from efflux transporters into influx transporters (**Figure 11D**) and are employed to retrieve sugar molecules from the periarbuscular space using the electrochemical proton gradient established by H^+-ATPases. Thus, the co-existence of active proton-coupled H/C-transporters and C diffusion facilitators transporting the same carbon source would not only promote the dissipation of the energy of the sugar gradient, it would also increase the apoplastic C concentration, with the concomitant risk of losing carbon from the periarbuscular space by diffusion, and would additionally provoke a waste of valuable energy via the creation of a futile cycle of sugar efflux and retrieval. In order to avoid this futile cycle, the model suggests that either the SWEETs are tightly regulated or separated from regions where proton-coupled co-transporters exist, which use the same substrate as the SWEETs.

DISCUSSION

In this study we elaborated the thermodynamic flexibility of the simple transporter system shown in **Figure 1** using computational cell biology. This approach allowed us to gain insights into the system that are far beyond the reach of any wet-lab experimental technique available at the moment. To evaluate the robustness of the obtained results we assessed the foundations and the limits of the model.

The Model is Based on Wet-Lab Experimental Evidence

Extensive molecular biology work and proteomic approaches provide clear evidence that proton-coupled phosphate and sugar transporters are present in the periarbuscular zone (Harrison and van Buuren, 1995; Gianinazzi-Pearson, 1996; Harrison, 1996, 2012; Rausch et al., 2001; Harrison et al., 2002; Paszkowski et al., 2002; Karandashov and Bucher, 2005; Javot et al., 2007; Helber et al., 2011; Doidy et al., 2012). However, at the moment it is not clear whether also other types of transporters like sugar channels or phosphate-permeable anion channels may contribute to the nutrient exchange as well. We therefore consider the model shown in **Figure 1** as a basic model that can be extended in future computational cell biology studies (as exemplarily shown in **Figure 11**) in order to evaluate the thermodynamic advantages and disadvantages of the expression and activation of these newly discovered transporters. A subsequent justification of the model design is provided by the conclusions drawn from this study. The results explain the big advantages of handling the nutrient exchange via H^+-coupled transporters, as in this case each organism maintains tight control over the exchange process (**Figure 7**).

The Simulation Covers a Broad Range of Biological Realities

The model is characterized by a large set of 20 free or partially dependent parameters. Namely these are: the distance between the two membranes, the concentrations of protons, sugar and phosphate in the three compartments, the activity/expression levels of the six transporters, the equilibrium voltages V_p^0 and

V_f^0 of the H^+-ATPase-dependent background conductances, and the voltages at the two membranes. To gain confidence in the reliability of the simulations the parameters were carefully assessed: (i) The size of the periarbuscular space was set to 100 nm, a value reported in literature (Balestrini and Bonfante, 2005). This value was used to calculate the volume of the apoplast between both membranes and to determine the concentration changes during the simulations. The increase or decrease of this value in the simulation by a factor of 10 (1 μm and 10 nm, respectively) affected only the initial equilibration process (time interval before the dashed line in **Figure 3**) by factor ∼3 and ∼0.8, respectively, but left the equilibrium conditions unaffected. Because in this study we considered the system always in its equilibrium, the results presented here do not depend on the exact size of the interfacial apoplast between plant and fungus. (ii) The pH values were set to physiological pH7.0 in the cytosols and to pH6.0 in the apoplast. A different apoplastic pH in the range <pH7.0 does not affect qualitatively the results. A far lower pH (Guttenberger, 2000) would result in even lower nutrient concentrations in the periarbuscular space. (iii) The activity levels of the six transporters were normalized to the activity of the plant H/C-transporter in a reference condition (**Figure 3**). When we changed all activities in the reference condition by factor 0.1 or factor 10 only the initial equilibration process was affected. It slowed down or increased by a factor of 10. Thus, the behavior of the system in equilibrium does not depend on the absolute expression/activity level of the transporters, but only on the relative activity levels toward each other. (iv) The other parameters were either determined in the simulations ($[C_{apo}]$, $[P_{apo}]$, V_p, V_f) or they were screened in the entire reasonable interval (from $-\infty$ to ∞ for V_p^0 and V_f^0, or from 0 to ∞ for the relative transporter activities and for $[C]_{plant}$, $[C]_{fungus}$, $[P]_{plant}$, $[P]_{fungus}$). In summary we can state that we have explored the entire parameter space of the system. Therefore, the results presented here represent a broad range of biological realities, rather than being restricted to a particular set of parameters.

The Molecular Model Explains Macroscopic Observations

The transporter network shown in **Figure 1** reflects the basic transporters needed by the plant and the fungus to selfishly accumulate phosphate and sugar from the closer environment. It is widely assumed that the bidirectional mutualism observed in arbuscular mycorrhizal symbiosis must involve other, so far unknown, transporters that mediate the efflux of phosphate from the fungus and of carbohydrates from the plant (Bonfante and Genre, 2010; Smith and Smith, 2011; Johri et al., 2015). Although we do not exclude the involvement of other transporters, here we provide evidence by computational cell biology that the simple system of proton-coupled transporters would be sufficient for the exchange of phosphate and sugar between plant and fungus at the arbuscular interface. In this special environment the proton-coupled H/P- and H/C-transporters ensure very low apoplastic sugar and phosphate concentrations. Under these conditions, the Nernst-equilibrium of the proton-coupled transporters is at moderately negative, physiological voltages and slight variations in membrane voltage and/or concentrations can change the flux direction through the transporters. Thus, H/P- and H/C-transporters can function as both, uptake and release pathways; the direction of flux depends on the electrochemical gradients. If plant and fungus optimize their economic benefits everyone for themselves, they establish a robust, tightly controllable, long-lasting trade in phosphate and sugar. The properties of the plant fungal P/C-economics of the transporter network (**Figure 1**) are well in line with those observed in ecological wet-lab experiments (Kiers et al., 2011). In other words, our model predicts precisely macroscopic observations. Indubitably, the dry-lab experiments presented here cannot provide an airtight proof of the accuracy of the working model but, the evidence provided manifests its validity.

Competition—the Basis of Cooperation in AM Symbiosis?

It might shake our idealistic picture of mutualist symbiosis when stating that plant and fungus compete with each other for the same resources. However, the model presented in this study paradoxically explains the nutrient exchange between plant and fungus with the simple assumption that each organism is only interested in maximizing the gain for reasonable costs. Such self-organizing processes are well-known in economics and were first described in 1776 by the Scottish philosopher Adam Smith (1776) for a selfish human economy. Adapted to AM symbiosis the famous statement of Smith would read: *both actors, plant and fungus, intending only their own gains are led by an invisible hand to promote an end that was no part of their intentions.*

AUTHOR CONTRIBUTIONS

ID conceived the project and supervised the research. SS, BV, DB, JG, TS, and ID planned and designed computational cell biology experiments; and analyzed the data. JG, TS, and ID wrote the manuscript. All authors had intellectual input on the project and commented on the manuscript.

FUNDING

This work was supported by the interdisciplinary Ph.D. program of the Universidad de Talca (SS, BV, DB) and the FONDECYT grant N° 1150054 of the Comisión Nacional Científica y Tecnológica of Chile (ID, JG, TS).

ACKNOWLEDGMENTS

We kindly acknowledge the KhanAcademy for the publically available online course in microeconomics (https://www.khanacademy.org/economics-finance-domain/microeconomics).

SUPPLEMENTARY MATERIAL

The Supplementary Material for this article can be found online at: http://journal.frontiersin.org/article/10.3389/fpls.2016.00912

REFERENCES

Balestrini, R., and Bonfante, P. (2005). The interface compartment in arbuscular mycorrhizae: a special type of plant cell wall? *Plant Biosyst.* 139, 8–15. doi: 10.1080/11263500500056799

Blatt, M. R., Wang, Y., Leonhardt, N., and Hills, A. (2014). Exploring emergent properties in cellular homeostasis using OnGuard to model K+ and other ion transport in guard cells. *J. Plant Physiol.* 171, 770–778. doi: 10.1016/j.jplph.2013.09.014

Bonfante, P., and Genre, A. (2010). Mechanisms underlying beneficial plant-fungus interactions in mycorrhizal symbiosis. *Nat. Commun.* 1, 48. doi: 10.1038/ncomms1046

Carpaneto, A., Geiger, D., Bamberg, E., Sauer, N., Fromm, J., and Hedrich, R. (2005). Phloem-localized, proton-coupled sucrose carrier ZmSUT1 mediates sucrose efflux under the control of the sucrose gradient and the proton motive force. *J. Biol. Chem.* 280, 21437–21443. doi: 10.1074/jbc.M501785200

Casieri, L., Ait Lahmidi, N., Doidy, J., Veneault-Fourrey, C., Migeon, A., Bonneau, L., et al. (2013). Biotrophic transportome in mutualistic plant-fungal interactions. *Mycorrhiza* 23, 597–625. doi: 10.1007/s00572-013-0496-9

Chen, L.-Q., Hou, B.-H., Lalonde, S., Takanaga, H., Hartung, M. L., Qu, X.-Q., et al. (2010). Sugar transporters for intercellular exchange and nutrition of pathogens. *Nature* 468, 527–532. doi: 10.1038/nature09606

Cowden, C. C., and Peterson, C. J. (2009). A multi-mutualist simulation: applying biological market models to diverse mycorrhizal communities. *Ecol. Modell.* 220, 1522–1533. doi: 10.1016/j.ecolmodel.2009.03.028

Derrer, C., Wittek, A., Bamberg, E., Carpaneto, A., Dreyer, I., and Geiger, D. (2013). Conformational changes represent the rate-limiting step in the transport cycle of maize sucrose transporter1. *Plant Cell* 25, 3010–3021. doi: 10.1105/tpc.113.113621

Doidy, J., Grace, E., Kühn, C., Simon-Plas, F., Casieri, L., and Wipf, D. (2012). Sugar transporters in plants and in their interactions with fungi. *Trends Plant Sci.* 17, 413–422. doi: 10.1016/j.tplants.2012.03.009

Dreyer, I., Gomez-Porras, J. L., Riaño-Pachón, D. M., Hedrich, R., and Geiger, D. (2012). Molecular Evolution of Slow and Quick Anion Channels (SLACs and QUACs/ALMTs). *Front. Plant Sci.* 3:263. doi: 10.3389/fpls.2012.00263

Fitter, A. H. (2006). What is the link between carbon and phosphorus fluxes in arbuscular mycorrhizas? A null hypothesis for symbiotic function. *New Phytol.* 172, 3–6. doi: 10.1111/j.1469-8137.2006.01861.x

Gajdanowicz, P., Michard, E., Sandmann, M., Rocha, M., Corrêa, L. G. G., Ramírez-Aguilar, S. J., et al. (2011). Potassium (K+) gradients serve as a mobile energy source in plant vascular tissues. *Proc. Natl. Acad. Sci. U.S.A.* 108, 864–869. doi: 10.1073/pnas.1009777108

Gianinazzi-Pearson, V. (1996). Plant cell responses to arbuscular mycorrhizal fungi: getting to the roots of the symbiosis. *Plant Cell* 8, 1871–1883. doi: 10.1105/tpc.8.10.1871

Guttenberger, M. (2000). Arbuscules of vesicular-arbuscular mycorrhizal fungi inhabit an acidic compartment within plant roots. *Planta* 211, 299–304. doi: 10.1007/s004250000324

Harrison, M. J. (1996). A sugar transporter from *Medicago truncatula*: altered expression pattern in roots during vesicular-arbuscular (VA) mycorrhizal associations. *Plant J.* 9, 491–503. doi: 10.1046/j.1365-313X.1996.09040491.x

Harrison, M. J. (2012). Cellular programs for arbuscular mycorrhizal symbiosis. *Curr. Opin. Plant Biol.* 15, 691–698. doi: 10.1016/j.pbi.2012.08.010

Harrison, M. J., Dewbre, G. R., and Liu, J. (2002). A phosphate transporter from *Medicago truncatula* involved in the acquisition of phosphate released by arbuscular mycorrhizal fungi. *Plant Cell* 14, 2413–2429. doi: 10.1105/tpc.004861

Harrison, M. J., and van Buuren, M. L. (1995). A phosphate transporter from the mycorrhizal fungus Glomus versiforme. *Nature* 378, 626–629. doi: 10.1038/378626a0

Helber, N., Wippel, K., Sauer, N., Schaarschmidt, S., Hause, B., and Requena, N. (2011). A versatile monosaccharide transporter that operates in the arbuscular mycorrhizal fungus Glomus sp is crucial for the symbiotic relationship with plants. *Plant Cell* 23, 3812–3823. doi: 10.1105/tpc.111.089813

Hills, A., Chen, Z. H., Amtmann, A., Blatt, M. R., and Lew, V. L. (2012). OnGuard, a computational platform for quantitative kinetic modeling of guard cell physiology. *Plant Physiol.* 159, 1026–1042. doi: 10.1104/pp.112.197244

Hoeksema, J. D., and Schwartz, M. W. (2003). Expanding comparative-advantage biological market models: contingency of mutualism on partners' resource requirements and acquisition trade-offs. *Proc. Biol. Sci.* 270, 913–919. doi: 10.1098/rspb.2002.2312

Javot, H., Penmetsa, R. V., Terzaghi, N., Cook, D. R., and Harrison, M. J. (2007). A *Medicago truncatula* phosphate transporter indispensable for the arbuscular mycorrhizal symbiosis. *Proc. Natl. Acad. Sci. U.S.A.* 104, 1720–1725. doi: 10.1073/pnas.0608136104

Johri, A. K., Oelmüller, R., Dua, M., Yadav, V., Kumar, M., Tuteja, N., et al. (2015). Fungal association and utilization of phosphate by plants: success, limitations, and future prospects. *Front. Microbiol.* 6:984. doi: 10.3389/fmicb.2015.00984

Karandashov, V., and Bucher, M. (2005). Symbiotic phosphate transport in arbuscular mycorrhizas. *Trends Plant Sci.* 10, 22–29. doi: 10.1016/j.tplants.2004.12.003

Kiers, E. T., Duhamel, M., Beesetty, Y., Mensah, J. A., Franken, O., Verbruggen, E., et al. (2011). Reciprocal rewards stabilize cooperation in the mycorrhizal symbiosis. *Science* 333, 880–882. doi: 10.1126/science.1208473

Klepek, Y.-S., Geiger, D., Stadler, R., Klebl, F., Landouar-Arsivaud, L., Lemoine, R., et al. (2005). Arabidopsis POLYOL TRANSPORTER5, a new member of the monosaccharide transporter-like superfamily, mediates H+-Symport of numerous substrates, including myo-inositol, glycerol, and ribose. *Plant Cell* 17, 204–218. doi: 10.1105/tpc.104.026641

Krajinski, F., Courty, P.-E., Sieh, D., Franken, P., Zhang, H., Bucher, M., et al. (2014). The H+-ATPase HA1 of *Medicago truncatula* is essential for phosphate transport and plant growth during Arbuscular Mycorrhizal Symbiosis. *Plant Cell* 26, 1808–1817. doi: 10.1105/tpc.113.120436

Loew, L. M., and Schaff, J. C. (2001). The Virtual Cell: a software environment for computational cell biology. *Trends Biotechnol.* 19, 401–406. doi: 10.1016/S0167-7799(01)01740-1

Manck-Götzenberger, J., and Requena, N. (2016). Arbuscular mycorrhiza symbiosis induces a major transcriptional reprogramming of the potato sweet sugar transporter family. *Front. Plant Sci.* 7:487. doi: 10.3389/fpls.2016.00487

Marschner, H. (2012). *Marschner's Mineral Nutrition of Higher Plants*, *3rd Edn*. London: Academic Press.

Minguet-Parramona, C., Wang, Y., Hills, A., Vialet-Chabrand, S., Griffiths, H., Rogers, S., et al. (2016). An optimal frequency in Ca2+ oscillations for stomatal closure is an emergent property of ion transport in guard cells. *Plant Physiol.* 170, 33–42. doi: 10.1104/pp.15.01607

Noë, R., and Hammerstein, P. (1995). Biological markets. *Trends Ecol. Evol.* 10, 336–339.

Nour-Eldin, H. H., Andersen, T. G., Burow, M., Madsen, S. R., Jørgensen, M. E., Olsen, C. E., et al. (2012). NRT/PTR transporters are essential for translocation of glucosinolate defence compounds to seeds. *Nature* 488, 531–534. doi: 10.1038/nature11285

Parniske, M. (2008). Arbuscular mycorrhiza: the mother of plant root endosymbioses. *Nat. Rev. Microbiol.* 6, 763–775. doi: 10.1038/nrmicro1987

Paszkowski, U., Kroken, S., Roux, C., and Briggs, S. P. (2002). Rice phosphate transporters include an evolutionarily divergent gene specifically activated in arbuscular mycorrhizal symbiosis. *Proc. Natl. Acad. Sci. U.S.A.* 99, 13324–13329. doi: 10.1073/pnas.202474599

Preuss, C. P., Huang, C. Y., and Tyerman, S. D. (2011). Proton-coupled high-affinity phosphate transport revealed from heterologous characterization in Xenopus of barley-root plasma membrane transporter, HvPHT1;1. *Plant Cell Environ.* 34, 681–689. doi: 10.1111/j.1365-3040.2010.02272.x

Ramos, A. C., Façanha, A. R., and Feijó, J. A. (2008). Proton (H+) flux signature for the presymbiotic development of the arbuscular mycorrhizal fungi. *New Phytol.* 178, 177–188. doi: 10.1111/j.1469-8137.2007.02344.x

Rausch, C., Daram, P., Brunner, S., Jansa, J., Laloi, M., Leggewie, G., et al. (2001). A phosphate transporter expressed in arbuscule-containing cells in potato. *Nature* 414, 462–470. doi: 10.1038/35106601

Schwartz, M. W., and Hoeksema, J. D. (1998). Specialization and resource trade: biological markets as a model of mutualisms. *Ecology* 79, 1029–1038. doi: 10.1890/0012-9658(1998)079[1029:SARTBM]2.0.CO;2

Smith, A. (1776). *An Inquiry into the Nature and Causes of the Wealth of Nations*. London: W. Strahan & T. Cadell.

Smith, F. A., and Smith, S. E. (2015). How harmonious are arbuscular mycorrhizal symbioses? Inconsistent concepts reflect different mindsets as well as results. *New Phytol.* 205, 1381–1384. doi: 10.1111/nph.13202

Smith, S. E., Jakobsen, I., Grønlund, M., and Smith, F. A. (2011). Roles of arbuscular mycorrhizas in plant phosphorus nutrition: interactions between pathways of phosphorus uptake in arbuscular mycorrhizal roots have important implications for understanding and manipulating plant phosphorus acquisition. *Plant Physiol.* 156, 1050–1057. doi: 10.1104/pp.111.174581

Smith, S. E., and Smith, F. A. (2011). Roles of arbuscular mycorrhizas in plant nutrition and growth: new paradigms from cellular to ecosystem scales. *Annu. Rev. Plant Biol.* 62, 227–250. doi: 10.1146/annurev-arplant-042110-103846

van der Heijden, M. G. A., Martin, F. M., Selosse, M.-A., and Sanders, I. R. (2015). Mycorrhizal ecology and evolution: the past, the present, and the future. *New Phytol.* 205, 1406–1423. doi: 10.1111/nph.13288

Verbruggen, E., and Kiers, T. E. (2010). Evolutionary ecology of mycorrhizal functional diversity in agricultural systems. *Evol. Appl.* 3, 547–560. doi: 10.1111/j.1752-4571.2010.00145.x

Wyatt, G. A. K., Kiers, E. T., Gardner, A., and West, S. A. (2016). Restricting mutualistic partners to enforce trade reliance. *Nat. Commun.* 7, 10322. doi: 10.1038/ncomms10322

Conflict of Interest Statement: The authors declare that the research was conducted in the absence of any commercial or financial relationships that could be construed as a potential conflict of interest.

Advantages of publishing in Frontiers

OPEN ACCESS
Articles are free to read, for greatest visibility

COLLABORATIVE PEER-REVIEW
Designed to be rigorous – yet also collaborative, fair and constructive

FAST PUBLICATION
Average 85 days from submission to publication (across all journals)

COPYRIGHT TO AUTHORS
No limit to article distribution and re-use

TRANSPARENT
Editors and reviewers acknowledged by name on published articles

SUPPORT
By our Swiss-based editorial team

IMPACT METRICS
Advanced metrics track your article's impact

GLOBAL SPREAD
5'100'000+ monthly article views and downloads

LOOP RESEARCH NETWORK
Our network increases readership for your article

Frontiers
EPFL Innovation Park, Building I • 1015 Lausanne • Switzerland
Tel +41 21 510 17 00 • Fax +41 21 510 17 01 • info@frontiersin.org
www.frontiersin.org

Find us on